The Role of Charge-Transfer Interactions and Delocalization in Annelated Nitronyl Nitroxides

by

Brynn Mary Dooley
B.Sc., Okanagan University College, 2005

A Dissertation Submitted in Partial Fulfillment
of the Requirements for the Degree of

DOCTOR OF PHILOSOPHY

in the Department of Chemistry

Supervisory Committee

The Role of Charge-Transfer Interactions and Delocalization in Annelated Nitronyl Nitroxides

by

Brynn Mary Dooley
B.Sc., Okanagan University College, 2005

Supervisory Committee

Dr. Natia L. Frank, (Department of Chemistry)
Supervisor

Dr. Reginald H. Mitchell, (Department of Chemistry)
Departmental Member

Dr. Cornelia Bohne, (Department of Chemistry)
Departmental Member

Dr. Chris Papadopoulos, (Department of Electrical and Computer Engineering)
Outside Member

Abstract

Supervisory Committee
Dr. Natia L. Frank, (Department of Chemistry)
Supervisor
Dr. Reginald H. Mitchell, (Department of Chemistry)
Departmental Member
Dr. Cornelia Bohne, (Department of Chemistry)
Departmental Member
Dr. Chris Papadopoulos, (Department of Electrical and Computer Engineering)
Outside Member

The design and synthesis of stable organic radicals with delocalized spin density distribution and low energy optical and redox processes is central to the development of magneto-conducting materials. Towards this end, a generalized synthetic methodology has been developed allowing for the synthesis of a series of annelated benzonitronyl nitroxide (BNN) radicals. The BNN radicals exhibited remarkably low reduction potentials (~0.0 V vs SCE) and a near-infrared absorption attributed to a HOMO–SOMO charge-transfer excitation.

The annelated BNN radicals were found to be less stable than the closely related tetramethyl nitronyl nitroxide radicals, particularly in solution. A series of π-delocalized and heteroaromatic radicals were synthesized to determine if the instability was due to the delocalization of electron density onto the carbon skeleton or the low reduction potential. DFT calculations with the EPR-II basis gave rise to calculated electronic structures that were consistent with EPR spectroscopy and suggested changes in spin density distribution are occurring with perturbation of the annelated ring. Cyclic voltammetry revealed the heteroaromatic and π-delocalized radicals had reduction potentials lower than BNN, with some systems reducing at potentials of 0.2 V vs SCE, comparable to that of 7,7,8,8-tetracyanoquinodimethane. The distribution of spin

throughout the molecular framework and the low reduction potential of the annelated nitronyl nitroxide radicals were both found to contribute to the lowered stability of the annelated nitronyl nitroxides relative to the far less redox active tetramethyl nitronyl nitroxides.

The low reduction potential of the BNN radicals suggested that incorporation into acceptor–donor (A–D) systems would allow for investigation of the role of charge transfer interactions on the electronic structure and properties of neutral open-shell A–D radicals. Two D–A–D radicals were prepared using metal catalyzed coupling and furoxan condensation methodologies which resulted in incorporation of a second donor in the *C*5 position of the BNN moiety. The radical D^1–A–D^2 triads, where D^1 = thiophene and D^2 = thiophene or phenyl, exhibited three intramolecular charge-transfer excitations (λ_{max} = 550, 580 and 1000 nm) that were investigated by variable temperature absorption spectroscopy. Structural characterization of the triads in the solid state by single crystal and powder X-ray diffraction revealed slipped π stacks that arise from intermolecular π–π and D–A interactions, providing pathways for antiferromagnetic (AFM) and ferromagnetic (FM) exchange. While the phenyl substituted triad (Th–BNN–Ph) exhibited antiferromagnetic interactions and a room temperature conductivity of σ_{RT} = 10^{-7} S cm^{-1}, the thienyl substituted derivative (Th–BNN–Th) exhibited short-range FM interactions and increased conductivity (σ_{RT} = 10^{-5} S cm^{-1}), giving rise to an organic semiconductor exhibiting FM exchange. The differences in conductivity and magnetic behavior were rationalized by the degree of slippage dictated by an interplay between π–π and intermolecular D−A interactions.

Finally, a series of BNN–D radicals were investigated where the donor ability of D was systematically varied from E_{ox} = 2.30 V vs SCE (benzene) to 0.32 V vs SCE (tetrathiafulvalene). Calculations of the near-infrared charge transfer excitation suggested that the HOMO–SOMO gap could be significantly decreased with increasing donor ability, consistent with charge transfer theory. A subset of the series of BNN–D radicals with D = anisole, benzo[*b*]thiophene, *N*-methylindole, *N*-ethylcarbazole, and *N,N*-diphenylaniline were synthesized. Solution state spectroscopic studies of the series by EPR and electronic absorption spectroscopy revealed spin-delocalized structures with extremely low reduction potentials (~0 V vs SCE). The solid state properties of the BNN–D radicals were investigated by magnetometry and room temperature conductivity measurements. Due to primarily steric interactions, weak D–A coupling was observed, with weak intermolecular interactions in the solid state leading to paramagnetic and insulating behaviour. The BNN-(*N,N*-diphenylaniline) radical structure was characterized by single crystal XRD and found to exist as well isolated radical moieties with extremely weak intermolecular interactions, consistent with magnetometry and conductivity measurements.

Table of Contents

List of Figures

List of Tables

List of Schemes

List of Numbered Compounds

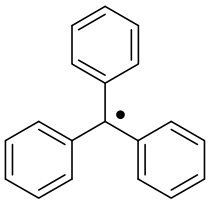

1.1

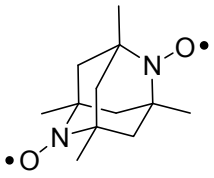

1.2

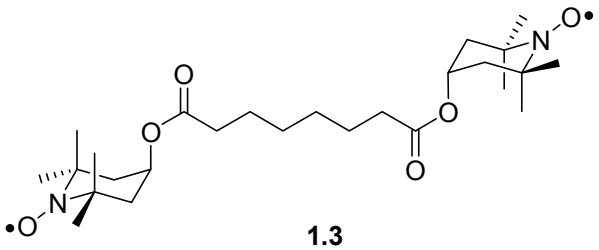

1.3

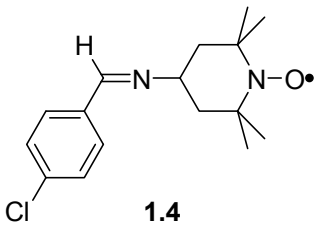

1.4

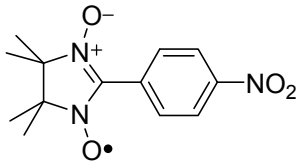

1.5

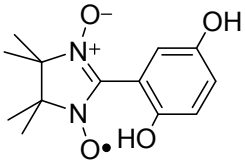

1.6

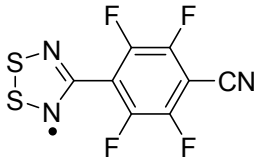

1.7

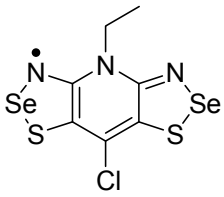

1.8

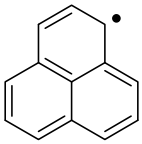

1.9

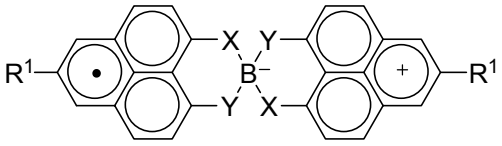

X = NR^2, O
Y = O

1.10

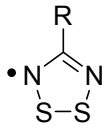

1.11

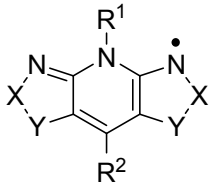

X, Y = S or Se

1.12

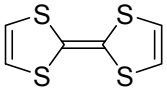

1.13

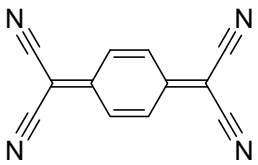

1.14

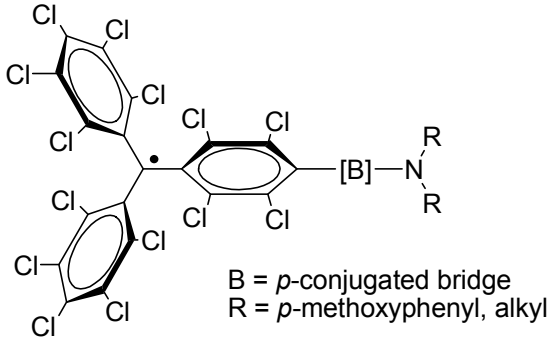

1.15

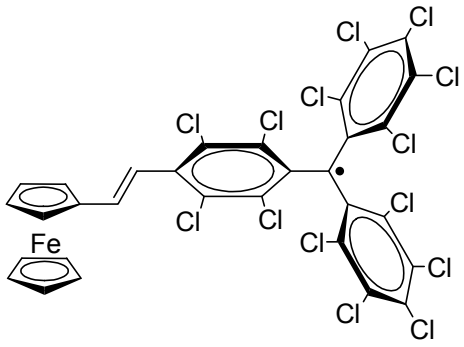

1.16

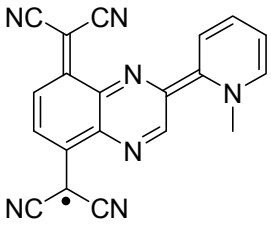

1.17

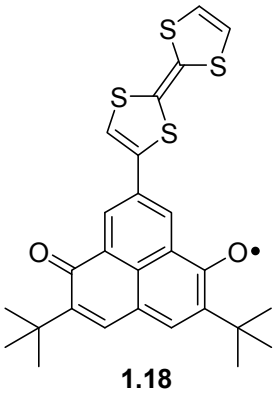

1.18

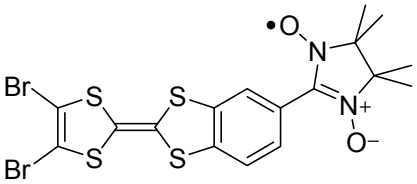

1.19

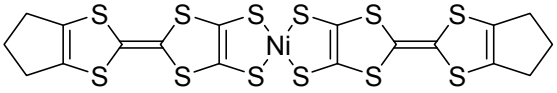

1.20

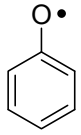

2.1

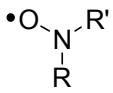

2.2

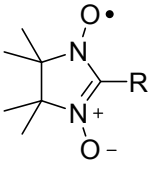

2.3

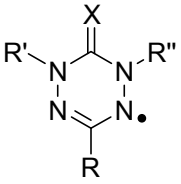

2.4

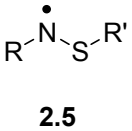

2.5

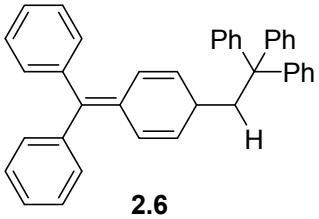

2.6

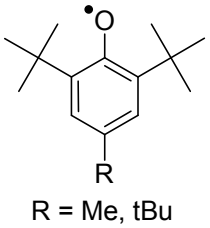

2.7

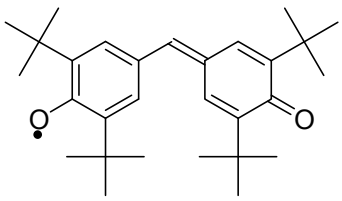

2.8

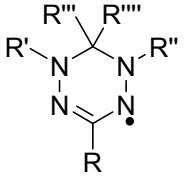

2.9

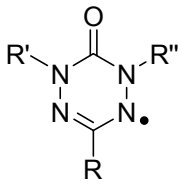

2.10

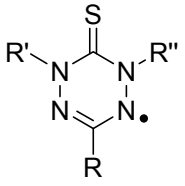

2.11

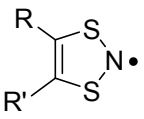

2.12

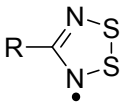

2.13

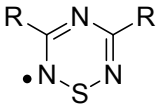

2.14

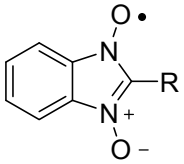

2.15

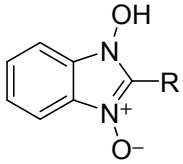

2.16

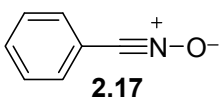

2.17

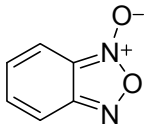

2.18

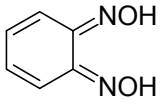

2.19

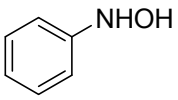

2.20

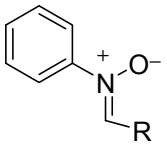

2.21a-l

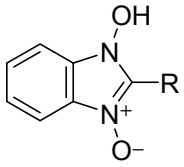

2.16a-l

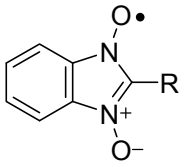

2.15a-e

R =

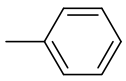

a

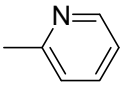

b

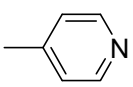

c

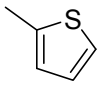

d

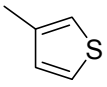

e

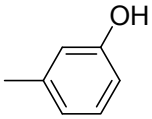

f

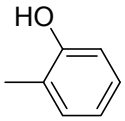

g

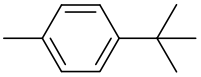

h

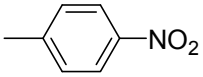

i

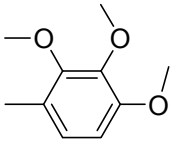

j

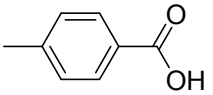

k

l

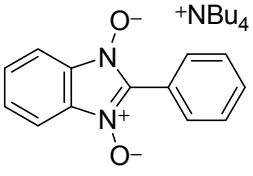

2.22

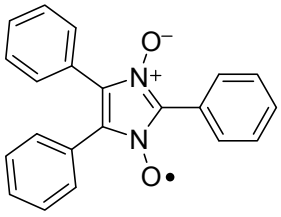

3.1

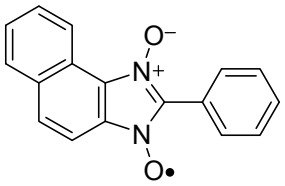

3.2

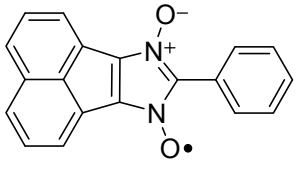

3.3

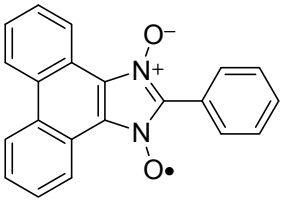

3.4

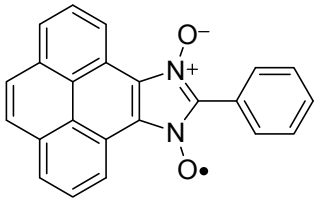

3.5

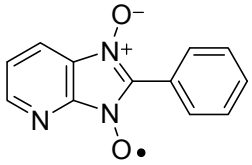

3.6

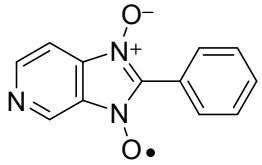

3.7

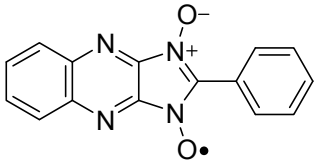

3.8

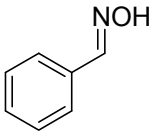

3.9

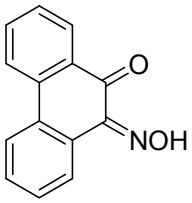

3.10

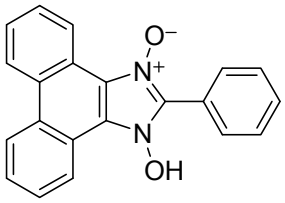

3.11

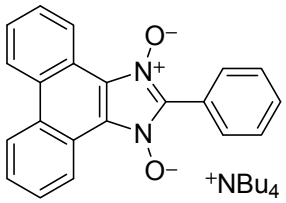

3.12

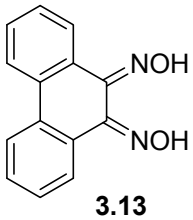

3.13

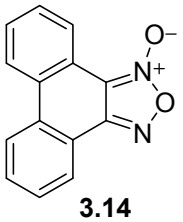

3.14

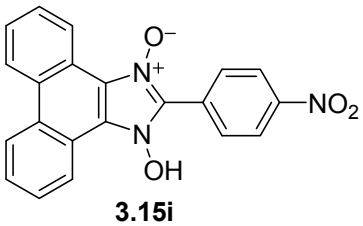

3.15i

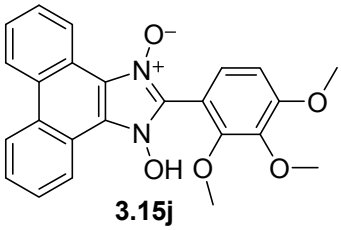

3.15j

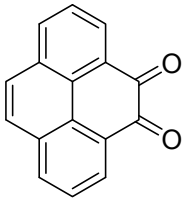

3.16

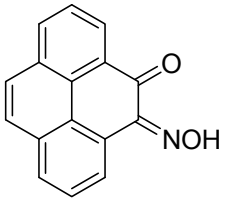

3.17

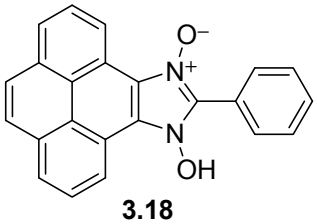

3.18

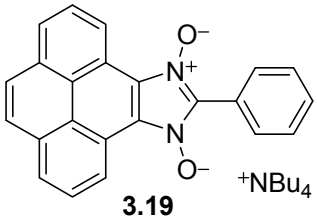

3.19

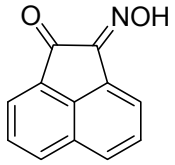

3.20

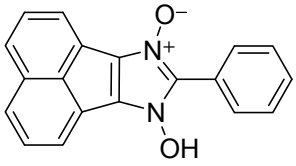

3.21

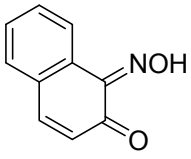

3.22

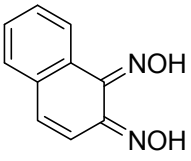

3.23

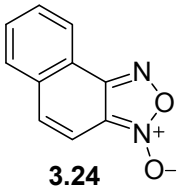

3.24

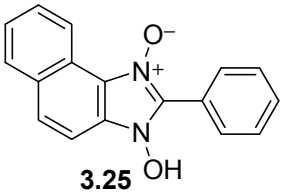

3.25

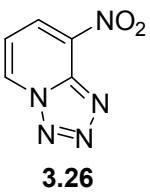

3.26

3.27

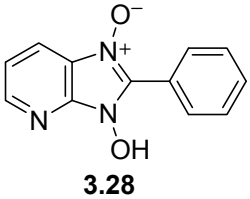

3.28

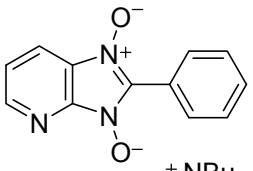

3.29

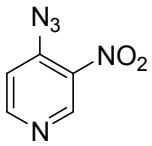

3.30

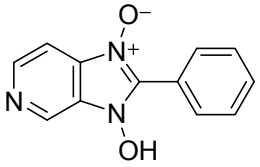

3.31

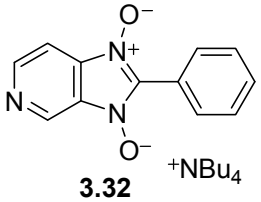

3.32

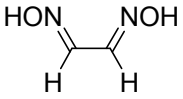

3.33

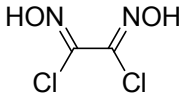

3.34

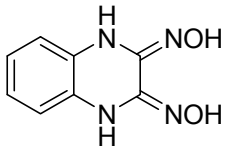

3.35

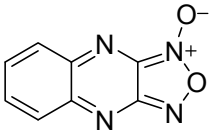

3.36

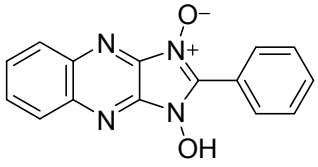

3.37

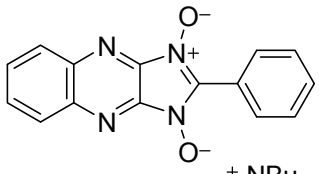

3.38

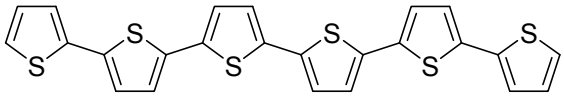

4.1

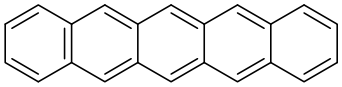

4.2

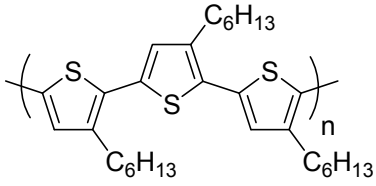

4.3

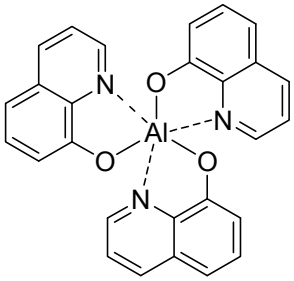

4.4

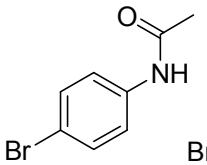

4.5

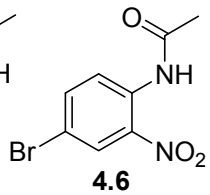

4.6

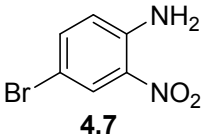

4.7

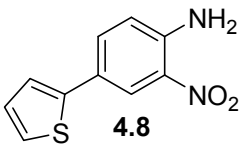

4.8

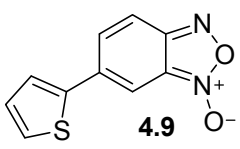

4.9

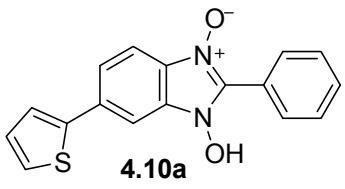

4.10a

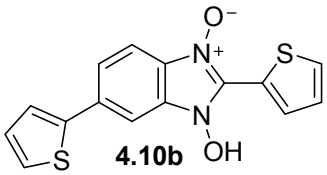

4.10b

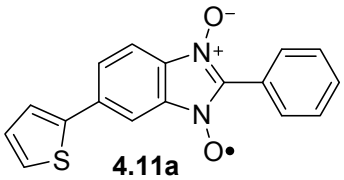

4.11a

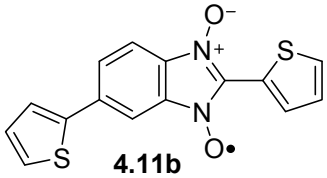

4.11b

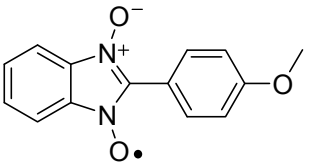

5.1a

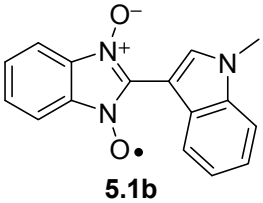

5.1b

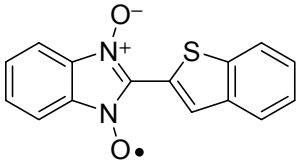

5.1c

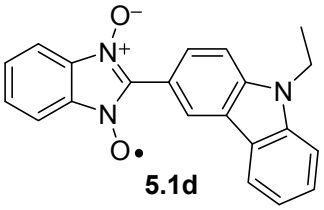

5.1d

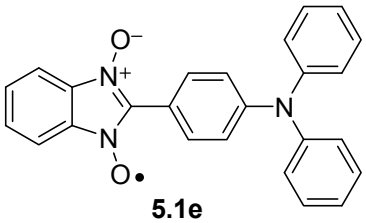

5.1e

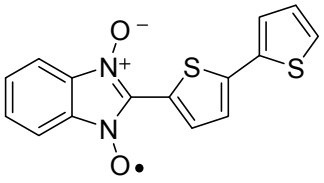

5.1f

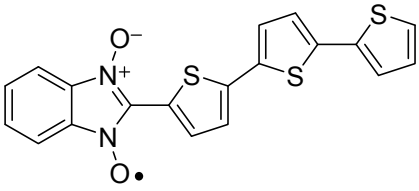

5.1g

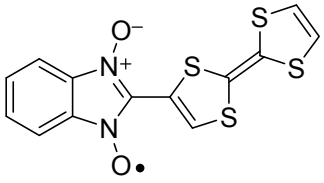

5.1h

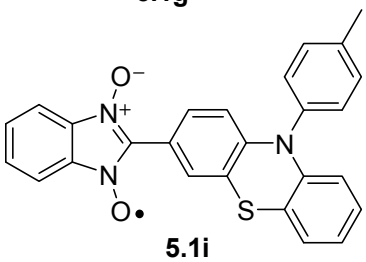

5.1i

R =

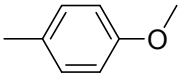

a

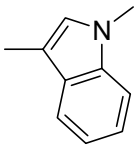

b

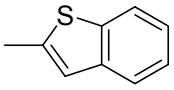

c

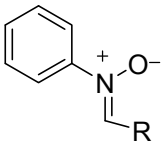

5.2a-e

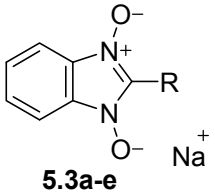

5.3a-e

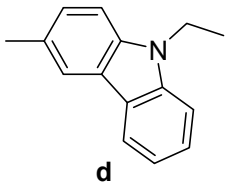

d

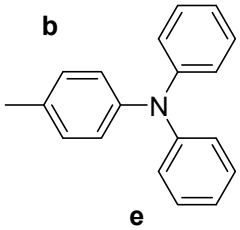

e

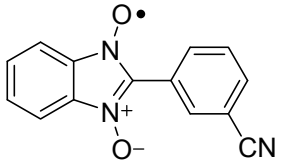

5.4

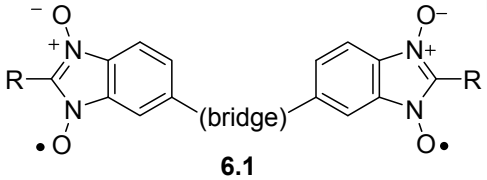

6.1

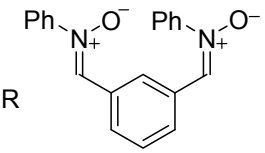

6.2

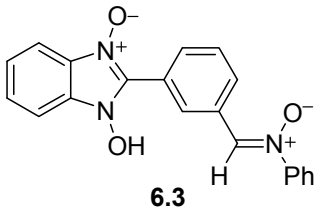

6.3

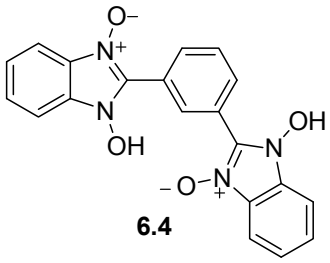

6.4

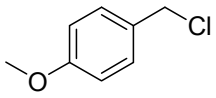

6.5

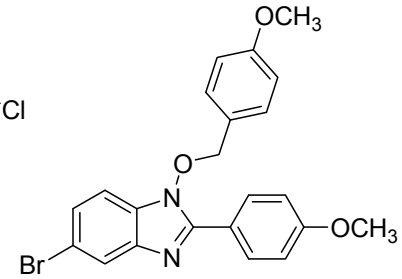

6.6

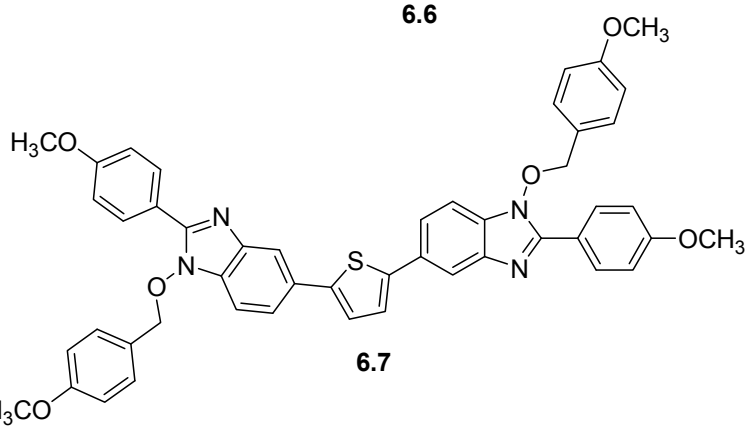

6.7

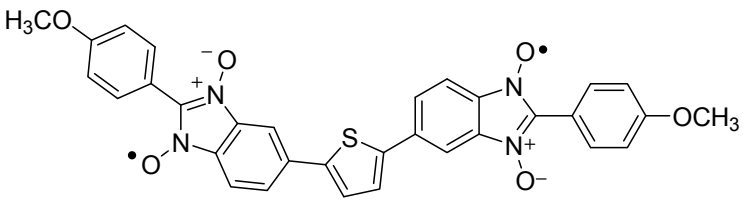

6.8

List of Abbreviations

α	crystalline phase
a	hyperfine coupling constant (also hfcc) or crystallographic *a* axis
A	acceptor or absorbance
Å	Angstrom
a.u.	absorbance unit
AC	alternating current
AFM	antiferromagnetic
Anal.	analysis
aq	aqueous
atm	atmosphere
β	Bohr magneton or crystalline phase
b	crystallographic *b* axis
BHT	butylhydroxytoluene
BNN	benzonitronyl nitroxide
BQ	benzoquinone
bs	broad singlet (NMR descriptor)
χ	magnetic susceptibility
$\chi_{M,p}$	molar paramagnetic susceptibility
c	crystallographic *c* axis
C	Curie constant
ºC	degrees Celsius
^{13}C NMR	carbon nuclear magnetic resonance

calcd	calculated
cm	centimeter
cm^{-1}	wavenumber
CPCM	conductor-like polarizable continuum model
CT	charge transfer
CV	cyclic voltammetry
δ	NMR chemical shift in parts per million downfield from a standard
Δ	difference or heat
ΔE_p	peak potential separation
ΔG^o	free energy
$\Delta G^‡$	free energy of activation
ΔR/R	relative magnetoresistance
d	doublet (NMR descriptor)
D	donor
1D	one-dimensional
2D	two-dimensional
3D	three-dimensional
DBU	1,8-diazabicyclo[5.4.0]undec-7-ene
dd	doublet of doublets (NMR descriptor)
ddd	doublet of doublet of doublets (NMR descriptor)
DDQ	2,3-dichloro-5,6-dicyanobenzoquinone
decomp	decompose
DFT	density functional theory

DMF	dimethylformamide
dmit	4,5-dimercapto-1,3-dithiole-2-thione
DMPH	5,10-dimethyl-5,10-dihydrophenazine
DMSO	dimethyl sulfoxide
DOS	density of states
DPPH	2,2-diphenyl-1-picrylhydrazyl
ε	dielectric constant or molar absorptivity
$E_{1/2}$	half-wave potential
EA	electron affinity or elemental analysis
E_{cell}	cell potential
E_F	Fermi energy
EI-MS	electron impact mass spectrometry
emu	electromagnetic unit
E_{op}	energy of optical transition
E_{ox}	oxidation potential
EPR	electron paramagnetic resonance
E_{red}	reduction potential
ESI-MS	electrospray ionization mass spectrometry
Et	ethyl
EtOH	ethanol
eV	electronvolt
f	oscillator strength or purity factor
Fc	ferrocene

Fc^+	ferrocenium
FC	field cooled
FET	field effect transistor
FM	ferromagnetic
FT-IR	Fourier transform infrared
γ	crystalline phase or gyromagnetic ratio
g	electron g-factor (Landé factor) or gram
G	Gauss
g_e	free electron g factor
GMR	giant magnetoresistance
h	hour
h	Planck's constant
$\hbar$	Planck's constant divided by 2π
H	external magnetic field
H	Hamiltonian
^{1}H NMR	proton nuclear magnetic resonance
H_{ab}	electron coupling matrix element
H_c	coercive field
hfcc	hyperfine coupling constant
HH	head-to-head
HOMO	highest occupied molecular orbital
HRMS	high-resolution mass spectrometry
HT	head-to-tail

Hz	hertz
I	nuclear spin quantum number
IP	ionization potential
i_{pa}	anodic peak potential
i_{pc}	cathodic peak potential
iR	uncompensated resistance
IR	infrared
J	coupling constant (NMR) or magnetic exchange coupling constant
k	rate constant
K	kelvin
k_B	Boltzmann constant
k_{ET}	rate of electron transfer
λ	wavelength
λ	reorganization energy
λ_i	inner-sphere reorganization energy
λ_{max}	wavelength of maximum absorption
λ_o	outer-sphere reorganization energy
LED	light emitting diode
lit	literature
LUMO	lowest unoccupied molecular orbital
LYP	Lee–Yang–Parr
μ	carrier mobility
m	multiplet (NMR descriptor)

m	meta
M	molar or magnetization
M^+	molecular ion
m/*z*	mass-to-charge ratio
mCPBA	*m*-chloroperoxybenzoic acid
Me	methyl
MeOH	methanol
MeTHF	2-methyltetrahydrofuran
mg	milligram
min	minute
mL	millilitre
mmol	millimole
MO	molecular orbital
mol	mole
mol %	mole percent
mp	melting point
m_s	spin state
mV	millivolt
ν	frequency
$\tilde{\nu}$	wavenumber
$\nu_{1/2}$	full width at half-maximum height
ν_{max}	frequency of maximum absorption
n	total number of individuals

N_A	Avogadro's number
NIR	near-infrared
nm	nanometer
NMR	nuclear magnetic resonance
o	ortho
Oe	Oersted
opt	optimization
[ox]	oxidation
p	para
PAHs	polycyclic aromatic hydrocarbons
PCTM	perchlorotriphenylmethyl
pH	negative logarithm of hydrogen ion concentration
Ph	phenyl
PND	polarized neutron diffraction
ppm	parts per million
PXRD	powder X-ray diffraction
q	quartet (NMR descriptor)
q	elementary charge
ρ	resistivity
ρ	spin density
R	goodness of fit factor or generic organic functional group
r_{DA}	distance between redox centres in Å
rt	room temperature

R_w	weighted goodness of fit factor
σ	conductivity
s	singlet (NMR descriptor) or second
S	siemens
S	spin multiplicity
SCE	saturated calomel electrode
SCI-PCM	self-consistent isodensity polarizable continuum model
SIE	self-interaction error
SOMO	singly occupied molecular orbital
SQUID	superconducting quantum interference device
τ	time constant
θ	angle or Weiss constant
t	triplet (NMR descriptor)
$t_{1/2}$	half-life
T	temperature or Tesla
TBAH	tetrabutylammonium hexafluorophosphate
T_c	critical or Curie temperature
TCNE	tetracyanoethylene
TCNQ	7,7,8,8-tetracyanoquinodimethane
td	triplet of doublets
TDDFT	time-dependent density functional theory
TEA	triethylamine
THF	tetrahydrofuran

TLC	thin layer chromatography
tmdt	trimethylenetetrathiafulvalenedithiolate
TMNN	tetramethylnitronyl nitroxide
T_N	Néel temperature
TPA	triphenylamine
TTF	tetrathiafulvalene
UB3LYP	unrestricted Becke three-parameter Lee–Yang–Parr functional
UV	ultraviolet
UV–vis	ultraviolet–visible
V	volt
V	electron coupling matrix element
vis	visible
vs	versus
w/v	weight per volume
w/w	weight per weight
XRD	X-ray diffraction
ψ	wavefunction
Z	number of molecules in the crystallographic unit cell
ZFC	zero-field cooled
$2zJ'$	mean-field approximation where z = # of nearest neighbors

Acknowledgments

First I must thank my supervisor, Natia Frank. I will always be grateful for her guidance, seemingly endless support, and constant encouragement. Over the past five years she has allowed me the freedom to grow as a scientist and an individual. In my time in the her group I have been constantly challenged and I leave here with an invaluable skill set and a confidence I did not possess at the start of my graduate school education. I will always be thankful for the role she has played in both my professional and personal development.

I would also like to thank the many UVic faculty and staff that have enriched my time here. In particular I would like to thank my committee members, Reg and Cornelia who always had time to discuss my research and propose new ideas. Thank you also to Fraser for giving me the unique opportunity to develop instructional materials and explore the pedagogy of teaching, this experience has been an integral part of my development as an instructor. Finally, I must thank Irina, who patiently taught me UNIX and allowed me unrestricted access to her cluster, without which much of the computational research presented in this dissertation would not have been possible.

I must thank my lab and office mates who made my time at UVic so enjoyable. In particular I would like to thank Mark who has been through much of this journey with me and has always been there to put things in perspective. Thank you also to Michelle, who without realizing pushed me to be a more conscientious researcher and who made a great second half of a rather feisty team. Finally, thank you to Joe who has been a true friend and taught me (among other things) how to have a respectable golf tantrum.

I could not have accomplished this without the love and encouragement of my family and friends. I will be forever grateful to my parents for their support (moral and otherwise) and to my sister, who always had kind, humorous, and reassuring words for me. I also would like to thank my dear friend Bev who taught me how much fun university could be.

Finally I would like to thank my best friend Kevin. His support, encouragement and companionship made graduate school the most special years of my life. This journey would not have been what it was without him.

Dedication

To my parents – thank you for believing in me.

Chapter 1: Stable Radicals as Building Blocks for Organic Spintronics

1.1 Preamble

Since Gomberg's discovery of triphenylmethyl radical **1.1**[1] many stable and persistent organic radicals have been reported. The structural motifs of today's radicals go well beyond the original triphenylmethyl framework and numerous examples of both charged and neutral stable radicals are now known.[2-4]

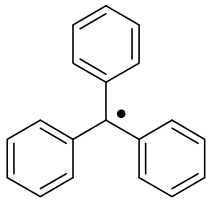

1.1

Figure 1.1. Triphenylmethyl radical.

Stable radicals have been used as *in vitro* and *in vivo* spin trapping agents[5-11] and spin labels[12-15] to obtain structural, environmental and reactivity information by means of electron paramagnetic resonance (EPR) spectroscopy. Radicals have also been investigated for their unique redox chemistry. This has led to the development of oxidation catalysts that transform alcohols to aldehydes,[16,17] stable-radical-mediated living radical polymerization[18] and more recently, organic radicals as charge storage layers in organic radical batteries.[19-24] Radical redox chemistry is often maintained upon metal complexation and the growing fields of ligand non-innocence[25-27] and valence tautomerism[28-32] focus on the ability of certain metal-bound radicals to undergo a one-electron transfer processes in response to external stimuli for switching applications.

Because of the presence of an unpaired electron, stable organic radicals have also been used as spin-containing building blocks for the development of organic magnetic and conducting materials (Sections 1.3 and 1.4). The conventional molecular approach relies on intermolecular overlap between spin density on neighboring organic radicals. Our design strategy incorporates strong electron accepting organic nitroxide-based radicals into donor–acceptor dyads (D–A) and triads (D–A–D) to investigate how intra- and intermolecular electron transfer affects the solid state intermolecular spin–spin interactions that give rise to magnetic exchange and conductivity in molecular organic materials. By systematically varying the donor appended to the accepting radical we hope to develop structure–property relationships between the degree of intramolecular electron transfer (more specifically the electronic coupling matrix element, V) and the observed solid state phenomena, such as magnetic exchange and conductivity. The electronic structure of each new D–A molecule will be fully characterized using solution phase techniques. Following this the solid state interactions will be evaluated and compared to solid state structural information (when available). This will allow for an investigation of how the molecular electronic structure dictates packing interactions which ultimately give rise to magnetic exchange and conductivity pathways.

This introductory chapter begins with an overview of the theory behind the motivation for our research program, organic spintronics. This is followed by a description of magnetism and magnetic exchange and a discussion of conductivity in molecular systems (from a chemist's perspective). Finally, a summary of electron transfer theory is presented and the chapter is closed with an introduction to organic D–A radicals and our design strategy towards the realization of molecular magneto-conductors.

1.2 Spintronics

An electron is an elementary particle that has both a negative electric charge and an intrinsic angular momentum or spin (m_s) of ½. Angular momentum is directly proportional to magnetic moment through a proportionality constant, the magnetogyric ratio (γ). The component of electron spin magnetic moment in the direction of an external magnetic field (conventionally along the z direction) can be expressed as $\mu_z = \gamma\hbar m_S = \pm\frac{1}{2}g_e\beta$ where g_e is the free electron g-factor (2.0023) and β is the Bohr magneton. As each electron spin has a magnetic moment associated with it, in the same way charges are manipulated by applying an electric field, spin can be manipulated upon application of a magnetic field. In this way the movement of spin, like the movement of charge, can transmit information.

In conventional electronics, electric fields are used to control the motion of electron charges and electron spins are altogether ignored. This began to change in 1988 with the discovery of giant magnetoresistance[33,34] (GMR) which gave rise to a new paradigm of electronics based on electron angular momentum; spintronics. This term was proposed by Bell Labs and Yale University during a press release in 1998 and was meant to describe devices intended for information storage based electron spin-encoded bits.[35] Today spintronics enjoys a less rigorous definition and is generally used to describe the field of spin-based or spin transport electronics in which information is transmitted via electron spin. The field of spintronics includes research on spin-valve transistors,[36-38] molecular spintronics,[39-41] single-electron spintronics[42,43] and magnetoelectronics,[44-46] which specifically describes devices that utilize ferromagnetic materials, for example the read-write heads present in computer hard drives.

1.2.1 Current spin-based electronic devices

The physics underlying spintronic devices as they exist today had been known for some time. In 1964, Mott proposed a two-current conduction model[47] which was used by Fert and Campbell[48,49] to explain the influence of spin on conductivity in itinerant ferromagnets, metals with an unequal population of spin up and spin down electrons at the Fermi level. In an attempt to observe direct evidence for spin-dependent electron transport, multilayered magnetic structures were fabricated. The simplest film developed was comprised of three layers, two ferromagnetic layers (F1, F2) of identical composition sandwiching a non-magnetic (M) metallic layer (Figure 1.2).

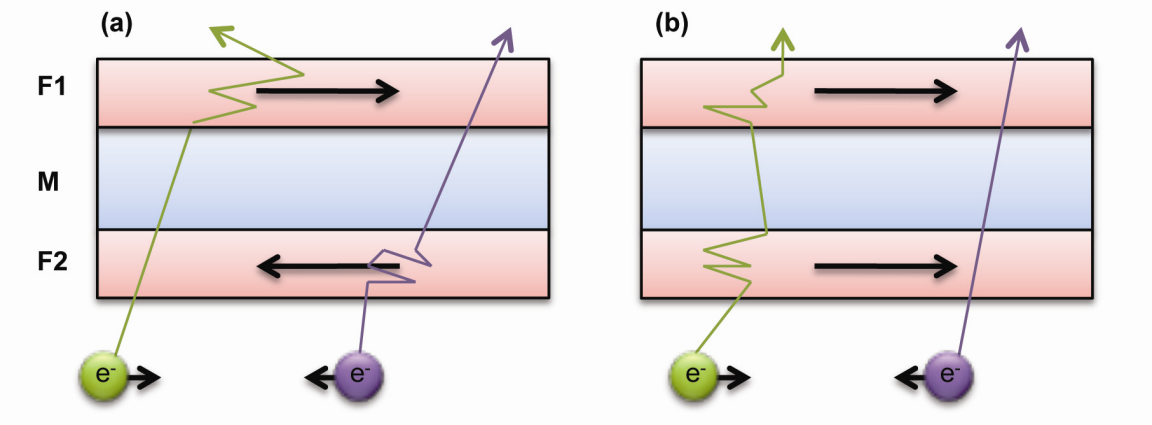

Figure 1.2. Schematic representation of the spin-valve effect in a three-layer film with the current circulating in-plane when the magnetic layers are aligned antiparallel (a) and parallel (b) to each other.[50]

When the magnetic dipole of the two magnetic layers are parallel (Figure 1.2, b), electrons whose spins are aligned antiparallel to those in the magnetic layers travel through the device virtually unscattered. In contrast, when the magnetic layers are antiparallel to each other (Figure 1.2, a), both electron spin states are scattered by one of the magnetic layers and the material exhibits high resistance. The net result is a large change in the electrical resistance in response to an applied magnetic field, termed

magnetoresistance. The relative magnetoresistance of the two configurations, ΔR/R, is expressed as the difference in resistance of the antiparallel configuration ($R_{\uparrow\downarrow}$) and the parallel configuration ($R_{\uparrow\uparrow}$) divided by the resistance of the parallel configuration ($\Delta R/R = (R_{\uparrow\downarrow} - R_{\uparrow\uparrow})/R_{\uparrow\uparrow}$).[51] Relative magnetoresistance has since become the figure of merit used to compare different device configurations. By tuning the composition and spatial configuration of the magnetic and spacer layers, these preliminary devices led to the development of spin-valve sensors which were introduced as read heads in magnetic hard disk drives by IBM in 1997. Since their introduction data storage density has increased by three orders of magnitude and the door was opened for mobile applications and unprecedented drive capacities (1 terabyte).[50] GMR, as applied to magnetic data storage, made a remarkably rapid transition from inception to commercialization and in 2007 Peter Grünberg and Albert Fert were awarded the Nobel Prize in Physics for their simultaneous discovery of GMR in Fe/Co/Fe layered ferromagnets.[52,53]

1.2.2 New materials for spintronics applications

All existing spintronic devices function in an analogous way to the spin-valves described above. They are magnetic memory devices or sensors that use the spin of the electron to store information. In addition to the improvement of spin-valve technology, there is also interest in adding a spin degree of freedom into semiconductor based technologies, namely field effect transistors (FETs) and light emitting diodes (LEDs). The development of spin-FETs and spin-LEDs requires magnetic semiconductors. These have been fabricated by doping inorganic semiconductors with ferromagnetic nanoparticles although thus far these materials are only ferromagnetic below room

temperature (T_c = 173 K in GaAs doped with Mn[54,55]) making them impractical for use in devices at ambient temperatures.

For the field of spintronics to go forward, new materials that can *inject* and *transport* spin must be developed (Figure 1.3). When non-magnetic metallic systems are used to transport spin, spin-polarized electrons can be injected at the interface, however, spin dephasing and spin relaxation lead to equilibration of spin up (S = +½) and spin down (S = −½) during transport. In metal conductors and semiconductors the nonequilibrium spin is relatively long lived (ns timescale)[56] making this technology viable, still, improvement on spin transport lifetime is necessary for advancement in this field.

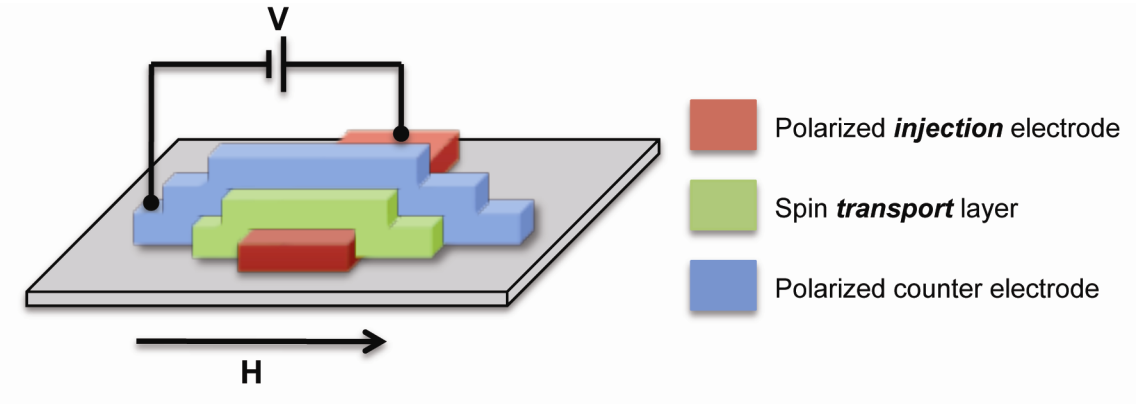

Figure 1.3. Schematic of a spin-valve.

Until recently, spintronic devices have been based exclusively on inorganic based metal[50] and semiconductor[57] technology. Although organic electronics have been intensely researched for some time, the integration of organic (semi)conductors into spintronic materials has been largely unexplored. Organic molecules and polymers are particularly attractive for use as spin carriers in spintronic devices for several reasons. In addition to the usual advantages touted in favour of organic materials, namely less expensive device fabrication, uncomplicated integration into current technologies, and

chemical versatility, organic materials have remarkably long spin relaxation lifetimes. In inorganic materials, spin scattering occurs primarily through spin-orbit coupling[58] which increases exponentially with atomic number. Carbon and other light organic elements (N, O) have negligible spin-orbit coupling and, as a result, slow spin dephasing rates. The weakness of the spin scattering mechanism means spin polarization may be maintained for long time periods (> 10 μs)[59,60] and distances (10 – 100 nm)[58] in organic materials, exceeding those detected in inorganic materials by orders of magnitude.[40,56] At present, a handful of devices have been fabricated where organic materials have been incorporated into spin-valves as the non-magnetic (spacer) layer.[61-71] Although the organic species have been shown to successfully transport spin, the observed magnetoresistance ($\Delta R/R$) is only on the order of a few % at room temperature.[64,71] Improvement in the magnitude of magnetoresistance and a fundamental understanding of spin transport in organics is therefore critical for future development of organic spintronics.

The discussion thus far has focused on the development of organic materials that can transport spin, however, there is also a need for materials that can inject spin (Figure 1.3). Development of these materials is challenging as it requires systems that are inherently spin polarized and interface well with the spin transport layer. Completely spin-polarized metallic compounds have been realized. The aptly named half-metallic ferromagnets[72] (usually metal oxides) have an unequal population between majority and minority spin at the Fermi level (E_F) (Figure 1.4). Additionally, a band gap is present in the minority density of states (DOS) resulting in a material whose conducting electrons are completely spin polarized.

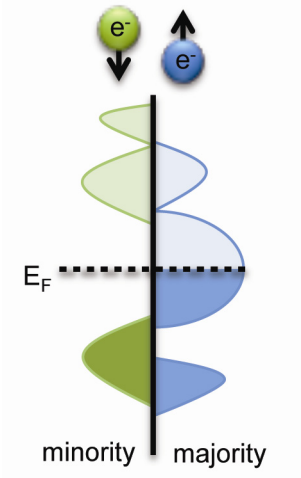

Figure 1.4. Theoretical DOS for a half-metallic ferromagnet with an uneven population of minority and majority spin at E_F and a band gap in the minority DOS.

Organic spin transport layers incorporated into organic spin-valves (discussed above) use the highly polarized half-metallic manganite $La_{0.7}Sr_{0.3}MnO_3$ (LSMO) or Co almost exclusively for the spin-injection layer.[58] For the field of organic spintronics to progress, different spin polarized injectors must be developed that exhibit a large degree of spin injection at room temperature. The spin injecting electrode must also interface well with the organic spin transport layer. The natural way to solve this problem is to use organic ferromagnets as the spin injecting electrodes. Organic ferromagnets would have a DOS similar to that in Figure 1.4 as ferromagnetism would give rise to an uneven population of minority and majority spins at E_F. The organic material may or may not have a band gap at E_F, and the size of the gap would dictate the conductivity. Organic materials that are ferromagnetic at or above room temperature have yet to be realized (see Section 1.3.2) although the ferrimagnetic vanadium tetracyanoquinone ($V(TCNE)_x$) polymers are often cited as examples of room temperature "organic" magnets. Amorphous organometallic $V(TCNE)_x$ was recently used as the spin injecting layer in a spin-valve configuration[73]

and successful injection of polarized electron was observed, however, even at low temperature the measured $\Delta R/R$ was small (2.3 % at 90 K, 0.5 V bias). Nevertheless, these results show that organic-based magnets can function as spin injectors suggesting the development of new organic ferromagnetic materials is critical to the advancement of organic spintronics. We propose using stable organic radicals, either as monomers or incorporated as spin bearing centres in the backbone of conjugated semiconducting organic polymers for investigation of molecular-based magneto-conducting materials that may find function in spin-based electronic devices.

1.3 Magnetic exchange in organic radicals

All materials are influenced to some extent by the presence of a magnetic field. Some materials are repelled by a magnetic field while others are attracted. The degree to which a material is influenced by an external field is its magnetic susceptibility χ. Susceptibility is defined as $M = \chi H$ where M is the magnetization (magnetic moment per unit of volume) and H is magnetic field strength. Magnetic susceptibility is a dimensionless quantity but is conventionally expressed in units of emu/cm^3. The molar magnetic susceptibility, χ_M, is obtained by multiplying χ by the molar volume and is reported as emu/mol. Magnetic susceptibility is a solid-state phenomenon arising from the bonding (intramolecular) and spatial (intermolecular) interactions between individual open-shell units in a crystal lattice. For this reason, a true understanding of the magnetic susceptibility of a system requires structural information obtained by crystallographic analysis.

The arrangement of spins in a bulk material can give rise to several different types of magnetism. The most common types of magnetic behaviours are diamagnetism, paramagnetism, antiferromagnetism, ferromagnetism, and ferrimagnetism (Figure 1.5). Diamagnetism and paramagnetism are discussed in some detail below.

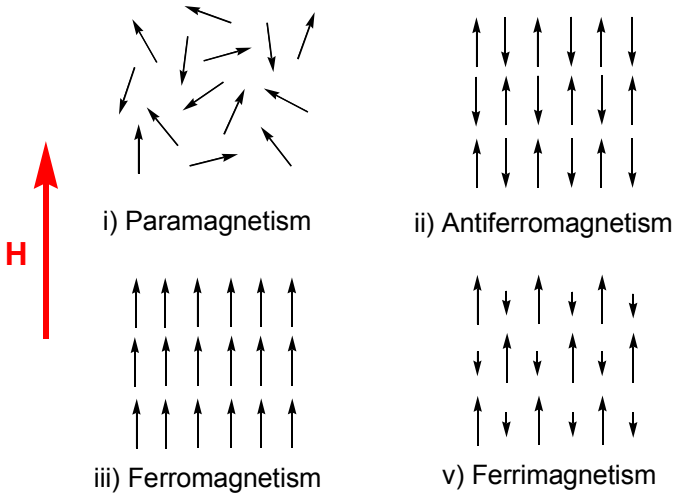

Figure 1.5. Different types of magnetism.

The total magnetic susceptibility of a material is the sum of the paramagnetic and diamagnetic contributions to the overall magnetization, that is $\chi_{tot} = \chi_P + \chi_D$. Diamagnetism is a property of all substances and arises from the interaction of paired electrons with a magnetic field. Diamagnetism was first modeled by Langevin[74] as a current circulating in a closed loop. This gives rise to a small induced magnetic field in opposition to the external magnetic field. Diamagnetic susceptibility is negative in sign and generally small, ranging from -1 to -10^{-4} emu/mol[75] and, to a first approximation, is independent of applied field and temperature. All molecules have filled orbitals with paired electrons that contribute to diamagnetic susceptibility. As diamagnetic susceptibility acts to diminish total magnetic susceptibility, it must be accounted for when calculating the paramagnetic susceptibility of an open-shell material. Diamagnetic

susceptibility of a molecular sample is additive[75,76] and may be approximated based on molecular formula using Pascal's constitutive corrections.[77-80] Alternatively diamagnetic susceptibility can be separated from paramagnetic susceptibility by measuring the temperature dependence of the susceptibility.[75]

1.3.1 Curie law

Paramagnetism is observed in systems with unpaired electrons where the electrons are magnetically dilute, and consequently cannot exchange couple. In a perfectly paramagnetic material the electrons also exist in isotropic environments (no g-anisotropy, spin-orbit coupling or zero-field splitting). The origin of paramagnetism can be attributed to the angular momentum of each individual electron (Section 1.2). In the absence of a magnetic field, the different spin (m_s) states are degenerate. The application of an external field resolves the degeneracy of the various states such that the spin states aligned with the field are stabilized relative to those antiparallel to the applied field (Figure 1.6). This Zeeman splitting gives rise to an energy gap between states of $\Delta E = g\beta SH$, where β is the Bohr magneton, g is the electron g-factor or Landé constant (2.0032 for a free electron), S is the spin state (m_s) and H is the magnitude of the external field.

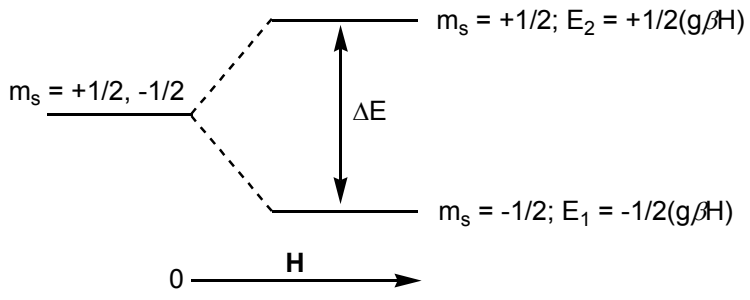

Figure 1.6. Energy levels of an electron in the presence of an applied field.

The population of the each spin state is governed by a Boltzmann distribution where $N_{upper}/N_{lower} \propto \exp(-\Delta E/k_B T)$, and k_B is the Boltzmann constant. When $\Delta E > k_B T$, only the lowest energy spin state is populated. This is akin to the classical physics model in which a system is described as having its spins "aligned with the external field" at lower temperature. When $\Delta E < k_B T$, each energy level is populated, resulting in the cancellation of individual magnetic moments and the net magnetization of the bulk material is small. At modest fields and temperatures, ($H/k_B T << 1$), the magnetization (M) can be defined as $M = Ng^2\beta^2 HS(S+1)/3k_B T$ (using a first approximation of the Brillouin function)[76] and the molar magnetic susceptibility is defined as $\chi = M/H$. Combining these two functions gives Equation 1 which is the Curie law, derived by Pierre Curie, where the Curie constant $C = Ng^2\beta^2 S(S+1)/3k_B$.

$$\chi = \frac{M}{H} = \frac{Ng^2\beta^2 S(S+1)}{3k_B T} = \frac{C}{T} \quad (1)$$

Perfect paramagnets (Curie law magnets) are rare as electrons rarely exist in a spin dilute isotropic environment. Those systems that only deviate slightly from spin-only magnetism due to the existence of an internal field, the Weiss field (θ), can be described using a small modification of the Curie law. This is referred to as Curie–Weiss law where $\chi = C/(T - \theta)$ and the Weiss constant θ has units of temperature. Rearranging this equation to that of a linear equation gives Equation 2.

$$\frac{1}{\chi} = \frac{C}{T} - \frac{\theta}{C} \quad (2)$$

Thus a plot of $1/\chi$ vs T has a slope equal to the Curie constant. The Weiss constant can be derived from the y-intercept and the sign and magnitude of the Weiss constant provides information about the nature and magnitude of the magnetic exchange interactions (Figure 1.7). A positive Weiss constant is consistent with ferromagnetic exchange, while a negative Weiss constant is consistent with antiferromagnetic exchange. Exchange interactions that occur in 2- or 3-dimensions lead to magnetic ordering with an ordering temperature referred to as T_c (critical temperature) when the interactions are ferromagnetic or T_N (Néel temperature) when the interactions are strongly antiferromagnetic. Above the ordering temperature all magnets are paramagnets.

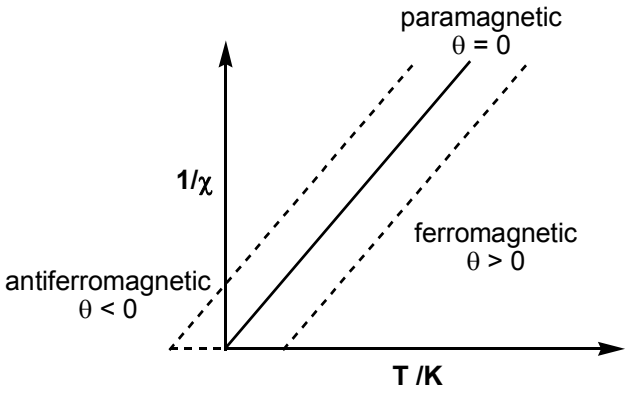

Figure 1.7. Reciprocal susceptibility $1/\chi$ vs temperature demonstrating perfect Curie behaviour (—) and ferromagnetic or antiferromagnetic deviations from Curie behaviour (---) (Curie–Weiss).

1.3.2 Intermolecular magnetic exchange interactions

As two spin-bearing centres come into close physical proximity the magnetic orbitals come into contact and magnetic exchange interactions arise. With respect to this dissertation, the observed magnetic exchange interactions discussed in Chapters 2, 4 and 5 occur exclusively via a direct exchange mechanism between two $S = ½$ units. For this

reason, the discussion of magnetic exchange pathways will be limited to McConnell I[81] and its extended version.[82,83]

The quantification of magnetic exchange integrals based on the sign of spin density overlap has become known as the McConnell I mechanism. McConnell's model for through-space magnetic exchange interactions was put forward in 1963[81] and suggests that when sites of spin density overlap, the sign and magnitude of the overlapping spin densities will determine the sign and magnitude of the magnetic exchange. The exchange interaction (J_{ij}^{AB}) between two π-delocalized radicals A and B can be described by the Hamiltonian (3) below, where S_i^A is the π-electron spin on atom i of molecule A and S_j^B is the π-electron spin on atom j of molecule B.

$$H^{AB} = -\sum_{ij} J_{ij}^{AB} S_i^A \cdot S_j^B \tag{3}$$

Equation 3 can be re-written to give 4, where S^A and S^B are the total spin operators for molecules A and B and ρ_i^A and ρ_j^B are the spin densities on atoms i and j of molecules A and B respectively.

$$H^{AB} = -S^A \cdot S^B \sum_{ij} J_{ij}^{AB} \rho_i^A \rho_j^B \tag{4}$$

Antiferromagnetic (−*J*) exchange is observed in systems that have overlap between atoms whose sign of ρ is the same (positive/positive or negative/negative). In π-delocalized radicals, much of the spin density is positive and this explains the antiparallel spin coupling commonly observed along the direction of the π stack. In certain solid configurations there could be an atom of positive spin density exchange coupled to an atom of negative spin density, this scenario would give rise to ferromagnetic exchange contribution (+*J*).

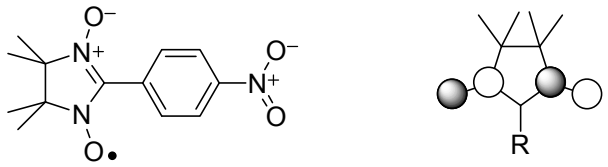

Figure 1.8. Structure of *p*-nitrophenyl nitronyl nitroxide (a) and SOMO of tetramethyl nitronyl nitroxide (b).

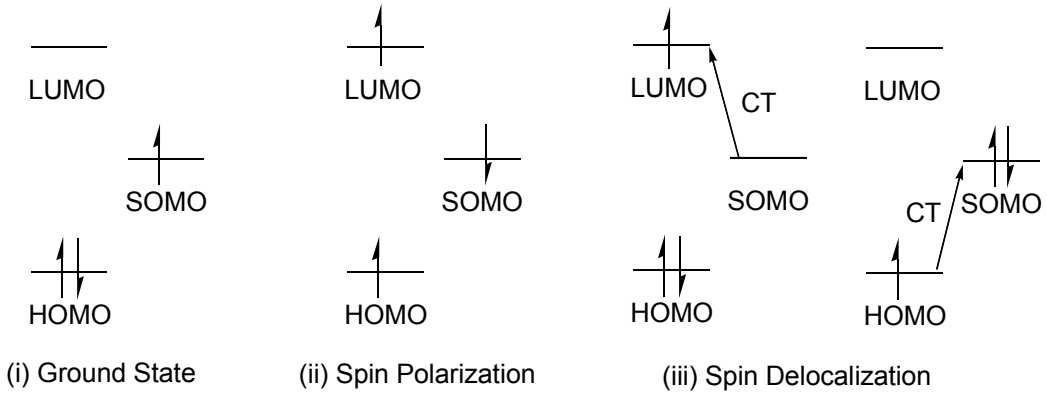

Figure 1.9. The ground state, spin polarization and spin delocalization configurations for an organic radical.

The McConnell I mechanism has since been expanded to distinguish between spin density induced by spin polarization and spin delocalization.[82] Consider the case in which a nitronyl nitroxide radical is covalently attached to closed-shell nitrobenzene. The SOMO is localized on nitronyl nitroxide (Figure 1.8) and the ground state electronic configuration can be described by differential population of the HOMO, LUMO, and SOMO in Figure 1.9.[83] The overall electronic structure of a radical is the sum of all available spin configurations. The spin polarization configuration described by the HOMO to LUMO triplet excitation (Figure 1.9, ii) gives rise to alternating negative and

positive spin density. Additionally, there are two charge-transfer configurations that contribute to the overall spin density distribution (Figure 1.9, iii). These charge-transfer configurations result in positive spin density distribution via spin delocalization. The charge-transfer configurations are usually not considered as they do not contribute significantly to the overall spin distribution, however, in open shell donor–acceptor molecules like *p*-nitrophenyl nitronyl nitroxide above, as well as systems presented in this dissertation, the charge-transfer contribution to overall spin density is non-zero.

Despite the number of structurally diverse organic radicals synthesized to date, ferromagnetic single component organic solids are extremely rare. For a system to be considered a ferromagnet, as opposed to exhibiting *ferromagnetic exchange*, it must show long range ordering of spins in the solid state. Because magnetic exchange between non-bonded $S = ½$ units relies solely on orbital overlap, the nature and magnitude of the observed exchange is dictated by solid-state packing interactions which are often weak. Although strategies can be employed to direct assembly (H-bonding, π-stacking, electrostatic interactions) there is no way of rationally designing an organic ferromagnet. All known organic ferromagnets are shown in Figure 1.10. Their critical temperatures (T_c) and coercive fields (H_c) are given in Table 1.1 and are in general lower than 2 K. Increased critical temperatures are observed in the main group organometallic radicals **1.7** and **1.8** in which spin-orbit coupling present in the larger S and Se atoms contributes to the magnetic anisotropy.

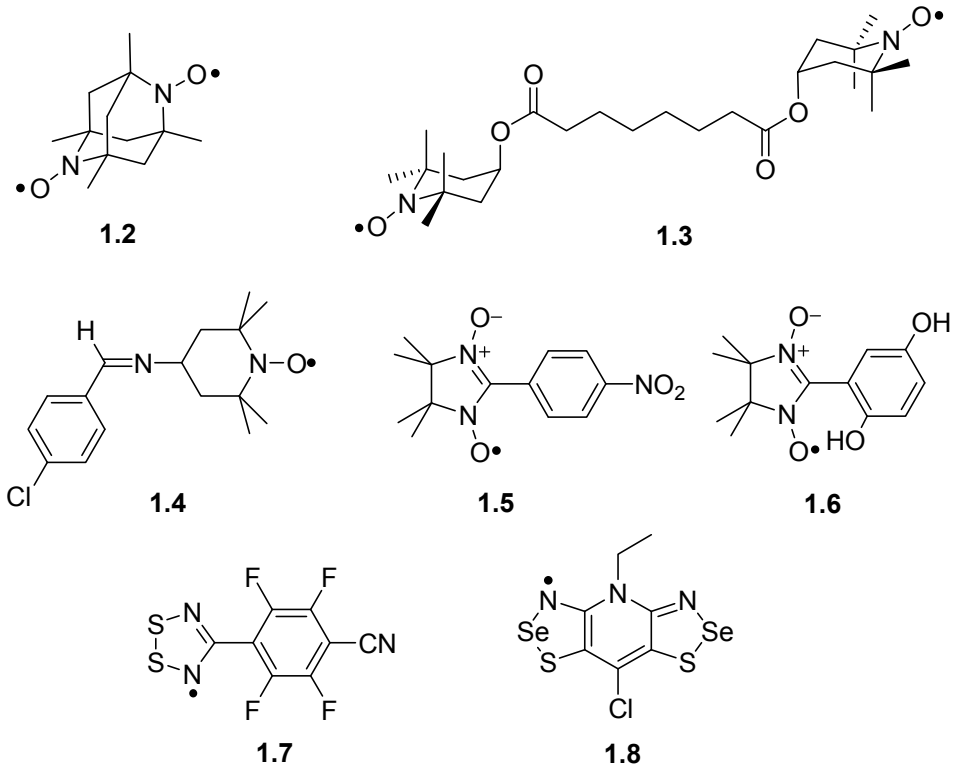

Figure 1.10. Organic ferromagnets.

Table 1.1. Summary of Weiss constant (θ) or magnetic exchange (*J*), critical temperature and coercive field for the known series of organic ferromagnets.

Magnet	θ (K)	J (cm^{-1})	T_c (K)	H_c (Oe)
1.2[a]	-	-	1.48	< 1
1.3[b]	0.7	-	0.38	-
1.4[c]	0.69	-	0.4	5
β-1.5[d]	1	-	0.60	1 - 2
γ-1.5[e]	-	~ 3	0.65	-
α-1.6[f]	-	0.93	0.51	< 20
β-1.7[g]	-	-	35.5	~ 1
1.8[h]	19.3	-	12.3	590

[a] See reference 84. [b] See reference 85. [c] See reference 86. [d] See reference 87. [e] See reference 88. [f] See reference 89. [g] See reference 90,91. [h] See reference 92.

A room temperature organic ferromagnet has yet to be realized although the *organometallic* donor–acceptor $V(TCNE)_x$ polymer (T_c ~ 400 K) is often cited as proof of principle.[93] Undoubtedly synthesizing an organic ferromagnet is challenging. We aim

to investigate how systematically varying molecular (and thereby electronic) structure gives rise to alternate magnetic exchange pathways and perhaps a generalized strategy for organic ferromagnets with higher critical temperatures.

1.4 Conductivity in organic radicals

Besides magnetic applications, organic radicals are researched for their potential use as molecular metals. Historically, research towards organic conductors, both molecular and polymeric, has used charge transfer (CT) to generate charge carriers.[94-99] Accordingly, these conductive systems are two component systems requiring both a donor (D) and acceptor (A) molecule (although more recently both D and A have been incorporated into a single molecule, Section 1.6). Neutral π-delocalized radicals have also been proposed as building blocks for organic electrical conductors.[100,101] In these systems the unpaired electrons act as the charge carriers.

1.4.1 A qualitative discussion of band theory

The notion of using organic π-delocalized radicals as units in molecular conductors arises from the idea that a stacked arrangement of radicals will, on the basis of band structure, be associated with a ½-filled energy band and a metallic ground state. In order to understand how molecular conduction could arise, and the limitations associated with this prediction, a brief discussion of electronic energy band structure is necessary.

For chemists, the theory of electronic structure in solids is often based on molecular orbital (MO) theory, where molecular orbitals are constructed from linear combinations of atomic orbitals. A facet of this theory is that the number of molecular orbitals is

equivalent to the number of atomic orbitals used in their construction. Consider an H_2 molecule. At the simplest level of theory there are two orbitals, the bonding and antibonding combinations shown in Figure 1.11. As hydrogen atoms are sequentially added to H_2 to give an H_n polymer, the number of molecular orbitals increases. Each orbital can be characterized by the number of nodes which in turn dictate the energy of each orbital. As n approaches Avogadro's number N_A (far right, Figure 1.11) the energy gap between individual levels decreases.[102,103]

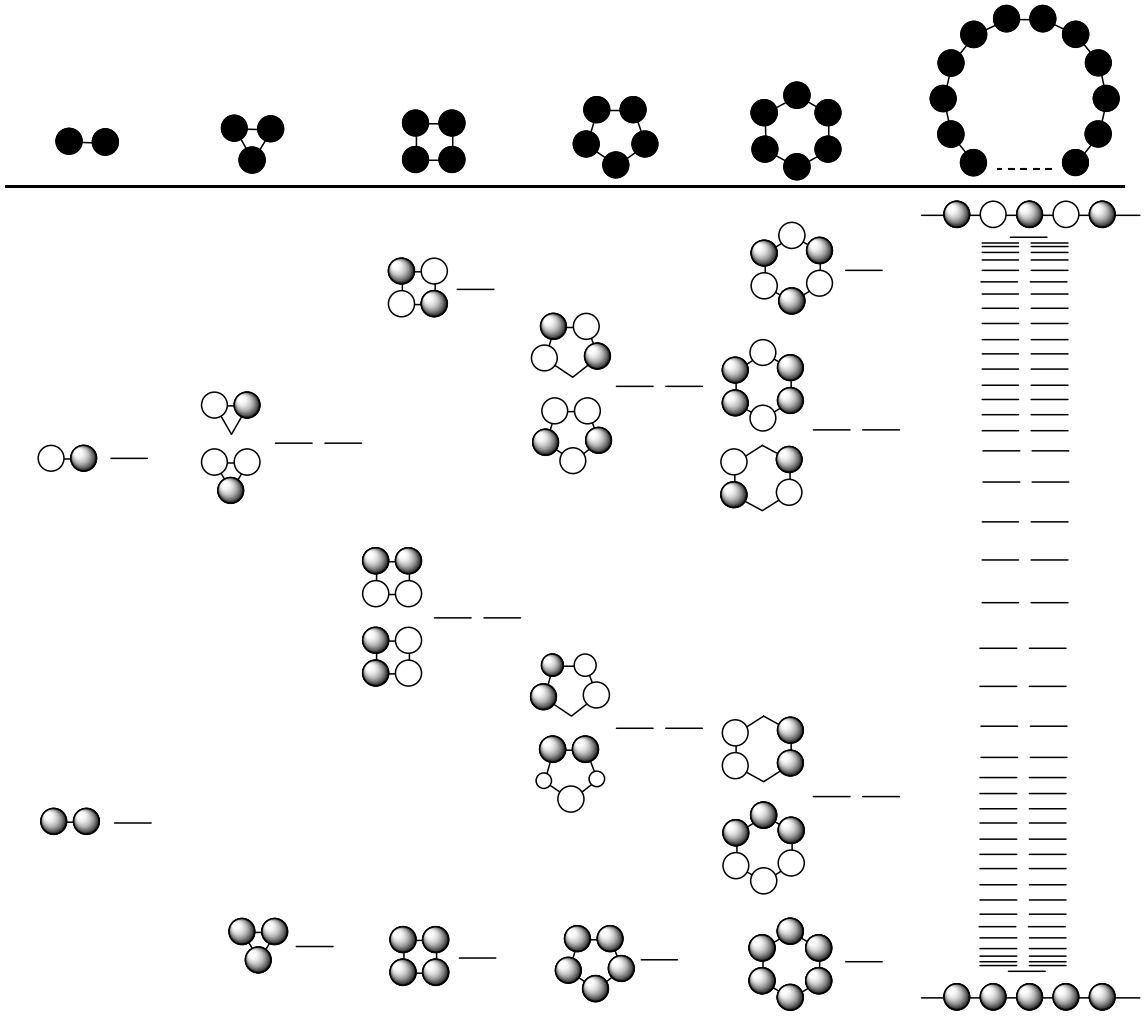

Figure 1.11. The progression of molecular orbitals for a hypothetical hydrogen polymer.[103]

The diagram in Figure 1.11 is often described in terms of a Bloch function, where Bloch's theorem states that the wave function (Ψ_k) for a periodic potential is equal to the product of a propagating wave multiplied by a function with periodicity in the crystal lattice.[104,105] If the hydrogen polymer above is described in terms of a lattice with n = 0, 1, 2, etc. where 0, 1 and 2 represent lattice points separated by a lattice spacing a, and there is an H 1s orbital (χ_0, χ_1, χ_2) at each lattice point (Figure 1.12), then a linear combination of the atomic 1s orbitals gives the wave function in equation 5.[103] The lattice spacing a is the length of the unit cell in one dimension and k is the wave vector.

$$\Psi_k = \sum_n e^{ikna}\chi_n \tag{5}$$

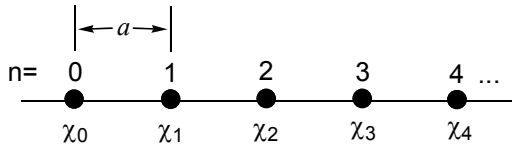

Figure 1.12. Notation used to describe the wave function of a linear chain of 1s H orbitals.

From equation 5 it can be shown that the wave function corresponding to k = 0 is the all bonding combination (Figure 1.13) which corresponds to the lowest energy MO in Figure 1.11, while $k = \pi/a$ gives rise to the all antibonding combination (Figure 1.13) which is the highest energy MO in Figure 1.11.

$$k = 0 \qquad \psi_0 = \sum_n e^0 \chi_n = \sum_n (1)\chi_n$$

$$= \chi_0 + \chi_1 + \chi_2 + \chi_3 + \chi_4 \ldots.$$

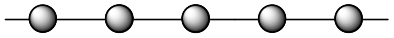

all bonding configuration

$$k = \pi/a \qquad \psi_{\pi/a} = \sum_n e^{\pi i n} \chi_n = \sum_n (-1)^n \chi_n$$

$$= \chi_0 - \chi_1 + \chi_2 - \chi_3 + \chi_4 \ldots.$$

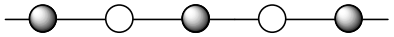

all antibonding configuration

Figure 1.13. Orbital combinations generated using two specific values of *k*: 0 and π/a.[103]

There is a unique range of values for *k* defined by $-\pi/a \leq k \leq \pi/a$ which is called the first Brillouin zone. The number of *k* values is defined by the number of discrete translations in the crystal which is simply the number of unit cells in the lattice. The variation in energy with *k* is defined as the dispersion of the band and a plot of E(*k*) vs *k* is a dispersion curve (Figure 1.14) or alternatively, a band structure. Although the dispersion curve appears to be a continuous function, *k* is both quantized and finite but can take on as many values as there is *n*.

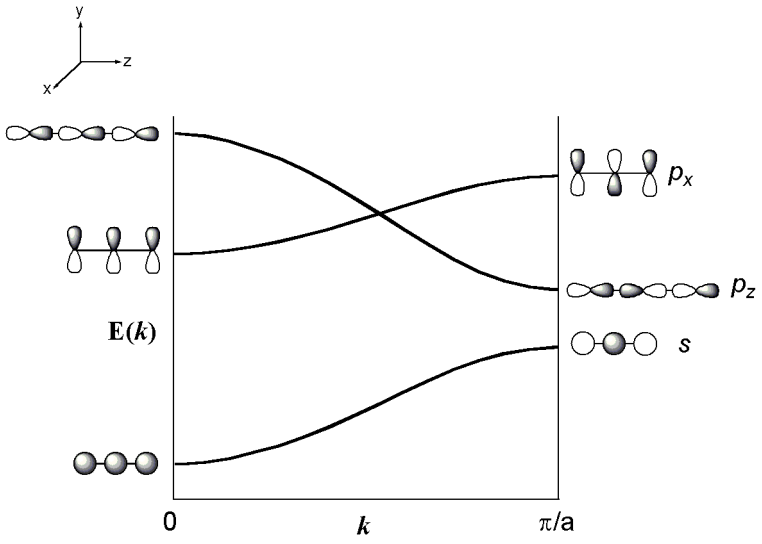

Figure 1.14. Dispersion curves for s- and p-orbitals in a theoretical array of atoms bonded along the *z*-axis.

An important feature of a band is its dispersion, or bandwidth. Bandwidth is determined by overlap of interacting orbitals and the greater the overlap, the larger the bandwidth. This is observed directly in a dispersion curve as bandwidth (or dispersion) is the difference in energy between the highest and lowest levels in the band. Bandwidth is clearly dependent on the physical distance between interacting species and in this dissertation, only distances less than the sum of the van der Waals radii of the two atoms under investigation will be considered significant. It is also apparent that in molecular systems (to a first approximation) bandwidth and magnetic exchange are complementary as the observation of significant values for either requires sufficient orbital overlap between neighbouring units. For this reason, molecules selected for use in molecular magneto-conducting materials must be free of steric bulk that would hamper close solid state packing.

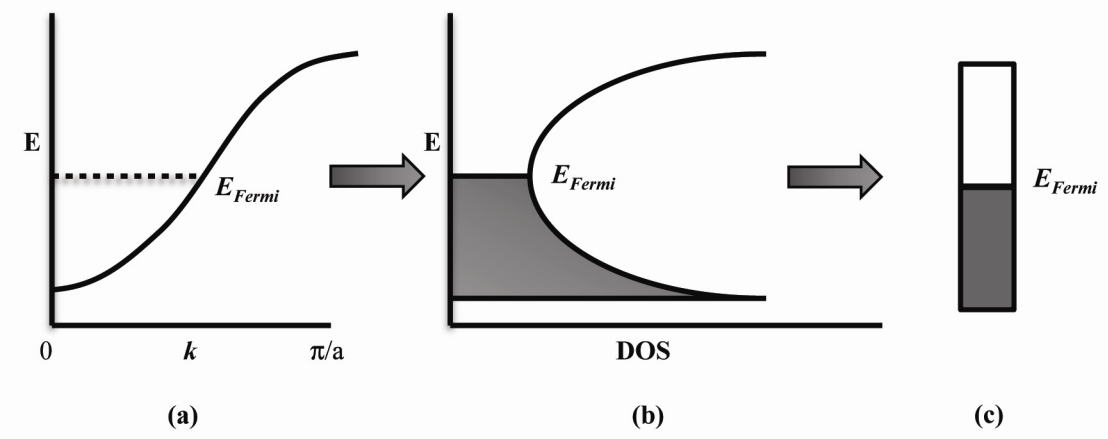

Figure 1.15. Projection of a theoretical dispersion curve (a) onto a DOS (b) and block diagram of a half filled band used to depict DOS (c).

Dispersion curves also provide information about the distribution of states at a given energy level. This distribution is referred to as the density of states (DOS) which is defined as the number of states between E and dE. For a 1D systme, the slope of a plot of E(*k*) vs *k* is inversely proportional to the number of states at that E. Projection of a plot of E(*k*) vs *k* onto a DOS diagram portrays the number of states present at a given energy (Figure 1.15, b). A DOS diagram can also be rendered as a block diagram (Figure 1.15, c) where the level of band filling is determined by the number of electrons in the system. The energy of the highest occupied state is the Fermi energy (E_F).

1.4.2 Peierls distortions and Mott Hubbard states

Metallic conduction occurs in solids where empty electronic states exist that are easily accessed by electrons at or near the Fermi level. This is often described as the absence of a gap between the highest occupied level and lowest unoccupied level. The filled band is the valence band and the unoccupied (empty) band is the conduction band. In a metal

there is no energetic barrier for promotion of electrons to the conduction band and electrons can migrate to the conduction band and are free to move throughout the solid.

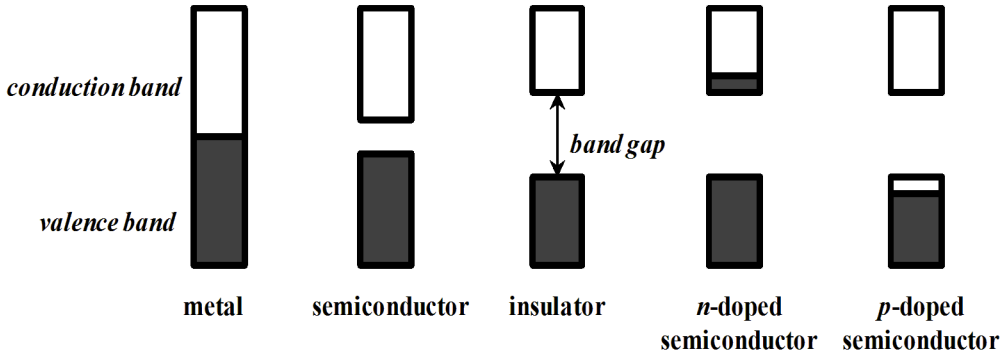

Figure 1.16. Block diagrams depicting the band structure of a different materials.

When a gap opens at the Fermi level, it is referred to as a band gap and it is the magnitude of the gap that dictates whether the material is semiconducting or insulating. If the gap is large ($E >> k_BT$) electrons cannot be thermally promoted to the conduction band and the material is insulating. When the band gap is small enough ($E > k_BT$) some electrons are promoted to the conduction band and the material is intrinsically semiconducting. Semiconductors can also be generated by doping, a process which results in the presence of holes in the valence band (*p*-doping) or electrons in the conduction band (*n*-doping). When an insulator is doped with an electron rich (relative to the parent system) dopant it is *n*-doped. Conversely doping with electron deficient species is referred to as *p*-doping. The block diagrams representing the different types of band structures for the above materials are shown in Figure 1.16.

Finally this discussion can return to the original goal of using organic $S = ½$ radical units as building blocks for molecular metals. On the basis of simple band theory, a stack of strongly interacting radicals should lead to the realization of a molecular system with a

metallic ground state in the same way the theoretical hydrogen network gave rise to a metallic band structure.

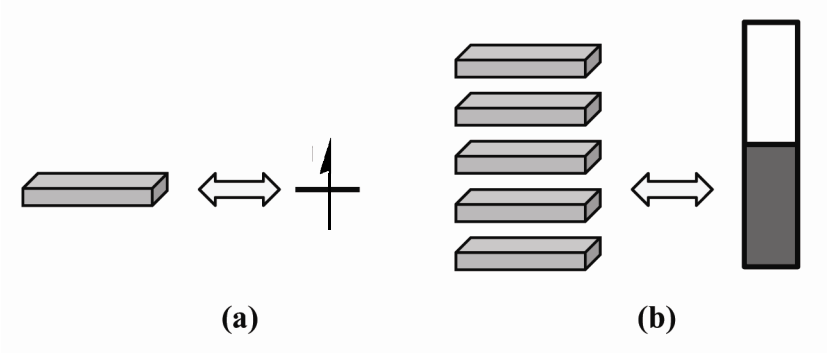

Figure 1.17. A single radical (a) and an ideal stack of strongly interacting radicals leading to formation of a metallic band (b).[101]

Unfortunately the ideal array presented in Figure 1.17 is prone to instabilities associated with 1D chains resulting in either a Peierls distortion or the formation of a Mott insulating state. A Peierls distortions is the solid state equivalent of a pseudo Jahn–Teller effect[102,106] whereby lattice distortions lower the overall energy of the solid. Peierls instabilities result in the formation of closed-shell or closely associated open-shell dimers and the opening of a band gap at the Fermi level. Polyacetylene is an example of a one-dimensional system with a half-filled band that is prone to Peierls instability.[107,108] The distortion in polyacetylene results in highly localized electronic states in which bond alternation and low conductivity are observed. Peierls distortions are somewhat intuitive as the formation of molecular H_2 is exactly what we as chemists would predict if our theoretical chain of hydrogen atoms were exposed to ambient conditions.

The most common synthetic strategy employed to suppress Peierls dimerization, the incorporation of sterically bulky groups, unfortunately also results in an insulating state, albeit for entirely different reasons. When radicals are stabilized towards dimerization by

incorporating steric bulk orbital dispersion is diminished. The net result is a decrease in bandwidth and radical spins become trapped on individual $S = ½$ units. The resulting low bandwidth and high Coulomb repulsion between each radical unit leads to formation of a Mott insulating state.

1.4.3 Single component molecular conductors

At this time a comprehensive review of all neutral radicals used to generate molecular metals is beyond the scope of this introduction, however, the majority of research in this field is based on phenalenyl **1.9** and thiazyl **1.11** radical derivatives and the resulting properties of the various materials are briefly reported below.

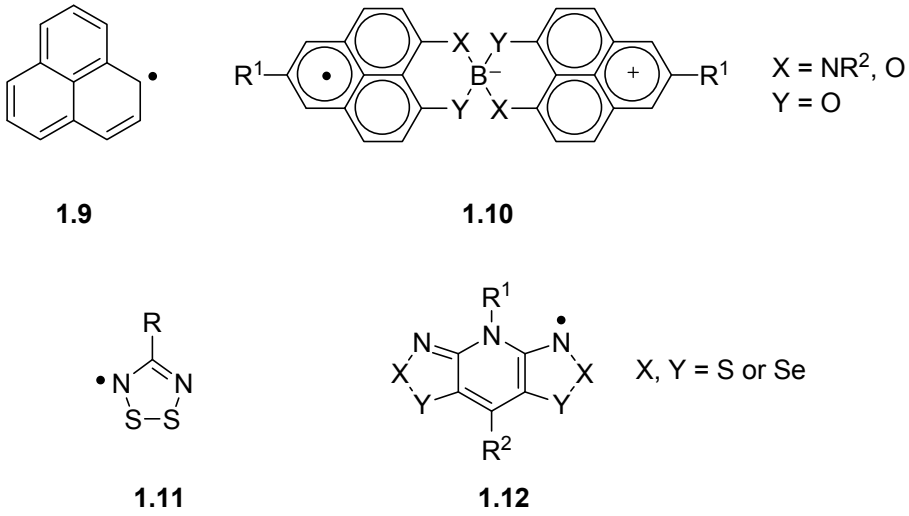

Figure 1.18. Phenalenyl **1.9**, spirobiphenalenyl **1.10**, thiazyl **1.11**, and thiadiazyl **1.12** radicals.

Unsubstituted phenalenyl radical **1.9** was the first neutral radical synthesized to test the theory presented above. Radical **1.9** was reported by Haddon et al. in 1975 but was prone to a Peierls instability and formed insulating σ dimers in the solid state.[100] The 2,5,8-tri-*tert*-butylphenalenyl and perchlorinated phenalenyl radicals were synthesized in an

attempt to overcome σ dimerization. The steric bulk of the *tert*-butyl groups inhibited σ dimerization, however, π dimerization was observed.[109] While the perchlorinated derivative did not dimerize, the chlorine atoms increased molecular separation and it behaved as a Mott insulator with a conductivity of only 10^{-10} S cm^{-1}.[110,111]

More recently the spirobiphenalenyl boron-centred radicals **1.10** based on the original phenalenyl framework have been investigated. Unlike the parent phenalenyl radicals, these systems have one spin per two phenalenyl units giving rise to a ¼-filled band in the solid state. This reduces the on-site Coulomb repulsion and allows for closer packing of the phenalenyl units. The properties of each individual material is highly dependent on substitution at R^1 (and R^2 when X = NR^2). In some systems σ dimerization[112] or face-to-face π dimerization[113] was observed, although interestingly when R^1 = H and R^2 = ethyl the conductivity was high despite π dimerization.[113] Worth noting was the synthesis of an X = N(cyclohexyl) derivative that formed superimposed phenalenyl π stacks in the solid state. In this system the C…C intermolecular distances were shorter than the sum of the van der Waals separation and a high room temperature conductivity (σ_{RT} = 0.3 S cm^{-1}) was observed.[114] Many of the X = Y = O spirobiphenalenyl radicals have been found to be conducting at room temperature, although the conductivity is still activated.[115] In many of the highly conducting spirobiphenalenyl systems close intermolecular contacts are present along more than one crystallographic axis and the dispersion of orbitals in more than one dimension may be giving rise to high room temperature conductivity.

Following the publication of the parent phenalenyl systems, Oakley et al. began preparing their first neutral radicals based on the thiadiazolyl framework **1.11** (Figure 1.18).[116,117] The thiadiazolyl class of radicals aimed to combine the delocalization of

phenalenyl with the conducting properties of the $(SN)_x$ polymer. The thiadiazolyl radicals **1.11** were stabilized (relative to the phenalenyl systems) by incorporating electronegative heteroatoms into the ring system. Much of the early work focused on **1.11** with various R groups. Numerous systems were prepared, however, the R substituent is located at a nodal position in the SOMO and little perturbation of the radical electronic structure was observed.[118] Regardless of substituent, intradimer S-S bonds formed below room temperature and the conductivity was on the order of 10^{-9} S cm^{-1}.[119-123] Replacing the sulfur in **1.11** with selenium resulted in an increase in conductivity,[124] consistent with the more diffuse selenium orbitals giving rise to a greater bandwidth.[125]

The greatest success in the Oakley group has come with the synthesis of the so called 'resonance stabilized' bisdithiazolyl (Figure 1.18, **1.12**) radicals. A number of derivatives of **1.12** differing in R^1 and R^2 have been isolated and characterized.[126-129] In these bisdithiazolyl systems spin density is delocalized evenly between the two dithiazolyl rings and the stability of these nitrogen-centred radicals improves accordingly. The room temperature conductivities were typically on the order of 10^{-6} S cm^{-1}. As before, the replacement of S with two or four Se atoms to give bisthiaselenazolyl[130] or bisdiselenazolyl[131] radicals increased the room temperature conductivity to as much as 10^{-3} S cm^{-1}, the highest observed yet for this class of radicals.[131]

1.4.4 Conducting donor–acceptor charge transfer salts

Molecular systems with high room temperature conductivities have also been explored through the synthesis of two-component donor–acceptor (D–A) charge transfer salts. These systems consist of co-crystallized donor and acceptor molecules whose redox potentials are such that they promote either partial or complete charge transfer between D

and A. In some cases these salts exhibit remarkable room temperature conductivity, metallic behavior, unusually strong magnetic exchange, and superconductivity.

The first reported example of a co-crystallized D–A complex exhibiting partial charge transfer and high conductivity came in 1973 from Ferraris et al.[132] In 1974 Wudl et al.[133,134] confirmed the electronic properties exhibited by the tetrathiafulvalene **1.13** 7,7,8,8-tetracyanoquinodimethane **1.14** (TTF:TCNQ) salt (Figure 1.19).

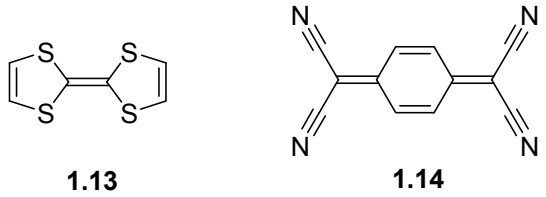

1.13 **1.14**

Figure 1.19. Tetrathiafulvalene (TTF, **1.13**) and tetracyano-*p*-quinodimethane (TCNQ, **1.14**).

The crystal structure of 1:1 TTF:TCNQ was reported soon after its synthesis.[135] 1:1 TTF:TCNQ packs parallel to the *b*-axis in separated uniform columns of TTF radical cations and TCNQ radical anions (Figure 1.20, a). The cationic TTF interplanar stacking distance is 3.47 Å, while the anionic TCNQ interplanar stacking distance is 3.17 Å. The columns themselves pack as slipped π-stacks in a herringbone motif (Figure 1.20, b). Charge transfer occurs between TTF and TCNQ molecules that are in the same plane, while the direction of conductivity is parallel to the column. This directional orthogonality between charge transfer and conductivity is common for charge transfer salts.

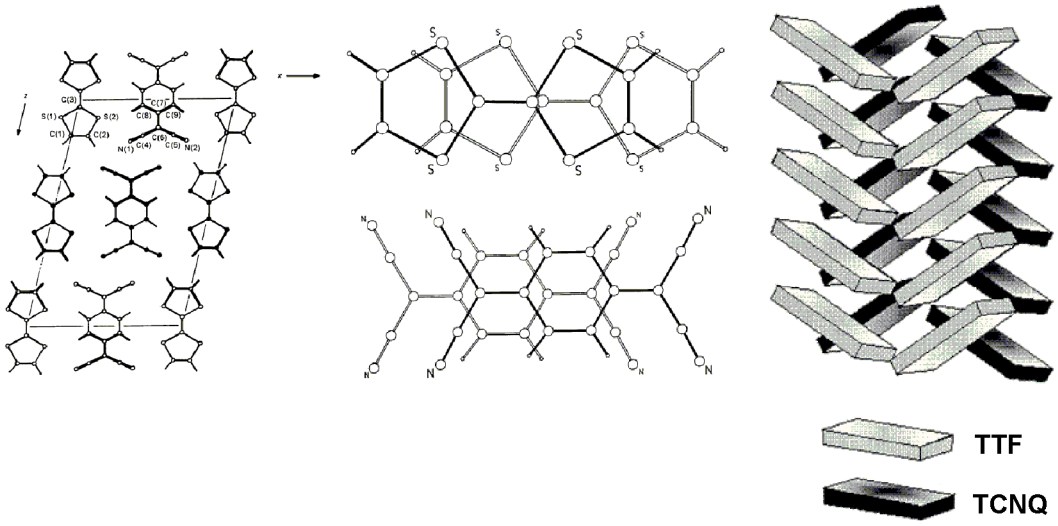

Figure 1.20. Segregated π-stacked columns (left, centre) and sketch illustrating 1D herringbone stacking (right) in a 1:1 TTF-TCNQ charge transfer salt.[135,136]

When considering organic charge transfer salts, the conductivity pathway is along the direction of greatest orbital overlap, giving rise to bandwidth parallel to the π stacks. Partial band filling as a result of incomplete electron transfer creates holes and is responsible for the conductivity observed along the stack. Partially filled bands can be deliberately introduced by controlling the stoichiometry of the donor and acceptor. If, for example, the donor and acceptor are present in a 2:1 ratio (complex salt), complete charge transfer will result in a non-integer oxidation state in two of the molecules.

Since the initial report of TTF-TCNQ,[132] hundreds of derivatized TTF-TCNQ charge transfer salts with a range of different properties have been reported.[94,95] Isostructural analogues of many of these systems have been synthesized with heavier selenium and tellurium atoms replacing sulfur atoms.[131,137] Aside from TTF derivatives, several charge transfer salts exist where benzo[1,2-*d*;4,5-*d'*]bis[1,3]dioxole derivatives, 1,2,5-thiadiazole derivates, N,N,N,N-tetramethyl-*p*-phenylenediamine and DMPH (5,10-dimethyl-5,10-

dihydrophenazine) act as donor molecules.[96,97] To date there is still a very small pool of acceptors and most acceptors are TCNQ/TCNE (TCNE = tetracyanoethylene) derivatives, although C_{60}[98] and quinones, such as dichlordicyanoquinone (DDQ),[96] have also been used as acceptors.

The conductivity in charge transfer salts is critically dependant on intermolecular interactions in the solid state. Crystal packing is manipulated through the use of planar π-delocalized molecules and nearly all molecules used in charge transfer salts fit this description. Planarity allows for the closest possible packing arrangement, while π delocalization results in strong π overlap, creating a pathway for the conducting electrons. Delocalization also stabilizes excess charge through resonance. Since partial charge transfer is desired, as it tends to result in higher conductivity,[94,138] the difference between the first oxidation potential of the donor and the first reduction potential of the acceptor is also considered. Partial charge transfer is estimated to occur when the donor and acceptor have a difference in redox potentials of $E_A - E_D \leq +0.25$ V.[138]

1.5 Electron transfer theory in organic donor–acceptor systems

As we propose using open-shell covalently bound donor–acceptor systems as building blocks for magnetic conductors, a short introduction to electron transfer theory is necessary. This includes a brief discussion of Marcus theory followed by an overview of the Robin–Day classification system.

Marcus' fundamental relationship in electron-transfer theory, namely the dependence of the rate of electron-transfer (k_{ET}) on the reorganization energy (λ) and free energy

(ΔG^o), can be derived mathematically by treating two overlapping potential energy wells (as described above) as simple parabolae (Figure 1.21).

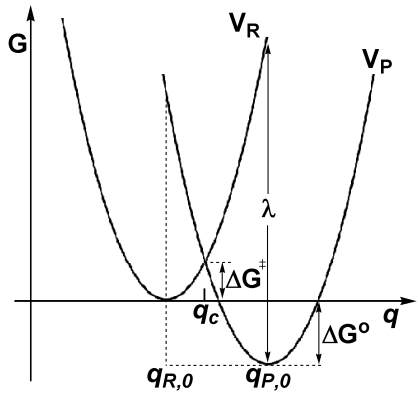

Figure 1.21. Free energy curve for an asymmetric ($\Delta G^o \neq 0$) electron transfer event. Reproduced as in reference 139.

The free energy curves in Figure 1.21 were solved in terms of the free energy barrier $\Delta G^{\ddagger}$ to give equation 6.[140,141]

$$\Delta G^{\ddagger} = \frac{1}{4\lambda}(\lambda + \Delta G^o)^2 \tag{6}$$

Substitution of 6 into the Arrhenius equation gives 7, which has since become the most influential relationship in electron transport theory.[139,142-144]

$$k_{ET} = A \exp\left[\frac{(-\Delta G^o + \lambda)^2}{4\lambda k_B T}\right] \tag{7}$$

This fundamental relationship describes how the rate of electron transfer depends critically on the reorganization energy and free energy of the reaction. The reorganization energy can be broken down into two parts as given in 8, where λ_i is the inner-sphere reorganization energy and λ_o is the outer-sphere reorganization energy.

$$\lambda = \lambda_o + \lambda_i \tag{8}$$

The inner-sphere reorganization energy is the energy associated with the population of various intramolecular vibrational modes. The outer-sphere reorganization energy is the energy required to reorient the permanent solvent dipole moment and polarized electron cloud before and after a charge transfer event. The redistribution of the electron cloud is rapid when compared to the rate of electron transfer, however, the reorientation of permanent dipole moments can be slow. For this reason, the rate of some electron transfer reactions may be controlled by the polarity of the solvent.[140-143]

Perhaps the most interesting and experimentally valuable phenomenon related to electron transfer is the ability to use the energy of the optical transition to calculate the thermal barrier to charge transfer. This relationship was derived by Hush and included as an addendum to Marcus theory resulting in the development of the experimentally practical Marcus–Hush theory.[145]

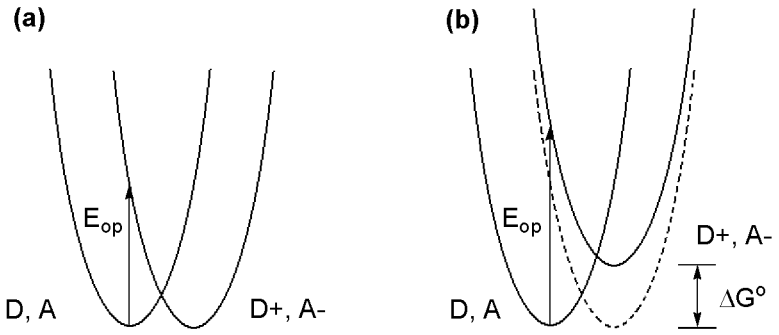

Figure 1.22. Potential energy curves illustrating an optically induced electron transfer for both the (a) symmetrical ($\Delta G^{o} = 0$) and (b) non-symmetrical ($\Delta G^{o} \neq 0$) cases. Adapted from reference 146.

An optically induced electron transfer is illustrated in Figure 1.22. The energy and shape of the absorption band is dictated by the intramolecular and solvent vibrations, λ_i and λ_o. These are the same λ_i and λ_o that determine the rate of thermal electron transfer.

When the potential energy curves in Figure 1.22 are considered, a relationship between the optical transition and λ can be derived for both symmetrical (equation 9) and unsymmetrical (equation 10) cases.[142,146]

$$E_{op} = \lambda = \lambda_o + \lambda_i \tag{9}$$

$$E_{op} = \lambda + \Delta G^o \tag{10}$$

If the unsymmetrical case is considered and 10 is substituted into equation 6, the thermal activation energy ($\Delta G^{\ddagger}$) may be determined from equation 11.[146,147]

$$\Delta G^{\ddagger} = \frac{(E_{op})^2}{4(E_{op} - \Delta G^o)} \tag{11}$$

Experimentally, Marcus–Hush theory is extremely useful as the energy of the optical absorption can be used to calculate the thermal barrier to electron transfer. In reality this relationship becomes much more complex but can still be used to calculate $\Delta G^{\ddagger}$ as well as several other electron transfer parameters, including the electronic coupling matrix element (V) and k_{ET}.[148]

1.5.1 Characterization of electronic coupling in solution

It has been over 40 years since Robin and Day first introduced their electron transfer classification system.[149] Robin and Day divided donor–acceptor systems into three classes based on the degree of the electronic coupling interaction; these three classes are depicted in Figure 1.23. It should be noted that the electronic coupling matrix element is represented in the literature by several different letters or symbols with the most common being V or H_{ab}. For the sake of continuity this dissertation will use V explicitly.

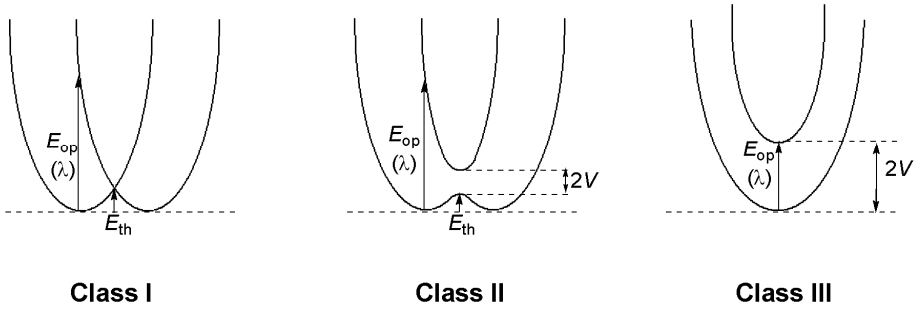

Figure 1.23. Potential wells depicting the Robin–Day classification system.[147]

The classification of a system as either class I, II or III depends on the strength of the electronic interaction (V) between the donor and acceptor moieties. In class I, the interaction between redox centers is negligible ($V = 0$)[150] and the complex only exhibits spectroscopic properties associated with each individual oxidation state. Class I systems are common when the system has a large internuclear separation or highly localized orbitals on the donor and acceptor. The class I systems are non-adiabatic (diabatic) as the electron must cross over a thermal barrier to a different potential energy surface during electron transfer.[146,147] In class I systems, the main mechanism for electron transfer is electron tunneling.

The class II systems are those which are weakly coupled electronically ($0 < V < \lambda/2$).[150,151] The weak electronic coupling will slightly alter the properties of each redox site and the system may also exhibit new spectroscopic properties that are not characteristic of either redox center. A thermal barrier to electron transfer still exists but the overlap is strong enough that the system is now classified as weakly adiabatic. In an adiabatic electron transfer process the electron remains on a single potential energy surface.[146,147] The class III systems are strongly electronically coupled ($V > \lambda/2$).[150,151] The electron is considered fully delocalized and a thermal barrier to electron transfer no

longer exists. The class III systems exhibit new spectroscopic properties owing to the fact that the redox sites now have an averaged valency. These new properties are often quite distinct from those of the original isolated redox sites.

Purely organic donor–acceptor systems were not investigated until well after electron transfer theory had been established with respect to inorganic complexes. This is predominantly because one-electron processes are much less common in organic chemistry. Additionally, organic donor–acceptor systems are theoretically more difficult to evaluate as the electron is usually delocalized over a number of atoms and the redox center is not well defined. This is contrary to inorganic complexes where the electron transfer occurs predominantly between the transition metal atoms. Although the decay in electronic coupling as a function of distance is similar in organic and metal compounds,[152] the electronic coupling in organic systems is stronger on average than that in metal-based systems.[153] This alone makes organic molecules attractive targets for use in molecular electronic devices.

1.6 Our stratagem towards organic magneto-conductors

We are interested in elucidating relationships between the electronic structure of the individual radical units and their observed bulk properties with the expectation that this will ultimately lead to rational design of magneto-conducting materials. For this reason we must be able to obtain structural information and have elected to study molecular systems. In particular, we are interested in understanding how D/A interactions affect the interplay between electronic structure and solid state packing which in turn affects magnetism, conductivity and solid state absorption spectroscopy. In some ways we are

bringing together the two schools of thought on molecular conductivity. We are still using the single molecule S = ½ subunits, however, we are introducing the D–A interactions used by the charge transfer salt community to realize high conductivities.

Chemically bonding the donor and acceptor removes some of the serendipity associated with packing in a two-component system, yet the conduction electrons can still be supplied by an electron transfer event between D and A. Our proposed molecular architecture covalently bonds accepting planar π-delocalized benzonitronyl nitroxide radicals with donors of varying strengths in D–A and D–A–D type motifs (Figure 1.24). Planar π-delocalized systems are attractive from a crystal engineering perspective as they often form π stacks with close intermolecular contacts. Electrostatic D–A interchain interactions are expected to lead to slippage along the stacks, leading to an offset of the Peierls distortions often associated with 1D π stacks. Maintaining a neutral charge is also important as coulomb repulsion between individual units will be minimal.

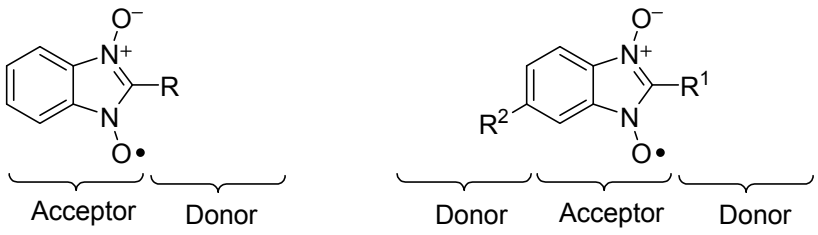

Figure 1.24. Donor–acceptor (left) and donor–acceptor–donor (right) benzonitronyl nitroxide radicals.

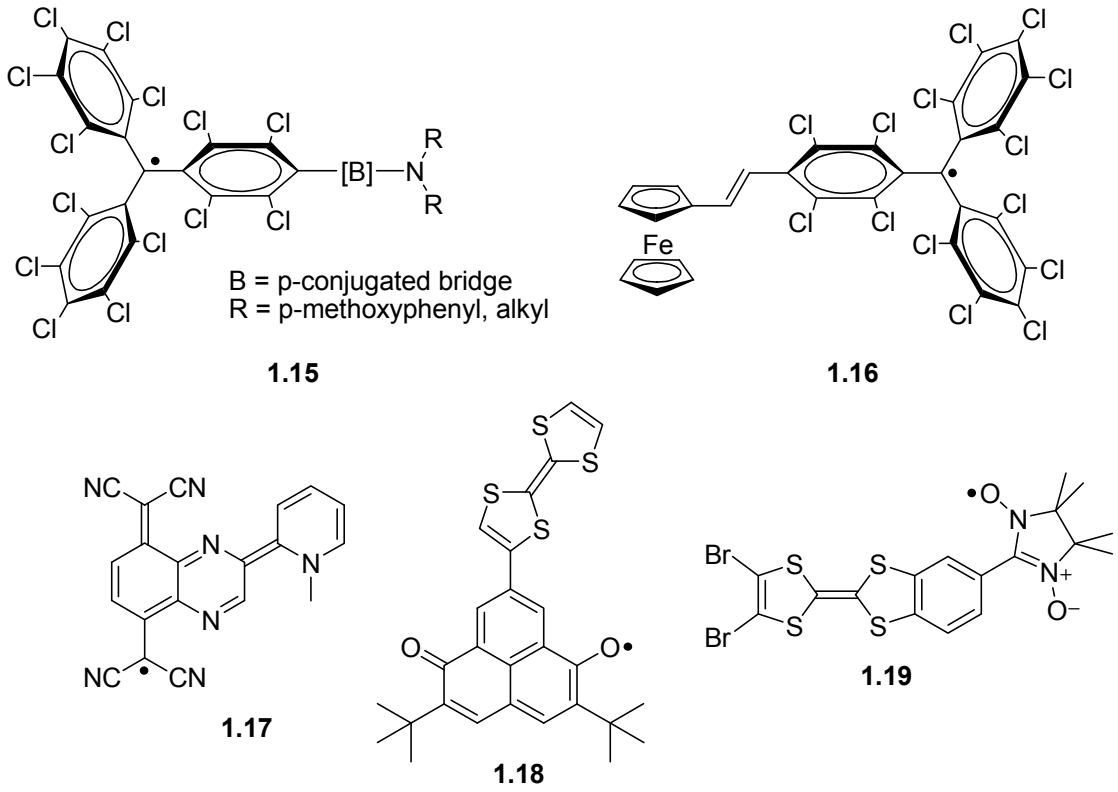

Figure 1.25. Neutral open-shell donor–acceptor systems.

There are very few examples of neutral delocalized open-shell donor–acceptor molecules, those known are shown in Figure 1.25. Solution phase electron transfer in parent electron-donating triphenylamine/electron-accepting perchlorinated triphenylmethyl radical **1.15** and its derivatives has been scrupulously studied. Each radical in series **1.15** exhibits weak absorption bands in the NIR (11 000 – 13 000 cm^{-1}) attributed to an optically induced charge transfer transition between the accepting perchlorinated phenylmethyl radical and the donating triphenylamine.[154,155] Charge transfer was confirmed by measuring the absorbance of the transition in twelve different solvents, ranging from nonpolar *n*-hexane to strongly polar acetonitrile. Although the solid state properties have not been investigated in these systems, this series of comprehensive solution phase experiments is important within the context of our work as

it demonstrates electron transfer in open-shell organic D–A systems behaves exactly as it would in a closed-shell analogue. Similar solution phase behavior, namely the observation of a low energy CT transition, was observed in ferrocene perchlorinated triphenylmethyl radical **1.16** and its derivatives.[156-158] The tetrathiafulvalene (TTF) 2,5-di-tert-butyl-6-oxophenalenoxyl **1.18** neutral D–A radical also exhibited a solvatochromic solution phase charge transfer band. EPR and UV–vis spectroscopy showed reversible thermochromic interconversion between the neutral radical and charge separated oxophenalenoxyl anion/TTF cation.[159] This temperature dependent equilibrium has been well studied in cationic dihydrazine D–A species[148,160,161] and is an interesting solution phase phenomena that, if present in the solid state, could lead to thermally accessible conducting and magnetic states and switching applications.

Conductivity was only measured in two of the above systems (Figure 1.25, **1.17** and **1.19**), both of which were found to be semiconducting at room temperature. In the case of the TCNQ derivative[162] **1.17** the powder conductivity was 3.2 x 10^{-5} S cm^{-1} while the conductivity of a polycrystalline sample of tetramethyl nitronyl nitroxide derivative[163] **1.19** was 9 x 10^{-4} S cm^{-1}. Magnetic exchange interactions have only been examined in **1.19** where the exchange was weakly ferromagnetic along π stacks (*intra*chain $J/k_B = 6.5$ K) and weakly antiferromagnetic between chains (*inter*chain $J/k_B = -1.1$ K).[163]

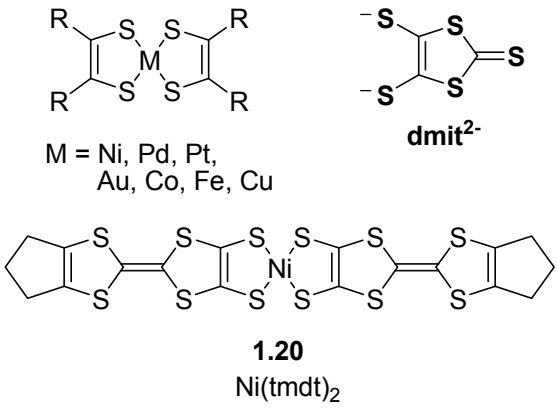

Figure 1.26. Metal dithiolene complexes.

Although not solely organic, metal dithiolene complexes (where A is an electron poor metal) are examples of neutral D–A−D systems. Bis-1,2-dithiolene complexes contain unpaired electrons and a planar delocalized electronic structure[164] that has resulted in the observation of ferromagnetic ordering (T_c = 4.5 K),[165-167] metallic conductivity,[168] and superconductivity. The first conducting $M(dmit)_2$ salt (dmit = 4,5-dimercapto-1,3-dithiole-2-thione), $(Bu_4N)_2[Ni(dmit)_2]_7 \cdot 2CH_3CN$ was reported in 1983.[169] Since then a number of metal dithiolene complexes have been reported.[164,168,170] The first metal dithiolenes were one-dimensional systems with dispersion along chains of stacked molecules with short S…S contacts.[168] They showed conductivities on the order of those observed for the 1D organic phenalenyl and thiadiazolyl radicals and were subject to the same types of lattice instabilities discussed above. Increasing the dimensionality of the solid state structure eliminated the Peierls instability and later bisdithiolene complexes, such as $Ni(tmdt)_2$ **1.20** (tmdt = trimethylenetetrathiafulvalenedithiolate)[171] in Figure 1.26, showed remarkably high conductivities, genuine 2- or 3D Fermi surface and metallic ground states.[168] Metal dithiolenes are important within the context of this research as they show both the importance of higher dimensionality band structure on conductivity

and that high conductivity can be achieved through orbital overlap between smaller p-block elements (in this case sulfur).

Only a handful of organic open-shell donor acceptor compounds have been synthesized, likely because very few organic radicals exist that are either strongly accepting or donating. Annelation of tetramethyl nitronyl nitroxide has provided us with a planar delocalized radical with redox properties appropriate for incorporation into D–A molecular systems.[172] By incorporating the benzonitronyl nitroxide radical into D–A molecules we aimed to investigate the effect of intramolecular electron transfer of the solid state properties of open-shell systems.

1.7 Scope and organization of this dissertation

Research in the Frank group has been driven by the need for new stable spin delocalized organic radicals with unique solid state properties for magneto-conducting applications. Prior to this work, the synthesis of a number of benzonitronyl nitroxide radicals was shown to be feasible, however, radical generation suffered from poor yield and reproducibility and the radicals were not isolated in high purity.

The second chapter of this dissertation describes the development of a mild synthetic methodology allowing for the synthesis of a number of benzonitronyl nitroxide precursors, of which a subset was selected for radical generation. The electronic structure of the series benzonitronyl nitroxide radicals were investigated through solution phase techniques (EPR, UV–vis–NIR, and cyclic voltammetry) and compared to computational results. Annelation was found to result in a remarkably low reduction potential (relative to the parent tetramethyl nitronyl nitroxide) making this class of radicals ideal for use as

electron acceptors in donor–acceptor systems. The solid state packing was investigated through X-ray crystallography and the crystallographic data was used to interpret the observed magnetic exchange.

The focus of the third chapter is on understanding the effect of increased conjugation in this class of benzannelated radicals. A series of π-delocalized and heteroaromatic radical precursors were synthesized and fully characterized. The electronic affinity (EA) and electronic structure of each radical was evaluated computationally and compared to their respective reduction potential and EPR spectrum in order to gain insight into the relationships between spin density distribution, redox potential and radical stability (solution phase lifetime).

The fourth chapter describes the synthetic methodology developed to allow for incorporation of benzonitronyl nitroxide radical acceptors into donor–acceptor–donor arrays. Solution phase techniques were used to evaluate the spin density distribution and electronic structure of these triads. A charge transfer excitation was observed in the visible region of the absorption spectrum and was studied using variable temperature spectroscopy and modeled computationally in order to gain insight into the solution phase structure, extent of radical delocalization and nature of the excited state. The solid state packing was determined by single crystal or powder diffraction crystallography. The effects of intermolecular donor–acceptor interactions on solid state packing, magnetic exchange and conductivity were explored.

Chapter five describes the synthesis of a series of benzonitronyl nitroxide donor–acceptor molecules where the difference in potential ($\Delta E = E_{ox} - E_{red}$) between donor ($E_{ox}$) and acceptor ($E_{red}$) was systematically decreased. The effects of decreasing ΔE on

radical electronic structure and electronic coupling (V) were assessed through solution phase spectroscopy and cyclic voltammetry. The conductivity and magnetism of the D–A radicals was measured and when possible interpreted in terms of solid state packing.

Chapter 2: Synthesis of π-Delocalized Benzannelated Nitronyl Nitroxide Radicals

2.1 Stable radicals for multifunctional materials

Radicals are often thought of as highly-reactive short-lived species. Loss of the spin bearing centre occurs through dimerization, hydrogen abstraction and disproportionation and often the activation barrier to these reaction pathways is negligible. When designing stable radicals, certain architectures can impart thermodynamic or kinetic stability. Radicals in which the spin density is delocalized over a number of atoms have greater thermodynamic stability toward dimerization and H-atom abstraction due to resonance stabilization. In addition, lower electrochemical disproportionation energies and lower lying excited states are typically observed, making them appropriate for use in materials science applications.

Many otherwise unstable radicals can be kinetically stabilized by the incorporation of sterically bulky substituents, however, the very features providing stability obstruct potentially interesting solid state interactions which would otherwise be observed through close intermolecular contacts. As our interests lie in designing magneto-conducing systems, we require organic radicals that are thermodynamically stable towards dimerization and whose kinetic stability does not rely on steric protection.

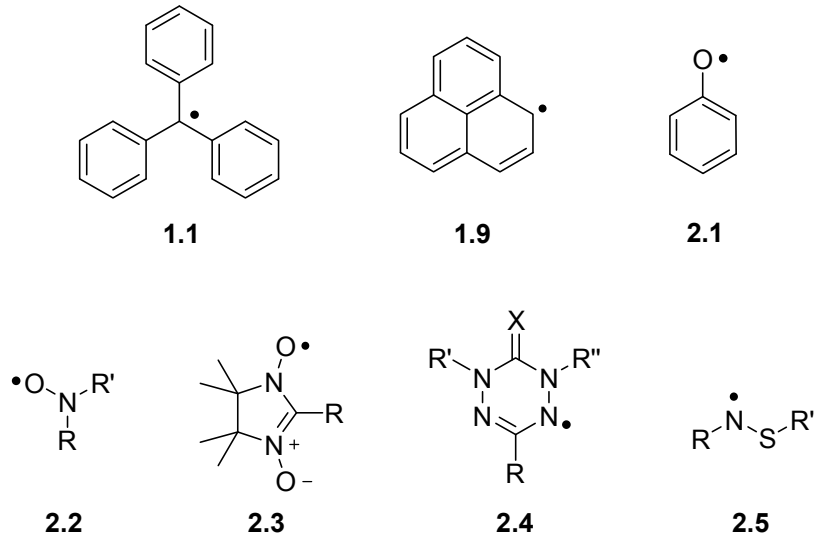

Figure 2.1. Classes of *neutral* stable organic radicals.

The oldest, and arguably most well-known example of a stable carbon-based radical is Gomberg's radical (triphenylmethyl radical **1.1**)[1] though it was not isolated in its free radical state for some time. At 5 ºC in benzene, only 2 – 3 % of triphenylmethyl radical is present in its dissociated form while the remainder exists as a head-to-tail dimer **2.6** (Figure 2.2).[173,174] The existence of such a dimer is evidence that the unpaired electron does not reside solely on the central carbon, but is delocalized into the phenyl rings. The SOMO (Figure 2.3) reflects this delocalization and is consistent with EPR spectroscopy which indicates ~30 % of the spin density resides on the central carbon, with significant spin populations at the *ortho* and *para* positions of the phenyl substituents.[175] Chlorination of triphenylmethyl radical **1.1** increases the radical stability towards dimerization by steric protection by the large chlorine atoms on the aryl rings with little change in spin density distribution.[176] This subset of triarylmethyl radicals, the perchlorotriphenylmethyl (PCTM) radicals are remarkably stable, having lifetimes on the order of decades – even when stored under ambient conditions.[176-178]

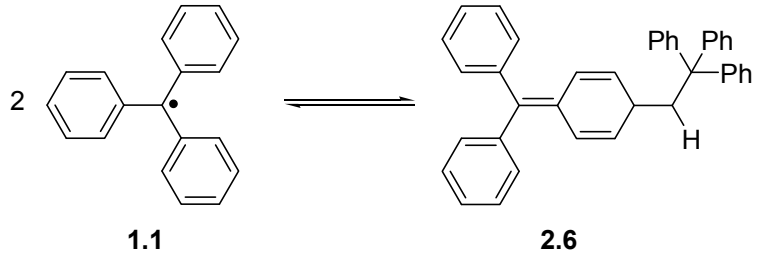

1.1 **2.6**

Figure 2.2. Equilibrium between triphenylmethyl radical and its dimer.

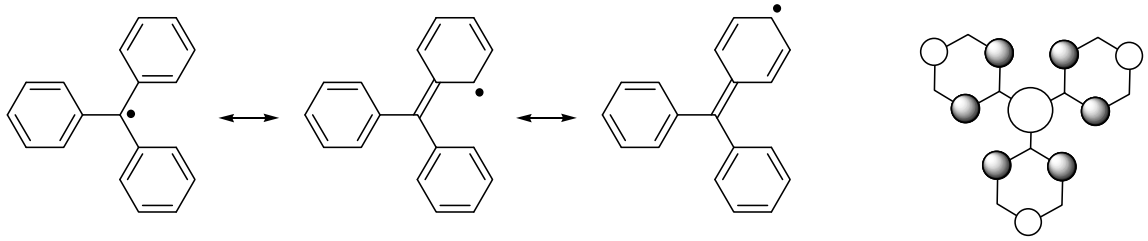

1.1

Figure 2.3. Resonance structures and SOMO of triphenylmethyl radical **1.1**.

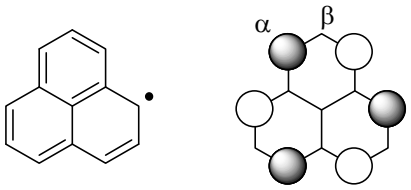

1.9

Figure 2.4. Phenalenyl radical and SOMO.

Phenalenyl **1.9** is a neutral π-conjugated hydrocarbon radical that is in many ways similar to the triphenylmethyl radical. Phenalenyl radicals possess a fused polycyclic planar structure whose unpaired spin is delocalized over the periphery of the molecular skeleton with the central carbon occupying a nodal position (Figure 2.4).[179,180] Unsubstituted phenalenyl is kinetically unstable and immediately undergoes σ dimerization, consequently it cannot be isolated in the solid state. Introducing

substituents at the β carbon renders phenalenyl radicals inert to σ dimerization,[109,111] however, certain derivatives have been shown to form face-to-face π dimers (Section 1.4.3).

Phenoxyl radicals **2.1** are electron deficient oxygen-centered radicals, with the majority of spin density located on the oxygen heteroatom.[181] A smaller percentage of spin density is located at the *ortho* and *para* positions and the overall spin density distribution is best described using resonance structures analogous to those described above for the triphenylmethyl radical **1.1**. To date, the most stable phenoxyl radicals are those substituted with bulky alkyl or aromatic groups at the *ortho* and *para* positions, with the *tert*-butyl and methyl (oxidized BHT) derivatives **2.7** being the most ubiquitous. Among phenoxyl radicals, the galvinoxyl radical[182] **2.8** (Figure 2.5) has received much attention due to the observed ferromagnetic-to-antiferromagnetic phase transition and exceptional stability.[183]

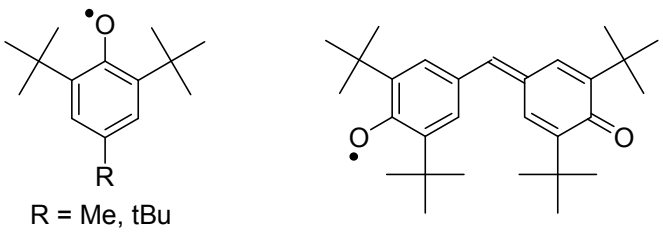

Figure 2.5. *tert*-Butylphenoxyl and galvinoxyl radicals.

The nitroxide **2.2** and nitronyl nitroxide **2.3** radicals (Figure 2.6) are undoubtedly the most comprehensively studied class of stable radicals.[184-192] Nitroxides have substantial spin density delocalized over both nitrogen and oxygen,[193] with little spin present on any other atoms in the molecule. Nitronyl nitroxides are further stabilized by delocalization of the unpaired electron over the O–N–C–N–O moiety with a node on the central (*C*2)

carbon atom. Nitroxides are inherently stable and σ dimers have never been observed as the N–O–O–N heteroatom chain formed upon dimerization would be a highly reactive species as a result of lone pair-lone pair repulsion. The overall nitroxide stability is dependent on the *N*-substituents and radical decomposition tends to occur by disproportionation. Nitroxides have been intensively studied for use as spin traps and labels,[194-198] while nitronyl nitroxides have been used as building blocks for magnetic materials[188,192,199-201] with *p*-nitrophenyl nitronyl nitroxide representing the first example of an organic ferromagnet.[83,87,88]

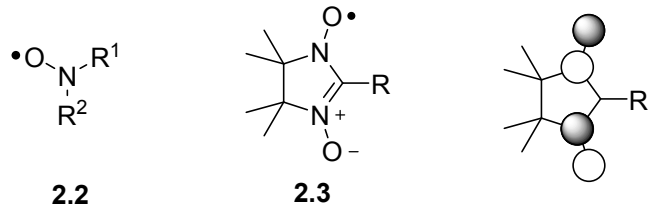

2.2 **2.3**

Figure 2.6. Nitroxide radical **2.2**, nitronyl nitroxide radical **2.3**, and nitronyl nitroxide SOMO.

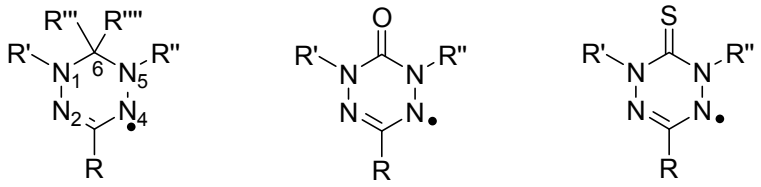

2.9 **2.10** **2.11**

Figure 2.7. Verdazyl **2.9**, oxoverdazyl **2.10** and thioxoverdazyl **2.11** radicals.

The nitrogen centered verdazyl radicals[202-205] have been extensively studied as a result of their exceptional chemical stability.[202] Verdazyls are categorized according to the nature of the *C*6 carbon which is either sp^3 or sp^2 hybridized and substituted with two

hydrocarbon R groups **2.9**, oxygen **2.10** or sulfur **2.11** (Figure 2.7). Verdazyl EPR spectra are dominated by a nine-line pattern arising from coupling to four nearly equivalent heterocyclic nitrogen atoms. Consistent with this, the greatest degree of positive spin density is present on the four nitrogen with a small amount of negative spin density at *C*3. Verdazyl radicals have primarily been investigated for use as spin-bearing centers in organic and metal-organic magnets,[203,206] although more recently they have been successfully used as radical initiators in 1,3-dipolar cycloadditions[207] and living polymerizations.[208]

Stable radicals based on the thiazyl (SN) fragment include the thioaminyl **2.5**, dithiazolyl **2.12**, dithiadiazolyl **2.13**, and thiatriazinyl **2.14** derivatives (Figure 2.8).[209-212] The SOMO of each derivative is heavily concentrated on the sulfur and nitrogen atoms, although the cyclic thiazyl radicals have non-negligible contributions to the SOMO elsewhere in the molecule.[209] In contrast to the verdazyl and nitroxide radicals, thiazyl-based radicals have a tendency to undergo both σ and π dimerization (Section 1.4.3). The conductivity and magnetism of thiazyl radicals has been extensively researched.[213-215] Certain thiazyl derivatives have been found to exhibit unique phenomena such as magnetic bistability[213,216-218] and exceptionally strong antiferromagnetic exchange[119] and ferromagnetic ordering.[90,91]

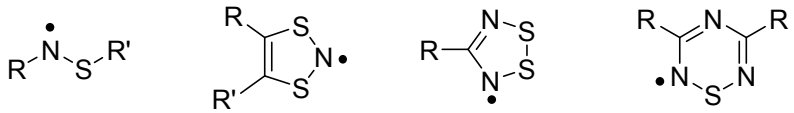

Figure 2.8. Organothiazyl radicals.

Among the stable radicals discussed above, nitroxide **2.3**, nitronyl nitroxide **2.3**, verdazyl **2.4**, and thiazyl **2.5** radicals have played a central role in the development of organic spin containing magnetic materials due to their ease of synthesis and high stability. The imidazolidinyl-based nitronyl nitroxides **2.3** are the most ubiquitous family of stable radicals used for magnetism pursuits, and have been intensely studied for the development of magneto-structural correlations in the solid state.[185] In an effort to develop new kinds of organic multifunctional materials, we have investigated a new class of spin-delocalized radicals, the annelated nitronyl nitroxides. Annelation of imidazolidinyl nitronyl nitroxide leads to a stable, planar spin-delocalized radical,[219-221] benzonitronyl nitronyl nitroxide (BNN **2.15**, Figure 2.9), which exhibits strong magnetic exchange through efficient π–π interactions in the solid state.[222,223]

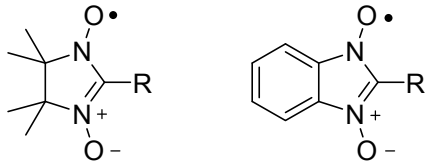

2.3 **2.15**

Figure 2.9. The tetramethyl nitronyl nitroxide **2.3** and benzonitronyl nitroxide **2.15** radicals.

Substitution of BNN at *C*2 with electron deficient aryl groups (more specifically, a series of halogenated phenyl rings and a 3-cyanophenyl group) was found to result in a factor of two increase in the magnitude of the exchange interactions.[223] Both antiferromagnetic and ferromagnetic exchange interactions were observed and were found to be entirely dependant on the crystal packing motif. Like the phenyl substituted BNN **2.15a**, the radicals adopted a nearly planar geometry with the exception of any systems containing ortho-substituted *C*2 substituents which exhibited high degrees of

torsion between the benzimidazole and phenyl rings.[223] This was also the first documented example of BNN radicals exhibiting ferromagnetic exchange in the solid state. Despite the unusual magnetic exchange interactions found in these systems, this class of radicals is poorly understood relative to the parent tetramethyl nitronyl nitroxides.

BNN radicals are of interest in that they possess (i) stability toward dimerization in solution and the solid state without the incorporation of bulky substituents giving rise to (ii), a planar topology for strong intermolecular interactions in the solid state, and (iii) delocalized spin density that provides multiple indirect and direct magnetic exchange pathways critical for conducting and magnetic materials development. Despite the unusually strong magnetic interactions found in these systems, there are precious few reports of the synthesis and magnetic characterization[219,222-224] of annelated nitronyl nitroxides, and virtually nothing is known about the effect of substitution on the spin density distribution and electronic structure of these systems.

2.2 Synthesis

Early synthetic approaches involve the preparation of radical precursor **2.16** by condensation of nitrosobenzene **2.17** with benzonitrile oxide,[225] acid-catalyzed condensation of *o*-benzoquinone dioxime **2.19** with arylaldehydes,[226] and base-catalyzed condensation of benzofuroxan **2.18** with primary nitroalkanes[227] (Scheme 2.1). These synthetic routes require either strongly acidic conditions, limiting the nature of the functionality, or suffer from poor reproducibility and low yields.

Scheme 2.1. Previous methodology for the preparation of BNN radicals.

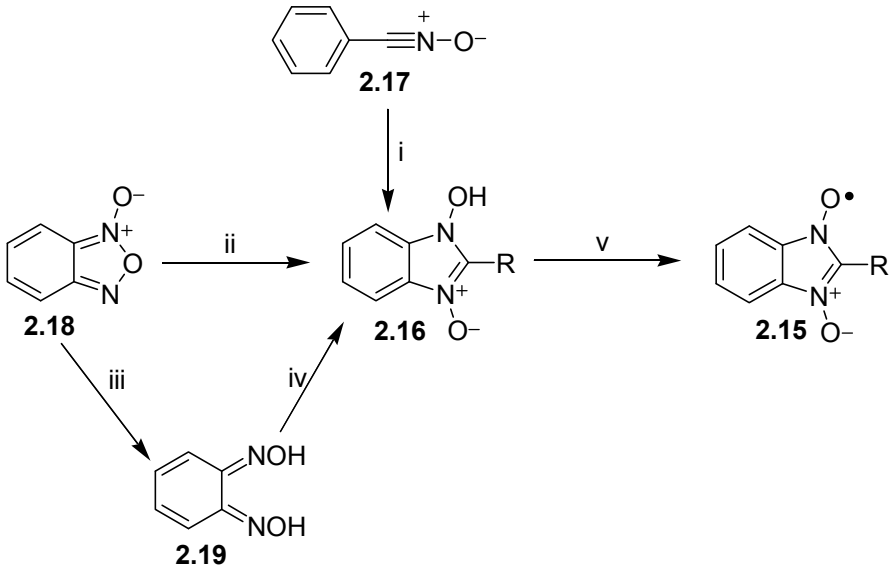

[a] Reagents and conditions: (i) PhNO; (ii) RCH_2NO_2, NR_3; (iii) NH_2OH; (iv) RCHO, H^+/EtOH; (v) PbO_2 or $NaIO_4$.

We have developed a generalized synthetic methodology for annelated nitronyl nitroxides with varying functionality based on the condensation of benzofuroxan with nitrone in nonpolar solvents. A series of radical precursors were synthesized in which heteroaromatic, aromatic, and alkyl substituents could be incorporated at the *C*2 position of the radical (Scheme 2.2).

Scheme 2.2. Synthesis methodology developed for the synthesis of BNN radical precursors **2.16a-l** and BNN radicals **2.15a-e**.[a]

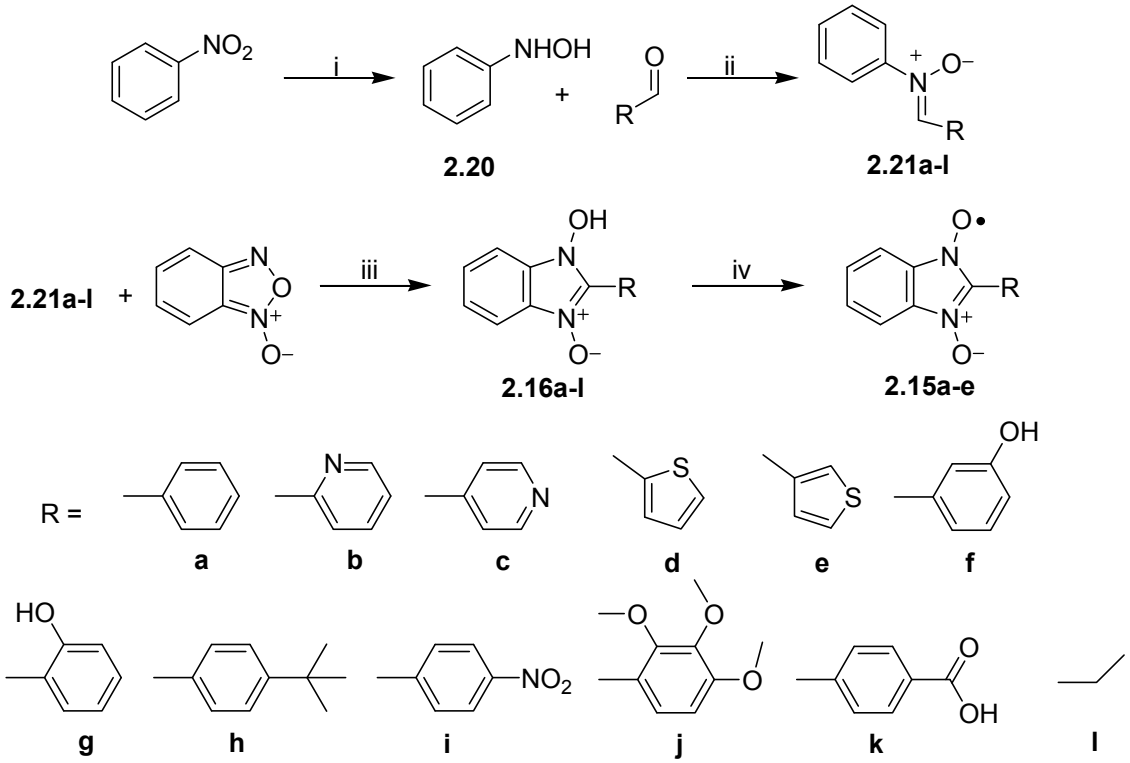

[a] Reagents and conditions: (i) NH_4Cl, Zn, H_2O, 80 %; (ii) EtOH, 70 – 90 %; (iii) toluene, Δ, 55 – 70 %; (iv) nBu_4NOH, toluene, followed by AgOTf, rt, 19 – 47 %.

The functionality of interest can be introduced via an aldehyde, which upon condensation with *N*-phenylhydroxylamine **2.20**[228] generates functionalized nitrones **2.21a-l** in good yield. Condensation of commercially available benzofuroxan with the nitrones of interest in refluxing toluene leads to precipitation of insoluble radical precursors **2.16a-l**. Thus, the radical precursors can be generated under neutral conditions in moderate yield. Initially oxidation was carried out on the protonated precursor in benzene with lead(IV) oxide.[172] This reaction consistently led to low yields of impure product as evidenced by the low magnetic moment of the isolated solid (measured by

SQUID magnetometry) and inaccurate elemental analysis.[223] Both lead(IV) oxide and the radical precursors are insoluble in all organic solvents, including DMF and DMSO. The insolubility of the radical precursors is attributed to the formation of strong hydrogen bonds between neighboring oxide and hydroxyl groups. The heterogeneity of the reaction mixture meant that most precursor was not being oxidized and was being discarded with the solid lead waste. Additionally, once cyclic voltammetry was obtained on the first BNN radical samples it became apparent that lead(IV) was too strong of an oxidant (1.70 V vs SCE, 25 ºC, 1 atm, aqueous solution)[229] as its oxidation potential is greater than the second radical/cation oxidation process ($BNN^{\bullet}/BNN^{+}$, Figure 2.12; $E_{1/2}$(ox), Table 2.2). It was believed that reducing the oxidation potential of the oxidant and selecting an oxidant that was soluble in organic solvents would lead to an increase in isolated yield. 2,3-Dichloro-5,6-dicyanobenzoquinone (0.53 V vs SCE, CH_3CN),[230] tris(4-bromophenyl)aminium hexachloroantimonate (1.1 V vs. SCE),[230] silver(I) trifluoromethanesulfonate, and silver(I) hexafluorophosphate (Ag^{+}/Ag redox couple is highly solvent dependant; 1.05 V vs SCE in CH_2Cl_2)[230] all successfully oxidized the radical precursors, however, the silver salts resulted in the cleanest reaction and were selected for routine use.

This methodology consistently led to clean generation of radical with the exception of 2-pyridyl derivative **2.16b**, which is a potentially good ligand. When oxidation of **2.16b** was attempted, the addition of silver(I) caused immediate precipitation of a bright red diamagnetic powder. While the identity of the solid was never confirmed it is likely a silver benzonitronyl nitroxide coordination complex arising from bidentate coordination

of the nitronyl nitroxide oxygen and pyridyl nitrogen lone pair. Precedence for this exists as (2-pyridyl)iminonitronyl nitroxides are known to coordinate silver.[231,232]

Although a cleaner reaction was observed with silver(I), the isolated yield of radical was still too low to allow for complete characterization of the system on a single batch of product. This was addressed by solubilizing the radical precursor through deprotonation with tetrabutylammonium hydroxide to generate a precursor anion salt **2.22** (Scheme 2.3). Initially this was done as a first step in the oxidation procedure but it was later found the tetrabutylammonium salt could be cleanly precipitated from nonpolar solvents and stored in the absence of light at room temperature for long periods of time without noticeable decomposition.

Scheme 2.3. Generation of [tetrabutylammonium][BNN] salt.[a]

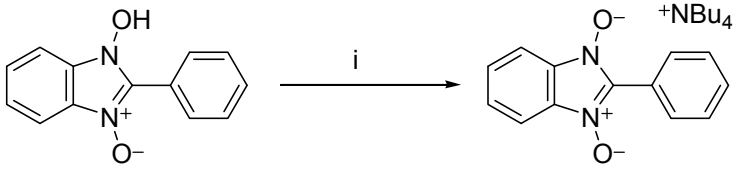

2.15a **2.22**

[a] Reagents and conditions: (i) NBu_4OH, toluene.

The improved methodology meant the radical anion and oxidizing agent could be combined to give a homogeneous solution. A subset of radical precursors (**2.16a-e**) were solubilized and oxidized in nonpolar solvents yielding yellow-green solutions with EPR spectra characteristic of nitronyl nitroxide radicals. Removal of the solvent under reduced pressure allowed for isolation of radicals **2.15a-e** in moderate yields (19 – 47 %, depending on radical solution stability). Analytically pure samples could be obtained by flash column chromatography on neutral alumina or low temperature (−78 ºC)

precipitation to yield brown microcrystalline needles. In general the series of radicals were stable in solution for up to 12 h and indefinitely stable in the solid state with the exception of **2.15b** which was found to decompose quickly in solution.

2.3 Solution phase characterization

The EPR spectra of annelated nitronyl nitroxides **2.15a-e** exhibit g-values of 2.007 ± 0.0003 and a five-line pattern with relative intensities of 1:2:3:2:1 consistent with hyperfine coupling to two equivalent nitrogen (Figure 2.10).

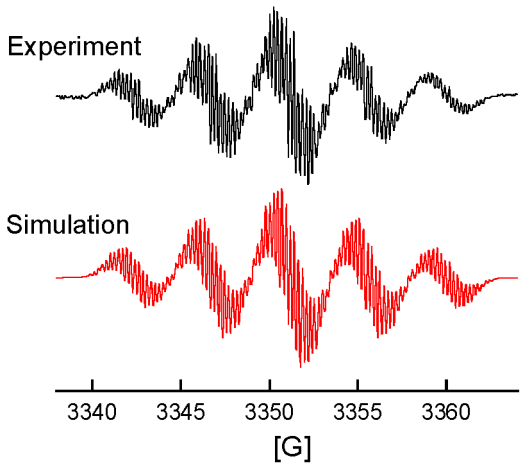

Figure 2.10. EPR spectrum of 2.15a (top = experimental, bottom = simulated, R > 0.99), 10^{-5} M solution in dry, degassed toluene at room temperature. Spectrum collected by Dr. Steven Bowles during earlier work on BNN radicals.[172]

Experimental hyperfine coupling constants (hfcc's) for each radical are reported in Table 2.1. Hyperfine coupling constants for the nitrogen in the benzimidazole moiety (N1 and N3) in **2.15a** were found to be $a(N_{1,3})$ = 4.328, roughly 60 % of that found for the parent radical **2.3** (7.4 G), consistent with significant spin delocalization into the annelated aromatic moiety. Superhyperfine coupling constants can be resolved for

coupling to two equivalent sets of protons on the annelated ring (H_α and H_β) and the aryl substituent protons, consistent with ~20 % of the total spin density residing in the annelated ring. The N_1, N_3, H_α and H_β hfcc's were nearly equivalent for the series of BNN radicals consistent with little perturbation of the spin system upon functionalization at *C*2.

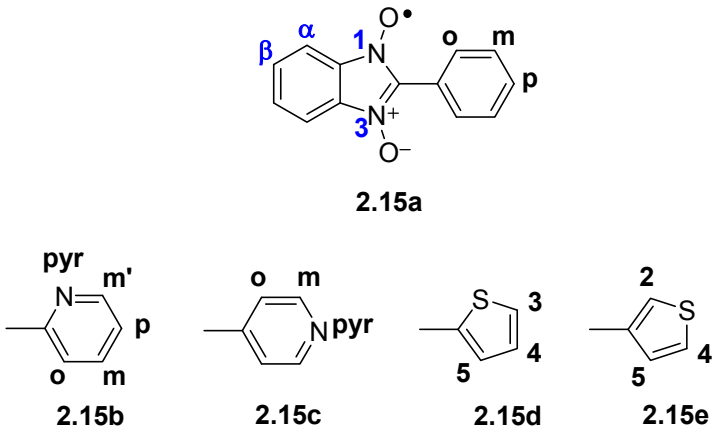

Figure 2.11. Labelled nitrogen and hydrogen atoms of radicals **2.15a-e**.

Table 2.1. Experimental g-values and hyperfine coupling constants[a] for radicals **2.15a-e**. Refer to Figure 2.11 for nitrogen and hydrogen labeling.

	2.3[b]	**2.15a**	**2.15b**	**2.15c**	**2.15d**	**2.15e**
g	2.007	2.007[c]	2.0073	2.0072	2.0070	2.0070
$a(N_{1,3})$	7.435	4.370	4.260	4.260	4.372	4.378
$a(N_{pyr})$	-	-	0.690	0.690	-	-
$a(H_\alpha)$	-	0.930	0.920	0.910	0.991	0.957
$a(H_\beta)$	-	0.650	0.690	0.730	0.742	0.698
$a(H_o)$	0.495	0.490	0.230	0.410	-	-
$a(H_m)$	0.173	0.220	0.200	0.220	-	-
$a(H_p)$	0.421	0.410	0.450	-	-	-
$a(H_{m'})$	-	-	0.200	-	-	-
$a(H_2)$	-	-	-	-	-	0.723
$a(H_3)$	-	-	-	-	0.728	-
$a(H_4)$	-	-	-	-	0.544	0.269
$a(H_5)$	-	-	-	-	0.174	0.079

Hyperfine coupling constants were simulated using the Winsim2002 software package assigned to specific atoms according to the spin density distribution determined from DFT calculations. [b] Reference 197. [c] Reference 219.

The electrochemical behavior of the series of BNN radicals **2.15a-e** was investigated by cyclic voltammetry. The parent radical **2.15a** exhibits a reversible one-electron reduction at −0.03 V vs SCE (ΔE_p = 80 mV) and an irreversible one electron oxidation at 1.60 V vs SCE in acetonitrile (Figure 2.12). By comparison, the cyclic voltammogram of TMNN **2.3** was found to have an irreversible one-electron reduction at −0.741 V versus SCE and a reversible one electron oxidation at 1.00 V versus SCE (ΔE_p = 90 mV).

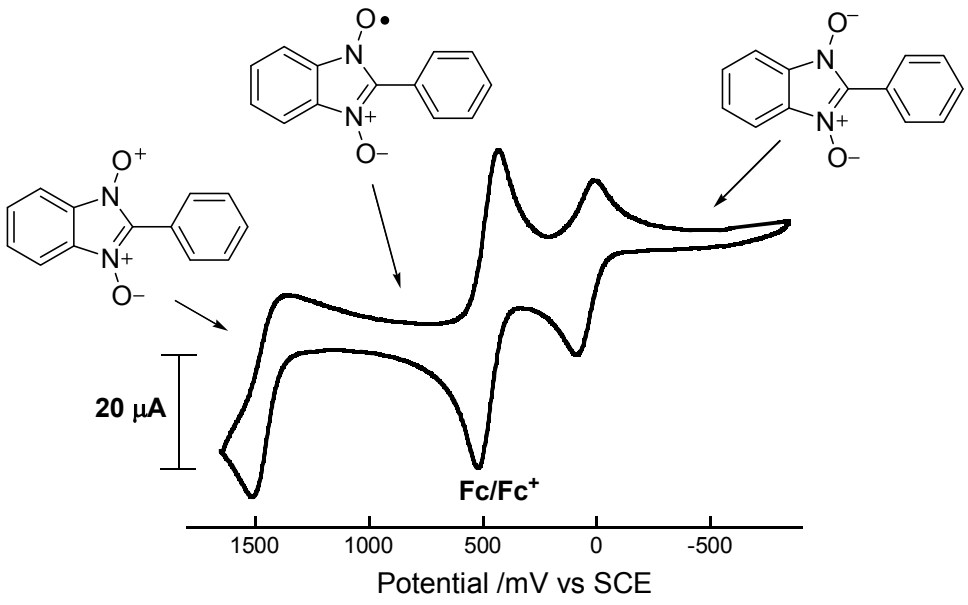

Figure 2.12. Cyclic voltammogram of 2.15a, 10 mM solution in CH_3CN, 0.1 M NBu_4PF_6, 50 mV s^{-1} scan rate, ferrocene added for reference.

Although both the oxidation and reduction processes of pyridyl radicals were found to be irreversible, the reduction potential is decreased relative to the parent **2.15a** by thienyl substitution (0.02 V vs SCE). The specific electrochemical properties of **2.15a** and **2.15c-e** are reported in Table 2.2. The very low reduction potential of the BNN radicals indicates that the radical moiety undergoes one-electron reduction at remarkably low

potentials, approaching that of 7,7,8,8-tetracyanoquinodimethane (TCNQ, 0.15 V vs SCE).[233]

Table 2.2. Electrochemical properties of BNN radicals **2.15a**, **2.15c-e** reported in V vs SCE.

	2.3	**2.15a**	**2.15c**[a]	**2.15d**	**2.15e**
$E_{1/2}$(red)	−0.74	−0.03	−0.18	0.02	0.02
ΔE_p (mV)	> 200	80	-	85	100
$E_{1/2}$(ox)	1.00	1.29	1.15	1.36	1.41
ΔE_p (mV)	90	171	-	170	140
E_{cell}	1.74	1.29	n/a	1.34	1.39

[a] Irreversible process, cathodic peak potential reported.

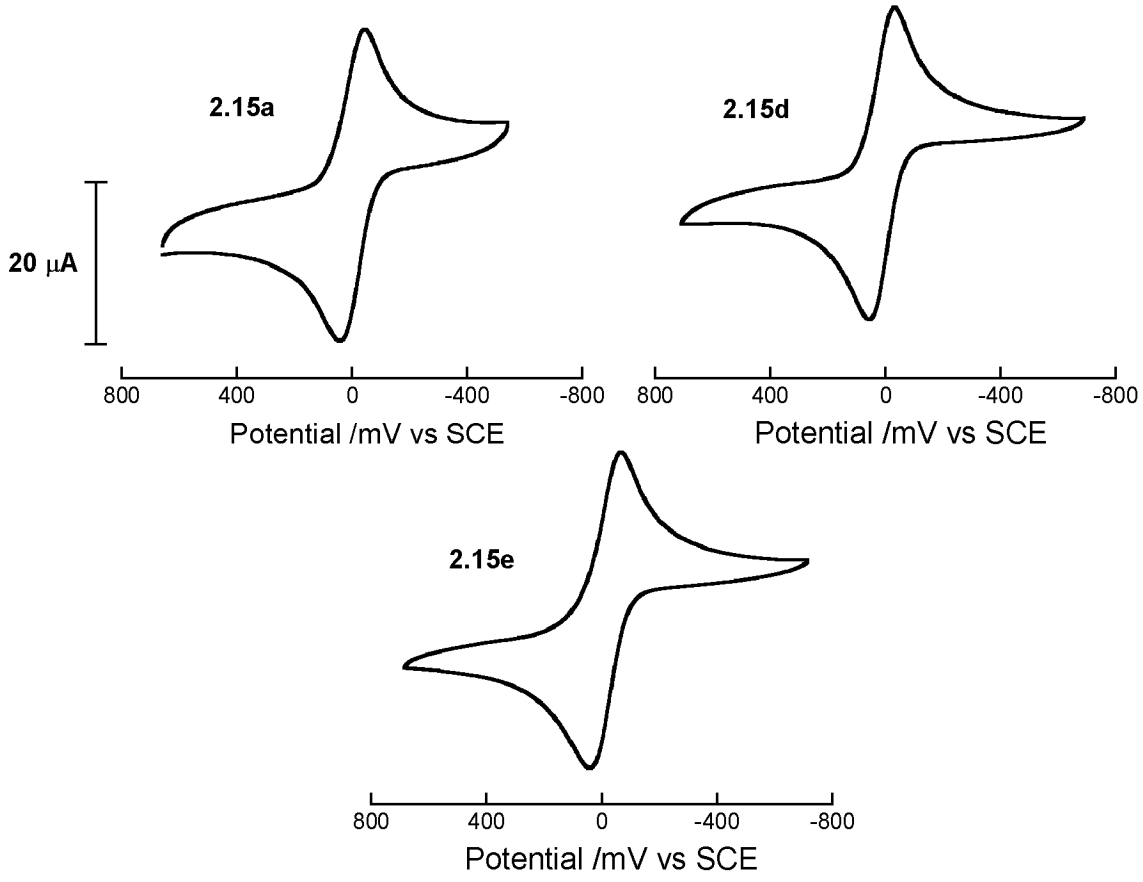

Figure 2.13. Cyclic voltammogram of reduction waves of **2.15a** (top left), **2.15d** (top right), and **2.15e** (bottom), 10 mM solution in CH_3CN, 0.1 M NBu_4PF_6, 50 mV s^{-1} scan rate.

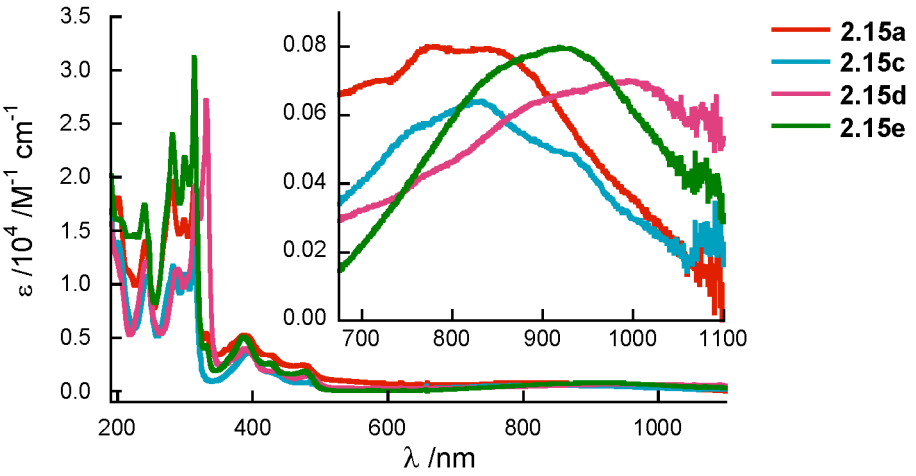

Figure 2.14. UV–vis spectra of nitronyl nitroxide radicals **2.15a** and **2.15c-e**, 10^{-5} M solutions in CH_3CN.

The absorption spectra of radicals **2.15a-e** possess absorptions in the UV region and a broad weak absorption band in the NIR (Table 2.3). The absorption maxima of the low-energy transition is dependent on the nature of the aryl substituent, lying at higher energy for electron acceptors (762 nm for 2-pyridyl **2.15b**) and lower energy for electron donors (930 – 990 nm for thienyl **2.15d-e**) (Figure 2.14). In contrast, the localized tetramethyl nitronyl nitroxide **2.3** exhibits a diagnostic absorption band in the visible region at 600 nm assigned to a SOMO–LUMO transition[197] (Figure 2.15). The low energy excitation observed in the benzannelated nitroxides has been assigned to a symmetry forbidden HOMO–SOMO transition (TDDFT computation; Section 2.5). Benzonitronyl nitroxide is a strong acceptor and the SOMO is localized primarily on the BNN moiety. As the energy of the donor approaches the energy of the acceptor, the HOMO–SOMO gap decreases and the energy of the excitation is shifted to longer wavelength.

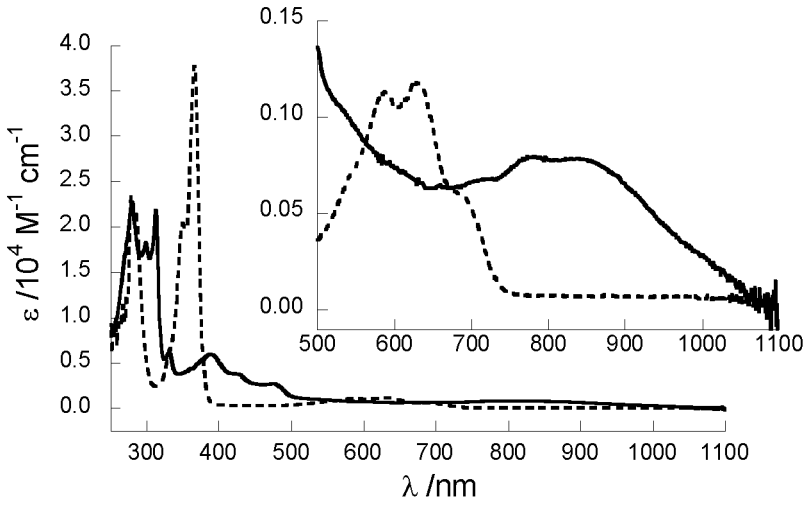

Figure 2.15. Electronic absorption spectrum of tetramethyl nitronyl nitroxide **2.3** (---) and benzimidazolyl nitronyl nitroxide **2.15a** (—), 10^{-5} M solutions in CH_3CN. Inset shows zoom of long wavelength absorptions.

Table 2.3. Absorption data for radicals **2.15a-e** (CH_3CN) reported as λ_{max} (nm) with ε (M^{-1} cm^{-1}) in brackets.

Radical	Short UV	Long UV	Visible	NIR
2.15a	200 (18000)	279 (20000)	388 (5500)	825 (800)
	241 (14000)	298 (16000)	421 (3500)	
		312 (19000)	475 (2500)	
2.15b[a]	242	280	392	762
		308	475	
2.15c	243 (11000)	281 (12000)	397 (3700)	831 (650)
		299 (11000)	427 (1800)	
		312 (14000)	483 (900)	
2.15d	243 (12000)	289 (12000)	390 (4000)	990 (750)
		315 (19000)	433 (2000)	
		331 (27000)	482 (1500)	
2.15e	240 (17000)	280 (24000)	386 (5100)	930 (800)
		299 (22000)	426 (2600)	
		313 (31000)	476 (1900)	
		330 (4300)		

[a] Concentration unknown as radical decomposes rapidly in solution.

2.4 Analysis of NIR excitation

Table 2.4. NIR excitation of **2.15a** in various solvents.

Solvent	Dielectric (ε)[a]	λ_{max} (nm)
carbon tetrachloride	2.2379	876
benzene	2.2825	881
chloroform	4.8069	860
acetonitrile	36.64	800

[a] Dielectric constants are those reported in the 91st CRC Handbook of Chemistry and Physics.[234]

The low energy transition was found to vary with substitution, and exhibit significant negative solvatochromism (Table 2.4), consistent with a charge-transfer band with a less polarized excited state. Given the strong acceptor strength found for the benzonitronyl moiety (0.0 V vs SCE), the charge-transfer band can be rationalized as a benzonitronyl nitroxide(A)−thiophene(D) interaction. Using generalized Mulliken–Hush theory[235,236] the strength of the electronic donor–acceptor coupling parameter (V) can be calculated using band shape analysis of the optical charge transfer transition using the following equation in which ν_{max} is the transition energy (cm^{-1}), $\Delta\nu_{1/2}$ is the bandwidth at half-height (cm^{-1}), ε is the molar extinction coefficient (M^{-1} cm^{-1}), and r_{DA} is the distance between donor and acceptor redox centers in Å.

$$V = (0.0205)\frac{\left[\varepsilon_{max}\Delta\nu_{1/2}\nu_{max}\right]^{1/2}}{r_{DA}}$$

When applying Hush theory, determination of the diabatic electron transfer distance (r_{DA}) in organic compounds suffers from the typically delocalized nature of the acceptor and donor, distinct from traditional inorganic systems where the redox centers are localized and the metal-metal distance can be explicitly determined. Here r_{DA} has been estimated to be the length of the benzonitronyl nitroxide-thiophene carbon-carbon bond

(1.43 Å, X-ray crystal structure) as the radical electron density on the benzonitronyl nitroxide moiety is highly delocalized over the ONCNO atoms and thiophene is aromatic. As r_{DA} is in the denominator of the Hush relationship describing the strength of the electronic donor–acceptor coupling parameter (V), a smaller value of r_{DA} will yield a larger V. Here, as r_{DA} is taken to be the length of the C-C bond between D and A, the values reported represent an upper limit of V. Computationally there is negligible electron density $C2$ and, as an alternative, the average distance between sites of high donor and acceptor electron density from the calculated molecular orbitals could be used to estimate r_{DA} providing a decreased but more accurate value of V.

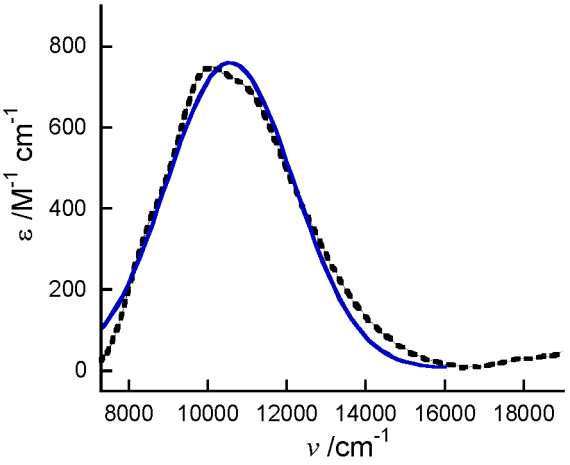

Figure 2.16. NIR band of radical **2.15d** (dashed line) and fit (solid blue line) with a Gaussian function.

Table 2.5. Electronic coupling energies of radicals **2.15a**, **2.15c-e**.

	r_{DA} (Å)	ε_{max} (M^{-1} cm^{-1})	$\Delta\nu_{1/2}$ (cm^{-1})	ν_{max} (cm^{-1})	R^2	V (cm^{-1})
2.15d	1.43	755	3231	10556	0.976	2000
2.15e	1.43	771	2571	11276	0.985	2100

The electronic coupling energy V for **2.15d** and **2.15e** was found to be the same within experimental error (Table 2.5). The similarity in coupling energy is not unexpected as the

magnitude of V depends strongly on bridge length and differences in redox potential between the donor and acceptor. Since neither of these variables differs dramatically between **2.15d** and **2.15e**, the donor–acceptor electronic coupling is comparable. For each of radical **2.15d** and **2.15e** the NIR CT excitation is weak (≤ 5000 M^{-1} cm^{-1}), Gaussian in shape and exhibits large bandwidths ($\Delta\nu_{1/2} \geq 2000$ cm^{-1}). This, coupled with the magnitude of electronic coupling V (2000 cm^{-1}, Table 2.5), confirms these systems are weakly-coupled Robin–Day Class II donor–acceptors.

2.5 Electronic structure calculations

Quantum mechanical electronic structure calculations were carried out at the UB3LYP/6-31G(d,p) level of theory[237,238] using the Gaussian 09 package[239] for the series of radicals **2.15a-e**. Analysis of the SOMO suggests that this orbital is primarily delocalized over the benzimidazole moiety, leading to spin delocalization onto the benzimidazole ring (Figure 2.17). Little perturbation of the energy of the SOMO is expected with substitution at *C*2, as it is a nodal position in the SOMO. In accord, spin densities in the *C*2 aryl group are dictated by spin polarization through the nodal *C*2 position, consistent with the larger class of nitronyl nitroxides.[193,240]

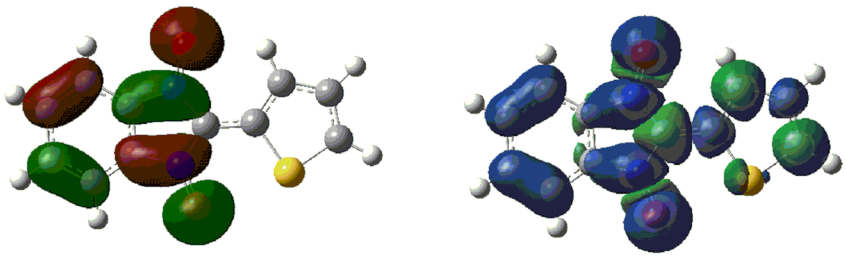

Figure 2.17. SOMO (left) and spin density (right) of radical 2.15d generated with GaussView 4.1.2, grid = coarse, isovalue = 0.02.

In order to better understand the nature of the low energy transition, vertical excitation energies and oscillator strengths for radical **2.15d** were computed by TDDFT[241] using the UB3LYP[237,238] functional with 6-31G(d,p) basis set and the Onsager solvation model.[242-244] TDDFT is known to predict vertical excitation energies of open-shell polycyclic aromatic hydrocarbons (PAHs) to within 0.3 eV of the experimental data and oscillator strengths that are consistent with the measured absorption spectra.[245] Solvation ($CHCl_3$) was included to better approximate the molecular structure and excitation energy in a somewhat polar environment.

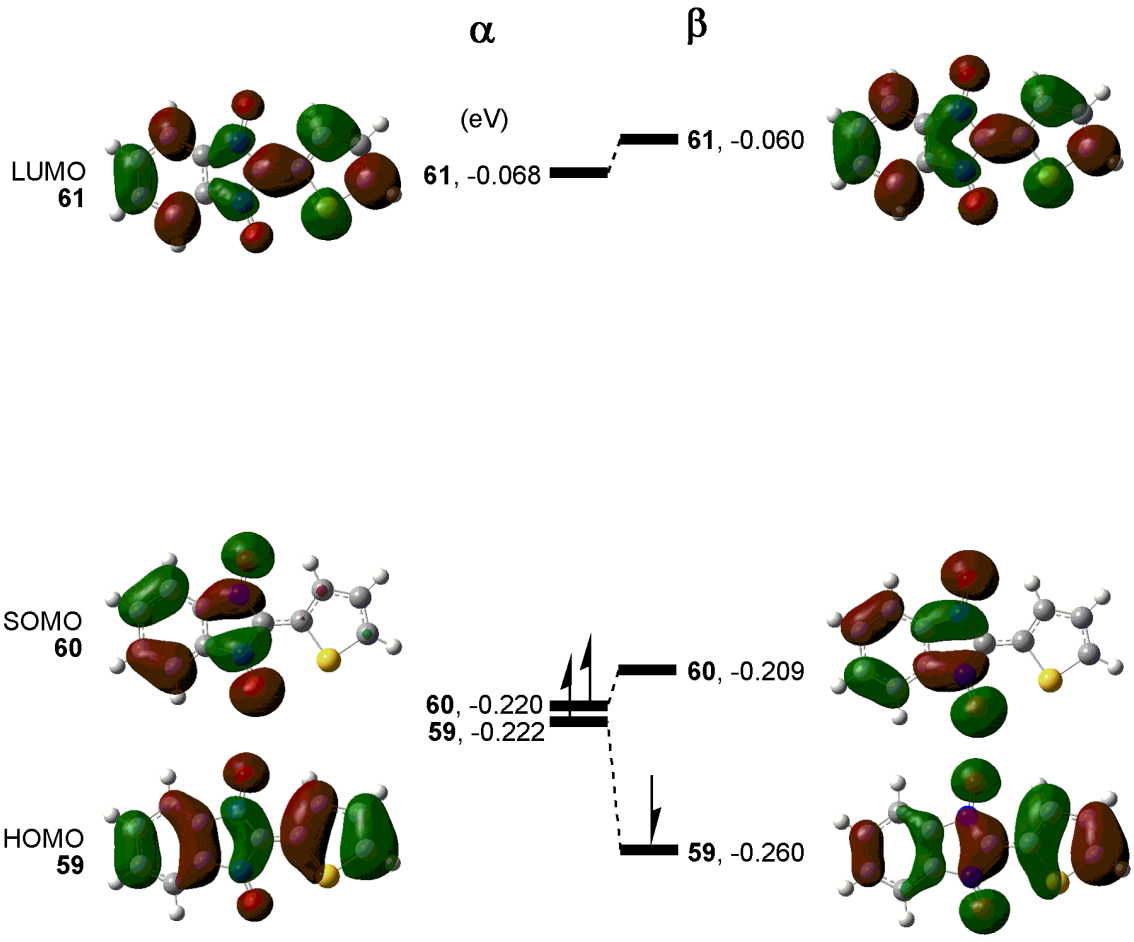

Figure 2.18. Computational (TDDFT UB3LYP/6-31G(d,p) scrf=chloroform) molecular orbital diagram of **2.15d** generated with GaussView4.1 (grid = coarse, isovalue 0.02).

TDDFT predicted a NIR transition at 881 nm with a force constant of 0.0138 which corresponds well with the experimentally observed weak intensity NIR excitation (990 nm in CH_3CN, 1010 nm in $CHCl_3$). The calculated excitation is dominated by a symmetry forbidden β–HOMO → β–SOMO transition (94 %). A small contribution to the NIR transition is computationally ascribed to a α–SOMO → α–LUMO transition. The relative contribution of this transition to the overall excitation increases when solvation is not included. The transition from the HOMO into the half-filled SOMO orbital is consistent with the triphenylmethyl[246] and benzothiazinyl[247] radicals, both of which have weak low energy transitions attributed to a HOMO–SOMO transition.

2.6 Structural analysis of thienyl derivatives by XRD

Maroon crystal plates of **2.15d** and dark red needles of **2.15e** were grown by slow evaporation of saturated n-pentane solutions, and their structures were determined by X-ray diffraction. The 2-thienyl derivative **2.15d** crystals were twinned and severely disordered. Refinement of the structure led to packing in the monoclinic $P2_1/c$ space group with two molecules per unit cell ($Z = 2$). The crystal structure is disordered with respect to rotation about a $C2$ axis perpendicular to the plane of the molecule, leading to superposition of two orientations each with 50 % occupancy, as shown in Figure 2.19. The molecule adopts an essentially planar geometry with a torsion angle of 1.7º between the benzimidazole and thiophene moieties. The 3-thienyl derivative **2.15e** exhibits monoclinic packing in the space group $P2_1/c$ with disorder with respect to rotation about a $C2$ axis parallel to the long axis of the molecule, with 50 % occupancy in each orientation, as shown in Figure 2.19. The degree of planarity is slightly less than that of

2.15d, with a torsion angle of 4.6º between benzimidazole and the *C*2 3-thienyl substituent. In contrast, when R = phenyl as in **2.15a**, a larger torsion angle of 10º is observed[222] and when the phenyl substituents are ortho substituted (Cl, F) much larger torsion angles (54 – 76º) are present.[223]

Table 2.6. Crystallographic data for **2.15d** and **2.15e**.

	2.15d	**2.15e**
formula	$C_{11}H_7N_2O_2S_1$	$C_{11}H_7N_2O_2S_1$
formula weight	231.25	231.25
color of crystal	maroon plates	dark red needles
crystal system	$P2_1/c$	$P2_1/c$
space group	monoclinic	monoclinic
a (Å)	7.3290(9)	4.8000(10)
b (Å)	4.6390(4)	17.022(4)
c (Å)	14.756(2)	12.5200(15)
volume (Å^3)	486.01(11)	953.3(3)
temperature (K)	130(2)	130(2)
Z	2	4
R_f [a]	0.1680	0.2504
R_w [b]	0.1678	0.1796
GOF	0.997	0.758

[a] $R_f = [\Sigma||F_o| - |F_c||]/[\Sigma|F_o|]$, $I > 2\sigma(I)$. [b] $R_w = ([\Sigma w||F_o|^2 - |F_c|^2|^2]/[\Sigma(w|F_o|^2)^2])^{1/2}$.

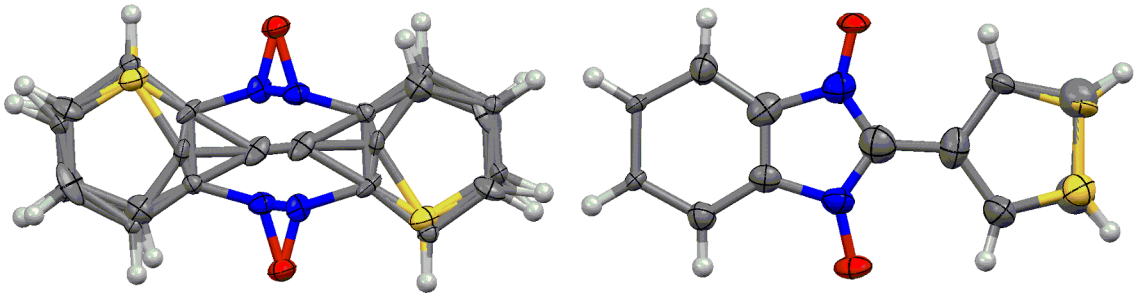

Figure 2.19. ORTEP representations of radical **2.15d** (left) and **2.15e** (right) with 50 % probability thermal ellipsoids. The packing disorder in **2.15d** arises from rotation about an axis perpendicular to the long axis of the molecule, while the disorder in **2.15e** arises from rotation about a *C*2 axis parallel to the long axis of the molecule.

The planarity of radicals **2.15d** and **2.15e** leads to edge-to-face and π-stacking interactions that cause packing in a herringbone motif (Figures 2.20 and 2.21). Radical **2.15a** packs in a sandwich herringbone motif which straddles the structural gap between γ and herringbone modes. The sandwich herringbone packing motif for aromatics is one in which both C…C and C…H interactions are important, leading to effective glide and stack stabilization. In both **2.15d** and **2.15e**, the surface area available for stacking C…C interactions and the edge surface area available for C…H interactions is nearly equal, leading to packing in which both stacking and edge-to-face interactions are efficient. Analysis of the interplanar angle between molecules creating an edge-to-face interaction (85º, **2.15d**; 89º, **2.15e**) and shortest crystallographic axes for **2.15d** (*b*-axis) and **2.15e** (*a*-axis), is consistent with a γ phase herringbone motif. Both C…C stacking and C…H edge-to-face interactions are energetically favored in the γ phase herringbone motif, consistent with prediction of packing based solely on topology.

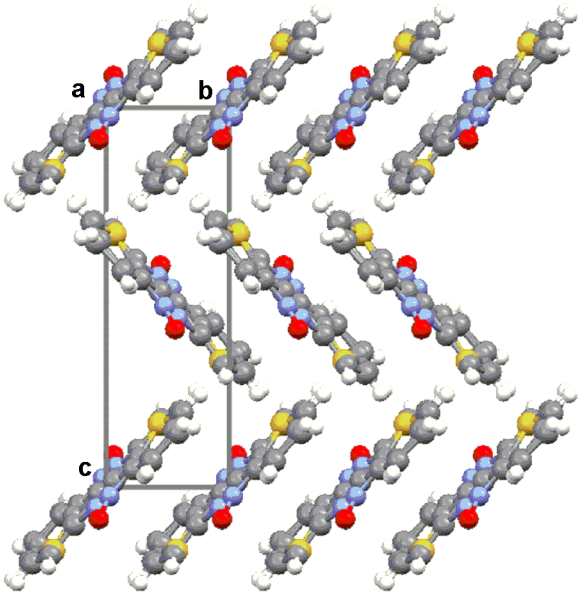

Figure 2.20. Packing diagram of radical **2.15d** viewed along the *a*-axis.

The nature of the edge-to-face interactions in **2.15e** arises from S…benzimidazole interactions, with a closest distance 3.50 Å for the benzimidazole plane-to-sulfur distance. The interplanar distance between stacked molecules is 3.42 Å for **2.15d** and 3.41 Å for **2.15e**, giving rise to short radical-radical contacts through π-stacking interactions. Unlike the *C*2-phenyl radical **2.15a**,[222] and electron deficient derivatives of **2.15a**,[223] no close radical-radical O…O contacts are present in **2.15d**, and **2.15e**, thus, the magnetic interactions in these systems arise from through-space π-stacking and C…H interactions rather than radical-radical contacts.

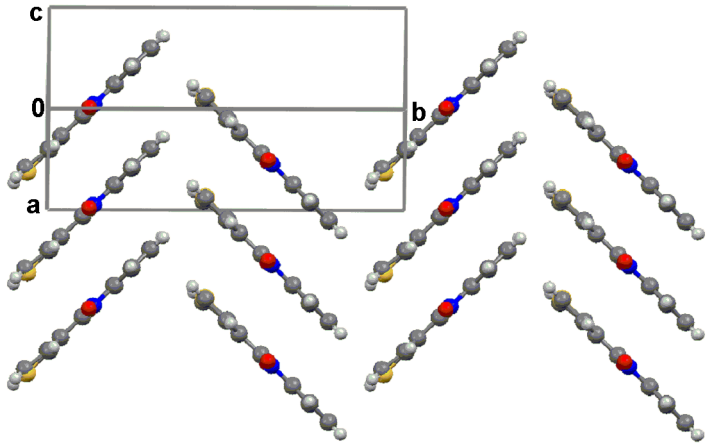

Figure 2.21. Packing diagram of **2.15e** viewed at a 45º angle bisecting the *a* and *b*-axis.

2.7 Magnetism of thienyl derivatives

The molar magnetic susceptibilities ($\chi_{M,p}$) were measured for polycrystalline samples of radicals **2.15d** and **2.15e** using a Quantum Design SQUID magnetometer in the temperature range of 2 – 300 K at DC fields of 0.1 – 5 Tesla (Figures 2.22 and 2.23). Diamagnetic corrections of the susceptibilities were made using Pascal's constitutive corrections.[80] The 2-thienyl **2.15d** and 3-thienyl **2.15e** derivatives exhibit magnetic moments close to the expected spin only value for a spin = ½ system (0.375 emu K

mol^{-1}), with temperature independent magnetic moments above 100 K. In both systems, the magnetic moment ($\chi_{M,p}T$) decreased with decreasing temperature, consistent with antiferromagnetic exchange interactions.

Analysis of the crystal structure suggests that the dominant pathway for magnetic exchange interactions is through the slipped π stack, with weak interchain interactions contributing to a minor extent. A fit of the magnetic moment as a function of temperature was obtained using the numerical solution for a Bonner–Fisher chain model[248] ($H = -JS_{rad}S_{rad+1}$) according to the following equation. In this numerical expression (and all other magnetic models from this point forward), *f* is used to denote purity. This factor does not necessarily represent the purity of the compound but rather the purity with respect to the number of spins that obey the applied magnetic exchange model.

$$\chi T = f\frac{Ng^2\beta^2}{k_B}\cdot\frac{0.25+0.074975x+0.075235x^2}{1.0+0.9931x+0.172135x^2+0.757825x^3}$$

$$x = \frac{|J|}{k_B T}; \quad J \leq 0$$

The g-value was fixed to the experimentally derived value of 2.007, to give $J = -7.5$ cm^{-1}, and a purity factor (*f*) of 0.98 for radical **2.15d**. Weaker exchange was found in radical **2.15e**, in which the exchange coupling *J* was found to be -1.9 cm^{-1} (f = 1.0). The inclusion of a mean field approximation ($2zJ'$) to account for the weak interchain interactions was not necessary, consistent with through chain interactions dominating the magnetic exchange pathway. Difficulties fitting the temperature dependent magnetic susceptibilities to reasonable magnetic models for both the parent radical **2.15a**[222] and a class of electron deficient benzannelated nitronyl nitroxides radicals[223] have been reported. Such effects have been attributed to diamagnetic

impurities[223] or the formation of high-spin spin clusters at low temperatures.[224] Neither phenomena was observed here and both radicals fit the mathematical expression for a uniform chain model quite well.

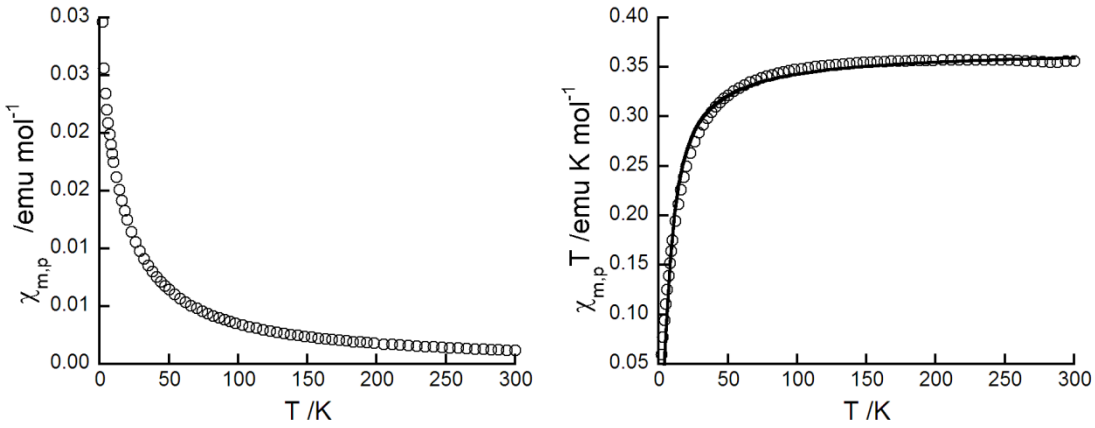

Figure 2.22. Temperature dependence of the molar magnetic susceptibility (left) and magnetic moment (right) for radical **2.15d** (2 – 300K) at 0.1 T fit to a Bonner–Fisher model. The solid line represents the best fit of the data to the model described in the text.

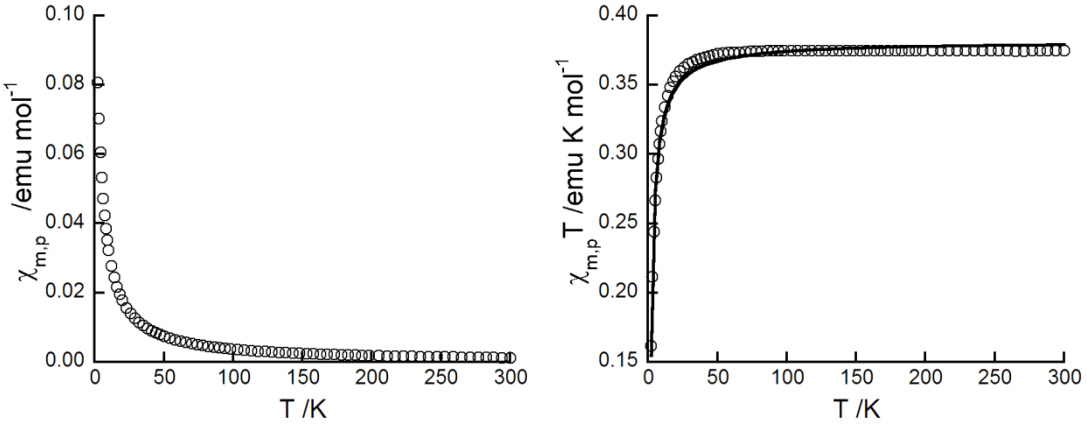

Figure 2.23. Temperature dependence of the molar magnetic susceptibility (top) and magnetic moment (bottom) for radical **2.15e** (2 – 300K) at 0.1 T fit to a Bonner–Fisher model. The solid line represents the best fit of the data to the model described in the text.

The surprisingly weak exchange relative to other benzannelated nitronyl nitroxides is attributed to the disorder observed in the solid state. This class of radicals is unique in that they are fully delocalized planar radicals that are stable toward dimerization in the solid state, unlike the phenalenyl or thiazyl classes of radicals. Directional non-covalent interactions are expected to be extremely weak or entirely absent, leading to little preference for molecular orientation in the crystalline state. The resulting disorder can cause complication of the dominant through-space pathways for magnetic exchange. Structural analysis of our systems indicates significant structural disorder in the solid state, leading to little preference for head-to-head (HH) vs. head-to-tail (HT) π stacking, or inversion about the molecular (long) axis. The distinction between HT and HH interactions discriminates between radical-radical contacts vs radical-aromatic contacts, providing two distinct pathways for magnetic exchange. As the spin density is highly delocalized, this will give rise to different exchange pathways as a function of topology (HH vs HT). Both types of packing were observed in **2.15d**, giving rise to competing magnetic exchange interactions and a weak overall exchange parameter.

2.8 Summary and conclusions

A robust and versatile synthetic methodology for annelated nitronyl nitroxides has been developed from which a series of heteroaromatic BNN radicals were successfully generated. The effect of annelation on the nitronyl nitroxide moiety has been examined spectroscopically and found to be consistent with a lowering of the SOMO energy. The resulting class of radicals possess extremely good electron acceptor ability, long-wavelength absorption spectra, and a spin delocalized electronic structure.

The magnetic behavior and structural characterization of acceptor–donor spin delocalized radicals **2.15d** and **2.15e** were reported. Electronic absorption spectroscopy accompanied by computation reveals that the near IR band can be assigned to a HOMO–SOMO charge transfer transition with electronic coupling of ~2000 cm^{-1} between the benzimidazole and thiophene moiety. Structural analysis of the thienyl radicals in the crystalline state reveals disorder due to the high symmetry of the planar delocalized radicals. The magnetic properties are therefore dictated by the topology of the radical and not by perturbations in the spin density induced by substitution at *C*2, which are minimal. The low reduction potentials and strength of the through-space magnetic exchange interactions demonstrated in the solid state make these particularly interesting systems for the development of multifunctional magnetic materials.

2.9 Experimental

2.9.1 General procedures

General Methods. Starting materials were purchased from commercial sources and used without further purification unless otherwise noted. ACS grade solvents were used as received. Dry solvents were obtained from an MBraun solvent purification system with the exception of THF which was distilled from Na/benzophenone prior to use and acetonitrile which was distilled from CaH_2 prior to use. Chromatography (including flash chromatography) was performed with 60 Å flash grade silica gel or neutral alumina. All reactions were monitored by TLC performed on plastic-backed silica gel plates and compounds were visualized under UV light or with an iodine chamber. Nuclear magnetic resonance spectra were taken on a Bruker AC300 operating at 300 MHz for ^1H or 75

MHz for ^{13}C and were recorded in $CDCl_3$ unless otherwise noted. Infrared spectra were recorded as dilute samples in KBr on a Perkin Elmer 1720 FTIR spectrophotometer unless otherwise noted. Mass spectra for routine characterization were obtained on either a Bruker Esquire~LC Ion Trap Electrospray Mass Spectrometer or a Kratos Profile HV-3 Direct Probe Mass Spectrometer. Elemental CHN analysis was performed by Canadian Microanalytical Services, Desert Analytics or University of British Columbia. Melting points were recorded (uncorrected) using a Gallenkamp melting point apparatus.

Electronic Absorption Spectra. Absorption spectra were recorded on an Agilent 8453 UV–vis spectrometer with photodiode array and peltier temperature controller or a Perkin Elmer Lambda 1050 UV–vis–NIR spectrometer equipped with a 3D WB detector module. Solutions of 10^{-5} M were measured at ambient temperatures in the reported solvents.

Cyclic Voltammetry. Voltammograms of degassed 1 mM radical solutions in 0.1 M n-Bu_4NPF_6/CH_3CN at ~300 K were obtained using a 3.0 mm diameter glassy carbon working electrode, platinum counter electrode, and Ag wire pseudo-reference electrode. Cyclic voltammograms were run from 0 to −1.5 V to +1.5 V at a scan rate of 50 mV s^{-1} unless otherwise stated. Ferrocene was used as an internal standard and all spectra are reported vs SCE (Fc/Fc^+ = 0.40 V vs SCE in acetonitrile/NBu_4PF_6).[230] Peak potentials (E_p) and peak currents (i_p) were extracted using BASi software.

Electron Paramagnetic Resonance. X-band EPR spectra were taken on a 9 GHz continuous wave Bruker EMX EPR spectrometer, typically using a modulation amplitude 0.1 G, microwave power 0.5 – 1 mW, and spectral width of 40.0 G. Radical solutions of 10^{-5} M in toluene were degassed via three freeze-pump-thaw cycles (N_2) prior to

measurement. DPPH was used as an external standard and reported g-values are relative to DPPH for all radical derivatives. Simulation of the EPR spectra was accomplished with the Winsim2002 software package which was used for numerical fitting of EPR spectra in solution using the nitroxide simulation. The resulting hfcc were perturbed and optimized with the downhill simplex algorithm until the global minimum for the fit was achieved. R-values for all fits obtained were > 0.99. Spectra used for simulation were used as measured.

Computations. Quantum mechanical calculations were carried out at the UB3LYP/6-31G(d,p) level of theory[237,238] (unless stated otherwise) using the Gaussian 09 package.[239] Geometry optimizations were performed without symmetry constraints (starting from C1). Vibrational frequencies were used to characterize the nature of stationary points. Electronic excitation energies for the both radicals were obtained at the UB3LYP/6-31 G(d,p) level using time dependent DFT calculations supplied in the Gaussian 03 package.[249]

X-ray Crystallography. X-ray diffraction data was collected on a Nonius KappaCCD diffractometer with graphite-monochromatized Mo-Kα radiation (λ = 0.71073 Å). The data was integrated and scaled using *hkl*-SCALEPACK.[250] The crystal structures were solved by direct methods (SIR92/7).[251] All hydrogen atoms were located using a riding model. All of the non-hydrogen atoms were refined anisotropically by full-matrix least-squares. Full structure reports are given in the appendix of this dissertation.

Magnetic Measurements. Magnetic measurements were performed on a Quantum Design MPMS 5.0 system, with fields in the range of 1–5 T, and temperature ranges between 2 and 300 K on polycrystalline samples. Diamagnetic corrections were made

using either Pascal's constants or the slope of the raw variable temperature magnetic moment in the paramagnetic (high temperature) regime.

2.9.2 Synthesis

Previously reported compounds. Phenylhydroxylamine **2.20**[228,252] was prepared according to literature methods. Nitrones **2.21f**,**g**,**i**[253] and **2.21l**[254,255] were prepared using the general methodology described below. Their identity and purity were confirmed using appropriate spectroscopic methods (^{1}H NMR, ^{13}C NMR, IR, MS) and were consistent with characterization as published.

General Procedure for nitrone generation: *C*-phenyl-*N*-phenylnitrone (2.21a).[253] A solution of phenylhydroxylamine (1.704 g, 15.6 mmol) and benzaldehyde (1.751 g, 16.5 mmol) in 23 mL 100% ethanol was heated briefly to reflux. The solution was then sonicated, capped with a rubber septum and allowed to stand in the absence of light for 24 h at room temperature. The solvent was removed under reduced pressure (*en vacuo*) and the resulting light yellow solid purified by either flash column chromatography on silica (60:40 hexane/ethyl acetate) or recrystallized from hot hexanes to yield 2.207 g (11.2 mmol, 72%) of a fluffy white solid. mp 112 – 114 ºC (lit[253] 114 ºC). IR (KBr) cm^{-1}: 3059, 1547, 1484, 1461, 1445, 1396. ^{1}H NMR (300 MHz, $CDCl_3$): δ 8.43 – 8.39 (m, 2H), 7.96 (s, 1H), 7.80 – 7.76 (m, 2H), 7.51 – 7.48 (m, 6H). ^{13}C NMR (75 MHz, $CDCl_3$): δ 149.0, 134.7, 130.9, 130.7, 129.9, 129.1, 129.0, 128.6, 121.7. EI-MS (70 eV) *m/z*: 197 $[M]^+$, 181 $[M - O]^+$.

***C*-2-Pyridyl-*N*-phenylnitrone (2.21b)**. Purified by flash column chromatography on silica with 90:10 $CHCl_3$/MeOH as eluent and dried under vacuum to yield a yellow solid (82%). mp 64 – 66 ºC. IR (KBr) cm^{-1}: 2993, 1713, 1577, 1548, 1483, 1460, 1451, 1435,

1385. ^{1}H NMR (300 MHz, $CDCl_3$): δ 9.26 (d, J = 8 Hz, 1H), 8.59 (d, J = 5 Hz, 1H), 8.21 (s, 1H), 7.78 – 7.72 (m, 3H), 7.42 – 7.38 (m, 3H), 7.25 – 7.21 (m, 1H). ^{13}C NMR (75 MHz, $CDCl_3$): δ 149.8, 149.7, 148.7, 136.8, 135.4, 130.3, 129.2, 124.5, 123.9, 121.6. EI-MS (70 eV) *m/z*: 198 $[M]^+$, 182 $[M - O]^+$. HRMS-EI (70 eV) *m/z*: $[M]^+$ calcd for $C_{12}H_{10}N_2O$, 198.07931; found, 198.07899. Anal. Calcd for $C_{12}H_{10}N_2O$: C, 72.71; H, 5.08; N, 14.13. Found: C, 72.79; H, 5.46; N, 13.98.

***C*-4-Pyridyl-*N*-phenylnitrone (2.21c)**. The suspension was heated briefly and filtered to remove salts that had formed. The filtrate was placed in the freezer for 24 h and the crystals were isolated using suction filtration, washed with hexanes (30 mL), and dried under vacuum yielding a fluffy white crystalline product (45%). mp 130 – 132 ºC. IR (KBr) cm^{-1}: 3059, 1591, 1556, 1458, 1406, 1209. ^{1}H NMR (300 MHz, $CDCl_3$): δ 8.66 (d, J = 6 Hz, 2H), 8.12 (d, J = 6 Hz, 2H), 7.94 (s, 1H), 7.73 – 7.70 (m, 2H), 7.46 – 7.44 (m, 3H). ^{13}C NMR (75 MHz, $CDCl_3$): δ 150.7, 148.9, 137.0, 132.4, 130.8, 129.4, 121.8, 121.6. EI-MS (70 eV) *m/z*: 198 $[M]^+$, 182 $[M - O]^+$. Anal. Calcd for $C_{12}H_{10}N_2O$: C, 72.71; H, 5.08; N, 14.13. Found: C, 72.35; H, 5.33; N, 14.15.

***C*-2-Thienyl-*N*-phenylnitrone (2.21d)**. The crude oil was recrystallized from hot ethyl acetate to give a light green crystalline product (73%). mp 95 – 97 ºC. IR (KBr) cm^{-1}: 3063, 1590, 1559, 1483, 1458, 1415, 1376. ^{1}H NMR (300 MHz, $CDCl_3$): δ 8.49 (s, 1H), 7.83 (dd, J = 8, 2 Hz, 2H), 7.61 (d, J = 4 Hz, 1H), 7.56 (d, J = 5 Hz, 1H), 7.51 – 7.43 (m, 3H), 7.21 (t, J = 5 Hz 1H). ^{13}C NMR (75 MHz, $CDCl_3$): δ 146.6, 133.2, 131.1, 130.2, 130.0, 129.3, 128.9, 127.1, 121.2. EI-MS (70 eV) *m/z*: 203 $[M]^+$, 186 $[M - OH]^+$. Anal. Calcd for $C_{11}H_9NOS$: C, 65.00; H, 4.46; N, 6.89. Found: C, 65.03; H, 4.07; N, 6.53.

***C*-3-Thienyl-*N*-phenylnitrone (2.21e)**. Bright yellow solid, purified by flash column chromatography (silica, 1:1 hexane/ethyl acetate) and dried under vacuum yielding a light yellow solid (79%). mp 71 – 73 ºC. IR (KBr) cm^{-1}: 3053, 1552, 1482, 1458, 1391. ^{1}H NMR (300 MHz, $CDCl_3$): δ 9.14 (d, J = 3 Hz, 1H), 8.05 (s, 1H), 7.78 – 7.74 (m, 2H), 7.49 – 7.43 (m, 4H), 7.35 (dd, J = 5, 3 Hz, 1H). ^{13}C NMR (75 MHz, $CDCl_3$): δ 136.8, 131.7, 129.9, 129.8, 129.2, 129.1, 128.2, 125.5, 121.6. EI-MS (70 eV) *m/z*: 203 $[M]^+$, 186 $[M - OH]^+$. Anal. Calcd for $C_{11}H_9NOS$: C, 65.00; H, 4.46; N, 6.89. Found: C, 64.84; H, 4.24; N, 6.85.

***C*-4-t-Butylphenyl-*N*-phenylnitrone (2.21h)**. The crude solution was concentrated under reduced pressure to give a yellow oil, which was purified by flash chromatography (silica, 1:1 ethyl acetate/hexane) yielding a pale yellow solid (71%). mp 88 – 90 ºC. IR (KBr) cm^{-1}: 2962, 2867, 1545, 1399, 1188, 1078, 1068. ^{1}H NMR (300 MHz, $CDCl_3$): δ 8.34 (d, J = 8 Hz, 2H), 7.90 (s, 1H), 7.78 – 7.74 (m, 2H), 7.50 – 7.41 (m, 5H), 1.34 (s, 9H). ^{13}C NMR (75 MHz, $CDCl_3$): δ 154.5, 149.1, 134.4, 129.8, 129.1, 129.0, 128.1, 125.6, 121.7, 35.1, 31.1. EI-MS (70 eV) *m/z*: 253 $[M]^+$, 237 $[M - O]^+$. Anal. Calcd for $C_{17}H_{19}NO$: C, 80.60; H, 7.56; N, 5.53. Found: C, 80.48; H, 7.45; N, 5.56.

***C*-2,3,4-Trimethoxylphenyl-*N*-phenylnitrone (2.21j)**. The crude solution was concentrated under reduced pressure to give a brown oil, which was subjected to flash chromatography (silica, 2:1 ethyl acetate/hexanes) yielding a yellow solid (84%). mp 78 – 80 ºC. IR (KBr) cm^{-1}: 2938, 2836, 1587, 1301, 1092. ^{1}H-NMR (300 MHz, $CDCl_3$): δ 9.24 (d, J = 9 Hz 1H), 8.17 (s, 1H), 7.71 (dd, J = 8, 2 Hz, 2H), 7.43 – 7.35 (m, 3H), 6.72 (d, J = 9 Hz, 1H), 3.88 (s, 3H), 3.86 (s, 3H), 3.80 (s, 3H). ^{13}C NMR (75 MHz, $CDCl_3$): δ 156.0, 152.5, 149.2, 141.3, 129.4, 128.9, 128.9, 124.4, 121.5, 117.8, 106.8,

61.7, 60.8, 56.1. EI-MS (70 eV) *m/z*: 287 $[M]^+$, 271 $[M - O]^+$, 256 $[M - OCH_3]^+$, 240 $[M - O_2CH_3]^+$. Anal. Calcd for $C_{16}H_{17}NO_4$: C, 66.89; H, 5.96; N, 4.88. Found: C, 66.81; H, 6.19; N, 4.82.

***C*-4-Carboxyphenyl-*N*-phenylnitrone (2.21k)**. A yellow microcrystalline solid formed on standing. The solid was isolated by suction filtration and washed with cold ethanol yielding a light yellow microcrystalline solid (68%). mp 200 – 202 ºC. IR (KBr) cm^{-1}: 2998, 1699, 1681, 1384, 1288, 1071, 862. ^{1}H-NMR (300 MHz, d_6-DMSO): δ 8.62 (s, 1H), 8.57 (d, J = 8 Hz, 2H), 8.05 (d, J = 8 Hz, 2H), 7.94 – 7.91 (m, 2H), 7.58 – 7.54 (m, 3H). ^{13}C NMR (75 MHz, d_6-DMSO): δ 166.8, 148.5, 134.7, 133.0, 131.9, 130.2, 129.4, 129.2, 128.6, 121.6. EI-MS (70 eV) *m/z*: 241 $[M]^+$, 225 $[M - O]^+$, 194 $[M - COOH]^+$. Anal. Calcd for $C_{14}H_{11}NO_3$: C, 69.70; H, 4.60; N, 5.81. Found: C, 69.61; H, 4.88; N, 5.51.

General procedure for the generation of 1-hydroxy-2-arylbenzimidazole-3-oxides: 1-Hydroxy-2-phenylbenzimidazole-3-oxide (2.16a). A solution of *C*-phenyl-*N*-phenylnitrone **2.21a** (1.012 g, 5.1 mmol) and benzofuroxan (1.231 g, 9.1 mmol) in 100 mL cyclohexane was refluxed gently for ~24 hours. The resulting precipitate was isolated by suction filtration, washed with cyclohexane and acetone, and dried en vacuo to yield a light brown powder. The powder was dissolved in 1 M NaOH, filtered through a Celite plug and then neutralized with 1 M HCl yielding an off-white precipitate. The precipitate was isolated by filtration, washed with methanol, acetone, and pentane and dried en vacuo yielding (0.641 g, 2.8 mmol, 55%) of an off-white powder. mp decomp. 210 – 211 ºC (lit[225] 216 ºC). IR (KBr) cm^{-1}: 3437, 1473, 1254, 1135, 1066. ^{1}H NMR (300 MHz, 0.2 M NaOD in D_2O): δ 7.85 (dd, J = 7, 4 Hz, 2H), 7.70 – 7.60 (m, 5H), 7.36 (dd, J

= 7, 4 Hz, 2H). ESI-MS (negative ion mode) *m/z*: 225 $[M - H]^-$. EI-MS (positive ion mode) *m/z*: 210 $[M - O]^+$, 194 $[M - 2O]^+$, 149 $[M - \text{phenyl}]^+$.

1-Hydroxy-2-(2-pyridinyl)benzimidazole-3-oxide (2.16b). Tan powder (59%). mp decomp. 209 – 212 ºC. IR (KBr) cm^{-1}: 3075, 1251, 745. ^1H NMR (300 MHz, 1.0 M NaOD in D_2O): δ 8.63 (d, J = 5 Hz, 1H), 7.88 (td, J = 8, 1 Hz, 1H), 7.73 (d, J = 8 Hz, 1H), 7.49 – 7.40 (m, 3H), 7.14 – 7.11 (m, 2H). ^{13}C NMR (75 MHz, 1.0 M NaOD in D_2O): δ 150.4, 142.8, 138.4, 135.6, 127.7, 127.3, 126.2, 124.2, 111.8. EI-MS (70 eV) *m/z*: 227 $[M]^+$, 211 $[M - O]^+$, 195 $[M - 2O]^+$, 149 $[M - (2\text{-pyridyl})]^+$. Anal. Calcd for $C_{12}H_9N_3O_2$: C, 63.43; H, 3.99; N, 18.49. Found: C, 62.96; H, 4.17; N, 18.22.

1-Hydroxy-2-(4-pyridinyl)benzimidazole-3-oxide (2.16c). Tan powder (70%). mp decomp. 228 – 230 ºC. IR (KBr) cm^{-1}: 3437, 1607, 1405, 1140, 1071. ^1H NMR (300 MHz, 1.0 M NaOD in D_2O): δ 8.54 (dd, J = 5, 1 Hz, 2H), 7.91 (dd, J = 5, 1 Hz, 2H), 7.43 (dd, J = 6, 3 Hz, 2H), 7.29 (dd, J = 6, 3 Hz, 2H). ^{13}C NMR (75 MHz, 1.0 M NaOD in D_2O): δ 149.5, 133.9, 132.3, 127.6, 124.4, 124.2, 111.7. EI-MS (70 eV) *m/z*: 210 $[M - OH]^+$, 194 $[M - O_2H]^+$, 149 $[M - (4\text{-pyridyl})]^+$. ESI-MS (negative ion mode) *m/z*: 226 $[M - H]^-$, 210 $[M - OH]^-$. Anal. Calcd for $C_{12}H_9N_3O_2$: C, 63.43; H, 3.99; N, 18.49. Found: C, 63.12; H, 4.01; N, 17.98.

1-Hydroxy-2-(2-thienyl)benzimidazole-3-oxide (2.16d). Tan powder (50%). mp decomp. 199 – 201 ºC (lit[226] 183 – 185 ºC). IR (KBr) cm^{-1}: 3436, 3102, 1559, 1464, 1407, 1351, 1261, 1138, 1073. ^1H NMR (300 MHz, 1.0 M NaOD in D_2O): δ 8.43 (d, J = 4 Hz, 1H), 7.55 (d, J = 5 Hz, 1H), 7.44 – 7.40 (m, 2H), 7.13 – 7.06 (m, 3H). ^{13}C NMR (75 MHz, 1.0 M NaOD in D_2O): δ 134.0, 130.6, 130.4, 127.6, 127.6, 123.6, 123.4, 111.0.

ESI-MS (negative ion mode) *m/z*: 230 $[M - H]^-$, 214 $[M - OH]^-$, 198 $[M - O_2H]^-$. Anal. Calcd for $C_{12}H_9N_3O_2$: C, 56.88; H, 3.47; N, 12.06. Found: C, 56.49; H, 3.37; N, 11.75.

1-Hydroxy-2-(3-thienyl)benzimidazole-3-oxide (2.16e). Tan powder (60%). mp decomp. 233 – 235 ºC. IR (KBr) cm^{-1}: 3436, 3124, 1566, 1461, 1350, 1255, 1197, 1135, 1069, 736. ^1H NMR (300 MHz, 1.0 M NaOD in D_2O): δ 8.35 (d, J = 3 Hz, 1H), 7.82 (d, J = 5 Hz, 1H), 7.42 – 7.36 (m, 3H), 7.07 – 7.03 (m, 2H). ^{13}C NMR (75 MHz, 1.0 M NaOD in D_2O): δ 134.4, 130.1, 127.5, 127.4, 126.5, 123.6, 123.1, 111.2. EI-MS (70 eV) *m/z*: 216 $[M - O]^+$, 200 $[M - 2O]^+$, 149 $[M – (3\text{-thienyl})]^+$. ESI-MS (negative ion mode) *m/z*: 230 $[M - H]^-$, 214 $[M - OH]^-$, 198 $[M - O_2H]^-$. Anal. Calcd for $C_{12}H_9N_3O_2$: C, 56.88; H, 3.47; N, 12.06. Found: C, 56.70; H, 3.77; N, 11.86.

1-Hydroxy-2-(3-hydroxyphenyl)benzimidazole-3-oxide (2.16f). Brown solid (51%). mp decomp. 234 – 236 ºC. IR (KBr) cm^{-1}: 3103, 1214, 741. ^1H NMR (300 MHz, 1.0 M NaOD in D_2O): δ 7.55 (dd, J = 6, 3 Hz, 2H), 7.28 – 7.23 (m, 3H), 6.93 – 6.87 (m, 2H), 6.75 (d, J = 8 Hz, 1H). ^{13}C NMR (75 MHz, 1.0 M NaOD in D_2O): δ 166.4, 139.3, 130.3, 127.5, 124.4, 123.7, 121.9, 120.5, 116.7, 111.4. EI-MS (70 eV) *m/z*: 242 $[M]^+$, 226 $[M - O]^+$, 210 $[M - O_2]^+$. Anal. Calcd for $C_{13}H_{10}N_2O_3$: C, 64.46; H, 4.16; N, 11.56. Found: C, 64.19; H, 4.43; N 11.18.

1-Hydroxy-2-(2-hydroxyphenyl)benzimidazole-3-oxide (2.16g). White/orange solid (48%). Recrystallized from EtOH. mp decomp. 239 – 242 ºC (lit[226] 227 - 228 ºC). IR (KBr) cm^{-1}: 3065, 1606, 1217, 1024, 733. ^1H NMR (300 MHz, 0.1 M KOH in D_2O): δ 7.58 (dd, J = 6, 3 Hz, 2H), 7.26 – 7.22 (m, 3H), 7.05 (dd, J = 8, 2 Hz, 1H), 6.65 (d, J = 8 Hz, 1H), 6.57 (t, J = 8 Hz, 1H). ^{13}C NMR (75 MHz, 1.0 M NaOD in D_2O): δ 167.7,

140.8, 133.4, 132.4, 127.5, 123.4, 120.8, 113.9, 112.8, 111.4. ESI-MS (negative ion mode) *m/z*: 241 $[M - H]^-$, 225 $[M - OH]^-$, 209 $[M - O_2H]^-$.

1-Hydroxy-2-(4-*tert*-butylphenyl)benzimidazole-3-oxide (2.16h). White solid (54%). Recrystallized from MeOH. mp decomp. 213 – 214 ºC. IR (KBr) cm^{-1}: 2961, 1269, 748. ^1H NMR (300 MHz, 1.0 M NaOD in D_2O): δ 7.76 (d, J = 8 Hz, 2H), 7.53 (d, J = 8 Hz, 4H), 7.23 – 7.17 (m, 2H), 1.19 (s, 9H). ^{13}C NMR (75 MHz, 1.0 M NaOD in D_2O): δ 154.9, 137.8, 130.2, 127.5, 126.0, 123.8, 120.4, 111.5, 34.7, 30.8. ESI-MS (negative ion mode) *m/z*: 281 $[M - H]^-$, 265 $[M - OH]^-$. Anal. Calcd for $C_{17}H_{18}N_2O_2$: C, 72.32; H, 6.43; N, 9.92. Found: C, 71.83; H, 6.27; N, 9.61.

1-Hydroxy-2-(4-nitrophenyl)benzimidazole-3-oxide (2.16i). Brown solid (70%). mp decomp. 222 – 224 ºC. IR (KBr) cm^{-1}: 1527, 1384, 1350, 1139, 1068. ^1H NMR (300 MHz, 1.0 M NaOD in D_2O): δ 8.13 (d, J = 9 Hz, 2H), 8.05 (d, J = 9 Hz, 2H), 7.42 (dd, J = 6, 3 Hz, 2H), 7.10 (dd, J = 6, 3 Hz, 2H). ^{13}C NMR (75 MHz, 1.0 M NaOD in D_2O): δ 148.2, 134.8, 131.0, 129.7, 127.6, 124.4, 123.9, 111.7. EI-MS (70 eV) *m/z*: 271 $[M]^+$.

1-Hydroxy-2-(2,3,4-trimethoxyphenyl)benzimidazole-3-oxide (2.16j). White fluffy solid (57%). mp decomp. 244 – 246 ºC. IR (KBr) cm^{-1}: 2944, 1300, 1093, 749. ^1H NMR (300 MHz, 1.0 M NaOD in D_2O): δ 7.50 (dd, J = 6, 3 Hz, 2H), 7.18 (dd, J = 6, 3 Hz, 2H), 7.03 (d, J = 9 Hz, 1H), 6.82 (d, J = 9 Hz, 1H), 3.74 (s, 3H), 3.72 (s, 3H), 3.45 (s, 3H). ^{13}C NMR (75 MHz, 1.0 M NaOD in D_2O): δ 156.0, 153.3, 141.2, 136.2, 128.1, 127.3, 123.8, 111.6, 109.4, 108.8, 61.7, 61.6, 56.5. HRMS-ESI (negative ion mode) *m/z*: $[M - H]^-$ calcd for $C_{16}H_{16}N_2O_5$, 315.0982; found, 315.0982. Anal. Calcd for $C_{16}H_{16}N_2O_5$: C, 60.75; H, 5.10; N, 8.86. Found: C, 60.37; H, 5.22; N, 8.68.

1-Hydroxy-2-(4-carboxyphenyl)benzimidazole-3-oxide (2.16k). Brown solid (36%). mp decomp. 225 – 227 ºC. IR (KBr) cm^{-1}: 3500, 3035, 1696, 1284, 694. ^{1}H NMR (300 MHz, 1.0 M NaOD in D_2O): δ 7.95 (d, J = 8 Hz, 2H), 7.89 (d, J = 8 Hz, 2H), 7.53 (dd, J = 6, 3 Hz, 2H), 7.22 (dd, J = 6, 3 Hz, 2H). ^{13}C NMR (75 MHz, 1.0 M NaOD in D_2O): δ 175.3, 138.7, 137.1, 130.3, 129.2, 127.5, 125.6, 124.0, 111.5. HRMS-ESI (negative ion mode) *m/z*: $[M - H]^-$ calcd for $C_{14}H_{10}N_2O_4$, 269.0562; found, 269.0570. Anal. Calcd for $C_{14}H_{10}N_2O_4$: C, 62.22; H, 3.73; N, 10.37. Found: C, 62.02; H, 3.88; N 10.36.

1-Hydroxy-2-ethylbenzimidazole-3-oxide (2.16l). White microcrystalline solid (40%). mp decomp. 211 – 213 ºC. IR (KBr) cm^{-1}: 1384, 1280, 1141, 1045. ^{1}H NMR (300 MHz, 1.0 M NaOD in D_2O): δ 7.31 (dd, J = 7, 3 Hz, 2H), 7.00 (dd, J = 6, 3 Hz, 2H), 2.81 (q, J = 8 Hz, 2H), 1.08 (t, J = 8 Hz, 3H). ^{13}C NMR (75 MHz, 1.0 M NaOD in D_2O): δ 142.4, 127.0, 123.0, 110.8, 15.3, 10.1. EI-MS (70 eV) *m/z*: 178 $[M]^+$, 145 $[M - O_2H]^+$. Anal. Calcd for $C_9H_{10}N_2O_2$: C, 60.66; H, 5.66; N, 15.72. Found: C, 60.23; H, 5.65; N, 15.63.

General Oxidation Procedure for 2.15a, 2.15c-e. Prior to oxidation, 1-hydroxy-2-phenylbenzimidazole-3-oxide **2.16a** (0.300 g, 1.3 mmol) was dissolved in 20 mL 1.0 M $NaOH_{(aq)}$, filtered twice through a Celite-545 plug, acidified with 1.0 M HCl, and isolated with suction. The wet clay was washed with water (5 mL), acetonitrile (5 mL), toluene (5 mL), and pentane (10 mL) and dried under a stream of N_2. The tan solid was suspended in toluene (5 mL) and, while sonicating, tetrabutylammonium hydroxide (1.3 mL as a 1.0 M MeOH solution, 1.3 mmol) was added to the suspension creating a yellow-orange solution. Silver(I) triflate (0.351 g, 1.4 mmol) was added to the sonicating solution causing immediate oxidation. The yellow-green solution was sonicated an additional 5

min, filtered through a Celite-545 plug and concentrated by rotary evaporation. The crude radical was subjected to flash column chromatography (neutral alumina, $CHCl_3$) and the combined fractions were concentrated under reduced pressure and dried under vacuum yielding a light brown solid (0.112 g, 38%). UV–vis (CH_3CN) λ_{max}, nm (ε): 200 (18000), 241 (14000), 279 (20000), 298 (16000), 312 (19000), 388 (5500), 421 (3500), 475 (2500), 825 (800).

2-(4-Pyridyl)benzimidazole N-N′-dioxide (2.15c): (27%). UV–vis (CH_3CN) λ_{max}, nm (ε): 243 (11000), 281 (12000), 299 (11000), 312 (14000), 397 (3700), 427 (1800), 483 (900), 831 (640). Anal. Calcd for $C_{12}H_8N_3O_2$: C, 63.71; H, 3.56; N, 18.58. Found: C, 63.42; H, 4.04; N, 18.80.

2-(2-Thienyl)benzimidazole N-N′-dioxide (2.15d): (47%). UV–vis (CH_3CN) λ_{max}, nm (ε): 243 (12000), 289 (12000), 315 (19000), 331 (27000), 390 (4000), 433 (2000), 482 (1500), 975 (750). Anal. Calcd for $C_{11}H_7N_2O_2S$: C, 57.13; H, 3.05; N, 12.11. Found: C, 57.02; H, 3.36; N, 11.91.

2-(3-Thienyl)benzimidazole N-N′-dioxide (2.15e): (42%). UV–vis (CH_3CN) λ_{max}, nm (ε): 240 (17000), 280 (24000), 299 (22000), 313 (31000), 330 (4300), 386 (5100), 426 (2600), 476 (1900), 930 (800). Anal. Calcd for $C_{11}H_7N_2O_2S$: C, 57.13; H, 3.05; N, 12.11. Found: C, 57.08; H, 3.15; N, 11.83.

2-(2-Pyridyl)benzimidazole N-N′-dioxide (**2.15b**): Prior to oxidation, 1-hydroxy-2-(2’-pyridyl)benzimidazole-3-N-oxide **2.16b** (0.075 g, 0.33 mmol) was dissolved in 5 mL 1.0 M $NaOH_{(aq)}$, filtered twice through a Celite-545 plug, acidified with 1.0 M HCl, and isolated with suction. The wet clay was washed with water (2 mL), acetonitrile (2 mL), toluene (2 mL), and pentane (5 mL) and dried under a stream of air. The tan solid was

suspended in benzene (10 mL) and, while sonicating, lead (IV) oxide (2.6 g, 11 mmol) was added to the solution and solution was sonicated under N_2 for 1 h. The bright green solution was filtered through a Celite-545 plug and concentrated by rotary evaporation. The crude radical was subjected to flash column chromatography (neutral alumina, 9:1 $CHCl_3$/MeOH) and the combined fractions were concentrated under reduced pressure and dried under vacuum yielding a light brown solid (0.014 g, 19%). UV–vis (CH_3CN) λ_{max}, nm (concentration unknown due to instability of radical): 242, 280, 308, 392, 475, 762. Anal. Calcd for $C_{12}H_8N_3O_2$: C, 63.71; H, 3.56; N, 18.58. Found: C, 62.96; H, 4.17; N, 18.22.

Chapter 3: Extended Aromatic and Heteroaromatic Annelated Nitronyl Nitroxides

3.1 Increasing radical stability

Although the term *stable* is used somewhat subjectively when describing organic radicals, one accepted definition of a stable radical is a substance that can be isolated and handled in the same manner as you would any other closed shell organic compound.[256] Radicals which can be characterized spectroscopically but cannot be isolated are considered persistent. The idea of using rational design to enhance radical stability was briefly introduced in Section 2.1. Thermodynamic stabilization of open-shell organics can be accomplished through the inclusion of heteroatoms and π delocalization.[2] Heteroatoms, particularly oxygen, nitrogen, and sulfur can effectively bear spin without a marked increase in their reactivity.

Delocalization of the unpaired spin over multiple atoms can also have a stabilizing effect, although the extent to which π delocalization contributes to stability is dependent on a number of factors. Delocalization is usually an effective means of decreasing reactivity as electron density is partitioned over a greater number of atoms. The result is that spin is not as heavily concentrated on any given atom and the reactivity at each centre decreases accordingly. More delocalization is not always better though, it is also important which atoms the spin is delocalized over. In diphenyl nitronyl nitroxide **3.1**, it is believed spin delocalization on the *C*4 and *C*5 aromatic groups acts to lower nitronyl nitroxide stability (relative to TMMN, **2.3**) as electron density is delocalized from

nitrogen atoms onto carbon atoms which are inherently less able to carry spin, due to a decreased electronegativity[257]

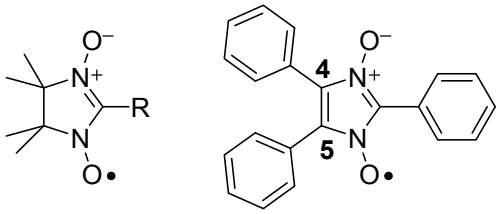

2.3 **3.1**

Figure 3.1. Tetramethyl nitronyl nitroxide **2.3** and diphenyl nitronyl nitroxide **3.1**.

Thus far we have shown BNN to be stable towards dimerization in solution and the solid state, as well as to be generally air and moisture stable. Still, the series of BNN radicals **2.15a** – **2.15e** were considerably less stable than TMNN **2.3**, especially in solution. We were interested in attempting to elucidate why, despite using design principles that typically have a stabilizing effect on open-shell systems, these radicals were some of the least stable nitronyl nitroxide radicals handled to date. It was shown that across the BNN series, roughly 20 % of the electron spin density is delocalized into annelated ring suggesting destabilization is occurring as a result of spin delocalization onto atoms which are less able to bear spin density.[221] When considering the stability (or lack thereof) of BNN and its derivatives, we must also consider how easily reduced they are. The reduction potential of BNN **2.15a** was lowered by nearly 750 mV relative to TMNN **2.3**. This is consistent with a significant lowering in energy of the singly occupied molecular orbital (SOMO) and the enhanced redox activity may trigger reaction pathways that ultimately lead to radical decomposition.

Prior to this work Dr. Steven Bowles attempted the synthesis of the systems shown in Figure 3.2 with limited success.[172] The acenapthalene **3.3** and naphthalene **3.2** radical

precursors could not be synthesized at all. While the synthesis of all other radical precursors was successful, the stability of the radicals was limited. The phenanthrene derivative **3.4** had previously been synthesized by Shiomi et al. and was found have a short (30 min) lifetime in solution and decomposed upon removal of solvent,[224] this reactivity was later confirmed in our own group.[172] Similarly, the pyrene derivative **3.5** decomposed so rapidly in solution detection of an EPR signal was not possible. Heteroaromatic radicals **3.6** – **3.8** were short lived in solution, however, characterization by EPR spectroscopy was possible.

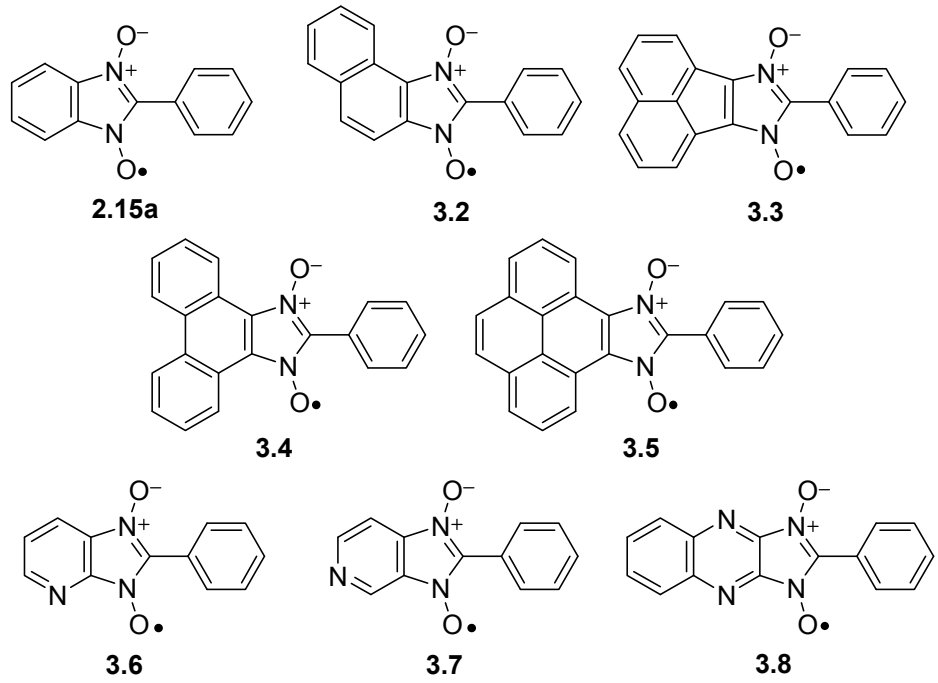

Figure 3.2. Aromatic and heteroaromatic annelated nitronyl nitroxide radicals.

Annelation, which results in an increase in conjugation length of TMNN **2.3** to give the π delocalized BNN derivatives **2.15a** and **3.2 – 3.8** in Figure 3.2, was found to yield a less stable class of radicals. Increasing the conjugation length increases the number of atoms the radical spin is delocalized over which, in this case, resulted in delocalization of

spin onto the carbon framework. Delocalization places spin density on atoms which are less electronegative and reactivity at these sites is increased, making dimerization a possible decomposition pathway. Additionally, extending the conjugation has a stabilizing effect leading to a decrease in SOMO energy. Decreasing the SOMO energy results in radicals with exceptionally low reduction potentials which may make them susceptible to disproportionation (Figure 3.3).

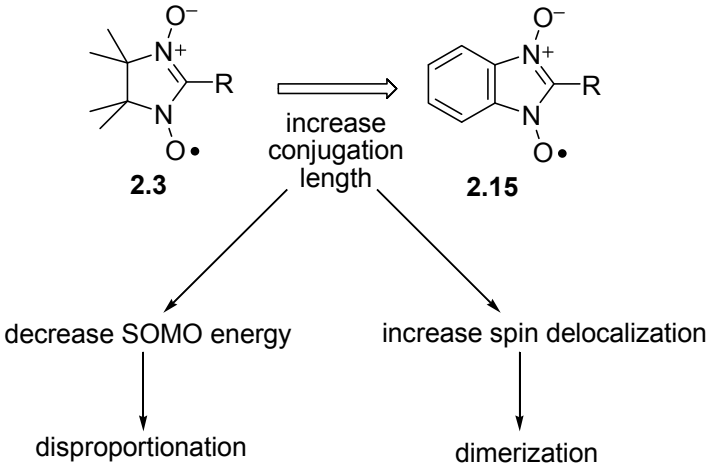

Figure 3.3. Potential decomposition pathways opened up upon annelation of TMNN **2.3** to give **2.15**.

We were interested in examining the series of π-delocalized nitronyl nitroxide radicals **2.15a** and **3.2 – 3.8** to ascertain whether the observed decrease in solution phase lifetime upon annelation can be attributed to delocalization of the radical spin onto less electronegative atoms or the exceptionally low reduction potential. The series of annelated nitronyl nitroxide radical targets (Figure 3.2) used to address this question include those that (a) exhibit an increase in π delocalization as in **3.2 – 3.5** (b) contain heteroatoms as in pyridyl derivatives **3.6** and **3.7** or (c) both, as in quinoxaline derivative **3.8**.

Prior to this work limited spectroscopy (EPR, UV–vis) had been used to characterize the electronic structure of **3.2 – 3.8**. Additionally, the electrochemical properties of **3.2 – 3.8** were unknown. Challenges arose in the generation of radicals **3.2 – 3.8** as the solution phase stability of the successfully generated radicals was poor and the radical precursors were highly insoluble. In Chapter 2 it was shown that the radical precursors could be solubilized by deprotonation. Given that the oxidation of the anion and the reduction of the radical are the same electrochemical process (Figure 3.4), we were interested in generating the radical precursor salts in order to evaluate their oxidation potential, and thus the reduction potential of the corresponding radical. If the low reduction potential is the source of radical instability, reduction potential should correlate with solution phase lifetime and be independent of spin density distribution.

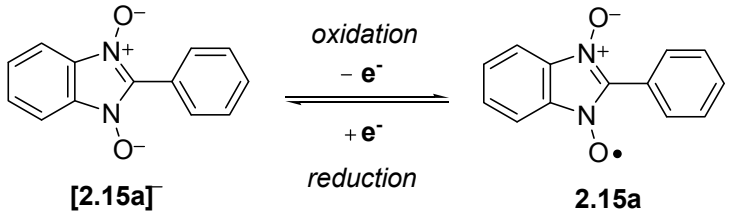

Figure 3.4. Electrochemical redox couple for BNN^{-}/$BNN^{\bullet}$.

Over the course of this work radical precursors **3.11**, **3.18**, **3.28**, **3.31**, and **3.37** were prepared in high purity and fully characterized in order to eliminate the possibility that the observed radical instability was due to the presence of impurities. Cyclic voltammetry was used to investigate the electrochemical reversibility and redox potentials of radicals **3.4** – **3.8**. Additionally, the electronic structure of π-delocalized and heteroaromatic systems **2.15a** and **3.2 – 3.8** were evaluated computationally with density functional

theory using unrestricted Becke's three-parameter hybrid exchange-correlation functional (UB3LYP)[238] with the EPR-II basis set.[258] Through the use of cyclic voltammetry, EPR spectroscopy and computational data we hoped to further our understanding of the roles of spin distribution and decreased reduction potential on the chemical stability of annelated nitronyl nitroxides.

3.2 Synthesis of extended aromatic nitronyl nitroxides

3.2.1 Synthesis of 1-hydroxyl-2-phenyl-phenanthro[9,10-*d*]imidazole 3-oxide

Although the EPR spectrum of **3.4** was reported in the literature,[224] the synthesis was not well described. The synthesis was accomplished via the acid catalyzed condensation between two monoxime fragments which has traditionally been the most common methodology for the synthesis of nitronyl nitroxides. This synthetic procedure was repeated and found to successfully generate the phenanthrene annelated nitronyl nitroxide salt, **3.12**. Benzaldehyde was condensed with hydroxylamine hydrochloride under basic conditions to give benzaldoxime **3.9** in 97 % yield. Analogous conditions were used to generate 9,10-phenanthrene monoxime **3.10** from commercially available 9,10-phenanthrenequinone. Following 9,10-phenanthrenequinone monoxime generation, **3.10** wa**s** reacted with benzaldoxime **3.9** under strongly acidic conditions to yield the annelated phenanthrene precursor **3.11**, which was deprotonated with tetrabutylammonium hydroxide to give the phenanthrene precursor salt **3.12** in high yield and purity. Treatment of the tetrabutylammonium precursor salt **3.12** with silver hexafluorophosphate yielded a deep blue solution that rapidly (< 1 min) turned yellow upon standing. This is consistent with previous reports on the colour and stability of

phenanthrene based radical **3.4**[172,224] and confirms deprotonation of the precursor with tetrabutylammonium hydroxide is not altering the chemical composition of the system.

Scheme 3.1. Synthesis of *C2*-phenyl phenanthrenimidazole nitronyl nitroxide precursor and corresponding tetrabutylammonium salt. [a]

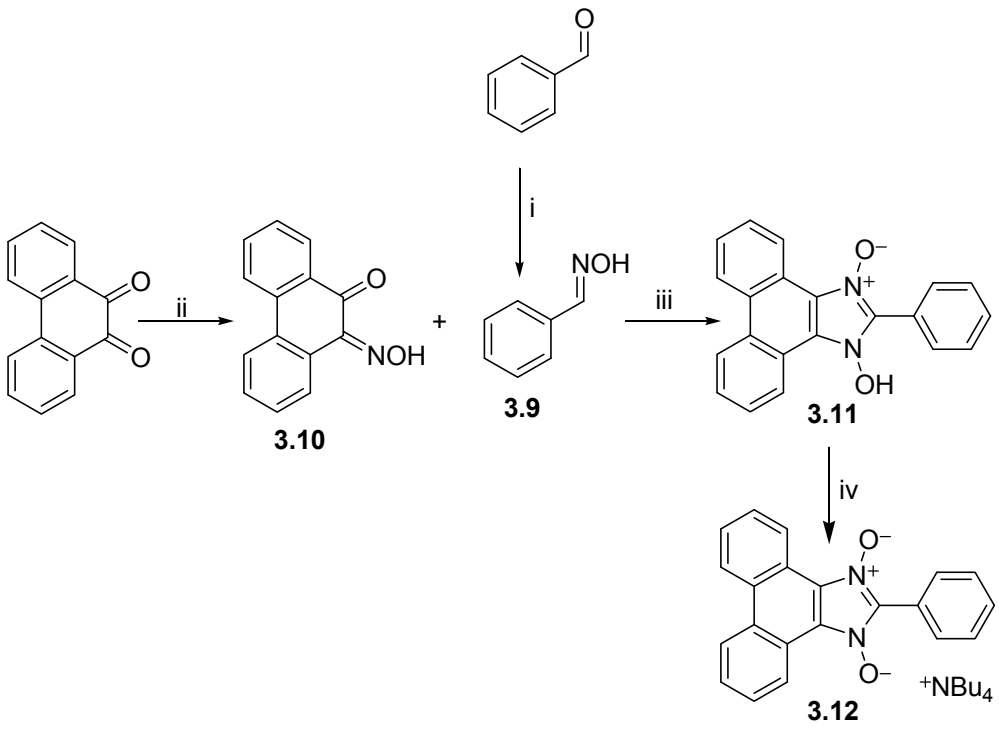

[a] Reagents and conditions: (i) $NH_2OH{\cdot}HCl$, pyridine, EtOH, 97 %; (ii) $NH_2OH{\cdot}HCl$, $BaCO_3$, EtOH, Δ, 87 %; (iii) $HCl_{(g)}$, EtOH, 98 %; (iv) $(nBu)_4NOH$, 5:1 acetone:EtOH, 95 %.

The use of $HCl_{(g)}$ in step iii (Scheme 3.1) limits the functional group tolerance of this synthesis. We were interested in utilizing the milder synthetic methodology developed in Chapter 2 for the synthesis of the larger aromatic systems presented here. Should the radicals show interesting solution or solid state properties, a series of derivatives would be attractive for further investigation of how functionalization perturbs electronic structure, solid state packing, and intermolecular spin-spin interactions. Additionally,

substitution, particularly on the annelated aromatic ring, could have a stabilizing effect creating π-delocalized radicals which are isolable in the solid state.

Scheme 3.2. Alternate route attempted for synthesis of **3.11**.[a]

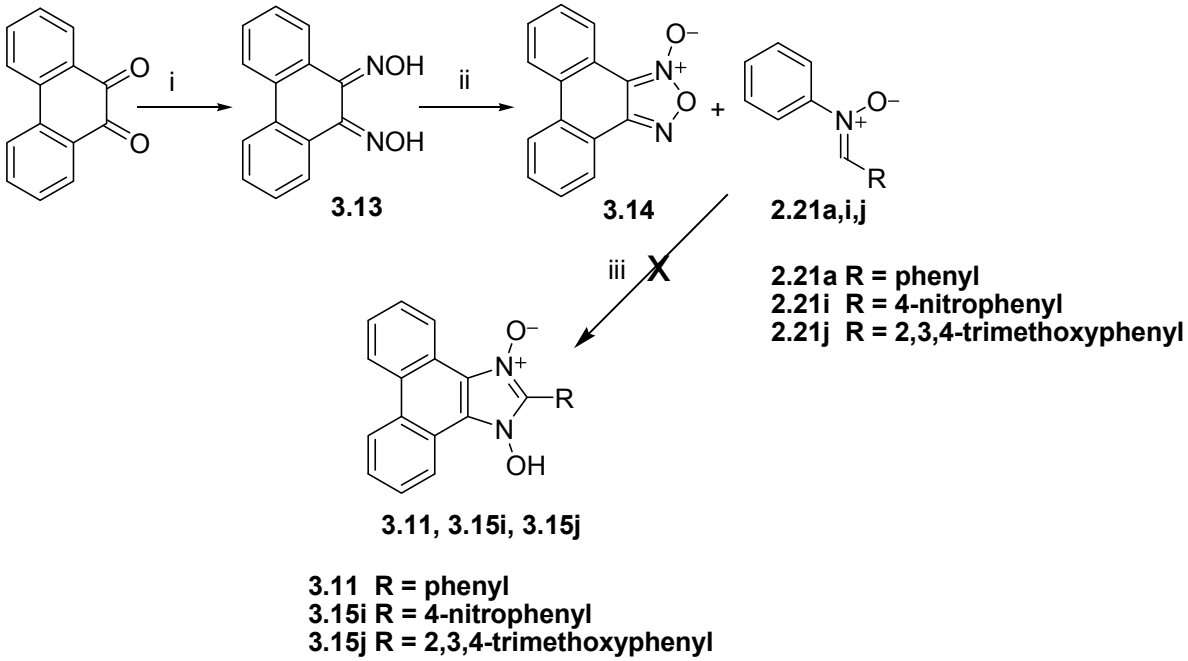

[a] Reagents and conditions: (i) $NH_2OH{\cdot}HCl$, pyridine, EtOH, Δ, 52 %; (ii) $NaOCl_{(aq)}$, KOH in EtOH, 84 %; (iii) toluene, Δ, 0 %.

Benzofurazan oxides can be synthesized by oxidation of *o*-nitroamine under acidic or basic conditions.[259-261] Given that dioximes are constitutional isomers of *o*-nitroamines we believed that oxidation of the dioxime under analogous conditions should yield the appropriate oxadiazole oxide (furoxan) and literature precedence for this exists.[262,263] 9,10-phenanthrenequinone was reacted with excess hydroxylamine hydrochloride to give dioxime **3.13**. Interpretation of the NMR data for dioxime **3.13** was difficult as dioximes exist in three different isomeric forms (ZZ, EE, and hydrogen bonded EZ; Figure 3.5).

Isomerization was observed in the NMR spectra of nearly all the monoxime and dioxime derivatives and the ratio between the different isomeric forms was dependant on solvent.

IR spectroscopy was more useful when attempting to determine whether mono or bis condensation had occurred. In the case of 9,10-phenanthrenequinone dioxime, the presence of stretches at 3186 and 1560 cm^{-1} are characteristic of ν(O–H) and ν(C=N) stretching in hydroxylamines.[264] Additionally, the IR spectrum did not contain the 1684 cm^{-1} ν(C=O) stretch present in 9,10-phenanthrenequinone[264] or the 1675 cm^{-1} stretch 9,10-phenanthrenequinone monoxime **3.10** confirming the twofold condensation with hydroxylamine was successful. Once synthesized, 9,10-phenanthrenequinone dioxime **3.13** was oxidized with sodium hypochlorite under basic conditions yielding phenanthrene furazan oxide **3.14** in 84 % yield. Again two isomeric forms were observed in ~2:1 ratio by NMR ($CDCl_3$), the closed oxadiazolo ring depicted in Scheme 3.2 and its open form, 9,10-dinitrosophenanthrene.

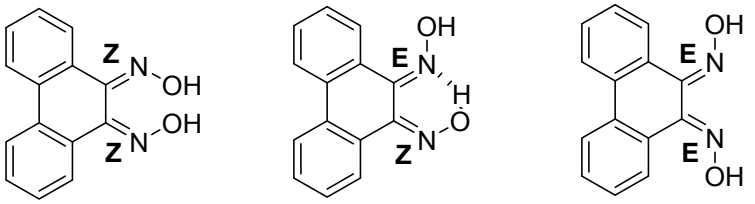

Figure 3.5. Isomers of dioxime.

Condensation of furazan oxide **3.14** with *C*-phenyl-*N*-phenyl nitrone **2.21a** in refluxing toluene did not yield any product after 4 days of heating. TLC revealed slow decomposition of **2.21a** over this time, however, the furazan oxide **3.14** remained unreacted and was recovered from the reaction. Following the failure of the first attempt at nitrone/furoxan coupling, both electron rich **2.21j** and electron poor **2.21i** nitrones

were reacted to test whether perturbing the electronics of the nitrone would facilitate a reaction. Again these condensations were unsuccessful and **3.14** was recovered quantitatively. There is no evidence **3.14** is reacting at all under these conditions suggesting, at least in this case, the milder methodology developed for the synthesis of benzannelated nitronyl nitroxides **2.21a-l** is not suitable for the generation of annelated phenanthrene nitronyl nitroxide radicals.

3.2.2 Synthesis of 1-hydroxyl-2-phenyl-pyreno[4,5-*d*]imidazole 3-oxide

Scheme 3.3. Synthesis of *C*2-phenyl pyreneimidazole nitronyl nitroxide precursor and corresponding tetrabutylammonium salt. [a]

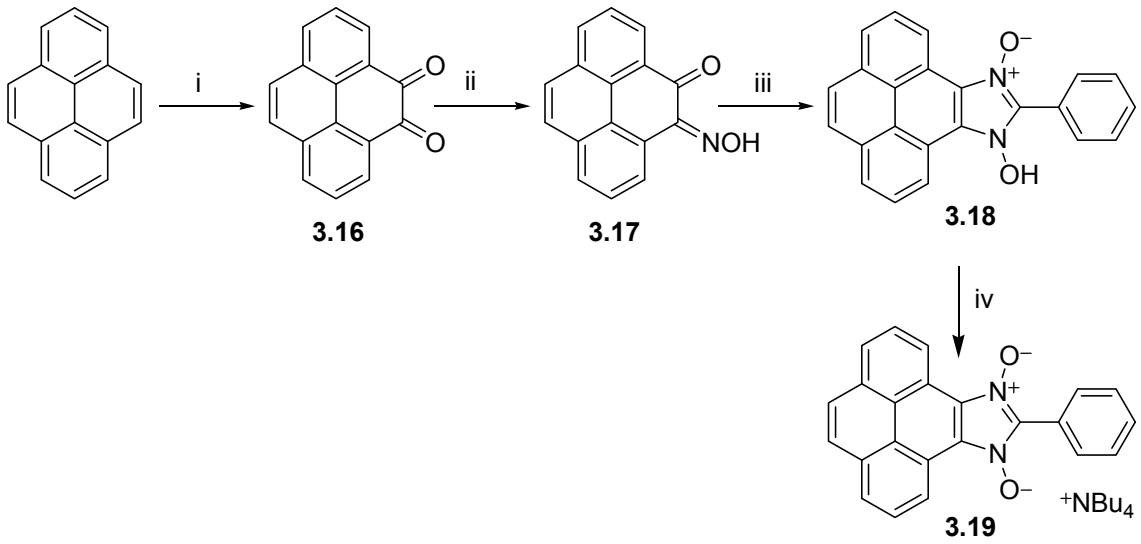

[a]Reagents and conditions: (i) $RuCl_3 \cdot xH_2O$, $NaIO_4$ in H_2O, 1:1 CH_3CN:CH_2Cl_2, 41 %; (ii) $NH_2OH \cdot HCl$, $BaCO_3$, EtOH, Δ, 93 %; (iii) PhC=NOH **3.9**, $HCl_{(g)}$, EtOH 71 %; (iv) $(nBu)_4NOH$, 2:1 acetone:EtOH, 67 %.

Pyrene radical precursor **3.18** was synthesized using acid catalyzed methodology analogous to that utilized during the synthesis of the phenanthrene derivative **3.11**. Pyrene was oxidized directly to pyrenedione **3.16** with ruthenium(III) chloride hydrate

and sodium periodate.[265] This was an improvement over previous multi-step synthetic methodology whereby the *C*4-*C*5 pyrene bond was oxidatively cleaved to generate phenanthrene-1,10-dicarboxylate which was subsequently protected by Fischer esterification and reductively coupled with sodium metal to give 4,5-pyrenedione **3.16**.[266]

Following purification, 4,5-pyrenedione **3.16** was reacted with one equivalent of hydroxylamine hydrochloride in the presence of barium carbonate to give 4,5-pyrenedione monoxime **3.17**. The monoxime was condensed with benzaldoxime **3.9** in acidic ethanol yielding pyrene nitronyl nitroxide precursor **3.18** as an insoluble tan powder. Precursor **3.18** was deprotonated with tetrabutylammonium hydroxide to give tetrabutylammonium pyrene precursor salt **3.19** which was used to investigate the pyrene nitronyl nitroxide radical/anion redox couple.

3.2.3 Attempted synthesis of acenaphthyl and naphthyl precursors

Scheme 3.4. Synthetic pathways attempted in the preparation of (2-phenyl)acenaphthylenimidazole 1-oxyl 3-oxide. [a]

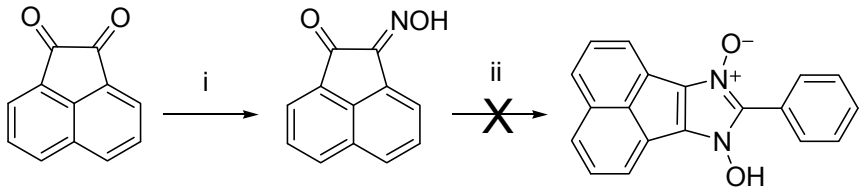

3.20 **3.21**

[a]Reagents and conditions: (i) $NH_2OH{\cdot}HCl$, pyridine, EtOH, 81 %; (ii) PhC=NOH **3.9**, $HCl_{(g)}$, EtOH, 0 %.

The synthesis of acenaphthyl **3.21** and naphthyl **3.25** radical precursors proved challenging. Bowles has previously shown the acenaphthyl and naphthyl derivatives

could not be synthesized by acid catalyzed condensation of dioxime with benzaldehyde or furoxan nitrone coupling.[172] This was confirmed during the course of this work.

Condensation of acenaphthyldioxime with hydroxyl amine gave 1,2-acenaphthylenedione monoxime **3.20** in 81 % yield. Reaction of the monoxime with benzaldoxime **3.9** in EtOH under strongly acidic conditions did not generate precursor **3.21**. Given the numerous synthetic pathways previously attempted and the lack of success associated with each, the synthesis of acenaphthyl nitronyl nitroxide precursor **3.21** was not explored further.

Scheme 3.5. Synthetic pathways attempted in the preparation of (2-phenyl)naphthalenimidazole 1-oxyl 3-oxide. [a]

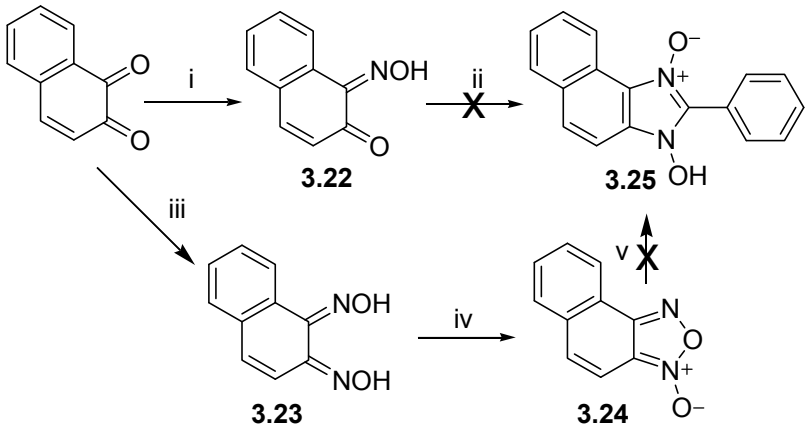

[a]Reagents and conditions: (i) $NH_2OH{\cdot}HCl$, $BaCO_3$, EtOH, 94 %;[172] (ii) PhC=NOH **3.9**, $HCl_{(g)}$, EtOH, 0 %; (iii) $NH_2OH{\cdot}HCl$, $BaCO_3$, EtOH, 83 %; (iv) $NaOCl_{(aq)}$, KOH in EtOH, 14 %; (v) *C*-phenyl-*N*-phenylnitrone **2.21a**, toluene, Δ, 0 %.

The synthesis of naphthyl radical precursor **3.25** was also revisited (Scheme 3.5). Bowles reported monoxime **3.22** could be successfully synthesized, however, no reaction was observed when **3.22** was combined with benzaldoxime **3.9** in anhydrous acidic EtOH. The synthesis of naphthyl nitronyl nitroxide precursor **3.25** was attempted here

using the furoxan nitrone coupling methodology developed in Chapter 2. Previously the synthesis of furoxan **3.24** was accomplished in four steps from 2-aminonaphthalene. We applied the dioxime oxidation developed for the synthesis of the phenanthrene furoxan **3.13** above to synthesize naphthalene furoxan (naphthaleno[1,2-*c*][1,2,5]oxadiazole N-oxide) **3.24** from 1,2-naphthoquinone in only two steps. Naphthoquinone was condensed to give 1,2-naphthoquinone dioxime **3.23** which was oxidized with aqueous sodium hypochlorite in basic EtOH to give naphthalene furoxan **3.24**. As before, although the furoxan could be generated it was unreactive towards *C*-phenyl-*N*-phenylnitrone **2.21a** and naphthyl precursor **3.25** was not isolated.

3.3 Synthesis of heteroaromatic nitronyl nitroxides

3.3.1 Synthesis of (2-phenyl)-4-azabenzimidazole nitronyl nitroxide

Scheme 3.6. Synthesis of (2-phenyl)-4-azabenzimidazole nitronyl nitroxide precursor salt. [a]

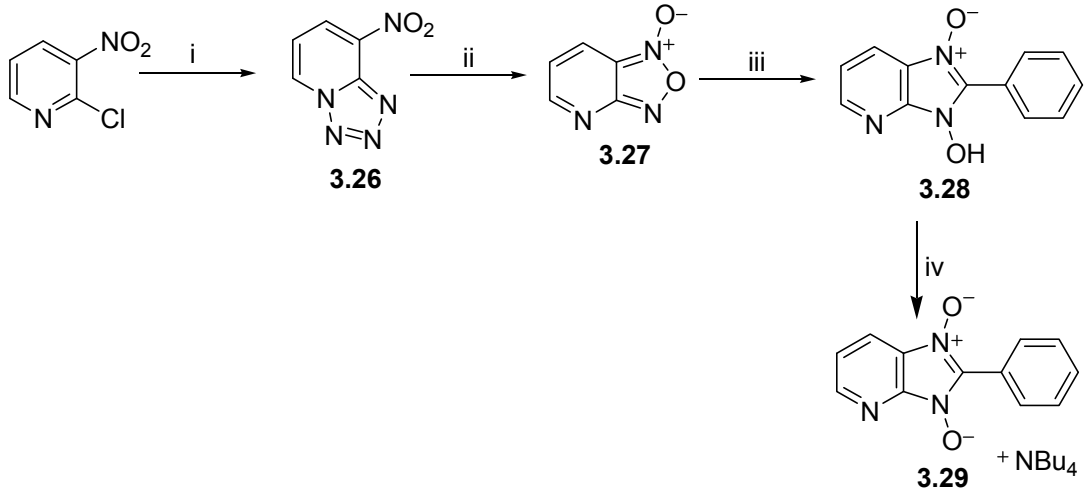

[a]Reagents and conditions: (i) NaN_3, 9:1 EtOH:H_2O, $HCl_{(aq)}$, Δ, 58 %; (ii) toluene, Δ, 85 %; (iii) *C*-phenyl-*N*-phenylnitrone **2.21a**, toluene, Δ, 80 %; (iv) $(nBu)_4NOH$, 1:1 acetone:EtOH, 57 %.

4-Azabenzimidazole nitronyl nitroxide precursor salt **3.29** was synthesized using the furoxan/nitrone condensation methodology developed for the synthesis of the benzannelated systems reported in Chapter 2. Nucleophilic attack on 2-chloro-3-nitropyridine with a source of azide gave **3.26**, which exists primarily in the tetrazole form depicted in Scheme 3.6. Gentle heating of the tetrazole resulted in loss of N_2 and formation of pyridine furoxan **3.27** in 49 % yield from 2-chloro-3-nitropyridine. Furoxan **3.27** was condensed with *C*-phenyl-*N*-phenylnitrone **2.21a** yielding precursor which could be deprotonated to give the tetrabutylammonium salt as a bright yellow-orange powder.

3.3.2 Synthesis of (2-phenyl)-5-azabenzimidazole nitronyl nitroxide

Scheme 3.7. Synthesis of (2-phenyl)-4-azabenzimidazole nitronyl nitroxide precursor salt. [a]

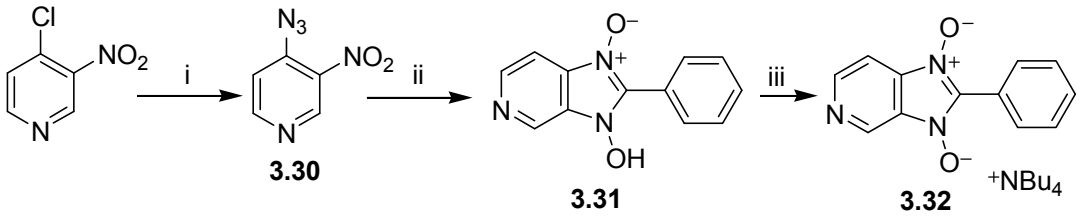

3.30 **3.31** **3.32**

[a]Reagents and conditions: (i) NaN_3, DMSO, 30 %; (ii) *C*-phenyl-*N*-phenylnitrone **2.21a**, toluene, Δ, 94 % (iii) $(nBu)_4NOH$, EtOH, 91 %.

5-Azabenzimidazole nitronyl nitroxide precursor salt **3.32** was synthesized using the same procedure as that used to prepare the 4-azabenzimidazole nitronyl nitroxide precursor salt **3.29**. Instead of substitution of chlorine with azide at the 2 position on pyridine (as in Scheme 3.6), 4-chloro-3-nitropyridine was used and azide substitution occurred at the 4-pyridyl position. Attempts at gently heating 4-azido-3-nitropyridine

3.30 to give furoxan resulted in formation of an insoluble black solid that was not the desired product. To combat this, azide **3.30** and *C*-phenyl-*N*-phenylnitrone **2.21a** were combined and gently heated. The in situ generation of the furoxan followed by immediate reaction with *C*-phenyl-*N*-phenylnitrone **2.21a** generated precursor **3.31** in nearly quantitative yield and formation of a black insoluble solid was not observed. Following isolation, precursor **3.31** was deprotonated with tetrabutylammonium hydroxide to give the 5-azabenzimidazole precursor salt **3.32** as a bright orange solid in 91 % yield.

3.3.3 Synthesis of 2-phenylimidazo[4,5-*b*]quinoxaline nitronyl nitroxide

The synthesis of 2-phenylimidazo[4,5-*b*]quinoxaline nitronyl nitroxide precursor salt was carried out according to Scheme 3.8. Glyoxal was condensed with two equivalents of hydroxylamine to give glyoxime **3.33** which was subsequently chlorinated with *N*-chlorosuccinimide to give dichloroglyoxime **3.34** as a white crystalline solid (69 % yield from glyoxal). 1,2-diaminobenzene was reacted with dichloroglyoxime **3.34** under mild basic conditions to give *N2,N3*-dihydroxy-2,3-quinoxalinediamine **3.35** in 82 % yield. Quinoxaline hydroxylamine **3.35** was oxidized with nitric acid to give furoxan **3.36** which reacted rapidly with *C*-phenyl-*N*-phenylnitrone to give quinoxaline precursor **3.37** as an orange powder in 44 % yield. Unfortunately, deprotonation of **3.37** with tetrabutylammonium hydroxide did not yield 2-phenylimidazo[4,5-*b*]quinoxaline nitronyl nitroxide precursor salt **3.38**. Instead a black solid was isolated whose ^{1}H and ^{13}C NMR spectra were inconsistent with that for **3.38**. Quinoxaline is susceptible to nucleophilic attack and hydroxide may be cleaving open the quinoxaline ring resulting in decomposition. Alternative methods of 2-phenylimidazo[4,5-*b*]quinoxaline nitronyl nitroxide precursor salt **3.38** generation were not explored.

Scheme 3.8. Synthesis of 2-phenylimidazo[4,5-*b*]quinoxaline nitronyl nitroxide precursor salt. [a]

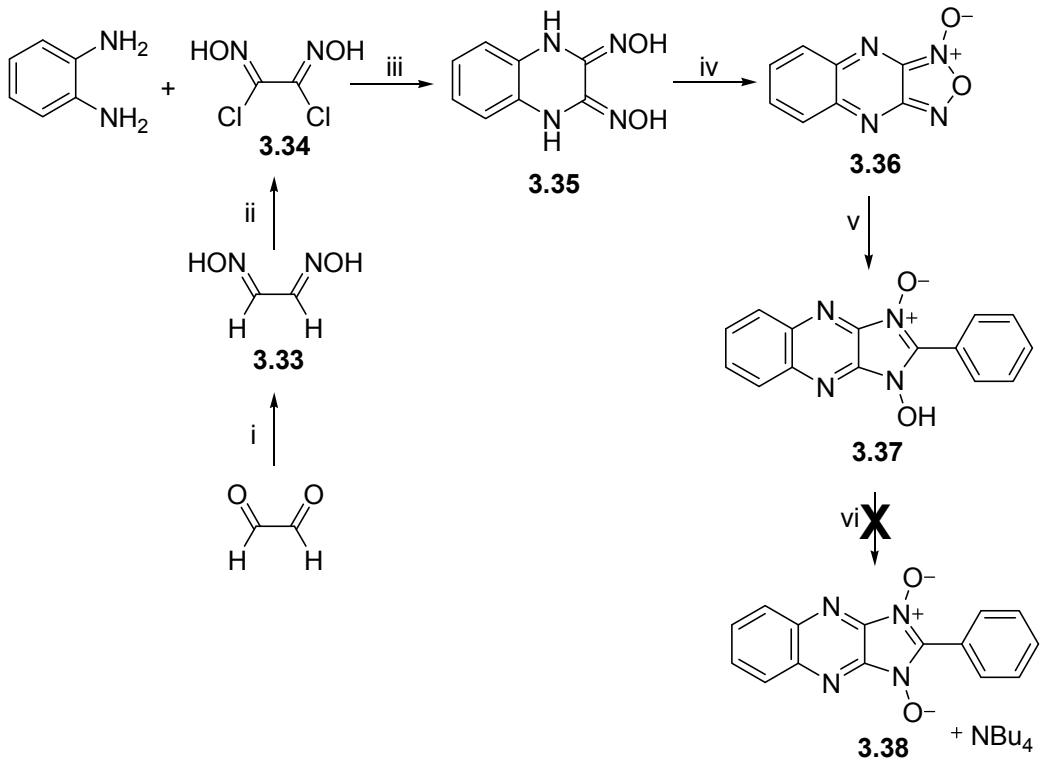

[a]Reagents and conditions: (i) $NH_2OH{\cdot}HCl$, KOH, H_2O, Δ, 79 %; (ii) NCS, DMF, 87 %; (iii) Na_2CO_3, CH_3CN, 0 °C to rt, 82 %; (iv) Conc HNO_3, CH_2Cl_2, 0 °C, 76 %; (v) *C*-phenyl-*N*-phenylnitrone **2.21a**, toluene, Δ, 44 %; (vi) $(nBu)_4NOH$, EtOH, 0 %.

3.4 Electrochemistry: cyclic voltammetry of precursor salts

The electrochemical behavior of the series of π-delocalized and heteroaromatic nitronyl nitroxide radicals **3.4 – 3.7** was investigated by cyclic voltammetry and compared to *C*2-phenyl substituted benzannelated nitronyl nitroxide radical **2.15a** (Table 3.1). With the exception of the quinoxaline nitronyl nitroxide anion [**3.8**]$^-$, the half-wave oxidation potential of each anion, and therefore reduction potential ($E_{1/2}$(red)) of each radical **3.4 – 3.7** was determined.

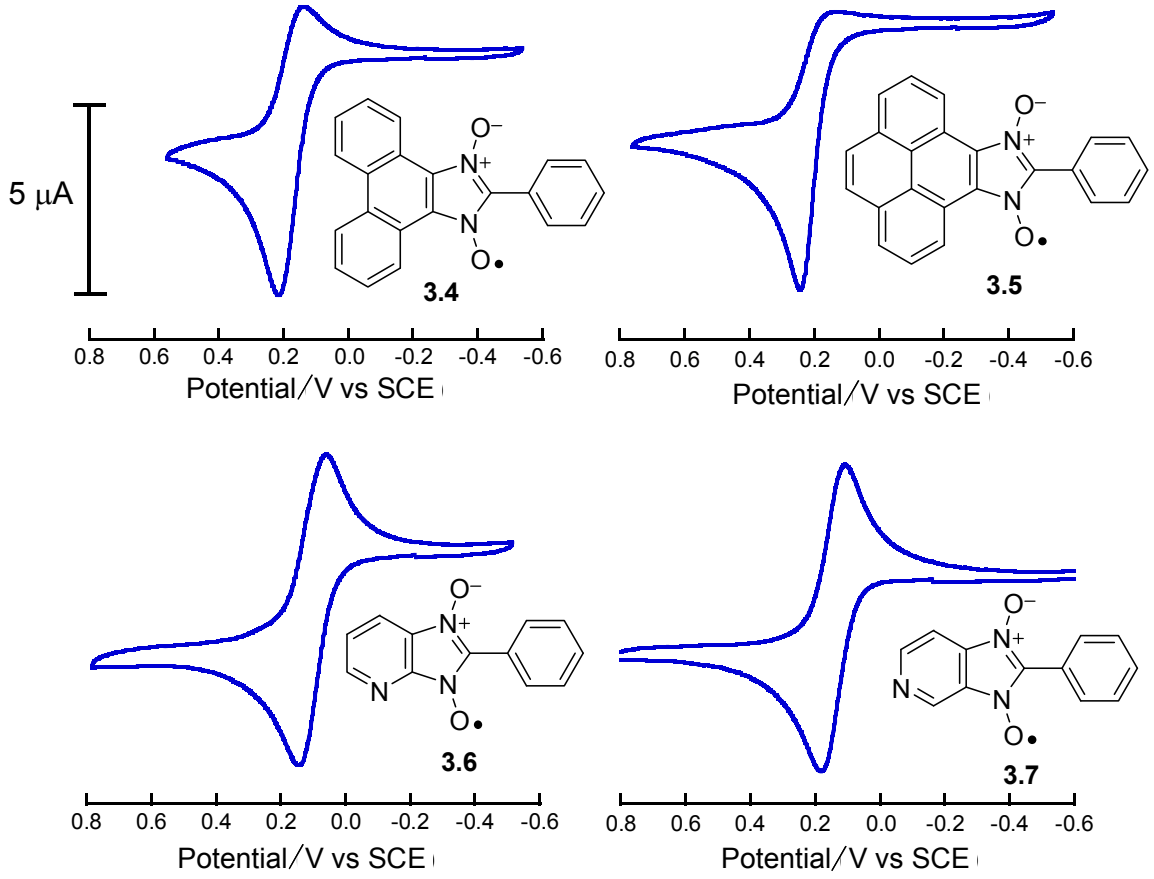

Figure 3.6. Cyclic voltammogram of reduction waves of **3.4 – 3.7**, 10 mM solution in CH_3CN, 0.1 M NBu_4PF_6, 50 mV s^{-1} scan rate.

Table 3.1. Half-wave reduction potentials and calculated electron affinities (EA) of radicals **2.15a**, **3.4 - 3.8**.

	2.15a	**3.4**	**3.5**	**3.6**	**3.7**	**3.8**
$E_{1/2}$(red) (V vs SCE)[a]	-0.03	0.19	0.18	0.09	0.17	-
ΔEp (mV)	75	77	93	89	80	-
i_{pa}/i_{pc}	1.18	1.96	2.95	1.39	1.18	-
EA (eV)[b]	2.11	2.50	2.55	2.24	2.41	2.35

[a] 10 mM solution in CH_3CN, 0.1 M NBu_4PF_6, 100 mV s^{-1} scan rate, Fc/Fc^+ internal standard. [b] Single point energies calculated using DFT UB3LYP/6-31+G(d,p), no zero point energy correction performed. Input structure was the geometry optimized structure determined from the UB3LYP/EPR-II calculation (Section 3.6).

The half-wave potentials determined for the reduction of radicals **3.4 – 3.7** are reported relative to SCE in Table 3.1 and depicted in Figure 3.6. In all cases the radicals reduce at potentials more positive than benzannelated nitronyl nitroxide **2.15a**. Moreover, with the exception of **3.6**, the radicals are more easily reduced than the strongly accepting 7,7,8,8-tetracyanoquinodimethane (TCNQ)[233] making them some of the strongest one-electron organic acceptors reported to date.

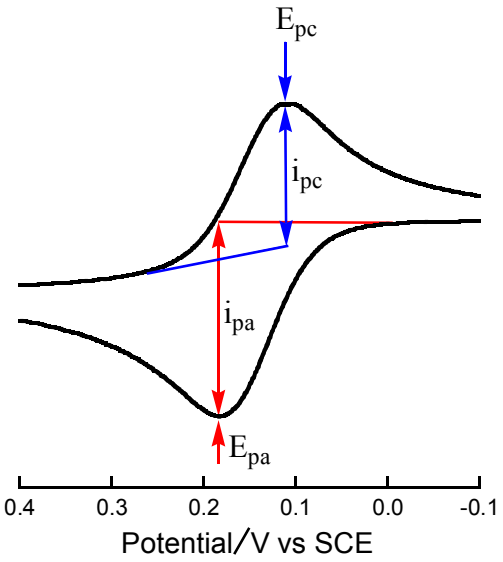

Figure 3.7. An archetypal voltammogram labelled with key peak parameters.

For a perfectly reversible electrochemical reaction the separation in the peak potentials ($\Delta E_p = E_{pc} - E_{pa}$, Figure 3.7) will be independent of scan rate and follow Nernstian behavior, that is ΔE_p will be close to $59/n$ mV (at 25 ºC), where n is the number of electrons transferred during the process.[267,268] In practice, a system is typically considered reversible provided that ΔE_p is less than ~80 mV. To be completely reversible the electron transfer event at the surface of the electrode must be fast relative to mass transport.[269] A quasi-reversible system can appear reversible when the applied voltage is

scanned slowly but will show an increase in ΔE_p at higher scan rates. The scan rate dependence of the separation between peak potentials for radicals **2.15a** and **3.4** – **3.7** is given in Table 3.2. As scan rate is increased, ΔE_p increases for **3.4**, **3.6** and **3.7**, consequently the electrochemical radical/anion redox couple is quasi-reversible. The ΔE_p for **2.15a** remains essentially constant over the scan rates evaluated, consistent with our previous assignment of this process as reversible.

Table 3.2. Scan rate dependence of the separation of peak potentials (ΔE_p, difference in anodic and cathodic peak potential, reported in mV) and ratio of peak currents (i_{pa}/i_{pc}) of radical reduction process. 10 mM solution in CH_3CN, 0.1 M NBu_4PF_6, 100 mV s^{-1} scan rate, Fc/Fc^+ internal standard.

Scan Rate	**2.15a**		**3.4**		**3.5**		**3.6**		**3.7**	
(mV s^{-1})	ΔE_p	i_{pa}/i_{pc}	ΔE_p	i_{pa}/i_{pc}	ΔE_p	i_{pa}/i_{pc}	ΔE_p	i_{pa}/i_{pc}	ΔE_p	i_{pa}/i_{pc}
50	75	1.18	76	1.96	112	2.95	85	1.39	73	1.18
100	75	1.26	77	1.80	93	3.34	89	1.41	80	1.20
150	79	1.24	78	1.75	85	3.41	96	1.38	86	1.20
200	82	1.21	83	1.56	86	3.39	99	1.42	90	1.18
250	76	1.22	75	1.49	75	3.23	93	1.44	85	1.18
300	77	1.22	78	1.40	75	3.16	97	1.40	87	1.17
500	-	-	80	1.27	76	2.81	97	1.42	98	1.18
750	-	-	85	1.18	81	2.62	-	-	-	-

The electrochemistry of pyrene radical **3.5** is more complex. The separation of peak potentials decreases with increasing scan rate, until the redox reaction appears reversible (scan rate $\geq$ 250 mV s^{-1}). This can be consistent with the coupling of a reversible or quasi-reversible electrochemical redox (E_r) process to an irreversible chemical reaction (C_i). Classification of an E_rC_i mechanism requires measurement of the ratio of the anodic peak current (i_{pa}) to that of the cathodic peak current (i_{pc}). When an electron transfer event is free of chemical complications or is followed by a reversible chemical reaction, the peak current ratio (i_{pa}/i_{pc}) is unity. However, if following oxidation a fraction of the

oxidized species chemically reacts before reduction can occur on the reverse scan, the heights of i_{pa} and i_{pc} will be inequivalent and $i_{pa}/i_{pc} \neq 1$. Each peak current is measured by extrapolating the preceding baseline current (horizontal lines in Figure 3.7) and taking the difference between the baseline and maximum peak current. In the case of pyrene radical **3.5**, the peak current ratio is far from unity at all scan rates. When tetrabutylammonium pyrene nitronyl nitroxide precursor salt **3.19** is oxidized to radical, the oxidation is rapidly followed by an irreversible chemical reaction. This significantly depletes the concentration of radical at the electrode surface and very little species is available for reduction during the cathodic sweep. The chemical instability of pyrene radical **3.5** observed by voltammetry is consistent with the rapid decomposition of **3.5** upon chemical oxidation.

The ratio of peak currents for phenanthrene nitronyl nitroxide **3.4** and **3.6** also deviate noticeably from unity. While i_{pa}/i_{pc} of **3.6** is constant with increasing scan rate, i_{pa}/i_{pc} of **3.4** decreases dramatically. A dependence of i_{pa}/i_{pc} on scan rate suggests electron transfer at the electrode and the irreversible chemical reaction are occurring on similar timescales. In the case of **3.4**, at low scan rates a chemical reaction occurs before the return reduction scan and i_{pa}/i_{pc} is 1.96 at 50 mV s^{-1}. As the scan rate is increased, the reverse electrochemical process occurs within a shorter timeframe, less chemical decomposition is observed prior to reduction and i_{pa}/i_{pc} is 1.18 at 750 mV s^{-1}. The ratio of peak current for **2.15a** and **3.7** are close to unity and very little, if any, chemical reactivity is observed between anion oxidation and radical reduction. The relative stability of radicals **2.15a** and **3.4** – **3.7** can be inferred by comparing the peak current ratios at a given scan rate. It would appear the benzannelated **2.15a** and 3,4-pyridine annelated **3.7** nitronyl nitroxide

radicals are more chemically stable (at 10^{-3} M in nBu_4PF_6/CH_3CN, 25 ºC) than the 2-pyridyl radical **3.6**. Pyridine radical **3.6** is relatively more stable than phenanthrene radical **3.4** while pyrene derivative **3.5** is has the shortest lifetime. The account of relative chemical stability derived from the voltammetry data presented here is consistent with that observed by Bowles.[172]

As discussed above, the tetrabutylammonium quinoxaline nitronyl nitroxide salt **3.38** could not be isolated, thus voltammetric data on the **3.8/[3.8]**$^-$ redox couple could not be obtained from pure salt **3.38**. As protonated quinoxaline precursor **3.37** was of high purity, cyclic voltammetry was attempted on **3.37**. Protonated quinoxaline precursor **3.37** could be solubilized in nBu_4PF_6/CH_3CN (~0.5 mg mL^{-1}, standard voltammetry conditions) by non-nucleophilic bases, such as Proton Sponge® (*N,N,N′,N′*-tetramethyl-1,8-naphthalenediamine), TEA (triethylamine) or DBU (1,8-diazabicyclo[5.4.0]undec-7-ene).

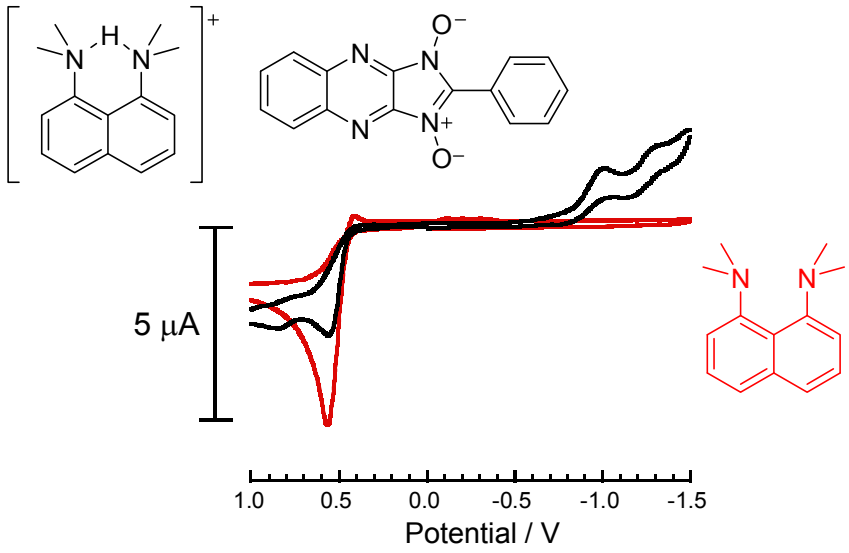

Figure 3.8. Cyclic voltammogram of Proton Sponge® before addition of quinoxaline nitronyl nitroxide precursor **3.37** (red) and after addition of **3.37** (black). 10 mM solution in CH_3CN, 0.1 M NBu_4PF_6, 50 mV s^{-1} scan rate. Peak potential has not been referenced to Fc/Fc^+ and is vs Ag wire pseudo-reference electrode.

The voltammogram of each base was recorded prior to dissolution of protonated precursor **3.37** and none had a redox process that would interfere with the reduction wave of quinoxaline nitronyl nitroxide radical **3.8**. Despite this, upon dissolution of **3.37** with any of the above amine bases, a peak associated with the **3.8/[3.8]**$^-$ redox couple was not observed. This is illustrated in Figure 3.8 where no redox processes are recorded between 0.6 and −0.9 V. The lack of an electrochemical redox process centred around 0 V and the presence of small irreversible processes at potentials greater than 0.5 V and less than −0.9 V is consistent with the species in solution no longer having annelated nitronyl nitroxide character. The difficulty encountered in isolation of the tetrabutylammonium quinoxaline nitronyl nitroxide salt **3.37** in combination with voltammetry data on protonated quinoxaline precursor **3.36** suggests the quinoxaline nitronyl nitroxide anion may not be chemically stable.

3.5 Stability: solution phase half-life

In order to properly quantify the relative stabilities of π-delocalized nitronyl nitroxide radicals **2.15a**, **3.4 – 3.8** spectroscopy was used in an attempt to determine the rate constant (k) and extrapolate a half-life ($t_{1/2}$) or time constant (τ) for the decay of each radical. It has been shown in our group that solid state isolation of phenanthrene **3.4** and pyrene **3.5** nitronyl nitroxide radicals is challenging as decomposition in solution occurs rapidly. Although all aza-subsituted nitronyl nitroxide radicals **3.6 – 3.8** were found to be more stable in solution,[172] concentration of the reaction solution resulted in a colour change and a product that was EPR silent.

In order to determine $t_{1/2}$, it was thought each radical could be oxidized with a source of silver(I) in situ and the decay, observed as decreasing radical absorbance, could be

monitored as a function of time. 10^{-5} M solutions of each radical precursor were prepared in distilled (dry, degassed) CH_2Cl_2 and transferred to a modified UV–vis cuvette which maintained an inert atmosphere over the course of the experiment. An equimolar amount of silver(I) hexafluorophosphate in distilled CH_2Cl_2 was added rapidly to the solution via syringe and the reaction was monitored by UV–vis spectroscopy (T = 24.4 ºC).

Unfortunately when this was attempted with the tetrabutylammonium phenanthrenimidazole salt **3.12** or pyreneimidazole salt **3.19** radical was never observed in any measurable quantity in solution. Pyreneimidazole nitronyl nitroxide radical has been reported to give a blue solution in benzene upon oxidation with PbO_2 or Ag_2O.[224] Most notably there is are two visible electronic transitions at 560 and 613 nm (benzene)[172] which were only observed as baseline perturbations and lasted no more than 4 min after silver(I) addition. Under these conditions, the rate constant for radical formation may be small when compared to the rate constant of radical decomposition ($k_{ox} << k_{decomp}$) for the pyrene and phenanthrene systems (Scheme 3.9). For this reason radical is not observed in any appreciable amount and any small transitions that appear are masked by peaks attributable to anion starting material and radical decomposition product(s).

Scheme 3.9. Proposed pathway for in situ generation of π-delocalized radicals.

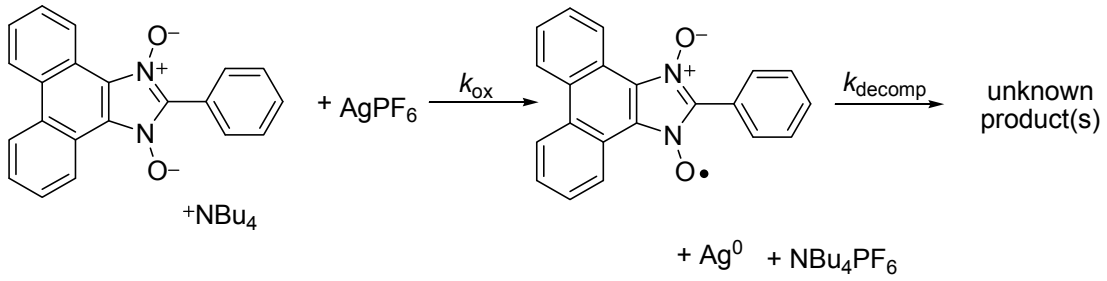

The oxidation potential of silver(I) is known to be dependent on solvent and counterion[230] and a variety of different silver(I) oxidation conditions were attempted. In addition a number of different oxidants were used in an attempt to increase k_{ox} relative to k_{decomp} (Table 3.5). None of the conditions proved successful and some oxidants, particularly lead dioxide and the nitrosonium salts, were too strong resulting in immediate formation of alternate product(s).

Table 3.3. Different conditions used when attempting in situ generation of phenanthrene nitronyl nitroxide radical **3.12**.

Oxidant	Solvent	Observations
$AgPF_6$	CH_2Cl_2	λ_{max} = 613 nm briefly observed
$AgPF_6$	CH_2Cl_2/EtOH[a]	λ_{max} = 613 nm briefly observed
AgOTf	CH_2Cl_2	λ_{max} = 613 nm briefly observed
$NOPF_6$	CH_3CN [b]	Over oxidation, radical not observed
$NOSbF_6$	CH_3CN	Over oxidation, radical not observed
$NOSbF_6$	CH_2Cl_2	Over oxidation, radical not observed
PbO_2	CH_2Cl_2	Over oxidation, radical not observed
BQ[c]	CH_2Cl_2	Over oxidation, radical not observed
Magic Blue[d]	CH_2Cl_2	Unknown if radical formed, aminium electronic transitions masked those for the radical

[a] Dichloromethane:ethanol solvent mixture in 3:1 ratio, ethanol was stirred over 4Å molecular sieves and purged with N_2 prior to use. [b] Acetonitrile is a common solvent for use with nitrosonium oxidants as it is one of the only solvents that dissolves the salt and is inert to the nitrosonium (aprotic). [c] BQ = benzoquinone. [d] Magic blue = tris(4-bromophenyl)aminium hexachloroantimonate.

The same methodology described above was used to measure k_{decomp} and $t_{1/2}$ for pyridine and quinoxaline nitronyl nitroxide radicals **3.6** – **3.8**. All nitrogen containing systems reacted immediately upon silver(I) addition to give bright orange insoluble powders. This reactivity was similar to that observed for *C*2-(4′-pyridyl) benzonitronyl

nitroxide **2.15b**. In all cases coordination of silver is suspected, although these products were difficult to characterize due to their insoluble nature.

In the end, in situ generation of these radicals may not be an appropriate way of determining kinetics parameters. This method was designed to gain insight into lifetime, however, the presence of anions, excess oxidant and any contaminants present in the oxidant (particularly silver(I) salts which are photosensitive) could be contributing to or providing new pathways for decomposition, skewing any kinetics derived from this method. Ideally each radical would be isolated as a pure solid, dissolved in a dry, degassed aprotic solvent and decomposition could be monitored without complicating factors such as the presence of ions. As previously discussed (Section 2.2) oxidation of the nitronyl nitroxide precursors is most commonly accomplished with PbO_2. The PbO_2 and its reduced by-products are removed by filtration and the crude reaction mixture is concentrated to dryness. In the case of radicals **3.4** – **3.8**, concentration results in the formation of EPR silent products. A new methodology was developed over the course of this work that allows for isolation of the radicals from solution by low temperature precipitation. This isolation technique may avoid the formation of closed shell products, unless the resulting species are a result of solid state dimerization. In addition to working out an isolation procedure that circumvents decomposition, an oxidation procedure employing an oxidant that does not bind nitrogen containing radicals must also be developed to allow for formation of pyridine and quinoxaline containing nitronyl nitroxide radicals. Finally, spectroelectrochemical experiments could be attempted and may allow for the observation of radical UV–vis spectra as well as the monitoring of radical decay, providing the radicals are stable under the electrochemical conditions.

3.6 Electronic structure calculations

A complete understanding of radical stability requires an exact knowledge of the location and degree of spin density residing on each atom in a given molecule. Polarized neutron diffraction (PND) measurements yield detailed spin density distribution maps. Unfortunately these measurements are costly and require large single crystals making the acquisition of PND data nontrivial. A more accessible spectroscopic technique, electron paramagnetic resonance (EPR) spectroscopy, can provide information on spin density distribution via determination of the isotropic hyperfine coupling constant (hfcc) for each nucleus. The hfcc for a given nucleus X, a(X) is directly proportional to spin density, $\rho(r_x)$ through the relationship in Equation 1[270] where g_e and g_0 are the isotropic g-values for a free electron and the radical respectively, γ_x is the gyromagnetic nuclear ratio and β_x is the nuclear magneton of nucleus X.

$$a(\mathrm{X}) = \frac{8\pi}{3}\frac{g_e}{g_0}\gamma_x\beta_x\rho(r_x) \qquad (1)$$

Although EPR spectroscopy will give the magnitude of spin density it cannot provide the sign. Additionally, the spin density can only be determined for atoms with a non-zero nuclear spin (I). Increasingly popular is the use of ab initio calculations to determine the sign and strength of spin density distribution on all nuclei, including those with values of I = 0. It was originally thought ab initio methods with large basis sets were necessary to predict hfcc's, however, more recently the use of density functional theory (DFT) with moderately sized basis sets has been shown to give reasonable results for spin density distribution in small radicals,[271] including simple nitronyl nitroxides such as **2.3**.[193,272-275] Of course the accuracy of DFT can range from poor to quite good depending on the basis set and functional used. Towards this end we have chosen to use the hybrid B3LYP[238]

functional with the EPR-II basis set,[258] a double-zeta plus polarization basis set which has been specifically optimized for computing hfcc's. DFT with UB3LYP/EPR-II has been shown to qualitatively reproduce experimental EPR and PND data well in simple imino nitroxide[276] and nitronyl nitroxide radicals.[270]

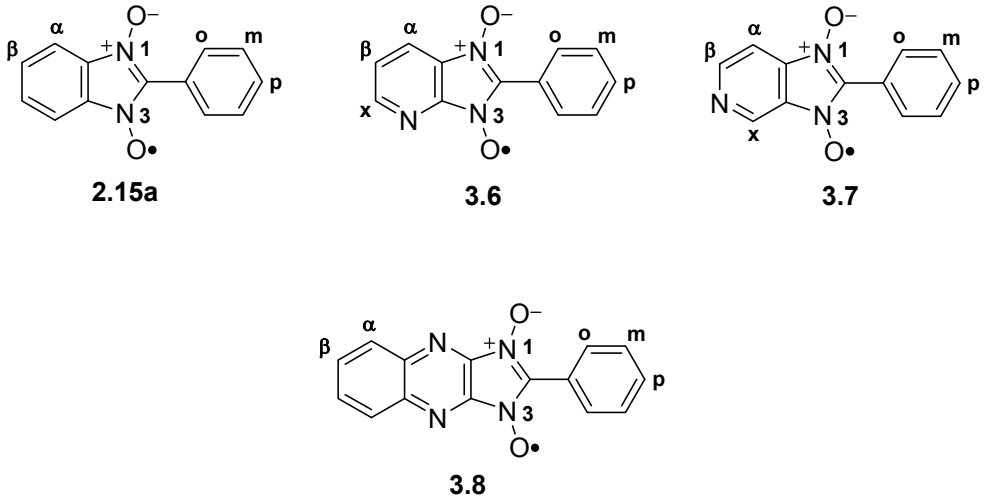

Figure 3.9. Labeled nitronyl nitroxide radicals for Table 3.4.

Table 3.4. Comparison of simulated and experimental[172] (EPR) hyperfine coupling constants (reported in Gauss) to nitrogen and hydrogen atoms in **2.15a** and **3.6 - 3.8**.

	2.15a		**3.6**		**3.7**		**3.8**	
atom	**calc**	**exptl**	**calc**	**exptl**	**calc**	**exptl**	**calc**	**exptl**
$a(N_1)$	2.86	4.37	2.51	4.139	2.59	3.990	2.78	4.232
$a(N_3)$	2.86	4.37	2.71	4.367	2.72	4.150	2.78	4.232
$a(N_{pyr})$	-	-	0.13	0.792	0.13	0.725	-	-
$a(N_{quin})$	-	-	-	-	-	-	0.38	0.440
$a(H_\alpha)$	-0.94	0.93	-0.67	0.725	-0.85	0.850	-0.29	0.407
$a(H_\beta)$	-0.72	0.65	-0.75	0.848	-1.18	0.906	-0.23	0.247
$a(H_x)$	-	-	-0.57	0.694	-0.81	0.703	-	-
$a(H_o)$	1.13	0.49	1.15	0.440	1.14	0.419	1.27	0.471
$a(H_m)$	-0.45	0.22	-0.46	0.201	-0.46	0.145	-0.50	0.190
$a(H_p)$	1.01	0.41	1.04	0.392	1.03	0.447	1.16	0.468

The hfcc's calculated using the EPR-II basis set can be compared to experimental hfcc's obtained by Steve Bowles (Table 3.4) for radicals for which well-resolved EPR spectra were collected (**2.15a** and **3.6** – **3.8**). Bowles was able to obtain an EPR spectrum of phenanthrene derivative **3.4**, however, the signal was broad due to decomposition of the sample and hydrogen hyperfine coupling could not be resolved.

Comparing the experimental data to the computational results presented in Table 3.4, we are confident the use of the UB3LYP functional with the EPR-II basis set is capable of qualitatively representing experimentally observed trend in hfcc among the series of annelated radicals. Most notably, the hfcc's to imidazolyl nitrogen ($a(N_1)$ and $a(N_3)$) are underrepresented computationally while the hfcc's to almost all hydrogen atoms are larger than those determined experimentally. This was not entirely unexpected and is, at least in part, due to the proclivity of density functional theory to over-delocalize π electrons. Nevertheless, experimental trends across the series, particularly the decrease in $a(N_1)$ and $a(N_3)$ with the incorporation of additional nitrogen atoms are reproduced well computationally. With confidence that our selected computational method was representing experimental trends we calculated the spin density distribution for the remaining radicals. These results are presented visually in Figure 3.10 and reported in Table 3.5 as Mulliken spin density, which is a direct representation of the spin population in the ground state.

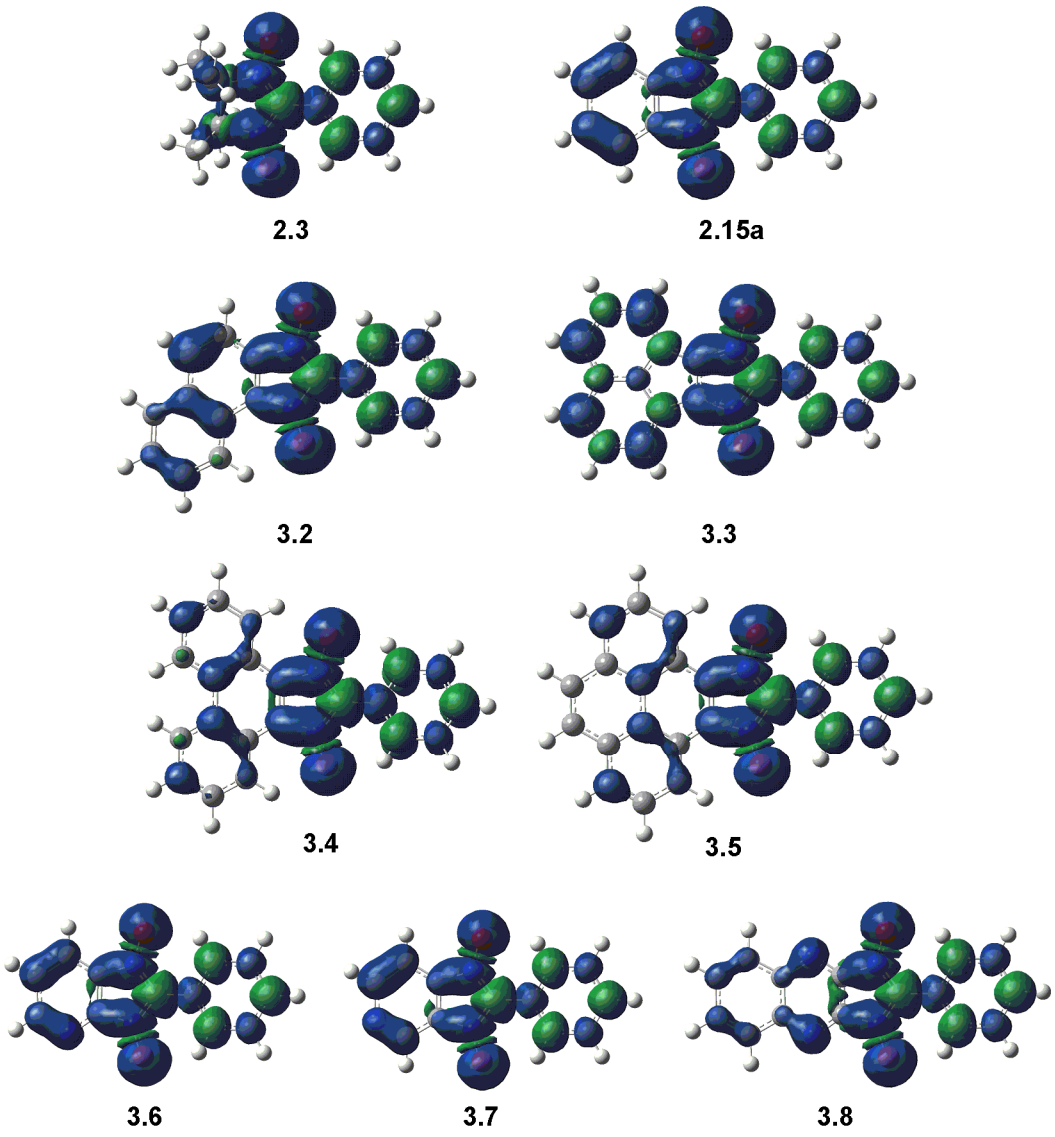

Figure 3.10. Spin density of radicals **2.3**, **2.15a**, **3.1 – 3.8** generated with GaussView 4.1.2, grid = coarse, isovalue = 0.02. Positive spin density is blue while negative spin density appears green.

In general we find the singly occupied molecular orbital (SOMO) to be largely concentrated on the N and O nitroxide atoms, consistent with the larger class of nitronyl nitroxide radicals. The spin populations on O and N are large and positive (blue, Figure 3.10; see also Table 3.5) due to the positive orbital coefficient present on these atoms.

Also observed in all of **2.1**, **2.15a** and **3.2 – 3.8** is a non-negligible negative spin population on *C*2 which originates from spin polarization of the bonding electrons.

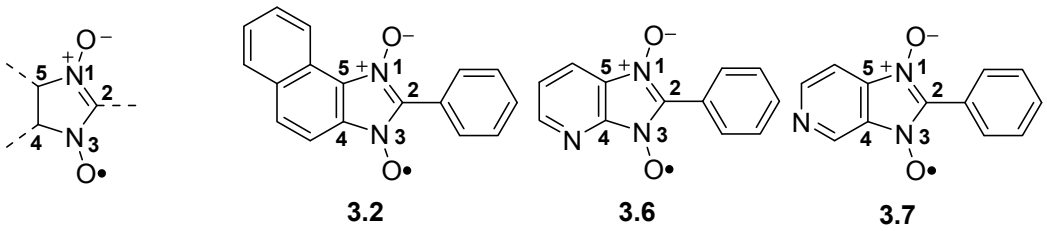

Figure 3.11. Labeled nitronyl nitroxide radicals. Left shows labeling scheme for nitronyl nitroxide when *N*1 = *N*1 and *C*4 = *C*5. The three radicals that do not contain C_{2v} symmetry are drawn in full to distinguish *C*4 from *C*5.

Table 3.5. Mulliken spin densities for N and C atoms in imidazole dioxide ring for radicals **2.3**, **2.15a**, **3.1 – 3.8** as calculated using UB3LYP/EPR-II.

atom	2.3	2.15a	3.2	3.3	3.4	3.5	3.6	3.7	3.8
N_1	0.278	0.188	0.176	0.158	0.176	0.177	0.178	0.178	0.182
N_3	0.278	0.188	0.183	0.158	0.176	0.177	0.181	0.182	0.182
C_2	-0.204	-0.175	-0.167	-0.159	-0.163	-0.165	-0.178	-0.176	-0.189
C_4	-0.012	0.0049	0.0046	0.034	0.027	0.025	0.020	0.0005	-0.0013
C_5	-0.012	0.0049	0.042	0.034	0.027	0.025	0.0092	0.020	-0.0014
N_{pyr}	-	-	-	-	-	-	0.024	0.014	-
N_{quin}	-	-	-	-	-	-	-	-	0.037

Perhaps the greatest difference across the series is the degree of spin density on the bridge carbons between the imidazole and benzannelated rings (*C*4 and *C*5). In tetramethyl nitronyl nitroxide **2.3** negative spin density is present on *C*4 and *C*5. The opposite is observed in benzonitronyl nitroxide **2.15a** where a small amount of positive spin density is observed on *C*4 and *C*5. Spin density at *C*4 and *C*5 is positive in **2.15a** as the SOMO extends over these carbon atoms, whereas in **2.3** it is highly localized on N and O. The least stable radicals, those based on phenanthrene **3.4** and pyrene **3.5** had positive spin densities nearly an order of magnitude greater than **2.15a** on *C*4/5. Initially

it was believed we would be able to correlate radical instability to the presence of a high degree of spin density on peripheral aromatic carbon atoms (those on the annelated ring furthest from the ONCNO core). This was based on the idea that the primary pathway for the generation of a diamagnetic species in triphenylmethyl radical **1.1** is through σ-dimerization[277] (Figure 3.12). It would seem this would be a possible spin annihilation mechanism here, if a large degree of spin were residing on peripheral phenanthrene or pyrene carbon atoms. Even a qualitative assessment of these systems (**3.4** and **3.5**, Figure 3.10) shows negligible spin density is delocalized over the annelated aromatic ring. Additionally, the spin density that is delocalized into the annelated ring is localized primarily on atoms that are sterically hindered, making σ-dimerization unlikely.

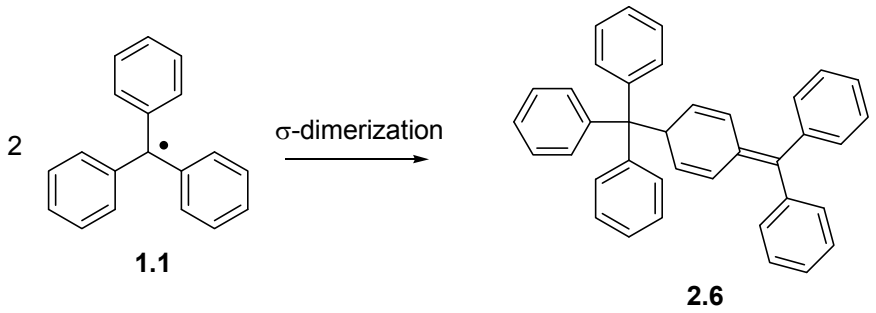

Figure 3.12. σ-dimerization pathway in triphenylmethyl radical **1.1** to give dimeric **2.6**.

Although a decomposition mechanism is not obvious, a large degree of spin density on a non-electronegative atom makes for a more reactive site. We are confident that the decomposition products are EPR silent, thus $S = ½$ units are no longer present in solution. It may be that the presence of large positive spin density at *C*4 and *C*5 (relative to **2.3**) makes these molecules particularly susceptible to disproportionation or dimerization.

Quinoxaline nitronyl nitroxide radical **3.8** has a spin density distribution more akin to tetramethyl nitronyl nitroxide **2.3** where negative spin density is present on *C*4 and *C*5.

Additionally, $E_{1/2}$(red) is predicted to be positive vs SCE, that is even more strongly accepting than benzonitronyl nitroxide **2.15a**. The strong acceptor ability of **3.8** makes it an attractive synthetic target as so few organic electron acceptors are known that can be reduced at such a low reduction potential. If radical stability is strongly dependent on spin density distribution, **3.8** would be predicted to be stable and should be isolable under the conditions described in Chapter 2 (precipitation at −78 ºC). Bowles demonstrated radical **3.8** could be generated by oxidation of protonated precursor **3.37** with lead dioxide in CH_2Cl_2 and an EPR spectrum was obtained, however, upon concentration of the solution diamagnetic products were formend. In the end, although **3.8** may be stable from a spin density perspective, alternate decomposition pathways such as hydrolysis of the fused quinoxaline-imidazole ring may be operative resulting in radical decomposition.

The experimentally determined half-wave reduction potential can be compared to the calculated electron affinity (EA) for each radical. The electron affinity was computed as the difference between the total energies for the ground state of the neutral radical and its respective anion. A single point calculation was performed for the closed-shell anion (singlet, charge = −1) and neutral radical (doublet, charge = 0) to determine the zero-point energy of each state. The gas-phase geometry optimized structure determined from the appropriate UB3LYP/EPR-II calculation was taken to be the ground state structure. Each energy calculation was performed using density functional theory (DFT) with the spin-unrestricted B3LYP functional (UB3LYP). The 6-31+G(d,p) basis set was selected as it includes diffuse functions to account for the more disperse orbitals on each anion. As

the geometry of the anion was not optimized this method of calculating EA assumes a vertical excitation (i.e. no structural relaxation).

The calculated electron affinity for each radical is reported in Table 3.1. As the radical half-wave reduction potential shifted to lower potential the calculated electron affinity increased accordingly, thus electron affinity and reduction potential correlate well across the series. Given that changes in reduction potential are well represented computationally by EA, the reduction potential of quinoxaline nitronyl nitroxide radical **3.8** can be approximated. The EA of quinoxaline radical **3.8** was calculated to be 2.35 eV, which is between that of **3.6** and **3.7**, suggesting the reduction potential of **3.8** would lie somewhere between 0.09 and 0.17 V vs SCE. This makes radical **3.8** a particularly desirable target as its spin density distribution is akin to the more stable tetramethyl nitronyl nitroxide **2.2**, while its reduction potential is estimated to be nearly as positive as TCNQ.

3.7 Conclusions

Of the targets described at the outset of this chapter, the tetrabutylammonium salts of phenanthrene, pyrene, and two pyridine nitronyl nitroxides were successfully synthesized. Each of these anions was studied by cyclic voltammetry and compared to benzonitronyl nitroxide **2.15a**. The reduction potential of each π-delocalized (**3.4**, **3.5**) or heterocyclic (**3.6**, **3.7**) radical shifted to more positive potential making these systems the most easily reduced organic radicals reported to date. In addition, the reduction potential was compared to calculated electron affinity of each radical and computational and experimental data were found to be in good agreement. In the case of **3.4** and **3.5**, the

formation of radical was followed by a rapid chemical reaction, consistent with the chemical instability previously observed for these systems. The peak current ratios provided information about the relative stability of the π-delocalized and heteroaromatic radicals. Using peak current ratios, the approximate relative stability of the series of nitronyl nitroxide radicals investigated is as follows: **2.15a** ≈ **3.7** > **3.6** >> **3.4** > **3.5**. Attempts at obtaining solution phase kinetic parameters to corroborate the stability derived from voltammetry data have thus far been unsuccessful due to difficulties associated with generation and isolation of this series of radicals.

Spin density distribution and hyperfine coupling constants were calculated for each of **2.3**, **2.15a**, **3.4** - **3.7** using the EPR-II basis set. Experimentally determined hyperfine coupling constants were compared to those determined computationally and although exact numerical values deviated significantly from experiment, the changes observed experimentally over the series were reproduced well computationally. Analysis of computed spin density distribution suggests that upon annelation spin density shifts from benzimidazole nitrogen atoms onto annelated carbon atoms. Interestingly, stabilization of the annelated radicals was not as simple as increasing spin delocalization as, in the case of the phenanthrene **3.4** and pyrene **3.5** nitronyl nitroxide radicals, increased delocalization resulted in a decrease in radical stability. The electronegativity of the atom bearing spin may be important, although it is not clear the inclusion of nitrogen atoms in the annelated ring stabilized **3.5** and **3.6** relative to **2.15a**. The least stable radicals had a greater proportion of spin density on bridging carbons potentially increasing reactivity at these sites. Most importantly, we were able to use DFT to reproduce experimental trends

across this series suggesting computational analysis of electron affinity and spin density distribution may be used to screen future targets prior to their synthesis.

Originally we intended to establish which of reduction potential or spin density distribution was the factor responsible for the observed instability of the annelated nitronyl nitroxide radicals. Cyclic voltammetry suggests low reduction potential is not the determining factor within the series as phenanthrene radical **3.4** and pyridine radical **3.6** have nearly identical reduction potentials yet the phenanthrene system **3.4** is undoubtedly less stable. The distribution of spin throughout the molecular framework is therefore more important than reduction potential when considering *relative* stability of the annelated radicals. However, the low reduction potential of the annelated nitronyl nitroxide radicals must contribute to the decrease in stability relative to the far less redox active tetramethyl nitronyl nitroxide series, suggesting that the overall stability of the annelated nitronyl nitroxides is dictated by a subtle interplay of spin density distribution and reduction potential.

3.8 Experimental

3.8.1 General procedures

General Methods. All general synthetic procedures employed have been previously reported in Chapter 2.9. 1,2-Naphthoquinone was recrystallized from benzene prior to use.

Computations. Quantum mechanical calculations were carried out at the UB3LYP[237,238] /epr-II[258] level of theory using the Gaussian 09 package.[239] Ionization potentials were calculated by taking the difference between the total energy of the anion

and neutral radical. Total energies were calculated using DFT UB3LYP[237,238]/6-31+G(d,p). No zero point energy correction was performed, as all structures would scale equally. The input structure was the geometry optimized structure determined from the #opt UB3LYP/EPR-II calculation. The single point energy of the anion was determined using geometry of neutral species, thus the excitations were assumed to be vertical.

Cyclic Voltammetry. Voltammograms were obtained from degassed 1 mM radical solutions in 0.1 M nBu_4PF_6/CH_3CN solutions at 300 K using a 3.0 mm diameter glassy carbon working electrode, platinum counter electrode, and Ag wire pseudo-reference electrode. The uncompensated resistance (iR) was measured and subtracted prior to the collection of each voltammogram. Ferrocene was used as an internal standard and all spectra are reported vs SCE (Fc/Fc^+ = 0.40 V vs SCE in acetonitrile/nBu_4PF_6).[230] Peak potentials (E_p) and peak currents (i_p) were extracted using BASi software.

3.8.2 Synthesis

Benzaldoxime (3.9).[278] Benzaldehyde (5.60 g, 53 mmol) and hydroxylamine hydrochloride (10.97 g, 158 mmol) were dissolved in 50 mL EtOH. Pyridine (5 mL) was added to the reaction flask and the solution was stirred at rt and monitored by TLC (CH_2Cl_2). After stirring for 4.5 h the reaction was complete by TLC. The EtOH was removed by rotary evaporation and the residue was suspended in 50 mL distilled water with sonication. The water layer was extracted with CH_2Cl_2 (3 x 50 mL) and the combined organic layers were washed with brine and dried over $MgSO_4$. The clear colorless solution was concentrated *en vacuo* to give 6.23 g (51 mmol, 97 %) of colourless oil. ^{1}H NMR confirmed further purification was not necessary. IR (KBr) cm^{-1}: 3306, 2896, 1632, 1577, 1493, 1445, 1304, 1289, 1210, 1075, 951. ^{1}H NMR (300 MHz,

$CDCl_3$): δ 9.58 (bs, 1H), 8.21 (s, 1H), 7.61 – 7.59 (m, 2H), 7.41 – 7.38 (m, 3H). ^{13}C NMR (75 MHz, $CDCl_3$): δ 150.5, 131.9, 130.2, 128.9, 127.2. EI-MS (70 eV) *m/z*: 121 $[M]^+$, 104 $[M - OH]^+$.

9,10-Phenanthrenequinone monoxime (3.10).[279] A suspension of 9,10-phenanthrenequinone (0.606 g, 2.6 mmol) and barium carbonate (1.57 g, 8.0 mmol, 3 eq) in EtOH (15 mL) was stirred at rt. Hydroxylamine hydrochloride (0.181 g, 2.6 mmol) was added to the suspension and the reaction was heated to reflux and monitored by TLC (CH_2Cl_2). After 5 h a bright yellow precipitate had formed and the reaction was complete by TLC. The reaction was cooled to rt and acetone (20 mL) was added to the stirring mixture. The suspension was filtered to remove salts and the orange solution was concentrated to dryness *en vacuo* yielding 0.560 g (2.3 mmol, 87 %) of an orange solid. mp 148 – 150 ºC (lit[280] 157 ºC). IR (KBr) cm^{-1}: 1675, 1599, 1526, 1449, 1342, 1281, 1117, 1091, 985, 757, 727. Note: *isomers present in NMR spectra.* ^1H NMR (300 MHz, d_6-DMSO): δ 9.39 (dd, J = 8, 2 Hz, 0.3H), 8.37 (ddd, J = 8, 2, 1 Hz, 0.9H), 8.32 (ddd, J = 8, 2, 1 Hz, 1.0H), 8.15 (dd J = 8, 1 Hz, 1.4H), 8.07 (dd, J = 8, 1 Hz, 0.9H), 7.98 (dd, J = 8, 2 Hz, 0.3H), 7.76 (ddd, J = 8,7, 2 Hz, 1.0H), 7.69 (ddd, J = 8, 7, 2 Hz, 0.3H), 7.59 – 7.39 (m, 3.4H). ^{13}C NMR (75 MHz, d_6-DMSO): δ183.3, 179.3, 179.0, 145.7, 144.0, 136.1, 136.0, 135.4, 135.3, 135.2, 134.9, 131.1, 130.6, 130.3, 129.8, 129.5, 129.2, 129.1, 129.0, 128.7, 128.5, 128.0, 127.1, 125.3, 124.4, 124.3, 124.0, 123.9, 123.8, 123.7. EI-MS (70 eV) *m/z*: 223 $[M]^+$.

1-Hydroxyl-2-phenyl-phenanthro[9,10-*d*]imidazole 3-oxide (3.11).[224] A solution of benzaldoxime **3.9** (0.253 g, 2.1 mmol) and 9,10-phenanthrenequinone monoxime **3.10** (0.441 g, 2.0 mmol) were combined in dry 100 % EtOH (15 mL) to give a bright orange

solution. $HCl_{(g)}$ was bubbled through the solution for 30 min, then the reaction was stirred at rt for 18 h. After 18 h the reaction a tan precipitate was present. The reaction was neutralized to pH = 7 with 10 % $NaHCO_3$ and the solids were isolated by vacuum filtration and washed with EtOH, acetone, and pentane and air dried to give 0.633 g (1.9 mmol, 98 %) of a tan powder. mp decomp. 180 – 182 ºC. IR (KBr) cm^{-1}: 3399, 3058, 1529, 1451, 1430, 1414, 1230, 1051, 1036, 746, 720, 690. For solubility reasons characterization by NMR and MS performed on deprotonated salt **3.12**.

[Tetrabutylammonium][2-Phenyl-phenanthro[9,10-*d*]imidazole 1,3-dioxide] (3.12). 1-hydroxyl-2-phenyl-phenanthro[9,10-*d*]imidazole 3-oxide **3.11** (0.035 g, 0.10 mmol) was suspended in 5:1 acetone:EtOH (6 mL) and sonicated for 5 min creating a fine tan suspension. While sonicating, 1.0 M NBu_4OH (0.10 mL, 0.10 mmol) was added dropwise creating a yellow-green solution. The solution was filtered through a Celite-545 pad and concentrated *en vacuo*. The resulting oil was dissolved in a minimum amount of acetone and poured into hexanes causing a fine yellow powder to precipitate. The powder was isolated by vacuum filtration, washed with hexanes and air dried yielding 0.054 g (0.095 mmol, 95 %) of a yellow-green powder. ^{1}H NMR (300 MHz, d_6-DMSO): δ 9.90 (d, J = 8 Hz, 2H), 9.31 (d, J = 8 Hz, 2H), 8.66 (d, J = 8 Hz, 2H), 7.56 – 7.43 (m, 6H), 7.31 (t, J = 8 Hz, 1H), 3.13 – 3.08 (m, 8H), 1.53 – 1.41 (m, 8H), 1.27 – 1.22 (m, 8H), 0.88 (t, 12H). ^{13}C NMR (75 MHz, d_6-DMSO): δ 131.4, 127.6, 127.0, 126.9, 126.1, 124.4, 122.8, 117.5, 57.4, 23.0, 19.1, 13.4. ESI-MS (negative ion mode) *m/z*: 325.6 $[M]^-$.

9,10-Phenanthrenequinone dioxime (3.13).[281,282] A mixture of 9,10-phenanthrenequinone (3.26 g, 15.7 mmol), hydroxylamine hydrochloride (20.17 g, 290 mmol), pyridine (10 mL) and EtOH (80 mL) were heated at reflux for 20 h during which

time the color of the solution changed from yellow to green. After 20 h the reaction was cooled to rt and left to stand for 2 h. Upon standing colorless needles of pyridine hydrochloride crystallized from solution and were removed by vacuum filtration. The filtrate was isolated and distilled water (150 mL) was added to the solution causing immediate formation of a light green precipitate. The precipitate was isolated by vacuum filtration and washed with water. The crude solid was recrystallized from MeOH/H_2O yielding 1.93 g (8.1 mmol, 52 %) of a green-yellow microcrystalline solid. mp decomp. 194 – 196 ºC (lit[283] 197 – 200 ºC). IR (KBr) cm^{-1}: 3186, 1560, 961, 947, 913, 756. Note: *isomers present in NMR spectra.* ^{1}H NMR (300 MHz, d_6-DMSO): δ 12.47 (s, 1.0H), 12.30 (s, 1.0H), 12.19 (d, J = 8 Hz, 1.6H), 8.68 (d, J = 8 Hz, 1.4H), 8.48 – 8.42 (m, 3.2H), 8.10 – 8.03 (m, 3.7H), 7.88 – 7.71 (m, 4.7H), 7.56 – 7.38 (m, 7.5H). ^{13}C NMR (75 MHz, d_6-DMSO): δ 147.7, 145.7, 144.7, 144.2, 132.7, 132.5, 131.8, 131.7, 131.1, 130.8, 130.6, 130.4, 130.3, 129.8, 129.6, 129.5, 129.2, 128.5, 128.3, 127.7, 127.4, 126.3, 125.9, 125.6, 124.8, 124.6, 124.4, 124.3, 124.2, 123.9, 119.4. EI-MS (70 eV) *m/z*: 238 $[M]^+$, 207 $[M - NOH]^+$.

Phenanthro[9,10-*c*][1,2,5]oxadiazole N-oxide (3.14). 9,10-phenanthrenequinone dioxime **3.13** (1.53 g, 6.4 mmol) was suspended in 10 % w/w KOH in EtOH (50 mL). Aqueous NaOCl (10.8 % w/w, 50 mL) was added dropwise over 30 min and the reaction was monitored by TLC (CH_2Cl_2). Once complete, the reaction was poured into H_2O (50 mL) and the aqueous layer was extracted with CH_2Cl_2 (3 x 100 mL). The combined organic layers were washed with brine, dried over $MgSO_4$ and concentrated *en vacuo* to give 1.27 g (5.4 mmol, 84 %) of a tan solid. mp 190 – 192 ºC. IR (KBr) cm^{-1}: 1626, 1612, 1602, 1523, 1510, 1468, 1452, 1420, 1088, 992, 955, 755, 722. Note: *isomers*

present in NMR spectra. ^{1}H NMR (300 MHz, $CDCl_3$): δ 8.61 (ddd, J = 8, 2, 1 Hz, 2H), 8.51 (dd, J = 8, 2 Hz, 3H), 8.43 (td, J = 8, 2 Hz, 5H), 8.35 (d, J = 8 Hz, 4H), 7.78 – 7.62 (m, 14H). ^{13}C NMR (75 MHz, $CDCl_3$): δ 150.8, 148.0, 132.2, 132.1, 131.5, 131.1, 130.6, 130.5, 129.1, 128.9, 128.8, 126.4, 124.2, 124.0, 123.8, 123.7, 121.2, 120.5, 118.2. ESI-MS (positive ion mode) *m/z*: 259.8 $[M + Na]^+$.

1-Hydroxyl-2-phenyl-phenanthro[9,10-*d*]imidazole 3-oxide (3.11). Phenanthro[9,10-*c*][1,2,5]oxadiazole 1-oxide **3.14** (0.207 g, 0.88 mmol) and *C*-phenyl-*N*-phenylnitrone **2.21a** (0.249 g, 1.26 mmol) were dissolved in dry toluene (25 mL) under an N_2 atm. The light brown solution was heated gently (60 ºC) for 48 h. No reaction was observed by TLC (CH_2Cl_2). After 48 h the temperature was increased and the reaction was refluxed an additional 48 h. No reaction was observed by TLC (CH_2Cl_2). The phenanthrenefuroxan **3.14** was recovered from the reaction mixture (flash chromatography, silica gel, CH_2Cl_2 as eluent) yielding 0.150 g (0.63 mmol, 72 % recovery).

1-Hydroxyl-2-(4-nitrophenyl)-phenanthro[9,10-*d*]imidazole 3-oxide (3.15i). Phenanthro[9,10-*c*][1,2,5]oxadiazole 1-oxide **3.14** (0.150 g, 0.63 mmol) and *C*-(4-nitrophenyl-*N*-phenylnitrone **2.21i** (0.241 g, 1.0 mmol) were dissolved in dry toluene (20 mL) under an N_2 atm. The yellow solution was heated gently (60 ºC) for 48 h. No reaction was observed by TLC (CH_2Cl_2). After 48 h the temperature was increased and the reaction was refluxed an additional 48 h. No reaction was observed by TLC (CH_2Cl_2). The phenanthrene furazan oxide **3.14** crystallized cleanly from the reaction mixture upon cooling and was recovered quantitatively.

1-Hydroxyl-2-(2,3,4-trimethoxyphenyl-phenanthro[9,10-*d*]imidazole 3-oxide (3.15j). Phenanthro[9,10-*c*][1,2,5]oxadiazole 1-oxide **3.14** (0.115 g, 0.49 mmol) and *C*-(2,3,4-trimethoxyphenyl-*N*-phenylnitrone **2.21j** (0.194 g, 0.68 mmol) were dissolved in dry toluene (10 mL) under an N_2 atm. The yellow solution was refluxed gently for 48 h. No reaction was observed by TLC (CH_2Cl_2). The phenanthrene furazan oxide **3.14** crystallized cleanly from the reaction mixture upon cooling and was recovered quantitatively.

4,5-Pyrenedione (3.16).[265,284,285] Pyrene (2.04 g, 10.1 mmol) and $RuCl_3 \cdot xH_2O$ (0.2 g, 1 mmol, 0.1 eq) were dissolved in 1:1 CH_3CN:CH_2Cl_2 (80 mL). Separately, $NaIO_4$ (10.0 g, 47 mmol, 4.7 eq) was dissolved in distilled H_2O (80 mL). The $NaIO_4$ solution was added in one portion to the stirring pyrene solution. The reaction was loosely capped with a rubber septum and stirred at room temperature. After 10 min the reaction was complete (TLC, CH_2Cl_2). The solution was poured into H_2O (500 mL) and the organic phase was separated. The aqueous phase was washed with CH_2Cl_2 (3 x 50 mL) and the organic layers were combined. The organics were washed with water (3 x 200 mL) and brine (1 x 200 mL), dried over $MgSO_4$ and concentrated *en vacuo* to give a brown solid. The crude solid was purified by column chromatography (silica gel, CH_2Cl_2 as eluent) yielding 0.95 g (4.1 mmol, 41 %) of a bright orange powder. A second product was isolated and confirmed by ^{1}H NMR to be bis-oxidized pyrene (4,5,9,10-pyrenetetrone). mp 285 – 287 ºC (lit[266] 302 – 304 ºC). IR (KBr) cm^{-1}: 1676, 1671, 1617, 1560, 1522, 1352, 1270, 836, 707. ^{1}H NMR (300 MHz, CD_2Cl_2) δ 8.43 (dd, J = 7, 1 Hz, 2H), 8.20 (dd, J = 8, 1 Hz, 2H), 7.87 (s, 2H), 7.79 (t, J = 8 Hz, 2H). ^{13}C NMR (75 MHz, CD_2Cl_2): δ 180.5, 136.2,

132.8, 131.8, 129.9, 129.2, 129.0, 128.4. ESI-MS (positive ion mode) *m/z*: 233.5 $[M + H]^+$.

4,5-Pyrenedione monoxime (3.17). A suspension of 4,5-pyrenedione **3.16** (0.507 g, 2.18 mmol) and $BaCO_3$ (1.31 g, 6.6 mmol, 3 eq) in EtOH (30 mL) was stirred at rt. Hydroxylamine hydrochloride (0.154 g, 2.21 mmol) was added to the suspension in one portion. The mixture was sonicated for 15 min, then refluxed for 18 h. Upon cooling, the solvent was removed under reduced pressure to give a light orange paste. 0.1 M HCl (50 mL) was added and the suspension was stirred for 30 min. The solid was isolated by vacuum filtration, washed with water and air dried yielding 0.500 g (2.02 mmol, 93 %) of a light orange solid. mp decomp. 232 – 234 ºC. IR (KBr) cm^{-1}: 3178, 1677, 1655, 1649, 1623, 1578, 1420, 1410, 1350, 1283, 1244, 1108, 1121, 1009, 1001, 832, 712. Note: *isomers present in NMR spectra.* ^1H NMR (300 MHz, d_6-DMSO) δ 9.30 (d, J = 1 Hz, 0.9H), 8.37 (dd, J = 7, 1 Hz, 1.0H), 8.29 (dd, J = 8, 1 Hz, 1.2H), 8.08 (dd, J = 8, 1 Hz, 1H), 7.94 – 7.72 (m, 4.4H). ^{13}C NMR (75 MHz, CD_2Cl_2): δ 179.3, 144.1, 134.8, 134.4, 134.2, 131.2, 131.1, 130.9, 130.2, 129.0, 128.9, 128.8, 128.5, 128.0, 127.7, 127.5, 127.4, 127.2, 127.0, 126.9, 126.5, 126.3, 124.5, 123.1, 122.7, 121.5. EI-MS (70 eV) *m/z*: 247 $[M]^+$, 231 $[M - O]^+$, 216 $[M - NOH]^+$.

1-Hydroxyl-2-phenyl-pyreno[4,5-*d*]imidazole 3-oxide (3.18). A solution of benzaldoxime **3.9** (0.519 g, 4.29 mmol) and 4,5-pyrenedione monoxime **3.17** (0.395 g, 1.60 mmol) were combined in dry 100 % EtOH (15 mL). $HCl_{(g)}$ was bubbled through the solution for 30 min, then the reaction was stirred at rt for 48 h. After 48 h the reaction a tan precipitate was present. The precipitate was isolated by vacuum filtration and washed with EtOH, acetone, and pentane and air dried to give 0.396 g (1.13 mmol, 71 %) of a tan

powder. mp decomp. 182 – 184 ºC. IR (KBr) cm^{-1}: 3050, 1602, 1459, 1438, 1388, 1317, 1190, 1161, 1106, 831, 763, 745, 716. Anal. Calcd for $C_{23}H_{14}N_2O_2$: C, 78.84; H, 4.03; N, 8.00. Found: C, 78.27; H, 3.72; N, 8.19. For solubility reasons characterization by NMR and MS performed on deprotonated salt **3.19**.

[Tetrabutylammonium][2-Phenyl-pyreno[4,5-*d*]imidazole 1,3-dioxide] (3.19). 1-hydroxyl-2-phenyl-pyrene[4,5-*d*]imidazole 3-oxide **3.18** (0.267 g, 0.76 mmol) was suspended in 2:1 acetone:EtOH (15 mL) and sonicated for 5 min creating a fine tan suspension. While sonicating, 1.0 M NBu_4OH (0.75 mL, 0.75 mmol) was added dropwise creating an orange solution. The solution was filtered through a Celite-545 pad and concentrated *en vacuo*. The resulting oil was dissolved in a minimum amount of acetone and added dropwise to 100 mL hexanes causing a fine yellow powder to precipitate. The powder was isolated by vacuum filtration, washed with cold pentane and air dried yielding 0.296 g (0.50 mmol, 67 %) of a yellow powder. ^{1}H NMR (300 MHz, d_6-DMSO): δ 10.03 (d, J = 7 Hz, 2H), 9.43 (d, J = 8 Hz, 2H), 8.10 – 8.06 (m, 4H), 7.96 (t, J = 8 Hz, 2H), 7.48 (t, J = 8 Hz, 2H), 7.32 (t, J = 8 Hz, 1H), 3.12 – 3.05 (m, 8H), 1.51 – 1.45 (m, 8H), 1.26 – 1.22 (m, 8H), 0.87 (t, 12H). ^{13}C NMR (75 MHz, d_6-DMSO): δ 132.7, 129.6, 128.9, 128.7, 128.6, 128.2, 127.3, 125.4, 124.8, 123.6, 121.3, 119.7, 59.1, 24.7, 20.8, 15.1. ESI-MS (negative ion mode): *m/z* 349.0 $[M]^-$.

1,2-Acenaphthylenedione Monoxime (3.20).[286] 1,2-acenaphthenequinone (1.074 g, 5.89 mmol) and hydroxylamine hydrochloride (0.406 g, 5.85 mmol) were suspended in EtOH (20 mL). Pyridine (2 mL) was added to the flask and the reaction was sonicated at rt and monitored by TLC (90:10 CH_2Cl_2:EtOH). After 2 h the reaction was complete by TLC. The yellow solution was concentrated by rotary evaporation yielding a yellow solid

that was purified by column chromatography (silica gel, CH_2Cl_2 as eluent) yielding 0.935 g (4.74 mmol, 81 %) of a light yellow solid. mp decomp. 200 – 202 ºC. IR (KBr) cm^{-1}: 3247, 1730, 1605, 1432, 1277, 1181, 1017, 995, 859, 830, 779. ^{1}H NMR (300 MHz, d_6-DMSO) δ 13.34 (s, 1H), 8.27 (t, J = 8 Hz, 2H), 8.09 (d, J = 8 Hz, 1H), 7.98 (d, J = 7 Hz, 1H), 7.84 – 7.70 (m, 2H). Note: *isomers present in ^{13}C NMR when DMSO used as NMR solvent.* ^{13}C NMR (75 MHz, d_6-DMSO): δ 188.1, 149.0, 138.9, 132.2, 132.0, 131.4, 130.1, 128.6, 128.3, 128.2, 127.7, 126.6, 124.8, 121.6, 121.1. EI-MS (70 eV) *m/z*: 197 $[M]^+$.

1-Hydroxyl-2-phenyl-acenaphthyleno[1,2-*d*]imidazole 3-oxide (3.21). A solution of benzaldoxime **3.9** (0.278 g, 2.3 mmol) and 1,2-acenaphthylenedione monoxime **3.20** (0.352 g, 1.8 mmol) were combined in dry 100 % EtOH (30 mL). $HCl_{(g)}$ was bubbled through the solution for 30 min, then the reaction was capped loosely with a rubber septum and stirred at rt for 72 h and monitored by TLC (9:1 CH_2Cl_2:EtOH). No reaction was observed.

1,2-Napthalenedione dioxime (3.23). A suspension of 1,2-naphthoquinone (1.31 g, 8.3 mmol) and $BaCO_3$ (9.79 g, 49.6 mmol, 6 eq) in EtOH (100 mL) was sonicated at rt. Hydroxylamine hydrochloride (1.69 g, 24.3 mmol) was added in one portion to the suspension. The reaction was sonicated for 2 h then stirred at room temperature for 14 h. After 14 h the reaction was neutralized (pH = 7) with 5 % HCl and left to stand at rt. A dark yellow solid precipitated from solution and was isolated by vacuum filtration, washed with distilled H_2O and dried *en vacuo.* The crude solid was recrystallized from EtOH yielding 1.29 g (6.9 mmol, 83 %) of a yellow-brown solid. mp 76 – 78 ºC. IR (KBr) cm^{-1}: 3247, 1670, 1655, 1594, 1438, 1384, 1309, 1066, 929. ^{1}H NMR (300 MHz,

d_6-DMSO) : δ 13.65 (bs, 0.9H), 8.02 (d, J = 8 Hz, 1H), 7.68 (td, J = 8, 2 Hz, 1H), 7.54 – 7.47 (m, 2H), 7.12 (d, J = 10 Hz, 1H), 7.02 (d, J = 10 Hz, 1H). ^{13}C NMR (75 MHz, d_6-DMSO): δ 181.3, 147.8, 136.4, 134.6, 131.2, 130.2, 129.1, 128.9, 127.0, 115.9. ESI-MS (positive ion mode) *m/z*: 211.8 $[M + Na]^+$.

Naphthaleno[1,2-*c*][1,2,5]oxadiazole N-oxide (3.24). 1,2-naphthalenedione dioxime **3.23** (1.211 g, 6.4 mmol) was suspended in 10 % w/w KOH in EtOH (45 mL). Aqueous NaOCl (10.8 % w/w, 45 mL) was added dropwise over 30 min and the reaction was monitored by TLC (CH_2Cl_2). Once complete, the reaction was poured over ice and the resulting tan precipitate was isolated by vacuum filtration and air dried. The crude product was purified by column chromatography (silica gel, CH_2Cl_2 as eluent) yielding 0.172 g (0.92 mmol, 14 %) of a pale yellow solid. mp 110 – 112 ºC. IR (KBr) cm^{-1}: 1625, 1604, 1590, 1550, 1520, 1481, 1438, 1275, 1211, 1099, 1079, 968, 805, 758. Note: *isomers present in NMR spectra.* ^{1}H NMR (300 MHz, CD_2Cl_2): δ 8.58 (dd, J = 7, 2 Hz, 2.7H), 8.47 (dd, J = 6, 3 Hz, 1.0H), 7.76 – 7.63 (m, 11.4H), 7.57 (d, J = 10 Hz, 2.8H), 7.43 (d, J = 10 Hz, 1.1H), 7.36 (d, J = 10 Hz, 2.7H), 7.13 (d, J = 9 Hz, 1.0H). ^{13}C NMR (75 MHz, CD_2Cl_2): δ 151.9, 151.4, 135.4, 133.6, 132.1, 131.8, 131.2, 130.2, 129.8, 129.6, 129.5, 129.2, 129.0, 123.8, 123.2, 122.2, 119.1, 114.8, 110.1, 109.8. EI-MS (70 eV): *m/z* 186 $[M]^+$, 170 $[M - O]^+$, 154 $[M - O_2]^+$.

1-Hydroxyl-2-phenyl-naphthyleno[1,2-*d*]imidazole 3-oxide (3.25). Naphthaleno[1,2-*c*]1,2,5-oxadiazole N-oxide **3.24** (0.146 g, 0.78 mmol) and *C*-phenyl-*N*-phenylnitrone **2.21a** (0.210 g, 1.07 mmol) were dissolved in dry toluene (5 mL) under an N_2 atm. The yellow solution was refluxed gently for 48 h. No reaction was observed by TLC (CH_2Cl_2) and no precipitate formed.

4-Nitrotetrazolo[1,5-*a*]pyridine (3.26).[287,288] Sodium azide (1.53 g, 23.5 mmol) was added slowly to a stirring solution of 2-chloro-3-nitropyridine (1.54 g, 9.7 mmol) in 9:1 EtOH:H_2O (150 mL) under an N_2 atm. 10 % $HCl_{(aq)}$ (15 mL) was added dropwise to the stirring solution and the reaction was refluxed for 22 h at which time it was complete by TLC (CH_2Cl_2). The reaction was cooled to rt and the contents of the flask were poured over ice and left to stand 1 h during which tan crystalline needles formed. The crystalline product was isolated by vacuum filtration, washed with water and dried *en vacuo* yielding 0.89 g (5.4 mmol, 58 %) of a copper colored solid. mp 166 – 168 ºC (lit.[288] 171 – 173 ºC). IR (KBr) cm^{-1}: 1633, 1541, 1517, 1484, 1342, 1318, 818. ^1H NMR (300 MHz, d_6-DMSO) δ 9.76 (dd, J = 7, 1 Hz, 1H), 8.88 (dd, J = 8, 1 Hz, 1H), 7.67 (dd, J = 8, 7 Hz, 1H). ^{13}C NMR (75 MHz, d_6-DMSO): δ 143.3, 135.8, 132.9, 132.0, 116.2. EI-MS (70 eV) *m/z*: 165 $[M]^+$.

[1,2,5]Oxadiazolo[3,4-*b*]pyridine 1-oxide (3.27).[288-290] A solution of 8-nitro-tetrazolo[1,5-*a*]pyridine **3.26** (0.315 g, 1.91 mmol) was refluxed in toluene (15 mL) under an N_2 atm. After 2 h the reaction was complete by TLC (CH_2Cl_2). The solution was concentrated to dryness and the solid was eluted through a short neutral alumina plug (CH_2Cl_2 as eluent) yielding 0.371 g (1.63 mmol, 85 %) of a pale yellow solid. mp 45 – 47 ºC (lit.[288,290] 52 – 53 ºC). IR (KBr) cm^{-1}: 1613, 1526, 1398, 1372, 1129, 1033, 805. Note: *isomerization occurring on NMR timescale, only broad peaks observed in ^1H and ^{13}C NMR. Not all C signals could be resolved, even on 500 MHz NMR with multiple scans.* ^1H NMR (300 MHz, $CDCl_3$) δ 8.77 (s, 1H), 7.82 (d, J = 6 Hz, 1H), 7.22 (d, J = 6 Hz, 1H). ^{13}C NMR (125 MHz, $CDCl_3$): δ 157.4, 122.0, 120.1. ESI-MS (positive ion mode) *m/z*: 138.1 $[M + H]^+$.

3-Hydroxy-2-phenyl-imidazo[4,5-*b*]pyridine 1-oxide (3.28). [1,2,5]oxadiazolo[3,4-*b*]pyridine 1-oxide **3.27** (0.068 g, 0.5 mmol) and *C*-phenyl-*N*-phenylnitrone **2.21a** (0.108 g, 0.52 mmol) were dissolved in dry toluene (3 mL) under an N_2 atm. The yellow solution was refluxed gently for 16 h by which time a yellow precipitate had formed. The solid was isolated by vacuum filtration, washed with acetone, toluene and pentane and air dried yielding 0.089 g (0.4 mmol, 80 %) of a bright yellow solid. mp decomp. 182 – 184 ºC. Anal. Calcd for $C_{12}H_9N_3O_2$: C, 63.43; H, 3.99; N, 18.49. Found: C, 63.02; H, 4.28; N, 18.44. For solubility reasons characterization by NMR and MS performed on deprotonated salt **3.29**.

[Tetrabutylammonium][2-Phenyl-imidazo[4,5-*b*]pyridine 1,3-dioxide] (3.29). 3-hydroxy-2-phenyl-imidazo[4,5-*b*]pyridine 1-oxide **3.28** (0.219 g, 0.96 mmol) was suspended in 1:1 acetone:EtOH (10 mL) with sonication. Tetrabutylammonium hydroxide (0.90 mL, 0.9 mmol) was added dropwise to the sonicating suspension creating a dark red solution. The solution was eluted through a short Celite-545 pad and concentrated *en vacuo*. The resulting oil was dissolved in a minimum amount of acetone and poured into diethyl ether causing a fine orange powder to precipitate. The powder was isolated by vacuum filtration, washed with hexanes and air dried yielding 0.259 g (0.55 mmol, 57 %) of a dark orange powder. ^{1}H NMR (300 MHz, d_6-DMSO): δ 9.39 (d, J = 8 Hz, 2H), 8.18 (dd, J = 5, 2 Hz, 1H), 7.91 (dd, J = 2, 8 Hz, 1H), 7.50 – 7.38 (m, 3H), 7.07 (dd, J = 8, 5 Hz, 1H) 3.18 – 3.13 (m, 8H), 1.59 – 1.44 (m, 8H), 1.30 – 1.22 (m, 8H), 0.89 (t, 12H). ^{13}C NMR (75 MHz, d_6-DMSO): δ 143.1, 138.3, 136.7, 128.6, 127.9, 127.1, 126.9, 120.7, 119.8, 116.2, 57.5, 23.0, 19.1, 13.4. ESI-MS (negative ion mode) *m/z*: 226.0 $[M]^-$.

4-Azido-3-nitropyridine (3.30).[289] A solution of 4-chloro-3-nitropyridine (1.05 g, 6.6 mmol) in DMSO (3 mL) was sonicated for 2 min. Sodium azide (0.43 g, 6.6 mmol) was added to the reaction and the reaction was sonicated a further 25 min. The yellow solution was poured over ice and the resulting cream colored precipitate was isolated by vacuum filtration, washed with cold water and air dried yielding 0.326 g (2.0 mmol, 30 %) of an off-white solid. mp decomp. 78 – 80 ºC (lit[289] 89 ºC). IR (KBr) cm^{-1}: 1611, 1535, 1517, 1484, 1356, 1318, 895, 818, 768. ^{1}H NMR (300 MHz, $CDCl_3$) δ 9.11 (s, 1H), 8.70 (d, J = 5 Hz, 1H), 7.24 (d, J = 5 Hz, 1H). ^{13}C NMR (75 MHz, d_6-DMSO): δ 153.9, 146.5, 142.9, 136.6, 116.5. EI-MS (70 eV) *m/z*: 165 $[M]^+$.

3-Hydroxy-2-phenyl-imidazo[4,5-*c*]pyridine 1-oxide (3.31). 4-azido-3-nitropyridine **3.30** (0.30 g, 1.8 mmol) and *C*-phenyl-*N*-phenylnitrone **2.21a** (0.64 g, 3.2 mmol) were combined in toluene (15 mL) and refluxed under an N_2 atm. After 5 h a tan precipitate had formed and the reaction was complete by TLC (7:3 hexane:EtOAc). The precipitate was isolated by vacuum filtration, washed with acetone and pentane and air dried yielding 0.394 g (1.7 mmol, 94 %) of an off-white powder. mp decomp. 228 – 231 ºC. IR (KBr) cm^{-1}: 3062, 1604, 1473, 1467, 1452, 1285, 1252, 1173, 1106, 1087. Anal. Calcd for $C_{12}H_9N_3O_2$: C, 63.43; H, 3.99; N, 18.49. Found: C, 63.43; H, 4.03 N, 18.15. For solubility reasons characterization by NMR and MS performed on deprotonated salt **3.32**.

[Tetrabutylammonium][2-Phenyl-imidazo[4,5-*c*]pyridine 1,3-dioxide] (3.32). 3-hydroxy-2-phenyl-imidazo[4,5-c]pyridine 1-oxide **3.31** (0.113 g, 0.50 mmol) was suspended in EtOH (10 mL) with sonication. Tetrabutylammonium hydroxide (0.45 mL, 0.45 mmol) was added dropwise to the sonicating suspension creating a dark brown solution. The solution was eluted through a short Celite-545 pad and concentrated *en*

vacuo. The resulting oil was dissolved in a minimum amount of acetone and poured into hexanes causing a fine yellow-orange powder to precipitate. The powder was isolated by vacuum filtration, washed with hexanes and air dried yielding 0.191 g (0.41 mmol, 91 %) of a yellow-orange powder. ^{1}H NMR (300 MHz, d_6-DMSO): δ 9.35 (d, J = 7 Hz, 2H), 8.77 (s, 1H), 8.05 (d, J = 6 Hz, 1H), 7.48 – 7.40 (m, 4H), 3.19 – 3.10 (m, 8H), 1.62 – 1.45 (m, 8H), 1.31 – 1.18 (m, 8H), 0.91 (t, 12H). ^{13}C NMR (75 MHz, d_6-DMSO): δ 139.1, 135.5, 135.4, 129.7, 128.8, 127.7, 127.2, 126.5, 124.8, 106.0, 57.5, 23.0, 19.1, 13.4. ESI-MS (negative ion mode) *m/z*: 226.9 $[M]^-$.

Glyoxime (3.33). A solution of glyoxal trimer hydrate (7.68 g, 110 mmol) and hydroxylamine hydrochloride (15.8 g, 227 mmol) in distilled H_2O (40 mL) was stirred at 0 ºC. KOH (12.3 g in 50 mL, 220 mmol) was added dropwise to the cooled solution over 30 min. Once all $KOH_{(aq)}$ was added, the reaction was heated (oil bath) to 90 ºC. As the reaction warmed it became cloudy yellow. Heating was continued until a clear yellow solution had formed (30 min) at which point the temperature of the bath was reduced slowly to rt. Upon slow cooling, large colourless plate-like crystals formed. The crystalline product was isolated by vacuum filtration, washed with minimal cold water and dried *en vacuo* yielding 7.62 g (86.5 mmol, 79 %) of a colorless crystalline solid. mp 178 – 180 ºC (lit[291] 178). IR (KBr) cm^{-1}: 3440, 1586. ^{1}H NMR (300 MHz, d_6-DMSO): δ 11.62 (s, 2H), 7.73 (s, 2H). ^{13}C NMR (75 MHz, MeOD): δ 146.9.

Dichloroglyoxime (3.34). Glyoxime **3.33** (6.80 g, 77 mmol) was dissolved in DMF (80 mL) and stirred at 0 ºC. *N*-chlorosuccinimide (25.04 g, 188 mmol) was added in small portions over a 1 h period so the temperature of the reaction did not exceed 20 ºC. After the addition of all *N*-chlorosuccinimide, the reaction was removed from the ice bath and

stirred at rt for 1 h after which the reaction was complete (TLC, 8:2 CH_2Cl_2:EtOH). The pale yellow solution was poured over 600 mL ice and a white microcrystalline solid formed upon standing. The solid was isolated by vacuum filtration, washed with water and hexanes and dried *en vacuo* yielding 10.63 g (67 mmol, 87 %) mp decomp. 198 – 200 ºC (lit[292] 213 ºC). IR (KBr) cm^{-1}: 3242, 3179, 1435, 1391, 1004, 855. ^1H NMR (300 MHz, d_6-DMSO): δ 13.14 (s, 2H). ^{13}C NMR (75 MHz, d_6-DMSO): δ 130.6. EI-MS (70 eV) *m/z*: 160 $[M + 4]^+$, 158 $[M + 2]^+$, 156 $[M]^+$, 139 $[M - OH]^+$.

***N2,N3*-Dihydroxy-2,3-quinoxalinediamine (3.35)**. 1,2-phenylenediamine (1.12 g, 10.4 mmol) and Na_2CO_3 (0.5 g, 6.0 mmol) were combined in CH_3CN (100 mL) and stirred at 0 ºC. Separately, dichloroglyoxime **3.34** (1.76 g, 11.2 mmol) was dissolved in CH_3CN (20 mL). The dichlorogloxime solution was added dropwise to the cold reaction mixture over a 1 h period. The reaction was warmed to rt and stirred for 2 h, by this time the reaction was complete (TLC, 9:1 CH_2Cl_2) and a white precipitate had formed. The solid material was isolated by vacuum filtration, washed with water, and air dried. The crude solid was recrystallized from hot EtOH yielding 1.61 g (8.5 mmol, 82 %) of an off white solid. mp 234 – 236 ºC (lit[293] 238 – 240 ºC). IR (KBr) cm^{-1}: 3375, 3282, 1647, 1529, 1458, 1438, 1123, 954, 927, 752. ^1H NMR (300 MHz, d_6-DMSO): δ 8.96 (bs, 4H), 7.18 (dd, J = 6, 3 Hz, 1H), 7.00 (dd, J = 6, 4 Hz, 1H), 6.82 (dd, J = 6, 3 Hz, 1H), 6.74 (dd, J = 6, 4 Hz, 1H). ^{13}C NMR (75 MHz, d_6-DMSO): δ 137.9, 125.3, 122.3, 120.6, 120.0, 114.1. ESI-MS (positive ion mode) *m/z*: 215.3 $[M + Na]^+$.

[1,2,5]Oxadiazolo[3,4-*b*]quinoxaline 1-oxide (3.36).[293,294] 2,3-bishydroxyimino-1,2,3,4-tetrahydroquinoxaline **3.35** (1.03 g, 5.4 mmol) was suspended in CH_2Cl_2 (25 mL). The reaction mixture was sonicated to give a fine suspension and then cooled to 0 ºC.

Concentrated HNO_3 (3 mL) was added dropwise to the stirring suspension. The reaction temperature was monitored so that it did not exceed 5 ºC and the reaction was followed by TLC (CH_2Cl_2). Once complete, the deep red solution was neutralized with aqueous $NaHCO_3$ to pH = 7 and the CH_2Cl_2 layer was isolated. The aqueous layer was extracted with CH_2Cl_2 (3 x 25 mL) and the combined organic layers were washed with brine, dried over $MgSO_4$ and concentrated to dryness to give a deep red solid. The crude solid was purified by column chromatography (silica gel, CH_2Cl_2) to give 0.78 g (4.1 mmol, 76 %) of a red crystalline solid. mp 160 – 162 ºC (lit[295] 161 – 162 ºC). IR (KBr) cm^{-1}: 1593, 1447, 1019, 776. ^1H NMR (300 MHz, $CDCl_3$): δ 7.89 – 7.85 (m, 2H), 7.74 – 7.70 (m, 2H). ^{13}C NMR (75 MHz, $CDCl_3$): δ 147.1, 132.6, 128.4, 128.0. EI-MS (70 eV) *m/z*: 188 $[M]^+$, 172 $[M - O]^+$.

3-Hydroxy-2-phenyl-imidazo[4,5-*b*]quinoxaline 1-oxide (3.37). *C*-phenyl-*N*-phenylnitrone **2.21a** (0.512 g, 2.6 mmol) and [1,2,5]oxadiazolo[3,4-*b*]quinoxaline 1-oxide **3.36** (0.351 g, 1.9 mmol) were suspended in toluene (15 mL) under an N_2 atm. The reaction was heated to reflux, the starting materials dissolved and an orange solid precipitated immediately formed. The mixture was stirred an additional 5 min, at which time the reaction was complete (TLC, CH_2Cl_2). The precipitate was isolated by vacuum filtration, washed with toluene, acetone and pentane and dried *en vacuo* yielding 0.236 g (0.84 mmol, 44 %) of a dark orange powder. mp decomp. 197 – 199 ºC. IR (KBr) cm^{-1}: 3064, 1522, 1465, 1445, 1330, 1223, 1080, 802, 759, 686. Anal. Calcd for $C_{12}H_9N_3O_2$: C, 64.74; H, 3.62; N, 20.13. Found: C, 65.01; H, 3.77 N, 19.88.

[Tetrabutylammonium][2-Phenyl-imidazo[4,5-*b*]quinoxaline 1,3-dioxide] (3.38). 3-hydroxy-2-phenyl-imidazo[4,5-*b*]quinoxaline 1-oxide **3.37** (0.100 g, 0.36 mmol) was

suspended in EtOH (5 mL) with sonication. Tetrabutylammonium hydroxide (0.30 mL, 0.3 mmol) was added dropwise to the sonicating suspension creating a black solution. The solution was eluted through a short Celite-545 pad and concentrated *en vacuo*. The resulting oil was sonicated with a minimum amount of toluene and concentrated by rotary evaporation to give a black solid. The solid was dissolved in acetone and precipitated from hexanes yielding a black powder. The powder was isolated by vacuum filtration, washed with hexanes and air dried yielding a black solid. Characterization was not consistent with product.

Chapter 4: Organic Open-Shell Benzonitronyl Nitroxide Donor–Acceptor Triads

4.1 Introduction

Organic semiconductors have been incorporated as the active layer in light emitting diodes (LEDs),[296-300] field effect transistors (FETs),[301-306] organic photovoltaics,[307-311] sensors,[312] lasers[313] and electrochromics.[314] While disadvantages arise due to decreased mobilities and intrinsic conductivities in disordered organics, efforts to increase figures of merit are driven by the low cost of solution-processing and direct-write printing used in the fabrication of flexible organic devices.[315,316]

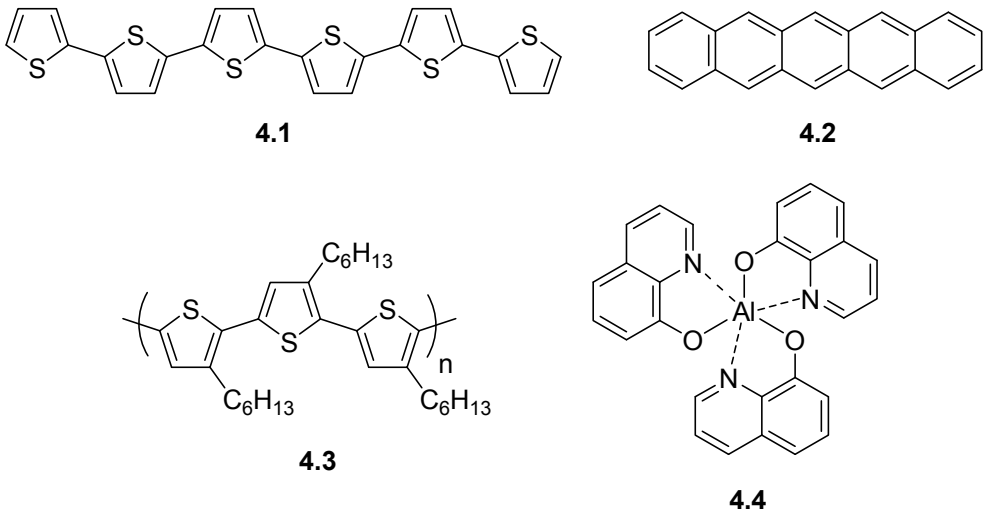

Figure 4.1. Common organic semiconductors.

The most common organic semiconductors, sexithiophene **4.1**, pentacene **4.2**, poly-3-hexylthiophene (P3HT) **4.3**, and *tris*(8-hydroxyquinoline)aluminum(III) (Alq_3) **4.4** are shown in Figure 4.1. Research towards the development of organic devices has thus far

focused on maximizing device performance by optimizing device fabrication and, despite the number of organic devices assembled, most contain one of the four organic semiconductors shown above.

To continue progress in this field, the synthesis of new organic systems affording semiconducting or conducting behavior will be necessary. If D–A coupling is strong and the barrier to electron transfer low, the conduction electrons can be supplied by electron transfer between donor and acceptor resulting in a system with intrinsic conductivity. An organic system in which the conductivity is high in the absence of doping is significant as organic materials typically require doping to achieve reasonable levels of conductivity. Doping decreases solubility thereby creating challenges for solution processing which is the major processing advantage for organic electronics.

The incorporation of unpaired electrons into D–A systems is a novel strategy towards developing organic D–A semiconductors in which the electrical conductivities can be modulated by changing the strength of the D or A and thereby modifying the electronic structure and intermolecular interactions. Planar radicals often form 1D chains which are predicted to give rise to a half-filled band structure[100] that could lead to semiconducting or metallic-like conductivities in the absence of Peierls distortions or the formation of Mott insulating states.

To date, a limited number of stable organic open-shell D–A systems have been realized.[154,155,159,317,318] Neutral paramagnetic donor–acceptor dyads comprised of triphenylamine (TPA)-perchlorinated triphenylmethyl (PCTM),[154,155] PTCM-ferrocene,[156-158] and tetrathiafulvalene (TTF) 2,5-di-tert-butyl-6-oxophenalenoxyl[159] have been investigated in solution and found to exhibit optically induced charge transfer (CT)

transitions in the NIR that are solvatochromic with varying degrees of charge separation in the ground state. The solid state behaviour has been investigated in only a few of these systems. A tetracyanoquinone (TCNQ) derivative[162] was found to exhibit a room temperature conductivity of 10^{-5} S cm^{-1} while a polycrystalline sample of TTF-tetramethylnitronyl nitroxide (TMNN)[163] exhibited a conductivity on the order of 10^{-4} S cm^{-1}, weak ferromagnetic exchange along the π-stacking axis (*intra*chain J/k_B = 6.5 K) and weak antiferromagnetic exchange between chains (*inter*chain $J/k_B = -1.1$ K).[163]

We have shown that benzonitronyl nitroxides **2.15** are remarkably strong acceptors (~0 V vs SCE), leading to a novel class of stable, planar, π-delocalized open-shell acceptors (Chapter 2). Given the exceptionally strong acceptor ability of BNN, stable open-shell D–A–D triads were designed in order to investigate the effect of CT interactions on the solid state behavior of neutral paramagnetic D–A systems. The triads are unique in that their planar topology allows for reasonably strong π–π interactions in the solid state. In contrast, the bulky propeller morphology of PCTM-based D–A radicals[176,177,319] does not allow for formation of close solid state contacts precluding the evaluation of the effect of intermolecular D–A interaction on solid state phenomena.

Two D^1–A–D^2 BNN triads were prepared, where D^1 = thiophene and D^2 = thiophene **4.11b** or phenyl **4.11a**. The electronic structure of each radical was elucidated through solution-phase spectroscopy, cyclic voltammetry and density functional theory (DFT). The solid state interactions were probed through the use of SQUID magnetometry, X-ray crystallography and diffuse reflectance spectroscopy. EPR spectroscopy and electrochemical studies reveal a spin-delocalized structure with a decreased SOMO energy and extremely low reduction potential. Structural characterization of the triads in

the solid state by PXRD and XRD reveal slipped π stacks arising from π–π and intermolecular D–A interactions, providing pathways for magnetic exchange and charge transport. The differences in conductivity and magnetic exchange in the two triads can be rationalized by the degree of slippage dominated by π–π interactions (**4.11a**) and intermolecular D–A interactions (**4.11b**). In addition, increased slippage along the 1D π stacks give rise to additional interactions between chains in **4.11b**, leading to increased dimensionality and pathways for charge transport and magnetic exchange.

4.2 Synthesis

Realization of radicals **4.11a-b** required thiophene functionalization of the benzannelated ring of parent BNN radical **2.15**. We previously developed a mild, generalizable methodology allowing for the synthesis of BNN radicals from aryl or alkyl nitrones and benzofuroxan.[221] Although the preparation of benzofuroxans can be accomplished via the oxidation of *ortho*-amino-nitro arenes,[259] and azido-nitro arenes,[320] the functionalization of benzofuroxans is not well known. Given their susceptibility to nucleophiles, we chose to form the necessary C-C bond prior to benzofuroxan formation. The thiophene ring could be installed at the *C*5 position of the benzannelated ring by modified palladium catalyzed coupling conditions originally developed for electron poor aryl halides.[321] Oxidative benzofuroxan generation and condensation with the corresponding nitrone led cleanly to the radical precursors for **4.10a** and **4.10b** from the same furoxan intermediate **4.9**. The synthetic methodology is shown in Scheme 4.1.

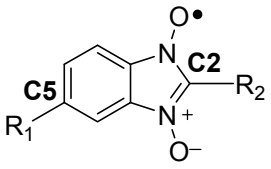

Figure 4.2. Labeled benzannelated nitroxide indicating *C*5 and *C*2 positions.

Scheme 4.1. Synthetic pathway affording bis-substituted benzonitronyl nitroxide radicals. [a]

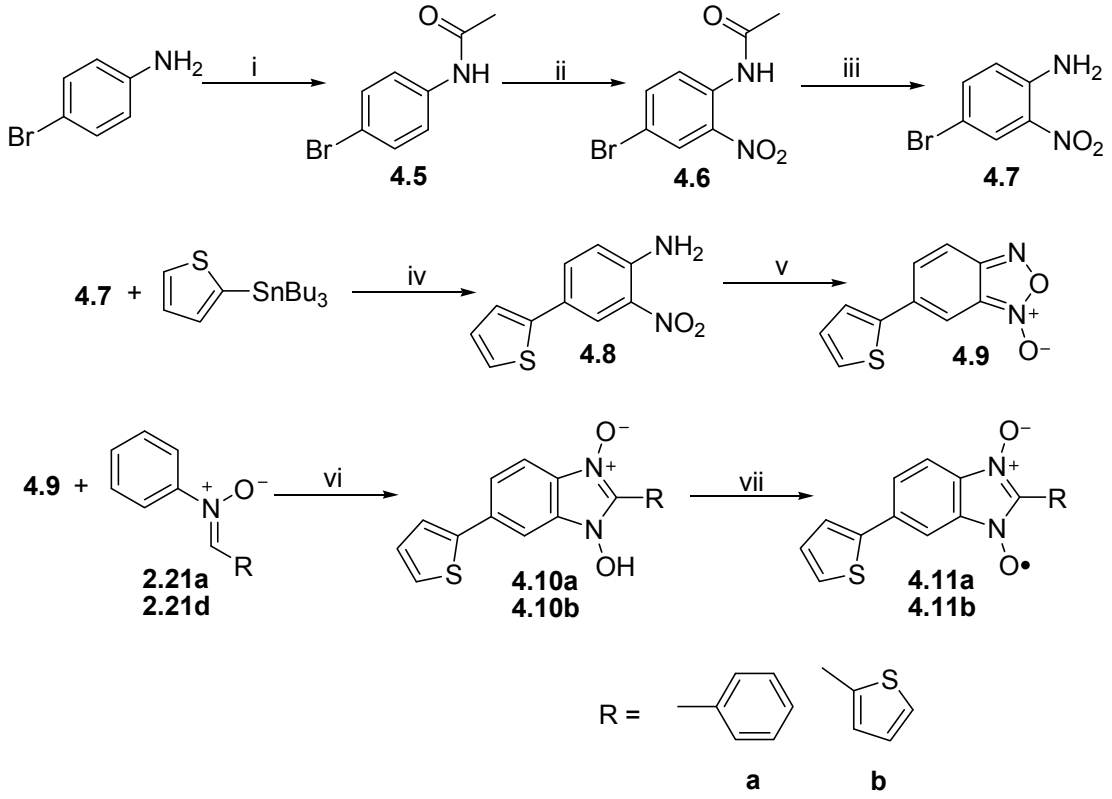

[a] Reagents and conditions: (i) acetic anhydride, Δ, 97 %; (ii) trifluoroacetic acid, fuming HNO_3, 0 ºC, 96 %; (iii) $HCl_{(aq)}$, Δ, 92 % (iv) Pd_2dba_3, (*o*-tolyl)$_3$P, CsF, THF, Δ, 92 %; (v) NaOH, EtOH, $NaOCl_{(aq)}$, 0 ºC, 91 %; (vi) toluene, Δ, 57 – 65 %; (vii) $(nBu)_4NOH$, EtOH, then 1:3 EtOH:CH_2Cl_2, $AgPF_6$, rt to −78 ºC, 20 %.

Acetylation, nitration and acid catalyzed deprotection of commercially available *p*-bromoaniline yielded 4-bromo-2-nitroaniline **4.7** in high yield (86% overall from *p*-bromoaniline). Stille coupling of **4.7** with 2-(tributylstannyl)thiophene installed the thiophene moiety at *C*5 to give **4.8** in 92% yield. Oxidation of the *o*-amino-nitroaromatic

4.8 with alcoholic base/sodium hypochlorite afforded 5-thienyl-benzofuroxan (**4.9**, 91%) which was then condensed with the appropriate nitrone (**2.21a** or **2.21d**) yielding the insoluble radical precursors **4.10a** and **4.10b** as tan powders in reasonable yield (57% and 65% yield respectively). The radical precursors were solubilized by deprotonation with sodium hydroxide, then oxidized with silver(I) hexafluorophosphate to yield the corresponding radicals. Isolation of radicals **4.11b** and **4.11a** by low temperature (−78 °C) recrystallization gave analytically pure samples which were found to be moderately unstable in solution but stable over a period of several months in the solid state in the absence of light.

4.3 Characterization of electronic structure in solution

X-band EPR spectra of radicals **4.11a** and **4.11b** were measured at room temperature in degassed toluene. The EPR spectra of nitronyl nitroxides **4.11a-b** (Figure 4.3) exhibit a five-line pattern with relative intensities of 1:2:3:2:1 and *g*-values of 2.0068 ± 0.0003. The nitrogen atoms in the benzimidazole ring (N1, N3) bear a large proportion of the spin density with hyperfine coupling constants of $a(N_1)$ = 4.27 G and $a(N_3)$ = 4.39 G for radical **4.11b** and $a(N_1)$ = 4.24 G and $a(N_3)$ = 4.41 G for radical **4.11a**. The magnitude of the nitrogen hyperfine coupling constants is consistent with those reported for other BNN derivatives[221-223,322] suggesting extended π conjugation via *C*5 functionalization does not significantly perturb the spin distribution in the benzannelated ring.

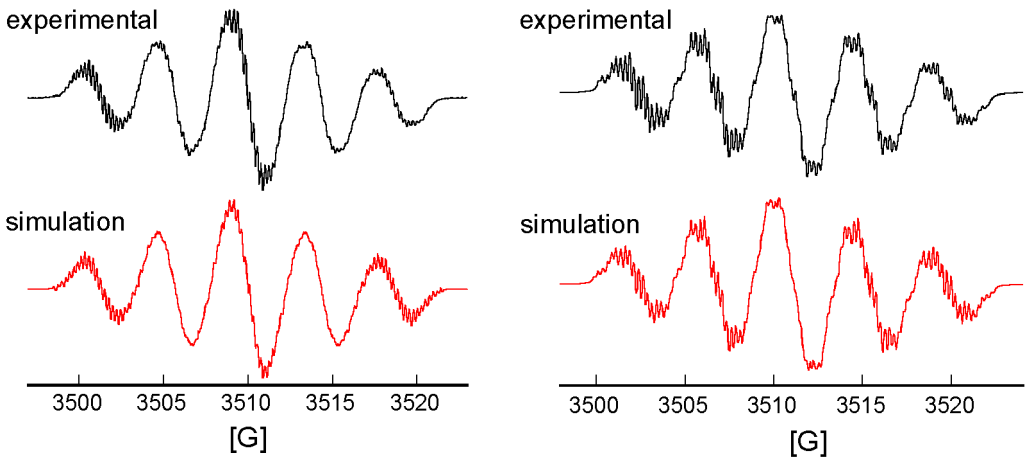

Figure 4.3. EPR spectrum of **4.11a** (left) and **4.11b** (right) (top = experimental, bottom = simulated, R > 0.99), 10^{-5} M solution in dry, degassed toluene at room temperature.

The electrochemical behavior of radicals **4.11a** and **4.11b** was investigated by cyclic voltammetry to determine the effect on reduction potential of a π-conjugated donor at *C*5. Both radicals exhibit a reversible one-electron reduction at 0.06 V vs SCE (ΔE_p = 80 mV)

(Figure 4.4) and an irreversible oxidation at 1.4 V vs SCE. The irreversible oxidation process results in deposition of an iridescent film on the glassy carbon electrode which completely passivates the system. Efforts towards growing thicker films for spectroscopic and structural characterization were unsuccessful. The reduction potentials of extended radicals **4.11a** and **4.11b** were found to be 60 mV lower than that of the parent radical. Although substitution on the benzannelated ring with a weakly donating group should make the central BNN radical moiety more difficult to reduce, extending the π conjugation of the benzannelated system lowers the SOMO energy thereby lowering the reduction potential. In this case the latter effect dominates leading to radicals that can undergo a one-electron reduction at remarkably low potentials, comparable to that of 7,7,8,8-tetracyanoquinodimethane (0.19 V vs SCE).[323]

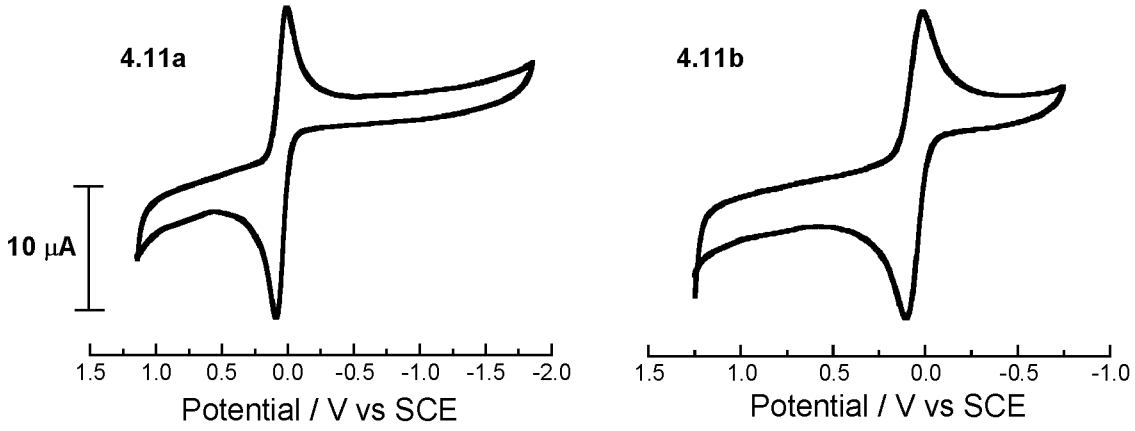

Figure 4.4. Cyclic voltammogram of the reductive process for radicals **4.11a-b**, mM solution in NBu_4PF_6/CH_3CN, 50 mV s^{-1} scan rate.

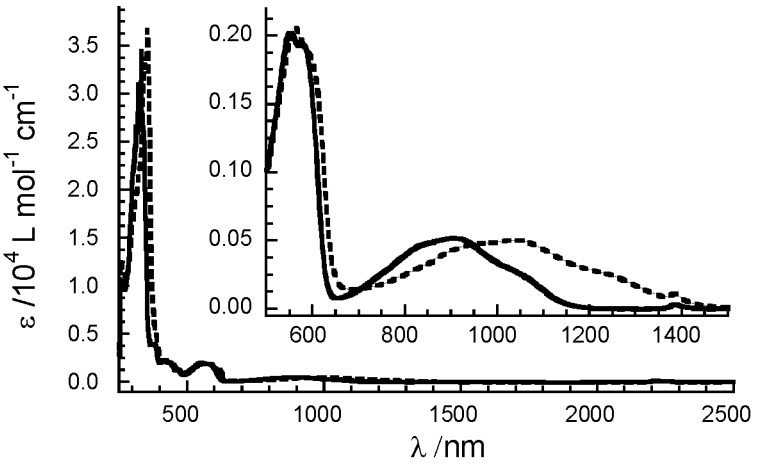

Figure 4.5. Absorption spectroscopy of **4.11a** (—) and **4.11b** (▪▪▪), 10^{-5} M THF, ambient T. Inset shows expansion of visible and NIR transitions (inset).

The electronic absorption spectra of radicals **4.11a** and **4.11b** (Figure 4.5) consist of several features in the UV and visible regions, as well as a broad absorption band in the NIR (λ_{max} = 900 for **4.11a** and 1025 nm for **4.11b**, $\varepsilon \approx 500$). The nature of the NIR transition has previously been shown to be dependent on the *C*2 substituent and is the result of a symmetry forbidden HOMO–SOMO transition.[220,221] The UV absorptions (between 200 – 400 nm) are characteristic of benzonitronyl nitroxide π–π^* transitions and are bathochromically shifted by roughly 100 nm relative to the parent BNN systems. This red shift is not unexpected given the increase in π conjugation as a result of *C*5 substitution.

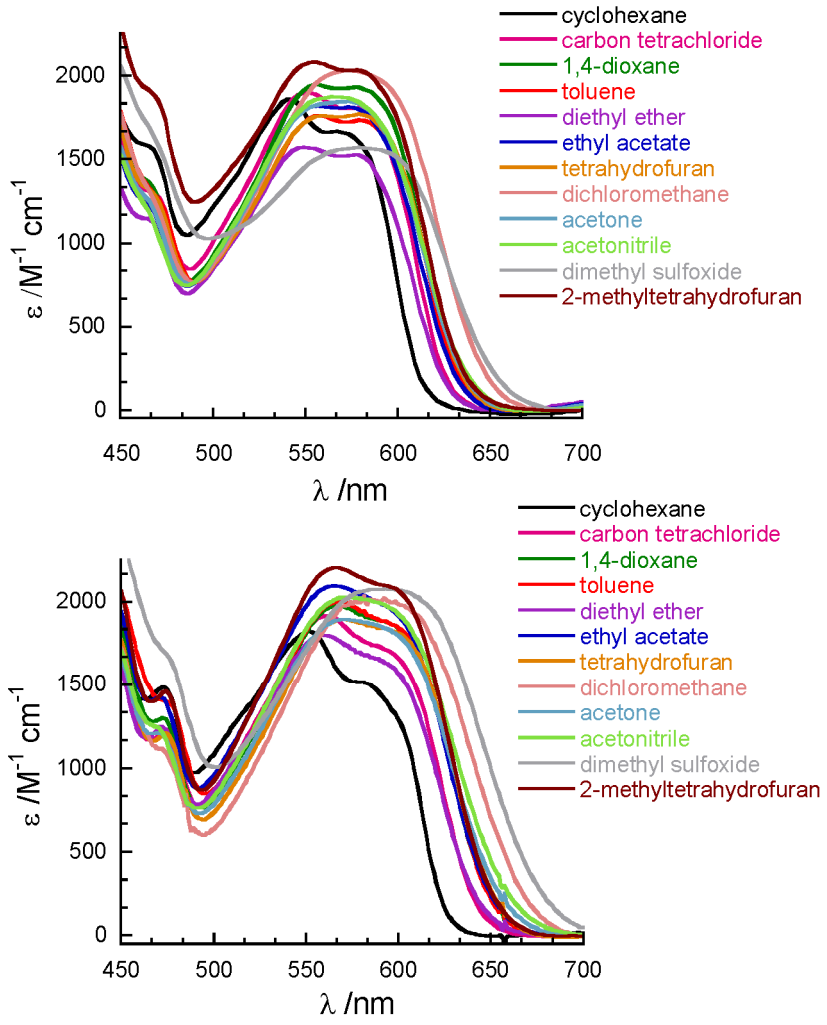

Figure 4.6. Charge transfer transition of **4.11a** (top) and **4.11b** (bottom) measured in solvents of varying dielectric (10^{-5} M, ambient T).

The visible transitions (λ_{max} = 557, ε ≈ 1500 and λ_{max} = 599 (sh), ε ≈ 1100, THF) have not previously been observed in any nitroxide system and are attributed to a CT excitation resulting from an interaction between the weakly donating *C*5 thiophene and strongly accepting nitronyl nitroxide moiety. The electronic absorption spectra of **4.11a** and **4.11b** were recorded in solvents ranging in polarity from cyclohexane to dimethyl sulfoxide (Figure 4.6). The transition at 550 nm exhibits a bathochromic shift and a decrease in extinction coefficient as the solvent polarity increases along the series, while

the transition at 580 nm exhibits a bathochromic shift and little change in extinction coefficient (by deconvolution, see Table 4.1) with increasing dielectric of the solvent. At dielectrics above ~22, a reversal in intensities of the two excitations is observed, such that the longer wavelength band is more intense in acetonitrile and DMSO. The observed positive solvatochromism is consistent with a CT excitation in which the excited state is preferentially stabilized with respect to the ground state in higher polarity solvents (Figure 4.7). The magnitude of the solvatochromism is not as large as that reported for other neutral open-shell D–A systems,[156] suggesting a highly delocalized ground state.

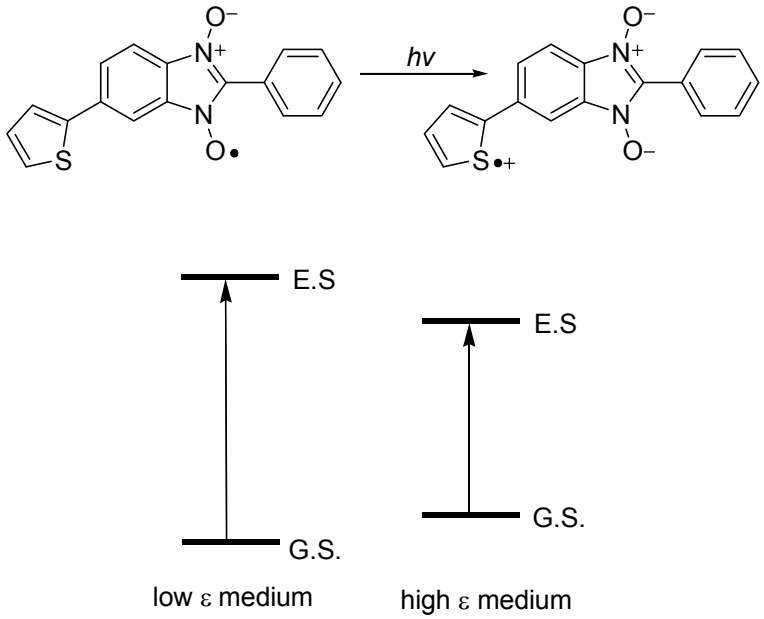

Figure 4.7. Energy absorption leads to a charge separated excited state (top). A stabilization of the excited state occurs in solvents that are more able to solvate molecules with large dipole moments (bottom).

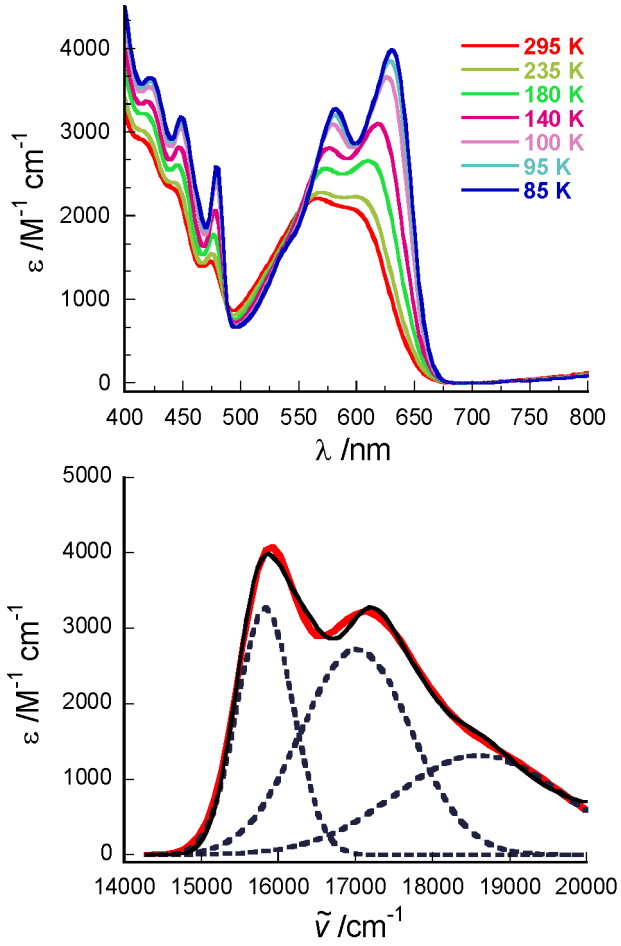

Figure 4.8. Variable temperature spectrum of **4.11a** in MeTHF (top) and deconvolution of charge transfer band of radical **4.11a** (MeTHF, 85 K) to give three transitions (bottom).

The electronic absorption spectra of **4.11a** and **4.11b** were investigated in the temperature range of 295 K to 85 K in 2-methyltetrahydrofuran (MeTHF) (Figure 4.8). As the temperature was decreased, an increase in intensity and ~20 nm bathochromic shift in the 550 nm and 580 nm transitions was observed. The variable temperature behavior of radicals **4.11a-b** was found to be fully reversible (Figure 4.9) thus the spectral changes cannot be the result of radical decomposition in solution nor are they due to aggregation as this would lead to peak broadening as opposed to the observed

sharpening. The bathochromic shift observed as temperature is decreased may be due to a planarization of the molecule, leading to an effective increase in electronic coupling and decrease in the energy of the CT excitation.

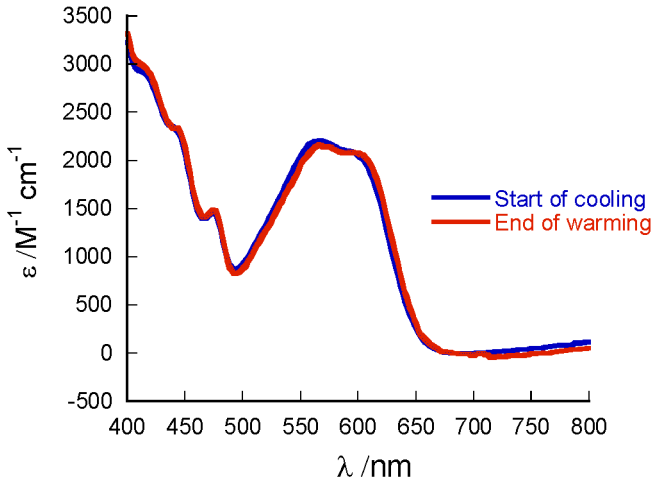

Figure 4.9. Spectrum of **4.11a** in MeTHF at 295 K before cooling (red) after cooling to 85 K and warming back to 295 K (blue).

In addition to the observed bathochromic shift and increase in molar absorptivity of the 550 nm and 580 nm excitations with decreasing temperature, a shoulder at ~530 nm became visible at 85 K (Figure 4.8). Because of this additional transition observed at low temperature, each CT excitation (500 – 700 nm) was deconvoluted into three Gaussian bands ($R^2 > 0.99$) (Figure 4.8, Table 4.1). In general, the two low energy transitions bathochromically shift with an increase in solvent polarity, while the high energy band (~530 nm) shows little dependence. The non-monotonic solvatochromic behavior may have contributions from specific and nonspecific solvent interaction as is observed for other neutral open-shell D–A molecules.[154-156]

Overall, an examination of the CT excitation in different polarity solvents reveals the presence of three distinguishable transitions, a shoulder at 535 nm and two transitions at

580 and 630 nm. The intensity of each transition is solvent dependent and the features of each individual band are better defined in low polarity dielectrics. Similar behavior was observed in the triphenylamine-perchlorinated triphenylamine (TPA–PCTM) acceptor radical systems, in which a shoulder is present in non-polar solvents while a broad asymmetric band is observed in more polar solvents. In the case of the TPA–PCTM radicals this behavior was attributed to vibrational fine structure,[154,324] however, these systems were not probed by variable temperature spectroscopy and their excited state spectroscopy was not modeled computationally. These experiments may prove valuable toward investigating the nature of the electronic transition in open-shell D–A systems, as was the case for the D–A–D BNN radicals **4.11a-b**. Though vibrational fine structure could not be conclusively ruled out, variable temperature spectroscopy and computational data (discussed below) support the origin of the visible band as arising from at least two distinct electronic transitions, and not vibrational fine structure.

4.4 Computational evaluation of charge transfer transitions

It is well established that the electronic structure of π-delocalized organic D–A molecules are difficult to characterize properly using DFT primarily as a result of the self-interaction error (SIE).[325,326] Computational evaluation of organic D–A systems using semi-empirical methods can be improved by utilizing hybrid exchange-correlation functionals[327,328] together with a polarizable solvent continuum model.[329] We chose to evaluate radicals **4.11a-b** using unrestricted TDDFT with Becke's three-parameter hybrid exchange functional[237,330] and the Lee-Yang-Parr correlation functional[238] (UB3LYP). The 6-31G(d,p) basis set was selected and all calculations were carried out using the

Gaussian 09 package.[239] X-ray crystal structure of **4.11a** (below) was used as the geometry input for each single point energy calculation. Three different solvation models (Onsager continuum model,[242-244] conductor-like polarizable continuum model (CPCM),[331,332] and self-consistent isodensity polarizable continuum model (SCI-PCM)[333]) were evaluated and compared to the experimentally observed CT excitations (Table 4.1). In all solvents the highest energy peak was broad (50 - 130 nm), overlapped strongly with transitions in the UV and was not predicted by TDDFT. The high energy shoulder (530 nm) may in fact be due to vibrational structure of the 580 nm transition, or may be too high in energy for TDDFT to calculate. As such, we focused on the two excitations that occur completely in the visible region and were predicted computationally.

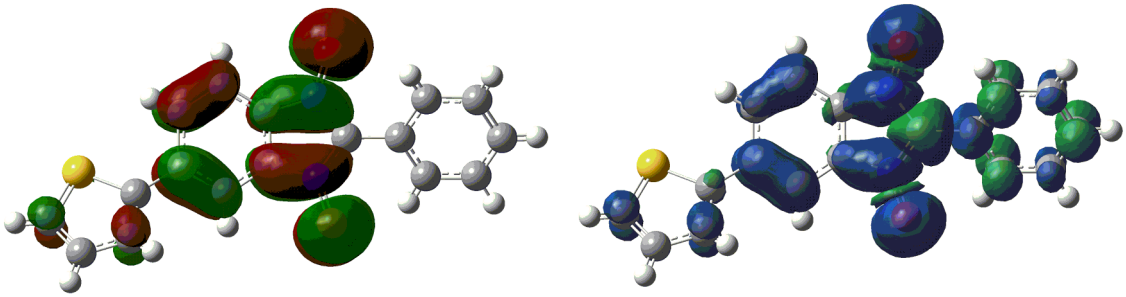

Figure 4.10. SOMO (left) and spin density (right) of radical **4.11a** generated with GaussView 4.1.2, grid = coarse, isovalue = 0.02. Calculated using TDDFT UB3LYP/6-31G(d,p) with SCI-PCM solvation, solvent = THF.

The SOMO and spin density distribution obtained for **4.11a** (Figure 4.10) are consistent with the electronic structure of the parent BNN.[221] There is some orbital population on the *C*5-thienyl due to π conjugation, and the node at *C*2 is maintained. The α and β–SOMO orbitals differ in energy and orbital population due to spin polarization effects (Figure 4.11).[83] The spin density distribution (Figure 4.10) is consistent with spin

delocalization in the BNN moiety with spin polarization dominating the spin density distribution in the *C*2 aryl ring.

Table 4.1. Excitation energies (λ) and oscillator strength (*f*) or molar absorptivity (ε) of the higher and lower energy visible absorption bands of **4.11a** determined computationally and experimentally in solvents of increasing dielectric strength.

		Onsager		**CPCM**		**SCI-PCM**		**experimental**	
Solvent	dielectric constant[a]	λ /nm	*f*	λ /nm	*f*	λ /nm	*f*	λ /nm	ε /$M^{-1}cm^{-1}$
cyclohexane	2.0243	535.1	0.0771	536.8	0.0798	530.0	0.0567	543	1700
		563.3	0.0022	561.7	0.0031	563.4	0.0013	584	1100
1,4-dioxane	2.2189	536.7	0.0770	538.3	0.0793	531.5	0.0569	556	1700
		562.6	0.0029	561.0	0.0041	562.7	0.0016	598	1200
CCl_4	2.2379	537.2	0.0783	538.8	0.0806	531.7	0.0570	553	1600
		562.5	0.0030	561.0	0.0044	562.7	0.0016	594	1200
toluene	2.379	538.5	0.0793	540.2	0.0814	532.7	0.0570	559	1400
		562.1	0.0037	560.6	0.0055	562.2	0.0018	599	1100
Et_2O	4.2666	544.3	0.0664	545.2	0.0628	539.9	0.0550	549	1400
		559.3	0.0133	558.6	0.0203	559.3	0.0060	591	1000
EtOAc	6.0814	546.4	0.0553	546.9	0.0484	542.4	0.0511	552	1600
		559.2	0.0263	559.1	0.0366	558.5	0.0107	595	1100
MeTHF[b]	6.97							555	1400
								596	1500
THF	7.52	547.2	0.0469	547.4	0.0397	543.5	0.0479	557	1500
		559.5	0.0366	559.8	0.0473	558.3	0.0143	599	1100
CH_2Cl_2	8.93	547.6	0.0403	547.7	0.0388	544.1	0.0448	556	1600
		560.0	0.0366	560.6	0.0544	558.2	0.0176	603	1400
acetone	21.01	547.1	0.0254	547.2	0.0224	545.3	0.0333	552	1500
		561.3	0.0574	562.2	0.0636	558.6	0.0299	595	1200
CH_3CN	36.64	546.8	0.0215	546.9	0.0196	545.4	0.0291	542	900
		562.0	0.0609	562.9	0.0660	559.0	0.0344	587	1300
DMSO	47.24	546.9	0.0195	547.1	0.0178	545.4	0.0277	560	850
		562.9	0.0662	563.9	0.0714	559.2	0.0358	606	1100

[a] Dielectric constants are those reported in the 91st CRC Handbook of Chemistry and Physics.[234] [b] MeTHF was not modeled computationally as it was not a solvent available in the Gaussian 09 package. Simply changing the dielectric in a polarizable continuum model (PCM) to that of MeTHF was not appropriate as dielectric is only one many internal parameters used to define solvents when using PCM.

Computationally, all three solvation models gave similar predicted excitation energies for the visible transitions and all calculated excitations were higher in energy than the experimentally determined λ_{max} values. TDDFT also reproduced the shifts in transition intensities with increasing solvent polarity, although only SCI-PCM accurately predicts the reversal of peak intensities observed in high dielectric solvents. The experimentally observed bathochromic shift in λ_{max} with increasing solvent polarity was reproduced well computationally. Each of the two transitions had major contributions from HOMO−4 → SOMO and HOMO−1 → SOMO excitations, however, the relative contribution of each was highly dependent on solvent polarity. Using the SCI-PCM solvation model, the higher energy band (~550 nm) ranged from being 83%:3% (HOMO−1 → SOMO) to (HOMO−4 → SOMO) in low polarity solvents (cyclohexane) to 45%:51% in high dielectric solvents (acetone). As solvent polarity increased further, the relative contribution of the HOMO−1 → SOMO transition decreased until it contributed just 36 % to the overall high energy excitation in DMSO. Conversely, the lower energy band (~580 nm) was predominantly (> 95 %) attributed to a HOMO−1 → SOMO transition in non-polar solvents (cyclohexane to toluene) whereas in polar solvents (acetone to DMSO) the contribution of the HOMO−1 and HOMO−4 → SOMO excitations were nearly equivalent.

The contribution of a deep lying state, such as a HOMO−4 appears unusual, however, the open-shell nature of these molecules results in a number of close lying occupied states (< 0.05 eV difference, Figure 4.11) and DFT may not be ordering these effectively degenerate orbitals correctly. It may be more appropriate to describe the second contribution to the CT excitation as a HOMO−*n* → SOMO excitation, especially

considering the CT transition is much more likely to arise from an electronic excitation from a molecular orbital with large coefficients in a π-type orbital (HOMO−2 or HOMO−3, Figure 4.11). This is in contrast to the HOMO−4 which is localized over the σ system, nonetheless, the HOMO-4 → SOMO transition would result in a redistribution of electron density and dipole moment.

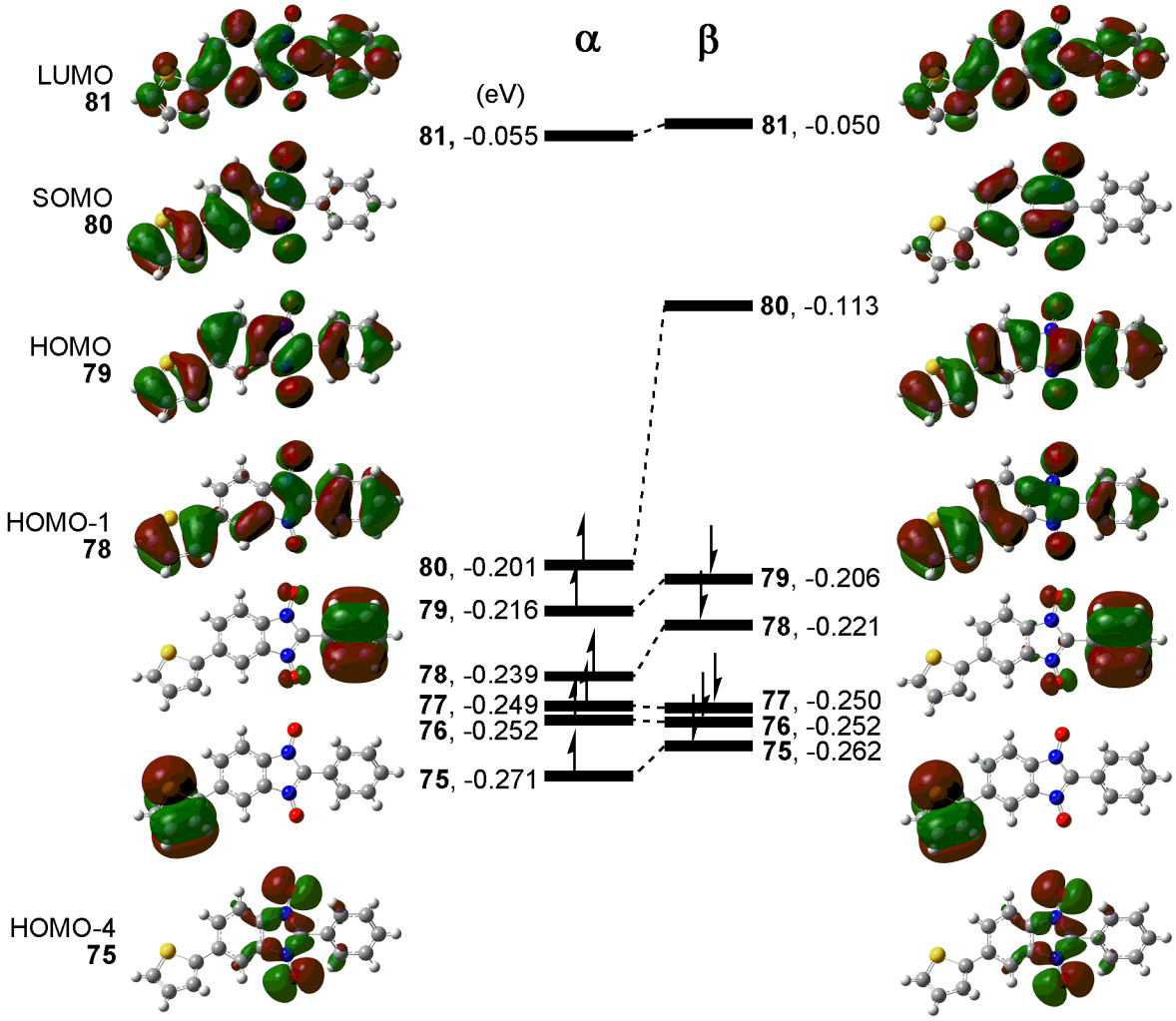

Figure 4.11. Molecular orbital diagram for **4.11a** with SCI-PCM solvation (THF), generated in GaussView 4.1, cube grid = coarse, isoval = 0.02.

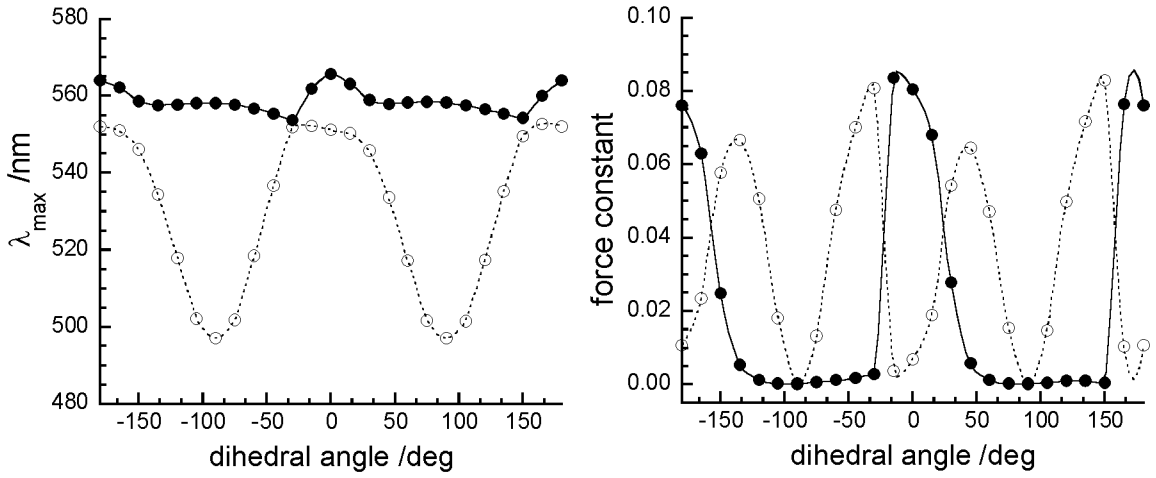

Figure 4.12. Force constant (right) and excitation energy (left) of the 550 nm (○) and 580 nm (●) transition as a function of torsion angle calculated using TDDFT with the UB3LYP functional and 6-31G(d,p) basis set with Onsager solvation (THF).

The effect of planarization on the energy of the CT excitations was examined computationally and the results are depicted in Figure 4.12. Experimentally, the CT transitions bathochromically shift by nearly 20 nm and double in intensity as the system is cooled. Computations suggest the higher energy (550 nm) transition is highly susceptible to changes in the *C*5-thienyl…BNN torsion angle while the lower energy (580 nm) transition is not. The force constants for the two transitions also differ in their dependence on torsion angle. The force constant for the 580 nm transition is at a maximum in the planar configuration (0º and 180º), while the force constant for the 550 nm transition is at a minimum in these configurations. Planarization of the system results in better orbital overlap between D and A which in turn leads to stronger electronic coupling and the experimentally observed enhancement of molar absorptivity. Contrary to that observed experimentally, computation suggests planarization would lead to a decrease in intensity (*f*) of the 550 nm band and an increase in the 580 nm. This discrepancy may be due to difficulties encountered when calculating excited state D–A

geometries using TDDFT, particularly when large changes in charge density are occurring.[334,335]

4.5 Structural analysis by XRD

Single crystals of **4.11a** were grown by slow evaporation of a saturated n-pentane/acetone solution to give purple plates, and analyzed by single crystal X-ray diffraction (XRD). Radical **4.11a** refined in the monoclinic crystal system, $P2_1/c$ space group, with four molecules per unit cell ($Z = 4$). Single crystals of **4.11b** of sufficient size for single-crystal XRD analysis could not be grown. Instead the structure was analyzed with powder X-ray diffraction (PXRD) which revealed the structure of **4.11b** to be closely related to that of **4.11a**, with subtle variations in the degree of slippage along the π stacks.

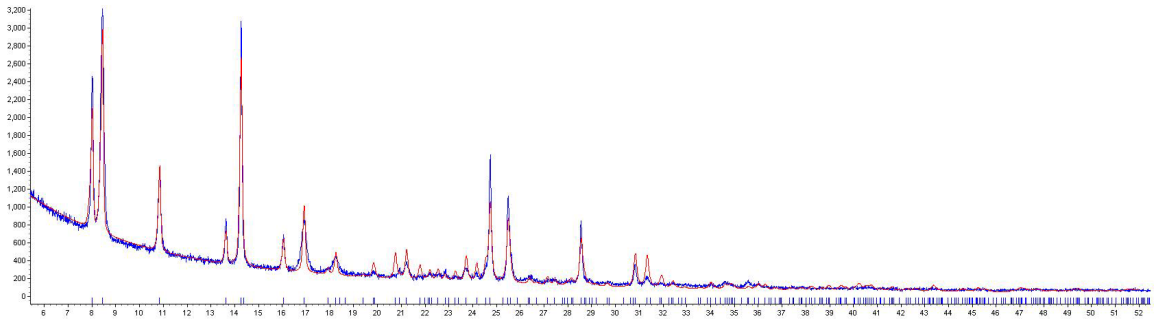

Figure 4.13. Experimental (blue) and calculated (red) X-ray powder pattern for radical **4.11b**.

The PXRD data (Figure 4.13) was analyzed using Topas,[336] starting from indexing the unit cell, determining the space group, and using a rigid body model with two variable torsion angles. As in **4.11a**, refinement of the structure led to packing in the monoclinic crystal system in the $P2_1/c$ space group with four molecules per unit cell ($Z = 4$). Detailed

structural information (bond lengths and angles) is not analyzed here given that the quality of the diffraction data did not allow for refinement of atomic positions. Select crystallographic data is reported in Tables 4.2 and 4.3, further metrics including a complete listing of bond lengths and angles are reported in Appendices A and B.

4.5.1 Crystallographic analysis of 4.11a

Table 4.2. Crystallographic data for **4.11a**.

	4.11a
formula	$C_{17}H_{11}N_2O_2S$
formula weight	307.35
color of crystal	dark purple
crystal system	monoclinic
space group	$P2_1/c$
a (Å)	14.1620 (2)
b (Å)	14.1493 (2)
c (Å)	7.03310 (10)
volume (Å^3)	1409.30 (3)
temperature (K)	296
Z	4
R_f [b]	0.0449
R_w [c]	0.1188
GOF	1.041

[a] $R_f = [\Sigma||F_o| - |F_c||]/[\Sigma|F_o|]$, $I > 2\sigma(I)$. [b] $R_w = ([\Sigma w||F_o|^2 - |F_c|^2|^2]/[\Sigma(w|F_o|^2)^2])^{1/2}$.

The single crystal structure and packing diagram of **4.11a** are shown in Figure 4.14. The benzimidazole skeleton, including the terminal oxygen atoms adopts a nearly planar geometry with an angle of just 1.2º between the plane of the benzannelated ring and the coplanar ONCNO atoms. The thiophene ring is twisted 27º from the plane of the central benzimidazole ring (*C*4-*C*5-*C*14-*S*1), while the phenyl ring is twisted 32º out of the plane (*C*9-*C*8-*C*1-*N*1). The radicals form slipped π stacks along the *c*-axis (Figure 4.14) with a

32º slippage angle and average interplanar distance of 3.31 Å between radicals. Interchain interactions occur between between *O*2…*C*3 at 3.074 Å along the *c*-axis. The well isolated π stacks would be expected to give rise to sizeable one-dimensional magnetic exchange via a direct exchange mechanism as there should be strong overlap between benzimidazole ring spin density along the stack, with very weak interchain interactions.

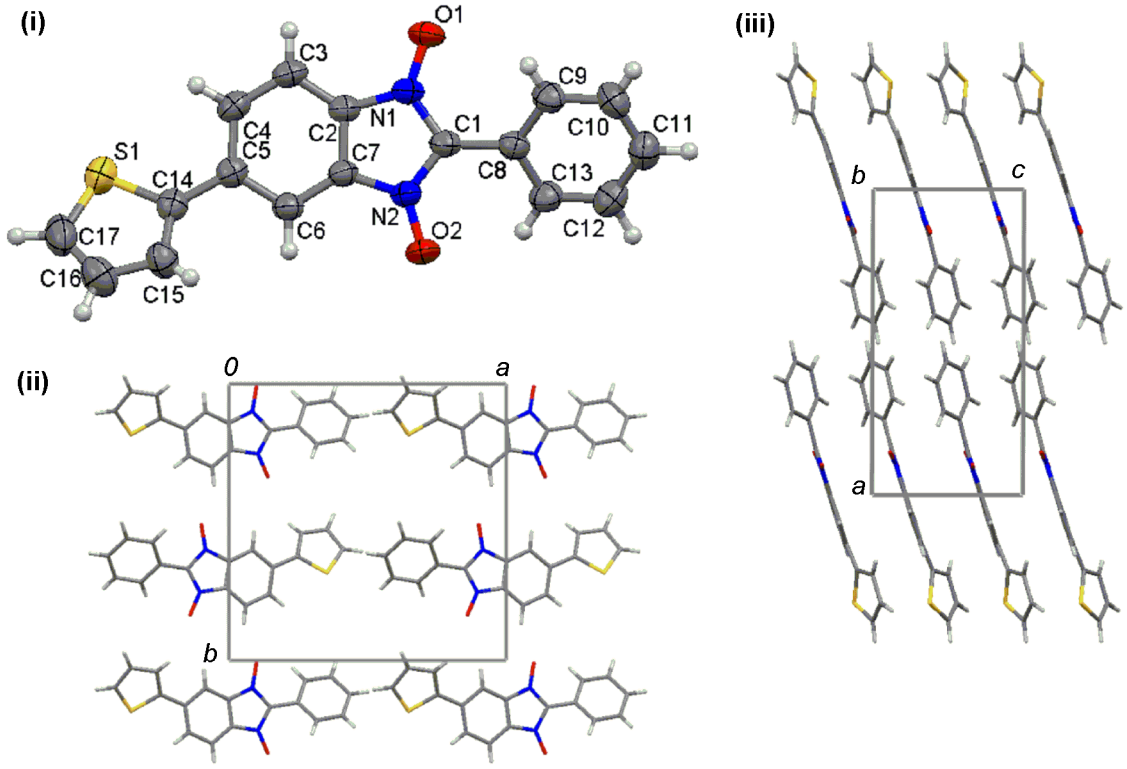

Figure 4.14. Single crystal structure of **4.11a** with 50 % probability thermal ellipsoids (i). Packing diagram of **4.11a** viewed down the *c*-axis (ii), and viewed down the *b*-axis (iii).

4.5.2 Crystallographic analysis of 4.11b

Table 4.3. Crystallographic data for **4.11b**.

	4.11b
formula	$C_{15}H_9N_2O_2S_2$
formula weight	313.37
color of crystal	green powder
crystal system	$P2_1/c$
space group	monoclinic
a (Å)	13.000 (1)
b (Å)	20.954 (2)
c (Å)	4.9518 (3)
volume (Å^3)	1347.86 (8)
temperature (K)	298
Z	4
R_f[a]	-
R_w[b]	-
GOF	-

The crystal structure and packing diagram of **4.11b** were determined by PXRD and are shown in Figure 4.15. As in **4.11a**, the benzimidazole skeleton adopts a planar geometry and the *C*5-thienyl ring is nearly coplanar (−7º torsion angle between *S*15-*C*11-*C*2-*C*3) with the benzimidazole moiety. The *C*2-thiophene imidazole torsion angle (*N*7-*C*8-*C*10-*S*19) is larger (31º) than that in 2-thienyl benzonitronyl nitroxide **2.15d** suggesting solid-state packing interactions are primarily responsible for the degree of ring torsion.

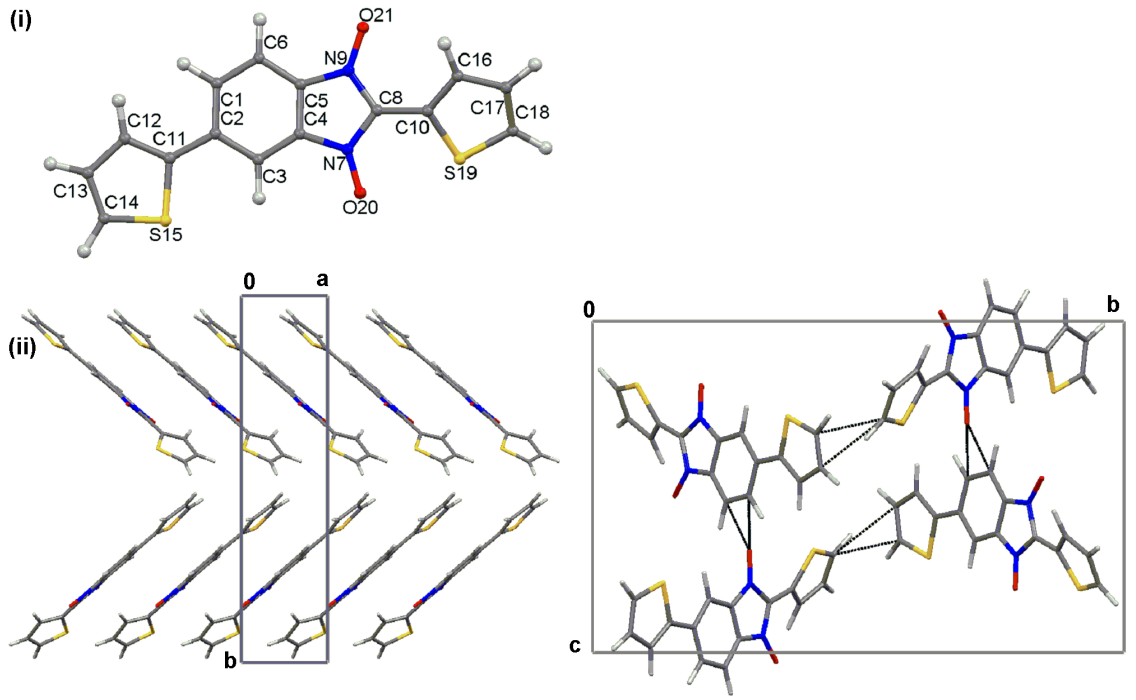

Figure 4.15. Labeled molecular structure of **4.11b** (i). Packing diagram of **4.11b** viewed along the *c*-axis (ii), and down the *a*-axis (iii).

Radical **4.11b** forms slipped π stacks along the *a*-axis separated by an interplanar distance of 3.26 Å with a 49º slippage angle between radicals along the chain. This large degree of slippage results in close contacts between electron rich (donor) thiophene rings and neighboring electron poor (acceptor) benzonitronyl nitroxide units (Figure 4.16), giving rise to intermolecular donor–acceptor interactions that are governed by electrostatic interactions. In addition to the close contacts within the π stack, close thiophene ring (*C*18…*C*14, 2.72 Å and *C*18…*C*13, 3.15 Å) and benzimidazole *O*20…*C*6 (2.25 Å) and *O*20…*C*1 (2.76 Å) contacts (Figure 4.15) exist between stacks, forming chains along the *b*- and *c*-axes. Analysis of the solid-state packing of **4.11b** suggests the presence of multiple exchange pathways and a higher dimensional structure when compared to **4.11a** which is predominantly 1D.

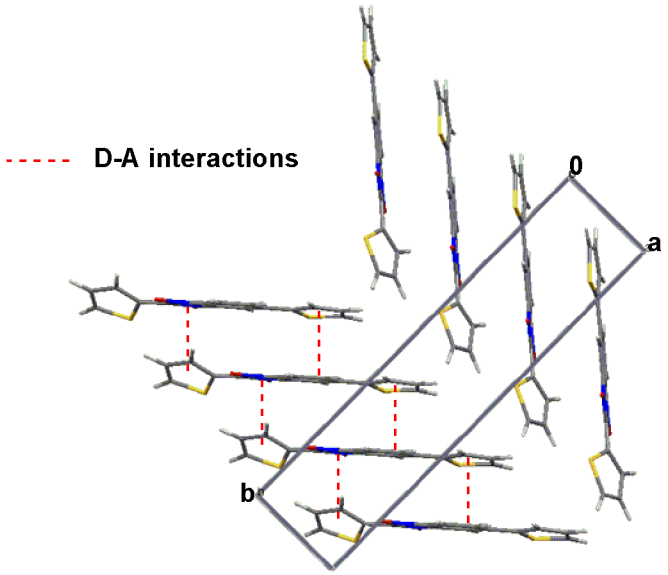

Figure 4.16. π stacks of **4.11b** viewed along the *c*-axis. Donor–acceptor interactions indicated by red dashed lines.

4.6 Magnetism of 4.11a and 4.11b

The molar magnetic susceptibilities ($\chi_{M,p}$) were measured for microcrystalline samples of radicals **4.11a-b** using a Quantum Design SQUID magnetometer in the temperature range of 2 – 300 K at DC fields of 0.1 – 5 T (Figures 4.17 and 4.18). At 300 K **4.11a** and **4.11b** exhibit magnetic moments close to the expected spin only value for an S = ½ system (0.375 emu K/mol). Below 250 K, the magnetic moment ($\chi_{M,p}T$) of phenyl derivative **4.11a** decreases with decreasing temperature (Figure 4.17, right) with a maximum in the molar magnetic susceptibility at 20.0 K (Figure 4.17, left), consistent with the presence of antiferromagnetic exchange interactions.

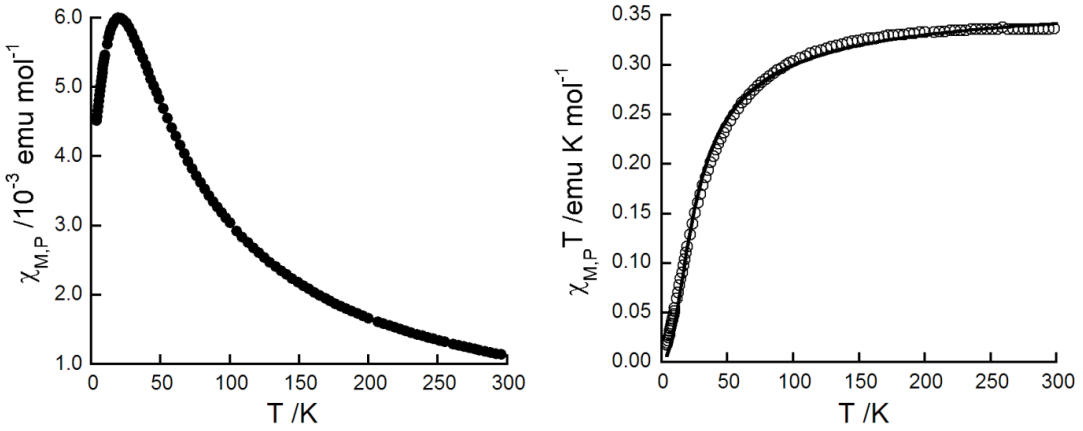

Figure 4.17. Temperature dependence of the molar magnetic susceptibility (top) and magnetic moment for radical **4.11a** (bottom). The solid line represents the best fit of the data to the model described in the text.

Based on the uniform 1D chain-like behaviour observed in the crystal structure, the Bonner–Fisher chain model[248] derived from the spin Hamiltonian $H = -JS_{rad}\cdot S_{rad+1}$ was used to fit the magnetic moment. A purity factor (f) was included to account for the percentage of spins behaving according to the model and the g-value was fixed at 2.0068 as determined by EPR.

$$\chi T = f\frac{Ng^2\beta^2}{k_B}\cdot\frac{0.25+0.074975x+0.075235x^2}{1.0+0.9931x+0.172135x^2+0.757825x^3}$$

$$x = \frac{|J|}{k_B T};\quad J \leq 0$$

The least-squares fit of the experimental data is very good (R = 1.0), leading to a exchange coupling parameter, J, of -33 cm^{-1} with f = 0.97. Moderate antiferromagnetic coupling on the order of that reported for **4.11a** has been observed in other BNN radicals[223] and can be attributed to the formation of 1D π stacks in the solid state. The system is well-described using a linear chain model suggesting that the O2…C3

interchain interactions do not contribute significantly to exchange pathways, thus, the inclusion of a mean-field parameter (*2zJ'*) was not necessary.

The magnetic moment of derivative **4.11b** is independent of temperature above 50 K with a magnitude of 0.378 at 300 K, slightly higher than the spin only value for an $S = ½$ system. The moment increases gradually below this temperature, suggesting ferromagnetic intermolecular interactions (Figure 4.18). The magnetic data was fit with a high-temperature series expansion of the Bonner-Fisher model (Padé approximant, below)[337] derived from the same spin Hamiltonian described above.[337] The data was not well represented by this model alone, which was not surprising as this analytical model only accounts for 1D magnetic chain interactions. Consequently a mean-field parameter was included in the analytical expression to account for the observed interchain magnetic interactions.

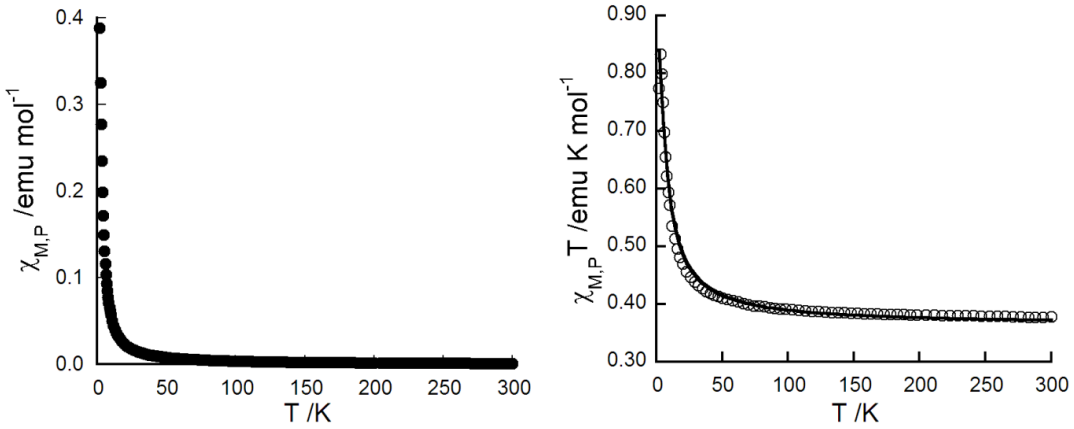

Figure 4.18. Temperature dependence of the molar magnetic susceptibility (top) and magnetic moment for radical **4.11b** (bottom). The solid line represents the best fit of the data to the model described in the text.

A fit of the magnetic data using a linear chain model with a mean field approximation gave a least squares fit of the experimental data with R = 0.99. The g-value was fixed to the experimentally derived value of 2.0067 (from EPR) to give J = +5 cm^{-1} and $2zJ'$ = +0.9 cm^{-1} with an f of 0.96. A fit of the magnetic data confirms the system cannot be accurately described by a simple 1D chain model as there is non-negligible through space spin density overlap in more than one direction in the solid state.

$$\chi'T = f\frac{Ng^2\beta^2}{4k_B}\cdot\left[\frac{N}{D}\right]^{2/3}$$

$$N = 1.0 + 5.7979916y + 16.902653y^2 + 29.376885y^3 + 29.832959y^4 + 14.036918y^5$$

$$D = 1.0 + 2.7979916y + 7.0086780y^2 + 8.6538644y^3 + 4.5743114y^4$$

$$y = J/2k_BT$$

$$\chi T = \frac{\chi'T}{1-\left(\frac{2zJ'}{Ng^2\beta^2}\right)\chi'T}$$

The maximum values of $\chi_{m,p}T$ were highly dependent on the applied field and saturation effects were observed below 15 K at higher field (Figure 4.20, a). More detailed studies of the magnetization at low temperatures (2 – 40 K) shed light on the nature of the low temperature ferromagnetic exchange interactions. The zero field cooled (ZFC) and field cooled (FC) magnetizations were measured and found not to diverge at low temperature (Figure 4.19), consistent with fast spin relaxation and the absence of a blocking temperature suggesting short-range magnetic interactions.

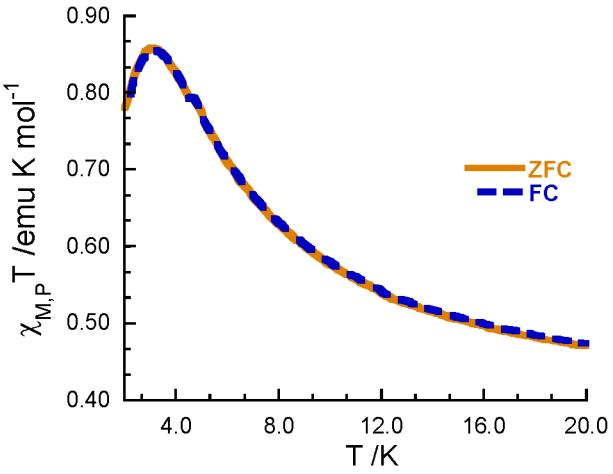

Figure 4.19. Temperature dependence of the molar magnetic susceptibility when cooled in the absence of an external field (ZFC) and in the presence of an external field (FC).

The temperature and frequency dependence of the AC magnetization was measured in the low temperature regime. The AC susceptibility was measured at frequencies between 1 and 999 Hz with a 2.57 Oe driving field, and 10 Oe external field between 2.0 and 10.0 K. While both imaginary and real components to χ_{ac} were observed, maxima were not observed above 2.0 K. A small frequency dependence was observed in the out-of-phase (χ'') AC susceptibility that was more pronounced at high frequency (Figure 4.20, c and d). AC susceptibility suggests there may be short range interactions at low temperature on the time scale of the high frequency AC experiments, however, spin relaxation is fast. Measurement of the field dependence of the magnetization at 2 K revealed a small (10 Oe) coercive field (Figure 4.20, b).

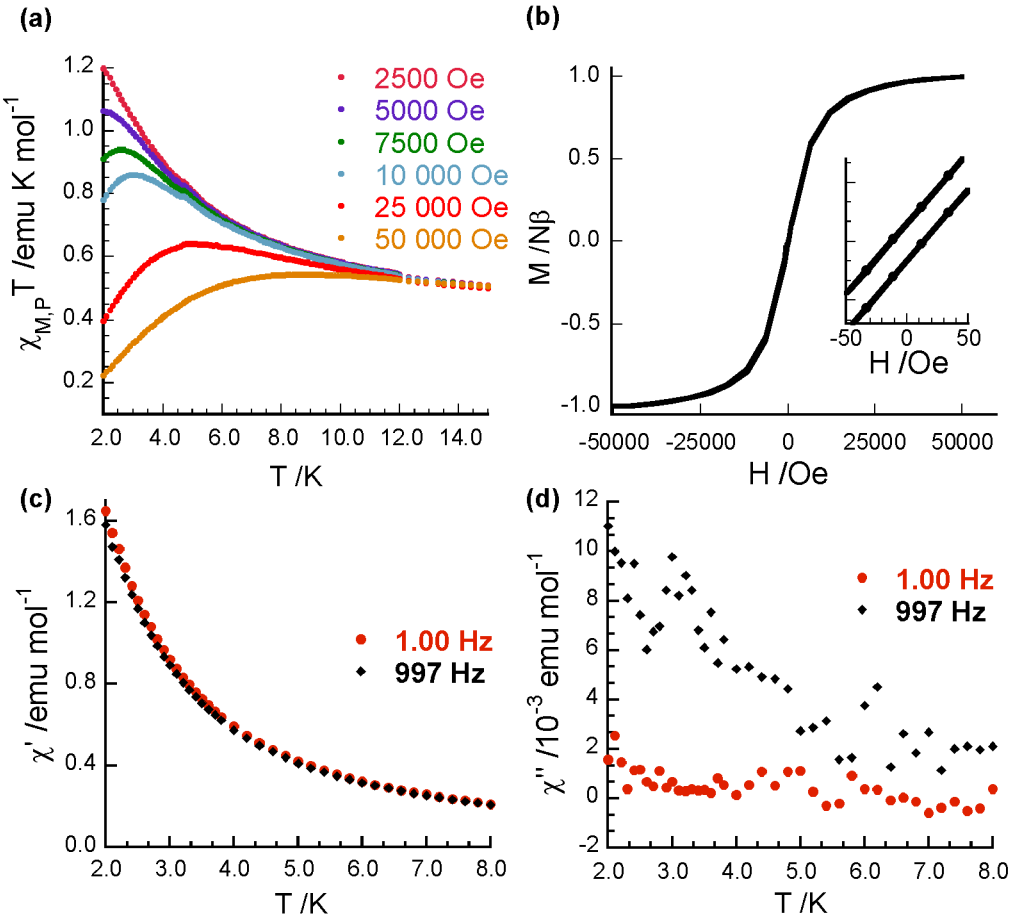

Figure 4.20. (a) Magnetic moment of **4.11b** as a function of temperature and field, 2 – 15 K. (b) Hysteresis loop at 2 K for **4.11b**, −5 to 5 T, H_c = 10 Oe. (c) In phase (χ′) AC susceptibility and (d) out of phase (χ″) AC susceptibility of **4.11b**, 2.57 Oe driving field, 10 Oe external field.

4.7 Magnetostructural analysis

Analysis of the intermolecular crystallographic packing interactions combined with unrestricted DFT methodology allow for computational evaluation of the magnetic exchange coupling constant *J*. This methodology is a first-principles bottom-up theoretical procedure[338] and allows for correlation of the experimentally measured magnetism, a macroscopic phenomena of the system, with the microscopic magnetic motif arising from the crystallographic packing.[339] Molecular packing in a crystal

structure can be described in terms of the distance between non-covalently bound molecules and the strength of the non-covalent interactions. The magnetic structure of a crystal can be described in an analogous way (Figure 4.21) where the overall magnetic solid state structure is the linear combination of all the dimeric magnetic exchange interactions J_{AB} between radical sites A and B. It is the repeat of the dominant exchange interactions in any given direction that ultimately gives rise to the overall bulk magnetism of the solid.

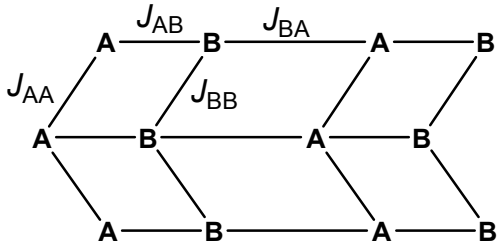

Figure 4.21. Different possible exchange interactions (*J*) between neighboring type A and type B radical sites in a theoretical solid.

The identification and calculation of the energy gap between each pairwise (AA, AB etc.) interaction allows for the calculation of each individual value of *J*. This is accomplished by isolating each closely packed (within van der Waals) dimer and using the nuclear crystallographic coordinates as geometry input for two single point DFT calculations which, in the case of an $S = ½$ pair of radicals, calculate the energy of the singlet $S = 0$ (antiferromagnetically coupled) and the triplet $S = 1$ (ferromagnetically coupled) states. Using the overall energy calculated for each state ($S = 0, 1$) the magnetic exchange can be determined based on the equation below where E_{BS} and E_T denote the energies of the broken symmetry singlet and triplet state and $\langle S^2 \rangle_{BS}$ and $\langle S^2 \rangle_T$ are represent average spin square values of the broken symmetry singlet and triplet state.[340] Broken

symmetry solutions often contain high degrees of spin contamination which can be partially accounted for using a spin projection technique which includes $\langle S^2 \rangle_{BS}$ and $\langle S^2 \rangle_T$ in the denominator of the expression used to calculate *J*. Additionally, when calculating the energy of the open-shell singlet the keyword "guess=mix" is included in the unrestricted formalism.

$$J = \frac{(E_{BS} - E_T)}{\langle S^2 \rangle_T - \langle S^2 \rangle_{BS}}$$

During analysis of the crystal packing of radical **4.11a** it was noted the radicals form well-isolated uniform chains. For this reason it was believed only one type of dimer interaction would significantly contribute to the bulk magnetism of the system. DFT calculations of the π-dimer using the hybrid UB3LYP functional with the 6-311+G(d,p) basis set[340] for the singlet and triplet states predicted a system with an exchange energy on the order of $J = -5$ cm^{-1} which is in good agreement with the experimentally derived value of -33 cm^{-1}. This certainly suggests the π stacked chains are providing the dominant exchange pathway and confirms the antiferromagnetic nature of the exchange.

Analysis of the crystal packing in radical **4.11b** led to evaluation of three sets of dimers, the π stacked dimer, as well as two sets of interchain dimers arising from close thiophene and benzimidazole ring contacts (Figure 4.22). The D–A π dimer was predicted computationally to possess a high spin ground state with an exchange energy on the order of $J = +33$ cm^{-1}. The thiophene C18…C13/14 dimer and O20…C1/6 dimers had much smaller exchange energies at +5 cm^{-1} and +1 cm^{-1} respectively. These computational values are in agreement with the sign of the experimentally derived magnetic exchange integrals ($J = +5$ cm^{-1} and $2zJ' = +0.9$ cm^{-1}) and suggest very strong exchange in radical **4.11b** would be possible in a more highly ordered state. The disorder

present in the system, as revealed by the poor quality of the PXRD data, leads to an effective decrease in the exchange, and suggests that highly ordered single crystalline materials are capable of three dimensional magnetic ordering to give exchange integrals of significant magnitude.

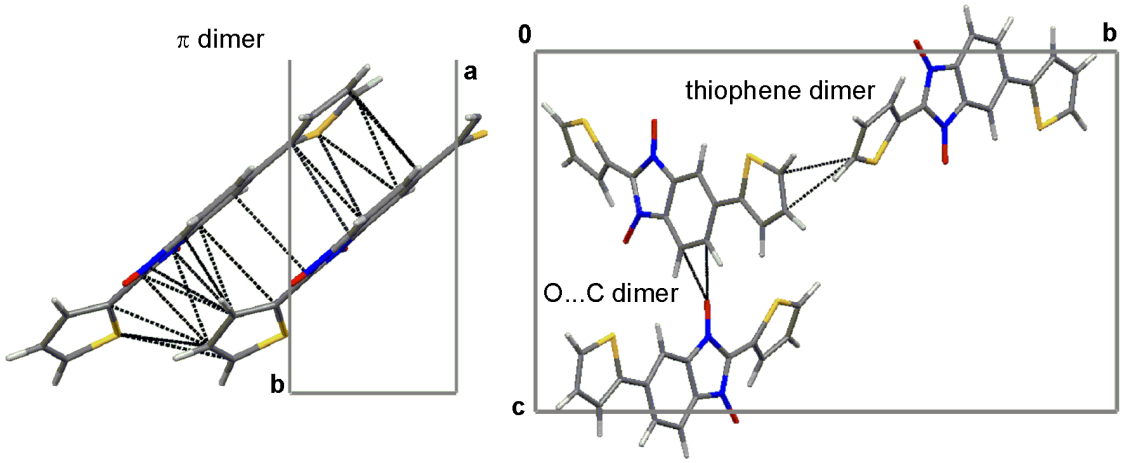

Figure 4.22. π dimer viewed along the *c*-axis (left) and thiophene C18…C13/14 and O20…C1/6 dimers viewed along the *a*-axis (right). Distances less than the sum of the van der Waals radii of two atoms (hydrogen excluded) indicated with black dashed lines.

4.8 Conductivity

The conductivity of **4.11a-b** was measured using a two-probe pressed pellet conductivity apparatus[341] externally calibrated with tetrathiafulvalene-tetracyanoquinodimethane (TTF-TCNQ).[132,342] The room temperature conductivity of **4.11b** was found to be on the order of 10^{-5} S cm^{-1} whereas **4.11a** showed a conductivity of 10^{-7} S cm^{-1}. These conductivities are accurate to within an order of magnitude and vary sample to sample, nevertheless, these preliminary measurements provide the conductivity regime of each material. The conductivity of **4.11b** implies it is semiconducting while **4.11a** lies on the semiconductor/insulator border. The higher

conductivity observed in **4.11b** is a direct result of the close atom-atom contacts in the solid state that give rise to multidimensional overlap and numerous well defined conduction pathways. Single-component neutral radical conductors are rare[100,119,120,343-347] and future work will involve elucidating the mechanism of charge transport and the nature of the charge carriers in order to evaluate the potential of these materials as intrinsic molecular magneto-conductors.

4.9 Solid state reflectance spectroscopy

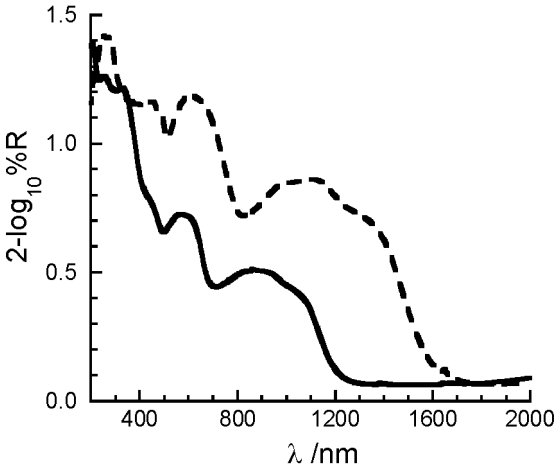

Figure 4.23. Diffuse reflectance spectra of films of **4.11a** (—) and **4.11b** (---) deposited from CH_2Cl_2 onto quartz slides, spectralon discs were used as a reflective background.

Solid state reflectance spectra were obtained on thin films of **4.11a-b** drop cast from dichloromethane. When compared to the solution phase absorption spectrum, the solid state absorbance (Figure 4.23) of **4.11a** does not contain any new transitions that could be attributed to intermolecular interactions. Conversely, when the solution and solid phase absorption spectra of **4.11b** are compared, the NIR transition is bathochromically shifted by ~200 nm in the solid state relative to the solution phase. The observed shift is

consistent with the presence of strong solid state intermolecular (donor–acceptor and π–π) interactions giving rise to an absorption onset on the order of 0.77 eV (1600 nm).This, in combination with the magnetic data, suggests isolation of a more ordered state of radical **4.11b** could lead to the realization of a purely organic ferromagnetic semiconductor with a moderately low activation energy.

4.10 Conclusions

We have shown that the structure of spin-delocalized acceptor BNN radicals can be modified to give paramagnetic donor–acceptor–donor triads that function as ferromagnetic or antiferromagnetic semiconductors, depending on a subtle interplay between π–π and donor–acceptor interactions in the solid state. We have developed synthetic methodology for installation of a thienyl moiety in the *C*5 position of benzonitronyl nitroxide radicals, resulting in extended π-conjugated systems with a D–A–D electronic structure. EPR spectroscopy was consistent with a spin delocalized structure, with hyperfine coupling to peripheral thienyl rings on the order of < 1 Gauss. A decrease in the SOMO energy results in a further decrease in the reduction potential of BNN, leading to a class of powerful electron acceptors for organic electronic materials.

Functionalization of the benzannelated ring leads to the appearance of two new electronic transitions attributed to charge transfer excitations as a result of a donor–acceptor interaction. The charge transfer excitations were investigated by solvatochromic and variable temperature electronic absorption spectroscopy. The lowest energy excitation at 1000 nm, observed in the parent BNN, is attributed to a HOMO–SOMO transition and was preserved in radicals **4.11a** and **4.11b** despite functionalization of the

benzannelated ring. Two close-lying charge transfer excitations in the visible (500 – 600 nm) were observed and assigned as HOMO−1 → SOMO and HOMO−*n* → SOMO transitions, the energy and intensity of which depend on solvent polarity and *C*5-thienyl…BNN torsion angle. TDDFT with the inclusion of a solvent continuum model provided a reasonable description of the observed spectroscopy and dependence of the transitions on geometry and dielectric medium, supporting the proposed assignment.

TDDFT electronic structure computations using the unrestricted formalism (UB3LYP) support a spin delocalized structure with differences in orbital coefficients and energy of the α– and β–SOMO orbitals arising from spin polarization effects. The spin density distribution is consistent with significant spin population in all positions of the molecule, leading to strong magnetic exchange interactions in the solid state via π–π interactions.

In the solid state, radical **4.11a** exhibits face-to-face π–π interactions that give rise to 1D chains responsible for the observed antiferromagnetic exchange and a room temperature conductivity of 10^{-7} S cm^{-1}. In contrast, radical **4.11b** exhibits slipped π stacks dominated by D/A interactions. The presence of additional interchain interactions leads to ferromagnetic exchange and an increase in conductivity (10^{-5} S cm^{-1}) due to higher dimensionality of the interaction lattice. The dominant exchange pathway is found to be intrachain with significant contributions from interchain interactions. Using a first principles bottom-up approach, the magnetic exchange was reproduced well computationally and was consistent with the experimentally observed magnetization. The solid state conductivity was found to be remarkably high for a non-doped organic system containing only light elements and future work will involve investigating carrier mobility and characterizing the nature of the charge carriers in these D–A–D systems.

4.11 Experimental

4.11.1 General procedures

All general synthetic procedures employed have been previously reported in Chapter 2.9.

Reflectance Spectra. Reflectance spectra were collected on a Perkin Elmer Lambda 1050 UV–vis–NIR spectrometer equipped with a 150 mm InGaAs integrating sphere. Solid samples were prepared by dropcasting films from concentrated dichloromethane solutions onto quartz slides under a stream of N_2. Spectralon discs were used as a 100 % R standards and were mounted behind the quartz slide to act as a reflective background.

Computations. Quantum mechanical calculations were carried out at the UB3LYP/6-31G(d,p) level of theory or the UB3LYP/6-311+G(d,p) level of theory[237,238] using the Gaussian 09 package.[239] All calculations were single point energy calculations where the input geometry was obtained from X-ray diffraction data. All single point energy calculations included a specified solvation model with the exception of the singlet-triplet gap dimer calculations.

X-ray Crystallography. A purple plate-like crystal of $C_{17}H_{11}N_2O_2S$ having approximate dimensions of 0.005 x 0.28 x 0.40 mm was mounted on a polymer loop. Single crystal X-ray diffraction data was collected on a Bruker SMART6000 CCD detector sitting on a Bruker D8 3-circle goniometer sitting on a Rigaku RU200 Cu rotating anode utilizing Cu/Kα radiation (λ = 1.54178 Å) and cross-coupled parallel focusing Göbel mirrors. The data were collected at a temperature of 23 ± 0.2 ºC to a maximum 2θ value of 68.3º. Of the 9124 reflections that were collected, 2508 were

unique (R_{int} = 0.0347). Data were corrected for absorption effects using the multi-scan technique with minimum and maximum transmission coefficients of 0.4847 and 0.9895, respectively. The structure was solved using the direct-methods procedure in the Bruker SHELXTL[288,348] program library and refined by a full-matrix least-squares refinement on F^2 based on 2508 reflections and 243 variable parameters. Upon convergence the maximum and minimum peaks on the final difference Fourier map corresponded to 0.186 and –0.344 e $Å^{-3}$, respectively.

Powder XRD Crystallography. A powder X-ray diffraction pattern (0.0042º steps) was obtained on a Panalytical X'Pert Pro diffractometer using a Cu−Kα_1 radiation with λ = 1.540598 Å source operating at 45 kV/35 mA at a temperature of 298 K. The X'Celerator linear detector was used to scan from 7 to 120º 2θ in a continuous scan. The powder X-ray data were analyzed using Topas[336] starting from the indexing of the cell, identification of the space group ($P2_1/c$), and random positioning of a geometry optimized structure. The position and orientation of the molecule was refined, as were the torsion angles of the thiophene linkages.

4.11.2 Synthesis

Synthetic Methodology. Phenylhydroxylamine was synthesized according to known literature methods.[349] *C*-phenyl-*N*-phenylnitrone and *C*-2-thienyl-*N*-phenylnitrone were synthesized as previously reported.[221] 2-nitro-4-(2-thienyl)-benzenamine **4.8** was synthesized by modifying the Stille reaction conditions developed by Littke et al.[321]

***N*-(4-Bromophenyl)-acetamide (4.5)**.[350] 4-bromoaniline (15.0 g, 87 mmol) was suspended in 70 mL acetic anhydride. The mixture was heated at 90 ºC until the reaction was complete (TLC, 1:1 hexane:ethyl acetate). The hot solution was poured over ice and

the crude solid was isolated by vacuum filtration, washed with water (2 x 50 mL) and air dried. Recrystallization from hot MeOH/H_2O afforded 17.9 g (84 mmol, 97 %) of a white crystalline solid. mp 156 – 158 ºC (lit[350,351] 168 ºC). IR (KBr) cm^{-1}: 3295, 2853, 2601, 1667, 1603, 1536. ^1H NMR (300 MHz, CD_3OD): δ 7.49 (d, J = 9 Hz, 2H), 7.42 (d, J = 9 Hz, 2H), 2.11 (s, 3H). ^{13}C NMR (75 MHz, CD_3OD) δ 171.7, 139.2, 132.7, 123.1, 117.4, 23.9. EI-MS (70 eV) *m/z* (relative intensity): 215 (M^+, 100 %), 217 ($[M + 2]^+$, 100 %).

***N*-(4-Bromo-2-nitrophenyl)-acetamide (4.5)**. N-(4-bromophenyl)-acetamide **4.5** (17.0 g, 79 mmol) was dissolved in a minimal amount of trifluoroacetic acid (~30 mL) and cooled to 0 ºC in an ice bath. Cold (4 ºC) fuming HNO_3 was added dropwise to the stirring solution until the reaction was deemed complete by TLC (1:1 hexane:ethyl acetate). The reaction mixture was poured slowly over ice. Upon standing a yellow precipitate formed. The precipitate was isolated by suction filtration, washed with water, and dried *en vacuo* yielding 19.7 g (76 mmol, 96 %) of a yellow powder. The product was used without subsequent purification. mp 98 – 99 ºC (lit[352] 104 ºC) IR (KBr) cm^{-1}: 3366, 1713, 1604, 1573, 1480. ^1H NMR (300 MHz, $CDCl_3$): δ 10.23 (bs, 1H), 8.70 (d, J = 9 Hz, 1H), 8.32 (d, J = 2 Hz, 1H), 7.70 (dd, J = 9, 2 Hz, 1H), 2.27 (s, 3H). ^{13}C NMR (75 MHz, $CDCl_3$) δ 169.0, 138.7, 136.5, 133.9, 128.1, 123.6, 115.2, 25.6. EI-MS (70 eV) *m/z* (relative intensity): 259.1 (M^+, 100 %), 261.1 ($[M + 2]^+$, 100 %). Anal. Calcd for $C_8H_7BrN_2O_3$: C, 37.09; H, 2.72; N, 10.81. Found: C, 37.00; H, 2.79; N, 10.68.

4-Bromo-2-nitro-benzenamine (4.7). *N*-(4-bromo-2-nitrophenyl)-acetamide **4.6** (10.0 g, 39 mmol) was suspended in 300 mL 9 M HCl. The reaction mixture was heated gently until all starting material had dissolved. Upon completion (TLC, CH_2Cl_2) the warm reaction solution was poured over ice yielding an orange precipitate. The precipitate was

isolated with vacuum filtration, washed with minimal water, and dried *en vacuo*. Recrystalization from hot MeOH/H_2O afforded 7.8 g (36 mmol, 92 %) of an orange crystalline solid. mp 102 – 104 ºC (lit[353] 109 – 110 ºC). IR (KBr) cm^{-1}: 3474, 3352, 1636, 1559, 1499. ^1H NMR (300 MHz, $CDCl_3$): δ 8.26 (d, J = 2 Hz, 1H), 7.42 (dd, J = 9, 2 Hz, 1H), 6.73 (d, J = 9 Hz, 1H), 6.10 (bs, 2H). ^{13}C NMR (75 MHz, $CDCl_3$) δ 143.7, 138.6, 132.6, 128.4, 120.5, 108.0. EI-MS (70 eV) *m/z* (relative intensity): 215.9 (M^+, 100 %), 217.9 ($[M + 2]^+$, 100 %) Anal. Calcd for $C_6H_5BrN_2O_2$: C, 33.21; H, 2.32; N, 12.91. Found: C, 33.20; H, 2.47; N, 12.78.

2-Nitro-4-(2-thienyl)-benzenamine (4.8). An oven dried two-neck flask was charged with 4-bromo-2-nitro-benzenamine **4.7** (1.109 g, 5.1 mmol), tris(dibenzylideneacetone)dipalladium(0) (0.070 g, 0.076 mmol, 1.5 mol %), tri-o-tolylphosphine (0.079 g, 0.26 mmol, 5 mol %) and cesium fluoride (1.580 g, 10 mmol). The flask was subject to three evacuation-backfill cycles (N_2). Dry, degassed THF (20 mL) and tributyl-2-thienyl-stannane (1.65 mL, 5.2 mmol) were added via syringe. The solution was gently refluxed for 10 h, cooled to room temperature, diluted with diethyl ether and eluted through a Celite-545/silica plug (diethyl ether as eluent). The filtrates were isolated and concentrated *en vacuo* to afford a crude solid. Recrystallization from hot MeOH/H_2O afforded 1.033 g (4.7 mmol, 92 %) of a dark red crystalline solid. mp 157 – 159 ºC. ^1H NMR (300 MHz, $CDCl_3$): δ 8.36 (d, J = 2 Hz, 1H), 7.62 (dd, J = 9, 2 Hz, 1H), 7.27 – 7.21 (m, 2H), 7.07 (dd, J = 5, 4 Hz 1H), 6.84 (d, J = 9 Hz, 1H), 6.12 (bs, 2H). ^{13}C NMR (75 MHz, $CDCl_3$): δ 143.7, 142.3, 133.6, 132.3, 128.1, 124.4, 124.2, 122.7, 122.7, 119.3. EI-MS (70 eV) *m/z* (relative intensity): 220 (M^+, 100 %), 174 ([M −

$NO_2]^+$, 15 %). Anal. Calcd for $C_{10}H_8N_2O_2S$: C, 54.53; H, 3.66; N, 12.72. Found: C, 54.28; H, 4.00; N, 12.42.

5-(2-Thienyl)-2,1,3-benzoxadiazole-3-oxide (4.9). 2-nitro-4-(2-thienyl)-benzenamine **4.9** (0.511 g, 2.3 mmol) was dissolved in 20 mL of a 10 % w/v NaOH/EtOH solution and cooled to 0 °C in an ice bath. A cold 10.8 % w/w NaOCl solution was added dropwise until the reaction mixture had lost its deep red color and a light yellow precipitate had formed. The precipitate was isolated by vacuum filtration, washed with minimal water and purified by flash column chromatography (silica gel, 50:50 hexane:ethyl acetate) yielding 0.458 g (2.1 mmol, 91 %) of a pale yellow solid. mp 131 – 132 ºC. IR (KBr) cm^{-1}: 2963, 2924, 1611, 1520, 1473. Note: *isomerization occurring on NMR timescale, only broad peaks observed in ^1H and ^{13}C NMR. C signals could be resolved, even on 500 MHz NMR with multiple scans.* ^1H NMR (300 MHz, $CDCl_3$): δ 7.70 – 7.40 (m, 5H), 7.15 (dd, J = 5, 4 Hz, 1H). EI-MS (70 eV) *m/z* (relative intensity): 218 (M^+, 100 %), 202 ([M − O]$^+$, 25 %), 172 ([M − NO_2]$^+$, 10 %). Anal. Calcd for $C_{10}H_6N_2O_2S$: C, 55.04; H, 2.77; N, 12.84. Found: C, 54.75; H, 2.68; N, 12.73.

1-Hydroxy-2,5-di-(2-thienyl)-benzimidazole-3-oxide (4.10b). 5-(2-thienyl)-2,1,3-benzoxadiazole-3-oxide **4.9** (0.506 g, 2.3 mmol) and *C*-(2-thienyl)-*N*-phenylnitrone **2.21d** (0.523 g, 2.6 mmol) were dissolved in 20 mL toluene. The reaction was warmed to 45 ºC for 16 hours. A tan precipitate formed in the flask and was isolated by vacuum filtration. The solid was washed with acetone and pentane and dried *en vacuo* yielding 0.401 g (1.3 mmol, 57 %) of a light tan powder. mp decomp. 200 − 202 ºC. ^1H NMR (300 MHz, 1.0 M NaOD in CD_3OD): δ 9.01 (dd, J = 4, 1 Hz, 1H), 7.94 (d, J = 1 Hz, 1H), 7.75 – 7.63 (m, 2H), 7.62 (dd, J = 9, 2 Hz, 1H), 7.45 (dd, J = 4, 1 Hz, 1H), 7.38 (dd, J = 5,

1 Hz, 1H), 7.31 (dd, J = 5, 4 Hz, 1H), 7.11 (dd, J = 5, 4 Hz, 1H). ^{13}C NMR (75 MHz, 1.0 M NaOD in CD_3OD): δ 145.7, 136.3, 131.3, 131.0, 130.7, 129.6, 129.2, 128.6, 127.7, 125.7, 125.6, 124.3, 122.7, 112.6, 108.6. EI-MS (70 eV) *m/z* (relative intensity): 314 (M^+, 15 %) 298 ($[M - O]^+$, 100 %). Anal. Calcd for $C_{15}H_{10}N_2O_2S$: C, 57.31; H, 3.21; N, 8.91. Found: C, 57.31; H, 3.01; N, 8.83.

1-Hydroxy-2-phenyl-5-(2-thienyl)-benzimidazole-3-oxide (4.10a). Light tan powder isolated in 65 % yield. mp decomp. 186 – 188 ºC. ^{1}H NMR (300 MHz, 1.0 M NaOD in CD_3OD): δ 8.59 (dd, J = 7, 5 Hz, 2H), 7.99 (dd, J = 2, 1 Hz, 1H), 7.77 (dd, J = 9, 1 Hz, 1H), 7.67 – 7.53 (m, 4H), 7.46 (dd, J = 4, 1 Hz, 1H), 7.39 (dd, J = 5, 1 Hz, 1H), 7.12 (dd, J = 5, 4 Hz, 1H). ^{13}C NMR (75 MHz, 1.0 M NaOD in CD_3OD): δ 145.6, 138.7, 131.6, 131.3, 130.9, 129.7, 129.2, 129.1, 128.7, 125.8, 125.6, 124.5, 122.9, 113.1, 109.0. EI-MS (70 eV) *m/z* (relative intensity): 308 (M^+, 10 %), 292 ($[M - O]^+$, 100 %). Anal. Calcd for $C_{17}H_{12}N_2O_2S$: C, 66.22; H, 3.92; N, 9.08. Found: C, 66.06; H, 3.63; N, 9.05.

2,5-Di-(2-thienyl)-benzimidazolyl N-N′-dioxide (4.11b). 1-hydroxy-2,5-di-(2-thienyl)-1H-benzimidazole-3-oxide **4.10b** (0.142 g, 0.45 mmol) was suspended in EtOH (15 mL) with sonication. An NaOH in ethanol (~0.6 M) solution was added dropwise to the sonicating suspension until all starting material had dissolved to give a yellow solution. The solution was filtered through a Celite-545 plug and concentrated by rotary evaporation. The crude solid was dissolved in a minimal amount of acetone and the solution was added dropwise to pentane. A yellow precipitate formed immediately and was isolated by suction filtration and air dried. The yellow precipitate was dissolved in 1:3 EtOH:CH_2Cl_2 (40 mL) with sonication. $AgPF_6$ (0.110 g, 0.44 mmol) was dissolved in minimal ethanol (~2 mL) and added in one portion to the sonicating solution. A brown

precipitate formed immediately. Further sonication led to formation of a dark green-black solution. The reaction mixture was eluted through a short neutral alumina column (CH_2Cl_2 as eluent). The filtrates were isolated and concentrated until the bulk of the dichloromethane had been removed. The ethanol solution was cooled to −78 ºC ($CO_{2(s)}$/acetone) for one hour. The solid material that formed was isolated on a cold filter stick, washed with cold pentane and dried *en vacuo*. The crude solid was dissolved in a minimal amount of dry diethyl ether and filtered through a Celite-545 plug (diethyl ether as eluent). The filtrates were isolated and cooled to −78 ºC ($CO_{2(s)}$/acetone). The diethyl ether was removed slowly at this temperature until a dark green solid was observed. The material was isolated on a cold filter stick and dried *en vacuo* yielding 0.024 g (0.08 mmol, 20 %) of a dark green powder. mp decomp. 132 – 134 ºC. HRMS Calcd for $C_{15}H_9N_2O_2S$, 313.0105; found: 313.0119. Anal. Calcd for $C_{15}H_9N_2O_2S$: C, 56.49; H, 2.89; N, 8.94. Found: C, 56.20; H, 3.04; N, 8.75. UV–vis (THF) λ_{max}, nm (ε): 352 (37000), 420 (sh, 2500), 444 (sh, 2100), 475 (1400), 560 (2100), 590 (sh, 1800), 1050 (500).

6-(2-Thienyl)-2-(phenyl)benzimidazolyl N-N′-dioxide (4.11a). Dark purple microcrystalline solid isolated in 20 % yield. mp decomp. 90 – 92 ºC. HRMS Calcd for $C_{17}H_{11}N_2O_2S$, 307.0541; found: 307.0692. Anal. Calcd for $C_{17}H_{11}N_2O_2S$: C, 66.43; H, 3.61; N, 9.11. Found: C, 66.30; H, 3.60; N, 9.08. UV–vis (THF) λ_{max}, nm (ε): 320 (31000), 330 (35000), 379 (4000), 414 (2200), 434 (sh, 2100), 466 (1300), 580 (1700), 910 (520).

Chapter 5: Synthesis and Characterization of Benzannelated Nitronyl Nitroxide Donor–Acceptor Dyads

5.1 Modulation of D–A coupling

Increased conductivities and mobilities have been observed in donor–acceptor (D–A) molecular[96,354] and polymeric systems.[309,355,356] In such systems the effective optical band gap is dictated by the energy of the charge transfer band, which is, to a first approximation, a function of the ionization potential (IP) and electron affinity (EA) of the donor and acceptor.[309,355,357-361]

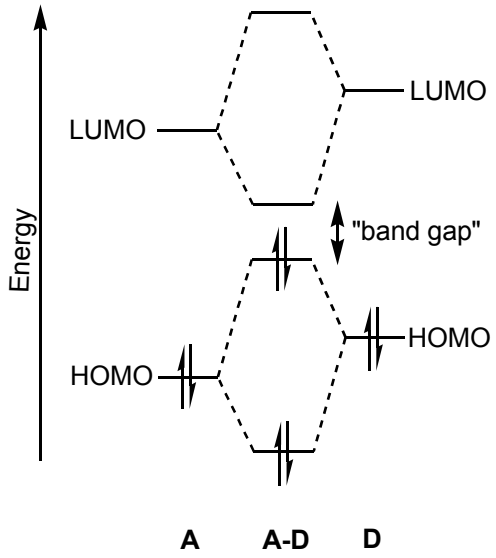

Figure 5.1. Theoretical donor (D) and acceptor (A) where hybridization of D and A energy levels results in a D–A monomer unit with a small HOMO–LUMO (band gap) separation.

When the IP of the donor and EA of the acceptor are close in energy, efficient mixing between D and A occurs resulting in a D–A molecule with an unusually small HOMO−LUMO separation (Figure 5.1). This D–A approach has been used to construct

closed-shell regioregular D–A copolymers that exhibit conductivities much greater than their homopolymer analogues.[355,356,362-364] Consequently, in closed-shell systems, physical properties such as band gap, frontier orbital energy levels, and carrier mobility can be modulated by appropriate choice of donor and acceptor.

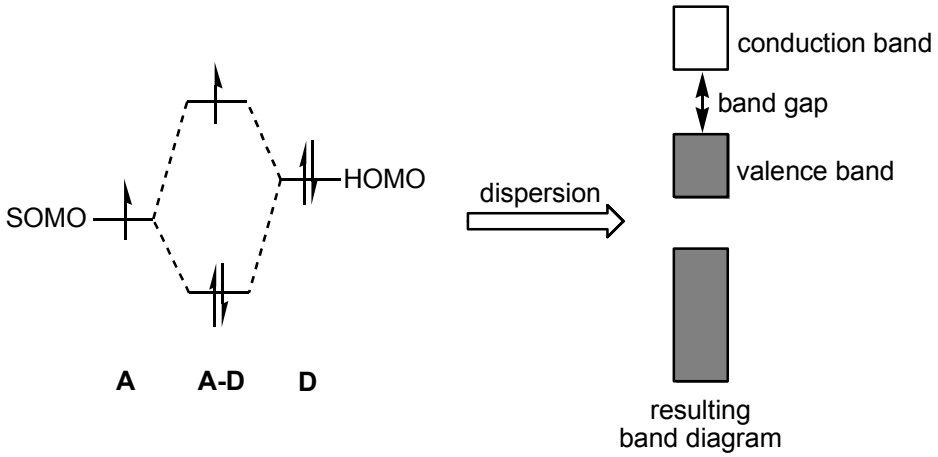

Figure 5.2. Mixing of an A and D where the HOMO of A is only half-filled (left) and the resulting band structure of the theoretical D–A system.

A similar molecular orbital diagram can be constructed to describe the mixing of an open-shell acceptor with a closed-shell donor (Figure 5.2), however, the net result is not simply a decrease in band gap. Dispersion of the orbitals presented in Figure 5.2 would result in formation of a filled band and a half-filled band. The half-filled band would be of radical character and susceptible to the same lattice deformations that typically lead to an opening of a band gap between the conduction and valence band in 1D $S = ½$ systems, that is Peierls distortions or the formation of Mott insulating states.

Nevertheless, D–A molecular architectures have resulted in systems that exhibit high conductivity in the absence of doping (Section 1.6), possibly due to the formation of 2- and 3D exchange pathways arising from electrostatic intermolecular D–A interactions that stabilize the system towards lattice deformations. We have also shown that close

solid-state intermolecular D–A contacts result in greater dimensionality (Chapter 4), leading to higher room temperature conductivity and ferromagnetic exchange. We became interested in designing a series of open-shell molecules using BNN as a strong acceptor and systematically varying the strength of the donor in order to investigate how modulation of the intramolecular D–A interaction affects molecular electronic structure, as well as solid state phenomena such as packing, magnetic exchange (*J*) and conductivity. Furthermore, this series may allow for elucidation of the mechanism by which charge carriers migrate through these D–A materials. Depending on orbital dispersion and the degree of crystallinity, a well defined band structure may not form and charge carrier migration would occur by hopping. Additionally, conductivity (σ) is defined as the product of the charge carrier mobility (μ) and the number of charge carriers (n), where q is the charge of the carrier (Equation 1). We hope to understand whether the bulk conductivity is higher in open-shell D–A systems as a result of an increase in mobility or the number of charge carriers present.

$$\sigma = nq\mu \tag{1}$$

In BNN radicals, the lowest energy excitation occurs in the NIR and has been attributed to a HOMO–SOMO CT transition that is dependent on the nature of the *C*2 substituent (Chapter 2). A theoretical model derived by Hush (Equation 2) describes the parameters responsible for the excitation energy of the CT transition (ν_{max}).[145,365] The Frank–Condon factors (λ_i and λ_o) correspond to the inner- and outer-sphere reorganization energy (Section 1.5). The redox asymmetry (ΔE_0) is the difference in redox potential between donor and acceptor and is typically assessed experimentally using electrochemical potential measurements, that is the oxidation potential of the donor

and reduction potential of the acceptor. Finally, any additional contributions due to spin-orbit coupling and ligand field asymmetry are included in the $\Delta E'$ term.

$$\nu_{max} = \lambda_i + \lambda_o + \Delta E_0 + \Delta E' \quad (2)$$

Assuming the molecular systems in question are similar in architecture, the inner- and outer-sphere reorganization energies should be of similar magnitude, thus they can be treated as a constant. Additionally, the systems presented here are organic and consequently spin orbit coupling and ligand field contributions are negligible ($\Delta E' \approx 0$). The net result is a change in the energy of the charge transfer excitation (ν_{max}) is dominated by differences in D–A redox potential for a series of structurally similar molecules. Although this may seem to be an oversimplification, Equation 2 is a powerful predictive tool, suggesting systematically reducing the oxidation potential of the donor while holding the reduction potential of the acceptor constant should result in a decrease in the HOMO–SOMO CT excitation energy. The CT excitation energy and intensity can be monitored spectroscopically and, using band shape analysis, the strength of the D–A interactions in each system can be quantitatively determined.

A initial series of BNN–donors (Figure 5.3) were designed such that the redox asymmetry between donor and acceptor (ΔE_0) ranged from ~2.3 V to 0.3 V. Each electron rich donor was selected based on oxidation potential and the ease by which it could be incorporated via an aldehyde into existing synthetic methodology. The solvated geometry optimized structure and excitation energy of the CT transition (ν_{max}) of each BNN–donor was calculated using time-dependent density functional theory (TDDFT) to determine if conclusions drawn from Equation 2 would hold across this series.

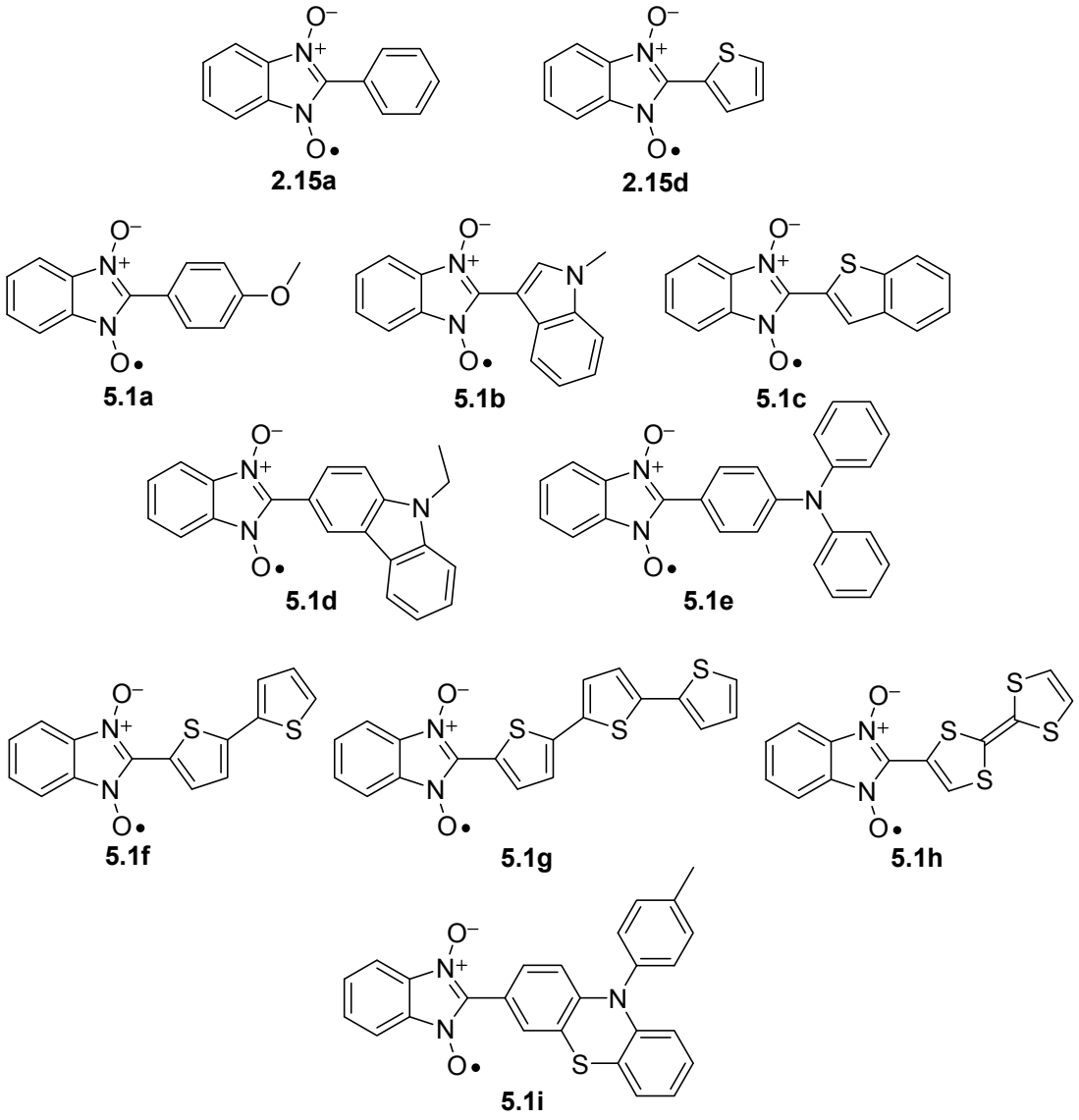

Figure 5.3. Series of BNN-donor radicals increasing in donor strength from phenyl to tetrathiafulvalene.

From the above proposed series (Figure 5.3) a subset of BNN–donor radicals **5.1a-e** were synthesized using the benzofuroxan/nitrone condensation methodology developed in Chapter 2. The electronic structure of each radical was elucidated through solution-phase spectroscopy and cyclic voltammetry. The solid state interactions were probed through the use of SQUID magnetometry, X-ray crystallography and diffuse reflectance

spectroscopy. EPR spectroscopy and electrochemical studies reveal a spin-delocalized structure with an extremely low reduction potential, although significant perturbations of the electronic structure with increasing donor ability were not observed. Weak intramolecular electronic coupling (V) between donor and acceptor was found to occur but was independent of donor strength and effectively constant across the series. Solid state magnetic interactions were weak suggesting little spin density overlap between molecules and, with the exception of *p*-methoxyphenyl BNN, the series of BNN–donor radicals were insulating at room temperature. This study highlights the importance of steric interactions and intramolecular torsion angles on the solid-state properties of organic materials as both result in a perturbation of the intra- or intermolecular electronic coupling pathways critical to magnetic exchange and electrical conductivity.

5.2 Calculation of BNN–D excitation energies

The absorption spectrum of each benzonitronyl nitroxide–donor (BNN–D) molecule was calculated using time dependent density functional theory (TDDFT) in order to determine the energy of the HOMO–SOMO CT excitation. Geometry optimization was accomplished using DFT with an unrestricted hybrid exchange-correlation functional (UB3LYP) and the 6-311+G(d,p) basis set. Solvation by chloroform (dielectric = 4.81)[234] using the conductor-like polarizable continuum model[331,332] (CPCM) was included in the calculation to better represent experimental spectroscopic conditions. All calculations were carried out using the Gaussian 09 package.[239] The oxidation potential and TDDFT predicted NIR λ_{max} (HOMO–SOMO energy gap) and force constant (f) for each donor group are reported in Table 5.1.

Table 5.1. Series of donors computationally evaluated for incorporation into BNN–D radicals. Absorption maximum (λ_{max}) and force constant (*f*) calculated using TDDFT UB3LYP/6-311+G(d,p) with the inclusion of CPCM solvation (chloroform).

Donor	Compound	E_{ox} (V vs SCE)[a]	λ_{max} (nm)	*f*
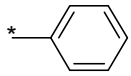	**2.15a**	2.30	721	0.0241
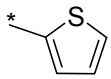	**2.15d**	2.15	930	0.0192
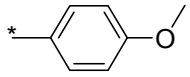	**5.1a**	1.76	905	0.0209
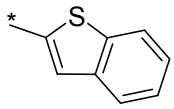	**5.1c**	-	947	0.0162
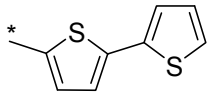	**5.1f**	1.30[b]	1165	0.0121
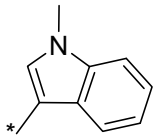	**5.1b**	1.2	1136	0.0154
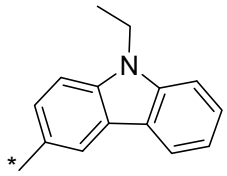	**5.1d**	1.14	1019	0.0146
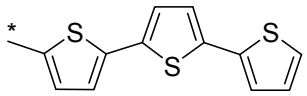	**5.1g**	1.05[c]	1302	0.0093
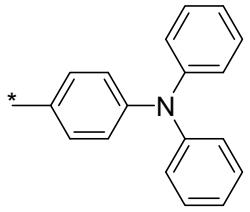	**5.1e**	0.86	1172	0.0092
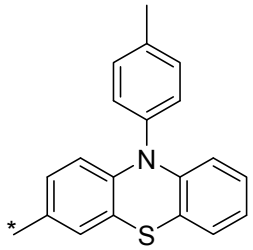	**5.1i**	0.59	1211	0.0076
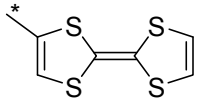	**5.1h**	0.32	2410	0.0188

[a] Oxidation potentials determined from reference 366 and are reported vs SCE in CH_3CN unless otherwise noted. [b] Reference 361. [c] Reference 367, CH_2Cl_2.

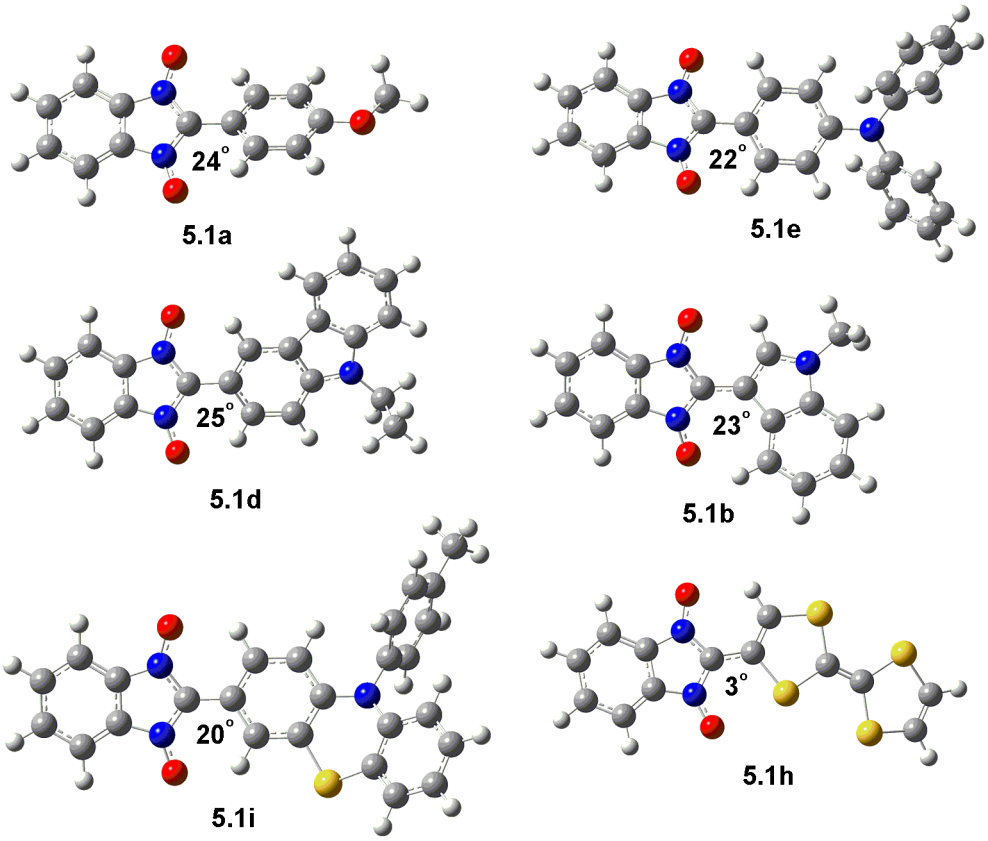

Figure 5.4. Geometry optimized structures of BNN-donors that exhibited torsion angles between benzimidazole and the donor ring. Visualized using GaussView 4.1.

Previously, all geometry optimizations of BNN based radicals have been carried out in the gas phase. The energy optimized molecular structure obtained when the calculation is carried out in the absence of solvent is always completely planar as a result of over-delocalization of the π system by DFT.[325,368,369] Here the inclusion of solvation has reduced over-delocalization in the larger five-six rotors **5.1a**, **5.1d**, **5.1e**, and **5.1i** as well as the *N*-methylindole **5.1b** and tetrathiafulvalene (TTF) **5.1h** derivatives as evidenced by the presence of a non-zero torsion angle between benzimidazole and the *C*2 aryl group (Figure 5.4). Placing the molecules in a solvation cavity during geometry optimization has resulted in calculated molecular geometries that better represent those typically

observed crystallographically. This series of calculations suggest the inclusion of a polarizable-continuum solvation model, even with a low polarity dielectric such as chloroform, may result in geometry optimized structures that better approximate the molecular geometry.

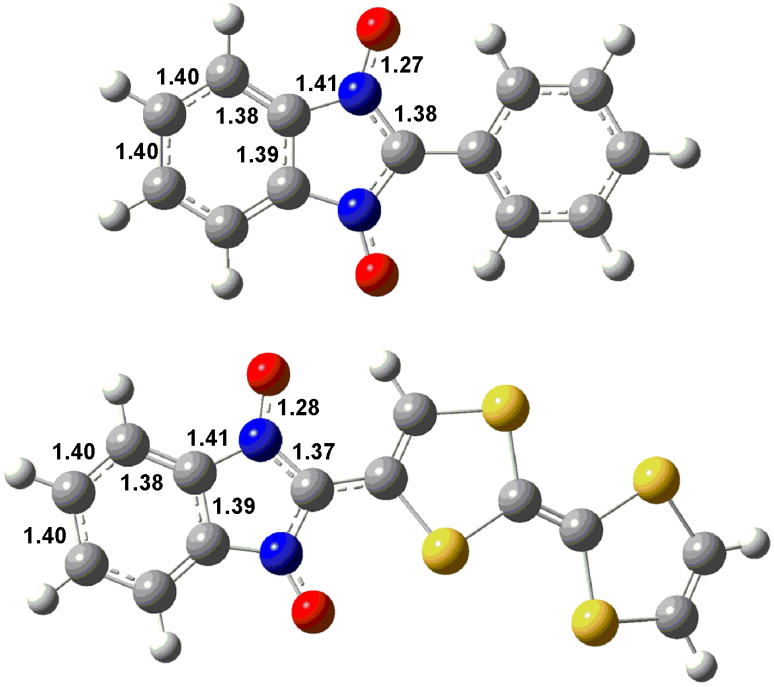

Figure 5.5. Differences in the bond lengths of the benzimidazole N,N′-dioxide ring upon *C*2 subsititution with phenyl **2.15a** and tetrathiafulvalene **5.1h**.

The benzimidazole bond lengths of the geometry optimized series of radicals **2.15a**, **2.15d**, and **5.1a-i** were compared to determine if functionalization with an increasingly electron rich group altered the geometry of the benzimidazole skeleton. Across the series the bond lengths of the benzimidazole N,N′-dioxide ring remained constant (Figure 5.5) suggesting little perturbation of the electronic structure with increasing donor ability. This is supported by comparing the SOMOs of the TTF and phenyl BNN derivatives as although the oxidation potential of these two aryl groups differs by ~2 V, the SOMO of

each radicals is indistinguishable (Figure 5.6). This is consistent with functionalization at *C*2, a nodal position in the SOMO, as little perturbation of the electronic structure is observed even when redox asymmetry (ΔE_0) is low.

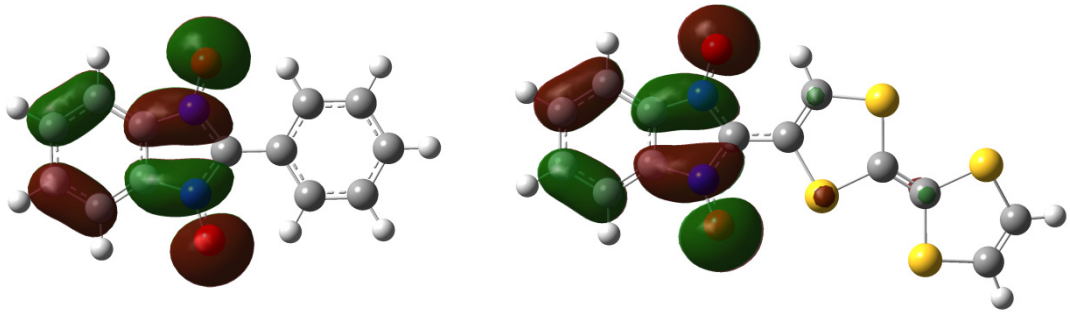

Figure 5.6. β SOMO of phenyl benzimidazole nitronyl nitroxide **2.15a** (left) and tetrathiafulvalene benzimidazole nitronyl nitroxide **5.8** (right), generated in GaussView 4.1, cube grid = coarse, isoval = 0.02.

The absorption maxima (λ_{max}) calculated using TDDFT support the conclusion based on Equation 2, that is decreasing the difference in redox potential between D and A will result in a decrease in the energy of the CT excitation. The shift in λ_{max} is not directly proportional to ΔE_0, suggesting contributions from inner- and outer-sphere reorganization energy cannot be assumed to be constant across the series. Given the variations in size and shape of the *C2* substituents, the contribution from reorganization energy must vary from system to system. As the NIR excitation is dominated by a β–HOMO → β–SOMO transition (~95 %), the optically induced CT excitation results in transfer of an electron from the HOMO (which is primarily located on the donor in the absence of strong mixing, i.e. the system is Robin–Day Class II) to the benzimidazole-based SOMO. Thus electron transfer results in the formation of a donor-based radical cation. For many of the above donors the reorganization energy would be large as there are significant geometric changes associated with oxidation of these molecules to their respective radical cations.

A computational analysis of the target D–A series suggests perturbation of the HOMO–SOMO CT excitation is possible by changing the strength of the donor at *C2*. The energy of the CT excitation can be measured directly through the use of absorption spectroscopy and Mulliken–Hush analysis of the CT absorption band gives the strength of electronic coupling (V) between D and A. As we are interested in understanding how intramolecular electronic coupling affects solid state interactions, the magnetic exchange, conductivity and solid state absorbance of each radical will be investigated using solid state techniques such as SQUID magnetometry, reflectance spectroscopy and X-ray diffraction.

5.3 Synthesis of D–A nitronyl nitroxide radicals

Scheme 5.1. Synthesis methodology developed for the synthesis of BNN-Donor radical radicals **5.1a-e**. [a]

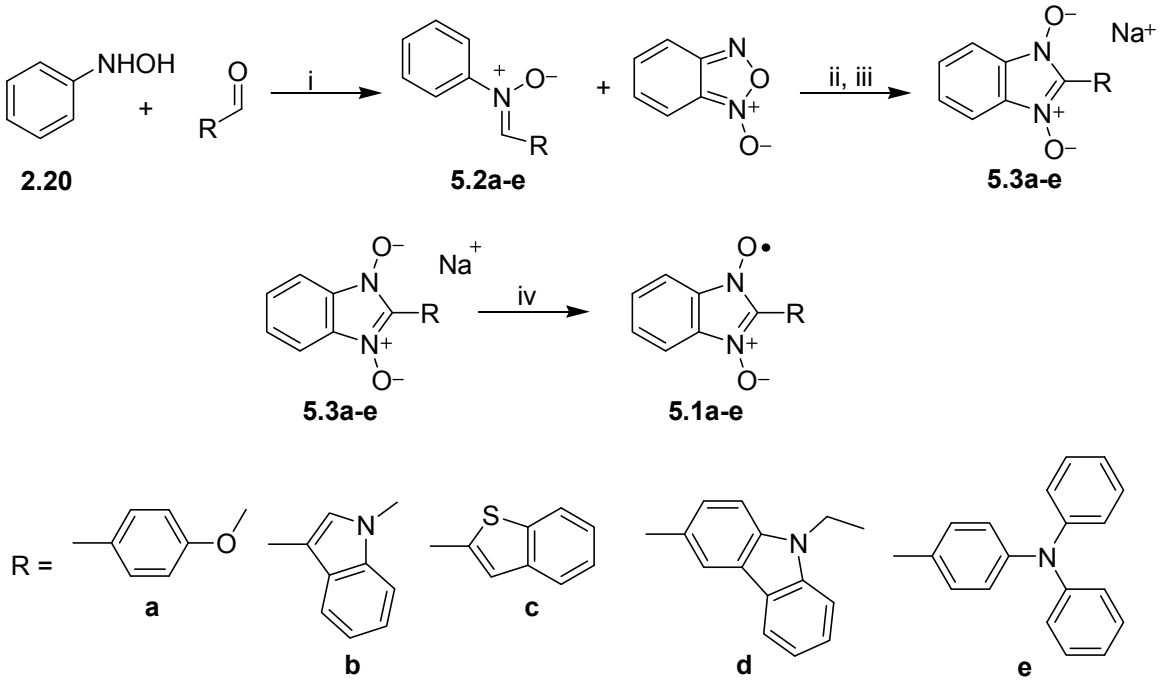

[a] Reagents and conditions: (i) EtOH, 71 – 95 %; (ii) toluene, Δ; (iii) NaOH, EtOH, 25 – 59 %; (iv) $AgPF_6$, rt to −78 ºC, 13 – 36 %.

An initial group of five donors (anisole **5.1a**, *N*-methylindole **5.1b**, benzo[*b*]thiophene **5.1c**, *N*-ethylcarbazole **5.1d**, and triphenylamine **5.1e**) were selected from the above series. The synthesis of the series of A–D type BNN radicals **5.1a-e** was accomplished using functionalized nitrones[221] (see Chapter 2) resulting in the incorporation of a series of donors at *C2* that ranged in donor strength from E_{ox} = 1.76 V vs SCE (anisole) to 0.86 V vs SCE (triphenylamine) (Scheme 5.1).

Phenylhydroxylamine was prepared according to literature methodology[228] and condensed with the appropriate aldehyde to give nitrones **5.2a-e** in 71 – 95 % yield. This series of donors represent the first examples of BNN radicals with strongly electron rich aryl groups, particularly triphenylamine, at *C*2. At the outset of the synthesis of this series we anticipated two potential problems, the first pertaining to the synthesis and stability of the nitrone and the second regarding the generation of radical. Condensation of phenylhydroxylamine with aldehyde requires nucleophilic attack by hydroxylamine at the aldehyde carbon. As the aldehyde was now more electron rich it was unknown if the synthesis would proceed as before, specifically whether the equilibrium would shift far enough to the right without the application of heat or other significant procedural modification. Along the same line, we were unsure if the isolated nitrone would be stable towards hydrolysis (Scheme 5.2). In the end, nitrone formation occurred using the same procedure as before and the isolated yields were comparable to those previously reported. No additional precautions were taken when handling the electron rich nitrones and each of **5.2a-e** were found to be stable (> 8 months) in the solid state when stored at −17 ºC in the absence of light.

Scheme 5.2. Condensation of phenylhydroxylamine and aldehyde yield nitrone, which is susceptible to a back reaction (hydrolysis).

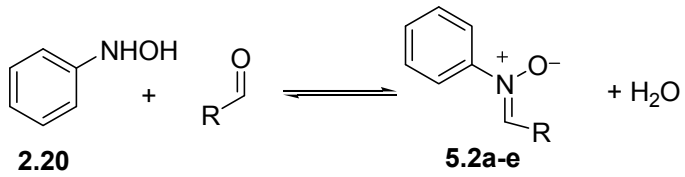

2.20 **5.2a-e**

Nitrone was reacted with benzofuroxan in refluxing toluene to give the corresponding radical precursor which was then deprotonated with sodium hydroxide in methanol to give precursor salts **5.3a-e** (25 – 59 %). This series of precursor salts marked the first time the $BNN^{-}/BNN^{\bullet}$ redox couple was close in oxidation potential to the redox couple of the *C*2 substituent ($D/D^{\bullet+}$). It was unknown if removal of a single electron from the [Na][BNN–D] salt (to generate neutral radical) would be possible, as the oxidation of potential of Ag(I) was high enough that BNN–D could be oxidized a second time to give diradical cation ($BNN^{\bullet}–D^{\bullet+}$). The doubly oxidized product was avoided by controlling the molar equivalents of oxidant added. Instead of adding Ag(I) in slight excess (as before), Ag(I) was used as the limiting reagent. This modification prevented diradical cation formation as we wished to isolate and fully characterize the series of neutral BNN–D radicals prior to examining them in an alternative oxidation state.

Oxidation of salts **5.3a** and **5.3c-e** with silver(I) hexafluorophosphate afforded radicals **5.1a** and **5.1c-e**. The major product generated during the oxidation of *N*-methylindole derivative **5.3b** was not a benzonitronyl nitroxide radical and radical **5.1b** was not isolated as evidenced by UV–vis spectroscopy. Radicals **5.1a** and **5.1c-e** were isolated from solution by precipitation from ~1:1 methanol:methylene chloride at low temperature (−78 °C) followed by low temperature recrystallization (−78 °C) which resulted in analytically pure samples in 13 – 36 % yield. Radicals **5.1a** and **5.1d-e** were stable in

solution for short periods of time (< 12 h) and indefinitely stable in the solid state when stored at ambient temperatures in the absence of light. Triphenylamine derivative **5.1e** was one of the most stable BNN radicals handled to date, likely as a result of kinetic stabilization of the radical centre by the bulky triphenylamine substituent. In contrast, radical **5.1c** was found to decompose rapidly (< 20 min) in solution as determined by EPR spectroscopy.

5.4 EPR spectroscopy

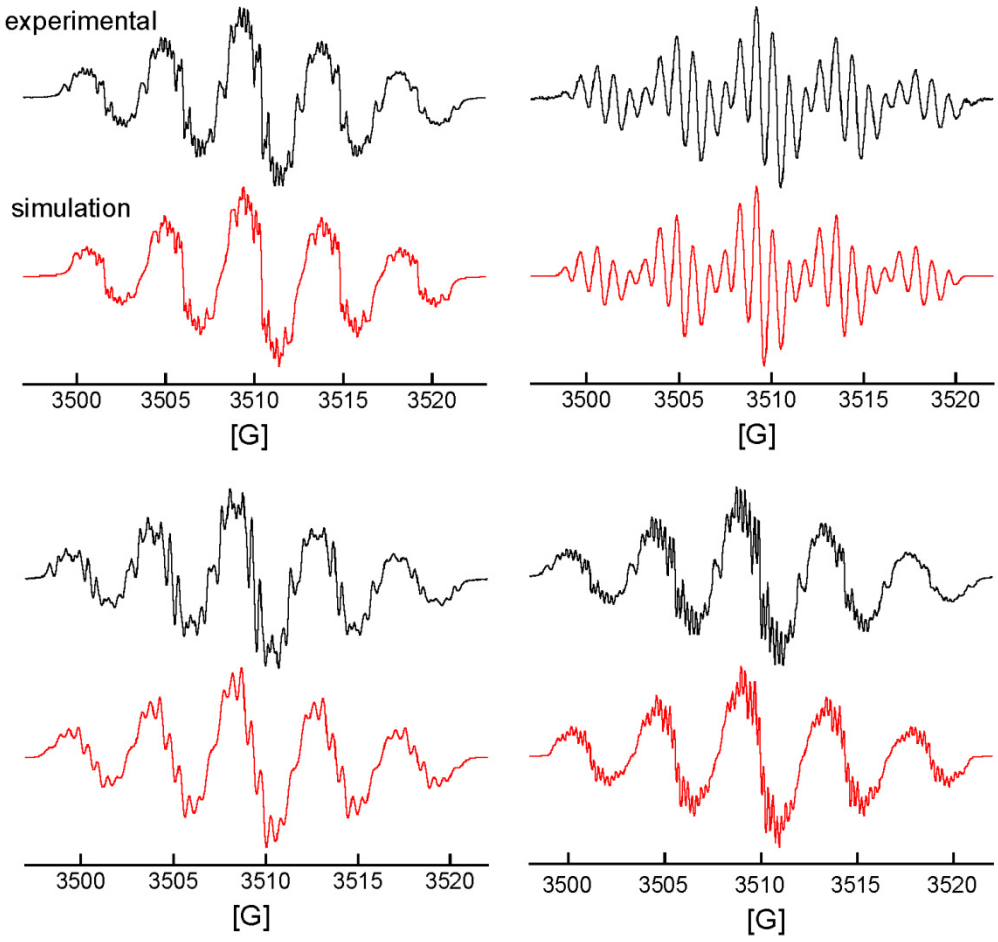

Figure 5.7. EPR spectrum of **5.1a** (top left, R > 0.98), **5.1c** (top right, R > 0.93), **5.1d** (bottom left, R > 0.97) and **5.1e** (bottom right, R > 0.97) (top = experimental, bottom = simulated), 10^{-5} M solution in dry, degassed toluene at ~300 K.

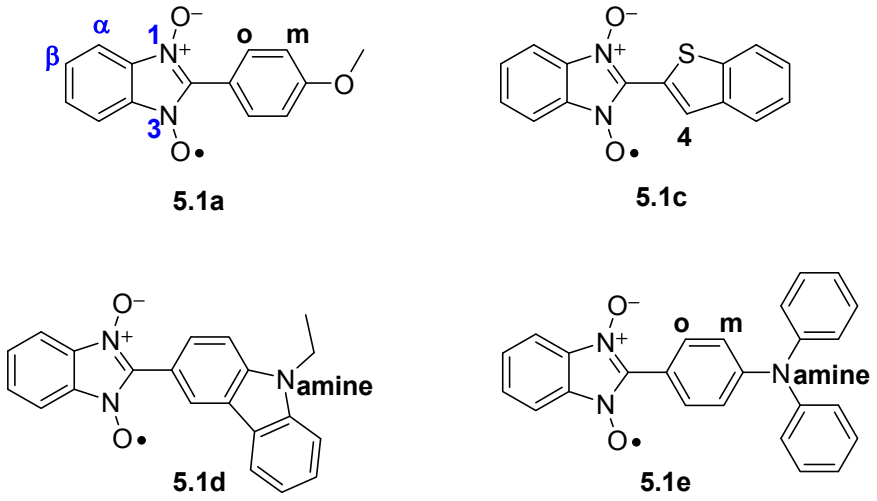

Figure 5.8. Labeled nitrogen and hydrogen atoms of radicals **5.1a** and **5.1c-e.**

Table 5.2. Experimental g-values and hyperfine coupling constants (Gauss) for radicals **5.1a** and **5.1c-e**. Parent phenyl benzonitronyl nitroxide **2.15a** included for reference. Refer to Figure 5.8 for nitrogen and hydrogen labeling.

	2.15a	**5.1a**	**5.1c**	**5.1d**	**5.1e**
g	2.007[a]	2.0076	2.0077	2.0082	2.0075
$a(N_{1,3})$	4.370	4.410	4.312	4.417	4.404
$a(N_{amine})$	-	-	-	0.517	0.188
$a(H_{\alpha})$	0.930	0.921	0.988	0.979	0.904
$a(H_{\beta})$	0.650	0.488	0.727	0.575	0.496
$a(H_o)$	0.490	0.200	-	-	0.227
$a(H_m)$	0.220	-	-	-	0.086
$a(H_p)$	0.410	-	-	-	-
$a(H_4)$	-	-	0.108	-	-
$a(H_{other})$	-	< 0.05	< 0.05	< 0.05	< 0.05

[a] Reference 219.

The spin density distribution and degree of spin delocalization in benzonitronyl nitroxide-donor radicals **5.1a** and **5.1c-e** was probed using EPR spectroscopy. X-band EPR spectra of **5.1a** and **5.1c-e** were recorded as a 10^{-5} M solutions in dry, degassed toluene at room temperature and are shown in Figure 5.7. Simulation of the spectra was accomplished using Winsim2002. Initial hyperfine coupling constants used as simulation input were those reported for phenylbenzyl nitronyl nitroxide in Chapter 2. Additional H

atoms were included as necessary, however, assignments of the superhyperfine coupling constants for H atoms reported in Table 5.2 are tentative assignments.

Each EPR spectrum exhibits a five-line pattern with relative intensities of 1:2:3:2:1 and a g-value of ~2.008 (Table 5.2), consistent with the larger class of benzonitronyl nitroxide radicals. The presence of a five-line hyperfine splitting pattern is significant as it suggests the bulk of the spin density is delocalized over two equivalent I = 1 atoms and confirms isolation of a neutral benzonitronyl nitroxide based radical and not a diradical cation. The nitrogen atoms in the benzimidazole ring (N1, N3) bear the largest proportion of the spin density with hyperfine coupling constants of $a(N_{1,3})$ = 4.31 – 4.42 G, while the triphenylamine **5.1e** and *N*-ethylcarbazole **5.1d** nitrogen bear a much smaller proportion of spin with $a(N_{amine})$ = 0.517 G in carbazole and 0.188 G in triphenylamine. Although the spin population on the triphenylamine nitrogen seems low, the triphenylamine group is covalently bound to BNN through *C*2, which is in a nodal position in the SOMO and bears a small amount of negative spin density. This, coupled with a moderate BNN-phenyl torsion angle (22º from calculation, 31º from X-ray structure), results in weak coupling to the triphenylamine nitrogen. A greater degree of spin density resides on the carbazole nitrogen, however, carbazole hydrogen atoms bear very little spin density, as evidenced by the almost negligible (H_{other}) hyperfine coupling constants reported for **5.1d**. Comparison of each isolated radical to parent phenyl benzonitronyl nitroxide **2.15a** shows little perturbation of the spin system has occurred with functionalization at *C*2, consistent with our observations in Chapter 2.

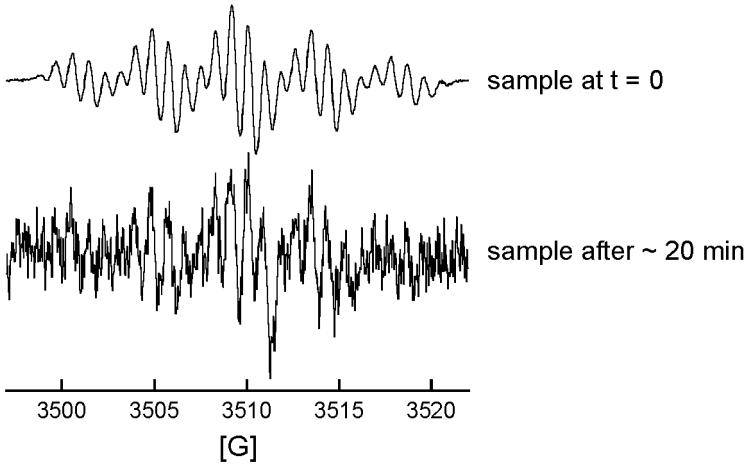

Figure 5.9. EPR spectrum of benzo[*b*]thienyl benzonitronyl nitroxide, 10^{-5} M solution in dry, degassed toluene at ~298 K in a sealed tube (**5.1c**, top) and sample after ~20 min had elapsed (bottom).

During collection of the EPR spectrum of benzo[*b*]thienyl derivative **5.1c** decomposition of the radical was observed after ~20 min, as evidenced by noticeable degradation of the EPR signal (bottom, Figure 5.9). The solution phase stability of this radical was poor, preventing analysis by cyclic voltammetry and growth of X-ray quality single crystals. The instability is also reflected in the magnetometry (see below) as the paramagnetic magnetic moment is lower than that calculated for an S = ½ species, consistent with the presence of diamagnetic impurities.

5.5 Cyclic voltammetry

The electrochemical behavior of the series of BNN radicals **5.1a** and **5.1d-e** were investigated by cyclic voltammetry. Initially the $BNN^{-}/BNN^{\bullet}$ redox couple was probed using the corresponding sodium salts **5.3a-e**, however, the solubility of the sodium salts was poor in CH_3CN. As a result the current detected during the potential scan was low and the resulting voltammogram was of inferior quality. The solubility and solution phase

stability of radicals **5.1a** and **5.1d-e** in acetonitrile was high enough that voltammetric data could be collected using the neutral radical.

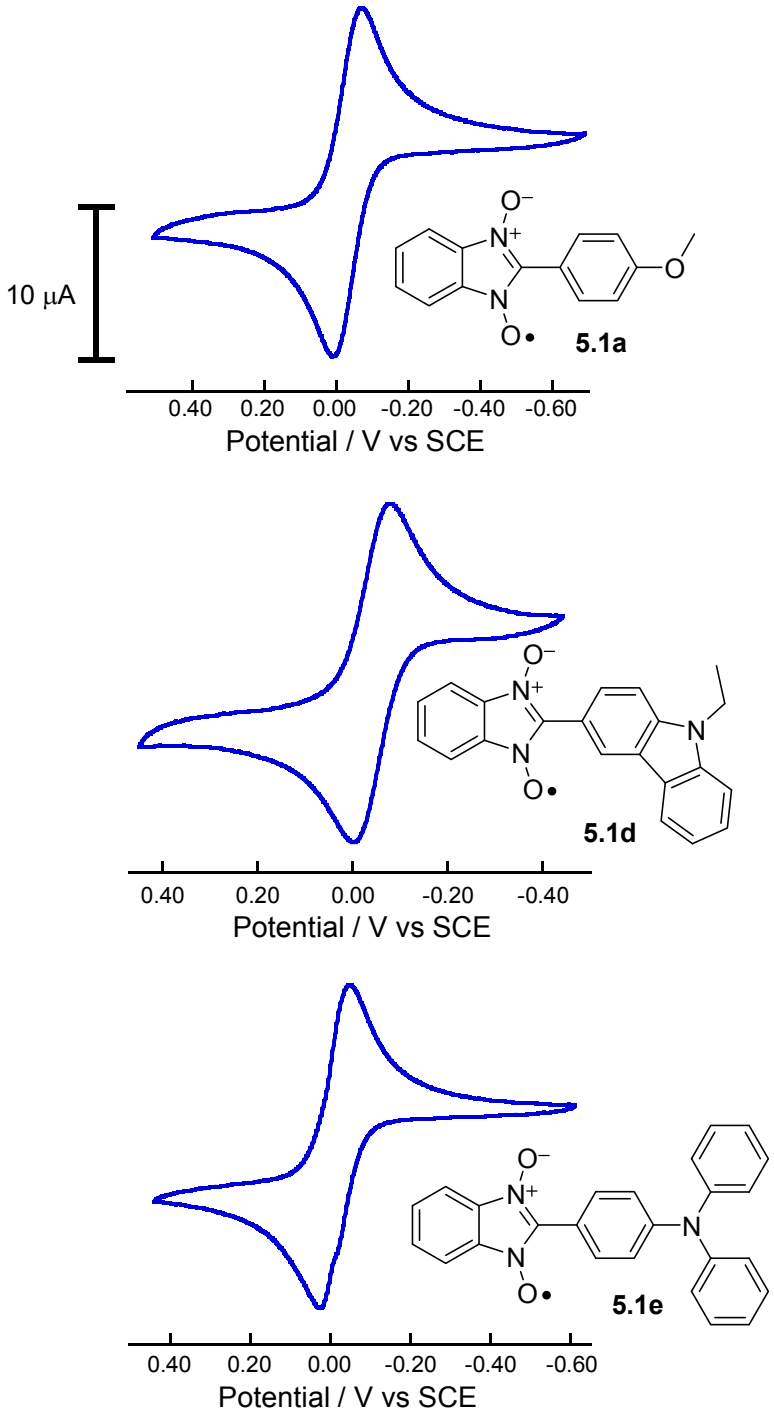

Figure 5.10. Cyclic voltammetry of the reduction process of **5.1a**, **5.1d**, and **5.1e**, 10 mM solution in CH_3CN, 0.1 M NBu_4PF_6, 50 mV s^{-1} scan rate, ferrocene used as reference (full voltammograms in Appendix C).

Cyclic voltammograms of **5.1a** and **5.1d-e** are shown in Figure 5.10. The parent phenyl BNN radical **2.15a** exhibits a reversible one-electron reduction at −0.03 V vs SCE (ΔE_p = 80 mV) and an irreversible one electron oxidation at 1.60 V vs SCE in acetonitrile (Section 2.3). BNN–D radicals **5.1a** and **5.1d-e** exhibited reduction potentials at similar potentials (~0 V vs SCE, Table 5.3) consistent with little electronic coupling between D and A. Little perturbation in the oxidation potential of the donor was also observed, with the oxidation of *N*-ethylcarbazole (1.17 V vs SCE) and triphenylamine (0.98 V vs SCE) occurring at only slightly more positive potentials, consistent with inductive effects slightly raising the oxidation potential as electron density is drawn towards the acceptor.

Table 5.3. Electrochemical properties of BNN radicals **2.15a**, **5.1a**, and **5.1d-e**. Redox processes reported in V vs SCE. 10 mM solution in CH_3CN, 50 mV s^{-1} scan rate.

	2.15a	**5.1a**	**5.1d**	**5.1e**
$E_{1/2}$(red)	−0.03	0.03	−0.04	−0.01
ΔE_p (mV)	80	77	74	78
$E_{1/2}$(ox)	1.29	1.35	1.17[a]	0.98
ΔE_p (mV)	171	82	-	75
E_{cell}	1.29	1.32	n/a	0.99

[a] Irreversible process, anodic peak potential reported.

The scan rate dependence of the reduction wave for **5.1a** and **5.1d-e** is summarized in Table 5.4. For all three radicals the separation of peak potentials (ΔE_p) increased with increasing scan rate, confirming the reduction process was quasi-reversible. The ratio of anodic to cathodic peak current (i_{pa}/i_{pc}) confirms the observed chemical stability of the radicals and their corresponding anions as for all three of **5.1a** and **5.1d-e** the peak current ratio is near unity at all scan rates.

Table 5.4. Scan rate dependence of the separation of peak potentials (ΔE_p, difference in anodic and cathodic peak potential, reported in mV) and ratio of peak currents (i_{pa}/i_{pc}) of radical reduction process. 10 mM solution in CH_3CN, 0.1 M NBu_4PF_6, 100 mV s^{-1} scan rate, Fc/Fc^+ internal standard.

Scan Rate	**5.1a**		**5.1d**		**5.1e**	
($mV\ s^{-1}$)	ΔE_p	i_{pa}/i_{pc}	ΔE_p	i_{pa}/i_{pc}	ΔE_p	i_{pa}/i_{pc}
50	77	1.02	74	1.13	78	1.15
100	73	1.02	70	1.04	88	1.07
150	78	1.01	74	1.05	97	1.04
200	81	1.01	78	1.05	103	1.05
250	85	1.01	78	1.07	105	1.03
500	98	1.01	90	1.03	125	1.00

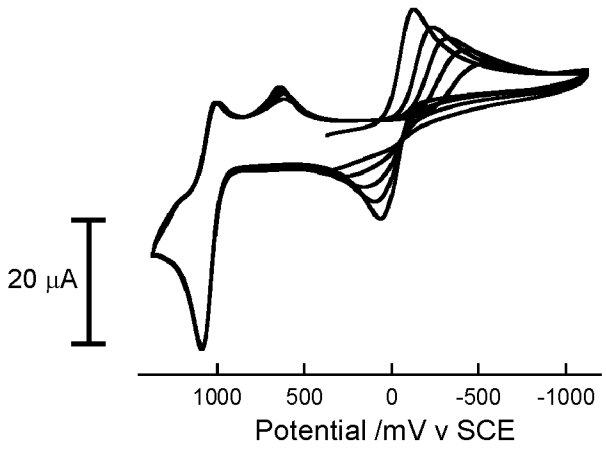

Figure 5.11. Cyclic voltammogram of **5.1e** cycled between positive and negative potential five times (10^{-3} M solution in 0.1 M NBu_4PF_6/CH_2Cl_2, 100 mV s^{-1} scan rate).

When potential was scanned multiple times over a larger window for **5.1e**, the radical reduction process became increasingly irreversible and after five complete scans a negligible concentration of radical remained in solution (Figure 5.11). This would normally be attributed to decomposition of the entire molecule, however, after multiple scans the triphenylamine oxidation peak remains virtually unchanged. During the oxidation and subsequent reduction of triphenylamine (~1 V vs SCE in CH_2Cl_2) a chemical process is occurring that is degrading the nitroxide radical. A comparison of the

quantity of current passed (i.e. the height of the redox wave) during the oxidation process at 1 V vs SCE and the reduction process at 0 V vs SCE, the oxidation process may be a $2e^-$ process where both triarylamine and BNN radical are oxidized at nearly equivalent potentials. Following oxidation a new species is observed on the reverse scan which exhibits an electrochemical process at ~600 mV V SCE. This species may be responsible for degradation of the radical as following generation of the new chemical species, i_{pc} of the radical reduction decreases and the potential is cathodically shifted. The fact that formation of triphenylamine radical cation results in degradation of benzonitronyl nitroxide unfortunately suggests isolation of the diradical cation, and subsequent examination of the *intra*molecular magnetic D–A exchange may not be possible.

5.6 UV–vis–NIR spectroscopy

The electronic absorption spectra of radicals **5.1a** and **5.1c-e** (Figure 5.12) include several features in the UV and visible regions, as well as a broad absorption band in the NIR (Table 5.5). The nature of NIR transition has previously been shown to be dependent on the *C*2 substituent and is the result of a symmetry forbidden HOMO–SOMO transition. The intense ($\varepsilon \approx 56000\ M^{-1}\ cm^{-1}$) UV absorption ($\lambda_{max}$ = 380 nm) observed in **5.1e** (Figure 5.9, red) is characteristic of triphenylamine absorption (λ_{max} = 303 nm).[370]

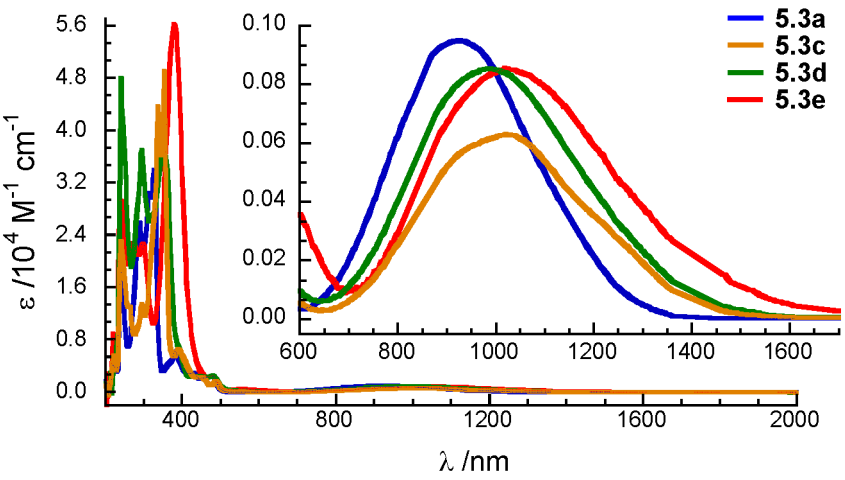

Figure 5.12. UV–vis–NIR spectra of nitronyl nitroxide radicals **5.1a** and **5.1c-e**, 10^{-5} M solutions in chloroform, ~298 K.

Given the strong acceptor strength found for benzonitronyl nitroxide (−0.03 V vs SCE), the low energy NIR transition observed in the spectrum of radicals **5.1a** and **5.1c-e** can be rationalized as a CT excitation between the accepting benzonitronyl nitroxide moiety and the *C*2 donor. As in Chapter 2, the strength of the electronic donor–acceptor coupling parameter (V) can be calculated using band shape analysis of the Gaussian-shaped optical charge transfer excitation. This is accomplished using the following equation in which ν_{max} is the excitation energy (cm^{-1}), $\Delta\nu_{1/2}$ is the bandwidth at half-height (cm^{-1}), ε_{max} is the molar extinction coefficient ($M^{-1}\ cm^{-1}$), and r_{DA} is the distance between the opposite charges in the charge separated $D^{\bullet+}A^{-}$ excited state (Å). Here r_{DA} has been estimated to be the length of the benzonitronyl nitroxide *C*2-phenyl carbon-carbon bond (1.45 Å) or *C*2-thienyl carbon-carbon bond (1.43 Å) as determined from the X-ray crystal structure of **5.1e** and **2.15d** respectively.

$$V = (0.0205)\frac{\left[\varepsilon_{max}\Delta\nu_{1/2}\nu_{max}\right]^{1/2}}{r_{DA}}$$

Table 5.5. Electronic coupling energies of radicals **5.1a**, **5c-e** determined using a Mulliken–Hush analysis.

		5.1a	**5.1c**	**5.1d**	**5.1e**
Experimental [a]	λ_{max}(exp) /nm	927	1019	982	1020
	ε /M^{-1} cm^{-1}	980	649	885	903
Calculated [b]	λ_{max}(calc) /nm	905	947	1019	1172
	f	0.0192	0.0162	0.0146	0.0092
Fit	r_{DA}	1.45	1.43	1.45	1.45
	$\Delta\nu_{1/2}$ /cm^{-1}	3334	3336	3457	3642
	ν_{max} /cm^{-1}	11059	10186	10367	9940
	R^2	0.985	0.982	0.985	0.993
	V /cm^{-1}	2700	2100[c]	2500	2600

[a] Experimental λ_{max} measured in chloroform. [b] Calculated λ_{max} determined by TDDFT UB3LYP/6-311+G(d,p) with CPCM (chloroform). [c] This value is approximate as the concentration of radical in solution was not known to a high degree of accuracy due to solution phase instability.

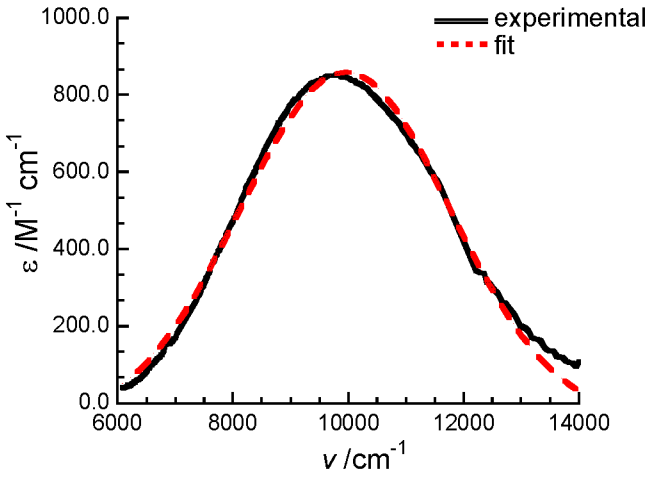

Figure 5.13. NIR band of **5.1e** fit with a Gaussian function, $R^2 > 0.99$. Fit parameters reported in Table 5.5.

For each of radical **5.1a** and **5c-e** the NIR CT excitation is weak ($\leq$ 5000 M^{-1} cm^{-1}), Gaussian in shape and exhibits large bandwidths ($\Delta\nu_{1/2} \geq 2000$ cm^{-1}). This, coupled with the magnitude of electronic coupling *V* (Table 5.5), confirms these systems are weakly-coupled Robin–Day Class II donor–acceptors. This is consistent with cyclic voltammetry

which showed little perturbation of the redox potentials of the acceptor and donor upon formation of a covalently bound molecule. The weak electronic coupling is likely a function of the site of substitution as we have previously shown *C*2 to be a nodal position in the SOMO, thus there is not a high degree of orbital mixing between donor and acceptor units.

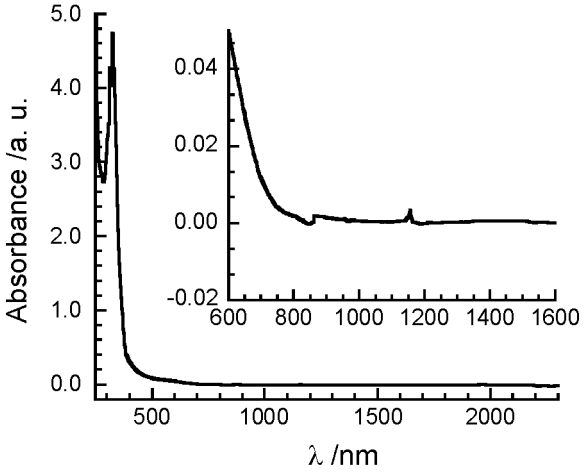

Figure 5.14. UV–vis–NIR of product isolated during attempted synthesis of **5.3b**. Solution of unknown concentration in chloroform, ~298 K.

The major product isolated from the oxidation of the *N*-methylindole sodium salt **5.3b** was EPR silent, suggesting the material was not paramagnetic. Additionally, the NIR HOMO–SOMO transition characteristic of BNN-based radicals was absent from the UV–vis–NIR spectrum (Figure 5.14). The reason radical **5.3b** could not be isolated is unknown, although the instability is consistent with the decreased stability of the 4-pyridyl **2.5c** and instability of the 2-pyridyl **2.5b** derivatives. The basicity of these groups may make the radical more susceptible to acidic impurities as protonation of the nitrogen in the aryl ring may open up alternate decomposition pathways. In contrast, the

N-ethylcarbazole **5.1d** and triphenylamine radicals **5.1e** exhibited good solution stability, suggesting proximity of the basic nitrogen to the nitronyl nitroxide may be important.

5.7 Structural analysis

Irregular black blocks of **5.1e**, long black needles of **5.1a** and small bronze needles of **5.1d** were grown by slow evaporation from saturated pentane/acetone solutions. Of the crystals grown, only **5.1e** diffracted X-ray irradiation well enough for crystal structure determination by single crystal XRD.

5.7.1 Crystal structure of diphenylaminophenyl derivative 5.1e by XRD

Table 5.6. Select crystallographic metrics for **5.1e**.

	5.1e
formula	$C_{25}H_{18}N_3O_2$
formula weight	392.42
crystal color, habit	black, irregular
crystal system	$P2_1/c$
space group	monoclinic
a (Å)	12.7544(6)
b (Å)	9.1449(5)
c (Å)	16.5677(8)
volume (Å^3)	1922.6(2)
temperature (K)	90.0(1)
Z	4
R_f[a]	0.048
R_w[b]	0.093
GOF	1.03

[a] $R_f = [\Sigma||F_o| - |F_c||]/[\Sigma|F_o|]$, $I > 2\sigma(I)$. [b] $R_w = ([\Sigma w||F_o|^2 - |F_c|^2|^2]/[\Sigma(w|F_o|^2)^2])^{1/2}$.

Refinement of the structure of **5.1e** led to packing in the monoclinic crystal system in the $P2_1/c$ space group with four molecules per unit cell (Z = 4). The detailed crystallographic data is reported in Table 5.6 and the single crystal structure and unit cell

of **5.1e** are shown in Figure 5.15. The benzimidazole ring, including the terminal oxygen atoms adopts a coplanar geometry with an angle of just 0.4º between the plane of the benzannelated ring and the coplanar ONCNO atoms. The *para*-substituted phenyl ring between BNN and diphenylamine is twisted 31º (*N*2-*C*1-*C*11-*C*12) from the plane of the central benzimidazole ring. This torsion angle was larger than expected as when the *C*2 group is substituted with an unsubstituted phenyl group, a torsion angle of just 10º is observed (Section 4.5.1 and phenyl benzonitronyl nitroxide[222]). It is only when the phenyl substituents are ortho substituted (Cl, F) that much larger torsion angles (54 – 76º) are present due to steric interaction.[223]

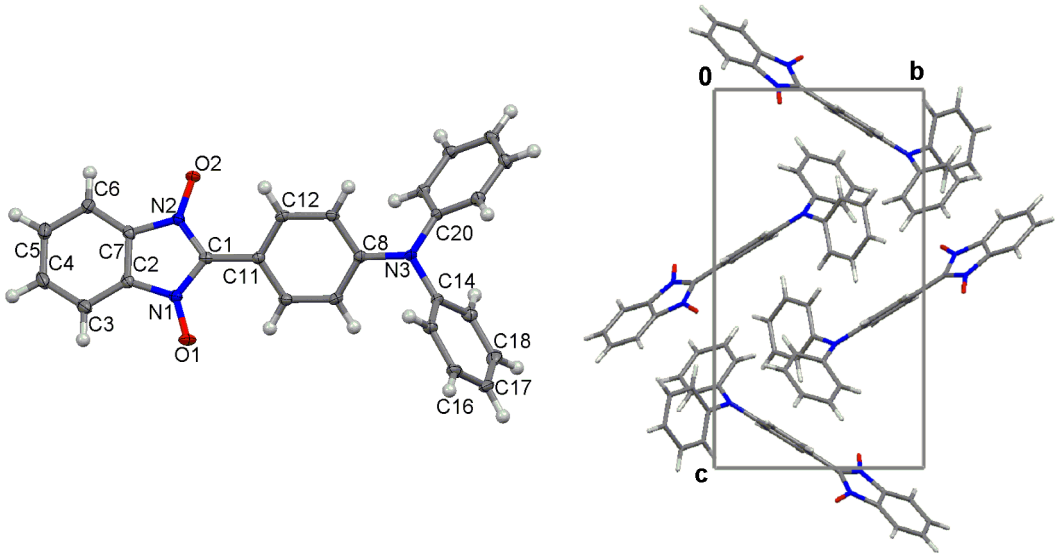

Figure 5.15. Single crystal structure of **5.1e** with 50 % probability thermal ellipsoids (left) and unit cell viewed along the *a*-axis of (right).

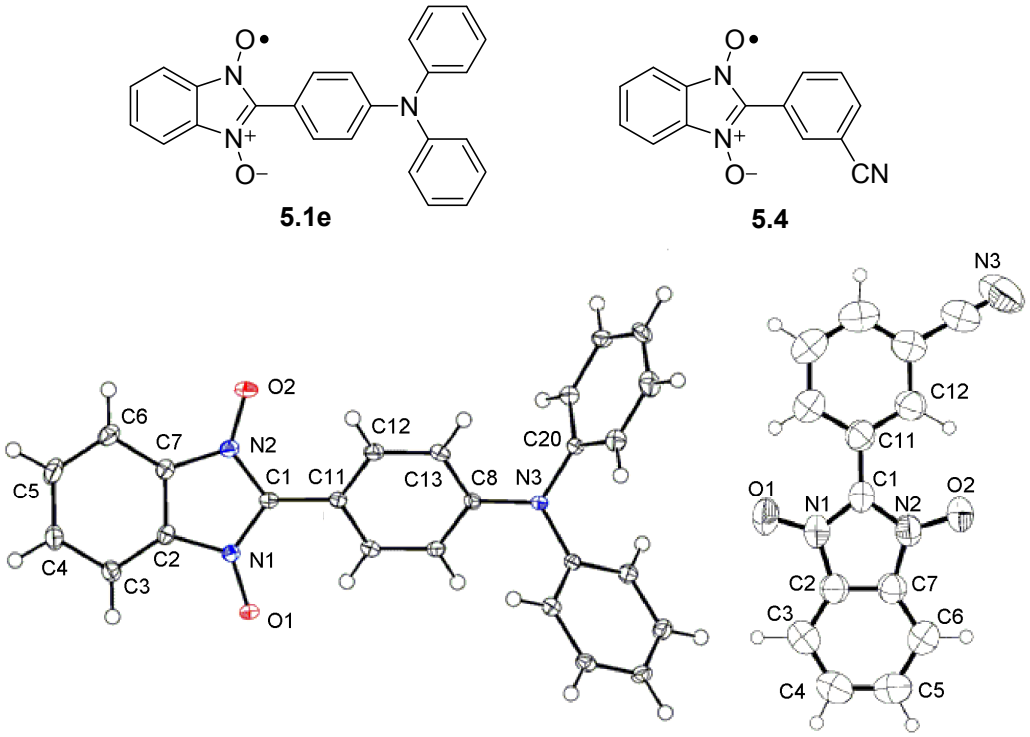

Figure 5.16. Triphenylamine benzonitronyl nitroxide **5.1e** (left) and 3-cyanophenyl benzonitronyl nitroxide **5.4**[223] (right), thermal ellipsoids at the 50 % probability level.

Table 5.7. Selected bond lengths (A), angles (deg) and torsions (deg) for triphenylamine benzonitronyl nitroxide **5.1e** determined crystallographically and from geometry optimization compared to 3-cyanophenylbenzonitronyl nitroxide **5.4**.

Atoms	**5.1e**	**5.4**[a]	**5.1e calcd**
*O*1–*N*1	1.283(1)	1.284(3)	1.275(1)
*O*2–*N*2	1.280(1)	1.284(3)	1.275(1)
*N*1–*C*1	1.371(2)	1.362(3)	1.377(5)
*N*1–*C*2	1.414(2)	1.414(3)	1.414(5)
*N*2–*C*7	1.411(2)	1.370(3)	1.414(5)
*N*2–*C*1	1.371(2)	1.370(3)	1.377(5)
*C*1–*C*11	1.448(2)	1.447(4)	1.449(0)
*C*2–*C*7	1.383(2)	1.373(4)	1.390(2)
*O*1–*N*1–*C*1	126.9(1)	126.6(2)	127.0(7)
*O*2–*N*2–*C*1	126.9(1)	126.9(2)	127.0(7)
*N*2–*C*1–*C*11	125.9(1)	126.4(2)	126.4(7)
*C*8–*N*3–*C*20	120.0(1)	-	120.5(9)
*N*2–*C*1–*C*11–*C*12	31.1(6)	21.0(3)	22.2(5)
*C*13–*C*8–*N*3–*C*20	43.5(5)	-	32.4(1)

[a] From reference 223, atom numbering has been changed to match that used for **5.1e**.

To evaluate if substitution with a strong donor leads to a perturbation in molecular structure, selected imidazole N,N′-dioxide bond lengths in and angles of **5.1e** were compared to electron poor 3-cyanophenyl benzonitronyl nitroxide **5.4**.[223] A comparison of the bond lengths and angles (Table 5.7) of **5.1e** and **5.4** reveals the imidazole rings are nearly identical and the only significant difference is in the length of the *C*2-*C*7 bond. Additionally, the ONC bond angles are nearly indistinguishable between the two molecules suggesting negligible difference in structure is occurring with substitution. This is consistent with spectroscopy and confirms little mixing between donor and acceptor is occurring upon functionalization at *C*2. Additionally comparison of the crystallographically determined structure to the geometry optimized structure (Section 5.2) reveals DFT calculations represented the solid state structure well, with the exception of the *N*2-*C*1-*C*11-*C*12 and *C*13-*C*8-*N*3-*C*20 torsion angles, which may be increased in the solid state as a result of packing effects.

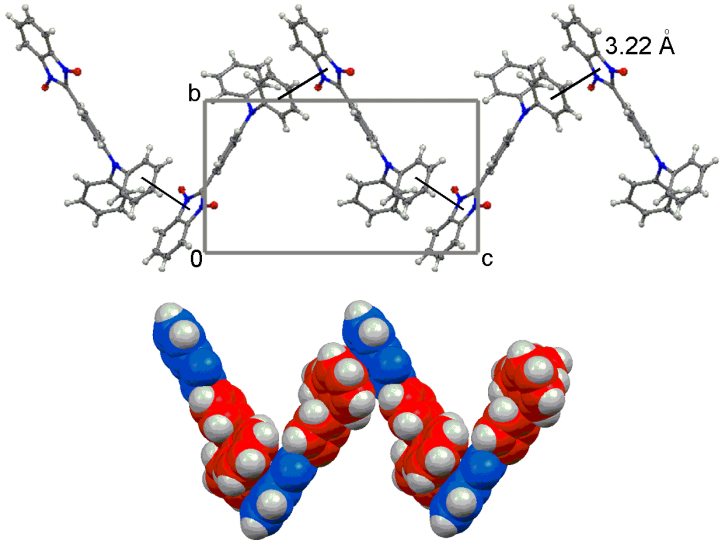

Figure 5.17. 1D chains of **5.1e** formed along the *c*-axis (top). A spacefill model shows the intermolecular interactions are between neighboring **donor** and **acceptor** units (bottom).

The bulky triphenylamine group results in a non-planar molecule and the closely packed π stacks common in other nearly planar BNN radicals are no longer observed. Consequently, intermolecular π overlap is virtually nonexistent and each BNN–triphenylamine molecule is well isolated from adjacent units. The only interactions present are the face-to-face contacts between the *C*14 phenyl ring of a triphenylamine donor and a neighboring accepting benzimidazole ring separated by an average distance of 3.22 Å (Figure 5.17). While the benzimidazole ring contains the bulk of the spin density, by EPR and calculation the spin density on the *C*14 aryl ring of triphenylamine is effectively zero (Figure 5.22). Accordingly, close contacts between rings of neighboring molecules is not predicted to result in strong magnetic exchange by way of a direct exchange mechanism.

5.8 Magnetism measurements

The molar magnetic susceptibilities ($\chi_{M,p}$) were measured for microcrystalline samples of radicals **5.1a** and **5.1c-e** using a Quantum Design SQUID magnetometer in the temperature range of 2 – 300 K at a DC field of 1 T. Without structural information the magnetic plots of **5.1a**, **5.1c**, and **5.1e** were analyzed using a Curie-Weiss analysis to obtain both the Curie and Weiss constants. Curie-law was used to analyze these systems as, in the absence of solid state packing information, it is inappropriate to use a spin Hamiltonian to extract the magnetic exchange coupling constant, *J*.

5.8.1 Magnetic exchange in *p*-methoxyphenyl derivative 5.1a

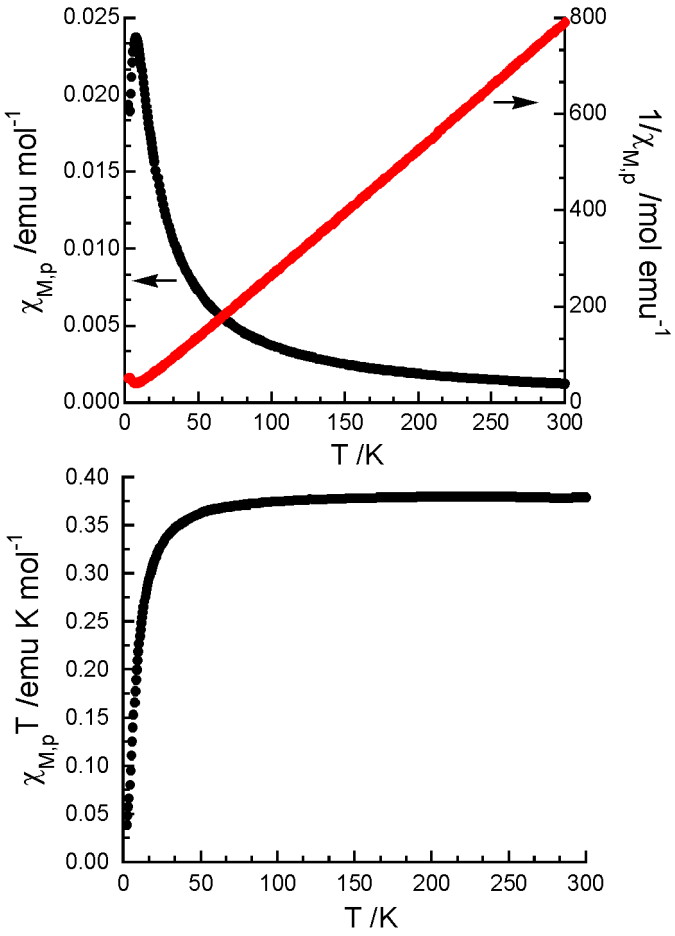

Figure 5.18. Temperature dependence of the molar magnetic susceptibility (top, black), inverse susceptibility (top, red) and magnetic moment for radical **5.1a** (bottom).

At 300 K **5.1a** exhibits a magnetic moment of 0.379 emu K mol^{-1}, close to the expected spin only value for a spin = ½ system (0.375 emu K mol^{-1}). Below 100 K, the magnetic moment ($\chi_{M,p}T$) of *p*-methoxyphenyl derivative **5.1a** began to decrease with decreasing temperature consistent with antiferromagnetic exchange interactions (Figure 5.18). A linear fit (R = 1.0) of the inverse magnetic susceptibility ($1/\chi$) in the paramagnetic regime (100 – 300 K) yielded a Curie constant, C, of 0.380 consistent with

a spin ½ material. The Weiss constant, θ was calculated to be −0.5 K confirming weak antiferromagnetic exchange.

5.8.2 Magnetic exchange in benzo[*b*]thienyl derivative 5.1c

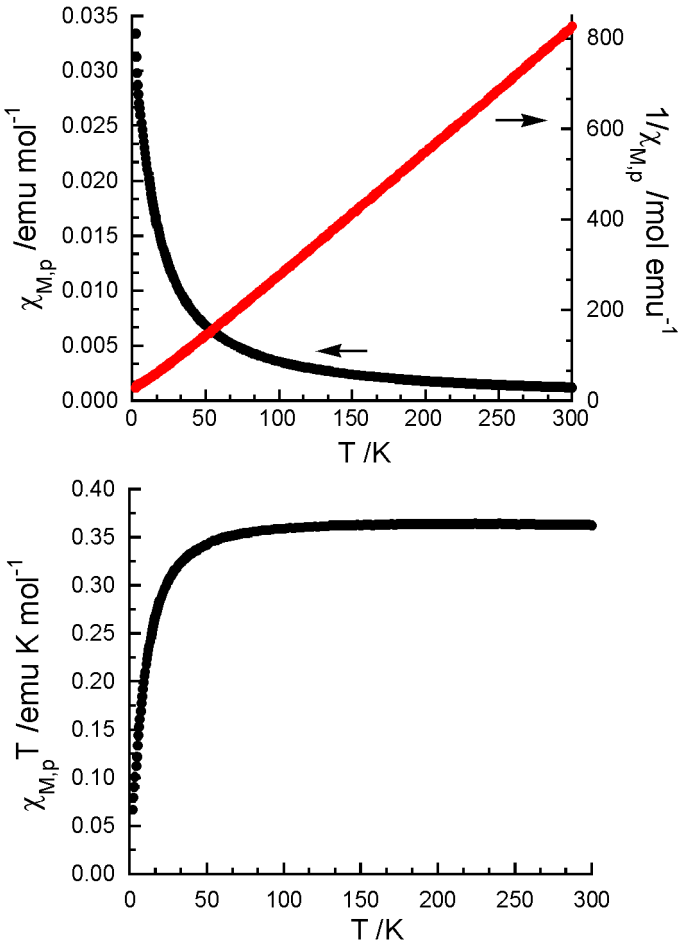

Figure 5.19. Temperature dependence of the molar magnetic susceptibility (top, black), inverse susceptibility (top, red) and magnetic moment for radical **5.1c** (bottom).

At 300 K **5.1c** exhibits a magnetic moment of 0.362 emu K mol^{-1}, slightly lower than the expected spin only value for a spin = ½ system (0.375 emu K mol^{-1}), consistent with the moderate instability observed for this system. Below 100 K, the magnetic moment ($\chi_{M,p}$T) of benzo[*b*]thienyl derivative **5.1c** began to decrease with decreasing temperature

consistent with antiferromagnetic exchange interactions (Figure 5.19). A linear fit (R = 1.0) of the inverse magnetic susceptibility ($1/\chi$) in the paramagnetic regime (100 – 300 K) yielded a Curie constant, C, of 0.364 and a Weiss constant, θ, of −1.0 K consistent with weak antiferromagnetic exchange.

5.8.3 Magnetic exchange in (*N*-ethyl)carbazole derivative 5.1d

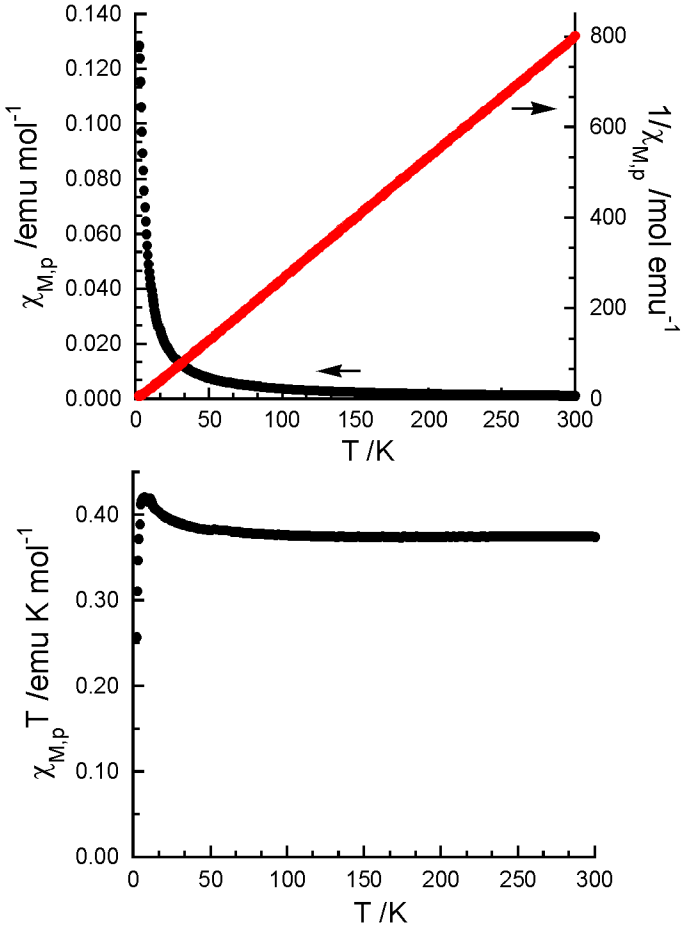

Figure 5.20. Temperature dependence of the molar magnetic susceptibility (top, black), inverse susceptibility (top, red) and magnetic moment for radical **5.1d** (bottom).

The temperature dependence of the magnetic moment of *N*-ethylcarbazole derivative **5.1d** is shown in Figure 5.16. At 300 K **5.1d** exhibits a magnetic moment of 0.374 emu K

mol^{-1}, close to the expected spin only value for an $S = ½$ system (0.375 emu K mol^{-1}). Below 50 K, the magnetic moment ($\chi_{M,p}T$) of **5.1d** began to increase with decreasing temperature consistent with ferromagnetic exchange interactions (Figure 5.20). A maximum magnetic moment of 0.421 emu K mol^{-1} was observed at 7 K. A linear fit (R = 1.0) of the inverse magnetic susceptibility ($1/\chi$) in the paramagnetic regime (50 – 300 K) yielded a Curie constant, C, of 0.374 consistent with a spin ½ material. The Weiss constant, θ was calculated to be +0.4 K confirming weak ferromagnetic exchange.

5.8.4 Magnetic exchange in triphenylamine derivative 5.1e

The molar magnetic susceptibility ($\chi_{M,p}$) was measured for a microcrystalline sample of radical **5.1e** in the temperature range of 2 – 300 K at a DC field of 1 T (Figure 5.17). At 300 K **5.1e** exhibits a magnetic moment consistent with the spin only value of 0.375 emu K mol^{-1} for an $S = ½$ system. The magnetic moment of **5.1e** is independent of temperature above ~50 K and begins to decrease gradually below this temperature, suggesting weak intermolecular antiferromagnetic interactions (Figure 5.17). Based on the uniform 1D chain-like behaviour observed in the crystal structure, the Bonner−Fisher chain model[248] derived from the spin Hamiltonian $H = -JS_{rad}.S_{rad+1}$ was used to fit magnetic moment. A purity factor (f) was included to account for the percentage of spins behaving according to the model and the g-value was set to 2.0075 as determined from EPR spectroscopy.

$$\chi T = f\frac{Ng^2\beta^2}{k_B}\cdot\frac{0.25+0.074975x+0.075235x^2}{1.0+0.9931x+0.172135x^2+0.757825x^3}$$

$$x = \frac{|J|}{k_B T};\quad J \leq 0$$

The least-squares fit of the experimental data to the above (R = 0.97) lead to a spin coupling, J, of -0.5 cm^{-1} and $f = 1.0$. The exceptionally weak antiferromagnetic exchange is consistent with the solid state packing where individual BNN-triphenylamine **5.1e** radicals are fairly well isolated.

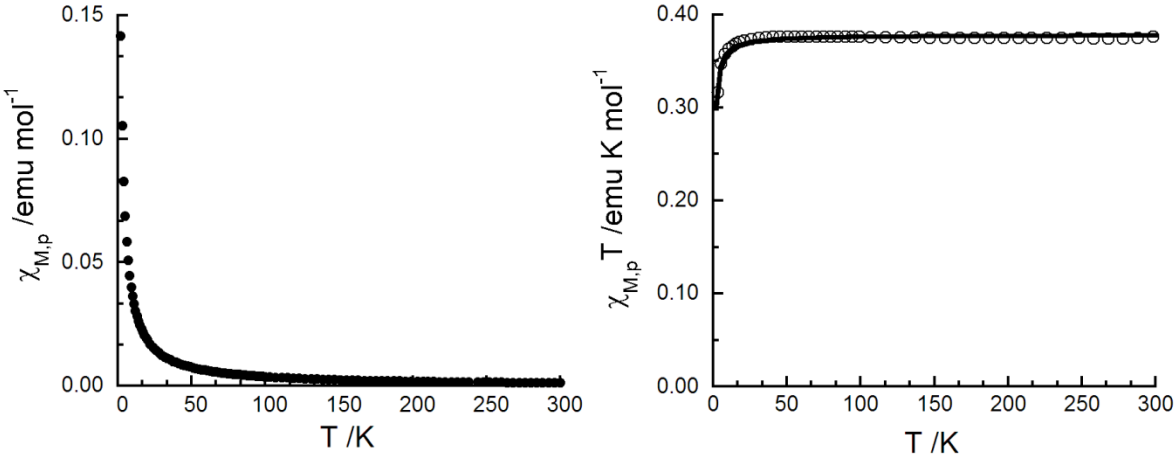

Figure 5.21. Temperature dependence of magnetic susceptibility, $\chi_{M,p}$ (left) and magnetic moment, $\chi_{M,p}T$ (right) for radical **5.1e**. The solid line represents the best fit of the data to the model described in the text.

5.9 Computational and magnetostructural analysis of 5.1e

Single point calculations were performed to determine the electronic structure and spin density distribution of radical **5.1e** using unrestricted TDDFT with Becke's three-parameter hybrid exchange functional[237,330] and the Lee–Yang–Parr correlation functional[238] (UB3LYP). The 6-311+G(d,p) basis set was selected and all calculations were carried out using the Gaussian 09 package.[239] The X-ray crystal structure of **5.1e** was used as the geometry input for the single point energy calculation. A conductor-like polarizable continuum model was used to solvate the system as the inclusion of solvation

reduces over delocalization of the π system in the calculated electronic structure of large π-delocalized D–A molecules.

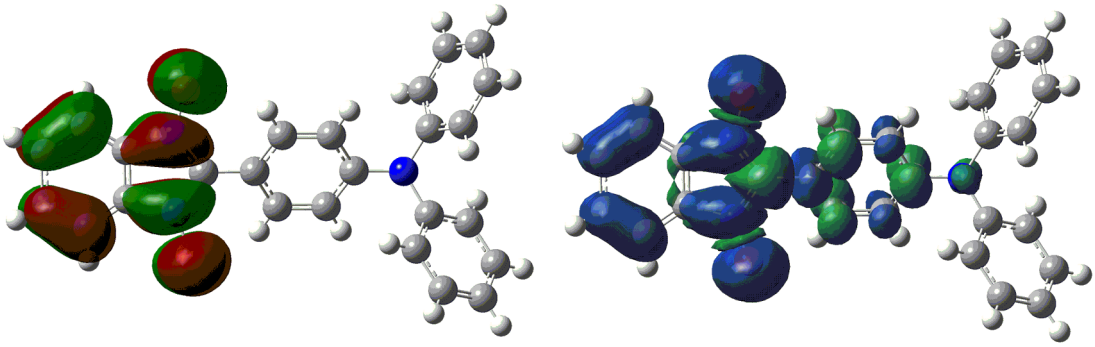

Figure 5.22. α SOMO (left) and spin density (right) of radical **5.1e** generated with GaussView 4.1, grid = coarse, isovalue = 0.02. Calculated using TDDFT UB3LYP/6-311+G(d,p) with CPCM solvation, solvent = chloroform.

The SOMO and spin density distribution obtained for **5.1e** (Figure 5.22) are consistent with the electronic structure of this class of nitroxide radicals.[221] The symmetry and node at *C*2 are maintained and the majority of the spin density is located in the benzannelated imidazole ring, consistent with EPR spectroscopy. The spin density distribution (Figure 5.22, right) indicates spin density is present in the benzimidazole ring through spin delocalization while spin polarization is dominating the spin density distribution in the *C*2 triphenylamine. Very little spin is found on the triphenylamine nitrogen, in agreement with the small hyperfine coupling constant ($a(N_{amine})$ = 0.188 G) determined by EPR spectroscopy.

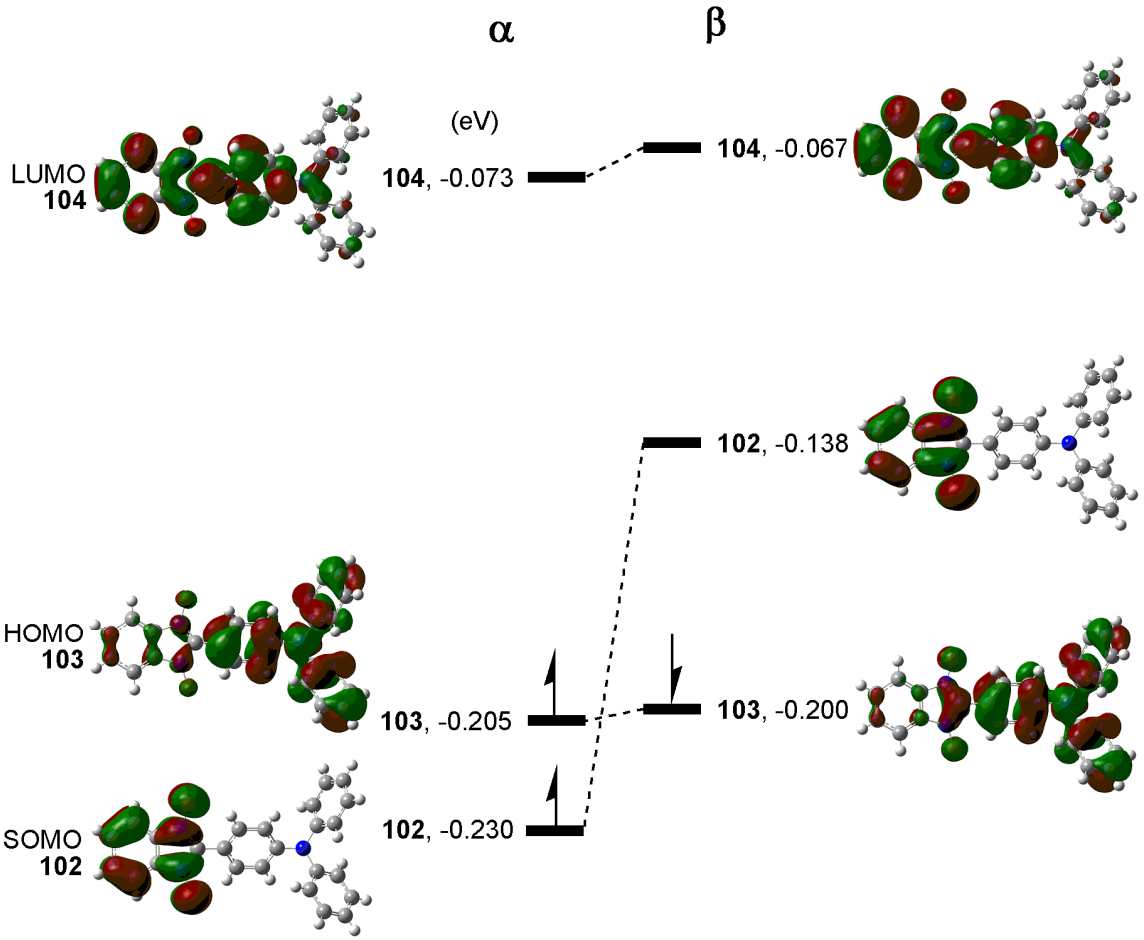

Figure 5.23. Molecular orbital diagram for **5.1e** with CPCM solvation ($CHCl_3$), generated in GaussView 4.1, cube grid = coarse, isoval = 0.02.

The molecular orbital diagram calculated for **5.1e** is shown in Figure 5.23. The α and β SOMO orbitals are significantly different in energy as a result of spin polarization arising from the mixing in of excited states.[83] Additionally, the HOMO has been calculated to be higher in energy than the α SOMO. When the HOMO and SOMO are close in energy, as they are here, the energy of the HOMO can be raised due to inclusion of an electron-electron repulsion term in the exchange correlation functional. Electron repulsion is not present in the SOMO as this orbital is singly occupied, thus the HOMO is artificially raised in energy relative to the SOMO and the calculation converges to give an electron

configuration that is not representative of the correct electronic structure. Analogous molecular orbital diagrams have been calculated for other open shell D−A molecules, most notably the nitronyl nitroxide(A)-tetrathiafulvalene(D) derivatives,[163,371-373] and used to rationalize the high conductivity and electron motility observed in these systems. Unfortunately, an explanation of the observed macroscopic properties based on this orbital configuration cannot be correct as this is not representative of the ground state electronic structure of the system.

As before (Section 4.7), a first principles bottom up approach was used to calculate the exchange parameter, J. Using the overall energy calculated for each state ($S = 0, 1$) the magnetic exchange was determined based on the equation below where E_{BS} and E_T correspond to the energies of the broken symmetry singlet and triplet state and $\langle S^2 \rangle_{BS}$ and $\langle S^2 \rangle_T$ are the spin expectation values of the broken symmetry singlet and triplet state.[340]

$$J = \frac{(E_{BS} - E_T)}{\langle S^2 \rangle_T - \langle S^2 \rangle_{BS}}$$

Analysis of the crystal packing of radical **5.1e** revealed the molecules were well isolated, with only one set of close contacts between benzimidazole and a neighboring triphenylamine aryl ring. For this reason it was believed only one type of solid state interaction would significantly contribute to the bulk magnetism of the system. DFT calculations of the dimer using the hybrid UB3LYP functional at the 6-311+G(d,p) level of theory[340] for the singlet (keyword guess=mix) and triplet states predicted a system with an exchange energy on the order of $J = +0.1$ cm^{-1} as compared to the experimentally derived value of -0.5 cm^{-1}. As the gap in energy between the singlet and triplet state is small, the degree of error is larger than the size of the singlet-triplet gap and the results are consistent with an essentially degenerate singlet and triplet state.

5.10 Conductivity

The conductivities of **5.1a** and **5.1c-e** were measured using a two-probe pressed pellet conductivity apparatus[341] externally calibrated with tetrathiafulvalene-tetracyanoquinodimethane (TTF-TCNQ).[132,342] With the exception of *p*-methoxyphenyl derivative **5.1a**, the room temperature conductivity of each radical was too low to be measured using our experimental setup, suggesting **5.1c-e** have conductivities at room temperature that are $\leq 10^{-9}$ S cm^{-1}. The room temperature conductivity of **5.1a** was on the order of 10^{-7} S cm^{-1} implying it may be semiconducting, although this would need to be confirmed by examining the temperature dependence of the conductivity. Although conclusions about solid state packing cannot be drawn without XRD data, the negligible magnetic exchange and low conductivities observed for **5.1a** and **5.1c-e** suggest very weak intermolecular interactions along the series.

5.11 Reflectance

Solid state reflectance spectra were obtained on thin films of **5.1a, 5.1c-e** dropcast from dichloromethane (Figure 5.24). Solid state absorption decreases in energy with decreasing oxidation potential of the donor. Taking the onset of absorption to be greater than 0.2 a.u., the onset of absorption ranges from 1430 nm (0.87 eV) for **5.1a** to 1610 nm (0.77 eV) for **5.1e**. Each transition is bathochromically shifted by ~100 nm, suggesting the presence of weak solid state π–π or D–A interactions. The emergence of a shoulder is observed on the low energy side of the NIR excitation in each of **5.1a**, **5.1c**, and **5.1d**. In the absence of variable temperature solution phase spectroscopy it is difficult to determine whether the shoulder is due to the emergence of vibrational fine structure or

whether we are observing a new excitation as a result of solid state D–A interactions. Further investigation of this excitation may provide insight into the nature of the solid state environment in the absence of a crystal structure.

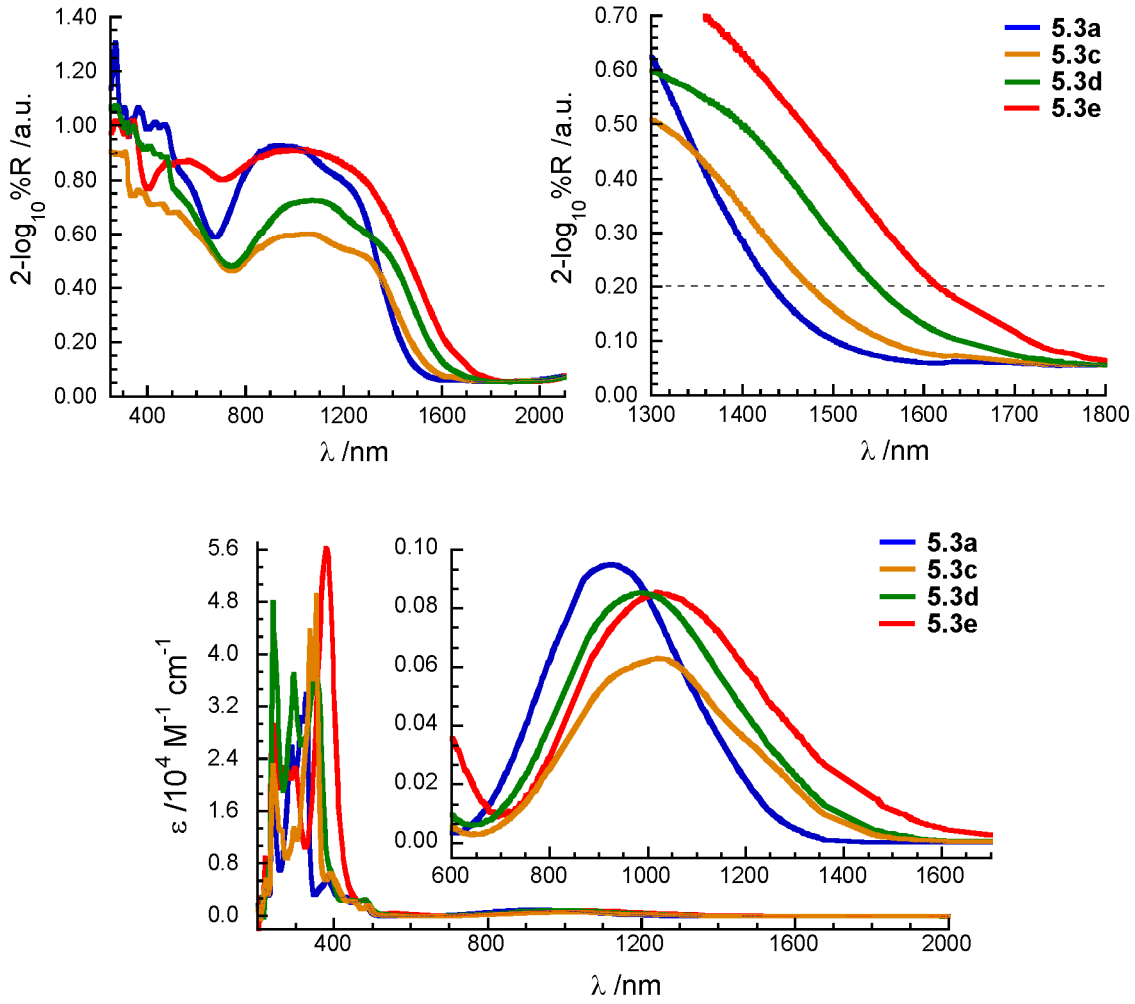

Figure 5.24. Solid state absorbance spectra of films of **5.1a** and **5.1c-e** deposited from CH_2Cl_2 onto quartz slides, spectralon discs were used as a reflective background (top). Solution phase absorbance spectrum of each radical shown for comparison (bottom).

5.12 Conclusion

Hush theory was used to design a series of benzonitronyl nitroxide-based D–A radicals that exhibited decreased NIR absorptions as the electron donor ability of the *C*2

substituent increased. The NIR excitation of each D–A radical was calculated using TDDFT and λ_{max} was found to decrease with decreasing donor oxidation potential, although the relationship was not linear as reorganization energy could not be assumed to be constant along the series.

Five donors ranging in oxidation potential were selected and incorporated at *C*2 in benzonitronyl nitroxide. The resulting D–A radicals are the first examples of BNN radicals substituted with strong donors. The isolation of such systems was significant as this confirmed a one-electron chemical oxidation of the precursor anion to yield a neutral radical was possible, even when the oxidation potential of the donor substituent was lower than that of the oxidant. EPR and UV–vis–NIR spectroscopy confirmed the isolated species were paramagnetic and benzonitronyl nitroxide based. The low energy HOMO–SOMO CT excitation characteristic of BNN radicals was observed and bathochromically shifted as the donor oxidation potential decreased. Band shape analysis of the optically induced CT transition suggested the donor and acceptor were weakly coupled Robin–Day Class II systems. This was confirmed by cyclic voltammetry as little perturbation of the acceptor reduction and donor oxidation potentials was observed.

Solid state spectroscopy and the temperature dependent magnetization suggests little interaction between individual molecules in the solid state. The magnetic exchange determined for each radical was weak and each system was effectively paramagnetic over the entire temperature range measured. A new low energy transition was observed in the solid state absorbance spectra of **5.1a** and **5.1c-e** which may be due to the presence of intermolecular D–A coupling. Furthermore, analysis of the solid state packing of triphenylamine derivative **5.1e** revealed the presence of close intermolecular D–A

contacts. Solid state absorption spectroscopy and X-ray diffraction suggest solid state D–A interactions are present and it may be that close D–A packing is attainable in more planar systems, for example the tetrathiafulvalene derivative.

We have shown substitution at *C*2 with a variety of substituents, including strong donors, is possible and calculations of the CT excitation energy suggest the HOMO–SOMO gap decreases with increasing donor ability. Despite this, high conductivity and strong magnetic exchange are not observed as strong D–A intermolecular interactions which would provide a pathway for conductivity and magnetic exchange were not present. As a result, the observed conductivity and magnetic exchange were very weak precluding elucidation of a relationship between the strength of the intramolecular D–A coupling and the bulk solid state properties.

5.13 Experimental

5.13.1 General procedures

All general synthetic procedures employed have been previously reported in Chapter 2.9. All starting materials were purchased from commercial suppliers and used without further purification.

Computations. Geometry optimizations were carried out at the UB3LYP/6-311+G(d,p) level of theory while single point calculations were carried out at the UB3LYP/6-311+G(d,p) or the UB3LYP/6-311+G(d,p) level of theory[237,238] using the Gaussian 09 package.[239] All geometry optimizations and single point energy calculations included a specified solvation model (CPCM, scrf = chloroform) with the exception of the singlet-triplet gap dimer calculations.

Cyclic Voltammetry. As in Chapter 2.9 with the exception of the multi-scan experiments performed on **5.1e** which were obtained in CH_2Cl_2 as the solubility of the radical was improved under these conditions. Solution was a degassed 1 mM radical solution in 0.1 M nBu_4NPF_6/CH_2Cl_2 at ~300 K with a 3.0 mm diameter glassy carbon working electrode, platinum counter electrode, and Ag wire pseudo-reference electrode. Ferrocene was used as an internal standard and **5.1e** was reported vs SCE (Fc/Fc^+ = 0.40 V vs SCE in acetonitrile and 0.46 V vs SCE in methylene chloride).[230] Peak potentials (E_p) and peak currents (i_p) were extracted using BASi software.

X-ray Crystallography. An irregular black crystal of $C_{25}H_{18}N_3O_2$ having approximate dimensions of 0.08 x 0.10 x 0.25 mm was mounted on a glass fiber. All measurements were made on a Bruker APEX DUO diffractometer with Mo-Kα radiation. The data were collected at a temperature of −183.0 ± 0.1ºC to a maximum 2θ value of 55.8º. Data were collected in a series of ϕ and ω scans in 0.5º oscillations with 5.0-second exposures. The crystal-to-detector distance was 40.00 mm. Of the 14080 reflections that were collected, 4513 were unique (Rint = 0.031); equivalent reflections were merged. Data were collected and integrated using the Bruker SAINT[374] software package. The linear absorption coefficient, μ, for Mo-Kα radiation is 0.88 cm^{-1}. Data were corrected for absorption effects using the multi-scan technique (SADABS[375]), with minimum and maximum transmission coefficients of 0.948 and 0.993, respectively. The data were corrected for Lorentz and polarization effects. The structure was solved by direct methods.[251] The final cycle of full-matrix least-squares refinement on F2 was based on 4513 reflections and 271 variable parameters and converged (largest parameter shift was 0.00 times its electrostatic discharge) with unweighted and weighted agreement factors of

0.048 and 0.093 respectively. The maximum and minimum peaks on the final difference Fourier map corresponded to 0.29 and –0.25 e $Å^{-3}$, respectively. All refinements were performed using the SHELXL-97[376] via the WinGX11[377] interface.

5.13.2 Synthesis

Previously reported compounds. Phenylhydroxylamine **2.20**[228,252] was prepared according to literature methods.

***C*-4-Methoxyphenyl-*N*-phenylnitrone 5.2a.** Phenylhydroxylamine (4.47 g, 41.0 mmol) and *p*-anisaldehyde (4.52 g, 33.2 mmol) were combined in 100 % EtOH (30 mL) to give a pale yellow solution. The reaction mixture was capped with a rubber septum and allowed to stand at rt in the absence of light for 16 h. The solvent was removed under reduced pressure and crude solid was purified by flash column chromatography (nitrone eluted in 90:10 CH_2Cl_2:EtOH, silica gel) yielding 5.66 g (24.9 mmol, 75 %) of a pale yellow solid. mp 107 – 109 ºC. IR (neat) cm^{-1}: 3052, 3009, 2933, 2837, 1601, 1572, 1553, 1507, 1458, 1397, 1306, 1258, 1176, 1063, 1029, 849, 755, 688. ^{1}H NMR (300 MHz, $CDCl_3$): δ 8.38 (d, J = 9 Hz, 2H), 7.83 (s, 1H), 7.74 (dd, J = 8, 2 Hz, 2H), 7.46 – 7.38 (m, 3H), 6.96 (d, J = 9 Hz, 2H). ^{13}C NMR (75 MHz, $CDCl_3$): δ 161.5, 148.9, 134.2, 131.2, 129.6, 129.1, 123.8, 121.6, 114.0, 55.4. EI-MS (70 eV) *m/z*: 227 $[M]^+$, 211 $[M - O]^+$.

***C*-(1-Methyl-3-indole)-*N*-phenylnitrone 5.2b.** Phenylhydroxylamine (1.07 g, 9.80 mmol) and 1-methylindole-3-carboxaldehyde (1.20 g, 7.54 mmol) were combined in 100 % EtOH (10 mL) to give a pale yellow solution. The reaction mixture was capped with a rubber septum and allowed to stand at rt in the absence of light for 48 h. The solvent was removed under reduced pressure and crude yellow oil was purified by recrystallization

from hexanes/ethyl acetate yielding 1.59 g (6.35 mmol, 84 %) of a yellow crystalline solid. mp 114 – 116 ºC. IR (neat) cm^{-1}: 3056, 1568, 1514, 1475, 1388, 1327, 1248, 1198, 1132, 1069, 1016, 764, 743, 688. ^{1}H NMR (300 MHz, $CDCl_3$): δ 9.14 (s, 1H), 8.32 (s, 1H), 7.84 (dd, J = 7, 1 Hz, 2H), 7.72 (d, J = 8 Hz, 1H), 7.49 – 7.21 (m, 6H), 3.84 (s, 3H). ^{13}C NMR (75 MHz, $CDCl_3$): δ 147.8, 136.7, 134.3, 129.1, 129.0, 127.5, 127.1, 123.1, 121.4, 121.0, 118.0, 110.2, 107.3, 33.4. EI-MS (70 eV) *m/z*: 250 $[M]^+$, 234 $[M - O]^+$.

***C*-2-Benzo[*b*]thienyl-*N*-phenylnitrone 5.2c.** Phenylhydroxylamine (1.30 g, 11.9 mmol) and benzo[*b*]thiophene-2-carboxaldehyde (1.42 g, 8.75 mmol) were combined in 100 % EtOH (10 mL) to give a pale yellow solution. The reaction mixture was capped with a rubber septum and allowed to stand at rt in the absence of light for 48 h. The solvent was removed under reduced pressure and crude solid was purified by recrystallization from ~9:1 CH_2Cl_2:EtOH, washed with cold hexanes and air dried yielding 1.80 g (8.29 mmol, 95 %) of pale yellow needles. mp 169 – 171 ºC. IR (neat) cm^{-1}: 3107, 3051, 1549, 1479, 1457, 1369, 1237, 1159, 1150, 1070, 840, 774, 751, 725, 692. ^{1}H NMR (300 MHz, $CDCl_3$): δ 8.51 (d, J = 1 Hz, 1H), 7.94 – 7.91 (m, 1H), 7.86 – 7.80 (m, 4H), 7.49 – 7.38 (m, 5H). ^{13}C NMR (75 MHz, $CDCl_3$): δ 146.8, 141.2, 138.0, 133.4, 130.2, 129.5, 129.3, 127.6, 126.1, 124.7, 123.8, 122.6, 121.2. EI-MS (70 eV) *m/z*: 253 $[M]^+$, 237 $[M - O]^+$.

***C*-(9-Ethyl-3-carbazole)-*N*-phenylnitrone 5.2d.** Phenylhydroxylamine (2.06 g, 18.9 mmol) and 9-ethyl-3-carbazole-carboxaldehyde (3.01 g, 13.5 mmol) were combined in 100% EtOH (20 mL) to give a yellow suspension. The reaction mixture was heated gently until all solids dissolved to give a clear solution, then capped with a rubber septum and allowed to stand at rt in the absence of light for 96 h. The solvent was removed under

reduced pressure and the resulting orange solid was purified by flash chromatography (nitrone eluted in 70:30 hexane:ethyl acetate) yielding 3.67 g (11.7 mmol, 87 %) of an orange oil that solidified upon standing. mp 158 – 160 ºC. IR (neat) cm^{-1}: 3060, 2977, 2934, 2893, 1709, 1625, 1592, 1491, 1471, 1457, 1378, 1348, 1290, 1238, 1177, 1132, 1067, 1022, 908, 768, 730, 689. ^{1}H NMR (300 MHz, $CDCl_3$): δ 9.56 (d, J = 1 Hz, 1H), 8.10 (td, J = 8, 2 Hz, 2H), 7.97 (s, 1H), 7.76 (dd, J = 7, 2 Hz, 2H), 7.38 – 7.24 (m, 6H), 7.18 (t, J = 8 Hz, 1H), 4.15 (q, J = 7 Hz, 2H), 1.27 (t, J = 7 Hz, 3H). ^{13}C NMR (75 MHz, $CDCl_3$): δ 148.9, 141.2, 140.4, 135.4, 129.4, 129.0, 128.1, 126.2, 123.2, 122.9, 121.9, 121.8, 121.5, 120.8, 119.8, 108.9, 108.4, 37.6, 13.8. EI-MS (70 eV) *m/z*: 314 $[M]^+$, 298 $[M - O]^+$.

***C*-4-Diphenylaminophenyl-*N*-phenylnitrone 5.2e.** Phenylhydroxylamine (0.72 g, 6.6 mmol) and 4-diphenylaminobenzaldehyde (1.33 g, 4.87 mmol) were combined in 100% EtOH (20 mL) to give a yellow suspension. The reaction mixture was heated gently until all solids dissolved to give a clear solution, then capped with a rubber septum and allowed to stand at rt in the absence of light for 48 h. The solvent was removed under reduced pressure and the resulting orange solid was purified by recrystallization from ethyl acetate yielding 1.26 g (3.46 mmol, 71%) of a bright yellow crystalline solid. mp 168 - 170 ºC. IR (neat) cm^{-1}: 3057, 1586, 1490, 1398, 1329, 1283, 1188, 1175, 1068, 757, 697. ^{1}H NMR (300 MHz, $CDCl_3$): δ 8.25 (d, J = 9 Hz, 2H), 7.80 (s, 1H), 7.75 (dd, J = 8, 2 Hz, 2H), 7.47 – 7.40 (m, 3H), 7.33 – 7.25 (m, 4H), 7.04 – 7.15 (m, 8H). ^{13}C NMR (75 MHz, $CDCl_3$): δ 150.0, 148.9, 146.7, 134.2, 130.5, 129.5, 129.1, 125.6, 124.3, 123.8, 121.6, 120.8. EI-MS (70 eV) *m/z*: 364 $[M]^+$, 348 $[M - O]^+$.

General procedure for the generation of radical precursor salts: [Sodium][2-(4-Methoxyphenyl)benzimidazole-1,3-dioxide] 5.3a. Benzofuroxan (1.78 g, 13.1 mmol) and *C*-(4-methoxyphenyl)-*N*-phenylnitrone **5.2a** (2.11 g, 9.3 mmol) were suspended in toluene (20 mL) and heated to gentle reflux under an N_2 atm. The reaction was heated for 6 h, by which time a tan precipitate had formed. The reaction mixture was cooled to ambient temperature and the precipitate was isolated by vacuum filtration. The solid was washed with toluene, acetone and pentane and air dried. The tan powder was suspended in EtOH (50 mL) with sonication to give a fine suspension. An ~0.7 M NaOH in EtOH solution (6.5 mL, 4.6 mmol, 0.9 eq) was added dropwise to the sonicating suspension until most (but not all) material had dissolved to give a yellow solution with some suspended particulate. The suspension was filtered through a Celite-545 plug and the resulting yellow solution concentrated to dryness by rotary evaporation. The crude solid was dissolved in a minimal amount of acetone and added dropwise to pentane. A yellow precipitate formed immediately, was isolated by vacuum filtration, washed with pentane and air dried yielding 1.3498 g (4.9 mmol, 53 %) of a bright yellow powder. mp decomp. 244 – 246 ºC. ^{1}H NMR (300 MHz, d_6-DMSO): δ 9.29 (d, J = 8 Hz, 2H), 7.52 (dd, J = 6, 3 Hz, 2H), 7.06 – 6.99 (m, 4H), 3.83 (s, 3H). ^{13}C NMR (75 MHz, d_6-DMSO): δ 158.9, 133.7, 129.4, 127.3, 120.2, 119.8, 112.5, 111.6, 111.3, 55.0. ESI-MS (negative ion mode) *m/z*: 533.61 $[(M)_2Na]^-$.

[Sodium][2-(3-*N*-Methylindole)benzimidazole-1,3-dioxide] 5.3b. Tan solid isolated in 50 % yield. mp decomp. 234 – 236 ºC. ^{1}H NMR (300 MHz, d_6-DMSO): δ 8.96 (s, 1H), 8.81 (s, 1H), 7.48 – 7.39 (m, 3H), 7.19 (t, J = 8 Hz, 1H), 7.06 – 6.98 (m, 3H), 3.84 (s,

3H). ^{13}C NMR (75 MHz, d_6-DMSO): δ 136.1, 135.3, 132.3, 127.5, 125.8, 125.7, 121.3, 119.7, 118.8, 110.7, 109.3, 100.5, 32.8. ESI-MS (negative ion mode) *m/z*: 378.44 $[M]^-$.

[Sodium][2-(2-Benzo[*b*]thienyl)benzimidazole-1,3-dioxide] 5.3c. Yellow solid isolated in 25 % yield. mp decomp. 306 – 308 ºC. ^{1}H NMR (300 MHz, CD_3OD): δ 9.29 (d, J = 1 Hz, 1H), 7.99 – 7.96 (m, 2H), 7.76 (dd, J = 6, 3 Hz, 2H), 7.43 (dd, J = 6, 3 Hz, 2H), 7.35 (dd, J = 6, 3 Hz, 2H). ^{13}C NMR (75 MHz, CD_3OD): δ 142.4, 139.9, 135.0, 129.4, 127.5, 126.7, 125.9, 125.7, 125.4, 124.4, 122.9, 112.2. ESI-MS (negative ion mode) *m/z*: 281.33 $[M]^-$.

[Sodium][2-(9-Ethyl-3-carbazole)benzimidazole-1,3-dioxide] 5.3d. Yellow solid isolated in 59 % yield. mp decomp. 256 – 258 ºC. ^{1}H NMR (300 MHz, d_6-DMSO): δ 10.12 (s, 1H), 9.49 (d, J = 8 Hz, 1H), 8.08 (d, J = 8 Hz, 1H), 7.64 (d, J = 8 Hz, 2H), 7.52 – 7.45 (m, 3H), 7.25 (t, J = 8 Hz, 1H), 7.03 (dd, J = 6, 3 Hz, 2H), 4.48 (q, J = 7 Hz, 2H), 1.36 (t, J = 7 Hz, 3H). ^{13}C NMR (75 MHz, d_6-DMSO): δ 139.2, 138.6, 134.1, 126.8, 125.6, 125.0, 122.1, 120.3, 119.7, 119.4, 118.4, 117.6, 110.5, 108.6, 107.0, 36.4, 13.1. ESI-MS (negative ion mode) *m/z*: 342.27 $[M]^-$.

[Sodium][2-(4-Diphenylaminophenyl)benzimidazole-1,3-dioxide] 5.3e. Yellow solid isolated in 47 % yield. mp decomp. 322 – 324 ºC. ^{1}H NMR (300 MHz, CD_3OD): δ 8.50 (d, J = 9 Hz, 2H), 7.73 (dd, J = 6, 3 Hz, 2H), 7.36 – 7.31 (m, 6H), 7.16 – 7.09 (m, 8H). ^{13}C NMR (75 MHz, CD_3OD): δ 150.9, 148.5, 138.1, 131.9, 130.6, 129.3, 126.5, 125.2, 124.0, 121.9, 118.4, 112.2. ESI-MS (negative ion mode) *m/z*: 392.12 $[M]^-$.

General procedure for the generation of radical 2-(4-Methoxyphenyl)-benzimidazolyl *N,N′*-dioxide 5.1a. [sodium][2-(4-methoxyphenyl)benzimidazole-1,3-dioxide] **5.3a** (0.562 g, 2.02 mmol) was dissolved in 1:2 EtOH:CH_2Cl_2 (60 mL) with

sonication. $AgPF_6$ (0.514 g, 1.85 mmol) was dissolved in minimal ethanol (~2 mL) and added in one portion to the sonicating solution. A grey precipitate formed immediately. Further sonication led to formation of a brown-green solution. The reaction mixture was eluted through a short neutral alumina column (CH_2Cl_2 as eluent). The filtrates were isolated and concentrated until the bulk of the dichloromethane had been removed. The ethanol solution was cooled to −78 ºC ($CO_{2(s)}$/acetone) for one hour. The solid material that formed was isolated on a cold filter stick, washed with cold pentane and dried *en vacuo*. The crude solid was dissolved in a minimal amount of dry acetone and filtered through a Celite-545 plug (diethyl ether as eluent). The filtrates were isolated and cooled to −78 ºC ($CO_{2(s)}$/acetone). The acetone was removed slowly at this temperature until a brown microcrystalline solid was observed. The material was isolated on a cold filter stick, washed with pentane and dried *en vacuo* yielding 0.106 g (0.41 mmol, 22 %) of a copper colored crystalline solid. HRMS Calcd for $C_{14}H_{11}N_2O_3$: 255.07697; Found: 255.07741. Anal. Calcd for $C_{14}H_{11}N_2O_3$: C, 65.88; H, 4.34; N, 10.97. Found: C, 65.68; H, 4.38; N, 10.92. UV–vis ($CHCl_3$) λ_{max}, nm (ε): 240 (18000), 288 (26000), 314 (30000), 327 (34000), 382 (6000), 430 (3000), 480 (2500), 925 (950).

2-(2-Benzo[*b*]thienyl)benzimidazolyl *N*,*N*′-dioxide 5.1c. Brown powder isolated in 13 % yield. Radical decomposes rapidly in solution, HRMS and EA not obtained. UV–vis ($CHCl_3$) λ_{max}, nm (ε): 240 (23000), 295 (14000), 236 (44000), 354 (49000), 390 (6000), 452 (sh, 2300), 488 (1700), 630 (1100).

2-(9-Ethyl-3-carbazole)benzimidazolyl *N*,*N*′-dioxide 5.1d. Bronze microcrystalline needles isolated in 25 % yield. HRMS Calcd for $C21H_{16}N_3O_2$: 342.12425; Found: 342.12400. Anal. Calcd for $C21H_{16}N_3O_2$: C, 73.67; H, 4.71; N, 12.27. Found: C, 71.76;

H, 4.70; N, 11.88. UV–vis ($CHCl_3$) λ_{max}, nm (ε): 240 (48000), 295 (37000), 350 (37000), 390 (sh, 7000), 480 (2500), 990 (850).

2-(4-Diphenylaminophenyl)-benzimidazolyl *N*,*N*′-dioxide 5.1e. Black microcrystalline solid isolated in 36 % yield. HRMS Calcd for $C_{15}H_9N_2O_2S$: 392.13990; Found: 392.13993. Anal. Calcd for $C_{15}H_9N_2O_2S$: C, 76.52; H, 4.62; N, 10.71. Found: C, 76.30; H, 4.79; N, 10.61. UV–vis ($CHCl_3$) λ_{max}, nm (ε): 240 (29000), 272 (23000), 297 (23000), 378 (56000), 480 (2500), 1030 (850).

Chapter 6: General Conclusions and Future Work

Research in the Frank group has been driven by the need for new stable spin delocalized organic radicals with unique solid state properties for magneto-conducting applications. BNN radicals are of interest in that they possess stability toward dimerization in solution and the solid state, a planar topology for strong intermolecular interactions, and delocalized spin density that provides multiple direct magnetic exchange pathways critical for conducting and magnetic materials development. Prior to this work, the synthesis of benzonitronyl nitroxide radicals was shown to be feasible, however, radical generation suffered from poor yield and reproducibility and the radicals were not isolated in high purity.

Significant advances in the design, synthesis, and chemistry of benzonitronyl nitroxide radicals have been made over the course of this research. A mild, generalizable methodology based on furoxan/nitrone condensation was optimized and used to generate a series of BNN precursors and radicals with aromatic, heteroaromatic and alkyl substituents. This methodology was subsequently modified to allow for the synthesis of BNN D–A–D triads and D–A dyads, where BNN radicals were substituted with a selection of strong donors. Unfortunately, the larger π-delocalized furoxans (naphthalene, phenanthrene and pyrene) did not condense with nitrones suggesting the synthesis of these larger π-delocalized systems cannot be accomplished using furoxan condensation methodology.

Not only was a mild synthetic methodology developed allowing for the synthesis of a number of benzonitronyl nitroxide precursors, but the oxidation procedure used to generate the radicals was significantly improved. The development of a mild

homogeneous oxidation procedure has allowed for the isolation and characterization of analytically pure samples, which is of particular importance when measuring bulk phenomena such as magnetism and conductivity.

The electronic structure of each series of benzonitronyl nitroxide radicals was investigated through solution phase techniques (EPR, UV–vis–NIR, and cyclic voltammetry) and compared to computational results. Annelation resulted in delocalization of ~20 % of the total spin density into the benzannelated ring and the appearance of a new NIR excitation attributed to a HOMO–SOMO charge transfer excitation. Cyclic voltammetry revealed the presence of a remarkably low reduction potential, attributed to a decrease in the energy of the SOMO upon annelation. The electronic structure of the BNN radicals was largely independent of substitution at *C*2 and only small perturbations in spin density and reduction potential were observed, even when the substituent was a strong electron donor. The magnitude of the observed changes were consistent with inductive effects and were minor, as *C*2 is located at a nodal position in the SOMO.

The D–A–D triads demonstrate larger changes in the electronic structure could be observed with functionalization at *C*5. This class of radicals exhibited further spin delocalization into the conjugated *C*5 thiophene ring and a reduction potential that was 50 mV more positive than that observed for phenyl BNN. A new weakly solvatochromic transition was observed in the visible spectrum and was investigated using variable temperature spectroscopy. The transition was deconvoluted into two excitations which were computationally attributed to a solvent dependant combination of a HOMO−n → SOMO and HOMO−1 → SOMO charge transfer excitations.

When available, the solid state packing was investigated through X-ray crystallography and the crystallographic data was used to interpret the observed magnetic exchange and electrical conductivity. With the exception of the D–A–D triads, the magnetic exchange and conductivity were weak as a result of either disorder or the absence of close intermolecular contacts. In the case of the D–A–D triads, an interplay between π–π and D–A interactions resulted in strong intermolecular interactions in the solid state. The solid state structure of thienyl-BNN-thienyl D–A–D derivative **4.11b** revealed the presence of additional interchain interactions that lead to ferromagnetic exchange and an increase in conductivity (10^{-5} S cm^{-1}) due to higher dimensionality of the interaction lattice. For all radicals, modeling of the magnetic exchange using a first principles bottom-up approach resulted in good agreement between the energy of the singlet-triplet gap and the observed magnetic exchange so long as the singlet-triplet gap was not effectively degenerate.

The solution phase properties and calculated electronic structure of the BNN radicals were in remarkably good agreement when the computational basis set and molecular environment were carefully selected. When DFT was used with either the EPR-II basis set or the UB3LYP basis set plus solvation, the calculated hyperfine coupling constants, spin density, electron affinity, and molecular geometry were all representative of the solution or solid state structure on the condition that the donor and acceptor were weakly coupled. Calculations also provided a reasonable description of the molecular orbital energies providing the redox asymmetry between donor and acceptor was large. As the donor and acceptor became close in energy, TDDFT artificially raised the HOMO level as a result an electron-electron repulsion term in the exchange correlation functional.

Overall, while it is possible to design and synthesize planar π-delocalized radicals with very low energy optical absorptions and extremely positive reduction potentials, packing effects preclude the observation of strong magnetic exchange and high conductivity. Moving forward, systems of interest may be those in which the electron coupling and magnetic exchange both occur by way of intramolecular exchange interactions. The synthesis of a series of donor bridged BNN diradicals (Figure 6.1) may allow for elucidation of a relationship between charge transfer (or donor strength) and magnetic exchange. If such a relationship could be realized, organic systems could be synthesized in which the magnetic exchange and charge transfer could be controlled at the molecular level giving rise to a new generation of organic magnetoelectronic materials.

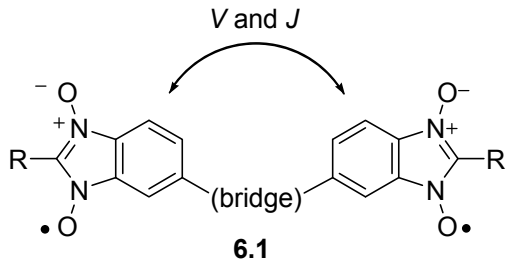

6.1

Figure 6.1. Acceptor–donor–acceptor benzonitronyl nitroxide diradical where bridge represents an electron rich donor.

Preliminary synthetic efforts towards these diradical systems suggests the furoxan/nitrone methodology is not amenable to bis-functionalization (Scheme 6.1). The synthesis of doubly-substituted nitrone **6.2** is possible, however, upon condensation with two equivalents of furoxan the monosubsituted intermediate **6.3** immediately precipiates. Attempts at solubilizing **6.3** through the use of non-nucleophilic amine bases (e.g. TEA, DBU, pyridine) results in decomposition of the starting materials (TLC) and bis-substituted **6.4** was never isolated. Moreover, this methodology yields an A–D–A

topology where the radicals are exchange coupled through the nodal *C*2 position. We have shown these radical-substituent interactions to be weak and are interested in substituting BNN at a site with a high molecular orbital coefficient, and therefore positive spin density.

Scheme 6.1. Proposed synthesis for *C*2 bridged A–D–A diradicals.[a]

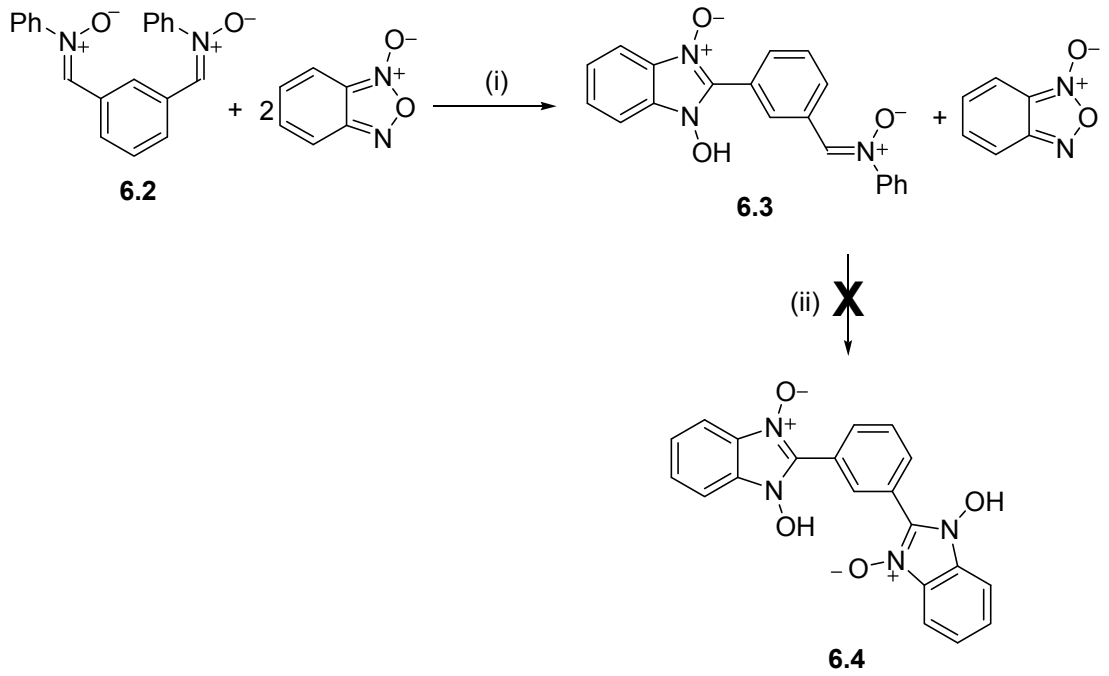

6.2 **6.3** **6.4**

[a] Reagents and conditions: (i) toluene, Δ; (ii) TEA, toluene, Δ.

Scheme 6.2. Proposed diradical synthesis.[a]

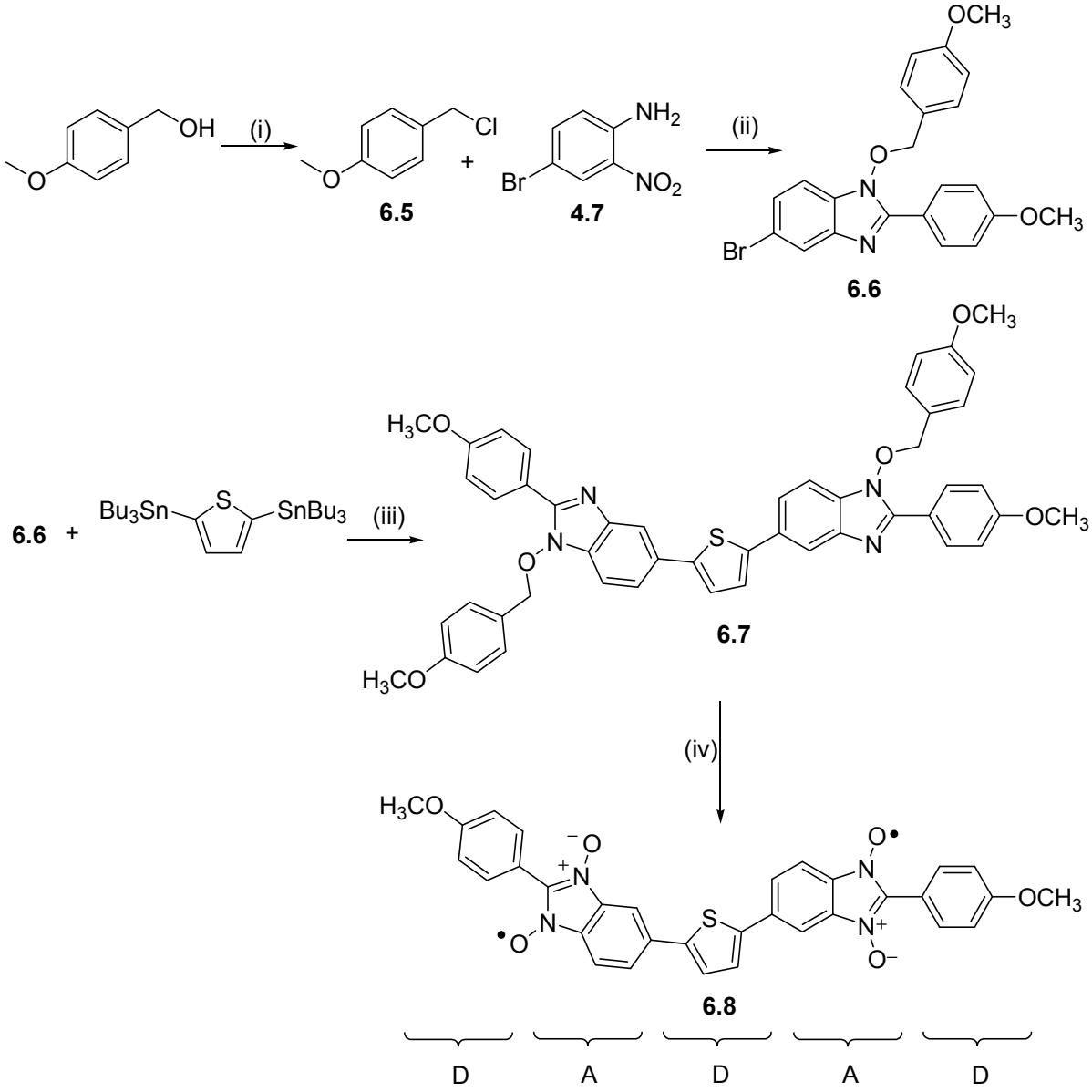

[a] Proposed reagents and conditions: (i) $HCl_{(aq)}$, sonication, rt; (ii) NaH, THF, Δ; (iii) Pd(0), $PtBu_3$, CsF, THF; (iv) mCPBA followed by DDQ, rt to –78 ºC

Over the course of this work an alternate synthetic methodology was briefly explored (Scheme 6.2) based on the work by Gardiner et al.[378-380] that yields benzyl-protected imidazole oxides **6.6** from *o*-nitrophenylamine **4.7** and two equivalents of benzyl halide. Preliminary results suggest the isolation of **6.6** in high yield is possible although the

reaction was sluggish when *p*-methoxybenzylchloride was used as the benzyl source. In this protected form, the benzimidazole-*N*-oxide exhibits excellent solubility and should be amenable to bis-functionalization using palladium catalyzed cross coupling to join two protected radical fragments to give diradical precursor **6.7**. Thiophene has been used as an example donor bridge, however, this methodology would be amenable to the insertion of a number of donor bridges through the use of bis-tin or bis-boronic acid/ester derivatized donors. Once **6.7** has been realized, the *N*-oxide could be formed by oxidation with *m*-chloroperoxybenzoic acid (mCPBA). DDQ (2,3-dichloro-5,6-dicyanobenzoquinone) is known to cleave the benzyl-oxygen bond,[378-380] which in this case should yield diradical **6.8**.

A series of A–D–A diradicals allowing for a systematic study of the effect of donor strength on intramolecular magnetic exchange could permit elucidation of a relationship between magnetic exchange and electron transfer. If the radicals were ferromagnetically coupled (S = 1 ground state) weak antiferromagnetic intermolecular interactions would still give rise to a *ferri*magnetic system and observation of a high T_c may be possible. Furthermore, intermolecular electrostatic D–A interactions can be expected to guide formation of a 3D solid state structure, resulting in increased conductivity through suppression of Peierls distortions.

Literature Cited

(1) Gomberg, M., An Instance of Trivalent Carbon: Triphenylmethyl. *J. Am. Chem. Soc.* **1900,** *22*(11), 757.

(2) Hicks, R. G., What's New in Stable Radical Chemistry? *Org. Biomol. Chem.* **2007,** *5*(9), 1321.

(3) Hicks, R. G., *Stable Radicals: Fundamentals and Applied Aspects of Odd-Electron Compounds*. John Wiley & Sons Inc.: West Sussex, 2010.

(4) Power, P. P., Persistent and Stable Radicals of the Heavier Main Group Elements and Related Species. *Chem. Rev.* **2003,** *103*(3), 789.

(5) Janzen, E. G., Spin Trapping. *Acc. Chem. Res.* **1971,** *4*(1), 31.

(6) Rehorek, D., Spin Trapping of Inorganic Radicals. *Chem. Soc. Rev.* **1991,** *20*(3), 341.

(7) Buettner, G. R., Spin Trapping - Electron-Spin-Resonance Parameters of Spin Adducts. *Free Radical Biol. Med.* **1987,** *3*(4), 259.

(8) Buettner, G. R.; Mason, R. P., Spin-Trapping Methods for Detecting Superoxide and Hydroxyl Free-Radicals In-Vitro and In-Vivo. *Methods Enzymol.* **1990,** *186*, 127.

(9) Rosen, G. M.; Rauckman, E. J., Spin Trapping of Superoxide and Hydroxyl Radicals. *Methods Enzymol.* **1984,** *105*, 198.

(10) Beckwith, A. L. J.; Bowry, V. W.; Ingold, K. U., Kinetics of Nitroxide Radical Trapping. 1. Solvent Effects. *J. Am. Chem. Soc.* **1992,** *114*(13), 4983.

(11) Bowry, V. W.; Ingold, K. U., Kinetics of Nitroxide Radical Trapping. 2. Structural Effects. *J. Am. Chem. Soc.* **1992,** *114*(13), 4992.

(12) Berliner, L. J., *Spin Labelling: Theory and Applications*. Academic Press: New York, 1979.

(13) Hubbell, W. L.; Cafiso, D. S.; Altenbach, C., Identifying Conformational Changes with Site-Directed Spin Labeling. *Nat. Struct. Mol. Biol.* **2000,** *7*(9), 735.

(14) Kosen, P. A., Spin Labeling of Proteins. *Methods Enzymol.* **1989,** *177*, 86.

(15) Pou, S.; Halpern, H. J.; Tsai, P.; Rosen, G. M., Issues Pertinent to the In Vivo In Situ Spin Trapping of Free Radicals. *Acc. Chem. Res.* **1999,** *32*(2), 155.

(16) Sheldon, R. A.; Arends, I.; Ten Brink, G. J.; Dijksman, A., Green, Catalytic Oxidations of Alcohols. *Acc. Chem. Res.* **2002,** *35*(9), 774.

(17) ten Brink, G. J.; Arends, I.; Sheldon, R. A., Green, Catalytic Oxidation of Alcohols in Water. *Science* **2000,** *287*(5458), 1636.

(18) Hawker, C. J.; Bosman, A. W.; Harth, E., New Polymer Synthesis by Nitroxide Mediated Living Radical Polymerizations. *Chem. Rev.* **2001,** *101*(12), 3661.

(19) Nesvadba, P.; Bugnon, L.; Maire, P.; Novak, P., Synthesis of A Novel Spirobisnitroxide Polymer and its Evaluation in an Organic Radical Battery. *Chem. Mater.* **2010,** *22*(3), 783.

(20) Suga, T.; Ohshiro, H.; Sugita, S.; Oyaizu, K.; Nishide, H., Emerging N-Type Redox-Active Radical Polymer for a Totally Organic Polymer-Based Rechargeable Battery. *Adv. Mater.* **2009,** *21*(16), 1627.

(21) Yonekuta, Y.; Susuki, K.; Oyaizu, K. C.; Honda, K. J.; Nishide, H., Battery-Inspired, Nonvolatile, and Rewritable Memory Architecture: A Radical Polymer-Based Organic Device. *J. Am. Chem. Soc.* **2007,** *129*, 14128.

(22) Suga, T.; Konishi, H.; Nishide, H., Photocrosslinked Nitroxide Polymer Cathode-Active Materials for Application in an Organic-Based Paper Battery. *Chem. Commun.* **2007,** (17), 1730.

(23) Bugnon, L.; Morton, C. J. H.; Novak, P.; Vetter, J.; Nesvadba, P., Synthesis of Poly(4-methacryloyloxy-TEMPO) via Group-Transfer Polymerization and its Evaluation in Organic Radical Battery. *Chem. Mater.* **2007,** *19*(11), 2910.

(24) Nishide, H.; Iwasa, S.; Pu, Y. J.; Suga, T.; Nakahara, K.; Satoh, M., Organic Radical Battery: Nitroxide Polymers as a Cathode-Active Material. *Electrochim. Acta* **2004,** *50*(2-3), 827.

(25) Kaim, W.; Moscherosch, M., The Coordination Chemistry of TCNE, TCNQ and Related Polynitrile π-Acceptors. *Coord. Chem. Rev.* **1994,** *129*(1-2), 157.

(26) Pierpont, C. G.; Lange, C. W., The Chemistry of Transition-Metal Complexes Containing Catechol and Semiquinone Ligands. *Prog. Inorg. Chem.* **1994,** *41*, 331.

(27) Chaudhuri, P.; Wieghardt, K., Phenoxyl Radical Complexes. *Prog. Inorg. Chem.* **2001,** *50*, 151.

(28) Vantamel, E.; Whitesid, T., Valence Tautomers of Heterocyclic Aromatic Species. *J. Am. Chem. Soc.* **1971,** *93*(23), 6129.

(29) Adams, D. M.; Dei, A.; Rheingold, A. L.; Hendrickson, D. N., Bistability in the [CO(II)(semiquinonate)$_2$] to [CO(III)(catecholate)(semiquinonate)] Valence-Tautomeric Conversion. *J. Am. Chem. Soc.* **1993,** *115*(18), 8221.

(30) Sato, O., Optically Switchable Molecular Solids: Photoinduced Spin-Crossover, Photochromism, and Photoinduced Magnetization. *Acc. Chem. Res.* **2003,** *36*(9), 692.

(31) Dei, A.; Gatteschi, D.; Sangregorio, C.; Sorace, L., Quinonoid Metal Complexes: Toward Molecular Switches. *Acc. Chem. Res.* **2004,** *37*(11), 827.

(32) Sato, O.; Tao, J.; Zhang, Y. Z., Control of Magnetic Properties Through External Stimuli. *Angew. Chem. Int. Ed.* **2007,** *46*(13), 2152.

(33) Baibich, M. N.; Broto, J. M.; Fert, A.; Vandau, F. N.; Petroff, F.; Eitenne, P.; Creuzet, G.; Friederich, A.; Chazelas, J., Giant Magnetoresistance of (001)Fe/(001)Cr Magnetic Superlattices. *Phys. Rev. Lett.* **1988,** *61*(21), 2472.

(34) Binasch, G.; Grunberg, P.; Saurenbach, F.; Zinn, W., Enhanced Magnetoresistance in Layered Magnetic-Structures with Antiferromagnetic Interlayer Exchange. *Phys. Rev. B: Condens. Matter* **1989,** *39*(7), 4828.

(35) Ivanov, V. A.; Aminov, T. G.; Novotortsev, V. M.; Kalinnikov, V. T., Spintronics and Spintronics Materials. *Russ. Chem. Bull.* **2004,** *53*, 2357.

(36) Gardelis, S.; Smith, C. G.; Barnes, C. H. W.; Linfield, E. H.; Ritchie, D. A., Spin-Valve Effects in a Semiconductor Field-Effect Transistor: A Spintronic Device. *Phys. Rev. B: Condens. Matter* **1999,** *60*(11), 7764.

(37) Jansen, R., The Spin-Valve Transistor: A Review and Outlook. *J. Phys. D: Appl. Phys.* **2003,** *36*(19), R289.

(38) Monsma, D. J.; Lodder, J. C.; Popma, T. J. A.; Dieny, B., Perpendicular Hot-Electron Spin-Valve Effect in a New Magnetic-Field Sensor - The Spin-Valve Transistor. *Phys. Rev. Lett.* **1995,** *74*(26), 5260.

(39) Bogani, L.; Wernsdorfer, W., Molecular Spintronics Using Single-Molecule Magnets. *Nat. Mater.* **2008,** *7*(3), 179.

(40) Rocha, A. R.; Garcia-Suarez, V. M.; Bailey, S. W.; Lambert, C. J.; Ferrer, J.; Sanvito, S., Towards Molecular Spintronics. *Nat. Mater.* **2005,** *4*(4), 335.

(41) Camarero, J.; Coronado, E., Molecular vs. Inorganic Spintronics: The Role of Molecular Materials and Single Molecules. *J. Mater. Chem.* **2009,** *19*(12), 1678.

(42) Seneor, P.; Bernand-Mantel, A.; Petroff, F., Nanospintronics: When Spintronics Meets Single Electron Physics. *J. Phys.: Condens. Matter* **2007,** *19*(16).

(43) Hanson, R.; Kouwenhoven, L. P.; Petta, J. R.; Tarucha, S.; Vandersypen, L. M. K., Spins in Few-Electron Quantum Dots. *Rev. Mod. Phys.* **2007,** *79*(4), 1217.

(44) Awschalom, D. D.; Kawakami, R. K., Magnetoelectronics - Teaching Magnets New Tricks. *Nature* **2000,** *408*(6815), 923.

(45) Prinz, G. A., Device physics - Magnetoelectronics. *Science* **1998,** *282*(5394), 1660.

(46) Prinz, G. A., Magnetoelectronics Applications. *J. Magn. Magn. Mater.* **1999,** *200*(1-3), 57.

(47) Mott, N. F., Electrons in Transition Metals. *Adv. Phys.* **1964,** *13*(51), 325.

(48) Fert, A.; Campbell, I. A., Two-Current Conduction in Nickel. *Phys. Rev. Lett.* **1968,** *21*(16), 1190.

(49) Fert, A.; Campbell, I. A., Electrical-Resistivity of Ferromagnetic Nickel and Iron Based Alloys. *J. Phys. F: Met. Phys.* **1976,** *6*(5), 849.

(50) Chappert, C.; Fert, A.; Van Dau, F. N., The Emergence of Spin Electronics in Data Storage. *Nat. Mater.* **2007,** *6*, 813.

(51) Felser, C.; Fecher, G. H.; Balke, B., Spintronics: A Challenge for Materials Science and Solid-State Chemistry. *Angew. Chem. Int. Ed.* **2007,** *46*(5), 668.

(52) Fert, A., Nobel Lecture: Origin, Development, and Future of Spintronics. *Rev. Mod. Phys.* **2008,** *80*(4), 1517.

(53) Fert, A., Origin, Development, and Future of Spintronics (Nobel Lecture). *Angew. Chem. Int. Ed.* **2008,** *47*(32), 5956.

(54) Chiba, D.; Matsukura, F.; Ohno, H., Electrical Magnetization Reversal in Ferromagnetic III-V Semiconductors. *J. Phys. D: Appl. Phys.* **2006,** *39*(13), R215.

(55) Macdonald, A. H.; Schiffer, P.; Samarth, N., Ferromagnetic Semiconductors: Moving Beyond (Ga, Mn)As. *Nat. Mater.* **2005,** *4*(3), 195.

(56) Zutic, I.; Fabian, J.; Das Sarma, S., Spintronics: Fundamentals and Applications. *Rev. Mod. Phys.* **2004,** *76*(2), 323.

(57) Awschalom, D. D.; Flatte, M. E., Challenges for Semiconductor Spintronics. *Nat. Phys.* **2007,** *3*, 153.

(58) Dediu, V. A.; Hueso, L. E.; Bergenti, I.; Taliani, C., Spin Routes in Organic Semiconductors. *Nat. Mater.* **2009,** *8*(9), 707.

(59) Harris, C. B.; Schlupp, R. L.; Schuch, H., Optically Detected Electron-Spin Locking and Rotary Echo Trains in Molecular Excited-States. *Phys. Rev. Lett.* **1973,** *30*(21), 1019.

(60) Krinichnyi, V. I.; Chemerisov, S. D.; Lebedev, Y. S., EPR and Charge-Transport Studies of Polyaniline. *Phys. Rev. B: Condens. Matter* **1997,** *55*(24), 16233.

(61) Wang, F. J.; Xiong, Z. H.; Wu, D.; Shi, J.; Vardeny, Z. V., Organic Spintronics: The Case of Fe/Alq(3)/Co Spin-Valve Devices. *Synth. Met.* **2005,** *155*, 172.

(62) Xiong, Z. H.; Wu, D.; Vardeny, Z. V.; Shi, J., Giant Magnetoresistance in Organic Spin-Valves. *Nature* **2004,** *427*(6977), 821.

(63) Wang, T. X.; Wei, H. X.; Zeng, Z. M.; Han, X. F.; Hong, Z. M.; Shi, G. Q., Magnetic/Nonmagnetic/Magnetic Tunnel Junction Based on Hybrid Organic Langmuir-Blodgett-Films. *Appl. Phys. Lett.* **2006,** *88*(24).

(64) Majumdar, S.; Laiho, R.; Laukkanen, P.; Vayrynen, I. J.; Majumdar, H. S.; Osterbacka, R., Application of Regioregular Polythiophene in Spintronic Devices: Effect of Interface. *Appl. Phys. Lett.* **2006,** *89*(12).

(65) Xu, W.; Szulczewski, G. J.; LeClair, P.; Navarrete, I.; Schad, R.; Miao, G. X.; Guo, H.; Gupta, A., Tunneling Magnetoresistance Observed in $La_{0.67}Sr_{0.33}MnO_3$/Organic Molecule/Co Junctions. *Appl. Phys. Lett.* **2007,** *90*(7).

(66) Pramanik, S.; Stefanita, C. G.; Patibandla, S.; Bandyopadhyay, S.; Garre, K.; Harth, N.; Cahay, M., Observation of Extremely Long Spin Relaxation Times in an Organic Nanowire Spin Valve. *Nature Nanotechnology* **2007,** *2*(4), 216.

(67) Wang, F. J.; Yang, C. G.; Vardeny, Z. V.; Li, X. G., Spin Response in Organic Spin Valves Based on $La_{2/3}Sr_{1/3}MnO_3$ Electrodes. *Phys. Rev. B: Condens. Matter* **2007,** *75*.

(68) Santos, T. S.; Lee, J. S.; Migdal, P.; Lekshmi, I. C.; Satpati, B.; Moodera, J. S., Room-Temperature Tunnel Magnetoresistance and Spin-Polarized Tunneling Through an Organic Semiconductor Barrier. *Phys. Rev. Lett.* **2007,** *98*.

(69) Shim, J. H.; Raman, K. V.; Park, Y. J.; Santos, T. S.; Miao, G. X.; Satpati, B.; Moodera, J. S., Large Spin Diffusion Length in an Amorphous Organic Semiconductor. *Phys. Rev. Lett.* **2008,** *100*(22).

(70) Morley, N. A.; Rao, A.; Dhandapani, D.; Gibbs, M. R. J.; Grell, M.; Richardson, T., Room Temperature Organic Spintronics. *J. Appl. Phys.* **2008,** *103*(7).

(71) Hueso, L. E.; Bergenti, I.; Riminucci, A.; Zhan, Y. Q.; Dediu, V., Multipurpose Magnetic Organic Hybrid Devices. *Adv. Mater.* **2007,** *19*, 2639.

(72) de Groot, R. A.; Müeller, F. M.; Engen, P. G. v.; Buschow, K. H. J., New Class of Materials: Half-Metallic Ferromagnets. *Phys. Rev. Lett.* **1983,** *50*(25), 2024.

(73) Yoo, J. W.; Chen, C. Y.; Jang, H. W.; Bark, C. W.; Prigodin, V. N.; Eom, C. B.; Epstein, A. J., Spin Injection/Detection Using an Organic-Based Magnetic Semiconductor. *Nat. Mater.* **2010,** *9*(8), 638.

(74) Langevin, P., Magnetism and Theory of the Electrons. *Ann. Chim. Phys.* **1905,** *4*(8), 70

(75) Carlin, R. L., *Magnetochemistry*. Springer-Verlag: Berlin, 1986.

(76) Kahn, O., *Molecular Magnetism*. Wiley-VCH: New York, 1993.

(77) Pascal, P., Magnetochemical Researches. *Ann. Chim. Phys.* **1910,** *19*, 5.

(78) Pascal, P., Magnetochemical Research II. *Ann. Chim. Phys.* **1912,** *25*, 289.

(79) Pascal, P., Magnetochemical Investigations III. *Ann. Chim. Phys.* **1913,** *28*, 218.

(80) Bain, G. A.; Berry, J. F., Diamagnetic Corrections and Pascal's Constants. *J. Chem. Educ.* **2008,** *85*(4), 532.

(81) McConnell, H. M., Ferromagnetism in Solid Free Radicals. *J. Chem. Phys.* **1963,** *39*(7), 1910.

(82) Yamaguchi, K.; Fueno, T.; Nakasuji, K.; Murata, I., Semiempirical Molecular-Orbital (MO) Calculations of the Effective Exchange Integrals for Sandwich Dimers of Free-Radical Species - Antimagnetic and Ferromagnetic Spin Couplings of Organic Free-Radicals. *Chem. Lett.* **1986,** (4), 629.

(83) Okumura, M.; Mori, W.; Yamaguchi, K., Theoretical-Studies of Magnetic Orderings in the β-Phase and γ-Phase of *p*-NPNN and Related Nitroxides. *Mol. Cryst. Liq. Cryst.* **1993,** *232*, 35.

(84) Chiarelli, R.; Novak, M. A.; Rassat, A.; Tholence, J. L., A Ferromagnetic Transition at 1.48 K in an Organic Nitroxide. *Nature* **1993,** *363*(6425), 147.

(85) Benoit, A.; Flouquet, J.; Gillon, B.; Schweizer, J., The Antiferromagnetic Structure of Tanol Substrate. *J. Magn. Magn. Mater.* **1983,** *31*(4), 1155.

(86) Nogami, T.; Ishida, T.; Tsuboi, H.; Yoshikawa, H.; Yamamoto, H.; Yasui, M.; Iwasaki, F.; Iwamura, H.; Takeda, N.; Ishikawa, M., Ferromagnetism in Organic Radical Crystal of 4-(*p*-Chlorobenzylideneamino)-2,2,6,6-tetramethylpiperidin-1-oxyl. *Chem. Lett.* **1995,** (8), 635.

(87) Tamura, M.; Nakazawa, Y.; Shiomi, D.; Nozawa, K.; Hosokoshi, Y.; Ishikawa, M.; Takahashi, M.; Kinoshita, M., Bulk Ferromagnetism in the Beta-Phase

Crystal of the Para-Nitrophenyl Nitronyl Nitroxide. *Chem. Phys. Lett.* **1991,** *186*(4-5), 401.

(88) Kinoshita, M.; Turek, P.; Tamura, M.; Nozawa, K.; Shiomi, D.; Nakazawa, Y.; Ishikawa, M.; Takahashi, M.; Awaga, K.; Inabe, T.; Maruyama, Y., An Organic Radical Ferromagnet. *Chem. Lett.* **1991,** (7), 1225.

(89) Matsushita, M. M.; Izuoka, A.; Sugawara, T.; Kobayashi, T.; Wada, N.; Takeda, N.; Ishikawa, M., Hydrogen-Bonded Organic Ferromagnet. *J. Am. Chem. Soc.* **1997,** *119*(19), 4369.

(90) Palacio, F.; Antorrena, G.; Castro, M.; Burriel, R.; Rawson, J.; Smith, J. N. B.; Bricklebank, N.; Novoa, J.; Ritter, C., High-Temperature Magnetic Ordering in a New Organic Magnet. *Phys. Rev. Lett.* **1997,** *79*(12), 2336.

(91) Banister, A. J.; Bricklebank, N.; Lavender, I.; Rawson, J. M.; Gregory, C. I.; Tanner, B. K.; Clegg, W.; Elsegood, M. R. J.; Palacio, F., Spontaneous Magnetization in a Sulfur–Nitrogen Radical at 36 K. *Angew. Chem. Int. Ed. Engl.* **1996,** *35*(21), 2533.

(92) Robertson, C. M.; Myles, D. J. T.; Leitch, A. A.; Reed, R. W.; Dooley, B. M.; Frank, N. L.; Dube, P. A.; Thompson, L. K.; Oakley, R. T., Ferromagnetism in a Heavy Atom Heterocyclic Radical Conductor. *J. Am. Chem. Soc.* **2007,** *129*(42), 12688.

(93) Manriquez, J. M.; Yee, G. T.; McLean, R. S.; Epstein, A. J.; Miller, J. S., A Room-Temperature Molecular Organic Based Magnet. *Science* **1991,** *252*(5011), 1415.

(94) Saito, G.; Yoshida, Y., Development of Conductive Organic Molecular Assemblies: Organic Metals, Superconductors, and Exotic Functional Materials. *Bull. Chem. Soc. Jpn.* **2007,** *80*(1), 1.

(95) Ogura, F.; Otsubo, T., Conductive Hetero-TCNQs. In *Handbook of Organic Conductive Molecules and Polymers*, Nalwa, H. S., Ed. John Wiley & Sons Inc.: New York, 1997; Vol. 1, pp 229

(96) Yamashita, Y.; Tomura, M., Highly Polarized Electron Donors, Acceptors and Donor-Acceptor Compounds for Organic Conductors. *J. Mater. Chem.* **1998,** *8*(9), 1933.

(97) Sun, D.; Rosokha, S. V.; Kochi, J. K., Reversible Interchange of Charge-Transfer Versus Electron-Transfer States in Organic Electron Transfer via Cross-Exchanges Between Diamagnetic (Donor/Acceptor) Dyads. *J. Phys. Chem. B* **2007,** *111*(24), 6655.

(98) Izuoka, A.; Tachikawa, T.; Sugawara, T.; Suzuki, Y.; Konno, M.; Saito, Y.; Shinohara, H., An X-ray Crystallographic Analysis of a $(BEDT\text{-}TTF)_2C_{60}$ Charge-Transfer Complex. *J. Chem. Soc., Chem. Commun.* **1992,** (19), 1472.

(99) Bryan, C. D.; Cordes, A. W.; Fleming, R. M.; George, N. A.; Glarum, S. H.; Haddon, R. C.; Oakley, R. T.; Palstra, T. T. M.; Perel, A. S.; Schneemeyer, L. F.; Waszczak, J. V., Conducting Charge-Transfer Salts Based on Neutral π-Radicals. *Nature* **1993,** *365*(6449), 821.

(100) Haddon, R. C., Design of Organic Metals and Superconductors. *Nature* **1975,** *256*(5516), 394.

(101) Cordes, A. W.; Haddon, R. C.; Oakley, R. T., A Molecule Like Sodium. *Phosphorus Sulfur Rel. Elem.* **2004,** *179*(4-5), 673.

(102) Hoffmann, R., How Chemistry and Physics Meet in the Solid-State. *Angew. Chem. Int. Ed. Engl.* **1987,** *26*(9), 846.

(103) Hoffmann, R., *Solids and Surfaces: A Chemist's View of Bonding in Extended Structures*. VCH: New York, 1988.

(104) Gersten, J. I.; Smith, F. W., *The Physics and Chemistry of Materials*. John Wiley & Sons, Inc.: New York, 2001; p 197.

(105) Kittel, C., *Introduction to Solid State Physics, 8th Ed.* John Wiley & Sons, Inc.: New York, 2005; p 167.

(106) Whangbo, M. H., Structural and Electronic-Properties of Linear-Chain Compounds and Their Molecular Analogies. *Acc. Chem. Res.* **1983,** *16*(3), 95.

(107) Chiang, C. K.; Fincher, C. R.; Park, Y. W.; Heeger, A. J.; Shirakawa, H.; Louis, E. J.; Gau, S. C.; Macdiarmid, A. G., Electrical-Conductivity in Doped Polyacetylene. *Phys. Rev. Lett.* **1977,** *39*(17), 1098.

(108) Shirakawa, H.; Louis, E. J.; Macdiarmid, A. G.; Chiang, C. K.; Heeger, A. J., Synthesis of Electrically Conducting Organic Polymers - Halogen Derivatives of Polyacetylene, (CH)X. *J. Chem. Soc., Chem. Commun.* **1977,** (16), 578.

(109) Goto, K.; Kubo, T.; Yamamoto, K.; Nakasuji, K.; Sato, K.; Shiomi, D.; Takui, T.; Kubota, M.; Kobayashi, T.; Yakusi, K.; Ouyang, J. Y., A Stable Neutral Hydrocarbon Radical: Synthesis, Crystal Structure, and Physical Properties of 2,5,8-tri-*tert*-butyl-phenalenyl. *J. Am. Chem. Soc.* **1999,** *121*(7), 1619.

(110) Haddon, R. C.; Chichester, S. V.; Stein, S. M.; Marshall, J. H.; Mujsce, A. M., Perchloro-7H-cycloprop[a]acenaphthylene and the Perchlorophenalenyl System. *J. Org. Chem.* **1987,** *52*(4), 711.

(111) Koutentis, P. A.; Chen, Y.; Cao, Y.; Best, T. P.; Itkis, M. E.; Beer, L.; Oakley, R. T.; Cordes, A. W.; Brock, C. P.; Haddon, R. C., Perchlorophenalenyl Radical. *J. Am. Chem. Soc.* **2001,** *123*(17), 3864.

(112) Liao, P.; Itkis, M. E.; Oakley, R. T.; Tham, F. S.; Haddon, R. C., Light-Mediated C-C σ-Bond Driven Crystallization of a Phenalenyl Radical Dimer. *J. Am. Chem. Soc.* **2004,** *126*(43), 14297.

(113) Chi, X.; Itkis, M. E.; Kirschbaum, K.; Pinkerton, A. A.; Oakley, R. T.; Cordes, A. W.; Haddon, R. C., Dimeric Phenalenyl-Based Neutral Radical Molecular Conductors. *J. Am. Chem. Soc.* **2001,** *123*(17), 4041.

(114) Pal, S. K.; Itkis, M. E.; Tham, F. S.; Reed, R. W.; Oakley, R. T.; Haddon, R. C., Resonating Valence-Bond Ground State in a Phenalenyl-Based Neutral Rdical Conductor. *Science* **2005,** *309*(5732), 281.

(115) Mandal, S. K.; Samanta, S.; Itkis, M. E.; Jensen, D. W.; Reed, R. W.; Oakley, R. T.; Tham, F. S.; Donnadieu, B.; Haddon, R. C., Resonating Valence Bond Ground State in Oxygen-Functionalized Phenalenyl-Based Neutral Radical Molecular Conductors. *J. Am. Chem. Soc.* **2006,** *128*(6), 1982.

(116) Boere, R. T.; Oakley, R. T.; Reed, R. W.; Westwood, N. P. C., Ultraviolet Photoelectron and ESR Studies of 1,2,4,6-Thiatriazinyl and 1,2,3,5-Dithiadiazolyl Radicals. *J. Am. Chem. Soc.* **1989,** *111*(4), 1180.

(117) Cordes, A. W.; Goddard, J. D.; Oakley, R. T.; Westwood, N. P. C., 1,2,3,5-Dithiadiazolium Cations and 1,2,3,5-Dithiadiazolyl Radicals: An Ab Initio Computational, Ultraviolet Photoelectron Spectroscopic, and Crystallographic Study of a Cation/Radical Pair. *J. Am. Chem. Soc.* **1989,** *111*(16), 6147.

(118) Fairhurst, S. A.; Johnson, K. M.; Sutcliffe, L. H.; Preston, K. F.; Banister, A. J.; Hauptman, Z. V.; Passmore, J., Electron-Spin-Resonance Study of $CH_3CNSSN^{\cdot}$, $C_6H_5CNSSN^{\cdot}$, AND $SNSSN^{\cdot+}$ Free Radicals. *J. Chem. Soc., Dalton Trans.* **1986,** (7), 1465.

(119) Andrews, M. P.; Cordes, A. W.; Douglass, D. C.; Fleming, R. M.; Glarum, S. H.; Haddon, R. C.; Marsh, P.; Oakley, R. T.; Palstra, T. T. M.; Schneemeyer, L. F.; Trucks, G. W.; Tycko, R.; Waszczak, J. V.; Young, K. M.; Zimmerman, N. M., One-Dimensional Stacking of Bifunctional Dithiadiazolyl and Diselenadiazolyl Radicals - Preparation and Structural and Electronic Properties of 1,3-$[(E_2N_2C)C_6H_4(CN_2E_2)]$ (E = S, Se). *J. Am. Chem. Soc.* **1991,** *113*(9), 3559.

(120) Cordes, A. W.; Haddon, R. C.; Oakley, R. T.; Schneemeyer, L. F.; Waszczak, J. V.; Young, K. M.; Zimmerman, N. M., Molecular Semiconductors From Bifunctional Dithiadiazolium and Diselenadiazolyl Radicals - Preparation and Solid-State Structural and Electronic Properties of 1,4-$[(E_2N_2C)C_6H_4(CN_2E_2)]$ (E = S, Se). *J. Am. Chem. Soc.* **1991,** *113*(2), 582.

(121) Cordes, A. W.; Haddon, R. C.; Hicks, R. G.; Oakley, R. T.; Palstra, T. T. M.; Schneemeyer, L. F.; Waszczak, J. V., Polymorphism of 1,3-Phenylene Bis(diselenadizaolyl) - Solid-State Structural and Electronic Properties of β-1,3-[$(Se_2N_2C)C_6H_4(CN_2Se_2)$]. *J. Am. Chem. Soc.* **1992,** *114*(5), 1729.

(122) Cordes, A. W.; Haddon, R. C.; Hicks, R. G.; Kennepohl, D. K.; Oakley, R. T.; Palstra, T. T. M.; Schneemeyer, L. F.; Scott, S. R.; Waszczak, J. V., Preparation and Solid-State Structural, Electronic, and Magnetic-Properties of teh 5-Cyano-1,3-benzene-Bridged Bis(1,2,3,5-dithiadiazolyl) and Bis(1,2,3,5-diselenadiazolyl) [5-CN-1,3-$C_6H_3(CN_2E_2)_2$] (E = S, SE). *Chem. Mater.* **1993,** *5*(6), 820.

(123) Cordes, A. W.; Haddon, R. C.; MacKinnon, C. D.; Oakley, R. T.; Patenaude, G. W.; Reed, R. W.; Rietveld, T.; Vajda, K. E., Preparation and Solid State Characterization of Isostructural Bifunctional 1,2,3,5-Dithiadiazolyls with Benzene, Bithiophene, and Piperazine Spacers. *Inorg. Chem.* **1996,** *35*(26), 7626.

(124) Cordes, A. W.; Glarum, S. H.; Haddon, R. C.; Hallford, R.; Hicks, R. G.; Kennepohl, D. K.; Oakley, R. T.; Palstra, T. T. M.; Scott, S. R., Preparation and Solid State Characterization of 1,2,3,5-Diselenadiazolyl $[HCN_2Se_2]^{\bullet}$. *J. Chem. Soc., Chem. Commun.* **1992,** (17), 1265.

(125) Cordes, A. W.; Bryan, C. D.; Davis, W. M.; Delaat, R. H.; Glarum, S. H.; Goddard, J. D.; Haddon, R. C.; Hicks, R. G.; Kennepohl, D. K.; Oakley, R. T.; Scott, S. R.; Westwood, N. P. C., Prototypal 1,2,3,5-Dithiadiazolyl and 1,2,3,5-Diselenadiazolyl $[HCN_2E_2]$.(E = S, SE) - Molecular and Electronic Structures of the Radicals and Their Dimers, By Theory and Experiment. *J. Am. Chem. Soc.* **1993,** *115*(16), 7232.

(126) Beer, L.; Britten, J. F.; Brusso, J. L.; Cordes, A. W.; Haddon, R. C.; Itkis, M. E.; MacGregor, D. S.; Oakley, R. T.; Reed, R. W.; Robertson, C. M., Prototypal Dithiazolodithiazolyl Radicals: Synthesis, Structures, and Transport Properties. *J. Am. Chem. Soc.* **2003,** *125*(47), 14394.

(127) Beer, L.; Brusso, J. L.; Cordes, A. W.; Godde, E.; Haddon, R. C.; Itkis, M. E.; Oakley, R. T.; Reed, R. W., Structure-Property Trends in π-Stacked Dithiazolo-Dithiazolyl Conductors. *Chem. Commun.* **2002,** (21), 2562.

(128) Beer, L.; Brusso, J. L.; Cordes, A. W.; Haddon, R. C.; Itkis, M. E.; Kirschbaum, K.; MacGregor, D. S.; Oakley, R. T.; Pinkerton, A. A.; Reed, R. W., Resonance-Stabilized 1,2,3-Dithiazolo-1,2,3-dithiazolyls as Neutral π-Radical Conductors. *J. Am. Chem. Soc.* **2002,** *124*(32), 9498.

(129) Beer, L.; Britten, J. F.; Clements, O. P.; Haddon, R. C.; Itkis, M. E.; Matkovich, K. M.; Oakley, R. T., Dithiazolodithiazolyl Radicals: Substituent Effects on Solid State Structures and Properties. *Chem. Mater.* **2004,** *16*(8), 1564.

(130) Brusso, J. L.; Derakhshan, S.; Itkis, M. E.; Kleinke, H.; Haddon, R. C.; Oakley, R. T.; Reed, R. W.; Richardson, J. F.; Robertson, C. M.; Thompson, L. K., Isostructural Bisdithiazolyl and Bisthiaselenazolyl Radicals: Trends in Bandwidth and Conductivity. *Inorg. Chem.* **2006,** *45*(26), 10958.

(131) Brusso, J. L.; Cvrkalj, K.; Leitch, A. A.; Oakley, R. T.; Reed, R. W.; Robertson, C. M., Resonance Stabilized Bisdiselenazolyls as Neutral Radical Conductors. *J. Am. Chem. Soc.* **2006,** *128*(47), 15080.

(132) Ferraris, J.; Cowan, D. O.; Walatka, V.; Perlstein, J. H., Electron Transfer in a New Highly Conducting Donor-Acceptor Complex. *J. Am. Chem. Soc.* **1973,** *95*(3), 948.

(133) Schafer, D. E.; Wudl, F.; Schmidt, P. H.; Thomas, G. A.; Ferraris, J. P.; Cowan, D. O., Some Attempts to Corroborate Existing Transport Measurements on TTF-TCNQ. *Solid State Commun.* **1974,** *14*(1), 99.

(134) Schafer, D. E.; Wudl, F.; Thomas, G. A.; Ferraris, J. P.; Cowan, D. O., Apparent Giant Conductivity Peaks in an Anisotropic Medium - TTF-TCNQ. *Solid State Commun.* **1974,** *14*(4), 347.

(135) Kistenmacher, T. J.; Phillips, T. E.; Cowan, D. O., The Crystal Structure of the 1:1 Radical Cation-Radical Anion Salt of 2,2'-Bis-l,3-dithiole (TTF) and 7,7,8,8-Tetracyanoquinodimethane (TCNQ). *Acta Crystallogr., Sect. B: Struct. Sci* **1974,** *30*(3), 763.

(136) Chi, X.; Itkis, M. E.; Reed, R. W.; Oakley, R. T.; Cordes, A. W.; Haddon, R. C., Conducting Pathways in Organic Solids: A Phenalenyl-Based Neutral Radical of Low Conductivity. *J. Phys. Chem. B* **2002,** *106*(33), 8278.

(137) Bendikov, M.; Wudl, F.; Perepichka, D. F., Tetrathiafulvalenes, Oligoacenenes, and Their Buckminsterfullerene Derivatives: The Brick and Mortar of Organic Electronics. *Chem. Rev.* **2004,** *104*(11), 4891.

(138) Wheland, R. C., Correlation of Electrical Conductivity in Charge-Transfer Complexes with Redox Potentials, Steric Factors, and Heavy Atom Effects. *J. Am. Chem. Soc.* **1976,** *98*(13), 3926.

(139) Barbara, P. F.; Meyer, T. J.; Ratner, M. A., Contemporary Issues in Electron Transfer Research. *J. Phys. Chem.* **1996,** *100*(31), 13148.

(140) Marcus, R. A., On the Theory of Oxidation-Reduction Reactions Involving Electron Transfer. I. *J. Chem. Phys.* **1956,** *24*(5), 966.

(141) Marcus, R. A., On the Theory of Oxidation-Reduction Reactions Involving Electron Transfer. II. Applications to Data on the Rates of Isotopic Exchange Reactions. *J. Chem. Phys.* **1957,** *26*(4), 867.

(142) Marcus, R. A., Electron-Transfer Reactions in Chemistry - Theory and Experiment. *Rev. Mod. Phys.* **1993,** *65*(3), 599.

(143) Marcus, R. A., Electron-Transfer Reactions in Chemistry - Theory and Experiment (Nobel Lecture). *Angew. Chem. Int. Ed. Engl.* **1993,** *32*(8), 1111.

(144) Atkins, P.; de Paula, J., Dynamics of Electron Transfer. In *Physical Chemistry*, 7 ed.; W. H. Freeman and Company: New York, 2002; p 1018.

(145) Hush, N. S., Intervalence-Transfer Absorption II. Theoretical Considerations and Spectroscopic Data. *Prog. Inorg. Chem.* **1967,** *8*, 391.

(146) Meyer, T. J.; Taube, H., Electron Transfer Reactions. In *Comprehensive Coordination Chemistry*, Wilkinson, G., Sir; Gillard, R. D.; McCleverty, J. A., Eds. Pergamon Press: Elmsford, New York, 1987; Vol. 1, pp 331

(147) Astruc, D., Concepts and Theories of Electron Transfer. In *Electron transfer and radical processes in transition-metal chemistry*, VCH: New York, 1995; pp 3

(148) Nelsen, S. F.; Ismagilov, R. F.; Trieber, D. A., Adiabatic Electron Transfer: Comparison of Modified Theory with Experiment. *Science* **1997,** *278*(5339), 846.

(149) Robin, M. B.; Day, P., Mixed Valence Chemistry A Survey and Classification. *Advances in Inorganic Chemistry and Radiochemistry* **1967,** *10*, 247.

(150) Rosokha, S. V.; Kochi, J. K., Mechanism of Inner-Sphere Electron Transfer via Charge-Transfer (Precursor) Complexes. Redox Energetics of Aromatic Donors with the Nitrosonium Acceptor. *J. Am. Chem. Soc.* **2001,** *123*(37), 8985.

(151) Lambert, C.; Noll, G., The Class II/III Transition in Triarylamine Redox Systems. *J. Am. Chem. Soc.* **1999,** *121*(37), 8434.

(152) Launay, J. P., Long-Distance Intervalence Electron Transfer. *Chem. Soc. Rev.* **2001,** *30*(6), 386.

(153) Nelsen, S. F.; Tran, H. Q.; Nagy, M. A., Comparison of *V* Values for Some Nitrogen- and Metal-Centered π-Bridged Mixed-Valence Compounds. *J. Am. Chem. Soc.* **1998,** *120*(2), 298.

(154) Heckmann, A.; Lambert, C., Neutral Organic Mixed-Valence Compounds: Synthesis and All-Optical Evaluation of Electron-Transfer Parameters. *J. Am. Chem. Soc.* **2007,** *129*(17), 5515.

(155) Heckmann, A.; Lambert, C.; Goebel, M.; Wortmann, R., Synthesis and Photophysics of a Neutral Organic Mixed-Valence Compound. *Angew. Chem. Int. Ed.* **2004,** *43*(43), 5851.

(156) Ratera, I.; Sporer, C.; Ruiz-Molina, D.; Ventosa, N.; Baggerman, J.; Brouwer, A. M.; Rovira, C.; Veciana, J., Solvent Tuning From Normal to Inverted Marcus Region of Intramolecular Electron Transfer in Ferrocene-Based Organic Radicals. *J. Am. Chem. Soc.* **2007,** *129*(19), 6117.

(157) Sporer, C.; Ratera, I.; Ruiz-Molina, D.; Gancedo, J. V.; Wurst, K.; Jaitner, P.; Rovira, C.; Veciana, J., Synthesis, X-ray Structure, EPR and Optical Properties of a Ferrocene Substituted Polychlorotriphenylmethyl Radical. *J. Phys. Chem. Solids* **2004,** *65*(4), 753.

(158) Sporer, C.; Ratera, I.; Ruiz-Molina, D.; Zhao, Y. X.; Vidal-Gancedo, J.; Wurst, K.; Jaitner, P.; Clays, K.; Persoons, A.; Rovira, C.; Veciana, J., A Molecular Multiproperty Switching Array Based on the Redox Behavior of a Ferrocenyl Polychlorotriphenylmethyl Radical. *Angew. Chem. Int. Ed.* **2004,** *43*(39), 5266.

(159) Nishida, S.; Morita, Y.; Fakui, K.; Sato, K.; Shiomi, D.; Takui, T.; Nakasuji, K., Spin Transfer and Solvato-/Thermochromism Induced by Intramolecular Electron Transfer in a Purely Organic Open-Shell System. *Angew. Chem. Int. Ed.* **2005,** *44*(44), 7277.

(160) Nelsen, S. F.; Ismagilov, R. F.; Powell, D. R., Charge Localization in a Dihydrazine Analogue of Tetramethyl-p-phenylenediamine Radical Cation. *J. Am. Chem. Soc.* **1996,** *118*(26), 6313.

(161) Nelsen, S. F.; Ismagilov, R. F.; Powell, D. R., Charge-Localized p-Phenylenedihydrazine Radical Cations: ESR and Optical Studies of Intramolecular Electron Transfer Rates. *J. Am. Chem. Soc.* **1997,** *119*(42), 10213.

(162) Tsubata, Y.; Suzuki, T.; Miyashi, T.; Yamashita, Y., Single-Component Organic Conductors Based on Neutral Radicals Containing the Pyrazino-TCNQ Skeleton. *J. Org. Chem.* **1992,** *57*(25), 6749.

(163) Komatsu, H.; Matsushita, M. M.; Yamamura, S.; Sugawara, Y.; Suzuki, K.; Sugawara, T., Influence of Magnetic Field upon the Conductance of a Unicomponent Crystal of a Tetrathiafulvalene-Based Nitronyl Nitroxide. *J. Am. Chem. Soc.* **2010,** *132*(13), 4528.

(164) Robertson, N.; Cronin, L., Metal bis-1,2-Dithiolene Complexes in Conducting or Magnetic Crystalline Assemblies. *Coord. Chem. Rev.* **2002,** *227*(1), 93.

(165) Allan, M. L.; Coomber, A. T.; Marsden, I. R.; Martens, J. H. F.; Friend, R. H.; Charlton, A.; Underhill, A. E., $NH_4Ni(mnt)_2$ H_2O - A Low-Dimensional Organic Ferromagnet. *Synth. Met.* **1993,** *56*(2-3), 3317.

(166) Coomber, A. T.; Beljonne, D.; Friend, R. H.; Bredas, J. L.; Charlton, A.; Robertson, N.; Underhill, A. E.; Kurmoo, M.; Day, P., Intermolecular Interactions in the Molecular Frromagnetic $NH_4Ni(mnt)_2$ Center Dot H_2O. *Nature* **1996,** *380*(6570), 144.

(167) Allan, M. L.; Martens, J. H. F.; Coomber, A. T.; Friend, R. H.; Marsden, I.; Marseglia, E. A.; Underhill, A. E.; Charlton, A., $NH_4Ni(mnt)_2$ H_2O - A New 1D Organic Ferromagnet. *Mol. Cryst. Liq. Cryst.* **1993,** *230*, 387.

(168) Kato, R., Conducting Metal Dithiolene Complexes: Structural and Electronic Properties. *Chem. Rev.* **2004,** *104*(11), 5319.

(169) Valade, L.; Bousseau, M.; Gleizes, A.; Cassoux, P., A New Two-Dimensional Conducting Mixed-Valence Compound Derived from a Nickel Bisdithiolato-Complex. *J. Chem. Soc., Chem. Commun.* **1983,** (3), 110.

(170) Faulmann, C.; Cassoux, P., Solid-State Properties (Electronic, Magnetic, Optical) of Dithiolene Complex-Based Compounds. *Progress in Inorganic Chemistry: Synthesis, Properties, and Applications* **2004,** *52*, 399.

(171) Tanaka, H.; Okano, Y.; Kobayashi, H.; Suzuki, W.; Kobayashi, A., A Three-Dimensional Synthetic Metallic Crystal Composed of Single-Component Molecules. *Science* **2001,** *291*(5502), 285.

(172) Bowles, S. E. Synthesis and Characterization of Annelated Nitronyl Nitroxides. Ph.D. Thesis, University of Washington, 2005.

(173) Lankamp, H.; Nauta, W. T.; Maclean, C., A New Interpretation of Monomer-Dimer Equilibrium of Triphenylmethyl- and Alkyl Substituted-Diphenyl Methyl-Radicals in Solution. *Tetrahedron Lett.* **1968,** (2), 249.

(174) McBride, J. M., Hexaphenylethane Riddle. *Tetrahedron* **1974,** *30*(14), 2009.

(175) Maki, A. H.; Allendoe.Rd; Danner, J. C.; Keys, R. T., Electron Nuclear Double Resonance in Solutions. Spin Densities in Triarylmethyl Radicals. *J. Am. Chem. Soc.* **1968,** *90*(16), 4225.

(176) Ballester, M., Inert Free Radicals (IFR): A Unique Trivalent Carbon Species. *Acc. Chem. Res.* **1985,** *18*(12), 380.

(177) Ballester, M.; Riera-Figueras, J.; Castañer, J.; Badfa, C.; Monso, J. M., Inert Carbon Free Radicals. I. Perchlorodiphenylmethyl and Perchlorotriphenylmethyl Radical Series. *J. Am. Chem. Soc.* **1971,** *93*(9), 2215.

(178) Armet, O.; Veciana, J.; Rovira, C.; Riera, J.; Castaner, J.; Molins, E.; Rius, J.; Miravitlles, C.; Olivella, S.; Brichfeus, J., Inert Carbon Free-Radicals. 8. Polychlorotriphenylmethyl Radicals - Synthesis, Structure, and Spin-Density Distribution. *J. Phys. Chem.* **1987,** *91*(22), 5608.

(179) Bennett, J. E., Study of the Oxidation of Hindered Phenols by Electron Spin Resonance. *Nature* **1960,** *186*(4722), 385.

(180) Morita, Y.; Nishida, S., Phenalenyls, Cyclopentadienyls, and Other Carbon-Centered Radicals. In *Stable Radicals: Fundamentals and Applied Aspects of Odd-Electron Compounds*, Hicks, R. G., Ed. John Wiley & Sons Inc.: West Sussex, 2010; pp 81.

(181) Armstrong, D. R.; Cameron, C.; Nonhebel, D. C.; Perkins, P. G., Oxidative Coupling of Phenols. 7. Spin-Density Calculations on the Phenoxyl Radical. *J. Chem. Soc., Perkin Trans. 2* **1983,** (5), 569.

(182) Coppinger, G. M., A Stable Phenoxyl Radical Inert to Oxygen. *J. Am. Chem. Soc.* **1957,** *79*(2), 501.

(183) Dietz, F.; Tyutyulkov, N.; Baumgarten, M., Nature of the Magnetic Interaction in Organic Radical Crystals. 3. Galvinoxyl Radicals in 1-D Crystals. *J. Phys. Chem. B* **1998,** *102*(20), 3912.

(184) Rozanstev, E. G., *Free Nitroxyl Radicals*. Plenum: New York, 1970.

(185) Karoui, H.; Le Moigne, F.; Ouari, O.; Tordo, P., Nitroxide Radicals: Properties, Synthesis and Applications. In *Stable Radicals: Fundamentals and Applied Aspects of Odd-Electron Compounds*, Hicks, R. G., Ed. John Wiley & Sons Inc.: West Sussex, 2010; pp 173.

(186) Volodarsky, L. B.; Reznikov, V. A.; Ovcharenko, V. I., *Synthetic Chemistry of Stable Nitroxides*. CRC Press Inc.: Boca Raton, 1993.

(187) Likhtenshtein, G.; Yamauchi, J.; Nakatsuji, S. i.; Smirnov, A. I., *Nitroxides: Applications in Chemistry, Biomedicine, and Materials Science* Wiley-VCH Verlag GmbH: Weinheim, 2008.

(188) Caneschi, A.; Gatteschi, D.; Rey, P., The Chemistry and Magnetic-Properties of Metal Nitronyl Nitroxide Complexes. *Prog. Inorg. Chem.* **1991,** *39*, 331.

(189) Nakatsuji, S.; Anzai, H., Recent Progress in the Development of Organomagnetic Materials Based on Neutral Nitroxide Radicals and Charge Transfer Complexes Derived From Nitroxide Radicals. *J. Mater. Chem.* **1997,** *7*(11), 2161.

(190) Tretyakov, E. V.; Ovcharenko, V. I., The Chemistry of Nitroxide Radicals in the Molecular Design of Magnets. *Russ. Chem. Rev.* **2009,** *78*(11), 971.

(191) Frank, N. L.; Clerac, R.; Sutter, J. P.; Daro, N.; Kahn, O.; Coulon, C.; Green, M. T.; Golhen, S.; Ouahab, L., Synthesis, Crystal Structure, Magnetic, and Electron Paramagnetic Resonance Properties of a Spiroconjugated Biradical: Evidence for Spiroconjugation Exchange Pathway. *J. Am. Chem. Soc.* **2000,** *122*(9), 2053.

(192) Stumpf, H. O.; Ouahab, L.; Pei, Y.; Grandjean, D.; Kahn, O., A Molecular-Based Magnet with a Fully Interlocked 3-Dimensional Structure. *Science* **1993,** *261*(5120), 447.

(193) Zheludev, A.; Barone, V.; Bonnet, M.; Delley, B.; Grand, A.; Ressouche, E.; Rey, P.; Subra, R.; Schweizer, J., Spin Density in a Nitronyl Nitroxide Free Radical - Polarized Neutron Diffraction Investigation and Ab Initio Calculations. *J. Am. Chem. Soc.* **1994,** *116*(5), 2019.

(194) Kocherginsky, N.; Swartz, H. M., *Nitroxide Spin Labels: Reactions in Biology and Chemistry* CRC Press Inc.: Boca Raton, 1995.

(195) Griffith, O. H.; Waggoner, A. S., Nitroxide Free Radicals - Spin Labels for Probing Biomolecular Structure. *Acc. Chem. Res.* **1969,** *2*(1), 17.

(196) Lagercra.C, Spin Trapping of Some Short-Lived Radicals By Nitroxide Method. *J. Phys. Chem.* **1971,** *75*(22), 3466.

(197) Ullman, E. F.; Siecki, J. H.; Boocock, D. G. B.; Darcy, R., Studies of Stable Free Radicals. 20. Nitronyl Nitroxide Monoradicals and Biradicals as Possible Small Molecule Spin Labels. *J. Am. Chem. Soc.* **1972,** *94*(20), 7049.

(198) Keana, J. F. W., Newer Aspects of Synthesis and Chemistry of Nitroxide Spin Labels. *Chem. Rev.* **1978,** *78*(1), 37.

(199) Stumpf, H. O.; Ouahab, L.; Pei, Y.; Bergerat, P.; Kahn, O., Chemistry and Physics of a Molecular-Based Magnet Containing 3 Spin Carriers, with a Fully Interlocked Structure. *J. Am. Chem. Soc.* **1994,** *116*(9), 3866.

(200) Luneau, D.; Rey, P., Magnetism of Metal-Nitroxide Compounds Involving Bis-Chelating Imidazole and Benzimidazole Substituted Nitronyl Nitroxide Free Radicals. *Coord. Chem. Rev.* **2005,** *249*(23), 2591.

(201) Bogani, L.; Sangregorio, C.; Sessoli, R.; Gatteschi, D., Molecular Engineering for Single-Chain-Magnet Behavior in a One-Dimensional Dysprosium-Nitronyl Nitroxide Compound. *Angew. Chem. Int. Ed.* **2005,** *44*(36), 5817.

(202) Hicks, R. G., Verdazyls and Related Radicals Containing the Hydrazyl [R_2N-NR] Group. In *Stable Radicals: Fundamentals and Applied Aspects of Odd-Electron Compounds*, Hicks, R. G., Ed. John Wiley & Sons Inc.: West Sussex, 2010; pp 245.

(203) Koivisto, B. D.; Hicks, R. G., The Magnetochemistry of Verdazyl Radical-Based Materials. *Coord. Chem. Rev.* **2005,** *249*(23), 2612.

(204) Mukai, K., Carbon-Based Magnetism. In *Carbon-Based Magnetism*, Makarova, T.; Palacio, F., Eds. Elsevier: Amsterdam, 2006; pp 75.

(205) Polumbrik, O. M., Advances in the Chemistry of Verdazyl Radicals. *Russ. Chem. Rev.* **1978,** *47*(8), 767.

(206) Mukai, K., In *Carbon-Based Magnetism*, Makarova, T.; Palacio, F., Eds. Elsevier: Amsterdam, 2006.

(207) Yang, A.; Kasahara, T.; Chen, E. K. Y.; Hamer, G. K.; Georges, M. K., 1,3-Dipolar Cycloaddition Reactions Initiated with the 1,5-Dimethyl-3-phenyl-6-oxoverdazyl Radical. *Eur. J. Org. Chem.* **2008,** (27), 4571.

(208) Chen, E. K. Y.; Teertstra, S. J.; Chan-Seng, D.; Otieno, P. O.; Hicks, R. G.; Georges, M. K., Verdazyl-Mediated Living-Radical Polymerization of Styrene and n-Butyl Acrylate. *Macromolecules* **2007,** *40*(24), 8609.

(209) Oakley, R. T., Cyclic and Heterocyclic Thiazines. *Prog. Inorg. Chem.* **1988,** *36*, 299.

(210) Chivers, T., Synthetic Methods and Structure Reactivity Relationships in Electron-Rich Sulfur Nitrogen Rings and Cages. *Chem. Rev.* **1985,** *85*(5), 341.

(211) Chivers, T., *A Guide to Chalcogen-Nitrogen Chemistry*. World Scientific: Singapore, 2005.

(212) Gleiter, R., Structure and Bonding in Cyclic Sulfur-Nitrogen Compounds—Molecular Orbital Considerations. *Angew. Chem. Int. Ed.* **1981,** *20*(5), 444.

(213) Rawson, J. M.; Palacio, F., Magnetic Properties of Thiazyl Radicals. *π-Electron Magnetism from Molecules to Magnetic Materials* **2001,** *100*, 93.

(214) Awaga, K.; Umezono, Y.; Fujita, W.; Yoshikawa, H.; Cui, H. B.; Kobayashi, H.; Staniland, S. S.; Robertson, N., Diverse Magnetic and Electrical Properties of Molecular Solids Containing the Thiazyl Radical BDTA. *Inorg. Chim. Acta* **2008,** *361*(14-15), 3761.

(215) Hicks, R. G., The Synthesis and Characterization of Stable Radicals Containing the Thiazyl (SN) Fragment and Their Use as Building Blocks for Advanced Functional Materials. In *Stable Radicals: Fundamentals and Applied Aspects of Odd-Electron Compounds*, Hicks, R. G., Ed. John Wiley & Sons Inc.: West Sussex, 2010; pp 317.

(216) Barclay, T. M.; Cordes, A. W.; George, N. A.; Haddon, R. C.; Itkis, M. E.; Mashuta, M. S.; Oakley, R. T.; Patenaude, G. W.; Reed, R. W.; Richardson, J. F.; Zhang, H., Redox, Magnetic, and Structural Properties of 1,3,2-Dithiazolyl Radicals. A Case Study on the Ternary Heterocycle $S_3N_5C_4$. *J. Am. Chem. Soc.* **1998,** *120*(2), 352.

(217) Fujita, W.; Awaga, K., Room-Temperature Magnetic Bistability in Organic Radical Crystals. *Science* **1999,** *286*(5438), 261.

(218) McManus, G. D.; Rawson, J. M.; Feeder, N.; van Duijn, J.; McInnes, E. J. L.; Novoa, J. J.; Burriel, R.; Palacio, F.; Oliete, P., Synthesis, Crystal Structures,

Electronic Structure and Magnetic Behaviour of the Trithiatriazapentalenyl Radical, $C_2S_3N_3$. *J. Mater. Chem.* **2001,** *11*(8), 1992.

(219) Gough, T. E.; Puzic, R., Electron-Spin Resonance Study of Stable Benzimidazole-3-oxyl-1-oxide Free-Radicals. *J. Magn. Reson.* **1976,** *23*(1), 31.

(220) Bowles, S. E.; Dooley, B. M.; Benedict, J. B.; Kaminsky, W.; Frank, N. L., The Competing Roles of Topology and Spin Density in the Magnetic Behavior of Spin-Delocalized Radicals: Donor-Acceptor Annelated Nitronyl Nitroxides. *Polyhedron* **2009,** *28*(9-10), 1704.

(221) Dooley, B. M.; Bowles, S. E.; Storr, T.; Frank, N. L., Synthesis of Neutral Spin-Delocalized Electron Acceptors for Multifunctional Materials. *Org. Lett.* **2007,** *9*(23), 4781.

(222) Kusaba, Y.; Tamura, M.; Hosokoshi, Y.; Kinoshita, M.; Sawa, H.; Kato, R.; Kobayashi, H., Isolation of Crystals of a Planar Nitronyl Nitroxide Radical: 2-Phenylbenzimidazol-1-yl N,N'-dioxide (PBIDO). *J. Mater. Chem.* **1997,** *7*(8), 1377.

(223) Zakrassov, A.; Shteiman, V.; Sheynin, Y.; Tumanskii, B.; Botoshansky, M.; Kapon, M.; Keren, A.; Kaftory, M.; Vos, T. E.; Miller, J. S., Synthesis, Structural, and Magnetic Characterization of Substituted Benzoimidazole-l-yl N,N'-dioxides. *J. Mater. Chem.* **2004,** *14*(12), 1827.

(224) Shiomi, D.; Sato, K.; Takui, T.; Itoh, K.; Tamura, M.; Nishio, Y.; Kajita, K.; Nakagawa, M.; Ishida, T.; Nogami, T., Possible Superhigh-Spin Cluster in the Crystals of a Novel Nitronyl Nitroxide Radical as Studied by FT Pulsed ESR. *Mol. Cryst. Liq. Cryst. Sci. Technol., Sect. A* **1999,** *335*, 1071.

(225) Minisci, F.; Galli, R.; Quilico, A., Addition Reaction of Nitrile Oxides on Aromatic Nitrosoderivatives. A Novel Synthesis of the Benzimidazole Ring. *Tetrahedron Lett.* **1963,** *4*(12), 785.

(226) Patzold, F.; Niclas, H. J.; Grundemann, E., Studies on the Reaction of Ortho-Benzoquinone Dioxime with Aldehydes - An Improved Procedure for 1-Hydroxybenzimidazole 3-oxides. *J. Prakt. Chem.* **1990,** *332*(3), 345.

(227) Abu El-Haj, M. J., Novel Synthesis of 1-Hydroxy-1H-benzimidazole 3-oxides and 2,2-Dialkyl-2H-benzimidazole 1,3-dioxides. *J. Org. Chem.* **1972,** *37*(15), 2519.

(228) Kamm, O., Phenylhydroxylamine. *Org. Synth. Coll. Vol. 1* **1941**, 455.

(229) Vanysek, P., Electrochemical Series. In *CRC Handbook of Chemistry and Physics, 2009 - 2010, 90th ed.*, Lide, D. R., Ed. CRC Press Inc.: Boca Raton, 2009; pp 8.

(230) Connelly, N. G.; Geiger, W. E., Chemical Redox Agents for Organometallic Chemistry. *Chem. Rev.* **1996,** *96*(2), 877.

(231) Lin, H. H.; Wei, H. H., Synthesis, Structure and Magnetic Properties of 1-D Silver(I) Complexes with Benzoic Acids Bearing Ortho-Imino Nitroxide and Para-Nitronyl Nitroxide Radical Ligands. *J. Chin. Chem. Soc.* **2008,** *55*(1), 45.

(232) Oshio, H.; Yamamoto, M.; Ito, T., Double Helical Assembly of Imino Nitroxyl Diradicals by Silver(I) Ions. *J. Chem. Soc., Dalton Trans.* **1999,** (15), 2641.

(233) Grosslannert, R.; Kaim, W.; Olbrichdeussner, B., Electron Delocalization in Molecule-Bridged Polymetallic Systems - Unique Neutral Complexes of TCNE or TCNQ and up to Four Organometallic Fragments $(C_5R_5)(CO)_2Mn$. *Inorg. Chem.* **1990,** *29*(25), 5046.

(234) *CRC Handbook of Chemistry and Physics, 2010 - 2011, 91st ed.* CRC Press Inc.: Boca Raton, 2010; p 15.

(235) Cave, R. J.; Newton, M. D., Generalization of the Mulliken-Hush Treatment for the Calculation of Electron Transfer Matrix Elements. *Chem. Phys. Lett.* **1996,** *249*(1-2), 15.

(236) Cave, R. J.; Newton, M. D., Calculation of Electronic Coupling Matrix Elements for Ground and Excited State Electron Transfer Reactions: Comparison of the Generalized Mulliken-Hush and Block Diagonalization Methods. *J. Chem. Phys.* **1997,** *106*(22), 9213.

(237) Becke, A. D., Density-Functional Thermochemistry. III. The Role of Exact Exchange. *J. Chem. Phys.* **1993,** *98*(7), 5648.

(238) Lee, C. T.; Yang, W. T.; Parr, R. G., Development of the Colle-Salvetti Correlation-Energy Formula Into a Functional of the Electron-Density. *Phys. Rev. B: Condens. Matter* **1988,** *37*(2), 785.

(239) Gaussian 09 Revision A.02, M. J. F., G. W. Trucks, H. B. Schlegel, G. E. Scuseria, M. A. Robb, J. R. Cheeseman, G. Scalmani, V. Barone, B. Mennucci, G. A. Petersson, H. Nakatsuji, M. Caricato, X. Li, H. P. Hratchian, A. F. Izmaylov, J. Bloino, G. Zheng, J. L. Sonnenberg, M. Hada, M. Ehara, K. Toyota, R. Fukuda, J. Hasegawa, M. Ishida, T. Nakajima, Y. Honda, O. Kitao, H. Nakai, T. Vreven, J. A. Montgomery, Jr., J. E. Peralta, F. Ogliaro, M. Bearpark, J. J. Heyd, E. Brothers, K. N. Kudin, V. N. Staroverov, R. Kobayashi, J. Normand, K. Raghavachari, A. Rendell, J. C. Burant, S. S. Iyengar, J. Tomasi, M. Cossi, N. Rega, J. M. Millam, M. Klene, J. E. Knox, J. B. Cross, V. Bakken, C. Adamo, J. Jaramillo, R. Gomperts, R. E. Stratmann, O. Yazyev, A. J. Austin, R. Cammi, C. Pomelli, J. W. Ochterski, R. L. Martin, K. Morokuma, V. G. Zakrzewski, G. A. Voth, P. Salvador, J. J. Dannenberg, S. Dapprich, A. D. Daniels, O. Farkas, J. B. Foresman, J. V. Ortiz, J. Cioslowski, and D. J. Fox Gaussian, Inc.: Wallingford CT, 2009.

(240) Deumal, M.; Lafuente, P.; Mota, F.; Novoa, J. J., A General Study of the Spin Population of α-Nitronyl Nitroxide Radicals: Radicals with Crystals Presenting Dominant Ferro or Antiferromagnetic Behavior. *Synth. Met.* **2001,** *122*(3), 477.

(241) Casida, M. E.; Jamorski, C.; Casida, K. C.; Salahub, D. R., Molecular Excitation Energies to High-Lying Bound States From Time-Dependent Density-Functional Response Theory: Characterization and Correction of the Time-Dependent Local Density Approximation Ionization Threshold. *J. Chem. Phys.* **1998,** *108*(11), 4439.

(242) Kirkwood, J. G., Theory of Solutions of Molecules Containing Widely Separated Charges with Special Application to Zwitterions. *J. Chem. Phys.* **1934,** *2*(7), 351.

(243) Onsager, L., Electric Moments of Molecules in Liquids. *J. Am. Chem. Soc.* **1936,** *58*(8), 1486.

(244) Wong, M. W.; Wiberg, K. B.; Frisch, M., Hartree-Fock Second Derivatives and Electric Field Properties in a Solvent Reaction Field: Theory and Application. *J. Chem. Phys.* **1991,** *95*(12), 8991.

(245) Hirata, S.; Head-Gordon, M.; Szczepanski, J.; Vala, M., Time-Dependent Density Functional Study of the Electronic Excited States of Polycyclic Aromatic Hydrocarbon Radical Ions. *J. Phys. Chem. A* **2003,** *107*(24), 4940.

(246) Anderson, L. C., The Absorption Spectra of Free Radicals. *J. Am. Chem. Soc.* **1935,** *57*(9), 1673.

(247) Zienkiewicz, J. z.; Kaszynski, P.; Young, V. G., Experimental and Theoretical Studies of Fused-Ring Persistent [1,2,4]Thiadiazinyl Radicals. *J. Org. Chem.* **2004,** *69*(22), 7525.

(248) Bonner, J. C.; Fisher, M. E., Linear Magnetic Chains with Anisotropic Coupling. *Phys. Rev.* **1964,** *135*(3A), A640.

(249) Gaussian 03 Revision C.02, F., M. J.; Trucks, G. W.; Schlegel, H. B.; Scuseria, G. E.; Robb, M. A.; Cheeseman, J. R.; Montgomery, Jr., J. A.; Vreven, T.; Kudin, K. N.; Burant, J. C.; Millam, J. M.; Iyengar, S. S.; Tomasi, J.; Barone, V.; Mennucci, B.; Cossi, M.; Scalmani, G.; Rega, N.; Petersson, G. A.; Nakatsuji, H.; Hada, M.; Ehara, M.; Toyota, K.; Fukuda, R.; Hasegawa, J.; Ishida, M.; Nakajima, T.; Honda, Y.; Kitao, O.; Nakai, H.; Klene, M.; Li, X.; Knox, J. E.; Hratchian, H. P.; Cross, J. B.; Bakken, V.; Adamo, C.; Jaramillo, J.; Gomperts, R.; Stratmann, R. E.; Yazyev, O.; Austin, A. J.; Cammi, R.; Pomelli, C.; Ochterski, J. W.; Ayala, P. Y.; Morokuma, K.; Voth, G. A.; Salvador, P.; Dannenberg, J. J.; Zakrzewski, V. G.; Dapprich, S.; Daniels, A. D.; Strain, M. C.; Farkas, O.; Malick, D. K.; Rabuck, A. D.; Raghavachari, K.; Foresman, J. B.; Ortiz, J. V.; Cui, Q.; Baboul, A. G.; Clifford, S.; Cioslowski, J.; Stefanov, B. B.; Liu, G.; Liashenko, A.; Piskorz, P.; Komaromi, I.; Martin, R. L.; Fox, D. J.; Keith, T.; Al-Laham, M. A.; Peng, C. Y.; Nanayakkara, A.; Challacombe, M.; Gill, P. M. W.; Johnson, B.;

Chen, W.; Wong, M. W.; Gonzalez, C.; and Pople, J. A.; Gaussian, Inc., Wallingford CT, 2004.

(250) Otwinowski, Z.; Minor, W.; Charles, W. C. J., Processing of X-ray Diffraction Data Collected in Oscillation Mode. In *Methods in Enzymology*, Academic Press: 1997; Vol. Volume 276, pp 307.

(251) Altomare, A.; Burla, M. C.; Camalli, M.; Cascarano, G. L.; Giacovazzo, C.; Guagliardi, A.; Moliterni, A. G. G.; Polidori, G.; Spagna, R., SIR97: A New Tool for Crystal Structure Determination and Refinement. *J. Appl. Crystallogr.* **1999,** *32*, 115.

(252) Corminboeuf, O.; Renaud, P., N-Alkoxyacrylamides as Substrates for Enantioselective Diels-Alder Reactions. *Org. Lett.* **2002,** *4*(10), 1735.

(253) Wheeler, O. H.; Gore, P. H., Absorption Spectra of Azo- and Related Compounds. II. Substituted Phenylnitrones. *J. Am. Chem. Soc.* **1956,** *78*(14), 3363.

(254) Aurich, H. G.; Franzke, M.; Kesselheim, H. P.; Rohr, M., Steric Effects on Regioselectivity in 1,3-Dipolar Cycloaddition of C,N-Dialkyl Nitrones with Acceptor-Substituted Alkynes. *Tetrahedron* **1992,** *48*(4), 669.

(255) Meske, M., Synthesis of 4-Alkoxy and 3-Nitro Substituted Isoxazolidines by Catalyzed 1,3-Dipolar Cycloaddition Reactions of Nitrones with Vinyl Ethers and Nitro Alkenes. *J. Prakt. Chem.* **1997,** *339*(5), 426.

(256) Griller, D.; Ingold, K. U., Persistent Carbon-Centered Radicals. *Acc. Chem. Res.* **1976,** *9*(1), 13.

(257) Volkamer, K.; Baumgart, H.; Zimmerma, H., N-oxides of Imidazolyls. *Angew. Chem. Int. Ed.* **1967,** *6*(11), 947.

(258) Barone, V., In *Recent Advances in Density Functional Methods, Part 1*, Chong, D. P., Ed. World Scientific Publishing Co.: Singapore, 1995; p 287.

(259) Mallory, F. B.; Smith, P. A. S.; Boyer, J. H., Benzofurazan Oxide. *Org. Synth.* **1957,** *37*, 1.

(260) Gaughran, R. J.; Picard, J. P.; Kaufman, J. V. R., Contribution to the Chemistry of Benzfuroxan and Benzfurazan Derivatives. *J. Am. Chem. Soc.* **1954,** *76*(8), 2233.

(261) Dyall, L. K.; Harvey, J. J.; Jarman, T. B., Oxidative Cyclizations. VIII. Mechanisms of Oxidation of ortho-Substituted Benzenamines and Improved Cyclizations by Bis(acetato-O)Phenyliodine. *Aust. J. Chem.* **1992,** *45*(2), 371.

(262) Das, O.; Paria, S.; Paine, T. K., Copper(II)-Mediated Oxidation of 1,2-Dioxime to Furoxan. *Tetrahedron Lett.* **2008,** *49*(41), 5924.

(263) Kropf, H.; Lambeck, R., Reaktionen mit Bleitetraacetat, II. Aldoximanhydrid-N-oxide aus Aromatischen Aldoximen. *Justus Liebigs Annalen der Chemie* **1966,** *700*(1), 18.

(264) Pretsch, E.; Clerc, T.; Seibl, J., *Tables of Spectral Data for Structure Determination of Organic Compounds*. 2nd ed.; Springer-Verlag: Berlin, 1989.

(265) Hu, J.; Zhang, D.; Harris, F. W., Ruthenium(III) Chloride Catalyzed Oxidation of Pyrene and 2,7-Disubstitued Pyrenes: An Efficient, One-Step Synthesis of Pyrene-4,5-diones and Pyrene-4,5,9,10-tetraones. *J. Org. Chem.* **2004,** *70*(2), 707.

(266) Young, E. R. R.; Funk, R. L., A Practical Synthesis of Pyrene-4,5-dione. *J. Org. Chem.* **1998,** *63*(26), 9995.

(267) Bard, A. J.; Faulkner, L. R., *Electrochemical Methods: Fundamentals and Applications*. John Wiley & Sons Inc.: New York, 1980.

(268) Wang, J., *Analytical Electrochemistry*. 3rd ed.; John Wiley & Sons Inc.: Hoboken, 2006.

(269) Mabbott, G. A., An Introduction to Cyclic Voltammetry. *J. Chem. Educ.* **1983,** *60*(9), 697.

(270) Cirujeda, J.; Vidal-Gancedo, J.; Jurgens, O.; Mota, F.; Novoa, J. J.; Rovira, C.; Veciana, J., Spin Density Distribution of α-Nitronyl Aminoxyl Radicals From Experimental and Ab Initio Calculated ESR Isotropic Hyperfine Coupling Constants. *J. Am. Chem. Soc.* **2000,** *122*(46), 11393.

(271) Gauld, J. W.; Eriksson, L. A.; Radom, L., Assessment of Procedures for Calculating Radical Hyperfine Structures. *J. Phys. Chem. A* **1997,** *101*(7), 1352.

(272) Pontillon, Y.; Akita, T.; Grand, A.; Kobayashi, K.; Lelievre-Berna, E.; Pecaut, J.; Ressouche, E.; Schweizer, J., Experimental and Theoretical Spin Density in a Ferromagnetic Molecular Complex Presenting Interheteromolecular Hydrogen Bonds. *J. Am. Chem. Soc.* **1999,** *121*(43), 10126.

(273) Romero, F. M.; Ziessel, R.; Bonnet, M.; Pontillon, Y.; Ressouche, E.; Schweizer, J.; Delley, B.; Grand, A.; Paulsen, C., Evidence for Transmission of Ferromagnetic Interactions through Hydrogen Bonds in Alkyne-Substituted Nitroxide Radicals: Magnetostructural Correlations and Polarized Neutron Diffraction Studies. *J. Am. Chem. Soc.* **2000,** *122*(7), 1298.

(274) Pontillon, Y.; Caneschi, A.; Gatteschi, D.; Grand, A.; Ressouche, E.; Sessoli, R.; Schweizer, J., Experimental Spin Density in a Purely Organic Free Radical: Visualisation of the Ferromagnetic Exchange Pathway in *p*-(Methylthio)phenyl Nitronyl Nitroxide, Nit(SMe)Ph. *Chem. Eur. J.* **1999,** *5*(12), 3616.

(275) Adamo, C.; di Matteo, A.; Rey, P.; Barone, V., Tuning of Structural and Magnetic Properties of Nitronyl Nitroxides by the Environment. A Combined Experimental and Computational Study. *J. Phys. Chem. A* **1999,** *103*(18), 3481.

(276) Barone, V.; Bencini, A.; di Matteo, A., Intrinsic and Environmental Effects in the Structure and Magnetic Properties of Organic Molecular Magnets: Bis(imino)nitroxide. *J. Am. Chem. Soc.* **1997,** *119*(44), 10831.

(277) Lankamp, H.; Nauta, W. T.; MacLean, C., A New Interpretation of the Monomer-Dimer Equilibrium of Triphenylmethyl- and Alkylsubstituted-Diphenylmethyl Radicals in Solution. *Tetrahedron Lett.* **1968,** *9*(2), 249.

(278) Fujiwara, H.; Ogasawara, Y.; Yamaguchi, K.; Mizuno, N., A One-Pot Synthesis of Primary Amides from Aldoximes or Aldehydes in Water in the Presence of a Supported Rhodium Catalyst. *Angew. Chem. Int. Ed.* **2007,** *46*(27), 5202.

(279) Katritzky, A. R.; Wang, Z.; Hall, C. D.; Akhmedov, N. G.; Shestopalov, A. A.; Steel, P. J., Cyclization of α-Oxo-oximes to 2-Substituted Benzoxazoles. *J. Org. Chem.* **2003,** *68*(23), 9093.

(280) Stankjavicius, A.; Yanusiene, L.; Zablockaite, D.; Pechura, R., Synthesis of Aliphatic Amides of 2-(2'-cyanophenyl)benzoic Acid. *Pharm. Chem. J.* **2007,** *41*(12), 646.

(281) Rai, B. K.; Chaudhary, S. K.; Rai, H. C., Co(II), Ni(II) and Cu(II) Chelates of Bis-9,10-phenanthroquinonedioxime and Their Nitrogen-Donor Adducts with NH_3 and Pyridine. *Asian J. Chem.* **2001,** *13*(1), 259.

(282) Boyer, J.; Mamikunian, G., 2-Nitro-9,10-*ψ*-dinitrosophenanthrene. *J. Org. Chem.* **1958,** *23*(11), 1807.

(283) Boyer, J. H.; Reinisch, R. F.; Danzig, M. J.; Stoner, G. A.; Sahhar, F., The Transformation of *ψ*-o-Dinitroso Aromatic Compounds into o-Nitroaryl Amines. *J. Am. Chem. Soc.* **1955,** *77*(21), 5688.

(284) Tabatabaeian, K.; Mamaghani, M.; Mahmoodi, N. O.; Khorshidi, A., Ultrasonic-Assisted Ruthenium-Catalyzed Oxidation of Aromatic and Heteroaromatic Compounds. *Catal. Commun.* **2008,** *9*(3), 416.

(285) Carroll, W. R.; Pellechia, P.; Shimizu, K. D., A Rigid Molecular Balance for Measuring Face-to-Face Arene-Arene Interactions. *Org. Lett.* **2008,** *10*(16), 3547.

(286) Bartczak, A. W.; Sangaiah, R.; Kelman, D. J.; Toney, G. E.; Deterding, L. J.; Charles, J.; Marbury, G. D.; Gold, A., Synthesis of N-6-Adenosine Adducts Expected From Cyclopenta-Ring Activation of Acenaphthylene and Aceanthrylene. *Tetrahedron Lett.* **1989,** *30*(25), 3251.

(287) Aguirre, G.; Boiani, L.; Boiani, M.; Cerecetto, H.; Maio, R. D.; González, M.; Porcal, W.; Denicola, A.; Piro, O. E.; Castellano, E. E.; Sant'Anna, C. M. R.; Barreiro, E. J., New Potent 5-Substituted Benzofuroxans as Inhibitors of Trypanosoma cruzi Growth: Quantitative Structure-Activity Relationship Studies. *Biorg. Med. Chem.* **2005,** *13*(23), 6336.

(288) Lowe-Ma, C. K.; Nissan, R. A.; Wilson, W. S., Tetrazolo[1,5-a]pyridines and Furazano[4,5-b]pyridine 1-oxides. *J. Org. Chem.* **1990,** *55*(12), 3755.

(289) Dyall, L. K.; Wah, W. M., Pyrolysis of Aryl Azides. VI. Identification of Neighboring Group Effects in Pyrolysis of Azidopyridines and Azidoquinolines. *Aust. J. Chem.* **1985,** *38*(7), 1045.

(290) Boyer, J. H.; McCane, D. I.; McCarville, W. J.; Tweedie, A. T., Pyrido-2,3-furoxane. *J. Am. Chem. Soc.* **1953,** *75*(21), 5298.

(291) Park, D. J.; Stern, A. G.; Wilier, R. L., A Convenient Laboratory Preparation of Cyanogen. *Synth. Commun.* **1990,** *20*(18), 2901

(292) Brintzinger, H.; Titzmann, R., Notiz Uber Einige Halogenierte Aliphatische Oxime. *Chem. Ber.* **1952,** *85*(4), 344.

(293) Alexandrou, N. E.; Nicolaides, D. N., 1,3-Addition Reactions of Cyanogen Di-N-oxide. *J. Chem. Soc. C* **1969,** (17), 2319.

(294) Gallos, J. K.; Lianis, P. S.; Rodios, N. A., Synthesis, Structure and Mass Spectral Fragmentation of a Series of Substituted Furazano[3,4-b]quinoxaline 1-Oxides and their Deoxides. *J. Heterocycl. Chem.* **1994,** *31*(2), 481.

(295) Nicolaides, D. N.; Gallos, J. K., A Convenient Synthesis of Furoxan[3,4-*b*]quinoxalines and Furazano[3,4-*b*]quinoxalines. *Synthesis* **1981,** (8), 638.

(296) Friend, R. H.; Gymer, R. W.; Holmes, A. B.; Burroughes, J. H.; Marks, R. N.; Taliani, C.; Bradley, D. D. C.; Dos Santos, D. A.; Bredas, J. L.; Logdlund, M.; Salaneck, W. R., Electroluminescence in Conjugated Polymers. *Nature* **1999,** *397*(6715), 121.

(297) Kamtekar, K. T.; Monkman, A. P.; Bryce, M. R., Recent Advances in White Organic Light-Emitting Materials and Devices (WOLEDs). *Adv. Mater.* **2010,** *22*(5), 572.

(298) Grimsdale, A. C.; Chan, K. L.; Martin, R. E.; Jokisz, P. G.; Holmes, A. B., Synthesis of Light-Emitting Conjugated Polymers for Applications in Electroluminescent Devices. *Chem. Rev.* **2009,** *109*(3), 897.

(299) Perepichka, I. F.; Perepichka, D. F.; Meng, H.; Wudl, F., Light-Emitting Polythiophenes. *Adv. Mater.* **2005,** *17*(19), 2281.

(300) Veinot, J. G. C.; Marks, T. J., Toward the Ideal Organic Light-Emitting Diode. The Versatility and Utility of Interfacial Tailoring by Cross-Linked Siloxane Interlayers. *Acc. Chem. Res.* **2005,** *38*(8), 632.

(301) Facchetti, A., Semiconductors for Organic Transistors. *Mater. Today* **2007,** *10*(3), 28.

(302) Dimitrakopoulos, C. D.; Malenfant, P. R. L., Organic Thin Film Transistors For Large Area Electronics. *Adv. Mater.* **2002,** *14*(2), 99.

(303) Dimitrakopoulos, C. D.; Mascaro, D. J., Organic Thin-Film Transistors: A Review of Recent Advances. *IBM J. Res. Dev.* **2001,** *45*(1), 11.

(304) Garnier, F.; Hajlaoui, R.; Yassar, A.; Srivastava, P., All-Polymer Field-Effect Transistor Realized by Printing Techniques. *Science* **1994,** *265*(5179), 1684.

(305) Mushrush, M.; Facchetti, A.; Lefenfeld, M.; Katz, H. E.; Marks, T. J., Easily Processable Phenylene-Thiophene-Based Organic Field-Effect Transistors and Solution-Fabricated Nonvolatile Transistor Memory Elements. *J. Am. Chem. Soc.* **2003,** *125*(31), 9414.

(306) Allard, S.; Forster, M.; Souharce, B.; Thiem, H.; Scherf, U., Organic Semiconductors for Solution-Processable Field-Effect Transistors (OFETs). *Angew. Chem. Int. Ed.* **2008,** *47*(22), 4070.

(307) Gunes, S.; Neugebauer, H.; Sariciftci, N. S., Conjugated Polymer-Based Organic Solar Cells. *Chem. Rev.* **2007,** *107*(4), 1324.

(308) Cheng, Y. J.; Yang, S. H.; Hsu, C. S., Synthesis of Conjugated Polymers for Organic Solar Cell Applications. *Chem. Rev.* **2009,** *109*(11), 5868.

(309) Chen, J. W.; Cao, Y., Development of Novel Conjugated Donor Polymers for High-Efficiency Bulk-Heterojunction Photovoltaic Devices. *Acc. Chem. Res.* **2009,** *42*(11), 1709.

(310) Helgesen, M.; Sondergaard, R.; Krebs, F. C., Advanced Materials and Processes for Polymer Solar Cell Devices. *J. Mater. Chem.* **2010,** *20*(1), 36.

(311) Coakley, K. M.; McGehee, M. D., Conjugated Polymer Photovoltaic Cells. *Chem. Mater.* **2004,** *16*, 4533.

(312) McQuade, D. T.; Pullen, A. E.; Swager, T. M., Conjugated Polymer-Based Chemical Sensors. *Chem. Rev.* **2000,** *100*(7), 2537.

(313) Samuel, I. D. W.; Turnbull, G. A., Organic Semiconductor Lasers. *Chem. Rev.* **2007,** *107*(4), 1272.

(314) Beaujuge, P. M.; Reynolds, J. R., Color Control in π-Conjugated Organic Polymers for Use in Electrochromic Devices. *Chem. Rev.* **2010,** *110*(1), 268.

(315) Forrest, S. R., The Path to Ubiquitous and Low-Cost Organic Electronic Appliances on Plastic. *Nature* **2004,** *428*(6986), 911.

(316) Gelinck, G. H.; Huitema, H. E. A.; Van Veenendaal, E.; Cantatore, E.; Schrijnemakers, L.; Van der Putten, J.; Geuns, T. C. T.; Beenhakkers, M.; Giesbers, J. B.; Huisman, B. H.; Meijer, E. J.; Benito, E. M.; Touwslager, F. J.; Marsman, A. W.; Van Rens, B. J. E.; De Leeuw, D. M., Flexible Active-Matrix Displays and Shift Registers Based on Solution-Processed Organic Transistors. *Nat. Mater.* **2004,** *3*(2), 106.

(317) Kirk, M. L.; Shultz, D. A.; Depperman, E. C.; Brannen, C. L., Donor-Acceptor Biradicals as Ground State Analogues of Photoinduced Charge Separated States. *J. Am. Chem. Soc.* **2007,** *129*(7), 1937.

(318) Shultz, D. A.; Bodnar, S. H.; Vostrikova, K. E.; Kampf, J. W., Synthesis and Structure of a Complex Having a Quartet Ground State with Three Entirely Different Spin Carriers: Nitronyl Nitroxide, *o*-Semiquinone, and Cu(II). *Inorg. Chem.* **2000,** *39*(26), 6091.

(319) Ballester, M.; Molinet, C.; Castañer, J., Preparation of Highly Strained Aromatic Chlorocarbons. 1. A Powerful Nuclear Chlorinating Agent - Relevant Reactivity Phenomena Traceable to Molecular Strain. *J. Am. Chem. Soc.* **1960,** *82*(16), 4254.

(320) Smith, P. A. S.; Boyer, J. H., Benzofurazan N-oxide. *Org. Synth.* **1951,** *31*, 14.

(321) Littke, A. F.; Fu, G. C., The First General Method for Stille Cross-Couplings of Aryl Chlorides. *Angew. Chem. Int. Ed.* **1999,** *38*(16), 2411.

(322) Esat, B.; Fidan, I.; Bahceci, S.; Yerli, Y.; Sari, L., Effect of Substituents on Spin Density in Benzimidazole Nitronyl Nitroxide Radicals Studied by Electron Spin Resonance. *Magn. Reson. Chem.* **2009,** *47*(8), 641.

(323) Mann, C. K.; Barnes, K. K., *Electrochemical Reactions in Nonaqueous Systems*. Marcel Dekker: New York (USA), 1970.

(324) Heckmann, A.; Dummler, S.; Pauli, J.; Margraf, M.; Kohler, J.; Stich, D.; Lambert, C.; Fischer, I.; Resch-Genger, U., Highly Fluorescent Open-Shell NIR Dyes: The Time-Dependence of Back Electron Transfer in Triarylamine-Perchlorotriphenylmethyl Radicals. *J. Phys. Chem. C* **2009,** *113*(49), 20958.

(325) Cohen, A. J.; Mori-Sanchez, P.; Yang, W. T., Insights into Current Limitations of Density Functional Theory. *Science* **2008,** *321*(5890), 792.

(326) Mori-Sanchez, P.; Cohen, A. J.; Yang, W. T., Many-Electron Self-Interaction Error in Approximate Density Functionals. *J. Chem. Phys.* **2006,** *125*(20), 4.

(327) Tozer, D. J., Relationship Between Long-Range Charge-Transfer Excitation Energy Error and Integer Discontinuity in Kohn-Sham Theory. *J. Chem. Phys.* **2003,** *119*(24), 12697.

(328) Day, P. N.; Nguyen, K. A.; Pachter, R., TDDFT Study of One- and Two-Photon Absorption Properties: Donor-π-Acceptor Chromophores. *J. Phys. Chem. B* **2005,** *109*(5), 1803.

(329) Renz, M.; Theilacker, K.; Lambert, C.; Kaupp, M., A Reliable Quantum-Chemical Protocol for the Characterization of Organic Mixed-Valence Compounds. *J. Am. Chem. Soc.* **2009,** *131*(44), 16292.

(330) Becke, A. D., Density-Functional Exchange-Engergy Approximation with Correct Asymptotic-Behavior. *Phys. Rev. A: At. Mol. Opt. Phys.* **1988,** *38*(6), 3098.

(331) Barone, V.; Cossi, M., Quantum Calculation of Molecular Enegies and Energy Gradients in Solution by a Conductor Solvent Model. *J. Phys. Chem. A* **1998,** *102*(11), 1995.

(332) Cossi, M.; Rega, N.; Scalmani, G.; Barone, V., Energies, Structures, and Electronic Properties of Molecules in Solution with the C-PCM Solvation Model. *J. Comput. Chem.* **2003,** *24*(6), 669.

(333) Foresman, J. B.; Keith, T. A.; Wiberg, K. B.; Snoonian, J.; Frisch, M. J., Solvent Effects. 5. Influence of Cavity Shape, Truncation of Electrostatics, and Electron Correlation Ab Initio Reaction Field Calculations. *J. Phys. Chem.* **1996,** *100*(40), 16098.

(334) Jamorski, C.; Foresman, J. B.; Thilgen, C.; Luthi, H. P., Assessment of Time-Dependent Density-Functional Theory for the Calculation of Critical Features in the Absorption Spectra of a Series of Aromatic Donor-Acceptor Systems. *J. Chem. Phys.* **2002,** *116*(20), 8761.

(335) Jodicke, C. J.; Luthi, H. P., Time-Dependent Density Functional Theory (TDDFT) Study of the Excited Charge-Transfer State Formation of a Series of Aromatic Donor-Acceptor Systems. *J. Am. Chem. Soc.* **2003,** *125*(1), 252.

(336) *TOPAS V4: General Profile and Structure Analysis Software for Powder Diffraction Data - User's Manual*. Bruker AXS: Karlsruhe, Germany, 2008.

(337) Baker, G. A.; Rushbrooke, G. S.; Gilbert, H. E., High-Temperature Series Expansions for the Spin-1/2 Heisenberg Model by the Method of Irreducible Representations of the Symmetric Group. *Phys. Rev.* **1964,** *135*(5A), A1272.

(338) Deumal, M.; Rawson, J. M.; Goeta, A. E.; Howard, J. A. K.; Copley, R. C. B.; Robb, M. A.; Novoa, J. J., Studying the Origin of the Antiferromagnetic to Spin-Canting Transition in the β-*p*-NCC_6F_4CNSSN Center Dot Molecular Magnet. *Chem. Eur. J.* **2010,** *16*(9), 2741.

(339) Deumal, M.; Bearpark, M. J.; Novoa, J. J.; Robb, M. A., Magnetic Properties of Organic Molecular Crystals via an Algebraic Heisenberg Hamiltonian. Applications to WILVIW, TOLKEK, and KAXHAS Nitronyl Nitroxide Crystals. *J. Phys. Chem. A* **2002,** *106*(7), 1299.

(340) Bhattacharya, D.; Misra, A., Density Functional Theory Based Study of Magnetic Interaction in Bis-Oxoverdazyl Diradicals Connected by Different Aromatic Couplers. *J. Phys. Chem. A* **2009,** *113*(18), 5470.

(341) Wudl, F.; Bryce, M. R., Apparatus for Two-Probe Conductivity Measurements on Compressed Powders. *J. Chem. Educ.* **1990,** *67*(8), 717.

(342) Wheland, R. C.; Gillson, J. L., Synthesis of Electrically Conductive Organic Solids. *J. Am. Chem. Soc.* **1976,** *98*(13), 3916.

(343) Haddon, R. C., Quantum Chemical Studies in Design of Organic Metals. 111* Odd-Alternant Hydrocarbons Phenalenyl (ply) System. *Aust. J. Chem.* **1975,** *28*(11), 2343.

(344) Oakley, R. T., 1993 Alcan Award Lecture - Chemical-Binding Within and Between Inorganic Rings - The Design and Synthesis of Molecular Conductors. *Can. J. Chem.* **1993,** *71*(11), 1775.

(345) Leitch, A. A.; Reed, R. W.; Robertson, C. M.; Britten, J. F.; Yu, X. Y.; Secco, R. A.; Oakley, R. T., An Alternating π-Stacked Bisdithiazolyl Radical Conductor. *J. Am. Chem. Soc.* **2007,** *129*(25), 7903.

(346) Robertson, C. M.; Leitch, A. A.; Cvrkalj, K.; Reed, R. W.; Myles, D. J. T.; Dube, P. A.; Oakley, R. T., Enhanced Conductivity and Magnetic Ordering in Isostructural Heavy Atom Radicals. *J. Am. Chem. Soc.* **2008,** *130*(26), 8414.

(347) Bag, P.; Itkis, M. E.; Pal, S. K.; Donnadieu, B.; Tham, F. S.; Park, H.; Schlueter, J. A.; Siegrist, T.; Haddon, R. C., Resonating Valence Bond and σ-Charge Density Wave Phases in a Benzannulated Phenalenyl Radical. *J. Am. Chem. Soc.* **2010,** *132*(8), 2684.

(348) Sheldrick, G. M., A short history of SHELX. *Acta Crystallographica Section A* **2008,** *64*, 112.

(349) Evans, D. A.; Song, H.-J.; Fandrick, K. R., Enantioselective Nitrone Cycloadditions of α,β-Unsaturated 2-Acyl Imidazoles Catalyzed by Bis(oxazolinyl)pyridine-Cerium(IV) Triflate Complexes. *Org. Lett.* **2006,** *8*(15), 3351.

(350) Ayyangar, N. R.; Srinivasan, K. V., Effect of Substituents in the Formation of Diacetanilides. *Can. J. Chem.* **1984,** *62*(7), 1292.

(351) Chrétien, J.-M.; Zammattio, F.; Le Grognec, E.; Paris, M.; Cahingt, B.; Montavon, G.; Quintard, J.-P., Polymer-Supported Organotin Reagents for Regioselective Halogenation of Aromatic Amines. *J. Org. Chem.* **2005,** *70*(7), 2870.

(352) Kharasch, M. S.; Lommen, F. W. M.; Jacobsohn, I. M., A Study of the Nitro-Anilines. *J. Am. Chem. Soc.* **1922,** *44*(4), 793.

(353) Heppolette, R. L.; Miller, J., The SN Mechanism in Aromatic Compounds. V. Halogen Substituents. *J. Am. Chem. Soc.* **1953,** *75*(17), 4265.

(354) Li, Y. W.; Guo, Q.; Li, Z. F.; Pei, J. N.; Tian, W. J., Solution Processable D-A Small Molecules for Bulk-Heterojunction Solar Cells. *Energy Environ. Sci.* **2010,** *3*(10), 1427.

(355) Liang, Y. Y.; Yu, L. P., A New Class of Semiconducting Polymers for Bulk Heterojunction Solar Cells with Exceptionally High Performance. *Acc. Chem. Res.* **2010,** *43*(9), 1227.

(356) van Mullekom, H. A. M.; Vekemans, J.; Havinga, E. E.; Meijer, E. W., Developments in the Chemistry and Band Gap Engineering of Donor-Acceptor Substituted Conjugated Polymers. *Mater. Sci. Eng., R* **2001,** *32*(1), 1.

(357) Burroughes, J. H.; Bradley, D. D. C.; Brown, A. R.; Marks, R. N.; Mackay, K.; Friend, R. H.; Burns, P. L.; Holmes, A. B., Light-Emitting Diodes Based on Conjugated Polymers. *Nature* **1990,** *347*, 539.

(358) Chen, H. Y.; Hou, J. H.; Zhang, S. Q.; Liang, Y. Y.; Yang, G. W.; Yang, Y.; Yu, L. P.; Wu, Y.; Li, G., Polymer Solar Cells with Enhanced Open-Circuit Voltage and Efficiency. *Nat. Photonics* **2009,** *3*(11), 649.

(359) Sirringhaus, H., Device Physics of Solution-Processed Organic Field-Effect Transistors. *Adv. Mater.* **2005,** *17*(20), 2411.

(360) Sirringhaus, H.; Brown, P. J.; Friend, R. H.; Nielsen, M. M.; Bechgaard, K.; Langeveld-Voss, B. M. W.; Spiering, A. J. H.; Janssen, R. A. J.; Meijer, E. W.; Herwig, P.; de Leeuw, D. M., Two-Dimensional Charge Transport in Self-Organized, High-Mobility Conjugated Polymers. *Nature* **1999,** *401*(6754), 685.

(361) Roncali, J., Synthetic Principles for Bandgap Control in Linear π-Conjugated Systems. *Chem. Rev.* **1997,** *97*(1), 173.

(362) Huang, H.; Pickup, P. G., In Situ Conductivity of a Low Band-Gap Conducting Polymer: Measurement of Intrinsic Conductivity. *Acta Polym.* **1997,** *48*(10), 455.

(363) Huang, H.; Pickup, P. G., A Donor-Accepter Conducting Copolymer with a Very Low Band Gap and High Itrinsic Conductivity. *Chem. Mater.* **1998,** *10*(8), 2212.

(364) Ajayaghosh, A., Donor-Acceptor Type Low Band Gap Polymers: Polysquaraines and Related Systems. *Chem. Soc. Rev.* **2003,** *32*(4), 181.

(365) Hush, N. S., Homogeneous and Heterogeneous Optical and Thermal Electron Transfer. *Electrochim. Acta* **1968,** *13*(5), 1005.

(366) Montalti, M.; Credi, A.; Prodi, L.; Gandolfi, M. T., *Handbook of Photochemistry, Third Edition*. CRC Press Inc.: Boca Raton, 2006.

(367) Casado, J.; Zgierski, M. Z.; Ewbank, P. C.; Burand, M. W.; Janzen, D. E.; Mann, K. R.; Pappenfus, T. M.; Berlin, A.; Pérez-Inestrosa, E.; Ortiz, R. P.; López Navarrete, J. T., Exploration of Ground and Excited Electronic States of Aromatic and Quinoid S,S-Dioxide Terthiophenes. Complementary Systems for Enhanced Electronic Organic Materials. *J. Am. Chem. Soc.* **2006,** *128*(31), 10134.

(368) Mori-Sanchez, P.; Cohen, A. J.; Yang, W., Localization and Delocalization Errors in Density Functional Theory and Implications for Band-Gap Prediction. *Phys. Rev. Lett.* **2008,** *100*(14), 146401.

(369) Zhang, Y. K.; Yang, W. T., A Challenge for Density Functionals: Self-Interaction Error Increases for Systems with a Noninteger Number of Electrons. *J. Chem. Phys.* **1998,** *109*(7), 2604.

(370) Hou, X.-Y.; Li, T. C.; Yin, C.-R.; Xu, H.; Lin, J.; Hua, Y.-R.; Chen, D.-Y.; Xie, L.-H.; Huang, W., Stable Hole-Transporting Molecular Glasses Based on Complicated 9,9-Diarylfluorenes (CDAFs). *Synth. Met.* **2009,** *159*(11), 1055.

(371) Izuoka, A.; Hiraishi, M.; Abe, T.; Sugawara, T.; Sato, K.; Takui, T., Spin Alignment in Singly Oxidized Spin-Polarized Diradical Donor: Thianthrene Bis(nitronyl nitroxide). *J. Am. Chem. Soc.* **2000,** *122*(13), 3234.

(372) Komatsu, H.; Mogi, R.; Matsushita, M. M.; Miyagi, T.; Kawada, Y.; Sugawara, T., Synthesis and Properties of TSF-Based Spin-Polarized Donor. *Polyhedron* **2009,** *28*(9-10), 1996.

(373) Sugawara, T.; Matsushita, M. M., Spintronics in Organic π-Electronic Systems. *J. Mater. Chem.* **2009,** *19*(12), 1738.

(374) *SAINT Version 7.68A*, Bruker AXS Inc.: Madison, Wisconsin, 1997-2010.

(375) *SADABS Bruker Nonius Area Detector Scaling and Absorption Correction - V2008/1*, Bruker AXS Inc.: Madison, Wisconsin, 2008.

(376) *SHELXL Version 2008/4*. Bruker AXS Inc.: Madison, Wisconsin, 2008.

(377) Farrugia, L. J., *WinGX* Suite for Small-Molecule Single-Crystal Crystallography. *J. Appl. Crystallogr.* **1999,** *32*, 837.

(378) Gardiner, J. M.; Loyns, C. R.; Schwalbe, C. H.; Barrett, G. C.; Lowe, P. R., Synthesis of 1-Alkoxy-2-alkyl-benzimidazoles from 2-Nitroanilines via Tandem N-Alkylation-Cyclization-O-Alkylation. *Tetrahedron* **1995,** *51*(14), 4101.

(379) Gardiner, J. M.; Procter, J., Synthesis of N-Alkoxybenzimidazoles with Differentiated C2 and O-Substituents. *Tetrahedron Lett.* **2001,** *42*(30), 5109.

(380) Gardiner, J. M.; Goss, A. D.; Majid, T.; Morley, A. D.; Pritchard, R. G.; Warren, J. E., Synthesis of N-Alkoxybenzimidazoles and N-Alkoxypyrimidazoles. *Tetrahedron Lett.* **2002,** *43*(43), 7707.

Appendix A: Crystallographic Parameters

Table A–1. Crystallographic parameters.

	2.15d	**2.15e**	**4.11a**
formula	$C_{11}H_7N_2O_2S_1$	$C_{11}H_7N_2O_2S_1$	$C_{17}H_{11}N_2O_2S$
formula weight	231.25	231.25	307.34
dimensions (mm)	0.15 × 0.10 × 0.05	0.41 × 0.05 × 0.02	0.005 × 0.28 × 0.40
color of crystal	maroon plates	dark red needles	dark purple
crystal system	$P2_1/c$	$P2_1/c$	$P2_1/c$
space group	monoclinic	monoclinic	monoclinic
Z	2	4	4
a (Å)	7.3290(9)	4.8000(10)	14.1620(2)
b (Å)	4.6390(4)	17.022(4)	14.1493(2)
c (Å)	14.756(2)	12.5200(15)	7.03310(10)
α (deg)	90.00	90.00	90.00
β (deg)	104.364(6)	111.273(6)	90.2230(10)
γ (deg)	90.00	90.00	90.00
volume (Å^3)	486.01(11)	953.3(3)	1409.30(3)
ρ_{calcd} (g cm^{-3})	1.580	1.611	1.449
μ (mm^{-1})	0.316	0.322	2.117
temperature (K)	130(2)	130(2)	296
λ (Å)	0.71073	0.71073	1.54178
$2\theta_{max}$ (deg)	27.50	23.77[a]	68.30
total reflections	1662	865	9124
unique reflections	925	282	2508
R_{int}	0.1030	0.3254	0.0347
solution method	direct	direct	direct
R_f [b]	0.1680	0.2504	0.0449
R_w [c]	0.1678	0.1796	0.1188
GOF	0.997	0.758	1.041

[a] To avoid problems with twinning, we needed to select a very small sample that then did produce a good data set that did not scatter well. As a result, more reflections at higher angle in theta turned out to be too low in intensity to be counted in the data statistics. [b] $R_f = [\Sigma||F_o| - |F_c||]/[\Sigma|F_o|]$, $I > 2\sigma(I)$. [c] $R_w = ([\Sigma w||F_o|^2 - |F_c|^2|^2]/[\Sigma(w|F_o|^2)^2])^{1/2}$.

Table A–1 (continued). Crystallographic parameters.

	4.11b[a]	**5.3e**
formula	$C_{15}H_9N_2O_2S_2$	$C_{25}H_{18}N_3O_2$
formula weight	313.37	392.42
dimensions (mm)	-	0.25 × 0.10 × 0.08
color of crystal	green powder	irregular black blocks
crystal system	$P2_1/c$	$P2_1/c$
space group	monoclinic	monoclinic
Z	4	4
a (Å)	13.000(1)	12.7520(7)
b (Å)	20.954(2)	9.1405(5)
c (Å)	4.9518(3)	16.5638(10)
α (deg)	90.00	90.00
β (deg)	92.265(89)	95.7950(10)
γ (deg)	90.00	90.00
volume (Å^3)	1347.86(8)	1920.80(19)
ρ_{calcd} (g cm^{-3})	-	1.357
μ (mm^{-1})	-	0.088
temperature (K)	298	90.0(1)
λ (Å)	1.540598	0.71073
$2\theta_{max}$ (deg)	-	27.86
total reflections	-	4541
unique reflections	-	3722
R_{int}	-	0.0311
solution method	-	direct
R_f[b]	-	0.0481
R_w[c]	-	0.0926
GOF	-	1.026

[a] Structure solved by PXRD. [b] $R_f = [\Sigma||F_o| - |F_c||]/[\Sigma|F_o|]$, $I > 2\sigma(I)$. [c] $R_w = ([\Sigma w||F_o|^2 - |F_c|^2|^2]/[\Sigma(w|F_o|^2)^2])^{1/2}$.

Appendix B: Complete Listing of Bond Lengths and Angles

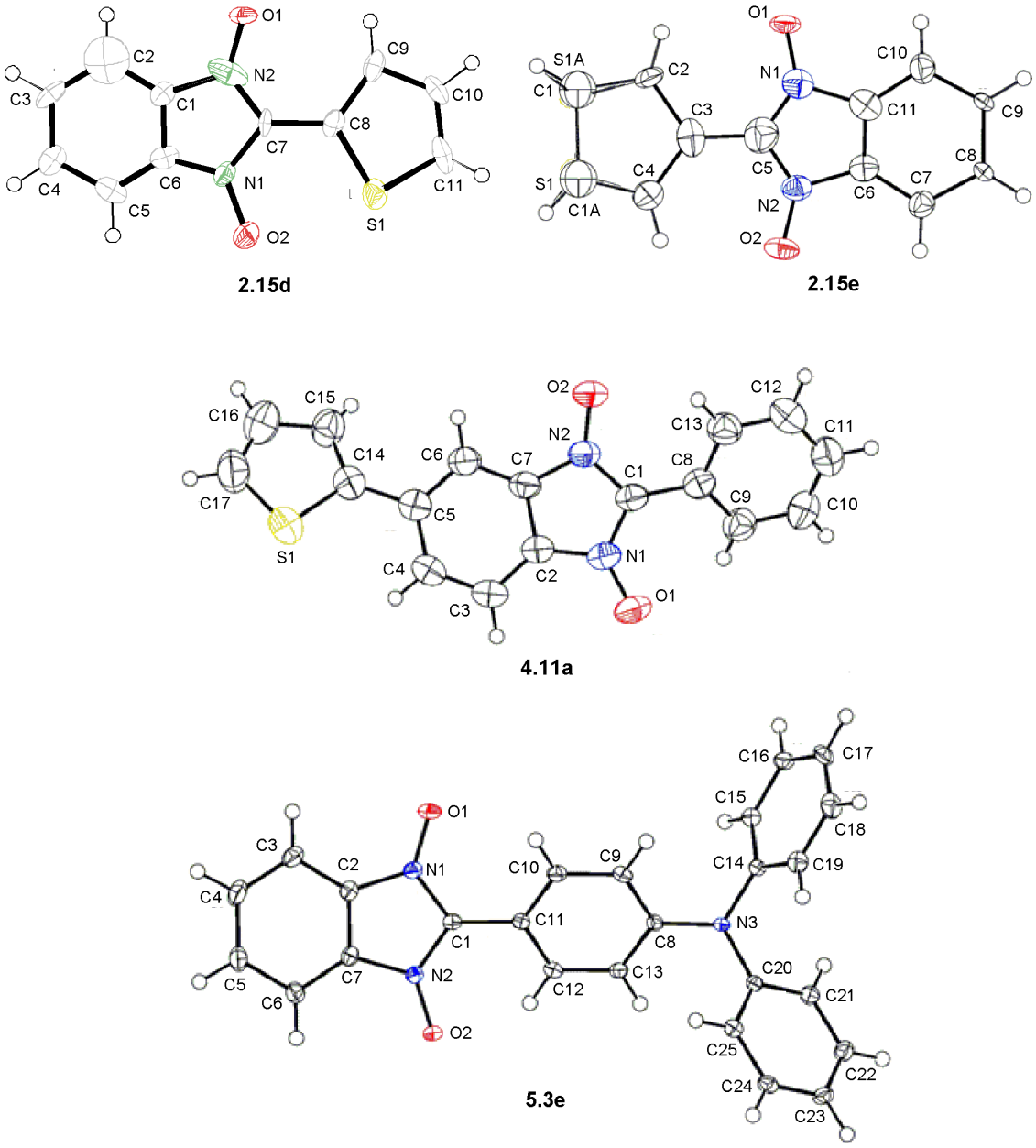

Figure B–1. ORTEP representations of all crystal structures for which bond lengths and angles are tabulated. Thermal ellipsoids presented at the 50 % probability level.

Table B–1. Bond lengths (Å) and angles (deg) for **2.15d.**

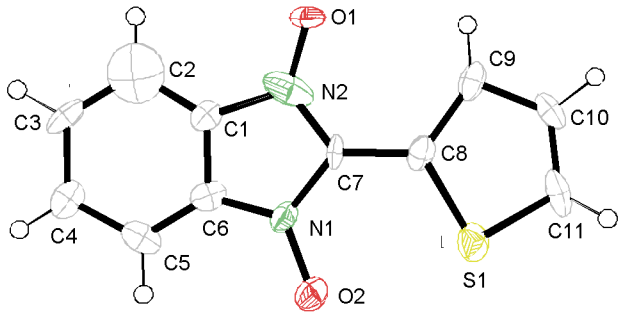

2.15d

S1	C6	1.242(12)	
S1	C11	1.67(2)	
S1	C8	1.706(14)	
O1	N2	1.230(11)	
O1	N1	1.333(10)	
N1	N2	0.709(8)	
N1	C7	1.014(13)	
N1	C7	1.344(17)	
N1	C1	1.384(14)	
N1	C8	1.821(14)	
N2	C7	1.187(15)	
N2	C7	1.362(16)	
N2	C6	1.428(14)	
N2	C8	1.933(14)	
C1	C8	0.631(12)	
C1	C7	1.375(15)	
C1	C6	1.390(12)	
C1	C2	1.395(17)	
C2	C3	1.46(2)	
C2	H2	0.95	
C3	C4	1.58(4)	
C3	H3	0.95	
C4	C5	1.48(4)	
C4	H4	0.95	
C5	C6	1.45(2)	
C5	H5	0.95	
C6	C8	0.805(11)	
C6	N2	1.428(14)	
C6	C7	1.499(14)	
C7	C7	0.887(15)	
C7	N2	1.187(15)	
C7	N1	1.344(17)	
C7	C8	1.430(12)	
C8	C9	1.370(18)	
C8	N2	1.933(14)	
C9	C10	1.41(3)	
C9	H9	0.95	
C10	C11	1.16(4)	
C10	H10	0.95	
C11	H11	0.95	
C6	S1	C11	117.5(12)
C11	S1	C8	91.4(11)

N2	N1	C7	103.1(18)
N2	N1	O1	66.1(14)
C7	N1	O1	169.1(11)
N2	N1	C7	61.8(13)
O1	N1	C7	127.8(9)
N2	N1	C1	170.4(19)
C7	N1	C1	67.9(8)
O1	N1	C1	122.9(9)
C7	N1	C1	109.2(11)
N2	N1	C8	154.4(18)
C7	N1	C8	51.5(7)
O1	N1	C8	139.3(9)
C7	N1	C8	92.8(9)
N1	N2	C7	86.5(15)
N1	N2	O1	82.2(15)
C7	N2	O1	168.6(9)
N1	N2	C7	46.5(12)
O1	N2	C7	128.6(9)
N1	N2	C6	155.5(19)
C7	N2	C6	69.3(8)
O1	N2	C6	122.0(9)
C7	N2	C6	109.2(10)
N1	N2	C8	133.9(17)
C7	N2	C8	47.5(6)
O1	N2	C8	143.8(8)
C7	N2	C8	87.5(8)
C8	C1	C7	82.0(16)
C8	C1	N1	125.1(18)
C7	C1	C6	65.7(9)
N1	C1	C6	108.8(10)
C8	C1	C2	105.2(18)
C7	C1	C2	172.8(11)
N1	C1	C2	129.7(9)
C6	C1	C2	121.5(10)
C1	C2	C3	119.3(13)
C1	C2	H2	120.4
C3	C2	H2	120.3
C2	C3	C4	114.2(19)
C2	C3	H3	122.9
C4	C3	H3	122.9
C5	C4	C3	127(3)
C5	C4	H4	116.4
C3	C4	H4	116.4

C6	C5	C4	106(2)
C6	C5	H5	127
C4	C5	H5	127
C8	C6	S1	111.1(14)
S1	C6	C1	123.8(10)
C8	C6	N2	117.1(13)
S1	C6	N2	131.8(10)
C1	C6	N2	104.4(9)
C8	C6	C5	118.7(17)
C1	C6	C5	131.4(14)
N2	C6	C5	124.1(14)
C8	C6	C7	69.4(11)
S1	C6	C7	179.1(11)
C1	C6	C7	56.7(8)
N2	C6	C7	47.8(6)
C5	C6	C7	171.7(15)
C7	C7	N1	89.7(18)
C7	C7	N2	80.7(17)
N1	C7	N2	170.4(9)
C7	C7	N1	48.9(13)
N1	C7	N1	138.7(9)
C7	C7	N2	59.3(14)
N2	C7	N2	140.0(8)
N1	C7	N2	108.2(6)
C7	C7	C1	159(2)
N1	C7	C1	68.9(10)
N2	C7	C1	120.6(10)
N1	C7	C1	152.3(12)
N2	C7	C1	99.3(11)
C7	C7	C8	175(2)
N1	C7	C8	94.8(11)
N2	C7	C8	94.8(10)
N1	C7	C8	126.5(12)
N2	C7	C8	125.2(12)
C7	C7	C6	144(2)
N1	C7	C6	126.6(10)
N2	C7	C6	63.0(8)
N1	C7	C6	94.7(11)
N2	C7	C6	156.9(11)
C1	C7	C6	57.7(6)
C1	C8	C6	151(2)
C1	C8	C9	56.0(16)
C6	C8	C9	153.0(16)

C1	C8	C7	72.1(16)
C6	C8	C7	78.8(13)
C9	C8	C7	128.1(13)
C1	C8	S1	166.2(18)
C9	C8	S1	110.2(9)
C7	C8	S1	121.7(10)
C6	C8	N1	112.5(13)
C9	C8	N1	94.4(11)
S1	C8	N1	155.3(8)
C1	C8	N2	109.9(16)
C9	C8	N2	165.8(11)
S1	C8	N2	83.9(7)
N1	C8	N2	71.4(4)
C8	C9	C10	105.5(16)
C8	C9	H9	127.3
C10	C9	H9	127.3
C11	C10	C9	122(3)
C11	C10	H10	119.2
C9	C10	H10	119.1
C10	C11	S1	111(2)
C10	C11	H11	124.6
S1	C11	H11	124.6

Table B–2. Bond lengths (Å) and angles (deg) for **2.15e**.

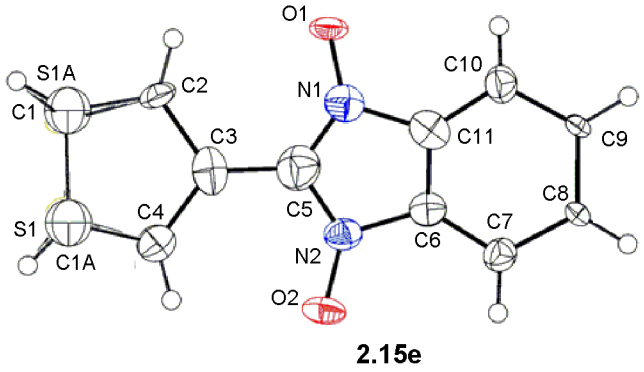

2.15e

S1	C4	1.547(15)	
S1	S1A	1.57(3)	
S1	C1	1.73(9)	
S1	H1A	1.0198	
C1A	C4	1.48(2)	
C1A	S1A	1.68(9)	
C1A	H1A	0.9602	
O1	N1	1.249(10)	
O2	N2	1.285(10)	
N1	C5	1.291(16)	
N1	C11	1.451(14)	
N2	C5	1.302(15)	
N2	C6	1.437(13)	
S1A	C2	1.545(16)	
S1A	H1	1.0279	
C1	C2	1.48(2)	
C1	H1	0.9601	
C2	C3	1.500(12)	
C2	H2	0.96	
C3	C5	1.444(16)	
C3	C4	1.468(11)	
C4	H4	0.9598	
C6	C11	1.297(12)	
C6	C7	1.391(15)	
C7	C8	1.429(13)	
C7	H7	0.95	
C8	C9	1.432(10)	
C8	H8	0.95	
C9	C10	1.426(13)	
C9	H9	0.95	
C10	C11	1.382(15)	
C10	H10	0.95	
C4	S1	S1A	105.8(10)
C4	S1	C1	104.9(12)
C4	S1	H1A	110.6
S1A	S1	H1A	141.4
C1	S1	H1A	142.3
C4	C1A	S1A	104(4)
C4	C1A	C1	103(4)
C4	C1A	H1A	120.2
S1A	C1A	H1A	134.5
C1	C1A	H1A	135.7

O1	N1	C5	132.6(11)
O1	N1	C11	119.2(9)
C5	N1	C11	108.0(10)
O2	N2	C5	132.3(11)
O2	N2	C6	120.1(9)
C5	N2	C6	107.4(10)
C2	S1A	S1	105.9(11)
C2	S1A	C1A	103.9(15)
C2	S1A	H1	125.7
S1	S1A	H1	128.4
C1A	S1A	H1	129.9
C2	C1	S1	101(4)
C2	C1	C1A	99(4)
C2	C1	H1	140.3
S1	C1	H1	118.6
C1A	C1	H1	120.2
C1	C2	C3	115(3)
C3	C2	S1A	109.2(10)
C1	C2	H2	114.9
C3	C2	H2	130
S1A	C2	H2	120.7
C5	C3	C4	128.3(10)
C5	C3	C2	122.6(10)
C4	C3	C2	108.9(9)
C3	C4	C1A	113(4)
C3	C4	S1	110.1(10)
C3	C4	H4	128.9
C1A	C4	H4	117.9
S1	C4	H4	121
N2	C5	N1	110.8(12)
N2	C5	C3	121.8(12)
N1	C5	C3	127.4(13)
C11	C6	C7	120.8(11)
C11	C6	N2	107.7(10)
C7	C6	N2	131.5(11)
C6	C7	C8	120.0(10)
C6	C7	H7	120
C8	C7	H7	120
C7	C8	C9	118.0(9)
C7	C8	H8	121
C9	C8	H8	121
C10	C9	C8	118.5(9)
C10	C9	H9	120.7

C8	C9	H9	120.7
C11	C10	C9	118.6(10)
C11	C10	H10	120.7
C9	C10	H10	120.7
C6	C11	C10	124.1(12)
C6	C11	N1	106.0(10)
C10	C11	N1	129.9(11)

Table B–3. Bond lengths (Å) and angles (deg) for **4.11a**.

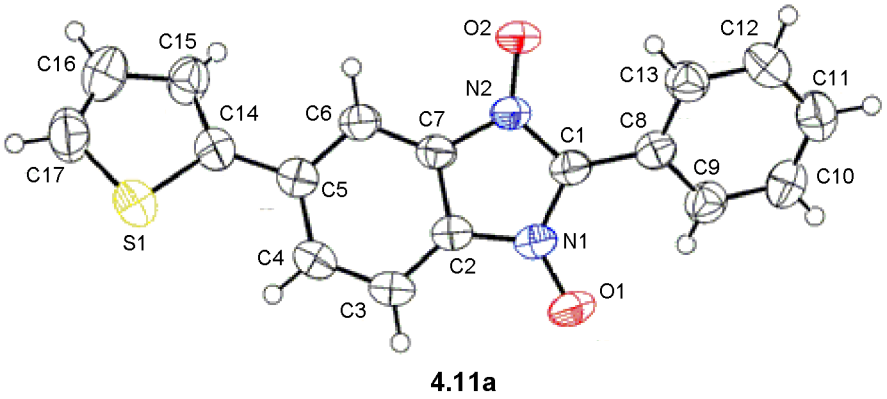

4.11a

S1	C17	1.692(3)	
S1	C14	1.7210(19)	
N1	O1	1.2813(18)	
N1	C1	1.373(2)	
N1	C2	1.408(2)	
N2	O2	1.2778(19)	
N2	C1	1.362(2)	
N2	C7	1.409(2)	
C1	C8	1.456(3)	
C2	C3	1.375(3)	
C2	C7	1.382(2)	
C3	C4	1.378(3)	
C3	H3	0.92(2)	
C4	C5	1.409(3)	
C4	H4	0.92(2)	
C5	C6	1.398(3)	
C5	C14	1.466(3)	
C6	C7	1.374(3)	
C6	H6	0.93(2)	
C8	C9	1.391(3)	
C8	C13	1.395(3)	
C9	C10	1.377(3)	
C9	H9	0.87(2)	
C10	C11	1.370(3)	
C10	H10	0.85(2)	
C11	C12	1.379(3)	
C11	H11	0.95(2)	
C12	C13	1.374(3)	
C12	H12	0.98(2)	
C13	H13	0.93(2)	
C14	C15	1.392(3)	
C15	C16	1.400(3)	
C15	H15	0.75(2)	
C16	C17	1.343(4)	
C16	H16	0.96(3)	
C17	H17	0.95(3)	
C17	S1	C14	92.21(12)
O1	N1	C1	126.45(16)
O1	N1	C2	123.95(14)
C1	N1	C2	109.58(14)
O2	N2	C1	126.27(15)
O2	N2	C7	123.77(14)

C1	N2	C7	109.94(14)
N2	C1	N1	106.87(15)
N2	C1	C8	126.10(15)
N1	C1	C8	126.98(16)
C3	C2	C7	121.81(17)
C3	C2	N1	131.32(16)
C7	C2	N1	106.87(14)
C2	C3	C4	116.26(17)
C2	C3	H3	123.7(14)
C4	C3	H3	120.0(14)
C3	C4	C5	122.83(17)
C3	C4	H4	119.6(13)
C5	C4	H4	117.5(13)
C6	C5	C4	119.64(17)
C6	C5	C14	119.30(16)
C4	C5	C14	120.99(17)
C7	C6	C5	116.81(17)
C7	C6	H6	120.1(13)
C5	C6	H6	123.0(13)
C6	C7	C2	122.63(16)
C6	C7	N2	130.65(16)
C2	C7	N2	106.72(15)
C9	C8	C13	119.07(18)
C9	C8	C1	120.36(17)
C13	C8	C1	120.56(16)
C10	C9	C8	119.8(2)
C10	C9	H9	121.5(15)
C8	C9	H9	118.6(15)
C11	C10	C9	120.8(2)
C11	C10	H10	121.9(15)
C9	C10	H10	117.3(15)
C10	C11	C12	119.8(2)
C10	C11	H11	118.4(14)
C12	C11	H11	121.8(14)
C13	C12	C11	120.3(2)
C13	C12	H12	119.3(14)
C11	C12	H12	120.2(14)
C12	C13	C8	120.1(2)
C12	C13	H13	119.4(14)
C8	C13	H13	120.4(14)
C15	C14	C5	127.67(18)
C15	C14	S1	109.84(15)
C5	C14	S1	122.44(14)

C14	C15	C16	112.3(2)
C14	C15	H15	120.9(19)
C16	C15	H15	126.7(19)
C17	C16	C15	113.2(2)
C17	C16	H16	122.1(18)
C15	C16	H16	124.6(18)
C16	C17	S1	112.36(19)
C16	C17	H17	130.2(18)
S1	C17	H17	117.4(18)

Table B–4. Bond lengths (Å) and angles (deg) for **5.3e**.

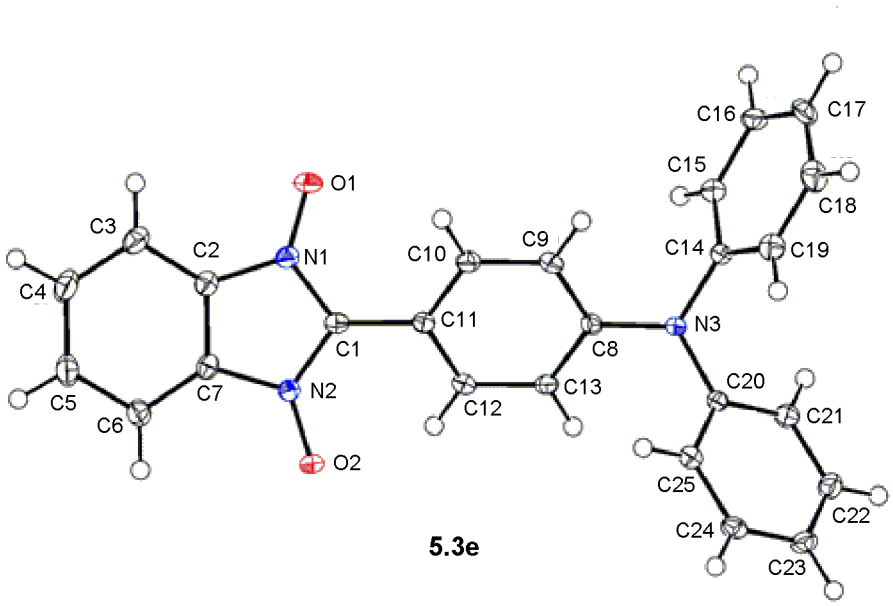

5.3e

C1	N1	1.3709(15)
C1	N2	1.3714(14)
C1	C11	1.4484(16)
C2	C3	1.3806(17)
C2	C7	1.3828(16)
C2	N1	1.4136(15)
C3	C4	1.3918(19)
C3	H3	0.95
C4	C5	1.3980(19)
C4	H4	0.95
C5	C6	1.3924(18)
C5	H5	0.95
C6	C7	1.3795(17)
C6	H6	0.95
C7	N2	1.4107(15)
C8	C9	1.3988(16)
C8	C13	1.4009(15)
C8	N3	1.4078(15)
C9	C10	1.3856(17)
C9	H9	0.95
C10	C11	1.4018(16)
C10	H10	0.95
C11	C12	1.4030(16)
C12	C13	1.3796(16)
C12	H12	0.95
C13	H13	0.95
C14	C19	1.3873(17)
C14	C15	1.3916(16)
C14	N3	1.4319(14)
C15	C16	1.3890(17)
C15	H15	0.95
C16	C17	1.387(2)
C16	H16	0.95
C17	C18	1.383(2)
C17	H17	0.95
C18	C19	1.3884(18)
C18	H18	0.95
C19	H19	0.95
C20	C25	1.3938(15)
C20	C21	1.3958(16)
C20	N3	1.4271(14)
C21	C22	1.3884(17)

C21	H21	0.95	
C22	C23	1.3903(17)	
C22	H22	0.95	
C23	C24	1.3843(17)	
C23	H23	0.95	
C24	C25	1.3888(16)	
C24	H24	0.95	
C25	H25	0.95	
N1	O1	1.2825(13)	
N2	O2	1.2798(12)	
N1	C1	N2	107.04(10)
N1	C1	C11	127.04(10)
N2	C1	C11	125.92(10)
C3	C2	C7	122.15(11)
C3	C2	N1	130.87(11)
C7	C2	N1	106.97(10)
C2	C3	C4	115.81(12)
C2	C3	H3	122.1
C4	C3	H3	122.1
C3	C4	C5	121.97(12)
C3	C4	H4	119
C5	C4	H4	119
C6	C5	C4	121.58(12)
C6	C5	H5	119.2
C4	C5	H5	119.2
C7	C6	C5	115.72(12)
C7	C6	H6	122.1
C5	C6	H6	122.1
C6	C7	C2	122.77(11)
C6	C7	N2	130.35(11)
C2	C7	N2	106.88(10)
C9	C8	C13	118.49(10)
C9	C8	N3	121.81(10)
C13	C8	N3	119.71(10)
C10	C9	C8	120.78(11)
C10	C9	H9	119.6
C8	C9	H9	119.6
C9	C10	C11	120.49(11)
C9	C10	H10	119.8
C11	C10	H10	119.8
C10	C11	C12	118.77(11)
C10	C11	C1	121.11(10)
C12	C11	C1	120.12(10)

C13	C12	C11	120.41(11)
C13	C12	H12	119.8
C11	C12	H12	119.8
C12	C13	C8	121.06(10)
C12	C13	H13	119.5
C8	C13	H13	119.5
C19	C14	C15	119.98(11)
C19	C14	N3	120.79(10)
C15	C14	N3	119.24(11)
C16	C15	C14	119.96(12)
C16	C15	H15	120
C14	C15	H15	120
C17	C16	C15	119.92(12)
C17	C16	H16	120
C15	C16	H16	120
C18	C17	C16	120.00(12)
C18	C17	H17	120
C16	C17	H17	120
C17	C18	C19	120.36(12)
C17	C18	H18	119.8
C19	C18	H18	119.8
C14	C19	C18	119.75(12)
C14	C19	H19	120.1
C18	C19	H19	120.1
C25	C20	C21	119.62(11)
C25	C20	N3	121.07(10)
C21	C20	N3	119.27(10)
C22	C21	C20	119.79(11)
C22	C21	H21	120.1
C20	C21	H21	120.1
C21	C22	C23	120.68(11)
C21	C22	H22	119.7
C23	C22	H22	119.7
C24	C23	C22	119.24(11)
C24	C23	H23	120.4
C22	C23	H23	120.4
C23	C24	C25	120.79(11)
C23	C24	H24	119.6
C25	C24	H24	119.6
C24	C25	C20	119.86(11)
C24	C25	H25	120.1
C20	C25	H25	120.1
O1	N1	C1	126.88(10)

O1	N1	C2	123.67(10)
C1	N1	C2	109.46(9)
O2	N2	C1	126.89(10)
O2	N2	C7	123.45(9)
C1	N2	C7	109.65(9)
C8	N3	C20	119.96(9)
C8	N3	C14	119.44(9)
C20	N3	C14	116.84(9)

Appendix C: Cyclic Voltammetry

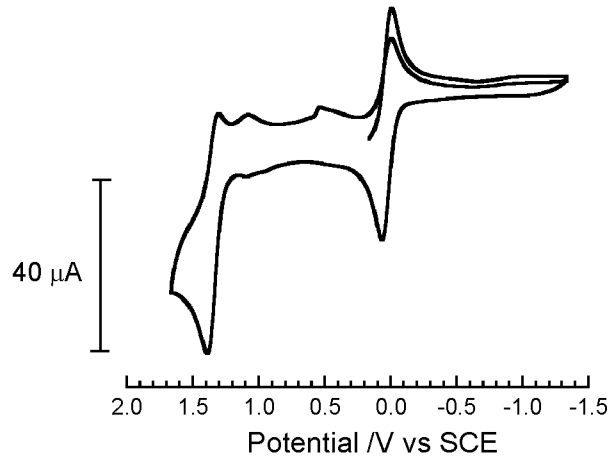

Figure C–1. Cyclic voltammogram of **5.1a**, 10^{-3} M solution in 0.1 M NBu_4PF_6/CH_3CN, 100 mV s^{-1} scan rate, ambient temperature.

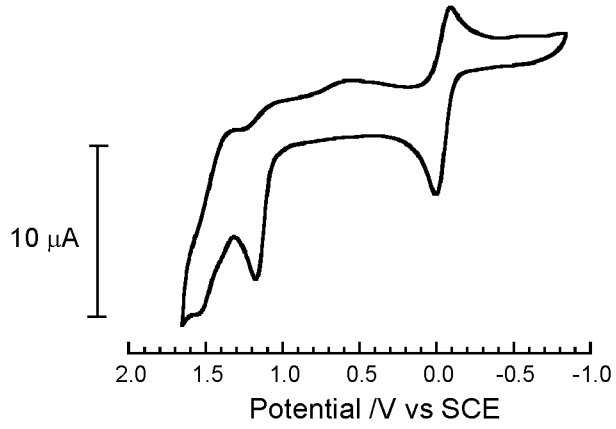

Figure C–2. Cyclic voltammogram of **5.1d**, 10^{-3} M solution in 0.1 M NBu_4PF_6/CH_3CN, 100 mV s^{-1} scan rate, ambient temperature.

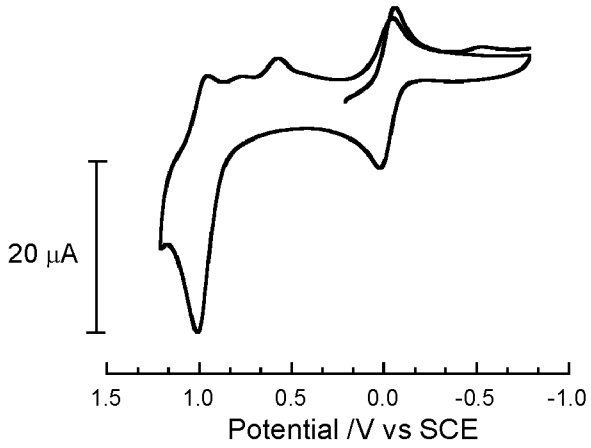

Figure C–3. Cyclic voltammogram of **5.1e**, 10^{-3} M solution in 0.1 M NBu_4PF_6/CH_3CN, 100 mV s^{-1} scan rate, ambient temperature.

Appendix D: ^{1}H and ^{13}C NMR Spectra

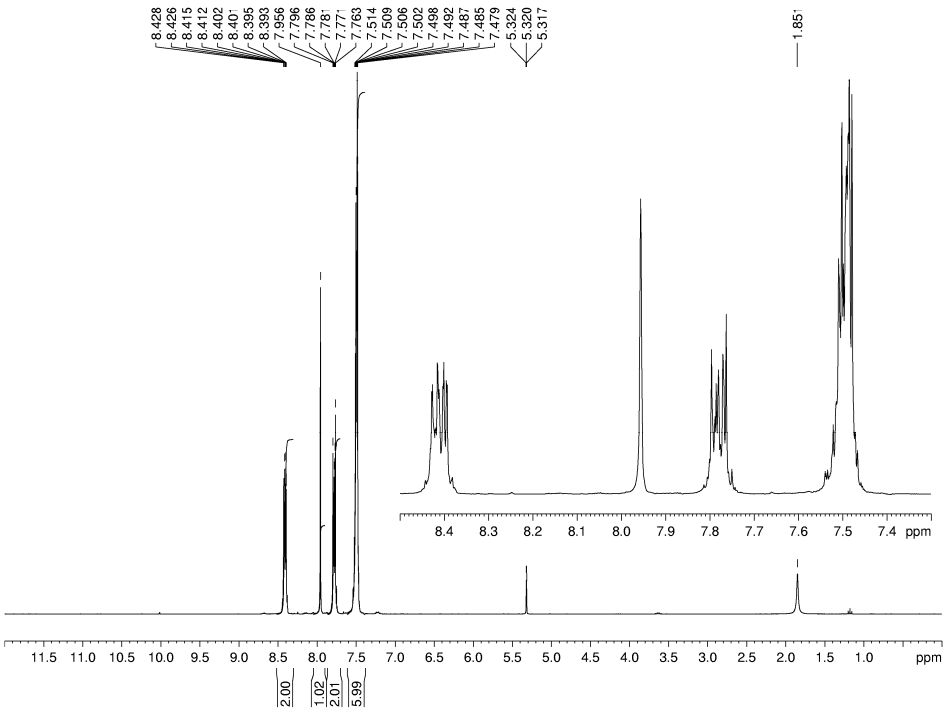

Figure D–1. ^{1}H NMR spectrum of **2.21a** (300 MHz, CD_2Cl_2).

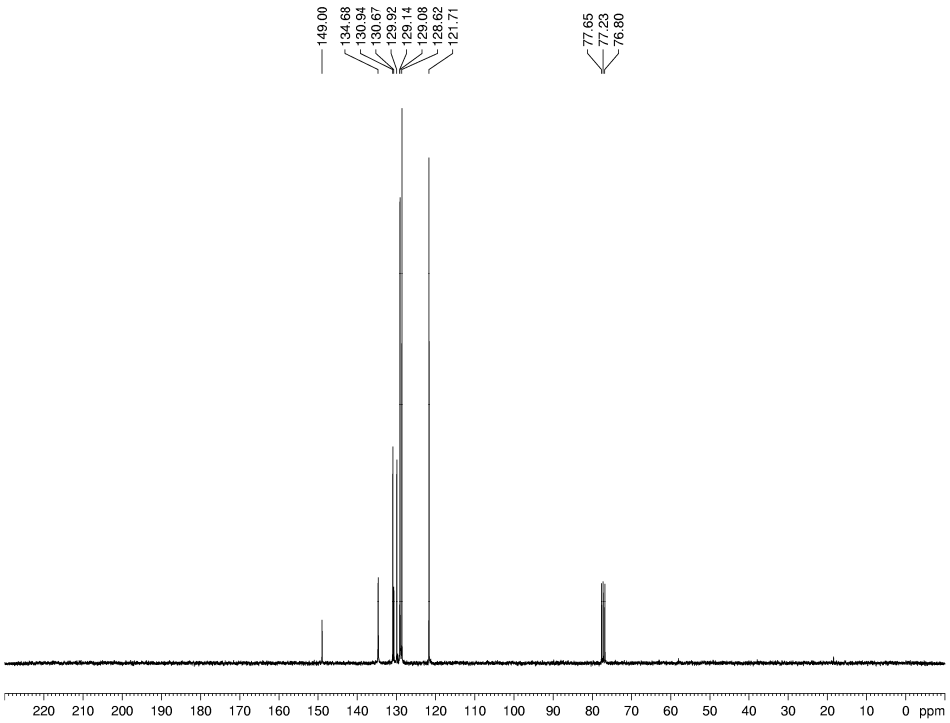

Figure D–2. ^{13}C NMR spectrum of **2.21a** (75 MHz, $CDCl_3$).

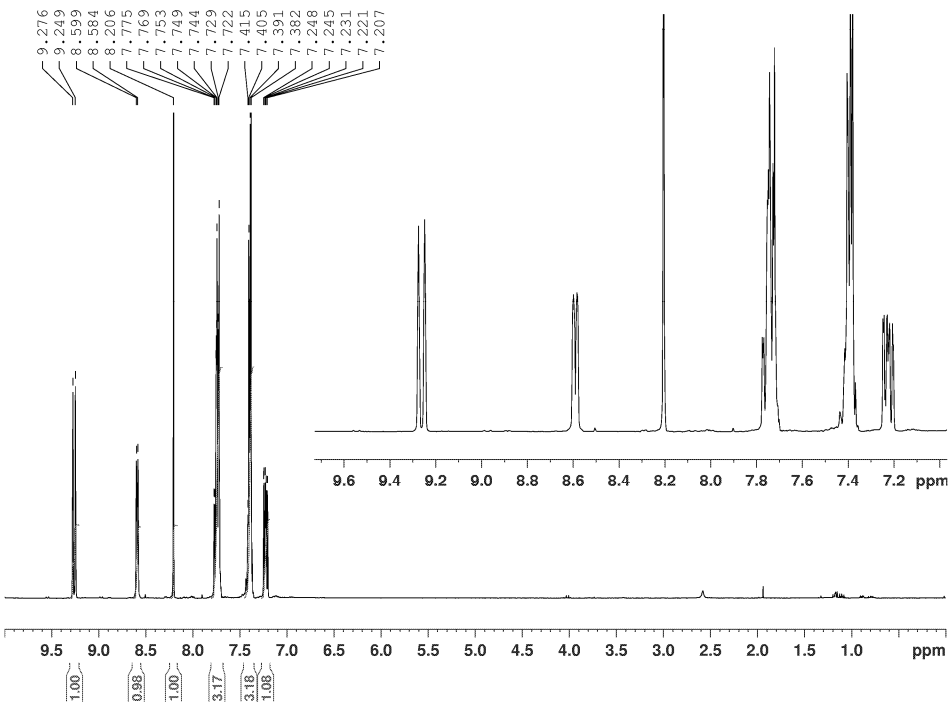

Figure D–3. ^{1}H NMR spectrum of **2.21b** (300 MHz, $CDCl_3$).

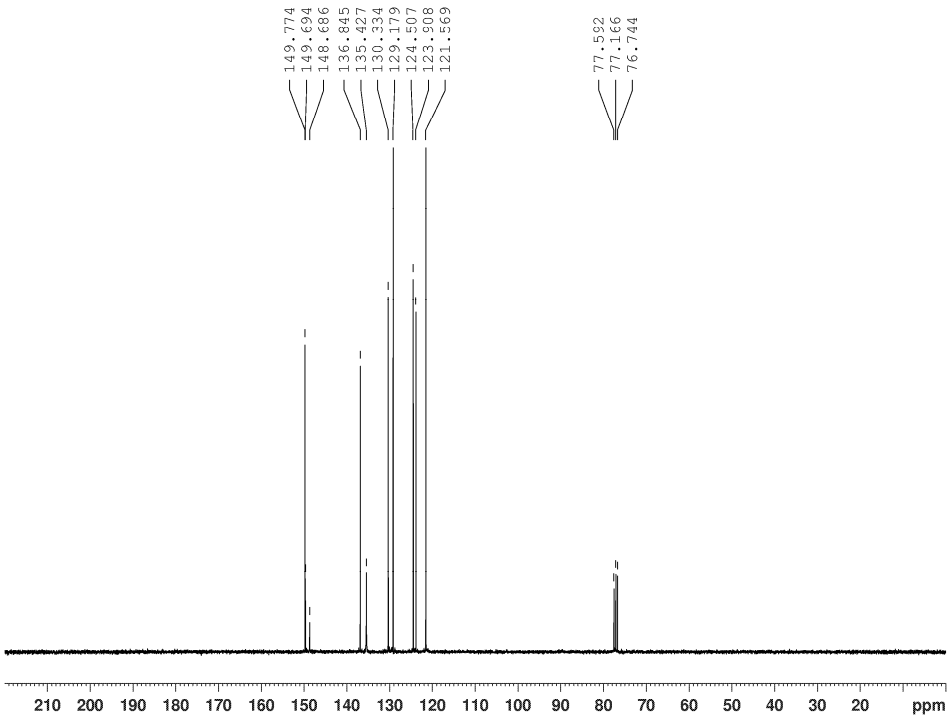

Figure D–4. ^{13}C NMR spectrum of **2.21b** (75 MHz, $CDCl_3$).

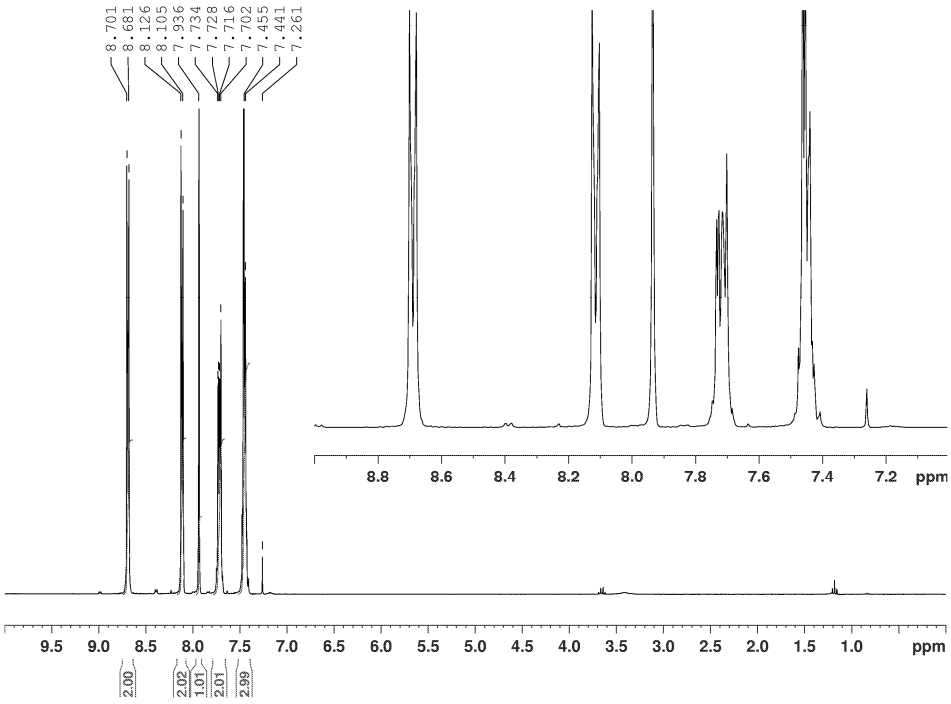

Figure D–5. ^{1}H NMR spectrum of **2.21c** (300 MHz, $CDCl_3$).

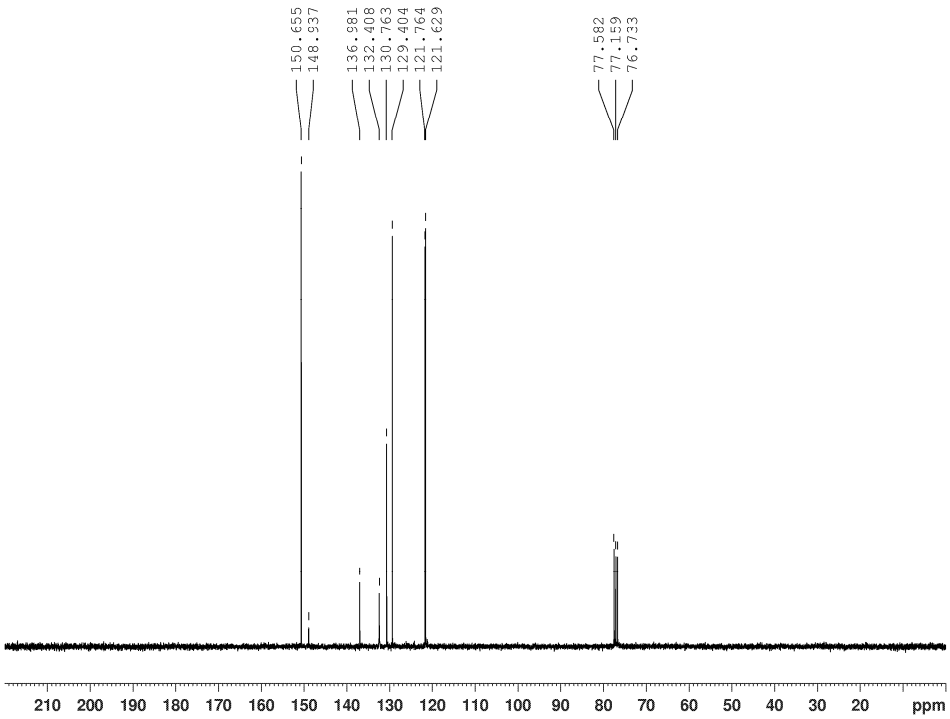

Figure D–6. ^{13}C NMR spectrum of **2.21c** (75 MHz, $CDCl_3$).

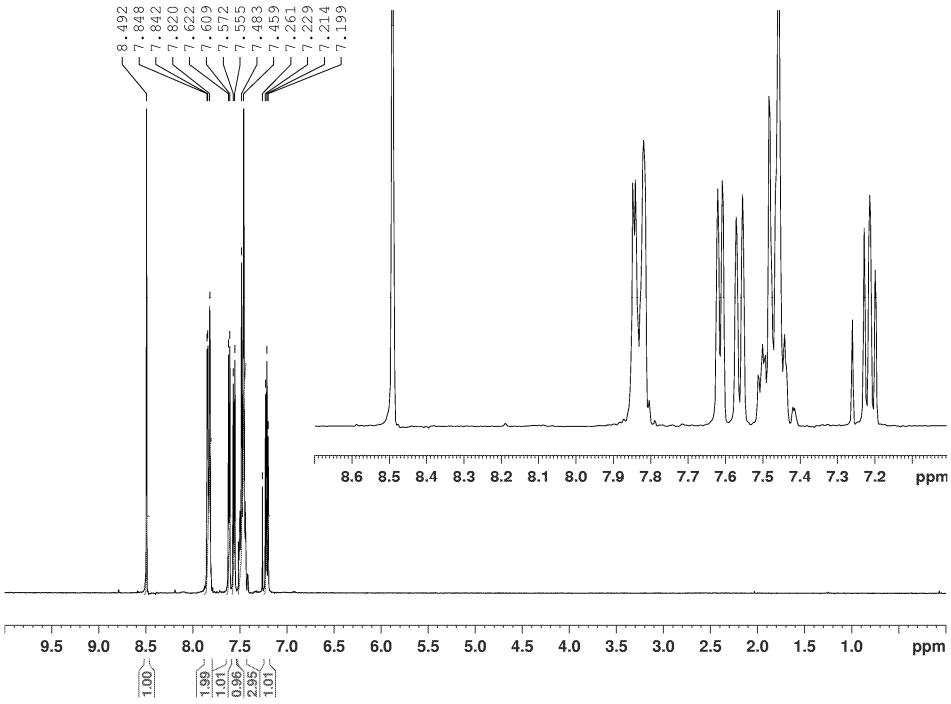

Figure D–7. ^{1}H NMR spectrum of **2.21d** (300 MHz, $CDCl_3$).

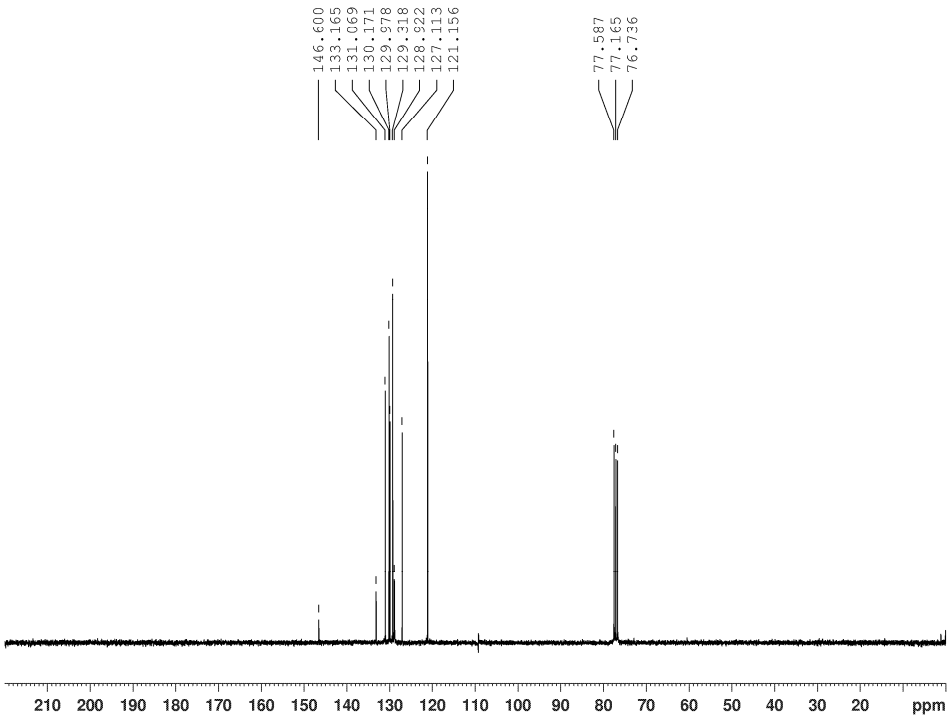

Figure D–8. ^{13}C NMR spectrum of **2.21d** (75 MHz, $CDCl_3$).

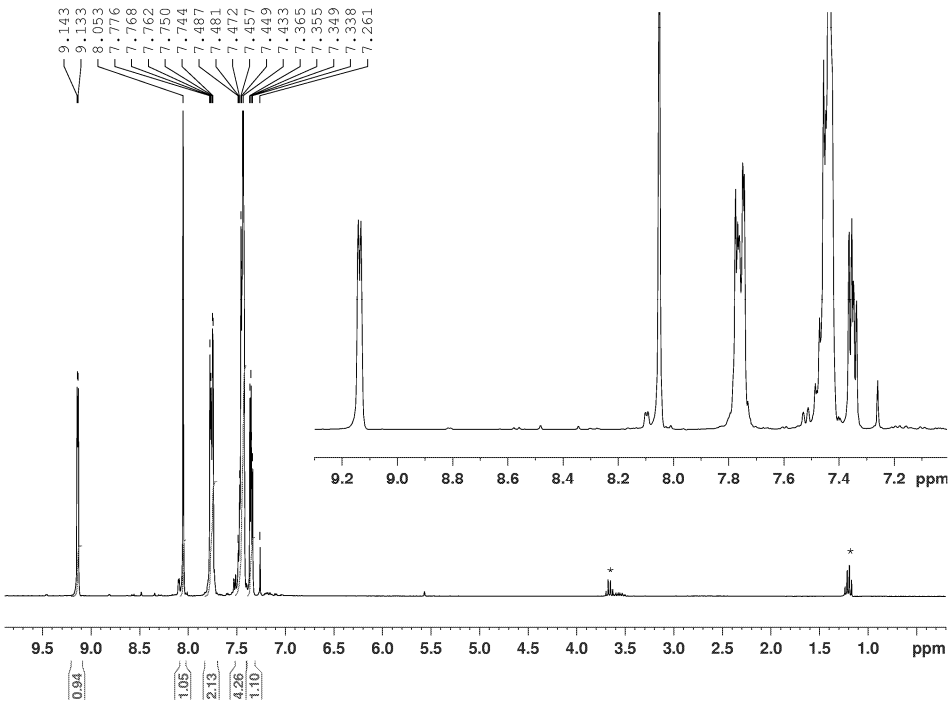

Figure D–9. ^{1}H NMR spectrum of **2.21e** (300 MHz, $CDCl_3$).

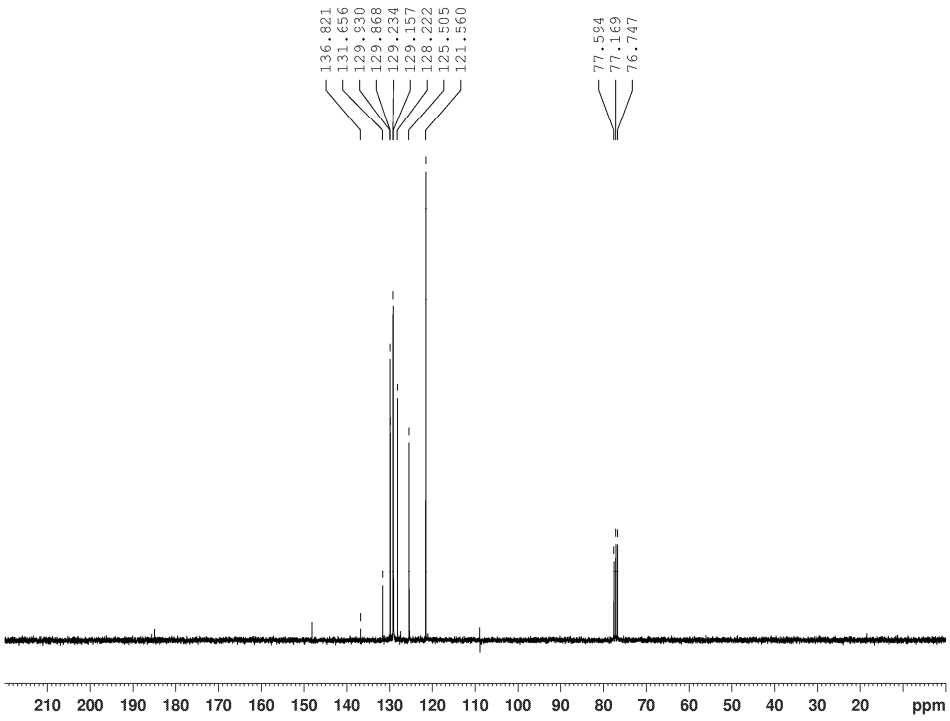

Figure D–10. ^{13}C NMR spectrum of **2.21e** (75 MHz, $CDCl_3$).

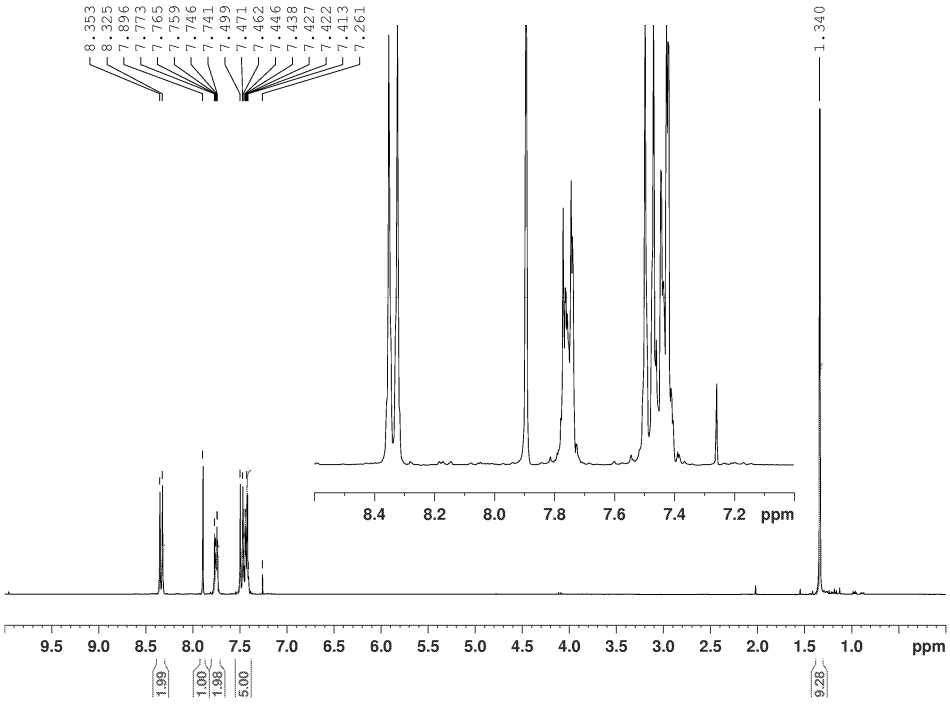

Figure D–11. ^{1}H NMR spectrum of **2.21h** (300 MHz, $CDCl_3$).

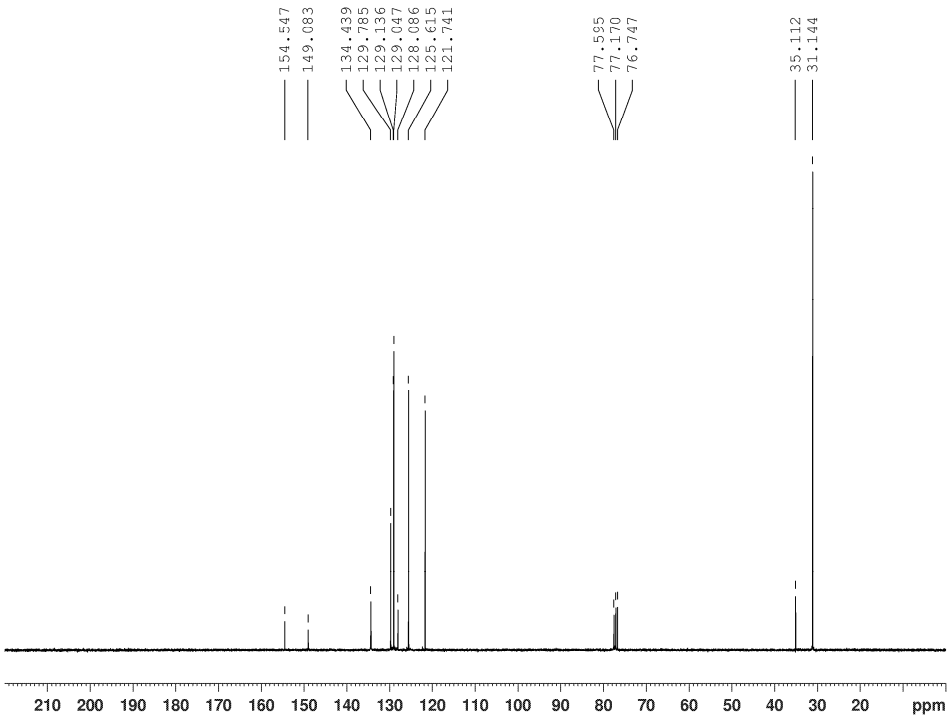

Figure D–12. ^{13}C NMR spectrum of **2.21h** (75 MHz, $CDCl_3$).

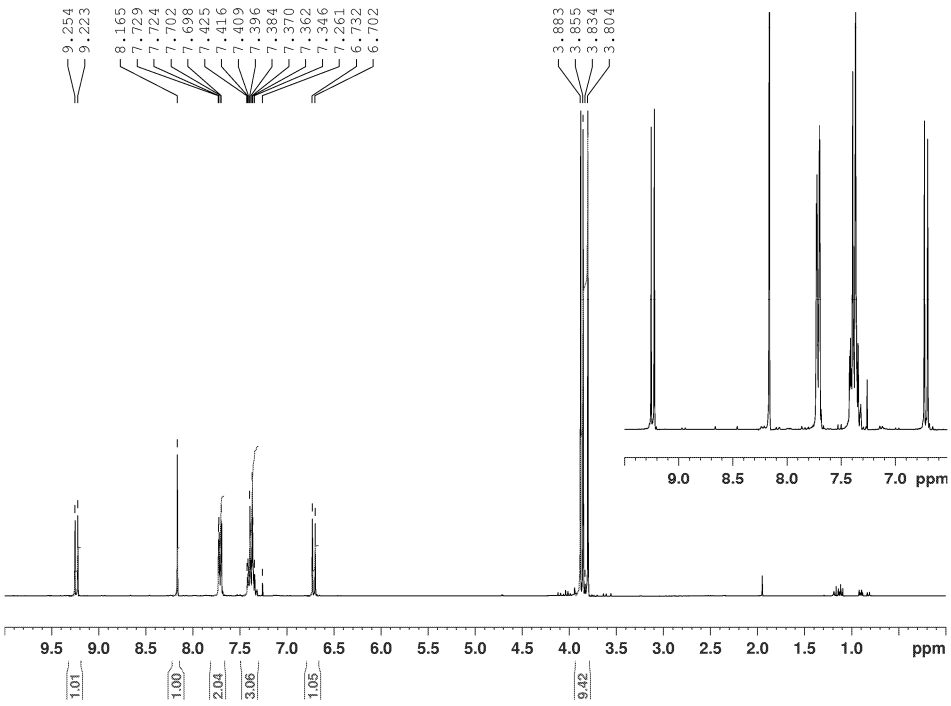

Figure D–13. ^{1}H NMR spectrum of **2.21j** (300 MHz, $CDCl_3$).

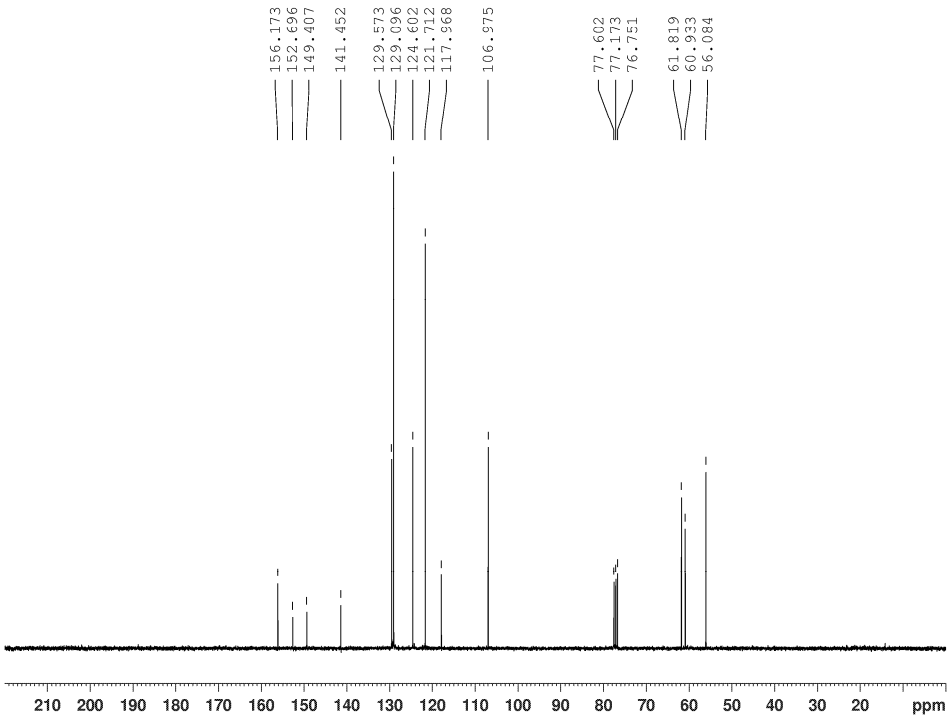

Figure D–14. ^{13}C NMR spectrum of **2.21j** (75 MHz, $CDCl_3$).

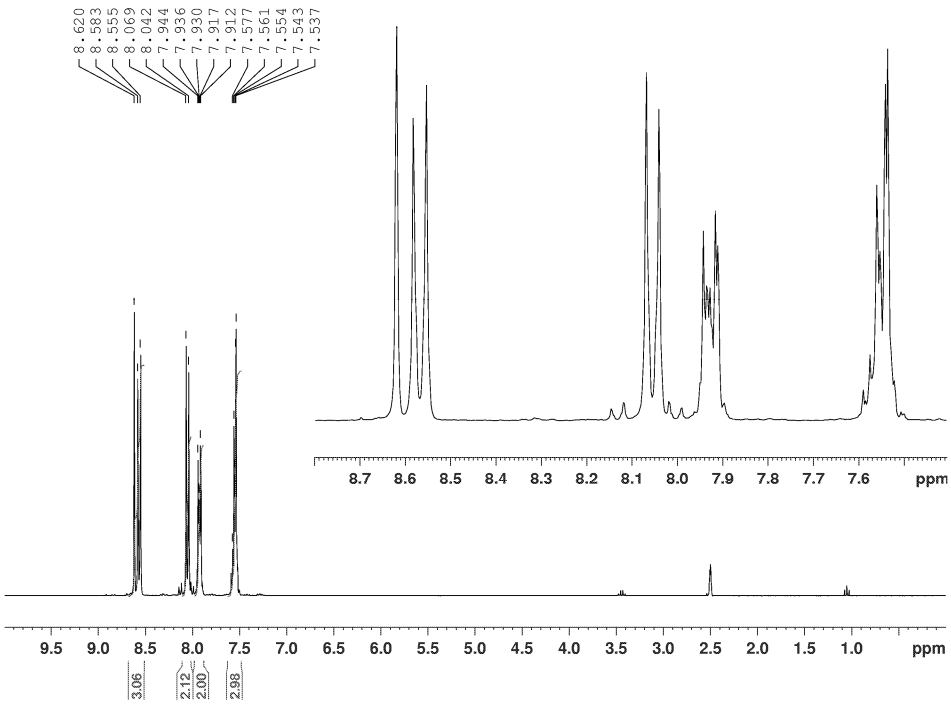

Figure D–15. ^{1}H NMR spectrum of **2.21k** (300 MHz, d_6-DMSO).

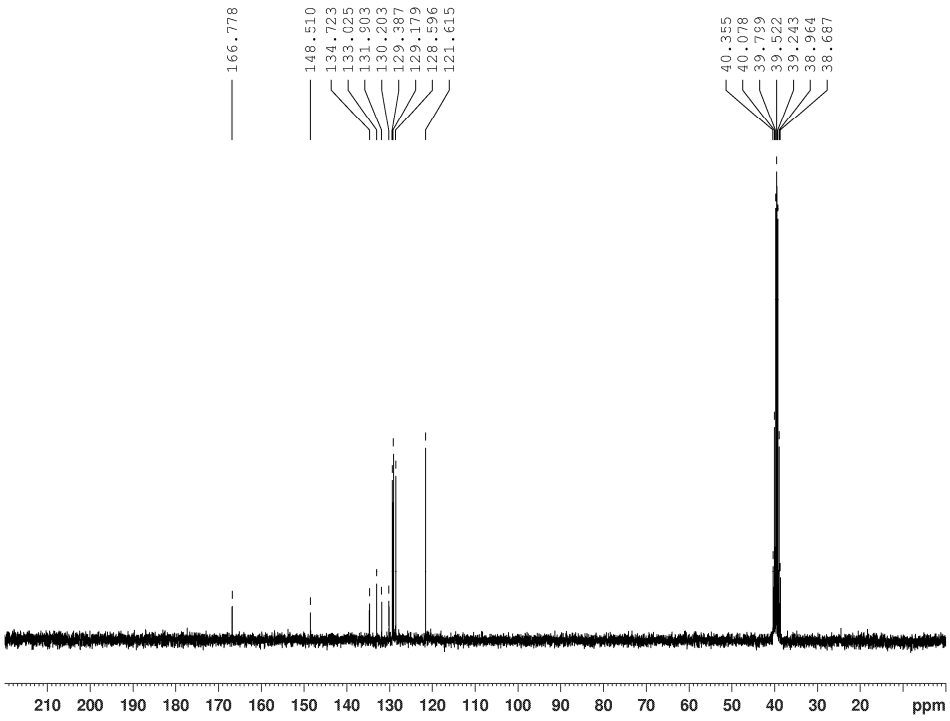

Figure D–16. ^{13}C NMR spectrum of **2.21k** (75 MHz, $CDCl_3$).

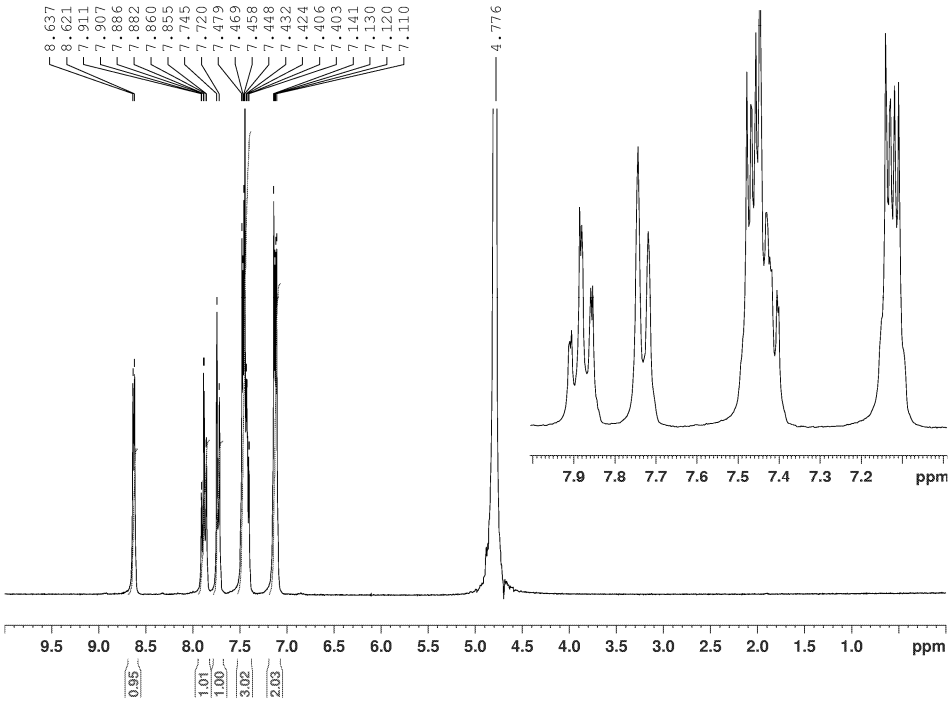

Figure D–17. ^{1}H NMR spectrum of **2.16b** (300 MHz, 1.0 M NaOD in D_2O).

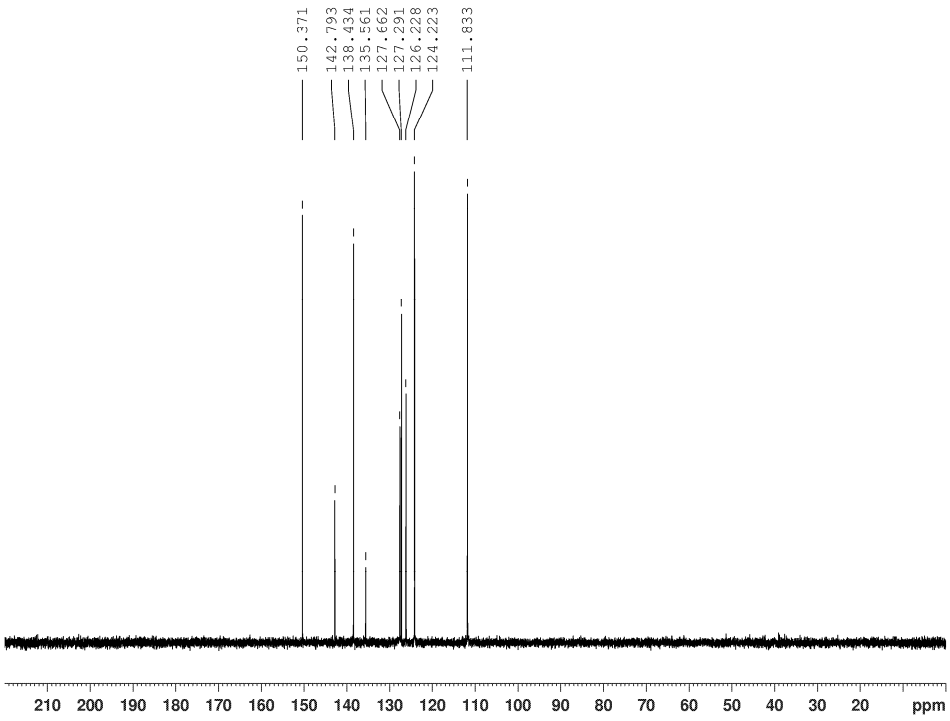

Figure D–18. ^{13}C NMR spectrum of **2.16b** (75 MHz, 1.0 M NaOD in D_2O).

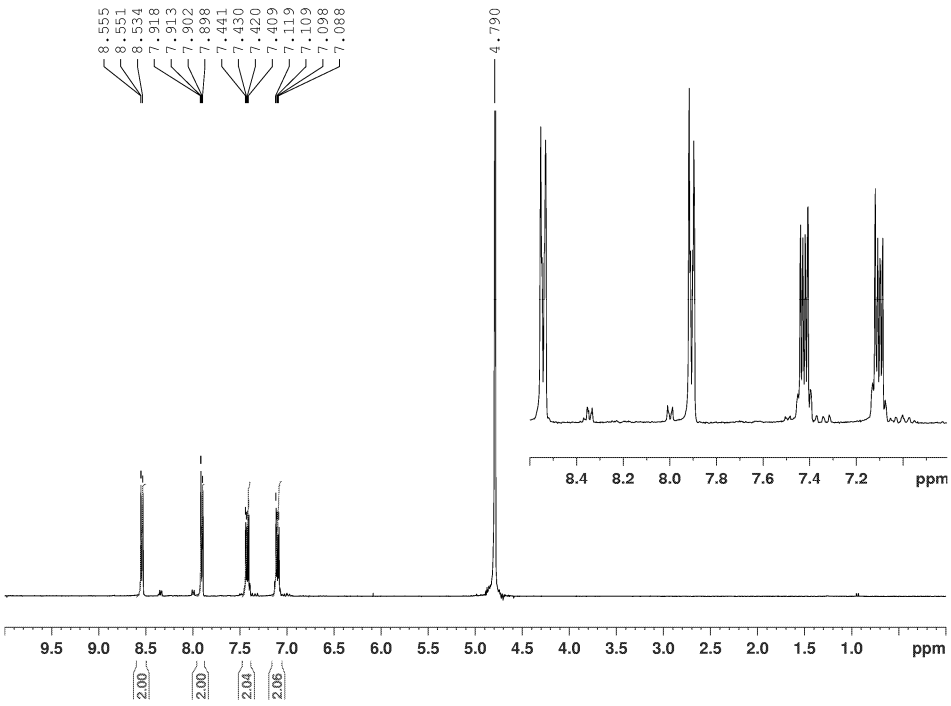

Figure D–19. ^{1}H NMR spectrum of **2.16c** (300 MHz, 1.0 M NaOD in D_2O).

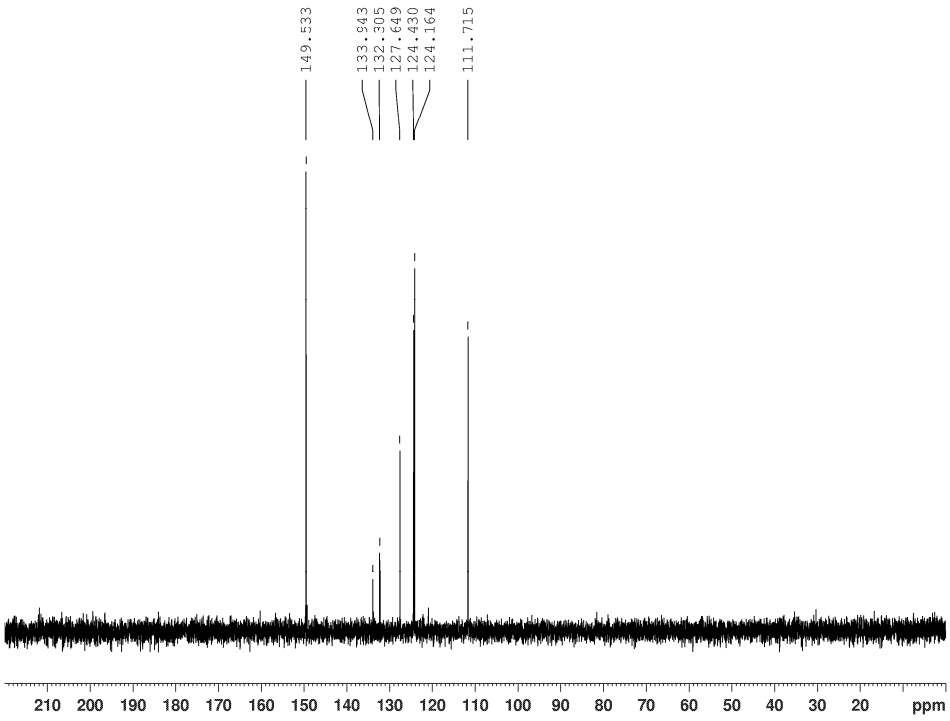

Figure D–20. ^{13}C NMR spectrum of **2.16c** (75 MHz, 1.0 M NaOD in D_2O).

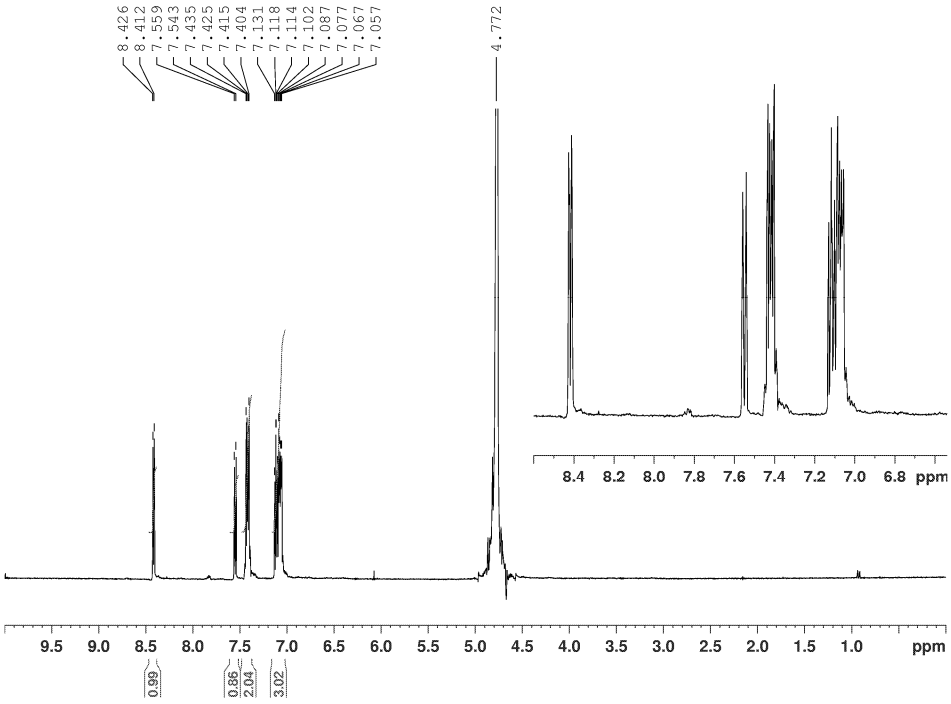

Figure D–21. ^{1}H NMR spectrum of **2.16d** (300 MHz, 1.0 M NaOD in D_2O).

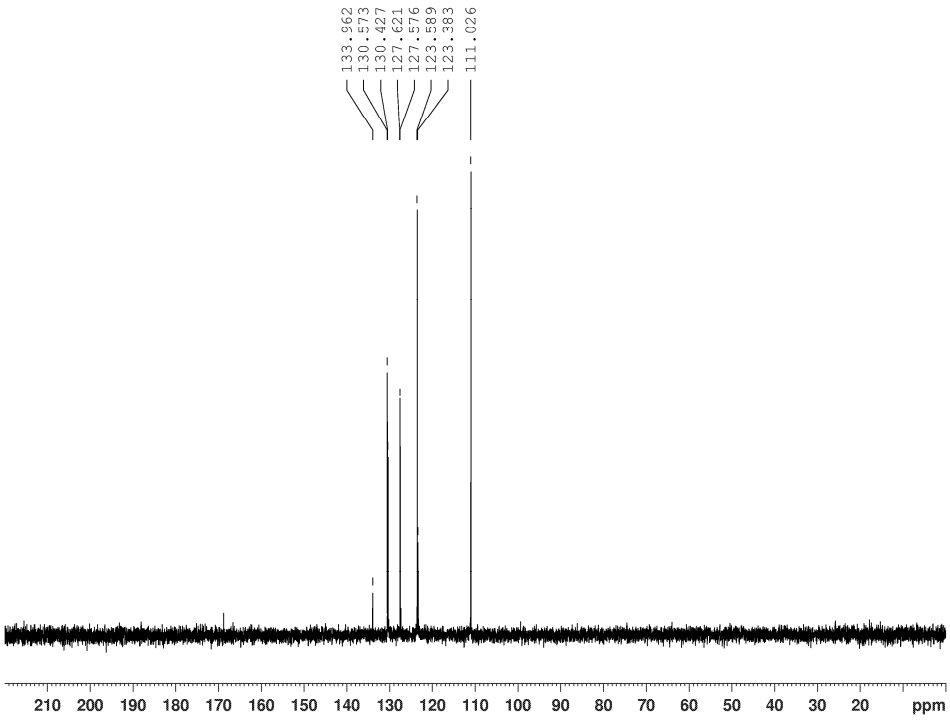

Figure D–22. ^{13}C NMR spectrum of **2.16d** (75 MHz, 1.0 M NaOD in D_2O).

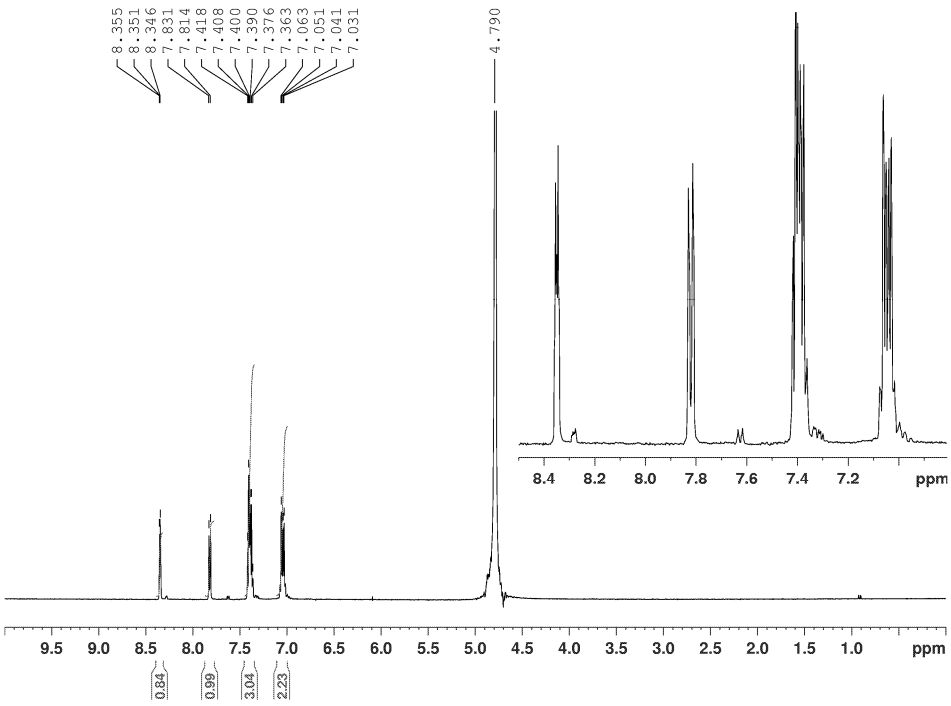

Figure D–23. ^{1}H NMR spectrum of **2.16e** (300 MHz, 1.0 M NaOD in D_2O).

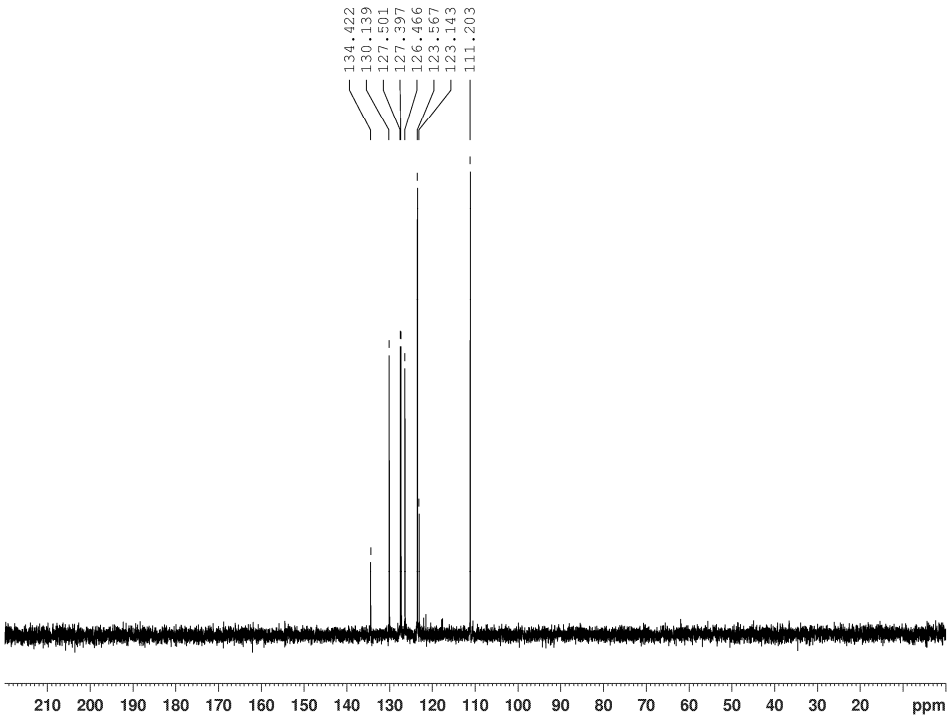

Figure D–24. ^{13}C NMR spectrum of **2.16e** (75 MHz, 1.0 M NaOD in D_2O).

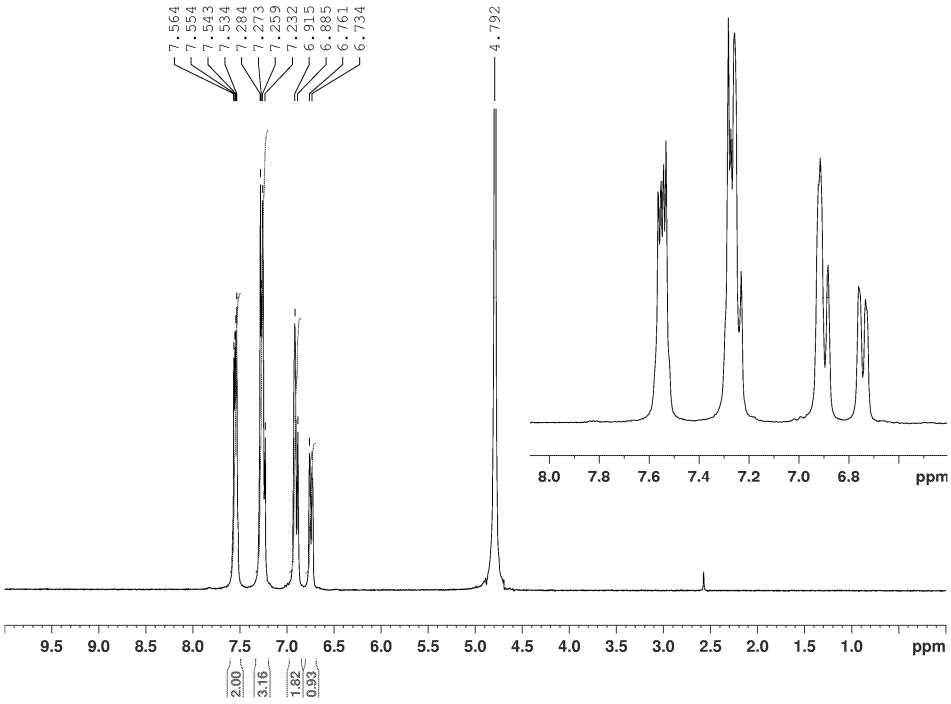

Figure D–25. ^{1}H NMR spectrum of **2.16f** (300 MHz, 1.0 M NaOD in D_2O).

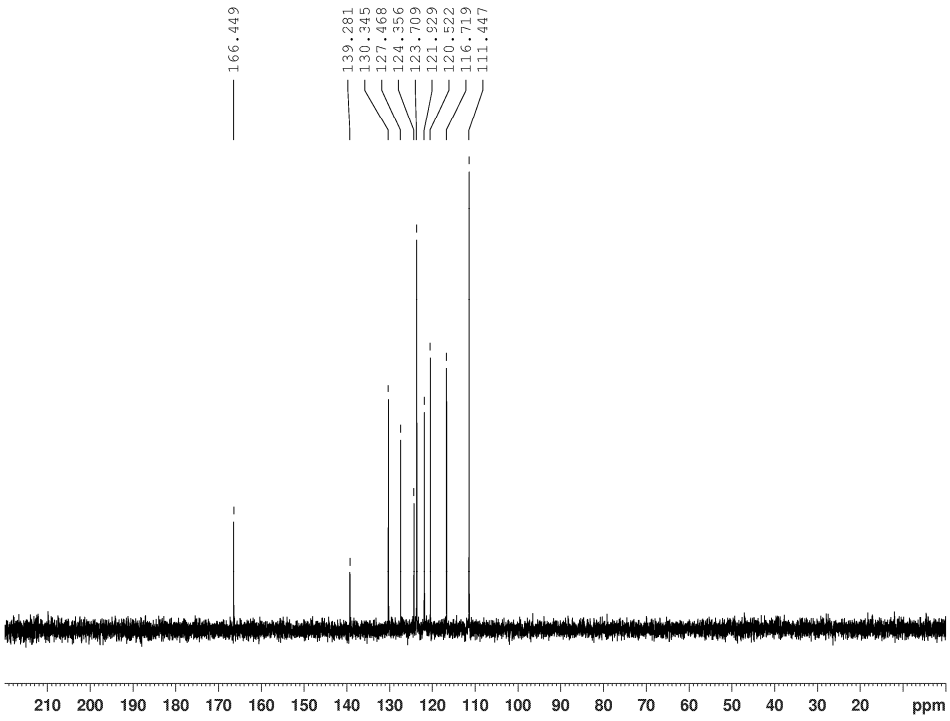

Figure D–26. ^{13}C NMR spectrum of **2.16f** (75 MHz, 1.0 M NaOD in D_2O).

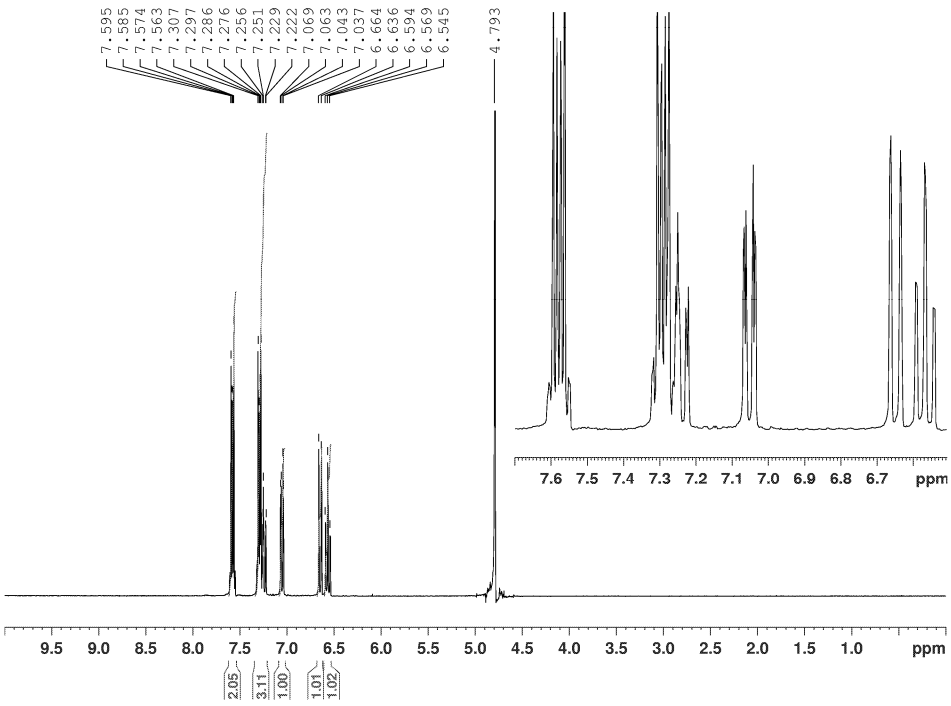

Figure D–27. ^{1}H NMR spectrum of **2.16g** (300 MHz, 1.0 M NaOD in D_2O).

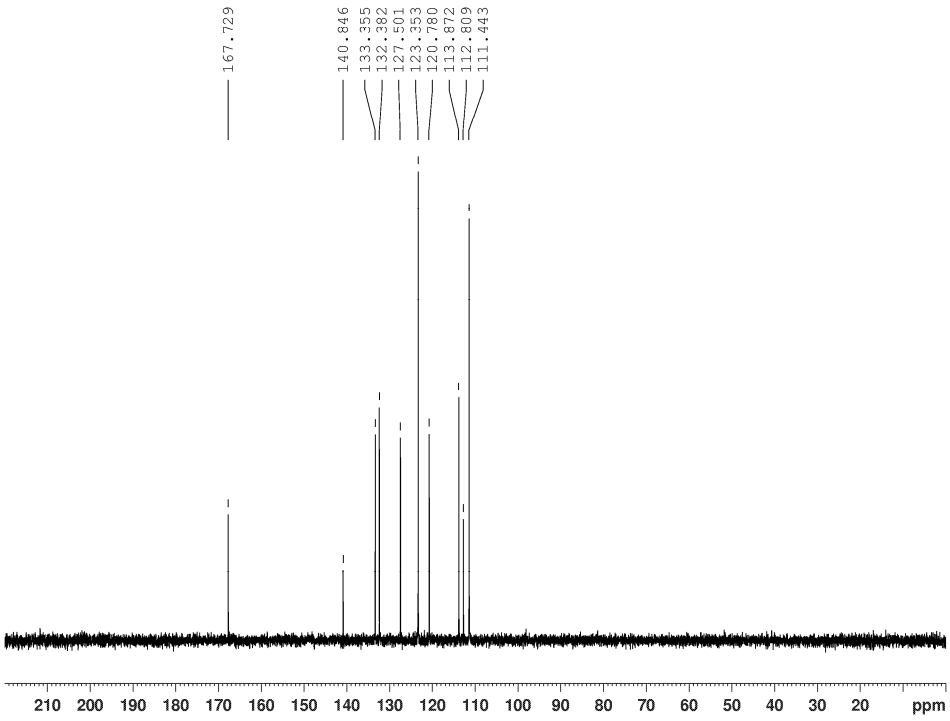

Figure D–28. ^{13}C NMR spectrum of **2.16g** (75 MHz, 1.0 M NaOD in D_2O).

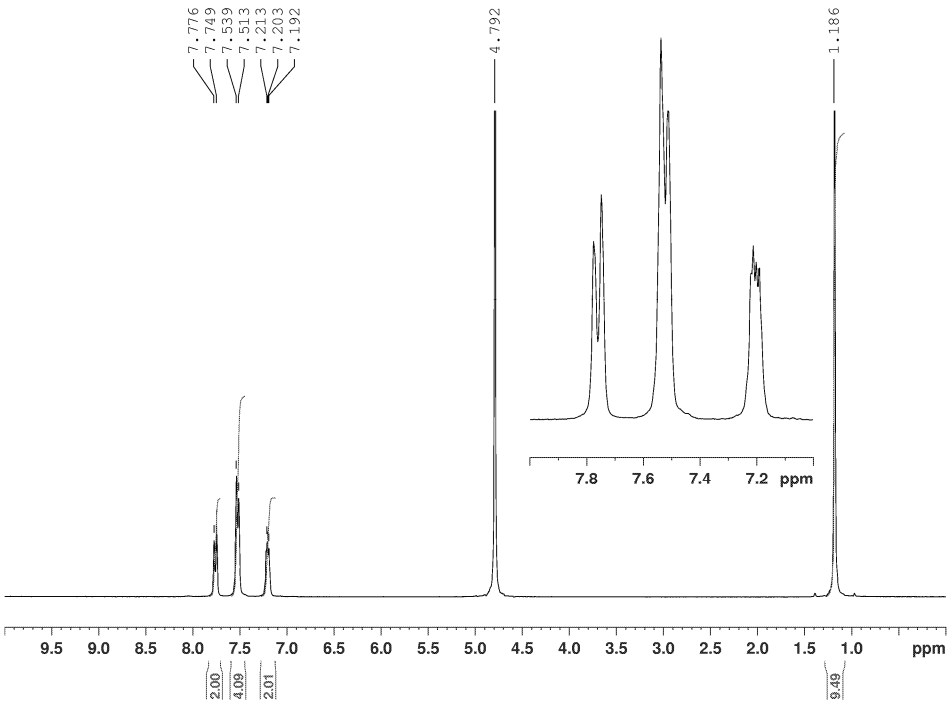

Figure D–29. ^{1}H NMR spectrum of **2.16h** (300 MHz, 1.0 M NaOD in D_2O).

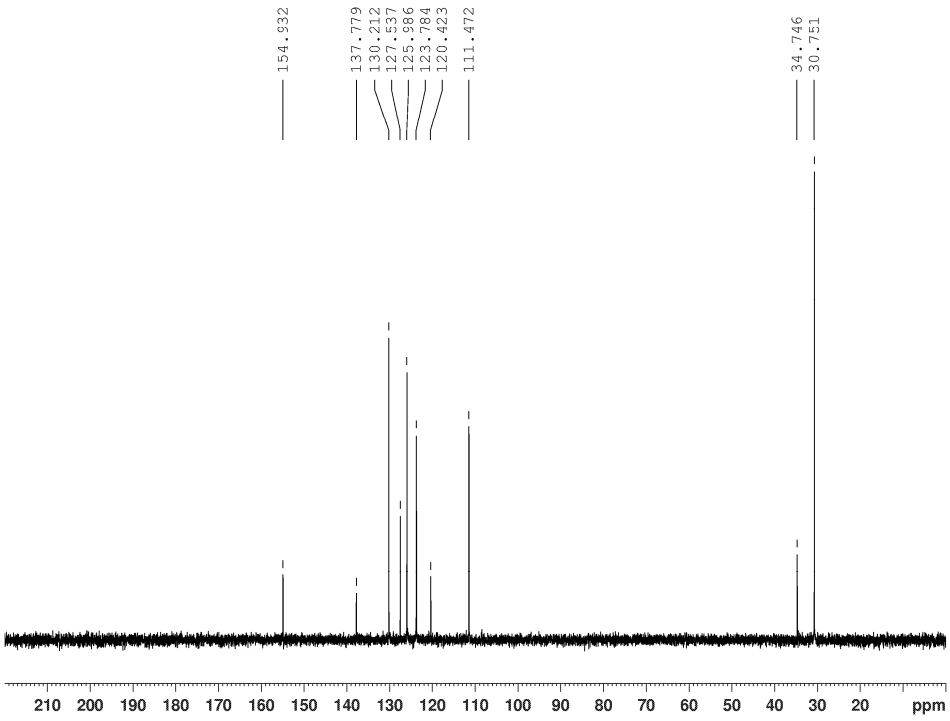

Figure D–30. ^{13}C NMR spectrum of **2.16h** (75 MHz, 1.0 M NaOD in D_2O).

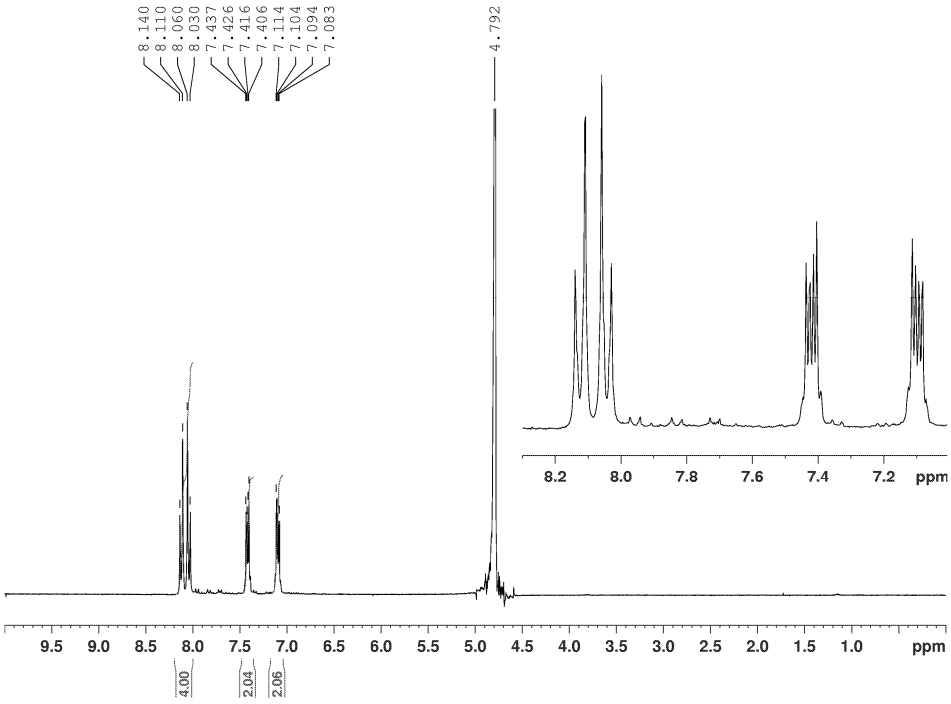

Figure D–31. ^{1}H NMR spectrum of **2.16i** (300 MHz, 1.0 M NaOD in D_2O).

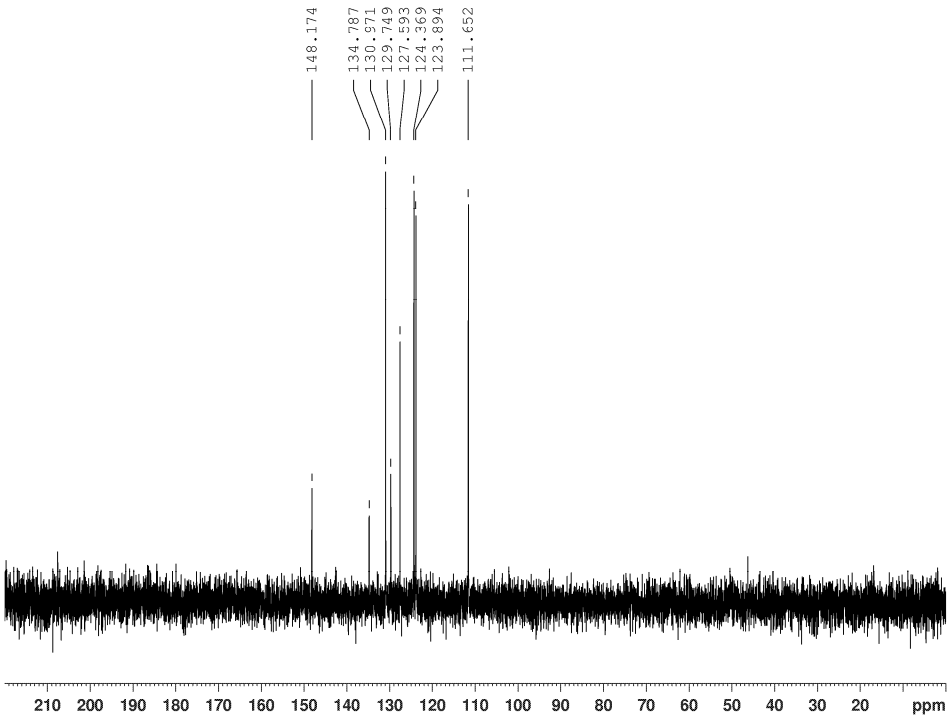

Figure D–32. ^{13}C NMR spectrum of **2.16i** (75 MHz, 1.0 M NaOD in D_2O).

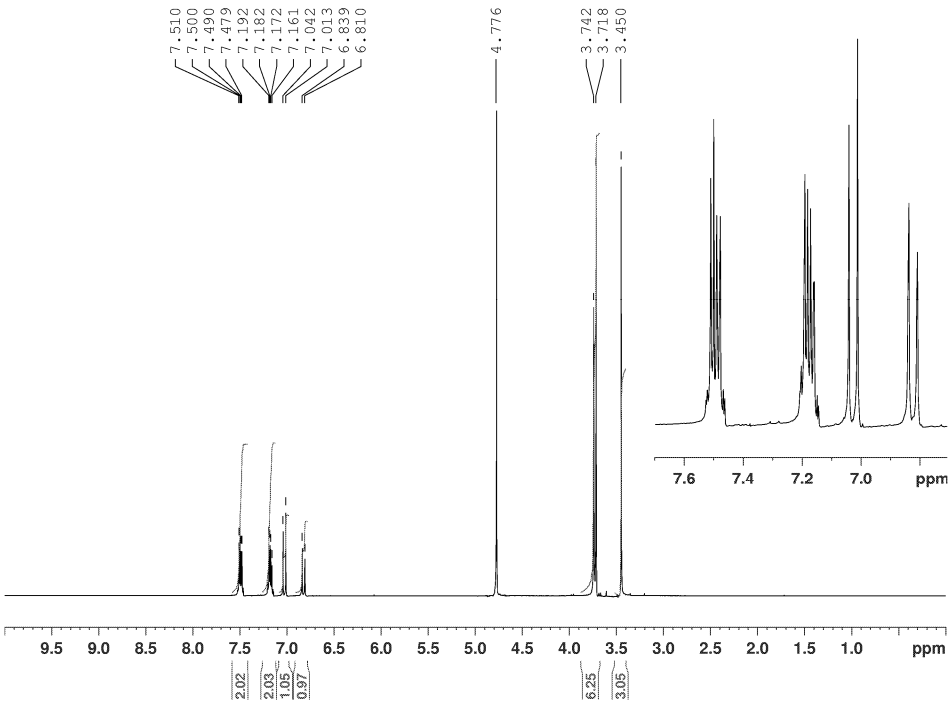

Figure D–33. ^{1}H NMR spectrum of **2.16j** (300 MHz, 1.0 M NaOD in D_2O).

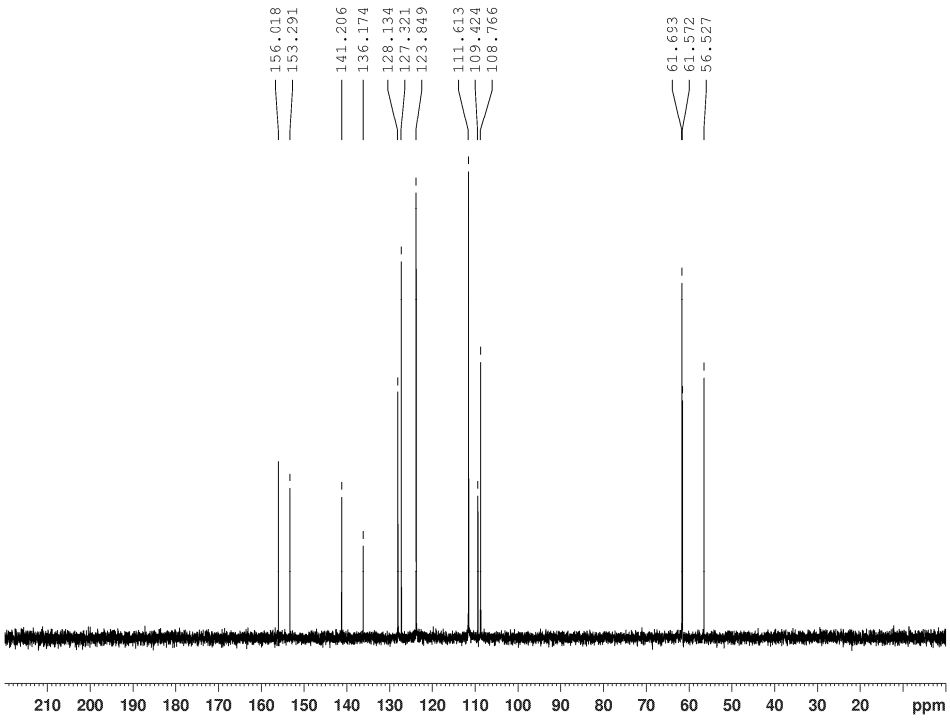

Figure D–34. ^{13}C NMR spectrum of **2.16j** (75 MHz, 1.0 M NaOD in D_2O).

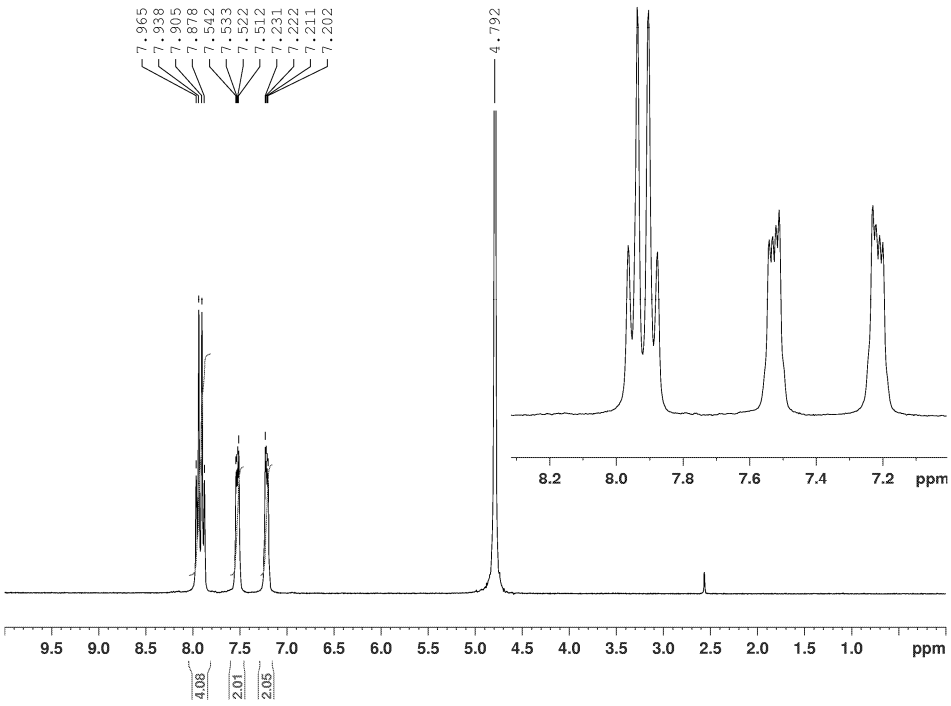

Figure D–35. ^{1}H NMR spectrum of **2.16k** (300 MHz, 1.0 M NaOD in D_2O).

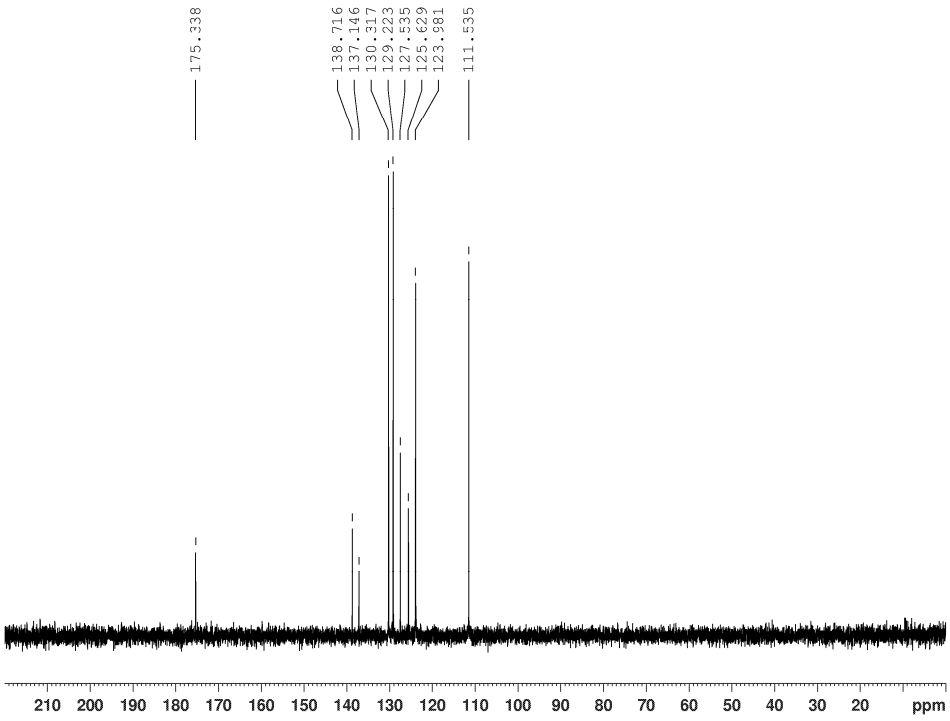

Figure D–36. ^{13}C NMR spectrum of **2.16k** (75 MHz, 1.0 M NaOD in D_2O).

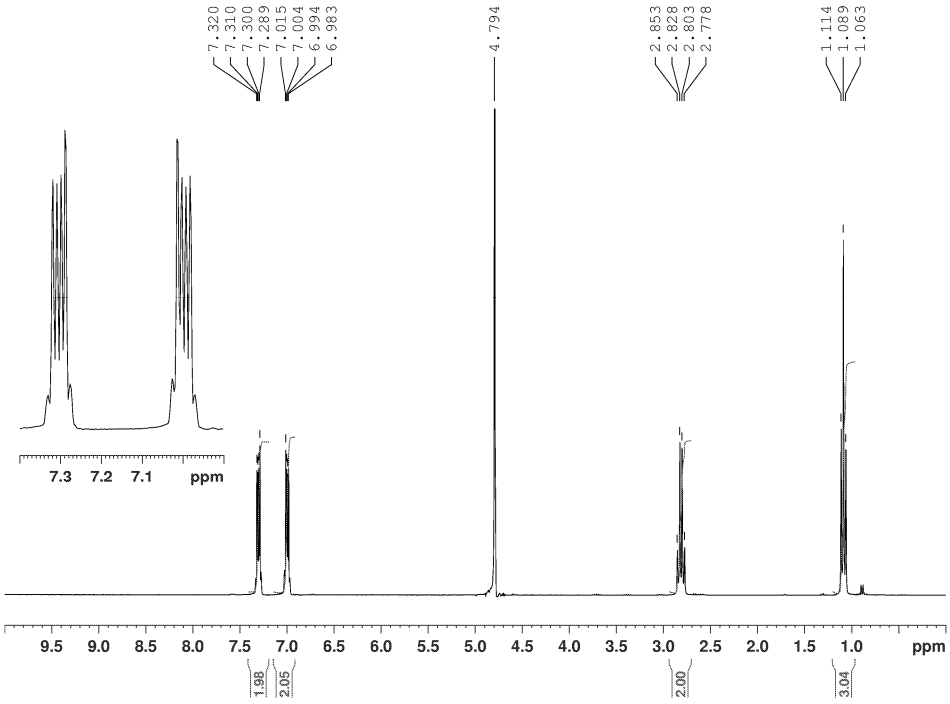

Figure D–37. ^{1}H NMR spectrum of **2.16l** (300 MHz, 1.0 M NaOD in D_2O).

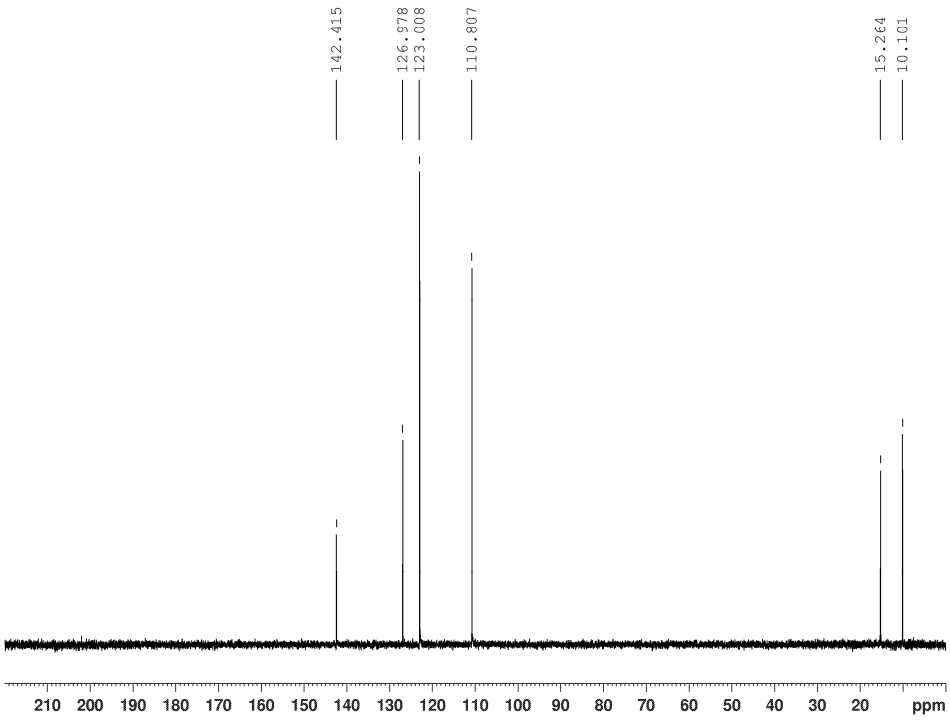

Figure D–38. ^{13}C NMR spectrum of **2.16l** (75 MHz, 1.0 M NaOD in D_2O).

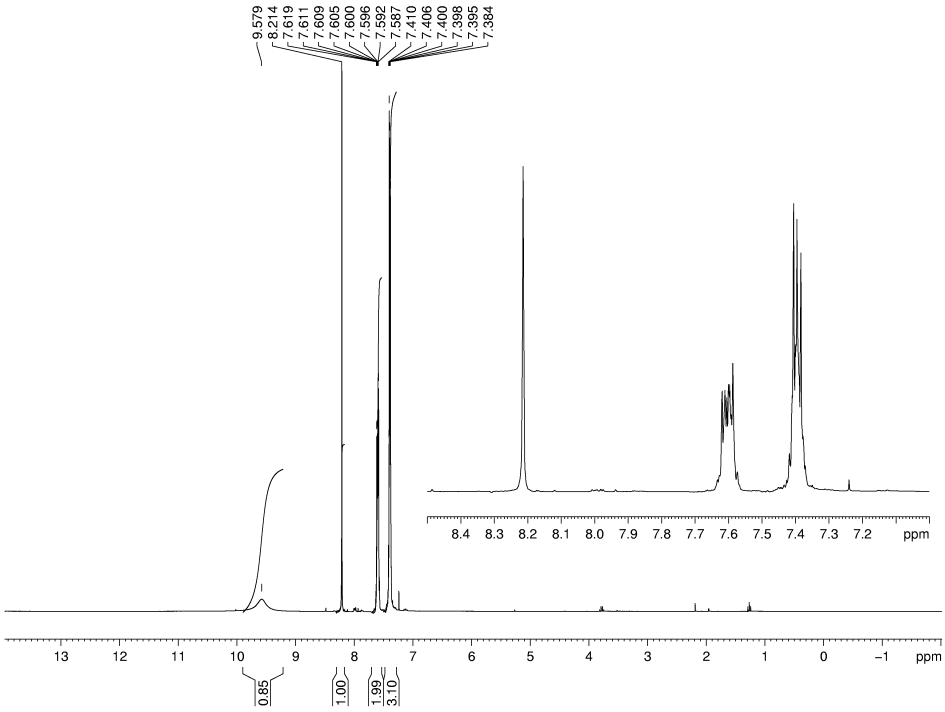

Figure D–39. ^{1}H NMR spectrum of **3.9** (300 MHz, $CDCl_3$).

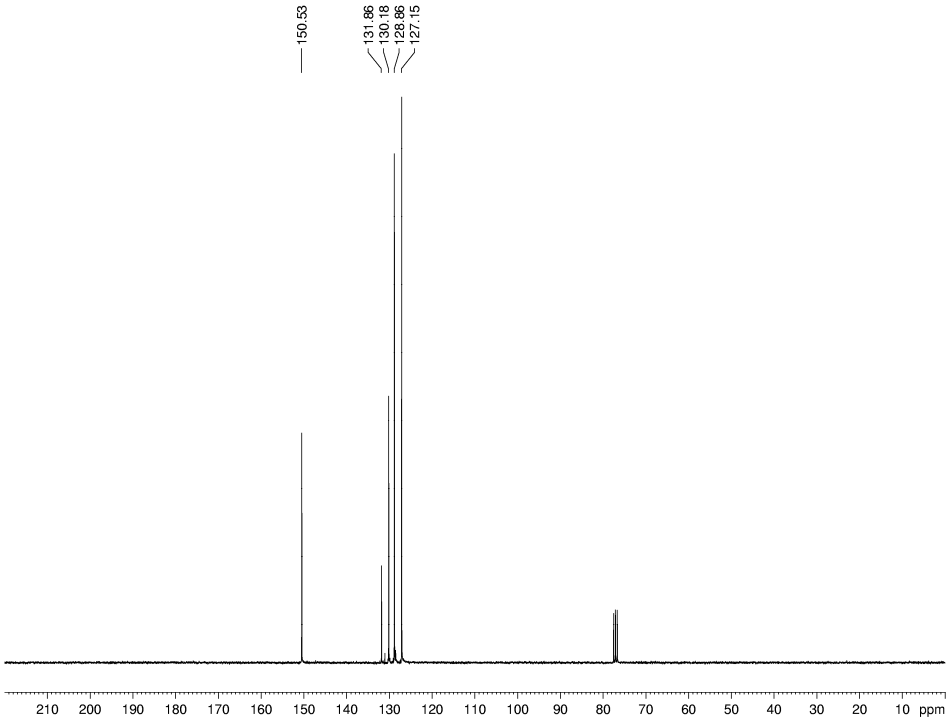

Figure D–40. ^{13}C NMR spectrum of **3.9** (75 MHz, $CDCl_3$).

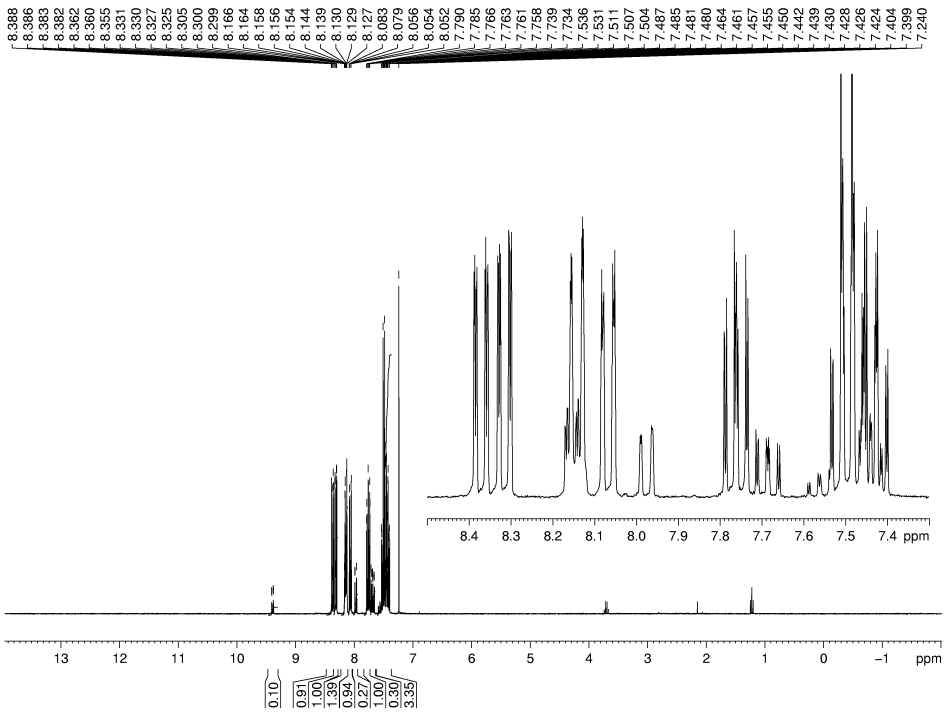

Figure D–41. ^{1}H NMR spectrum of **3.10** (300 MHz, $CDCl_3$).

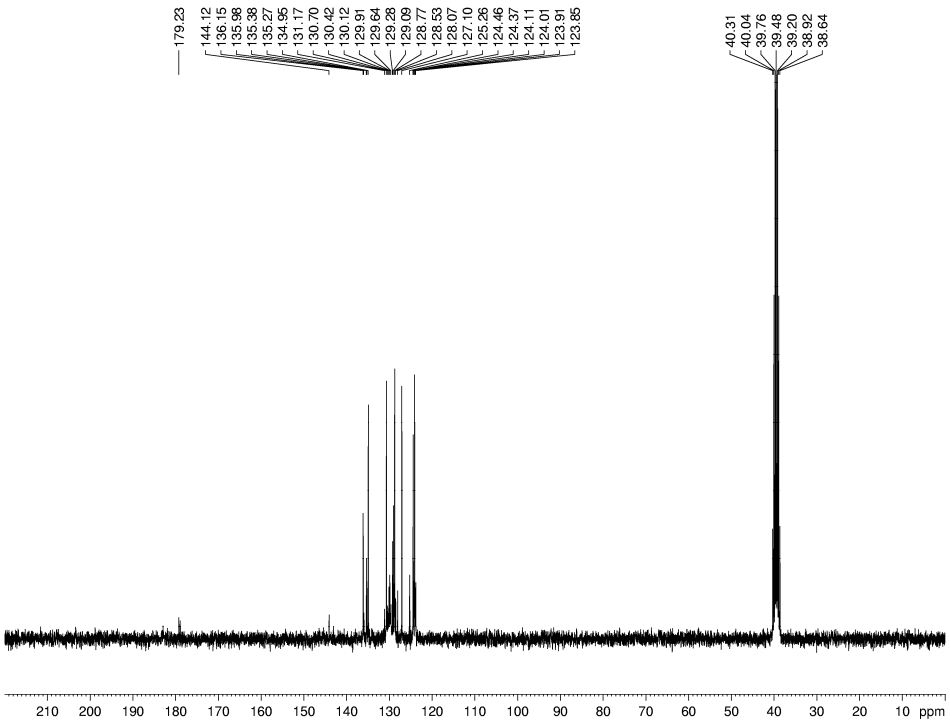

Figure D–42. ^{13}C NMR spectrum of **3.10** (75 MHz, d_6-DMSO).

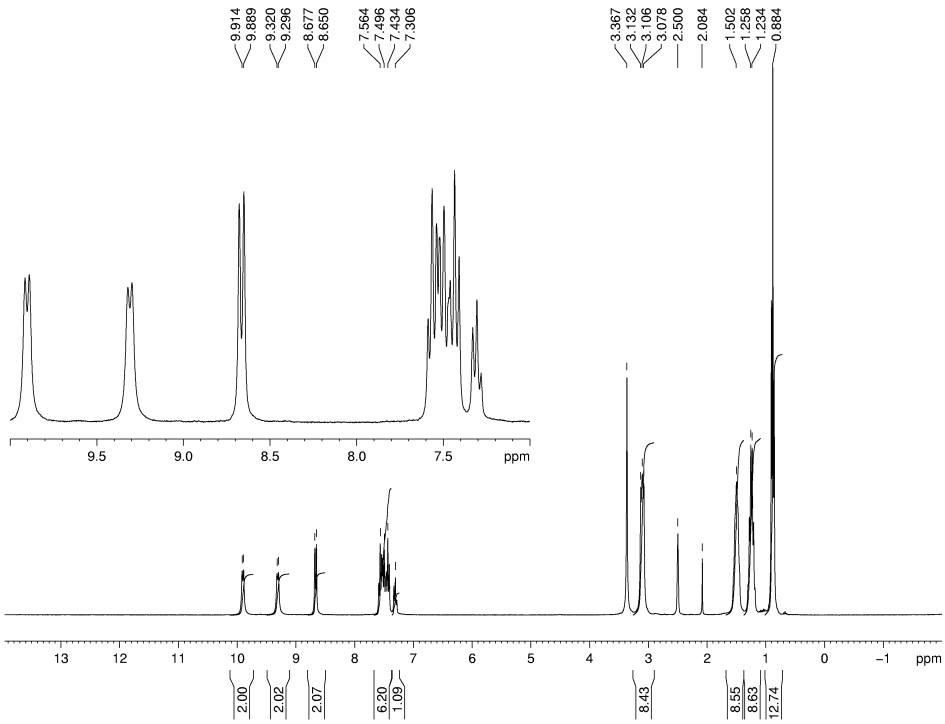

Figure D–43. ^{1}H NMR spectrum of **3.12** (300 MHz, d_6-DMSO).

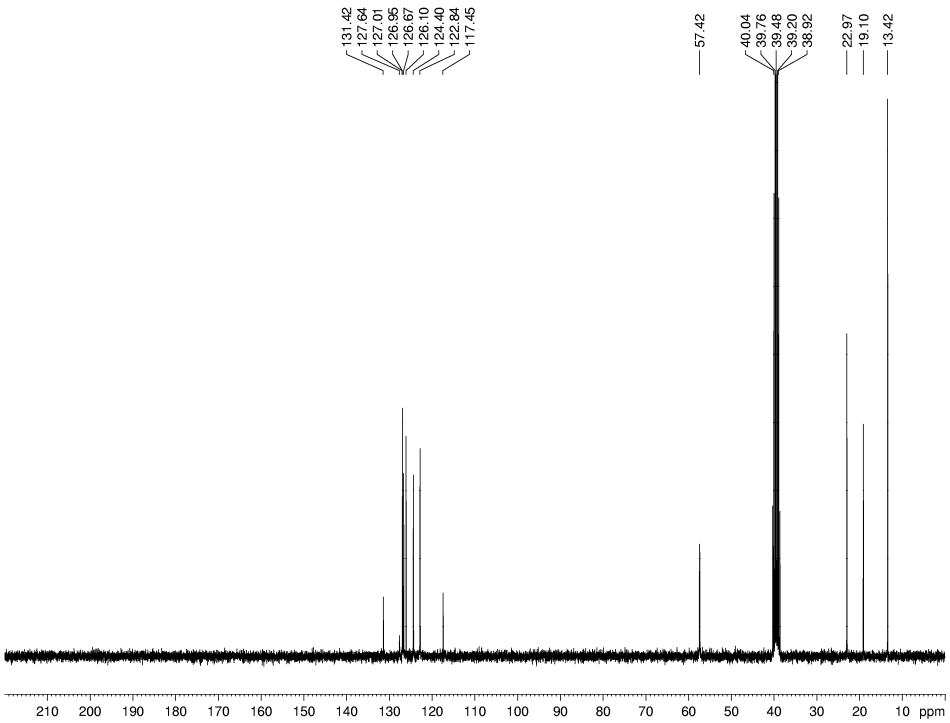

Figure D–44. ^{13}C NMR spectrum of **3.12** (75 MHz, d_6-DMSO).

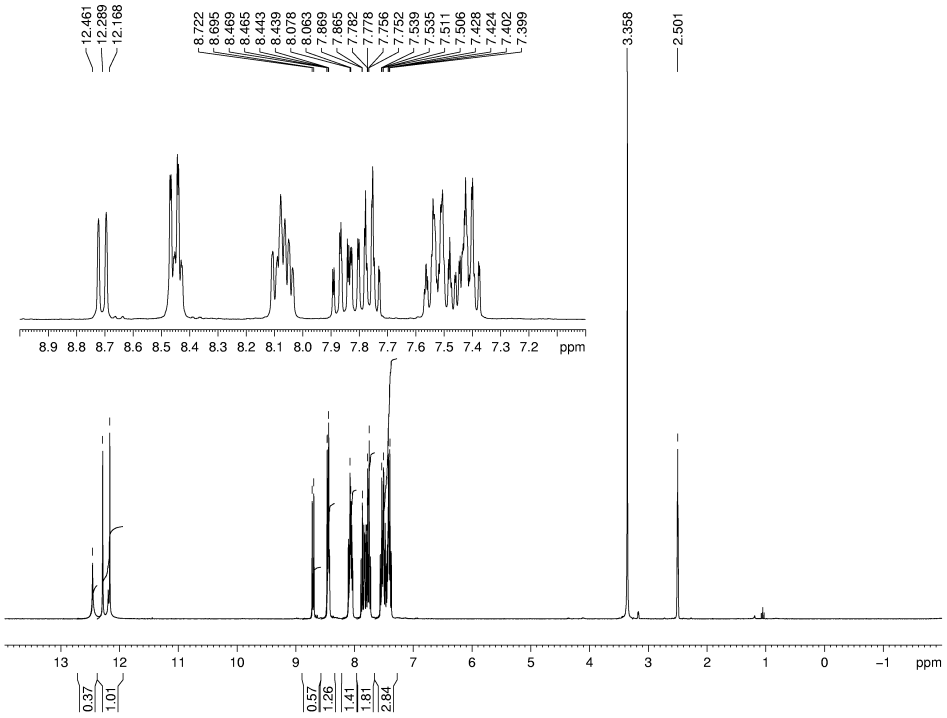

Figure D–45. ^{1}H NMR spectrum of **3.13** (300 MHz, d_6-DMSO).

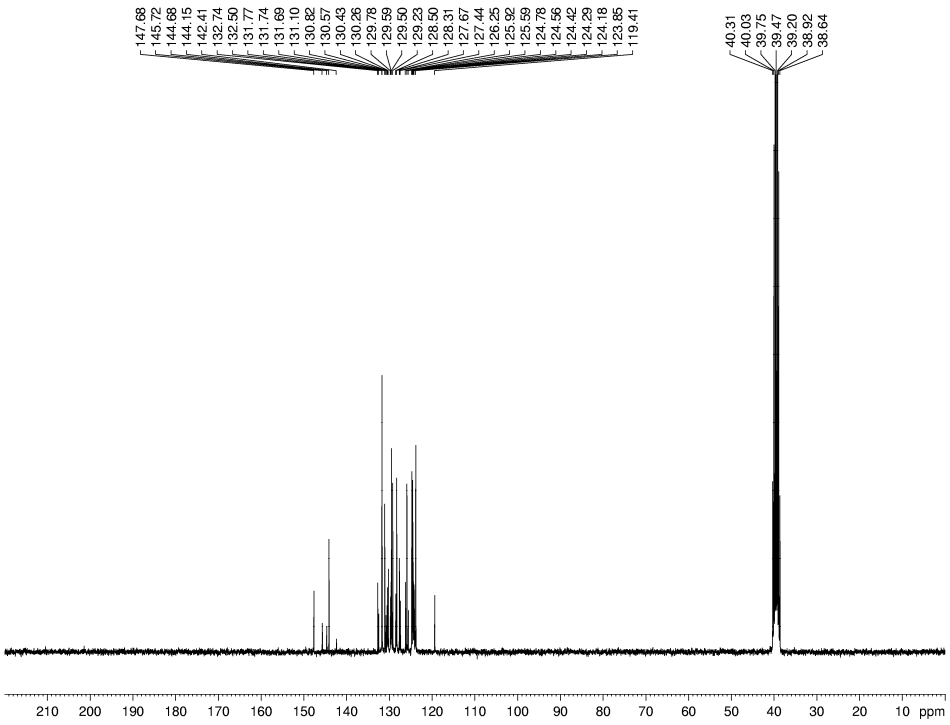

Figure D–46. ^{13}C NMR spectrum of **3.13** (75 MHz, d_6-DMSO).

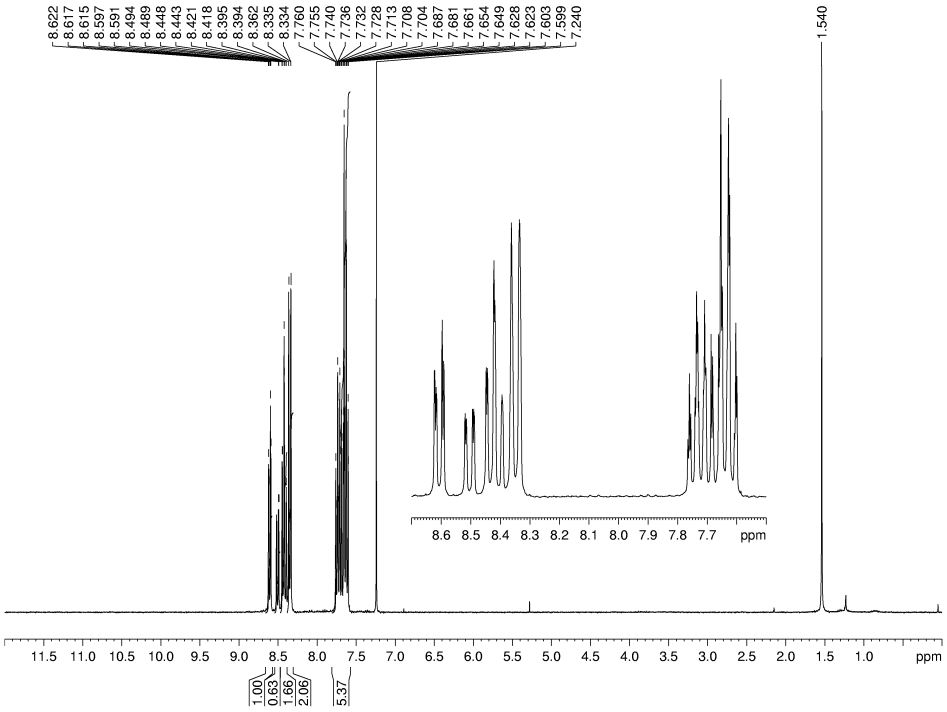

Figure D–47. ^{1}H NMR spectrum of **3.14** (300 MHz, $CDCl_3$).

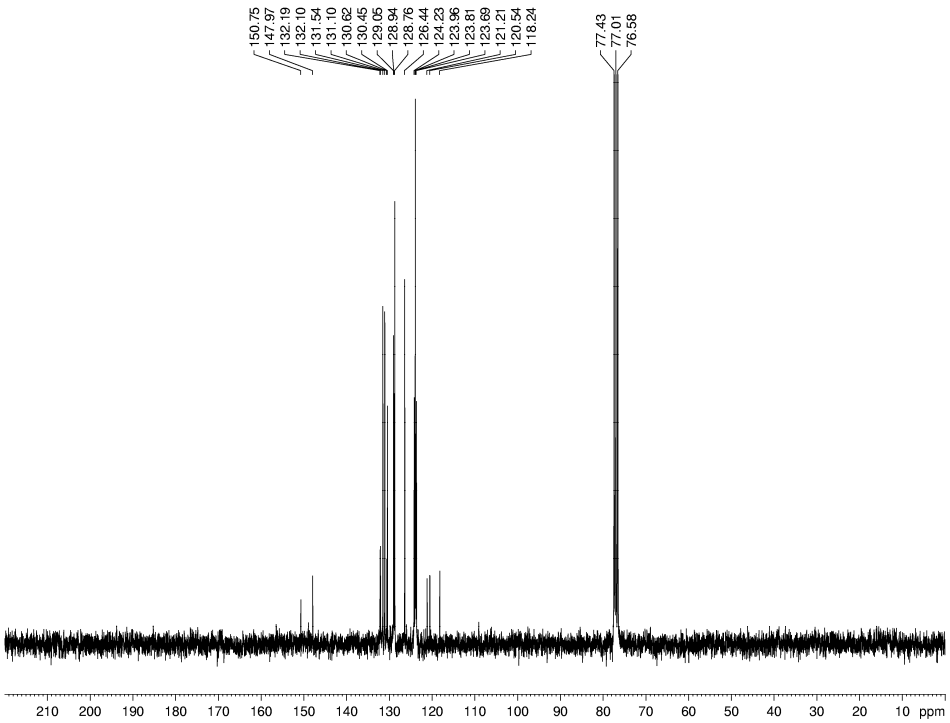

Figure D–48. ^{13}C NMR spectrum of **3.14** (75 MHz, $CDCl_3$).

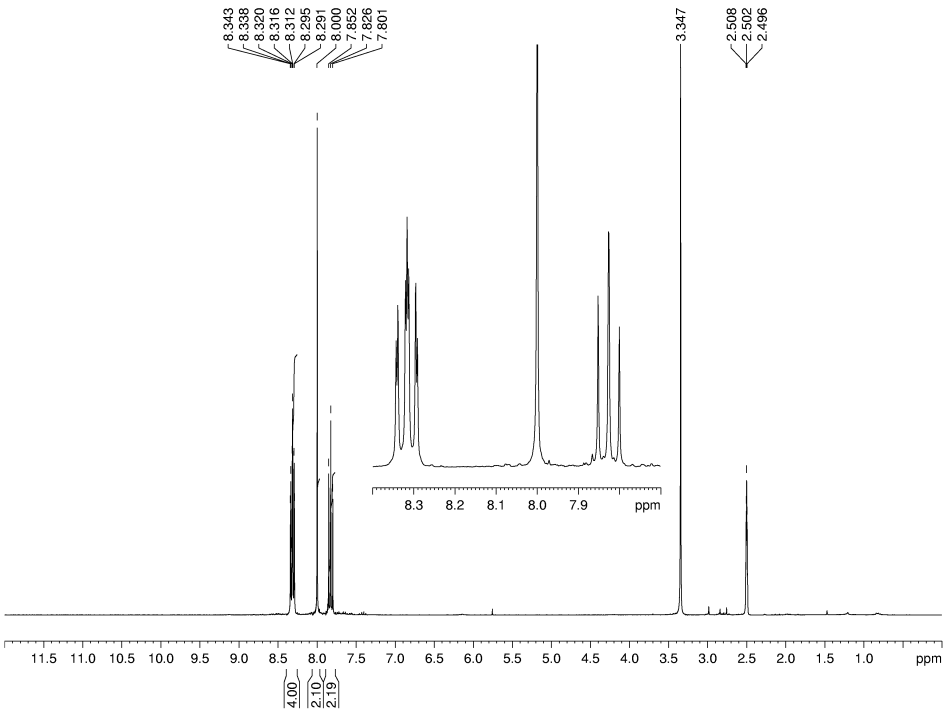

Figure D–49. ^{1}H NMR spectrum of **3.16** (300 MHz, d_6-DMSO).

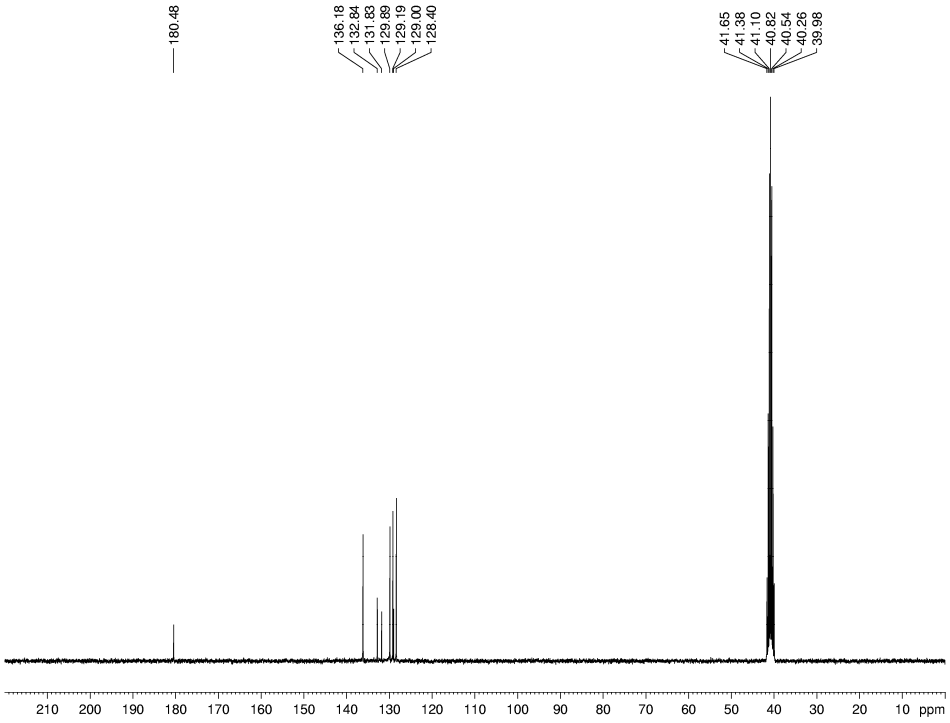

Figure D–50. ^{13}C NMR spectrum of **3.16** (75 MHz, d_6-DMSO).

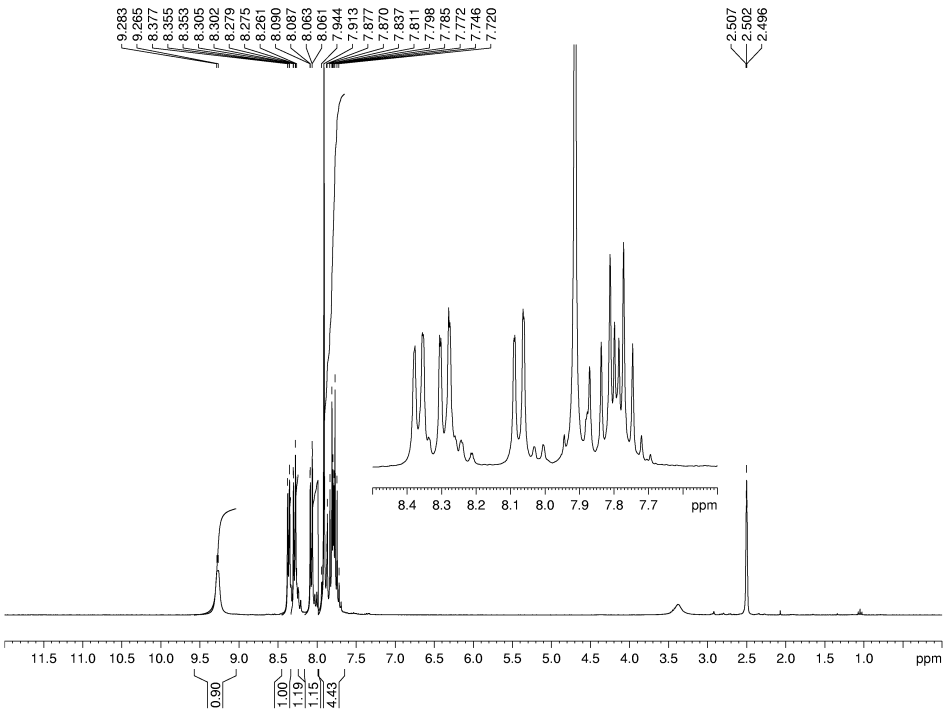

Figure D–51. ^{1}H NMR spectrum of **3.17** (300 MHz, d_6-DMSO).

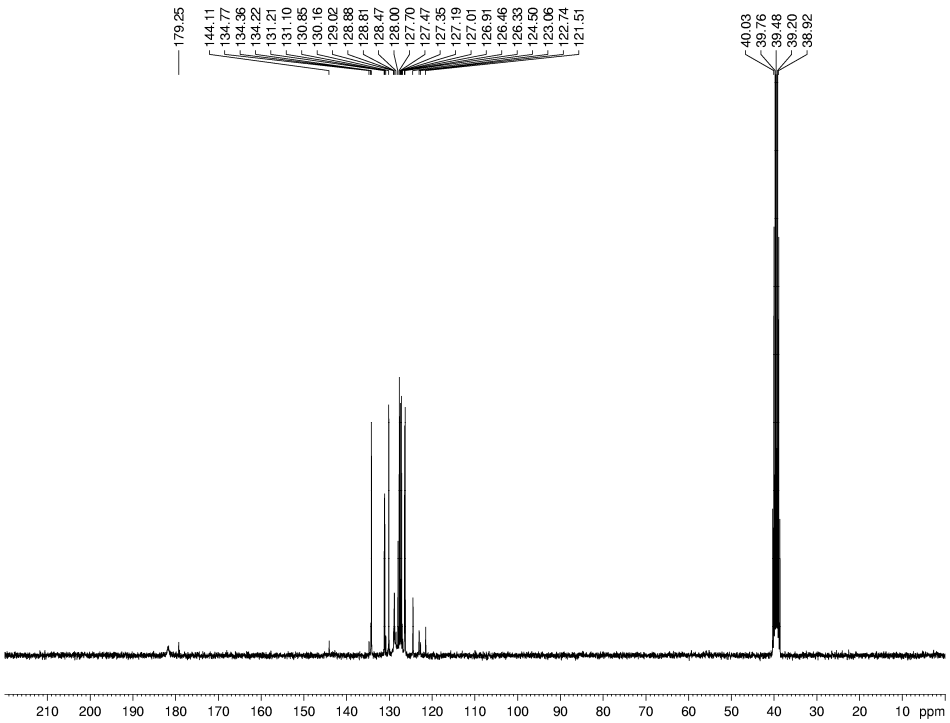

Figure D–52. ^{13}C NMR spectrum of **3.17** (75 MHz, d_6-DMSO).

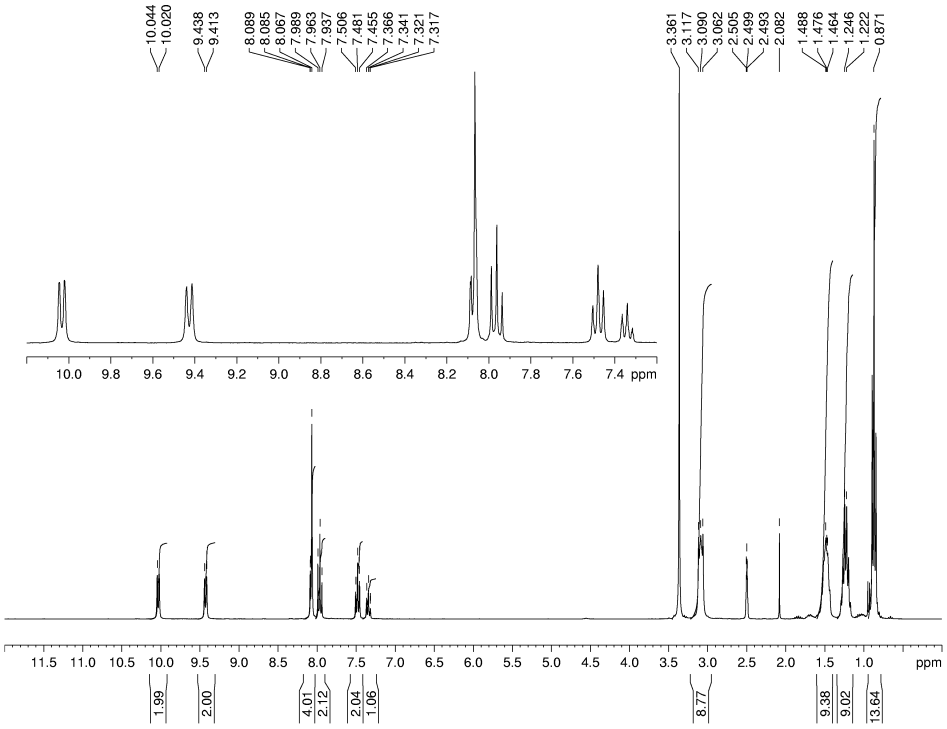

Figure D–53. ^{1}H NMR spectrum of **3.19** (300 MHz, d_6-DMSO).

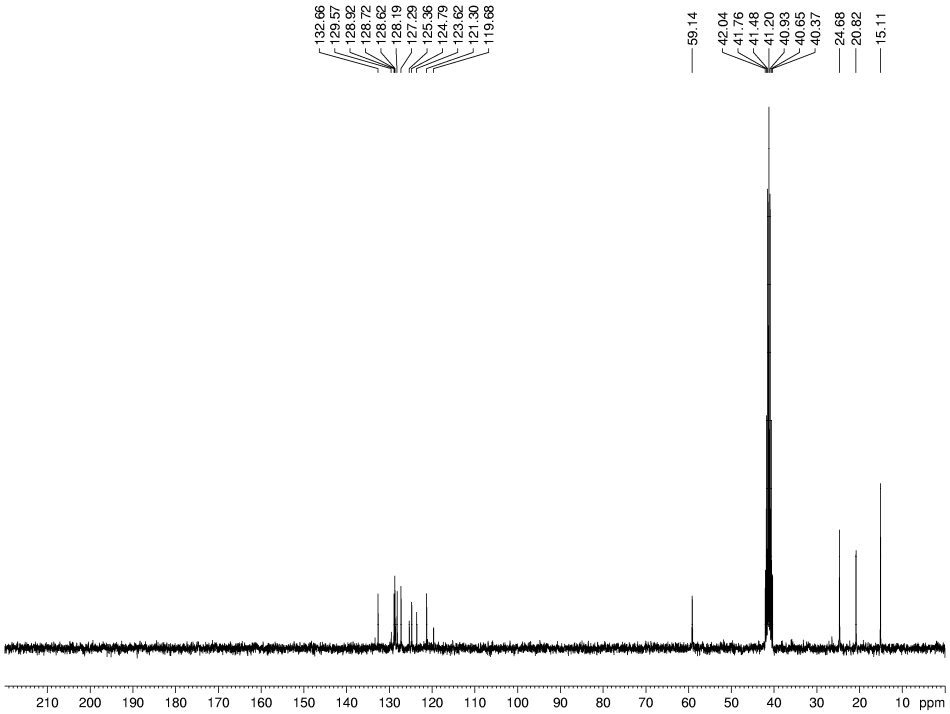

Figure D–54. ^{13}C NMR spectrum of **3.19** (75 MHz, d_6-DMSO).

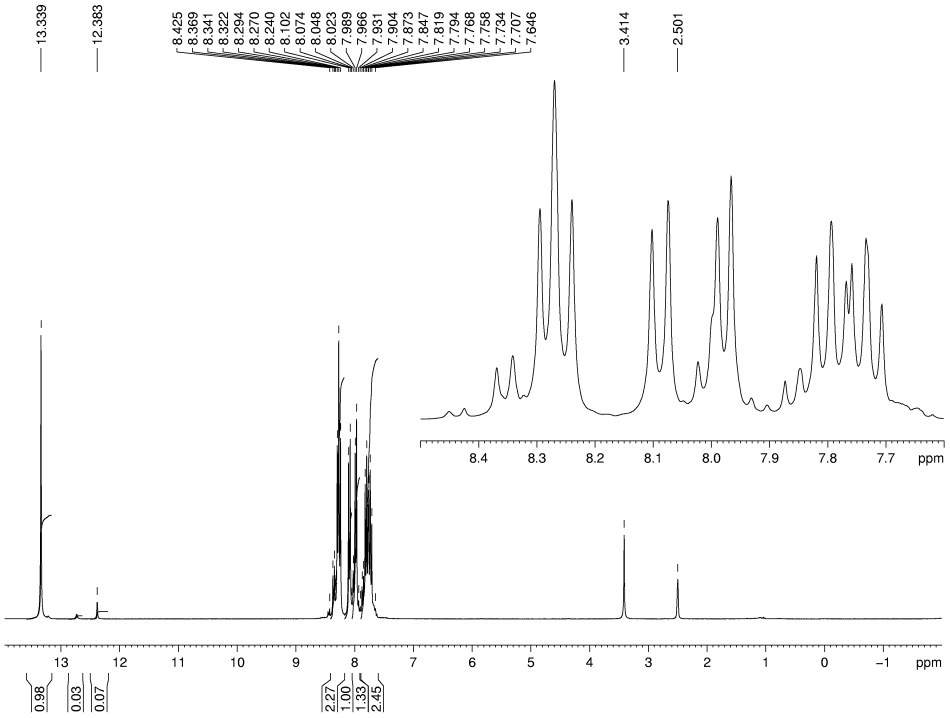

Figure D–55. ^{1}H NMR spectrum of **3.20** (300 MHz, d_6-DMSO).

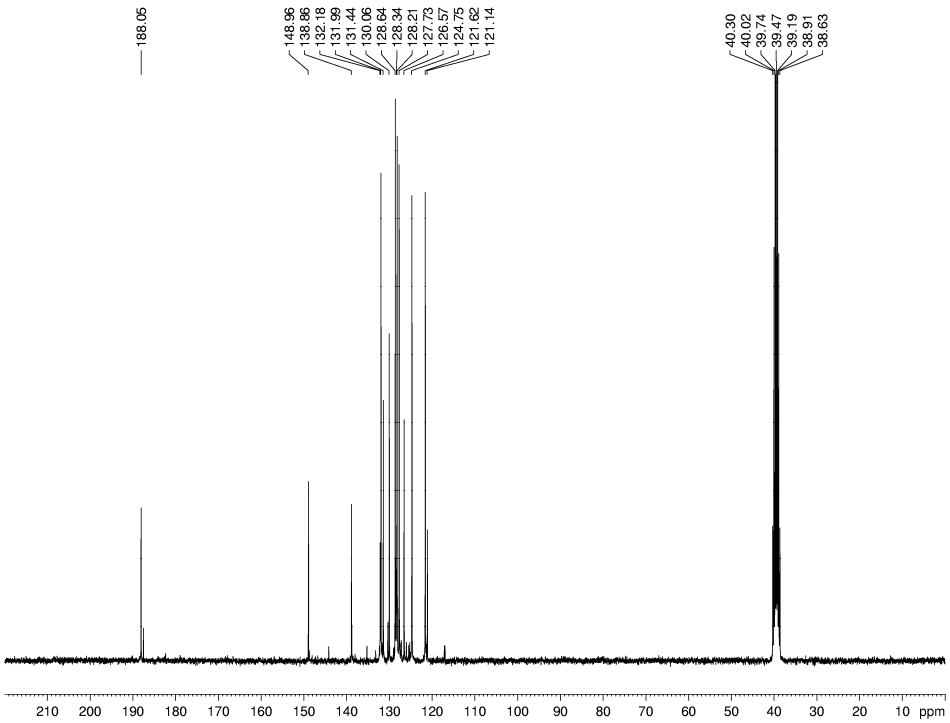

Figure D–56. ^{13}C NMR spectrum of **3.20** (75 MHz, d_6-DMSO).

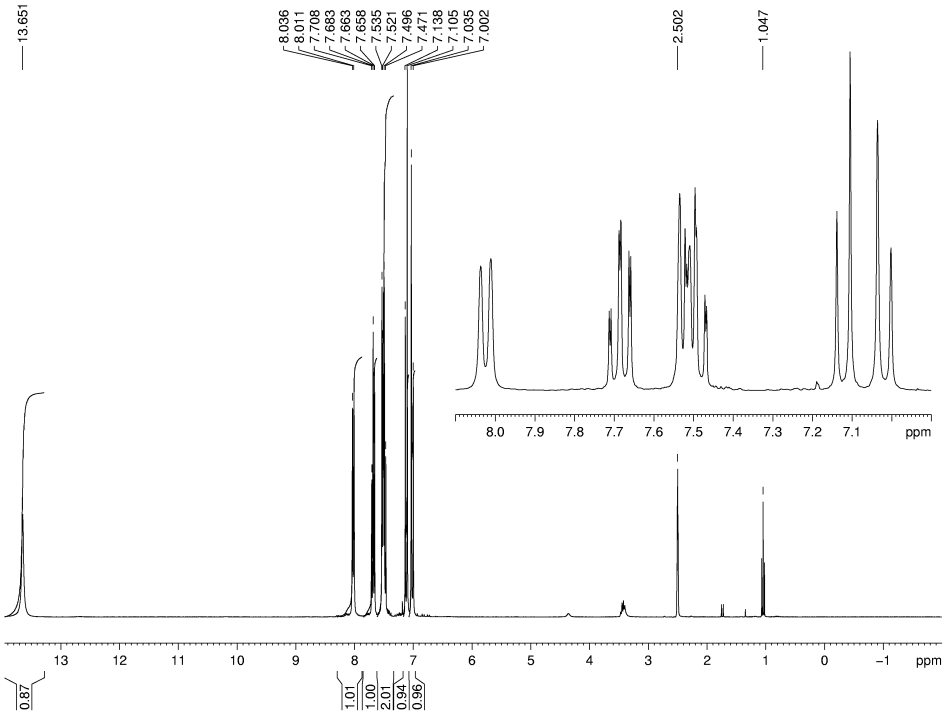

Figure D–57. ^{1}H NMR spectrum of **3.23** (300 MHz, d_6-DMSO).

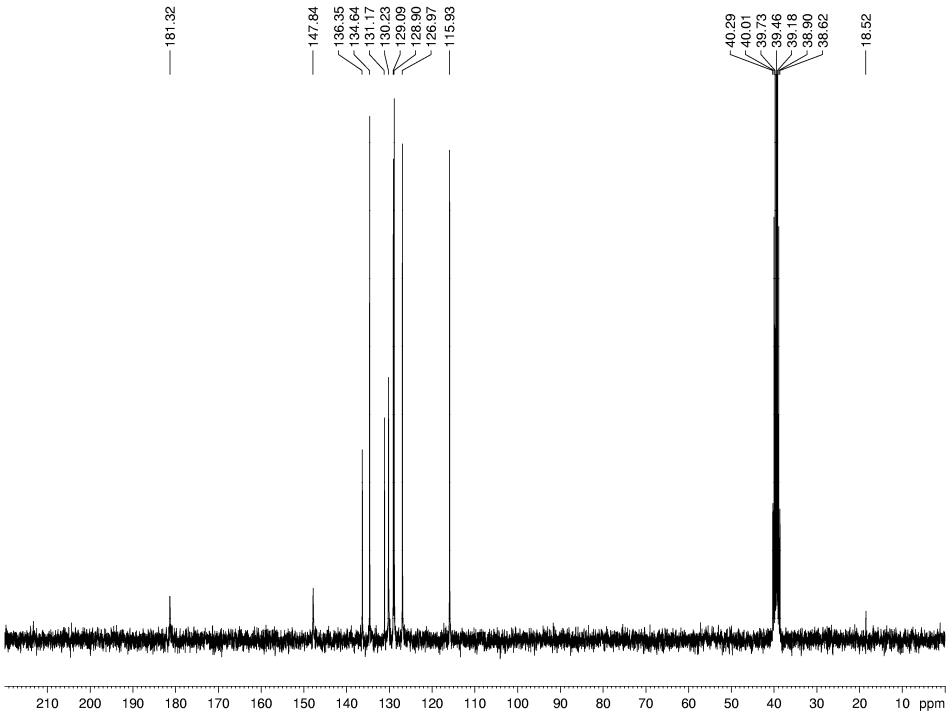

Figure D–58. ^{13}C NMR spectrum of **3.23** (75 MHz, d_6-DMSO).

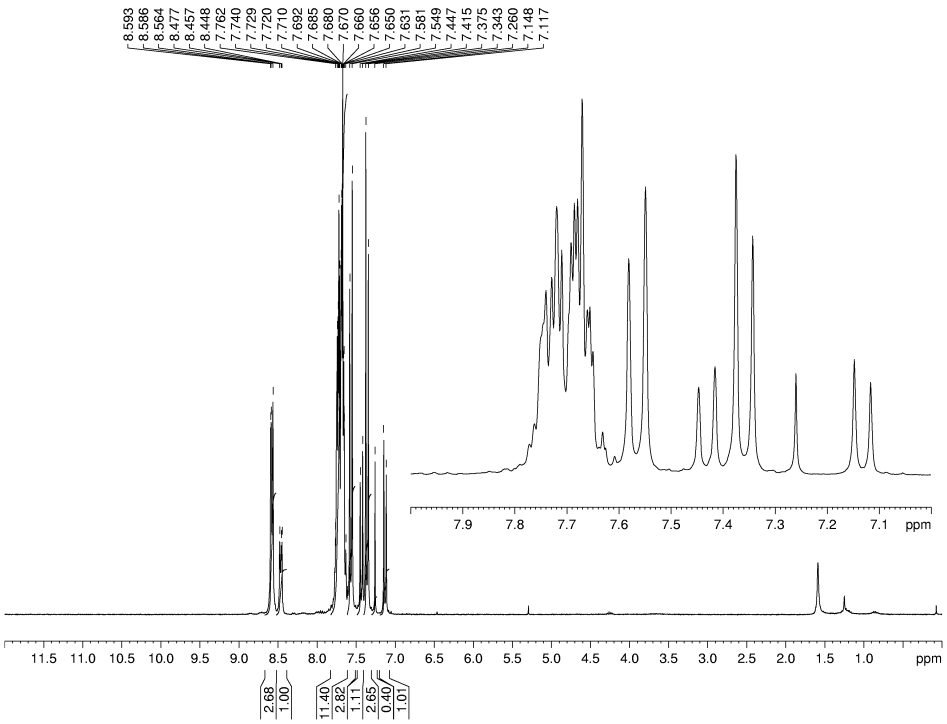

Figure D–59. ^{1}H NMR spectrum of **3.24** (300 MHz, $CDCl_3$).

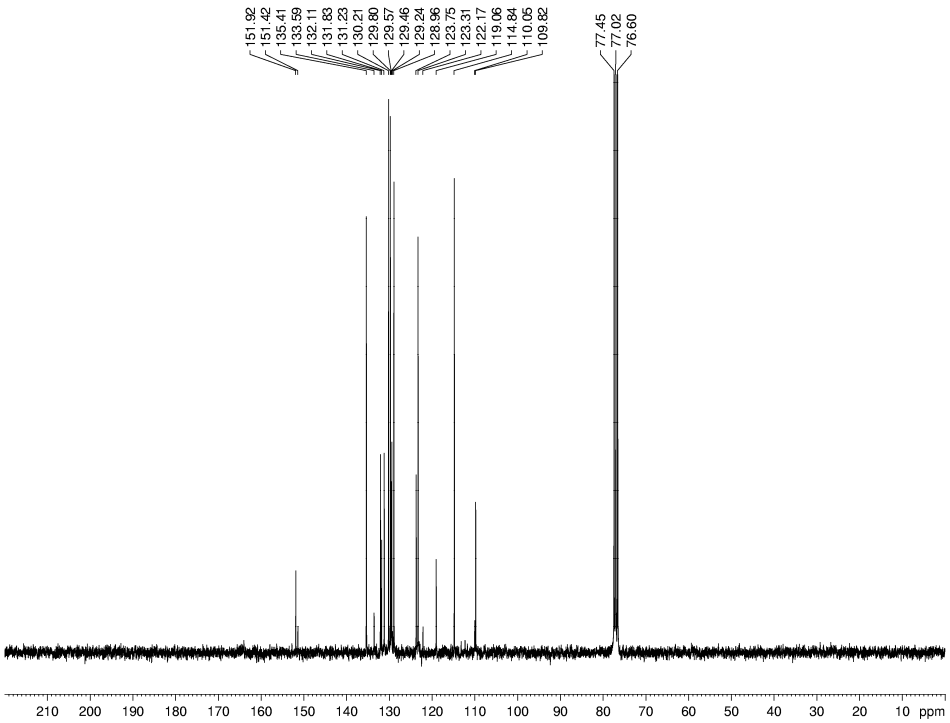

Figure D–60. ^{13}C NMR spectrum of **3.24** (75 MHz, $CDCl_3$).

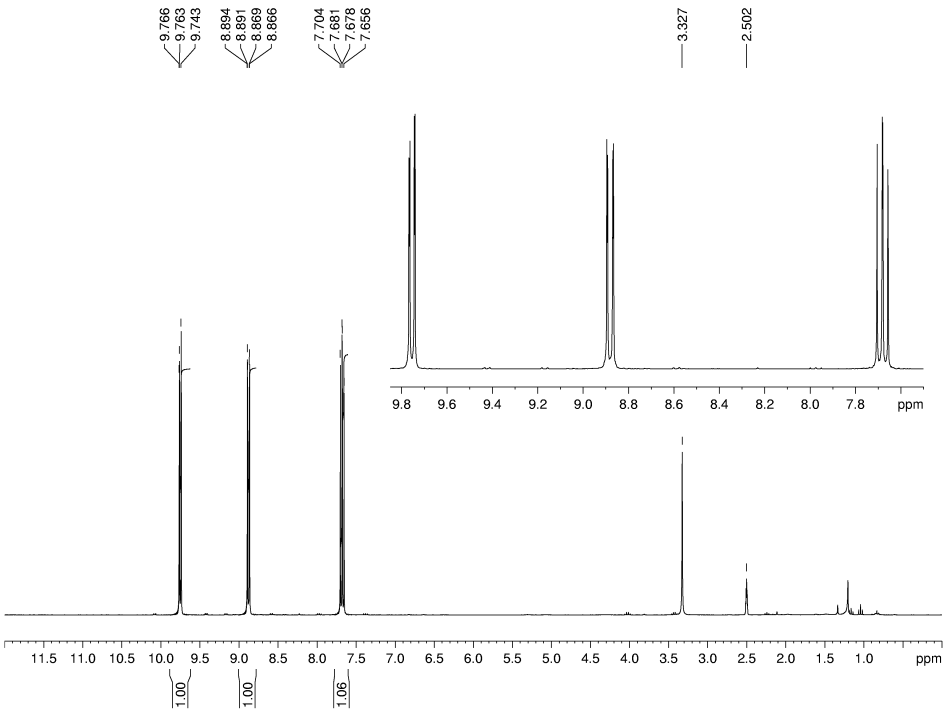

Figure D–61. ^{1}H NMR spectrum of **3.26** (300 MHz, d_6-DMSO).

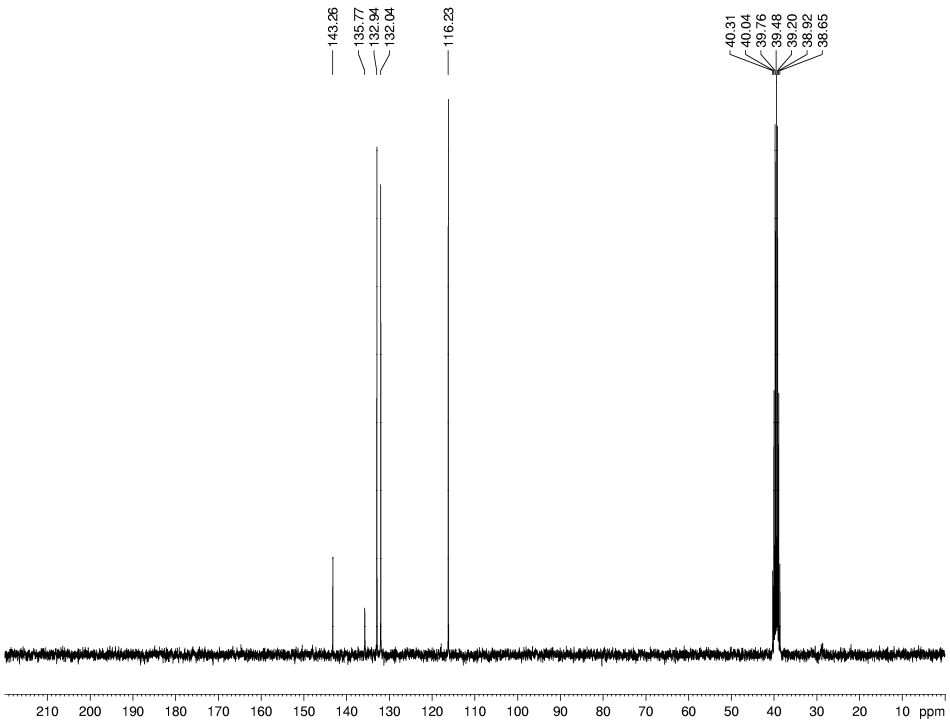

Figure D–62. ^{13}C NMR spectrum of **3.26** (75 MHz, d_6-DMSO).

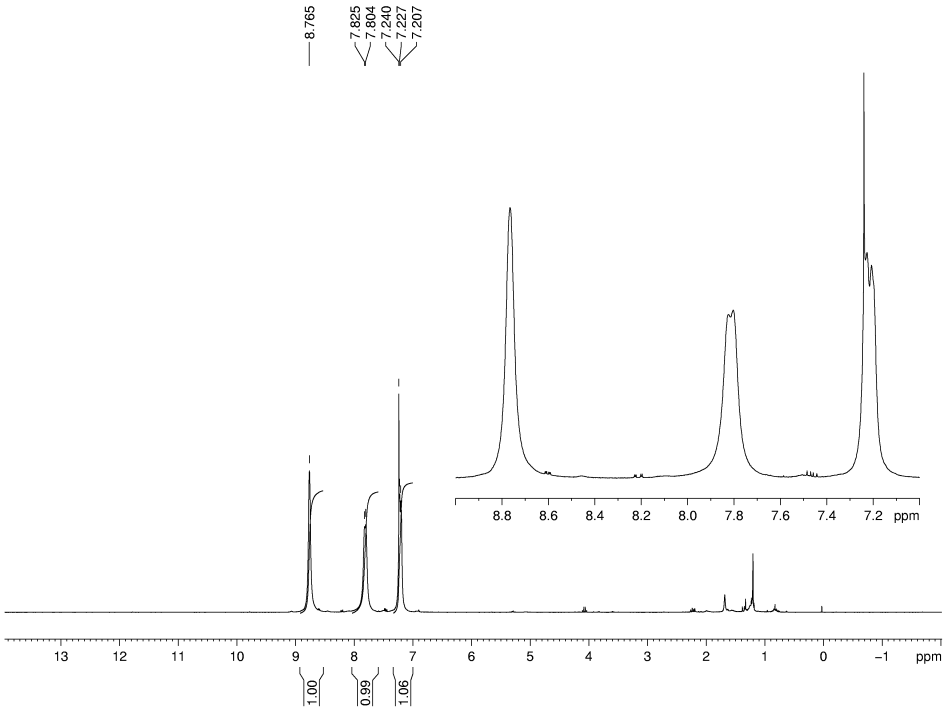

Figure D–63. ^{1}H NMR spectrum of **3.27** (300 MHz, $CDCl_3$).

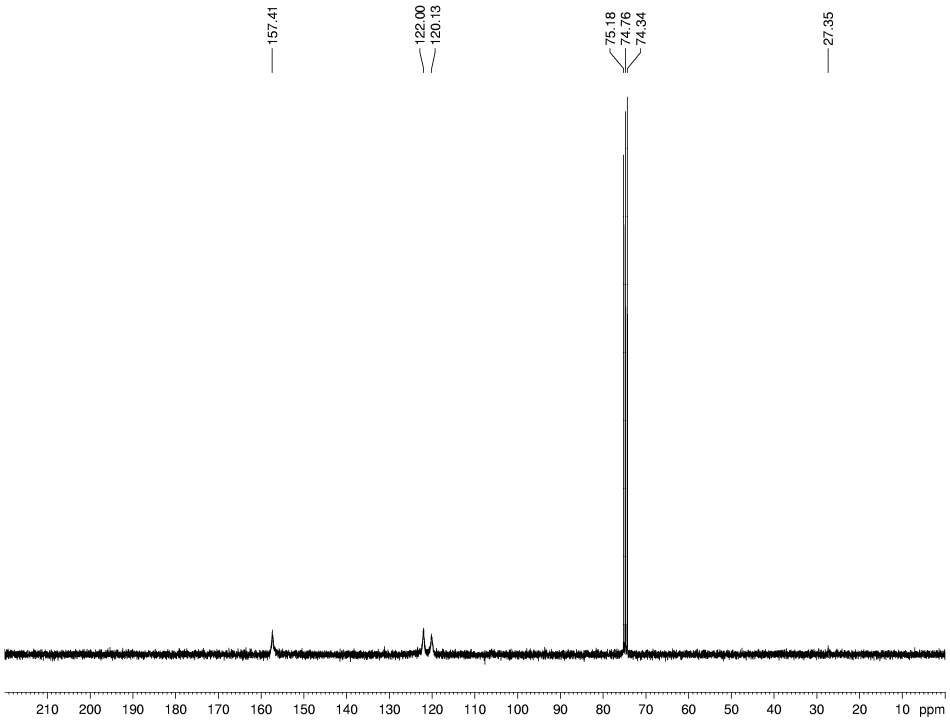

Figure D–64. ^{13}C NMR spectrum of **3.27** (75 MHz, $CDCl_3$).

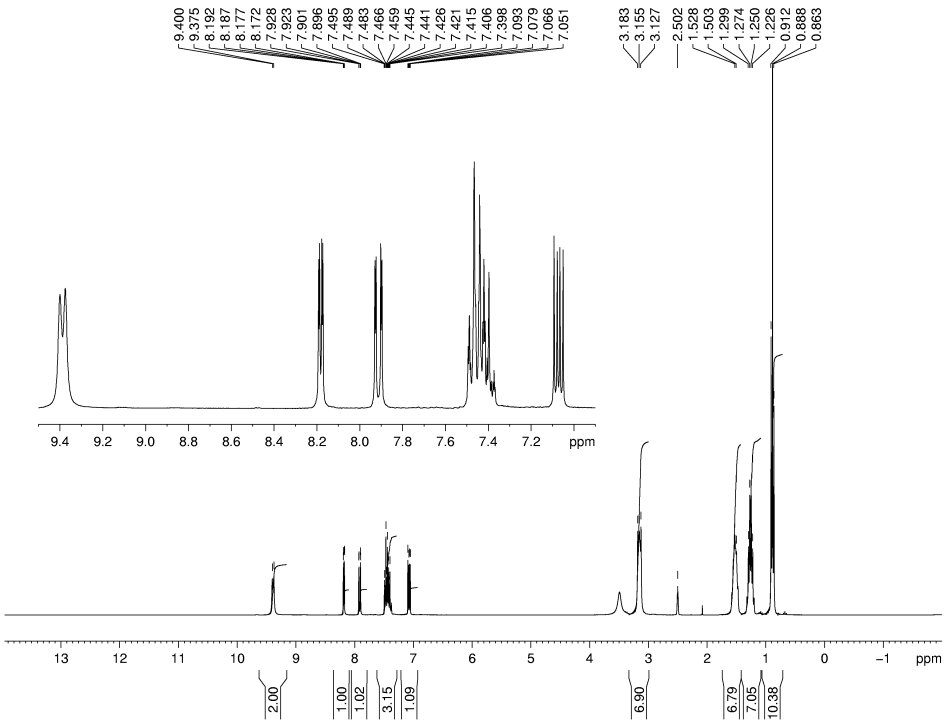

Figure D–65. ^{1}H NMR spectrum of **3.29** (300 MHz, d_6-DMSO).

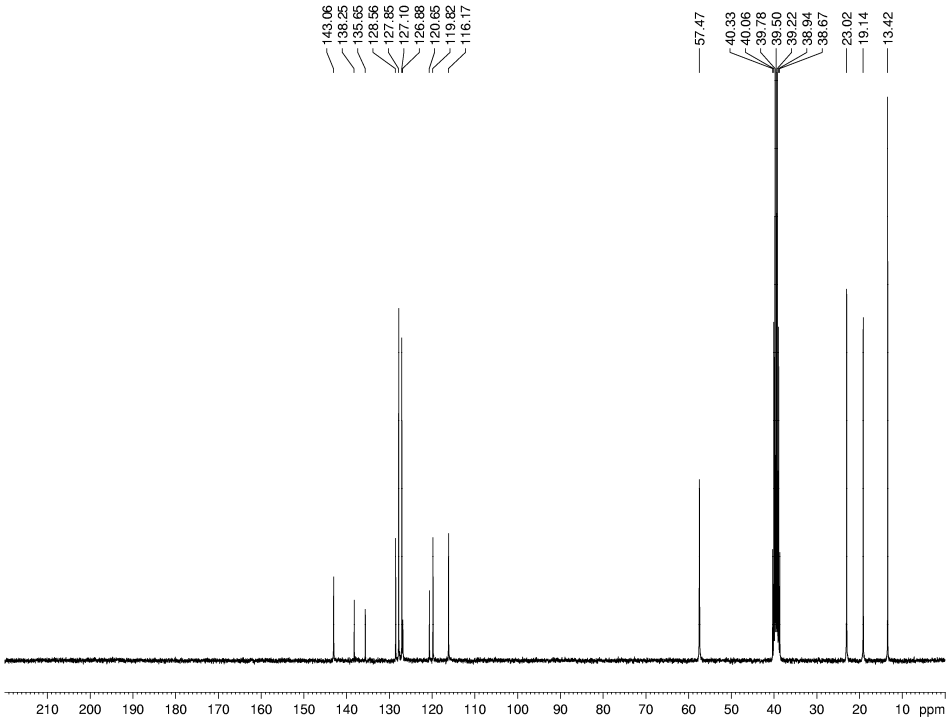

Figure D–66. ^{13}C NMR spectrum of **3.29** (75 MHz, d_6-DMSO).

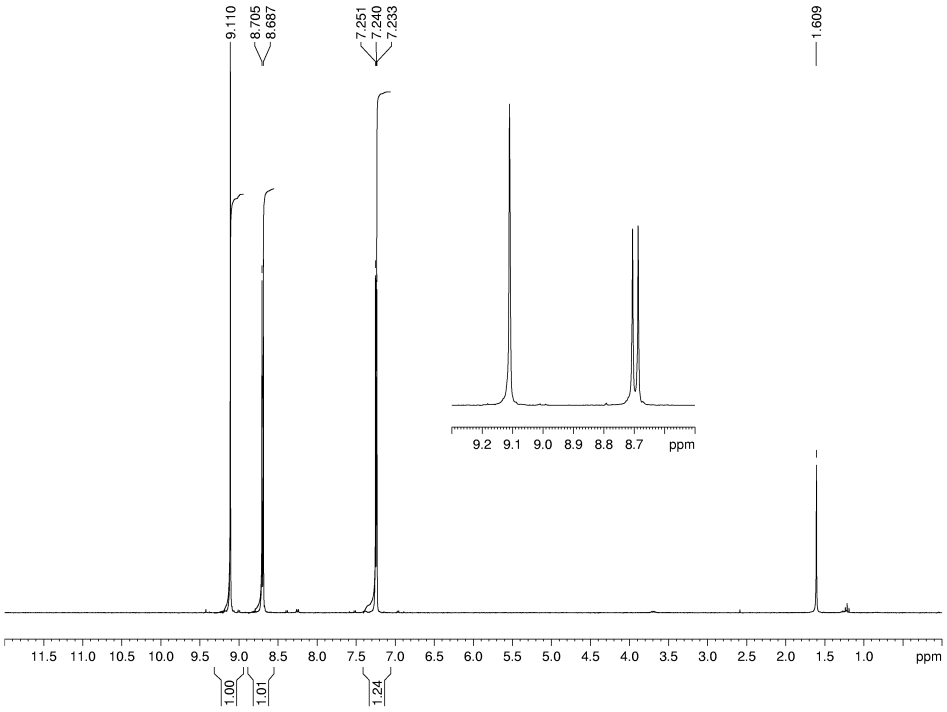

Figure D–67. ^{1}H NMR spectrum of **3.30** (300 MHz, $CDCl_3$).

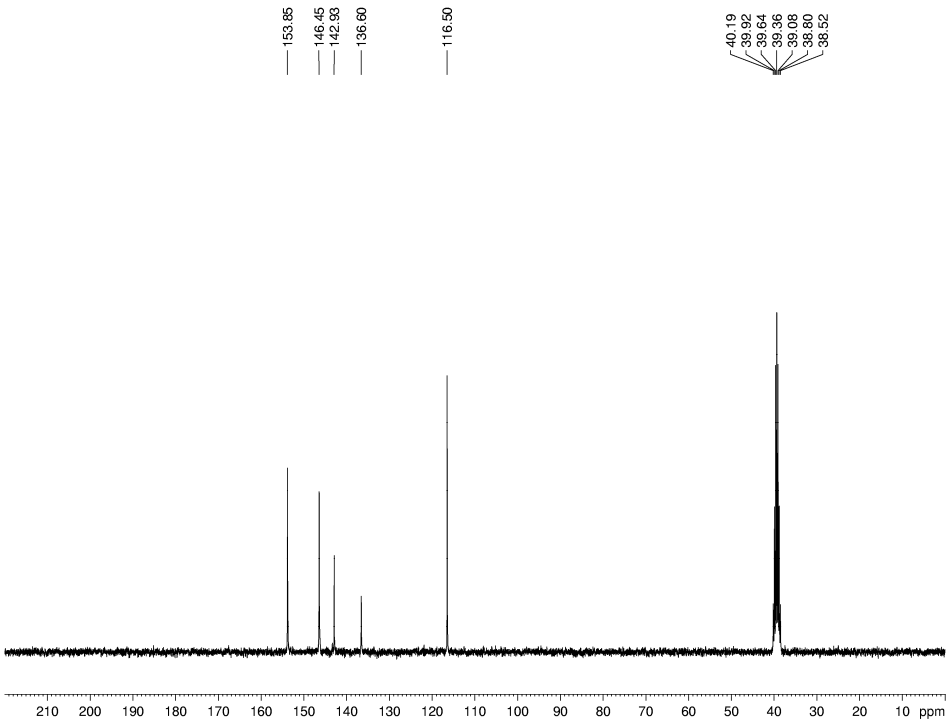

Figure D–68. ^{13}C NMR spectrum of **3.30** (75 MHz, d_6-DMSO).

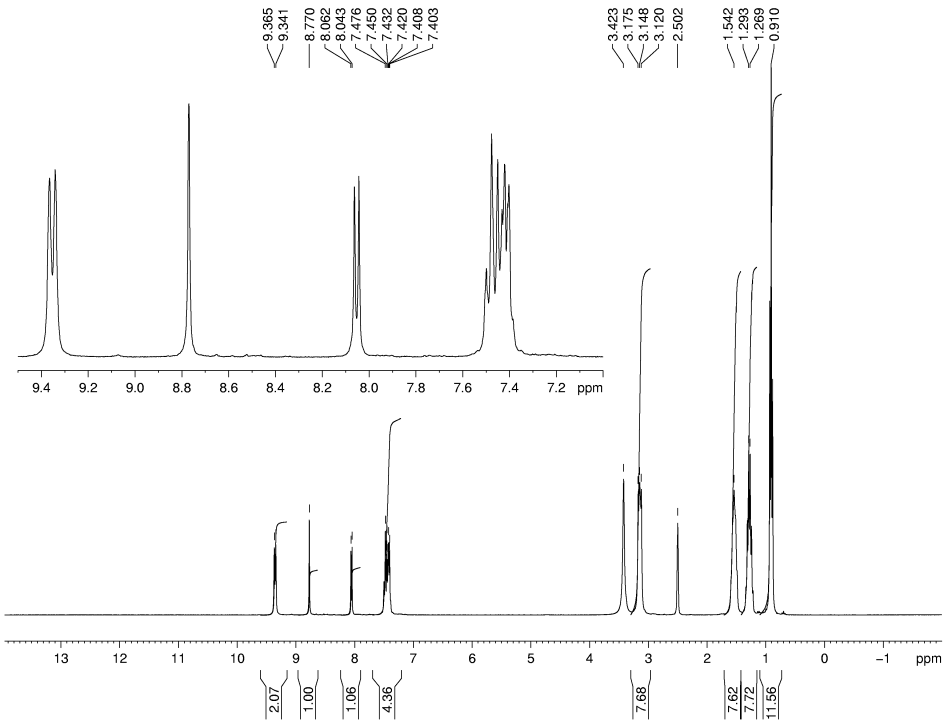

Figure D–69. ^{1}H NMR spectrum of **3.32** (300 MHz, d_6-DMSO).

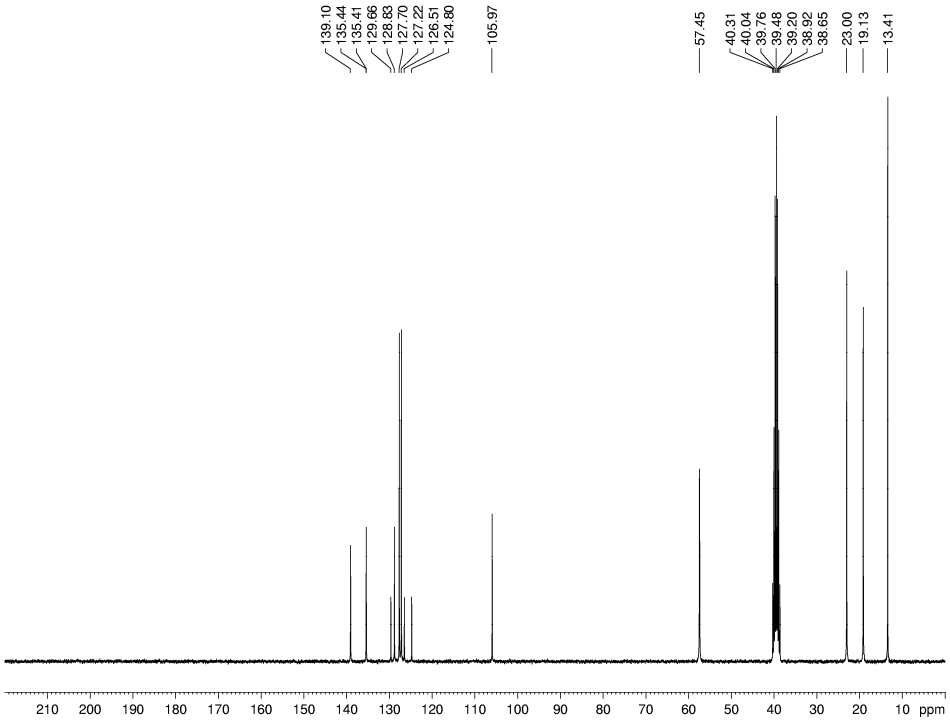

Figure D–70. ^{13}C NMR spectrum of **3.32** (75 MHz, d_6-DMSO).

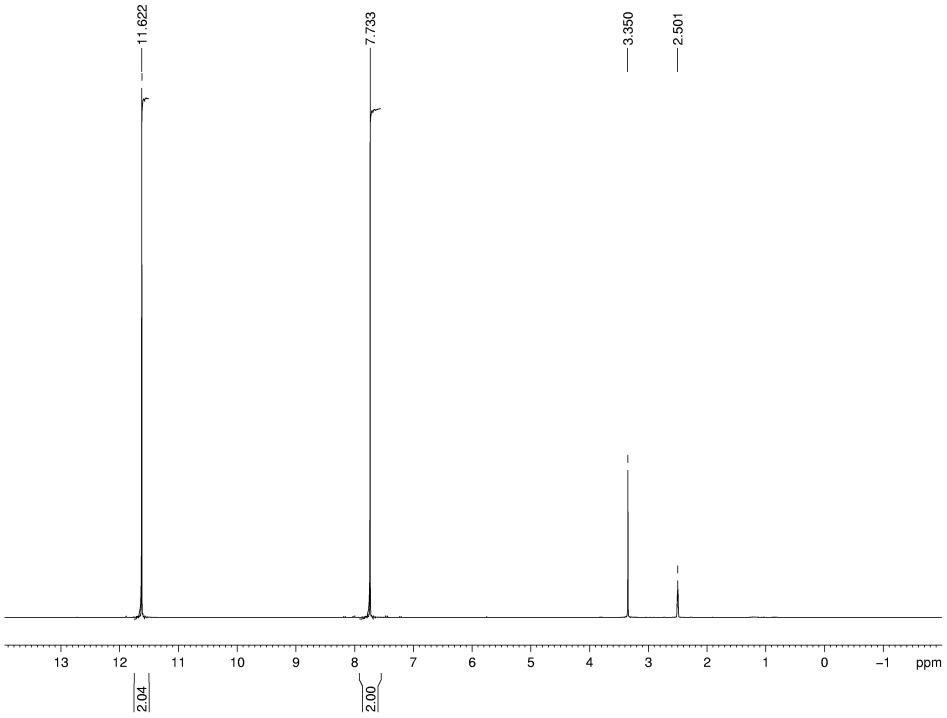

Figure D–71. ^{1}H NMR spectrum of **3.33** (300 MHz, d_6-DMSO).

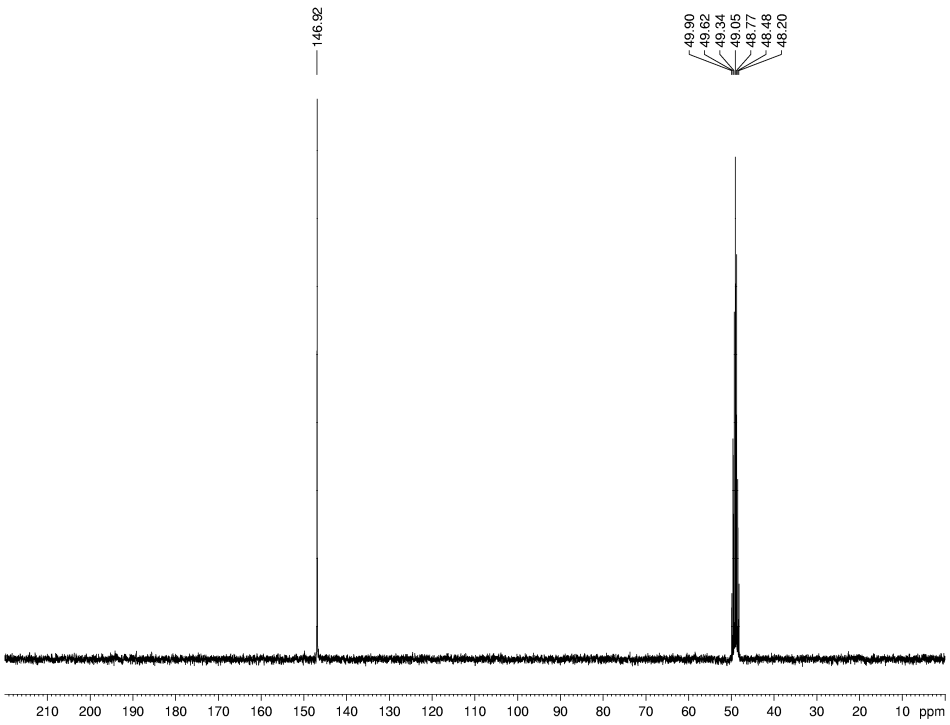

Figure D–72. ^{13}C NMR spectrum of **3.33** (75 MHz, MeOD).

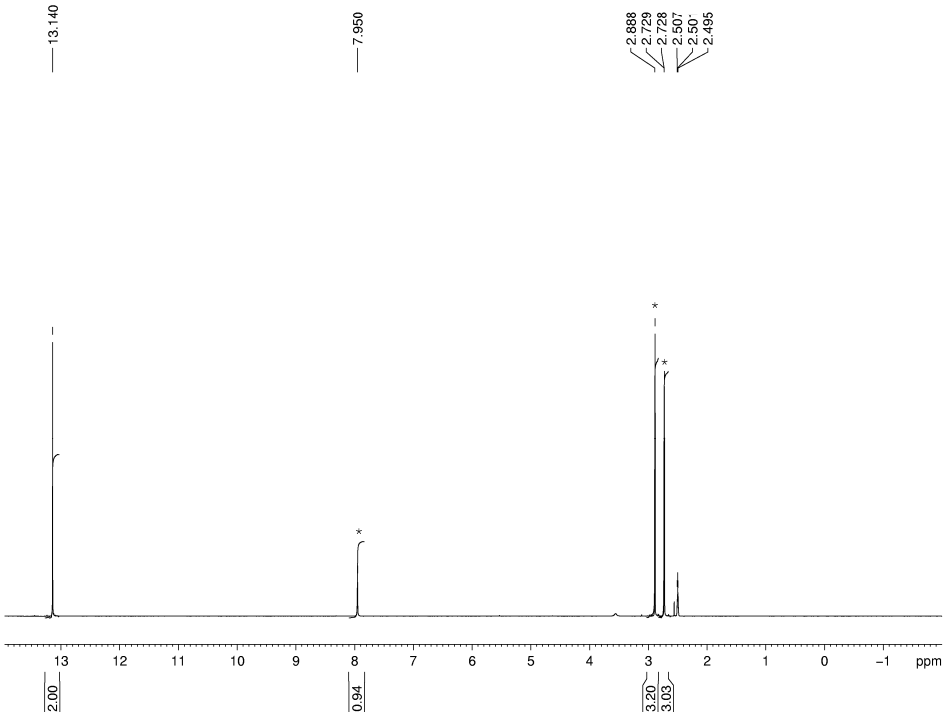

Figure D–73. ^{1}H NMR spectrum of **3.34** (300 MHz, d_6-DMSO). Asterisk indicates peaks due to DMF.

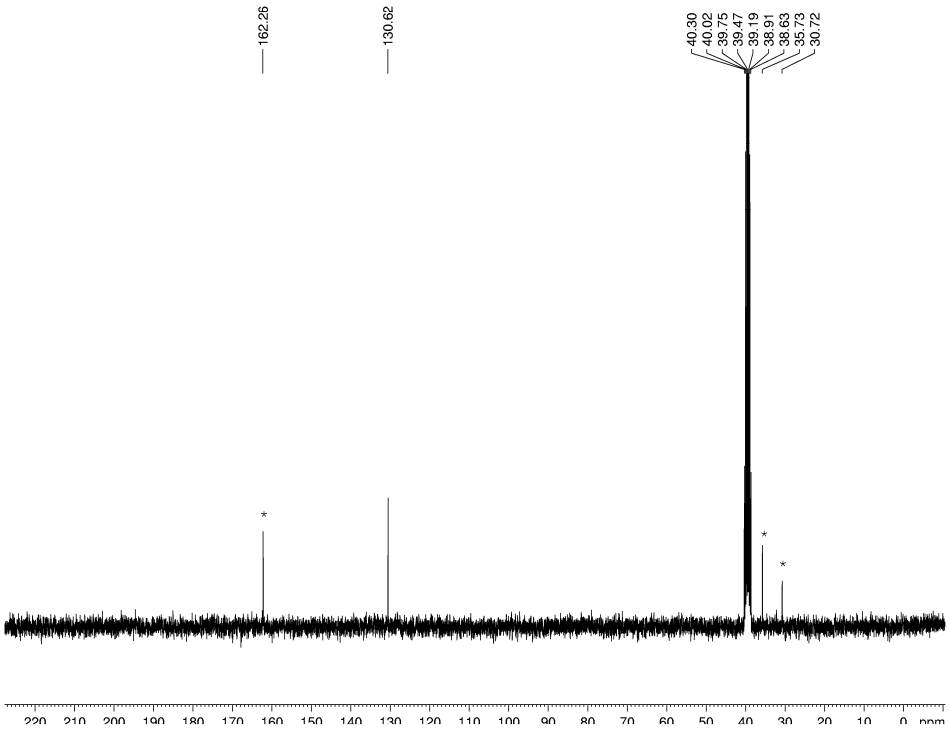

Figure D–74. ^{13}C NMR spectrum of **3.34** (75 MHz, d_6-DMSO). Asterisk indicates peaks due to DMF.

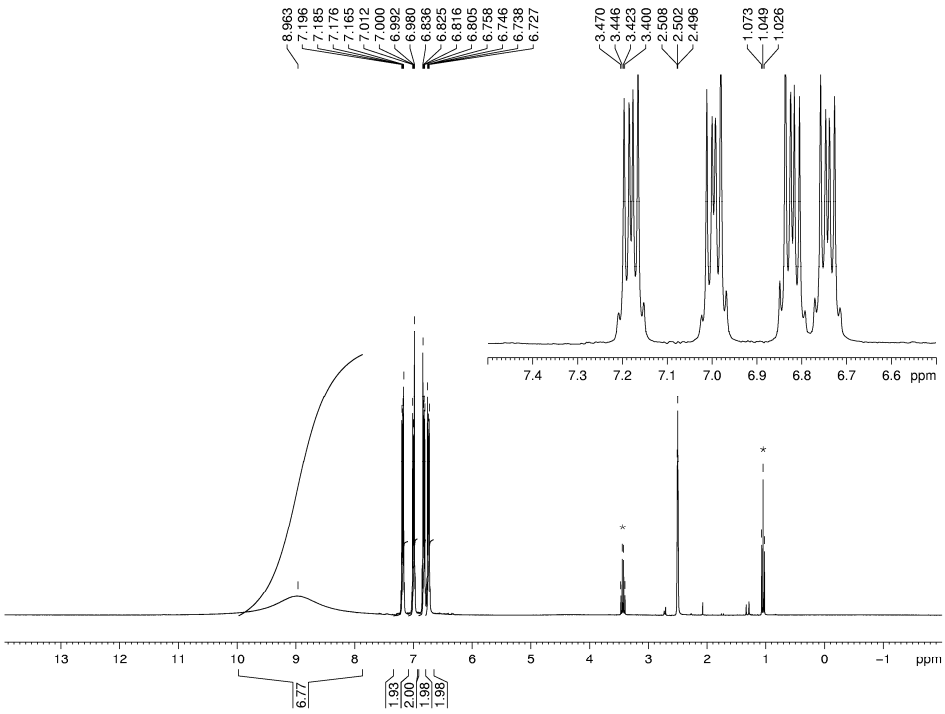

Figure D–75. ^{1}H NMR spectrum of **3.35** (300 MHz, d_6-DMSO). Asterisk indicates peaks due to EtOH.

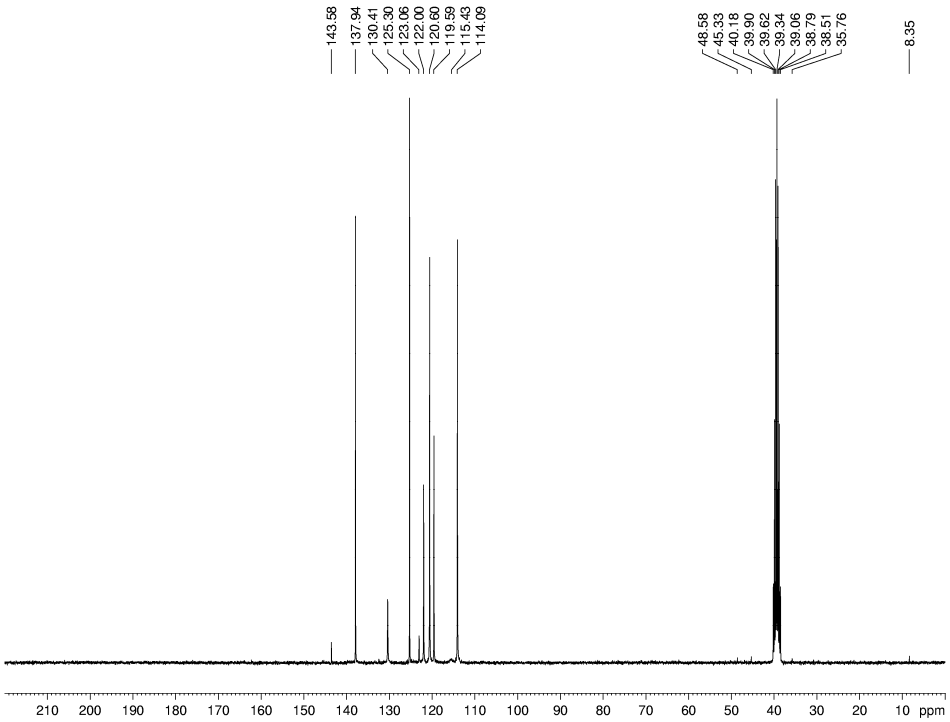

Figure D–76. ^{13}C NMR spectrum of **3.35** (75 MHz, d_6-DMSO).

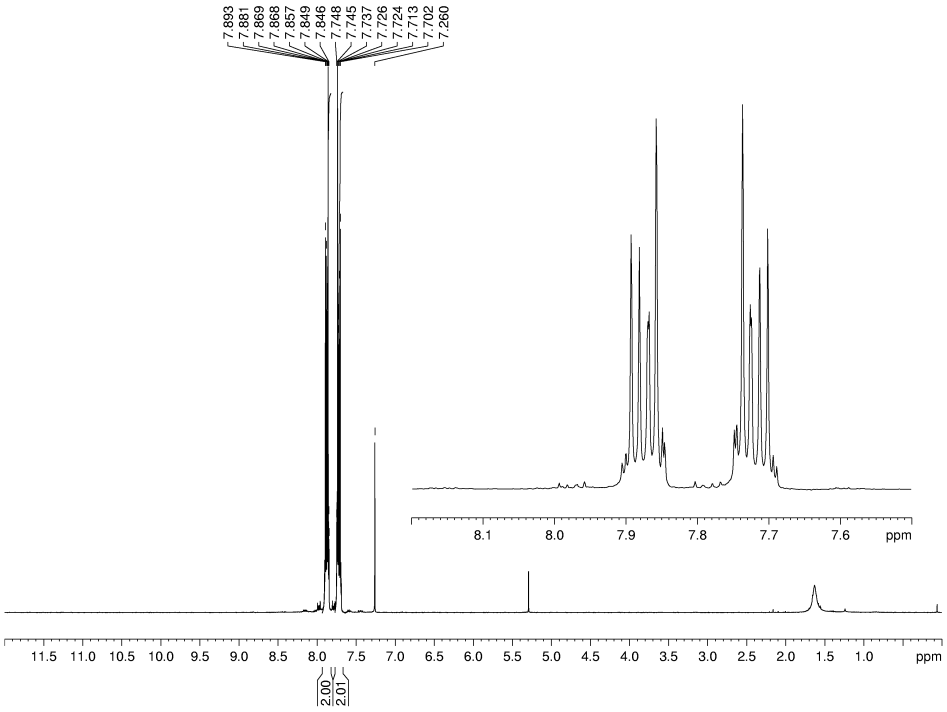

Figure D–77. ^{1}H NMR spectrum of **3.36** (300 MHz, $CDCl_3$).

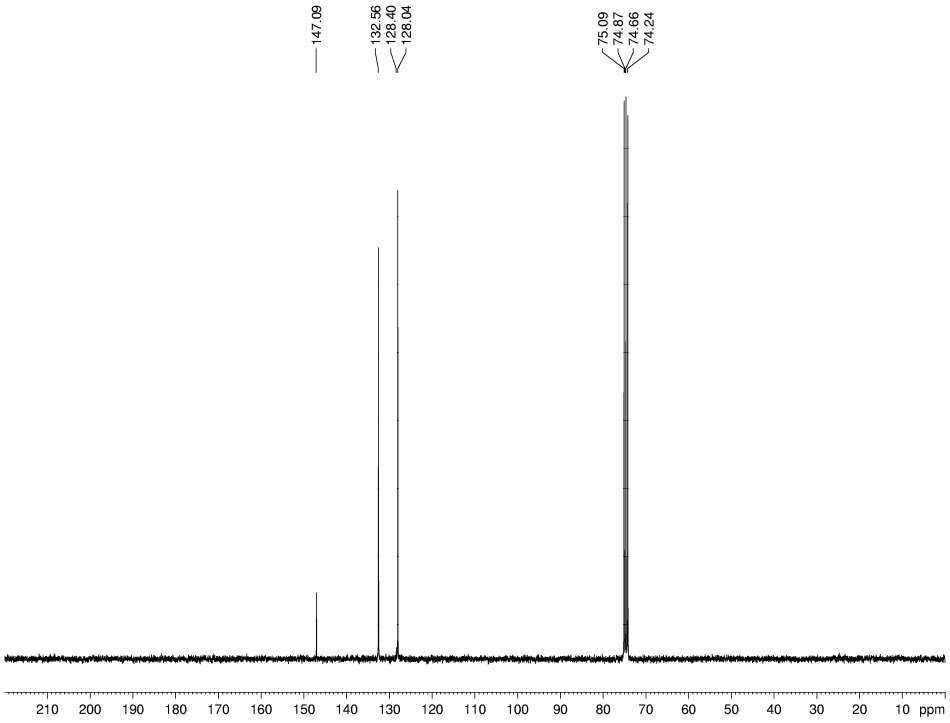

Figure D–78. ^{13}C NMR spectrum of **3.36** (75 MHz, $CDCl_3$).

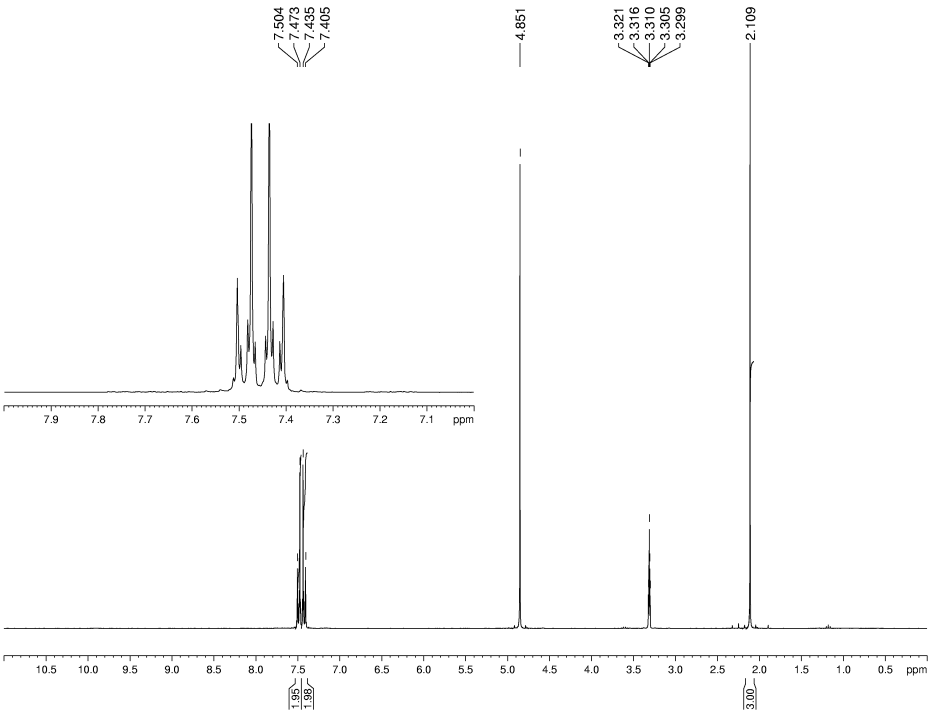

Figure D–79. ^{1}H NMR spectrum of **4.5** (300 MHz, MeOD).

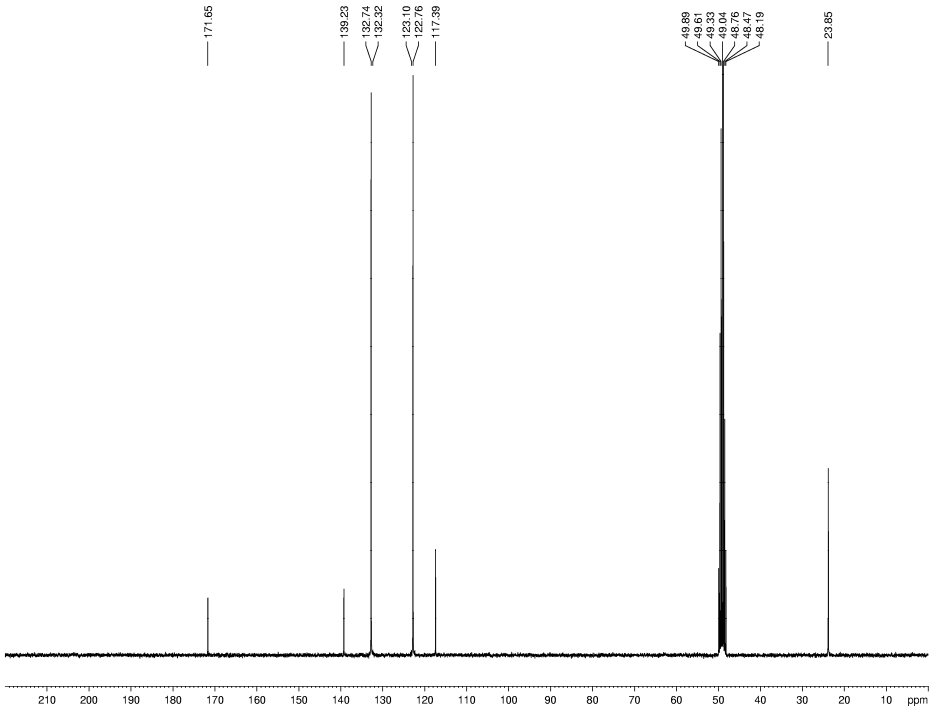

Figure D–80. ^{13}C NMR spectrum of **4.5** (75 MHz, MeOD).

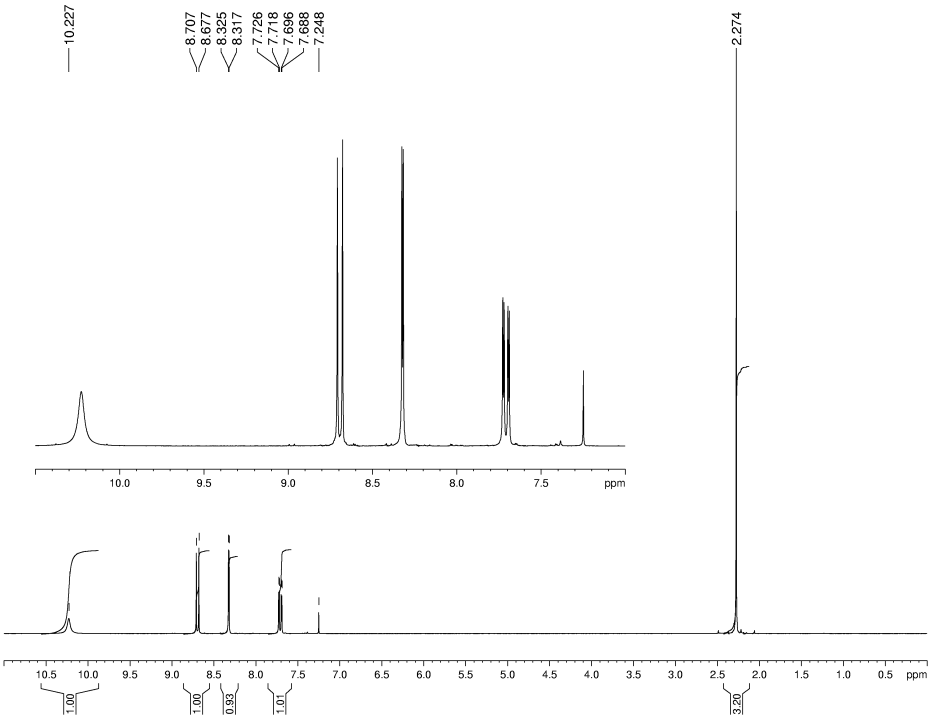

Figure D–81. ^{1}H NMR spectrum of **4.6** (300 MHz, $CDCl_3$).

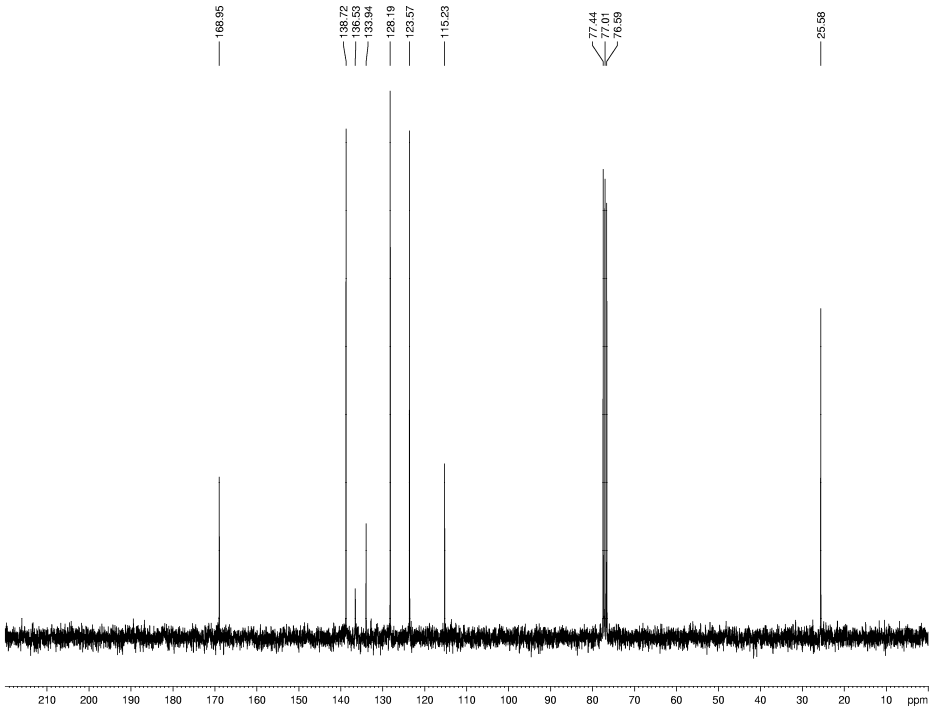

Figure D–82. ^{13}C NMR spectrum of **4.6** (75 MHz, $CDCl_3$).

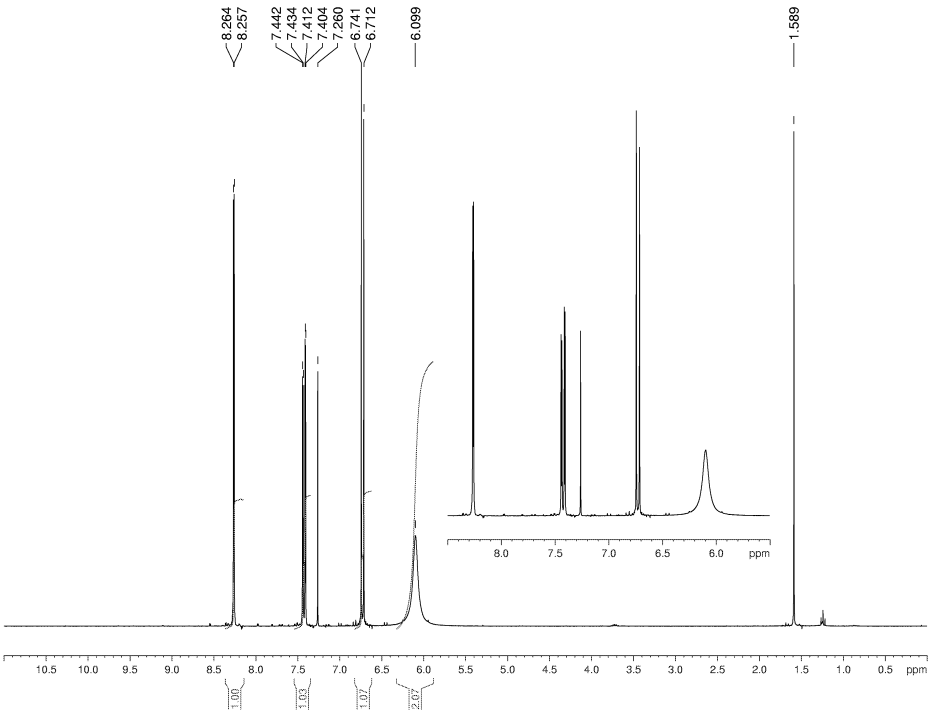

Figure D–83. ^{1}H NMR spectrum of **4.7** (300 MHz, $CDCl_3$).

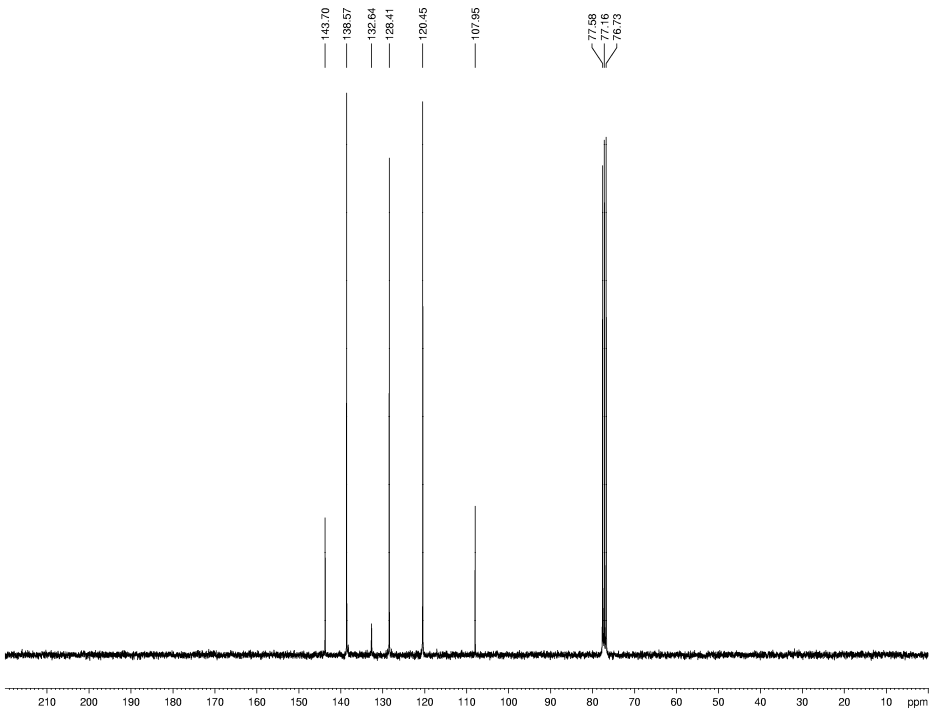

Figure D–84. ^{13}C NMR spectrum of **4.7** (75 MHz, $CDCl_3$).

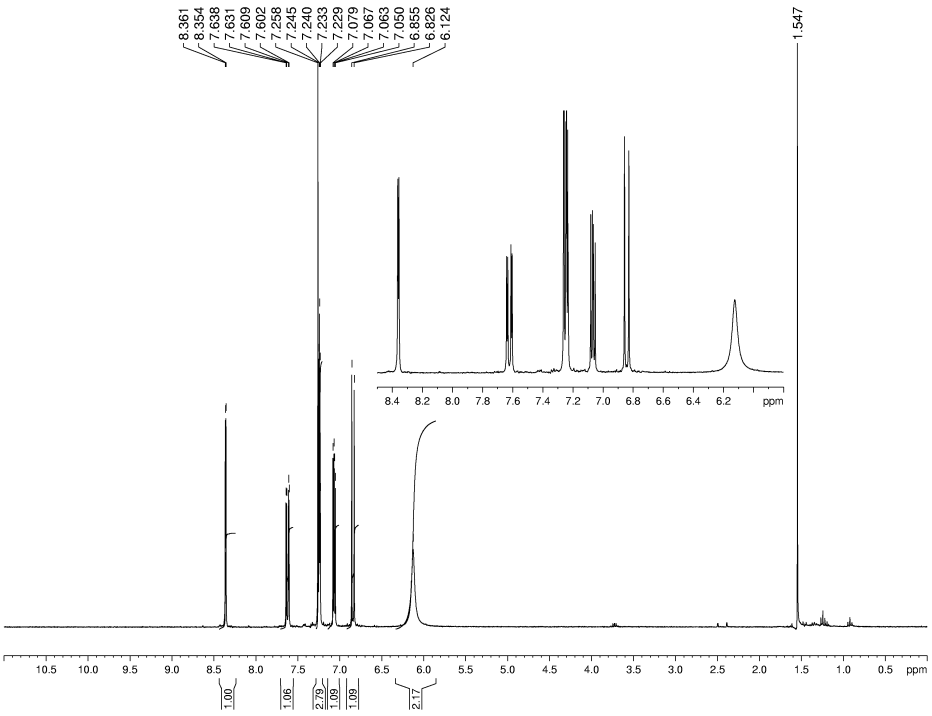

Figure D–85. ^{1}H NMR spectrum of **4.8** (300 MHz, $CDCl_3$).

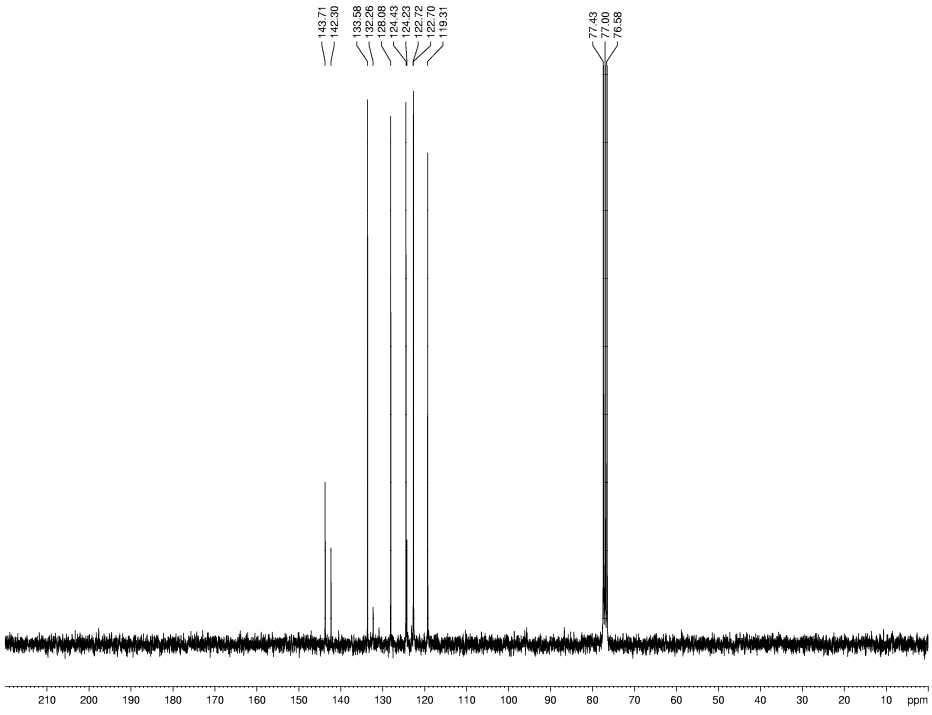

Figure D–86. ^{13}C NMR spectrum of **4.8** (75 MHz, $CDCl_3$).

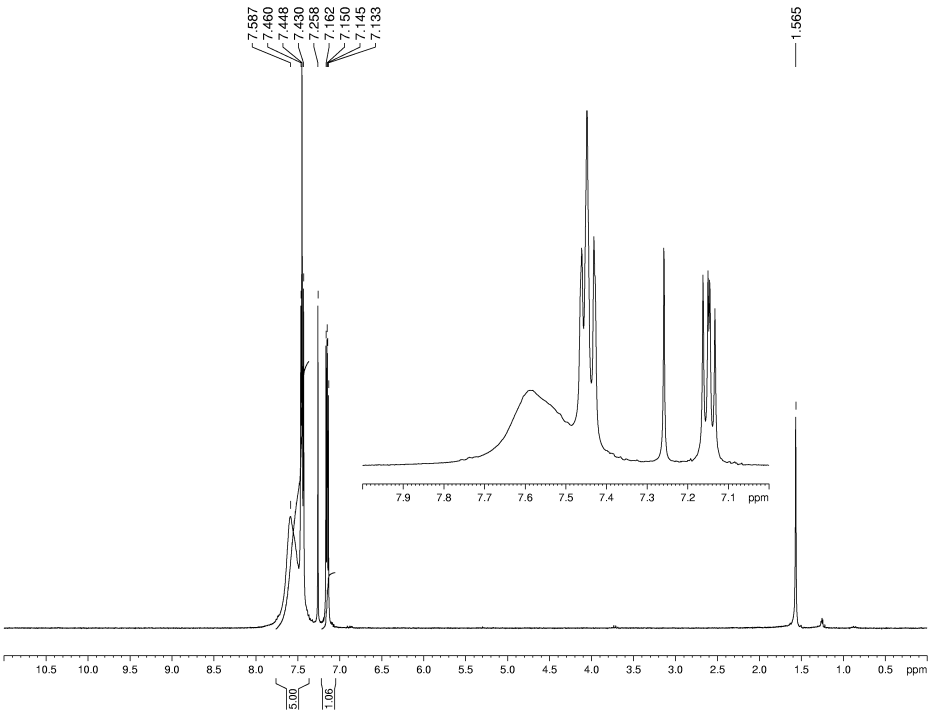

Figure D–87. ^{1}H NMR spectrum of **4.9** (300 MHz, $CDCl_3$).

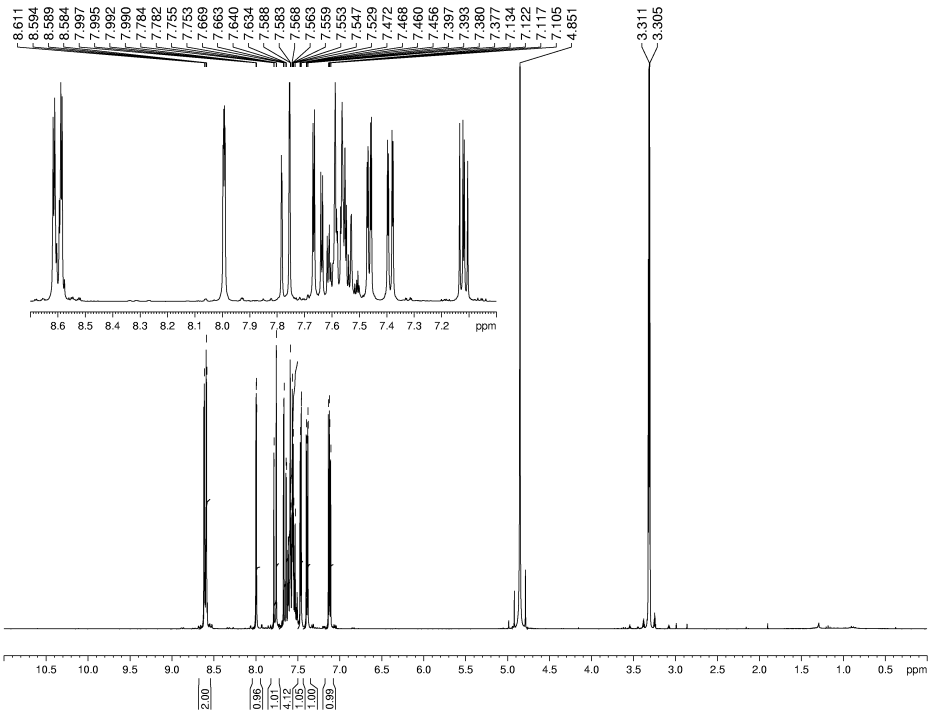

Figure D–88. ^{1}H NMR spectrum of **4.10a** (300 MHz, 1.0 M NaOD in MeOD).

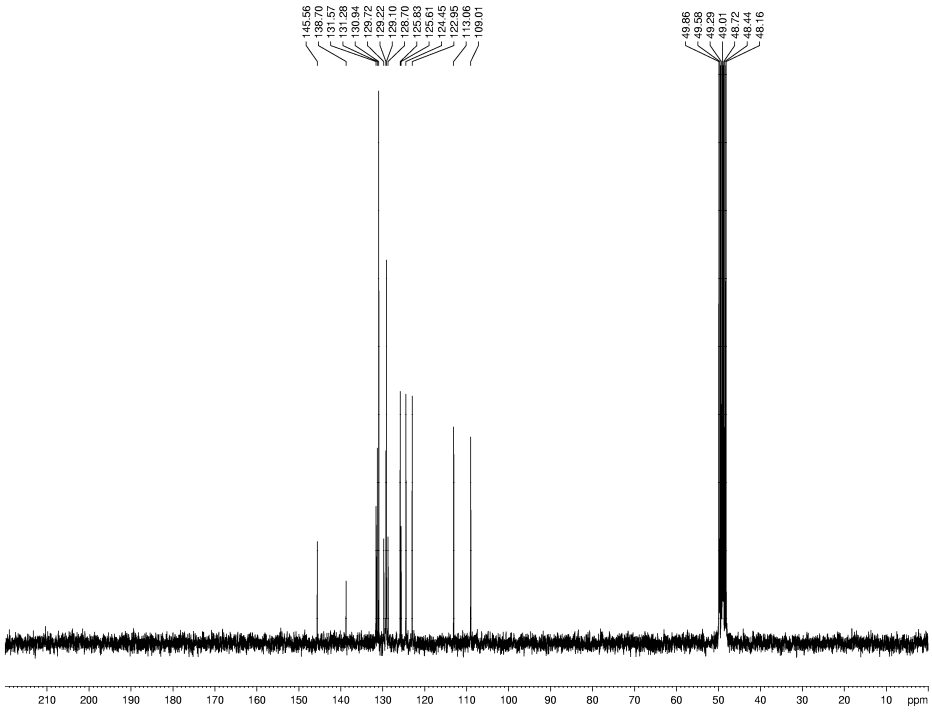

Figure D–89. ^{13}C NMR spectrum of **4.10a** (75 MHz, 1.0 M NaOD in MeOD).

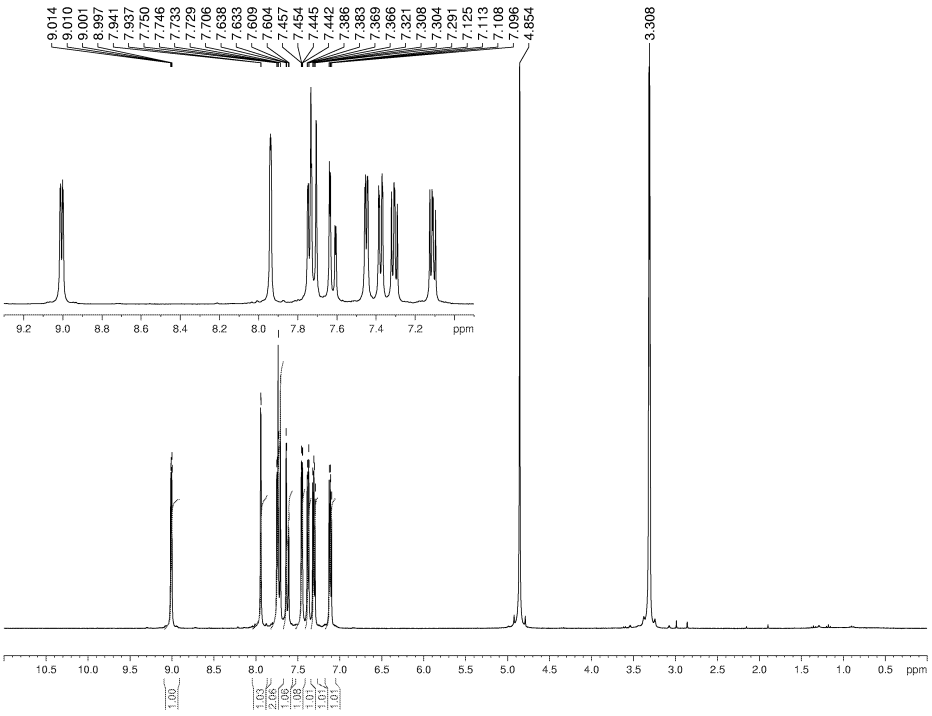

Figure D–90. ^{1}H NMR spectrum of **4.10b** (300 MHz, 1.0 M NaOD in MeOD).

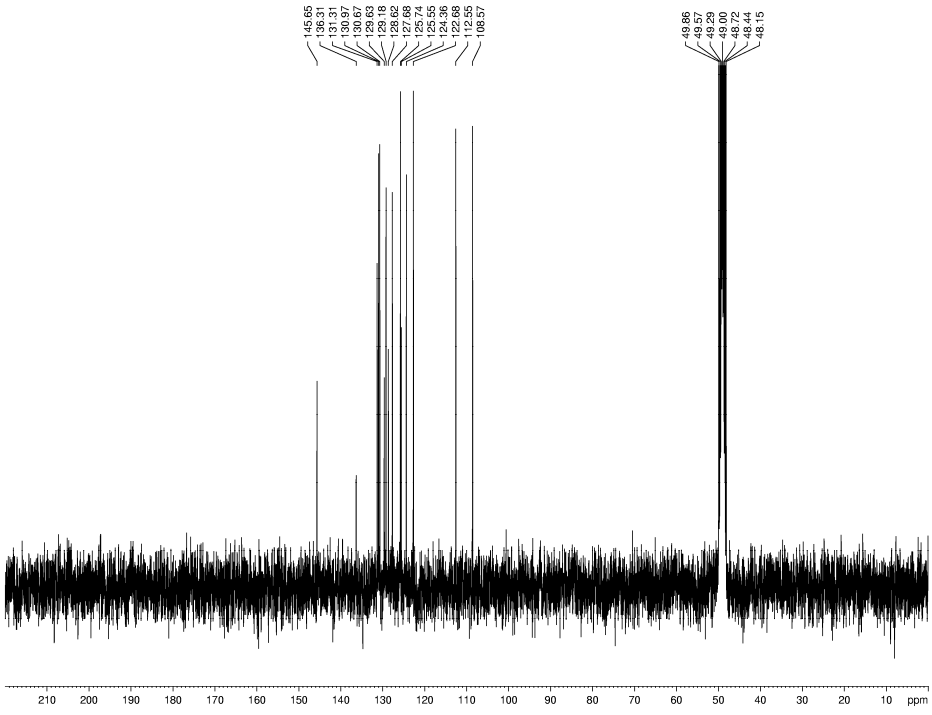

Figure D–91. ^{13}C NMR spectrum of **4.10b** (75 MHz, 1.0 M NaOD in MeOD).

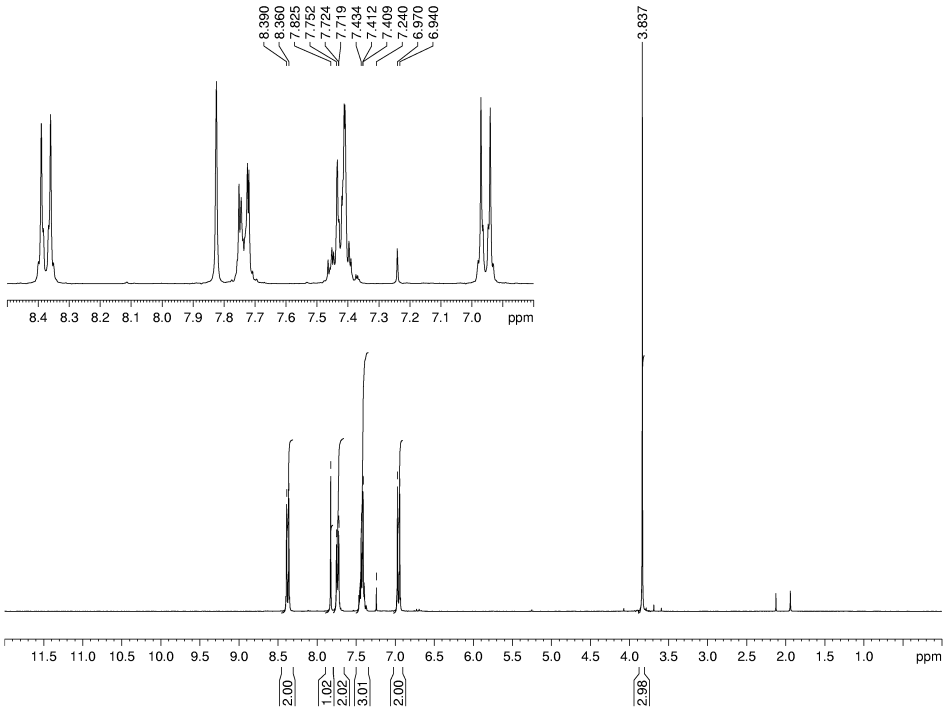

Figure D–92. ^{1}H NMR spectrum of **5.2a** (300 MHz, $CDCl_3$).

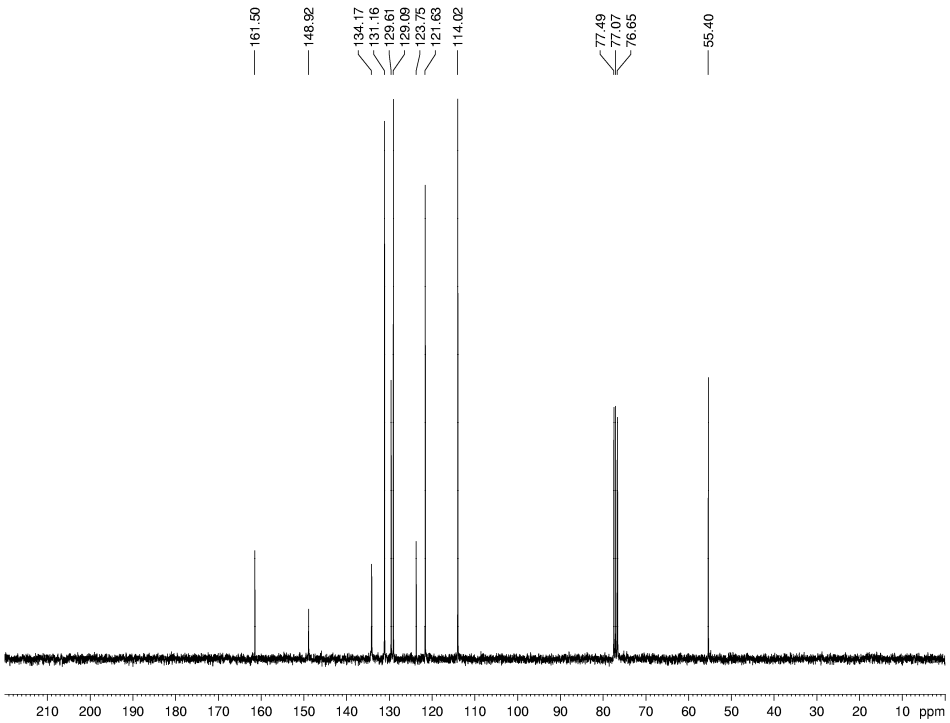

Figure D–93. ^{13}C NMR spectrum of **5.2a** (75 MHz, $CDCl_3$).

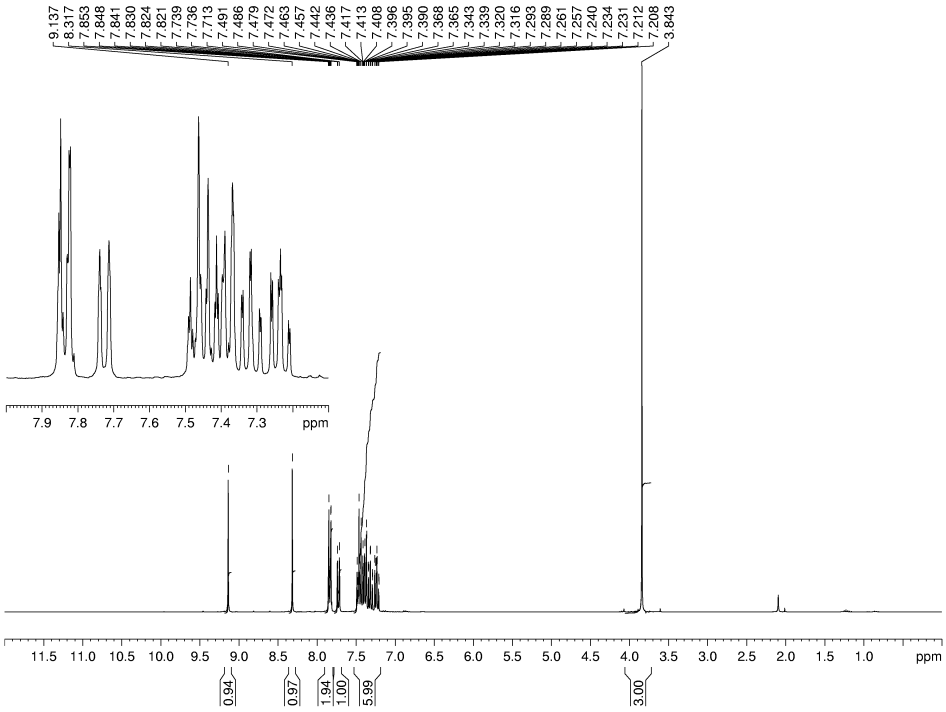

Figure D–94. ^{1}H NMR spectrum of **5.2b** (300 MHz, $CDCl_3$).

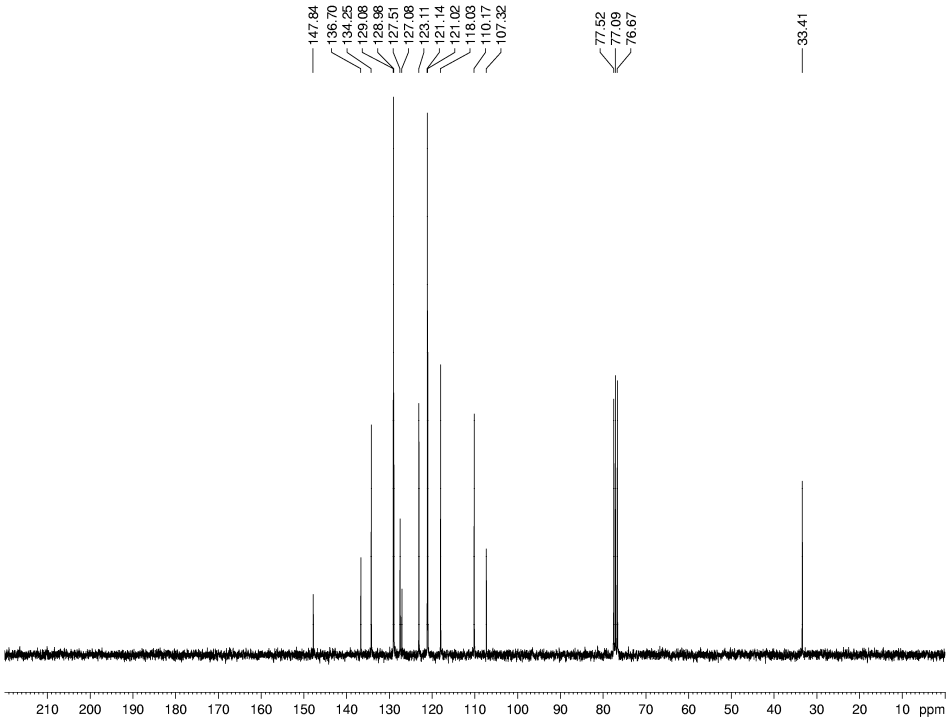

Figure D–95. ^{13}C NMR spectrum of **5.2b** (75 MHz, $CDCl_3$).

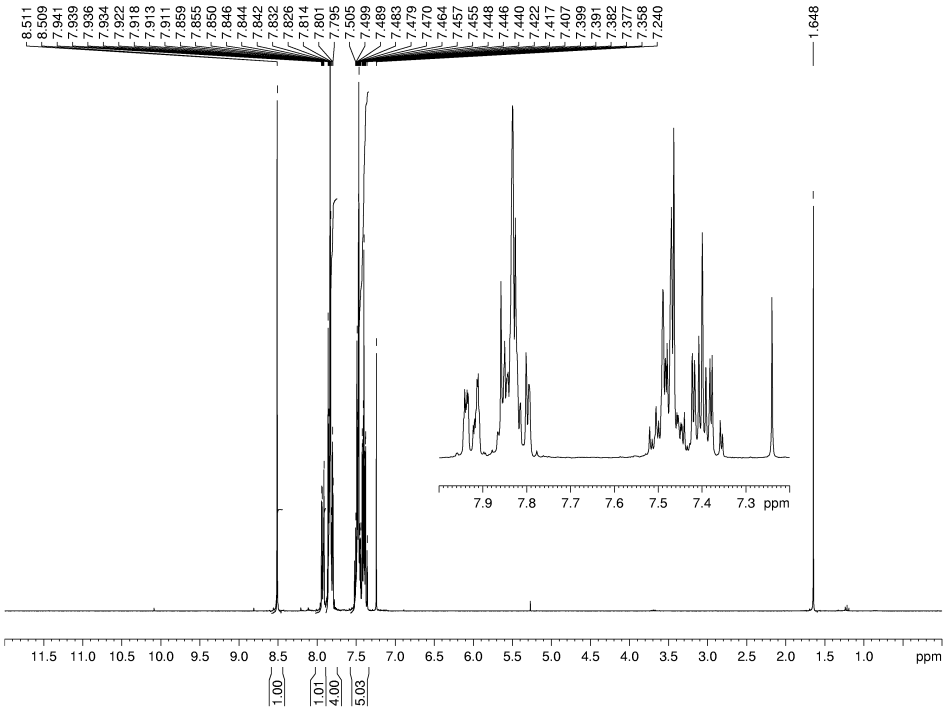

Figure D–96. ^{1}H NMR spectrum of **5.2c** (300 MHz, $CDCl_3$).

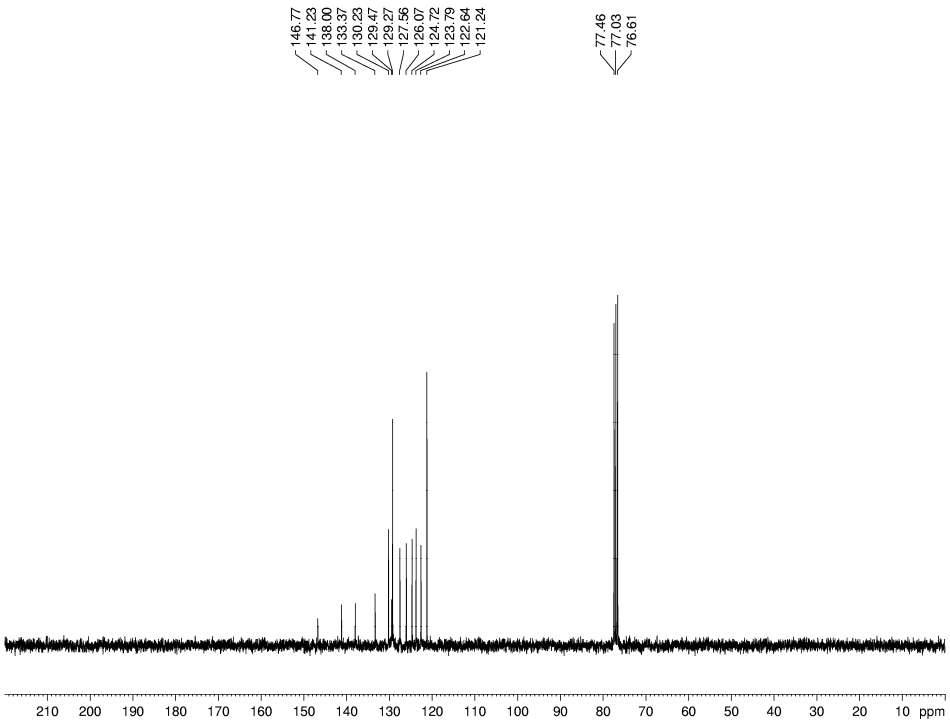

Figure D–97. ^{13}C NMR spectrum of **5.2c** (75 MHz, $CDCl_3$).

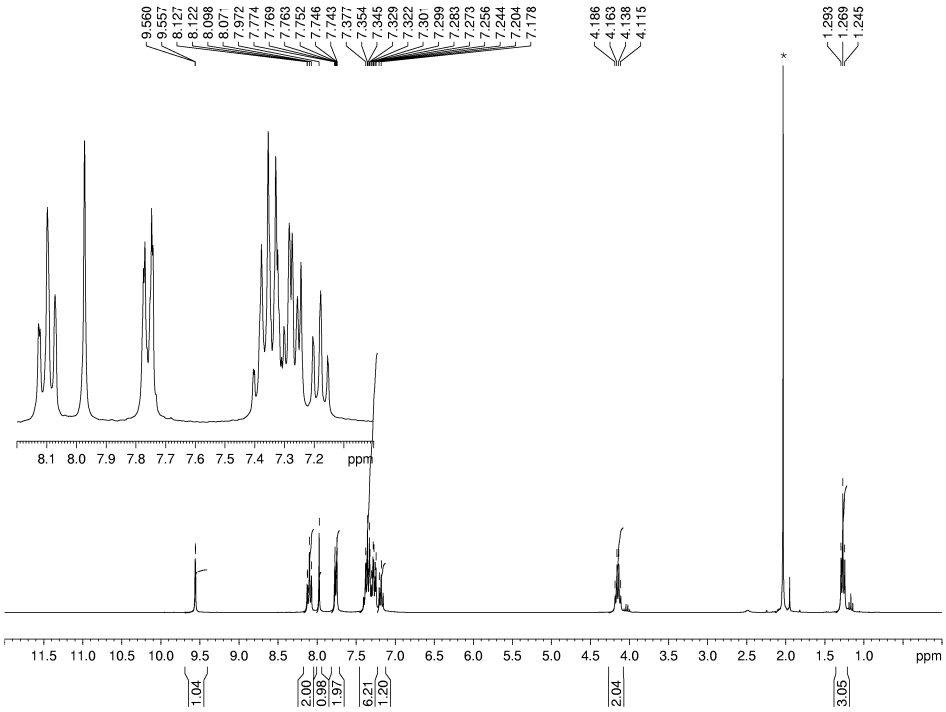

Figure D–98. ^{1}H NMR spectrum of **5.2d** (300 MHz, $CDCl_3$). Asterisk indicates peak due to acetone.

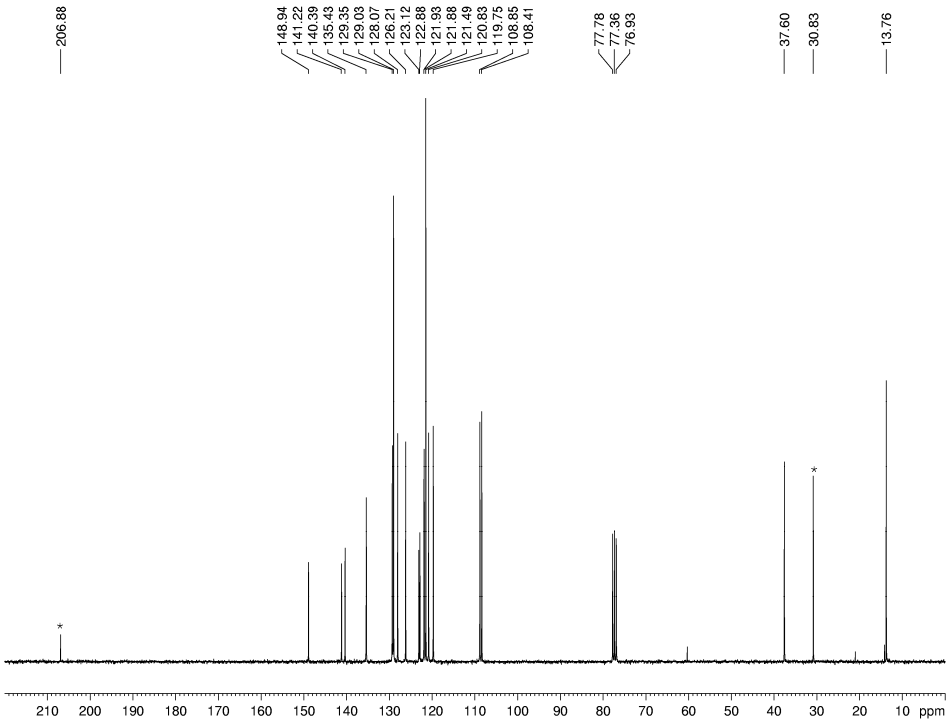

Figure D–99. ^{13}C NMR spectrum of **5.2d** (75 MHz, $CDCl_3$). Asterisk indicates peaks due to acetone.

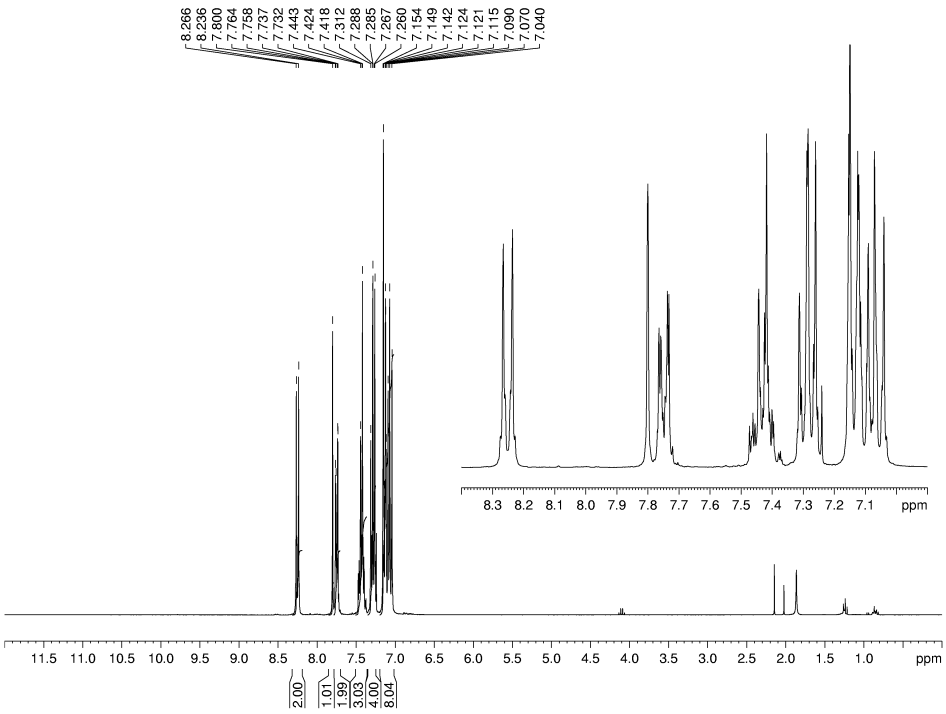

Figure D–100. ^{1}H NMR spectrum of **5.2e** (300 MHz, $CDCl_3$).

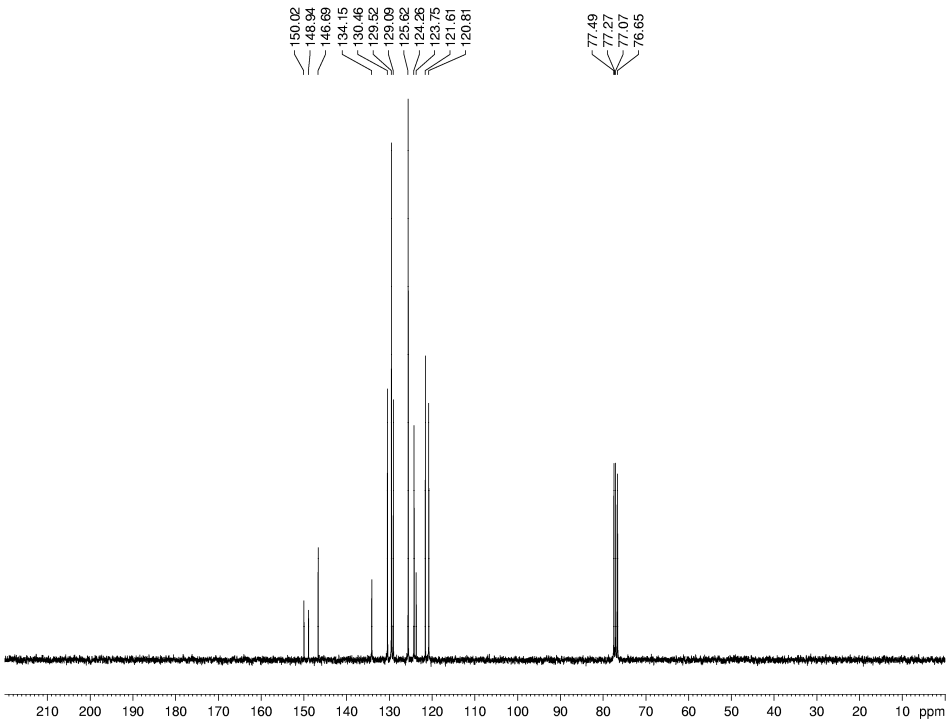

Figure D–101. ^{13}C NMR spectrum of **5.2e** (75 MHz, $CDCl_3$).

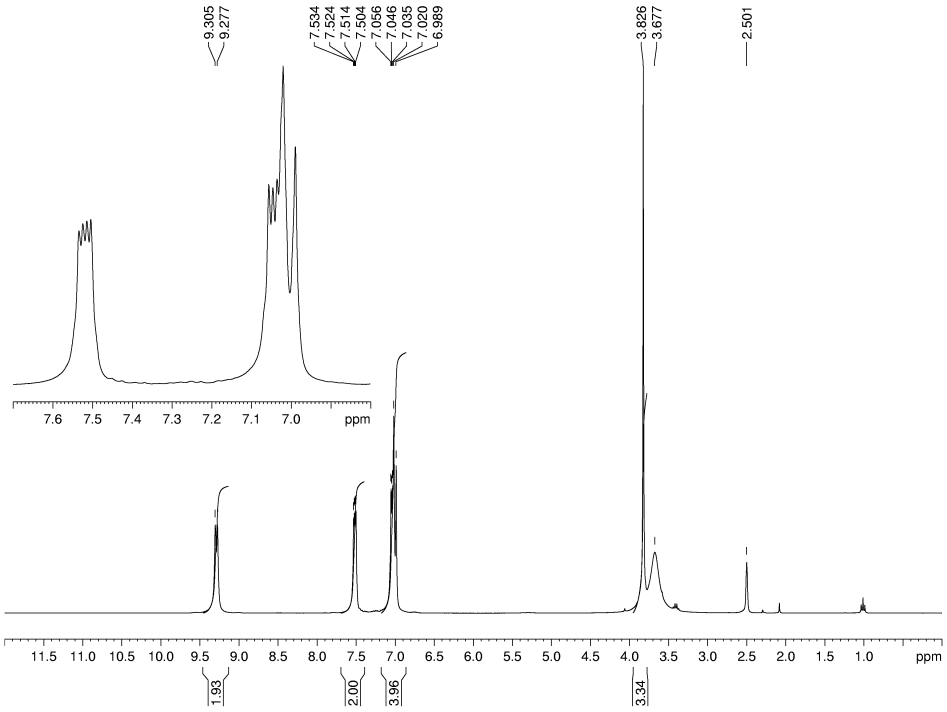

Figure D–102. ^{1}H NMR spectrum of **5.3a** (300 MHz, d_6-DMSO).

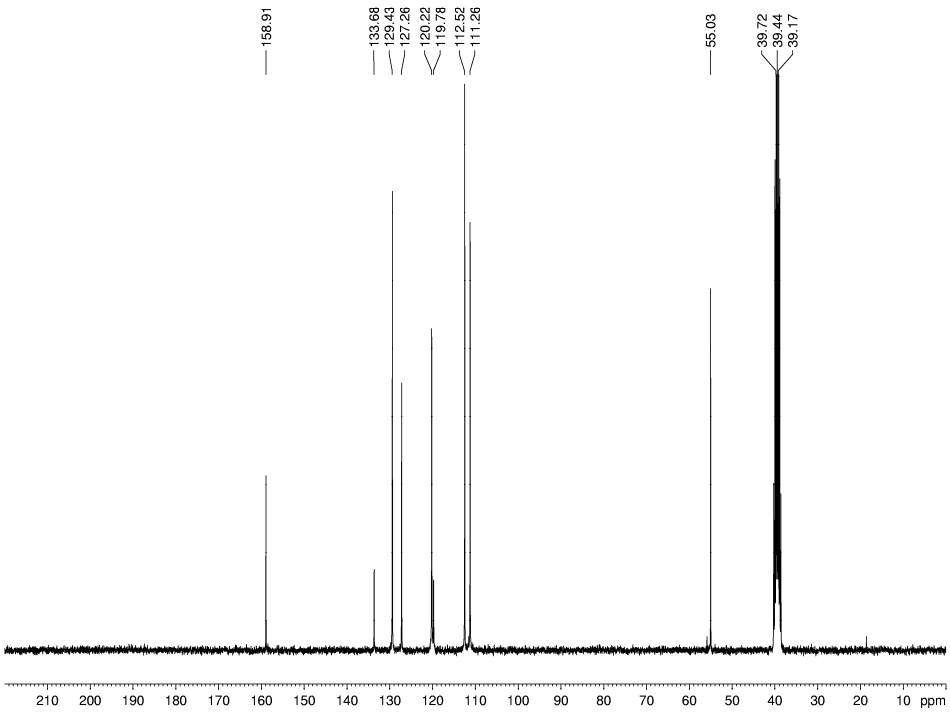

Figure D–103. ^{13}C NMR spectrum of **5.3a** (75 MHz, d_6-DMSO).

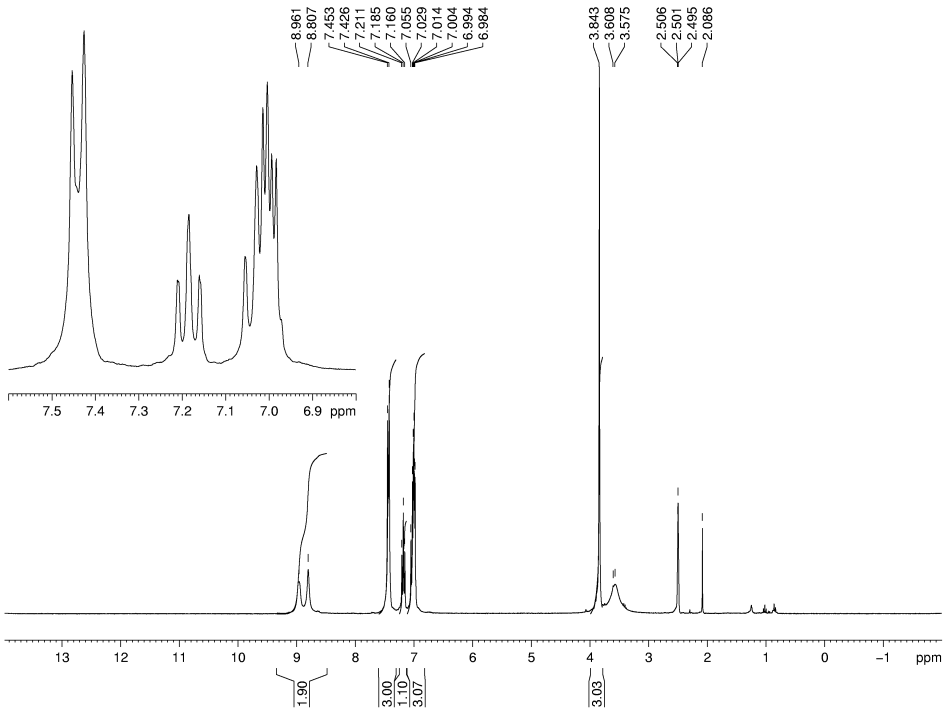

Figure D–104. ^{1}H NMR spectrum of **5.3b** (300 MHz, d_6-DMSO).

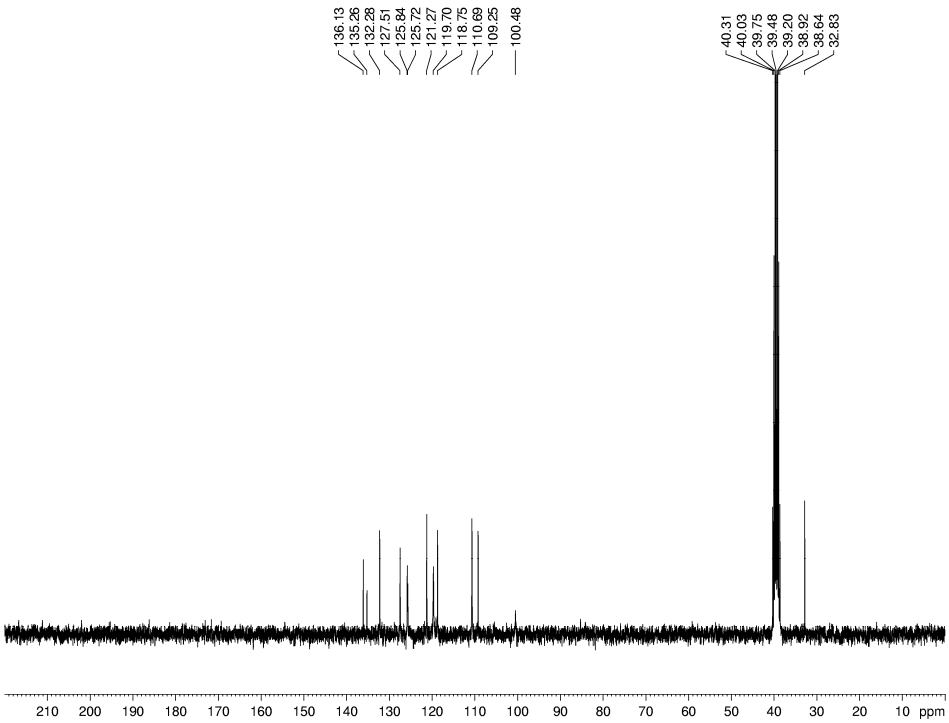

Figure D–105. ^{13}C NMR spectrum of **5.3b** (75 MHz, d_6-DMSO).

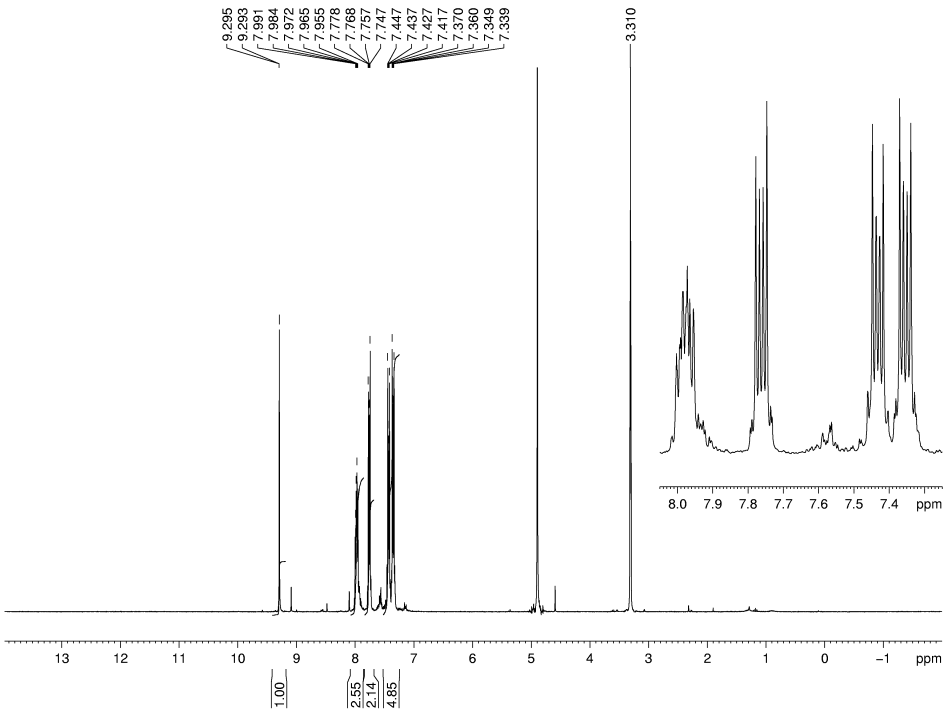

Figure D–106. ^{1}H NMR spectrum of **5.3c** (300 MHz, MeOD).

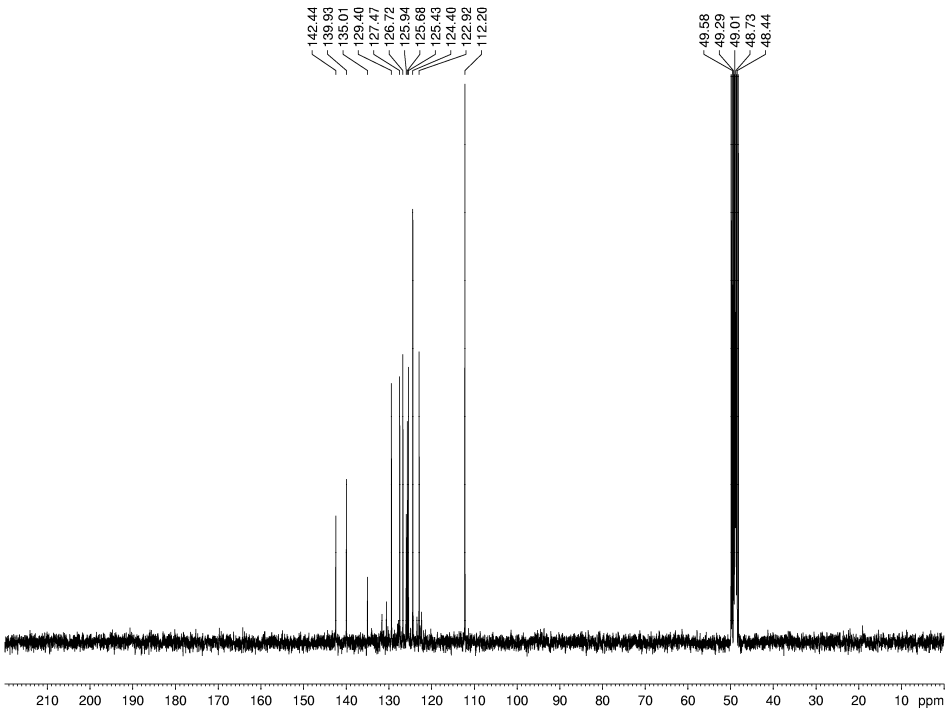

Figure D–107. ^{13}C NMR spectrum of **5.3c** (75 MHz, MeOD).

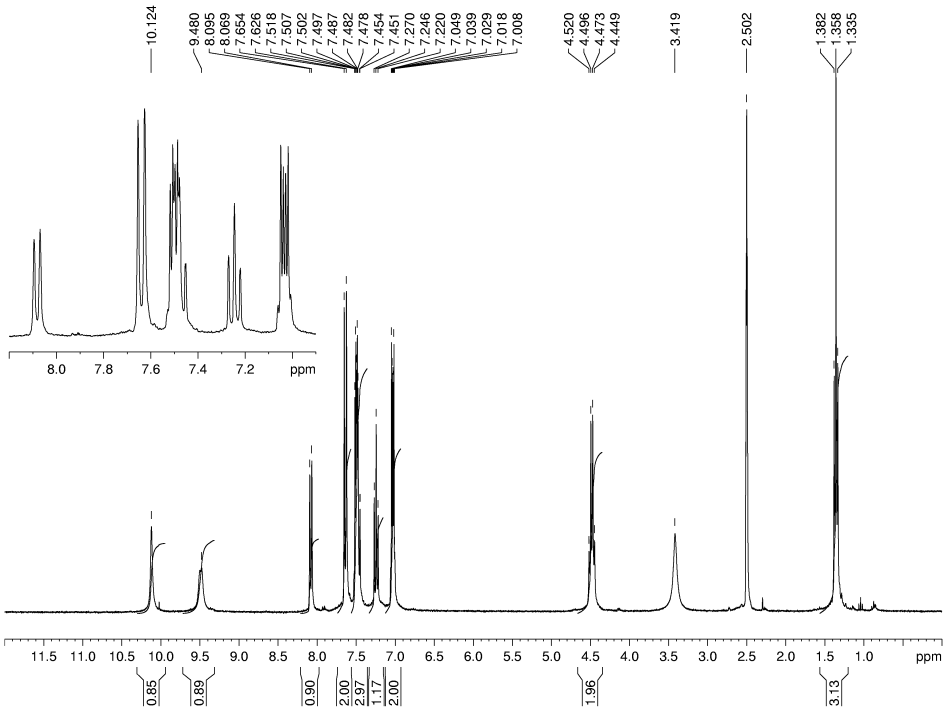

Figure D–108. ^{1}H NMR spectrum of **5.3d** (300 MHz, d_6-DMSO).

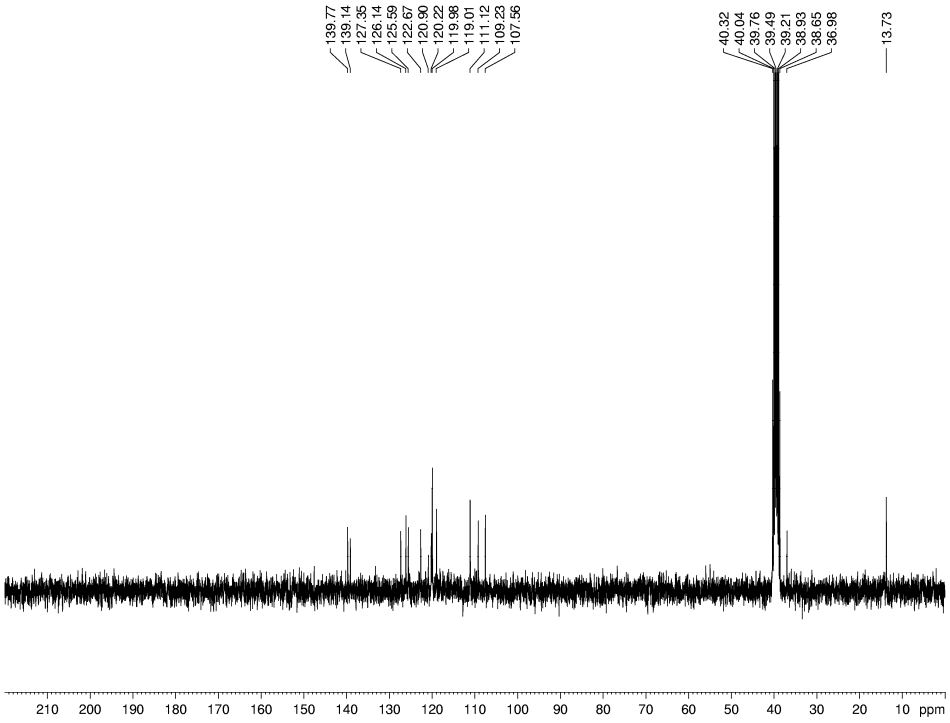

Figure D–109. ^{13}C NMR spectrum of **5.3d** (75 MHz, d_6-DMSO).

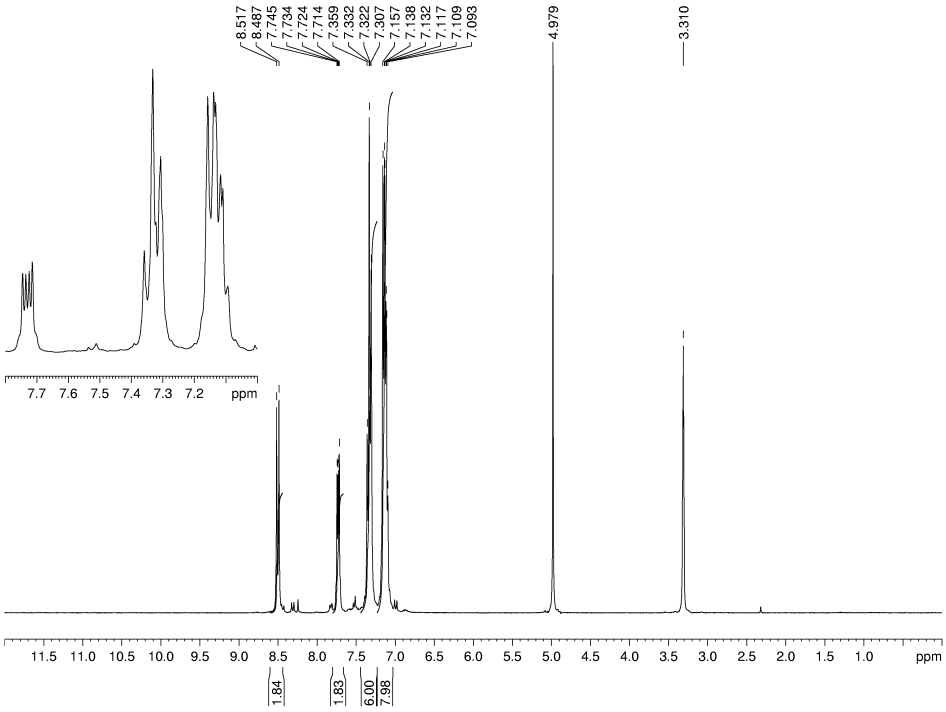

Figure D–110. ^{1}H NMR spectrum of **5.3e** (300 MHz, MeOD).

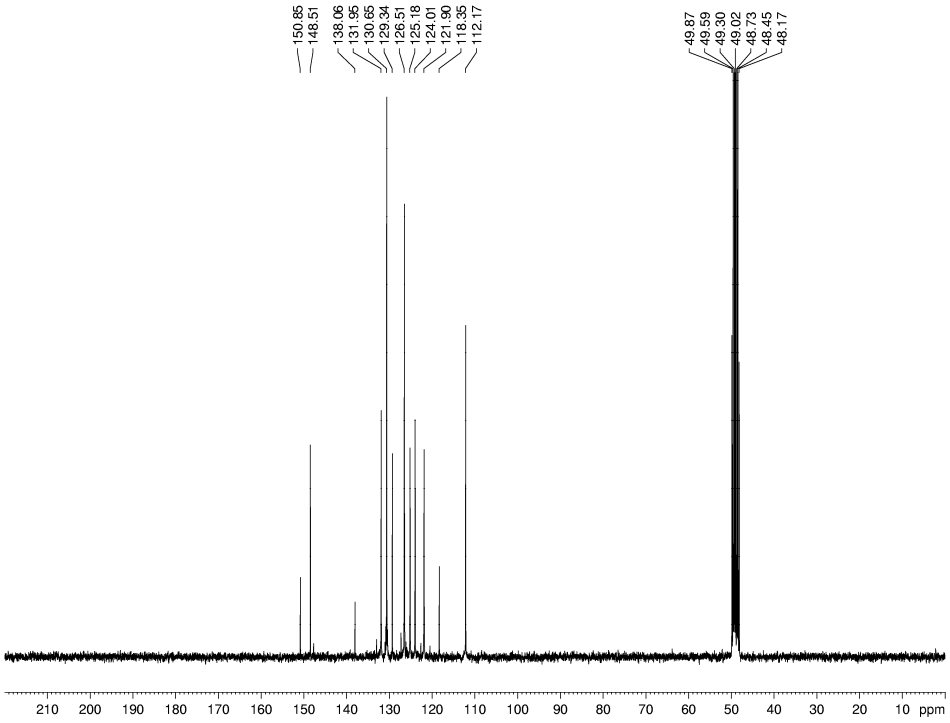

Figure D–111. ^{13}C NMR spectrum of **5.3e** (75 MHz, MeOD).

Appendix E: DFT Calculation Output Parameters

Table E–1. Output parameters for **2.15d**.

N-N= 1.139349524138D+03 E-N=-7.207947321593D+03 KE= 1.609251365430D+03
1\1\GINC-COMPUTE-0-0\SP\UTD-B3LYP-FC\6-31G(d,p)\C11H7N2O2S1(2)\BRYNND\
20-May-2010\0\\# td ub3lyp/6-31g(d,p) scrf=(solvent=chloroform,a0=4.72
)\\2ThBNN TDDFT ACN\\0,2\C,0,-4.139458,-0.845231,0.000335\C,0,-4.22947
3,0.556653,0.000472\C,0,-3.087542,1.365182,0.000201\C,0,-1.869922,0.70
4066,-0.000288\C,0,-1.780938,-0.687803,-0.000421\C,0,-2.903179,-1.5004
05,-0.000081\N,0,-0.548875,1.208999,-0.000284\N,0,-0.406519,-1.012563,
-0.000516\O,0,-0.258495,2.449607,0.00025\O,0,0.061583,-2.198422,-0.000
214\H,0,-5.050537,-1.434674,0.000598\H,0,-3.132146,2.447589,0.000294\H
,0,-2.80841,-2.579596,-0.000178\H,0,-5.208627,1.024411,0.000835\C,0,0.
331369,0.147473,-0.000648\C,0,4.194159,-0.246874,0.00047\C,0,3.921265,
1.096409,-0.000234\C,0,2.531093,1.374519,-0.00018\C,0,1.756884,0.22573
3,-0.000001\H,0,5.162214,-0.729158,0.000858\H,0,4.686223,1.863983,-0.0
00299\H,0,2.091208,2.36178,-0.000491\S,0,2.761099,-1.217325,0.000372\\
Version=AM64L-G09RevA.02\State=2-A\HF=-1081.4063644\S2=0.805773\S2-1=0
.\S2A=0.750504\RMSD=5.657e-09\PG=C01 [X(C11H7N2O2S1)]\\@

Table E–2. Output parameters for **2.3**, EPR-II.

1\1\GINC-COMPUTE-0-5\FOpt\UB3LYP\EPR-II\C13H17N2O2(2)\BRYNND\04-Sep-20
10\0\\#T opt ub3lyp/epr-II geom=connectivity density=current\\TMNN epr
-II\\0,2\N,-0.5781754178,1.100041174,-0.1302079932\C,0.2278309745,-0.0
000003772,0.0000007918\N,-0.5781753349,-1.1000419591,0.1302097925\O,-0
.2181282192,2.317131453,-0.2798234586\O,-0.2181280145,-2.3171322783,0.
2798244324\C,1.6970075342,-0.0000003236,0.0000003135\C,2.4212993548,1.
2202096581,-0.0491413806\C,2.4212996531,-1.2202101542,0.0491413874\C,3
.8204711684,1.210280172,-0.0467922459\H,1.8812244259,2.1549014787,-0.0
963187367\C,3.8204714575,-1.210280334,0.0467912389\H,1.8812251127,-2.1
549021716,0.0963190575\C,4.5291823555,0.0000000004,-0.000000744\H,4.35
69497326,2.1545167582,-0.0840917998\H,4.3569502765,-2.1545167918,0.084
0903617\H,5.6159109399,0.0000001073,-0.0000011519\C,-2.0270052382,-0.7
695420258,-0.1303060343\C,-2.0270052361,0.7695412806,0.1303081206\C,-2
.9205253655,1.5978572584,-0.7987483282\H,-2.7831714755,2.6577107059,-0
.5791059453\H,-3.9698885846,1.3388887184,-0.6297354246\H,-2.6841102783
,1.4395982168,-1.8518557243\C,-2.296809963,1.1597308598,1.5997864867\H
,-2.0775466482,2.2227741346,1.7234695892\H,-1.6661081979,0.5955810963,
2.2920909207\H,-3.3441173475,0.9881287416,1.8609915205\C,-2.9205258451
,-1.5978589177,0.7987493352\H,-3.969888987,-1.3388899411,0.6297365627\
H,-2.6841109965,-1.439601402,1.8518569501\H,-2.7831722612,-2.657712131
1,0.5791056577\C,-2.2968100812,-1.1597300055,-1.5997846942\H,-1.666109
817,-0.5955777966,-2.2920885365\H,-2.0775447206,-2.2227726431,-1.72346
95495\H,-3.3441179558,-0.988129468,-1.8609888754\\Version=AM64L-G09Rev
A.02\State=2-A\HF=-765.5994308\S2=0.813486\S2-1=0.\S2A=0.750666\RMSD=9
.581e-09\RMSF=2.639e-06\Dipole=-0.9536772,-0.000004,0.0000007\Quadrupo
le=11.5234324,-8.7723654,-2.751067,0.000001,-0.0000046,1.947859\PG=C01
[X(C13H17N2O2)]\\@

Table E–3. Output parameters for **2.15a**, EPR-II.

1\1\GINC-COMPUTE-0-21\FOpt\UB3LYP\EPR-II\C13H9N2O2(2)\BRYNND\16-Aug-20
10\0\\#T opt ub3lyp/epr-II geom=connectivity density=current\\BNN epr
II\\0,2\N,-0.9506118249,-0.2723574256,0.5918425006\C,-1.9597509395,-0.
1977317323,-0.357982988\N,-1.3513507284,0.1017572857,-1.5688587357\O,-
1.0641219712,-0.5258923292,1.8375519101\O,-1.9069331658,0.2608893482,-
2.7068227635\C,-3.3896295267,-0.3955611615,-0.127037744\C,-3.878453643
8,-0.6988133655,1.1718503187\C,-4.3179027615,-0.2878461796,-1.19696074
67\C,-5.2484436875,-0.8855568804,1.3824131067\H,-3.1846789681,-0.78407
66405,1.995832556\C,-5.6839947423,-0.4782220288,-0.9653720843\H,-3.961
3316363,-0.0578132905,-2.1906821071\C,-6.1597456976,-0.7774879463,0.32
05940597\H,-5.6031929605,-1.116763869,2.3829649465\H,-6.3785238233,-0.
391652144,-1.7963612019\H,-7.2225151342,-0.9237950933,0.4923702932\C,0
.0470302826,0.2155379808,-1.3795190323\C,1.0650083121,0.4995843946,-2.
2874366585\C,0.2982846675,-0.0190109941,-0.024933674\C,2.3689450909,0.
5380786016,-1.7622698862\C,1.5839856815,0.0150725672,0.5108348222\C,2.
6229366728,0.3009163538,-0.3925947129\H,1.7565159891,-0.1700544777,1.5
647509854\H,3.6449948283,0.3402381437,-0.0285991179\H,3.2005826024,0.7
552426101,-2.4255090161\H,0.8478634943,0.6782300228,-3.3342005801\\Ver
sion=AM64L-G09RevA.02\State=2-A\HF=-760.7508538\S2=0.802734\S2-1=0.\S2
A=0.750445\RMSD=6.232e-09\RMSF=5.233e-05\Dipole=0.7374101,0.103027,-0.
118865\Quadrupole=13.7043762,-7.2121975,-6.4921787,2.9271977,-3.333998
6,-0.5804068\PG=C01 [X(C13H9N2O2)]\\@

Table E–4. Output parameters for **3.2**, EPR-II.

1\1\GINC-COMPUTE-0-1\FOpt\UB3LYP\EPR-II\C17H11N2O2(2)\BRYNND\15-Aug-20
10\0\\#T opt ub3lyp/epr-II geom=connectivity density=current\\naphNN E
PR II\\0,2\N,0.422642126,-1.9988544543,-0.8058699986\C,0.7974060026,-1
.7780703999,0.5138653061\N,2.085524736,-2.266210459,0.6407109045\O,-0.
6954593506,-1.6961036811,-1.3438224999\O,2.8256236263,-2.2731555568,1.
6805191274\C,-0.0091598621,-1.1537092806,1.561825974\C,-1.3259203669,-
0.6937319561,1.2932854855\C,0.5116077007,-0.9948101938,2.8740336199\C,
-2.0849820334,-0.0985293295,2.3063631681\H,-1.7386287566,-0.8061448306
,0.3013521716\C,-0.2635128627,-0.3970539857,3.8731645903\H,1.511534950
5,-1.3388281502,3.096270475\C,-1.5636735543,0.054899369,3.6001036623\H
,-3.0901468101,0.2466339366,2.0800218588\H,0.1540142767,-0.2852667977,
4.8700677281\H,-2.1597872306,0.5182417868,4.3814404765\C,0.7847035329,
-3.3701321613,-5.1342801254\C,0.5641811056,-2.915493036,-3.8438312951\
C,1.5856270671,-3.05294203,-2.8602467797\C,2.845923366,-3.6654751679,-
3.2130225396\C,3.0271710099,-4.118001307,-4.5524353872\C,2.021119724,-
3.9746916813,-5.4931785985\C,1.4813702684,-2.6278654734,-1.5071575758\
C,3.890906539,-3.8158835046,-2.2414759394\C,3.7486213061,-3.3875364043
,-0.9315944479\C,2.5162063341,-2.7923898572,-0.6002483842\H,0.00417741
12,-3.2640616367,-5.8823143509\H,-0.3735094444,-2.4540800421,-3.561259
9317\H,3.9728689017,-4.5796762883,-4.824308792\H,2.1731883114,-4.32421
34424,-6.5103305202\H,4.5274303038,-3.4934531017,-0.1856813219\H,4.820
0775217,-4.2828332929,-2.5557691501\\Version=AM64L-G09RevA.02\State=2-
A\HF=-914.4108252\S2=0.79874\S2-1=0.\S2A=0.750417\RMSD=8.413e-09\RMSF=
7.754e-06\Dipole=0.3530462,-0.3827158,-0.8450966\Quadrupole=-0.0800761
,-5.4477901,5.5278662,-5.7907153,-6.5211821,6.979282\PG=C01 [X(C17H11N
2O2)]\\@

Table E–5. Output parameters for **3.3**, EPR-II.


```
1\1\GINC-COMPUTE-0-17\FOpt\UB3LYP\EPR-II\C19H11N2O2(2)\BRYNND\16-Aug-2
 010\0\\#T opt ub3lyp/epr-II geom=connectivity density=current\\aceNN e
 pr II\\0,2\N,1.1370875481,-1.7008719894,-1.1649037004\C,0.7276976933,-
 0.3811499747,-1.3673534954\N,1.8203350309,0.2949495487,-1.9144232909\O
 ,0.4520420311,-2.6632822397,-0.6824310894\O,1.8852057001,1.5231061549,
 -2.2546056145\C,-0.5870079896,0.1822048497,-1.0657118246\C,-1.61337267
 15,-0.6259020341,-0.5070112686\C,-0.8682616314,1.550629486,-1.32439700
 32\C,-2.8680190231,-0.0772715555,-0.2220014505\H,-1.4189192942,-1.6690
 235485,-0.3030329507\C,-2.1294827663,2.0800546013,-1.032174736\H,-0.10
 07238053,2.1815353622,-1.7490914292\C,-3.1379861395,1.2753054462,-0.48
 04240665\H,-3.6379557063,-0.7142286964,0.2050769276\H,-2.3221081297,3.
 1294720348,-1.2384061499\H,-4.1151290643,1.6940136703,-0.2562316595\C,
 5.0191652336,-4.7206590307,-1.7043020806\C,6.0637052892,-3.9793640447,
 -2.2518844494\C,5.88221871,-2.5898751881,-2.5499876062\C,4.6206535087,
 -2.0492912276,-2.2605388671\C,3.5414704949,-2.8073320096,-1.6968260992
 \C,3.739527847,-4.152641162,-1.4158067287\H,7.8427108924,-2.0510845777
 ,-3.3569291881\H,5.1767709607,-5.7728122118,-1.4854412191\H,7.01940444
 87,-4.4560288459,-2.4537655394\C,6.8469200263,-1.6915308157,-3.1110677
 564\C,4.2702020534,-0.6786482926,-2.4962415113\H,2.9522186124,-4.76527
 18538,-0.989115833\C,5.2208553054,0.1744355129,-3.0408165327\C,6.51224
 93404,-0.3592403169,-3.3422089946\H,5.0007777389,1.2187341679,-3.23637
 62534\H,7.257760354,0.3059250083,-3.7682775523\C,2.4666492343,-1.82885
 04212,-1.5843664478\C,2.8861375613,-0.6034911134,-2.0445433578\\Versio
 n=AM64L-G09RevA.02\State=2-A\HF=-990.6014467\S2=0.79801\S2-1=0.\S2A=0.
 750647\RMSD=5.286e-09\RMSF=1.211e-04\Dipole=1.3450982,-0.5763793,-0.30
 86135\Quadrupole=10.1891271,-1.0810633,-9.1080637,-6.6676765,-5.508428
 ,-0.3161116\PG=C01 [X(C19H11N2O2)]\\@
```


Table E–6. Output parameters for **3.4**, EPR-II.


```
1\1\GINC-COMPUTE-0-26\FOpt\UB3LYP\EPR-II\C21H13N2O2(2)\BRYNND\23-Aug-2
 010\0\\#T opt ub3lyp/epr-II geom=connectivity density=current\\Phenant
 hrene NN epr II\\0,2\N,-0.9758126002,-0.2223964938,0.597765329\C,-1.97
 92978907,-0.1903483167,-0.3520123772\N,-1.3635343619,0.0790402868,-1.5
 596220287\O,-1.1252616288,-0.4235885573,1.8498139372\O,-1.9368287418,0
 .174166135,-2.696608401\C,-3.4091489327,-0.3999645506,-0.1243384276\C,
 -3.8755920408,-0.9430745539,1.1012838441\C,-4.3588065406,-0.0643882766
 ,-1.1244536425\C,-5.2445706447,-1.1420658443,1.3091943808\H,-3.1680477
 367,-1.1951044611,1.8782320615\C,-5.7242564072,-0.266132864,-0.8969174
 648\H,-4.0215193604,0.3407646242,-2.0677857261\C,-6.1777854575,-0.8057
 086397,0.3165580693\H,-5.5809358597,-1.5610448955,2.2536364125\H,-6.43
 51769469,-0.0005868774,-1.6745634643\H,-7.239715637,-0.9613403345,0.48
 56651549\C,0.0365969465,0.2191542117,-1.3636447768\C,1.0721051598,0.49
 9044512,-2.3138441721\C,0.2786084135,0.0268255738,-0.0208791829\C,2.40
 61226398,0.5742172813,-1.7861910817\C,0.8295694534,0.700444526,-3.6993
 262654\C,1.5888982427,0.0908355059,0.5557873093\C,3.4531236777,0.85430
 17568,-2.7036742876\C,2.6640508799,0.3688520039,-0.355496495\C,1.88468
 62829,0.9720489697,-4.5591296169\H,-0.1869543605,0.6358654864,-4.06350
 84142\C,3.2038501431,1.0491182151,-4.0570994529\H,1.6951531795,1.12514
 64185,-5.6175233185\C,3.1442927886,-0.0349142609,2.4240134188\C,4.2142
 450513,0.238242594,1.5415455436\C,3.9749058576,0.4344577602,0.18652978
 42\C,1.8459709081,-0.1083588508,1.9389643962\H,3.3365713673,-0.1875699
 787,3.4819759818\H,5.2301978294,0.2955008461,1.9216787138\H,1.01315174
 82,-0.3149186078,2.5976476499\H,4.0292524367,1.2618420296,-4.730448239
```

\H,4.818890298,0.6410568418,-0.4602845966\H,4.4762011441,0.9214543251,
-2.3541524351\\Version=AM64L-G09RevA.02\State=2-A\HF=-1068.0698274\S2=
0.795416\S2-1=0.\S2A=0.750342\RMSD=7.131e-09\RMSF=3.413e-06\Dipole=1.0
024504,0.147105,-0.1595688\Quadrupole=12.1340558,-10.6444669,-1.489588
9,2.877255,-1.761582,-3.5456392\PG=C01 [X(C21H13N2O2)]\\@

Table E–7. Output parameters for **3.5**, EPR-II.

1\1\GINC-COMPUTE-0-25\FOpt\UB3LYP\EPR-II\C23H13N2O2(2)\BRYNND\15-Aug-2
010\0\\#T opt ub3lyp/epr-II geom=connectivity density=current\\Pyrene
NN epr II\\0,2\N,-0.9890369107,-0.2559007239,0.59477466\C,-1.999528261
9,-0.1925471536,-0.3484691045\N,-1.384245521,0.1132762055,-1.549588086
6\O,-1.1223176901,-0.5126197968,1.8383981955\O,-1.9552465375,0.2650489
765,-2.6814929047\C,-3.4294424453,-0.4055749708,-0.1216131384\C,-3.921
4590131,-0.7185045069,1.1739072106\C,-4.3584427807,-0.304417759,-1.191
7096171\C,-5.2900612811,-0.9204489471,1.3804624098\H,-3.2318612522,-0.
7999272417,2.0011135061\C,-5.7232662669,-0.5098931703,-0.9646570208\H,
-4.0049682843,-0.0675466769,-2.1843795503\C,-6.2008401721,-0.818642103
6,0.3180210407\H,-5.6435499056,-1.1588759065,2.3799430356\H,-6.4153810
186,-0.4273772365,-1.7982823265\H,-7.262480223,-0.9769277774,0.4864237
403\C,0.0161175175,0.241407229,-1.3559626027\C,1.0469829948,0.54712997
16,-2.3054465936\C,0.2624479133,0.0112531327,-0.0195394335\C,2.3795616
237,0.5986862186,-1.7612930524\C,0.8286198921,0.7877137895,-3.67755854
62\C,1.5747679469,0.0540612211,0.5581074516\C,3.4705316663,0.898116991
3,-2.6418450432\C,2.6367118874,0.3584296509,-0.3660660189\C,1.91276736
15,1.0780903006,-4.5154307276\H,-0.1797981864,0.7442846015,-4.06640062
61\C,3.2154835731,1.1334503536,-4.0095965556\H,1.7351583437,1.26204575
73,-5.5710507108\C,3.1828484809,-0.1086221682,2.3755701173\C,4.2303425
574,0.1851829369,1.496703056\C,3.9810324773,0.4211145615,0.1279899225\
C,1.8602180757,-0.1761467833,1.9196321627\H,3.3933682966,-0.2873846909
,3.4260162011\H,5.2525113196,0.2347086093,1.8626643045\H,1.0483899528,
-0.4032073432,2.597395352\H,4.0484822945,1.3597491733,-4.6699790202\C,
5.0547727652,0.7248623864,-0.7860052675\C,4.8105695193,0.9530409888,-2
.1109513867\H,6.0675354214,0.7681982749,-0.3942058698\H,5.6254538795,1
.1812847862,-2.7928174426\\Version=AM64L-G09RevA.02\State=2-A\HF=-1144
.3110397\S2=0.79608\S2-1=0.\S2A=0.750353\RMSD=4.157e-09\RMSF=1.415e-05
\Dipole=1.0326343,0.1536278,-0.1638259\Quadrupole=11.8164616,-11.62348
12,-0.1929804,3.185632,-1.6347243,-2.6016783\PG=C01 [X(C23H13N2O2)]\\@

Table E–8. Output parameters for **3.6**, EPR-II.

1\1\GINC-COMPUTE-0-2\FOpt\UB3LYP\EPR-II\C12H8N3O2(2)\BRYNND\16-Aug-201
0\0\\#T opt ub3lyp/epr-II geom=connectivity density=current\\4pyBNN ep
r II\\0,2\N,-0.9470398866,-0.277133513,0.6172272364\C,-1.9419136356,-0
.1981157786,-0.3433353477\N,-1.3218705053,0.1022097628,-1.556645962\O,
-1.0690105452,-0.5306792314,1.8635432985\O,-1.8756760155,0.26113743,-2
.6890176216\C,-3.3737486175,-0.3930013923,-0.126523666\C,-3.8728246312
,-0.6985628132,1.1685780685\C,-4.2941509074,-0.2815052811,-1.203305431
\C,-5.2444221211,-0.8838584251,1.3684425379\H,-3.1857950891,-0.7866866
914,1.9978131321\C,-5.6619501288,-0.4704851435,-0.9819604373\H,-3.9318
328043,-0.0499976067,-2.1943477622\C,-6.14736998,-0.7719844115,0.29988
90584\H,-5.6068603608,-1.1168986306,2.3657790423\H,-6.3500549958,-0.38
10617027,-1.817901066\H,-7.2116064363,-0.9173601209,0.4633094421\C,0.0
839032546,0.211423289,-1.3445360985\C,0.3041047044,-0.0275394312,0.015
7591141\C,2.2602039105,0.5244552484,-1.7626748162\C,1.5950162275,0.010

4010992,0.5331407084\C,2.5968927413,0.2993638265,-0.4097890541\H,1.796
140749,-0.1706801639,1.5829618133\H,3.6377267222,0.3523814269,-0.10844
94361\H,3.0414228968,0.7473485186,-2.4852074941\N,1.0045290942,0.48502
02557,-2.2534762792\\Version=AM64L-G09RevA.02\State=2-A\HF=-776.788207
3\S2=0.805523\S2-1=0.\S2A=0.750449\RMSD=8.230e-09\RMSF=2.003e-05\Dipol
e=0.6582208,-0.0604542,0.6779269\Quadrupole=17.3926782,-6.2015178,-11.
1911604,2.3711804,0.8013656,1.0236817\PG=C01 [X(C12H8N3O2)]\\@

Table E–9. Output parameters for **3.7**, EPR-II.

1\1\GINC-COMPUTE-0-2\FOpt\UB3LYP\EPR-II\C12H8N3O2(2)\BRYNND\16-Aug-201
0\0\\#T opt ub3lyp/epr-II geom=connectivity density=current\\5pyBNN ep
r II\\0,2\N,-0.9601950367,-0.2800337169,0.6068964753\C,-1.9655860574,-
0.2058261227,-0.3496158605\N,-1.3517770181,0.086635156,-1.5607073807\O
,-1.0761803542,-0.5267813691,1.8535836676\O,-1.902074011,0.2430573941,
-2.6999965189\C,-3.3959811218,-0.3986760462,-0.1228579189\C,-3.8887987
381,-0.6952719944,1.1761973043\C,-4.3200097536,-0.2927463217,-1.196862
9052\C,-5.2597971553,-0.877863491,1.3829909076\H,-3.1986489036,-0.7789
443786,2.0033299492\C,-5.6869730917,-0.4789176804,-0.9686907247\H,-3.9
60757278,-0.0676442878,-2.1906809248\C,-6.1668017666,-0.7718183575,0.3
173470439\H,-5.618509395,-1.1041216167,2.3831499166\H,-6.3788269098,-0
.3941456782,-1.8019539589\H,-7.2304304991,-0.9149770567,0.4862558805\C
,0.0445732851,0.1961727391,-1.3624901362\C,0.2880814602,-0.0331306385,
-0.0078268523\C,1.582127212,0.0072997577,0.4990766577\C,2.5788029209,0
.2913944605,-0.4550291369\H,1.8050323836,-0.1660932798,1.5449717408\H,
3.6189175358,0.3415950908,-0.1414327394\N,2.3564866487,0.5150995288,-1
.7674610745\C,1.0975333472,0.470908379,-2.2356348341\H,0.9321825765,0.
6524163804,-3.2932910973\\Version=AM64L-G09RevA.02\State=2-A\HF=-776.7
878221\S2=0.804451\S2-1=0.\S2A=0.750468\RMSD=6.770e-09\RMSF=2.770e-05\
Dipole=-0.2657463,-0.1150624,0.4640834\Quadrupole=7.8460395,-3.2539684
,-4.5920711,0.5748218,3.0965019,0.5826623\PG=C01 [X(C12H8N3O2)]\\@

Table E–10. Output parameters for **3.8**, EPR-II.

1\1\GINC-COMPUTE-0-3\FOpt\UB3LYP\EPR-II\C15H9N4O2(2)\BRYNND\16-Aug-201
0\0\\#T opt ub3lyp/epr-II geom=connectivity density=current\\QNN epr I
I\\0,2\N,-0.1789569796,-1.1373898086,-0.0992738925\C,-1.1078189446,-0.
2227211681,-0.5954270262\N,-0.4220607721,0.7049815399,-1.3791257773\O,
-0.3998019698,-2.1373904442,0.6561889031\O,-0.905815893,1.699239402,-2
.0090676017\C,-2.5431992833,-0.2344717763,-0.3396844628\C,-3.126371471
8,-1.2393723658,0.4817233795\C,-3.3899571802,0.7587711756,-0.906355181
\C,-4.5034118941,-1.2410598576,0.7201948641\H,-2.4982119662,-2.0009424
108,0.9198530587\C,-4.7644850677,0.7380259721,-0.6546445928\H,-2.96386
68811,1.5289463735,-1.5323030205\C,-5.3310605873,-0.2572025375,0.15696
46626\H,-4.9300105657,-2.0165086398,1.3500137393\H,-5.3945311467,1.504
8569773,-1.0962236698\H,-6.4006180361,-0.2659260637,0.3475051311\C,0.9
576718419,0.3744481549,-1.3797221152\C,1.1106097823,-0.785145863,-0.57
41670487\C,3.3131158229,-0.7797867289,-0.9574983031\C,3.1568457742,0.4
049734577,-1.780533706\C,4.61056795,-1.3358449617,-0.7821235652\C,5.70
72587391,-0.7495681545,-1.3916824458\C,5.5538600902,0.4137117953,-2.19
98025704\C,4.3050545556,0.9809013751,-2.3915445876\H,4.7029527943,-2.2
221187223,-0.1622183135\H,6.6956692368,-1.1781198533,-1.254535322\H,6.
4272595613,0.8573627443,-2.6685674313\H,4.1636641947,1.8667821083,-3.0
027242631\N,2.2442600151,-1.3846390777,-0.339409013\N,1.9308483869,0.9
910893413,-1.9897835031\\Version=AM64L-G09RevA.02\State=2-A\HF=-946.48

58994\S2=0.813542\S2-1=0.\S2A=0.750613\RMSD=6.993e-09\RMSF=2.141e-04\D
ipole=0.5932767,0.0047552,-0.1056318\Quadrupole=22.0678664,-12.392841,
-9.6750254,0.6952488,-5.8603876,2.2780762\PG=C01 [X(C15H9N4O2)]\\@

Table E–11. Output parameters for **2.15a**, E_{anion}.

1\1\GINC-COMPUTE-0-12\SP\UB3LYP\6-311+G(d,p)\C13H9N2O2(1-)\BRYNND\10-S
ep-2010\0\\# ub3lyp/6-311+g(d,p)\\BNN anion\\-1,1\N,0,-0.50706791,-1.1
1457633,-0.00011778\C,0,0.31985275,0.00000938,0.00052621\N,0,-0.507053
49,1.11459034,0.00006342\O,0,-0.16494285,-2.3441724,0.00068391\O,0,-0.
16492534,2.34418557,0.00112017\C,0,1.78170954,-0.00000304,0.00054659\C
,0,2.50606802,-1.22202031,0.00059956\C,0,2.50608319,1.22200832,-0.0000
1359\C,0,3.90462616,-1.21118151,-0.00009571\H,0,1.96917346,-2.15972178
,0.00107554\C,0,3.9046416,1.21115666,-0.00071878\H,0,1.96920134,2.1597
1738,0.00005012\C,0,4.61363211,-0.00001663,-0.00075391\H,0,4.44096393,
-2.15603582,-0.00011029\H,0,4.44099036,2.15600471,-0.00122834\H,0,5.70
009031,-0.00002347,-0.00147624\C,0,-1.86033419,0.69878217,-0.00043043\
C,0,-3.03791055,1.44349026,-0.00008598\C,0,-1.86036489,-0.69873125,-0.
00053256\C,0,-4.23557316,0.70651154,-0.00027003\C,0,-3.03791895,-1.443
44821,-0.0003168\C,0,-4.23554376,-0.70655889,-0.00037932\H,0,-3.015133
1,-2.52708052,-0.0002206\H,0,-5.18306599,-1.23650573,-0.00047377\H,0,-
5.18318147,1.23632845,-0.00025017\H,0,-3.01505081,2.5271223,0.00013012
\\Version=AM64L-G09RevA.02\State=1-A\HF=-760.9068171\S2=0.\S2-1=0.\S2A
=0.\RMSD=2.413e-09\Dipole=0.3239974,-0.0000657,-0.0012734\Quadrupole=-
1.1123631,-5.5073374,6.6197006,0.0005444,-0.0028247,-0.0031289\PG=C01
[X(C13H9N2O2)]\\@

Table E–12. Output parameters for **2.15a**, $E_{radical}$.

1\1\GINC-COMPUTE-0-14\SP\UB3LYP\6-311+G(d,p)\C13H9N2O2(2)\BRYNND\10-Se
p-2010\0\\# ub3lyp/6-311+g(d,p)\\BNN radical\\0,2\N,0,-0.50706791,-1.1
1457633,-0.00011778\C,0,0.31985275,0.00000938,0.00052621\N,0,-0.507053
49,1.11459034,0.00006342\O,0,-0.16494285,-2.3441724,0.00068391\O,0,-0.
16492534,2.34418557,0.00112017\C,0,1.78170954,-0.00000304,0.00054659\C
,0,2.50606802,-1.22202031,0.00059956\C,0,2.50608319,1.22200832,-0.0000
1359\C,0,3.90462616,-1.21118151,-0.00009571\H,0,1.96917346,-2.15972178
,0.00107554\C,0,3.9046416,1.21115666,-0.00071878\H,0,1.96920134,2.1597
1738,0.00005012\C,0,4.61363211,-0.00001663,-0.00075391\H,0,4.44096393,
-2.15603582,-0.00011029\H,0,4.44099036,2.15600471,-0.00122834\H,0,5.70
009031,-0.00002347,-0.00147624\C,0,-1.86033419,0.69878217,-0.00043043\
C,0,-3.03791055,1.44349026,-0.00008598\C,0,-1.86036489,-0.69873125,-0.
00053256\C,0,-4.23557316,0.70651154,-0.00027003\C,0,-3.03791895,-1.443
44821,-0.0003168\C,0,-4.23554376,-0.70655889,-0.00037932\H,0,-3.015133
1,-2.52708052,-0.0002206\H,0,-5.18306599,-1.23650573,-0.00047377\H,0,-
5.18318147,1.23632845,-0.00025017\H,0,-3.01505081,2.5271223,0.00013012
\\Version=AM64L-G09RevA.02\State=2-A\HF=-760.8286423\S2=0.801238\S2-1=
0.\S2A=0.750453\RMSD=2.099e-09\Dipole=-0.7494659,-0.0000575,-0.0010277
\Quadrupole=14.9692361,-7.2953691,-7.6738669,0.0004962,-0.0029964,-0.0
024348\PG=C01 [X(C13H9N2O2)]\\@

Table E–13. Output parameters for **3.4**, E_{anion}.

1\1\GINC-COMPUTE-0-35\SP\UB3LYP\6-311+G(d,p)\C21H13N2O2(1-)\BRYNND\10-
Sep-2010\0\\# ub3lyp/6-311+g(d,p)\\PhenNN anion\\-1,1\N,0,-0.930748,-1

.106061,0.022784\C,0,-1.759118,0.,-0.000051\N,0,-0.930752,1.106047,-0.
022935\O,0,-1.300498,-2.327452,0.066676\O,0,-1.300493,2.327444,-0.0669
37\C,0,-3.222077,0.000005,-0.000044\C,0,-3.946526,-1.192897,-0.258589\
C,0,-3.946511,1.192902,0.258576\C,0,-5.345392,-1.182841,-0.258716\H,0,
-3.412023,-2.112887,-0.447563\C,0,-5.345377,1.182832,0.258853\H,0,-3.4
11995,2.112896,0.447494\C,0,-6.054808,-0.000009,0.000113\H,0,-5.881161
,-2.10624,-0.461053\H,0,-5.881135,2.106215,0.461299\H,0,-7.141323,-0.0
00014,0.000167\C,0,0.427269,0.688837,-0.011879\C,0,1.627325,1.471869,-
0.026798\C,0,0.427272,-0.688847,0.011892\C,0,2.859804,0.733994,-0.0124
46\C,0,1.634757,2.892568,-0.049263\C,0,1.627334,-1.471874,0.026803\C,0
,4.066029,1.483228,-0.02266\C,0,2.859812,-0.733988,0.012441\C,0,2.8387
22,3.582993,-0.058407\H,0,0.688663,3.416875,-0.060571\C,0,4.060943,2.8
72948,-0.045066\H,0,2.840132,4.668927,-0.075818\C,0,2.838759,-3.582982
,0.058506\C,0,4.060973,-2.872929,0.045133\C,0,4.066045,-1.48321,0.0226
68\C,0,1.634784,-2.892571,0.049343\H,0,2.840163,-4.668917,0.075957\H,0
,5.002978,-3.413778,0.052198\H,0,0.688706,-3.416905,0.060641\H,0,5.002
938,3.413813,-0.052105\H,0,5.021195,-0.972384,0.012243\H,0,5.021179,0.
972403,-0.012204\\Version=AM64L-G09RevA.02\State=1-A\HF=-1068.275303\S
2=0.\S2-1=0.\S2A=0.\RMSD=6.967e-09\Dipole=1.2444755,-0.0000227,0.00019
37\Quadrupole=-6.7120454,-1.743938,8.4559835,0.0000487,-0.0007016,1.63
81108\PG=C01 [X(C21H13N2O2)]\\@

Table E–14. Output parameters for **3.4**, $E_{radical}$.

1\1\GINC-COMPUTE-0-29\SP\UB3LYP\6-311+G(d,p)\C21H13N2O2(2)\BRYNND\10-S
ep-2010\0\\# ub3lyp/6-311+g(d,p)\\PhenNN rad\\0,2\N,0,-0.930748,-1.106
061,0.022784\C,0,-1.759118,0.,-0.000051\N,0,-0.930752,1.106047,-0.0229
35\O,0,-1.300498,-2.327452,0.066676\O,0,-1.300493,2.327444,-0.066937\C
,0,-3.222077,0.000005,-0.000044\C,0,-3.946526,-1.192897,-0.258589\C,0,
-3.946511,1.192902,0.258576\C,0,-5.345392,-1.182841,-0.258716\H,0,-3.4
12023,-2.112887,-0.447563\C,0,-5.345377,1.182832,0.258853\H,0,-3.41199
5,2.112896,0.447494\C,0,-6.054808,-0.000009,0.000113\H,0,-5.881161,-2.
10624,-0.461053\H,0,-5.881135,2.106215,0.461299\H,0,-7.141323,-0.00001
4,0.000167\C,0,0.427269,0.688837,-0.011879\C,0,1.627325,1.471869,-0.02
6798\C,0,0.427272,-0.688847,0.011892\C,0,2.859804,0.733994,-0.012446\C
,0,1.634757,2.892568,-0.049263\C,0,1.627334,-1.471874,0.026803\C,0,4.0
66029,1.483228,-0.02266\C,0,2.859812,-0.733988,0.012441\C,0,2.838722,3
.582993,-0.058407\H,0,0.688663,3.416875,-0.060571\C,0,4.060943,2.87294
8,-0.045066\H,0,2.840132,4.668927,-0.075818\C,0,2.838759,-3.582982,0.0
58506\C,0,4.060973,-2.872929,0.045133\C,0,4.066045,-1.48321,0.022668\C
,0,1.634784,-2.892571,0.049343\H,0,2.840163,-4.668917,0.075957\H,0,5.0
02978,-3.413778,0.052198\H,0,0.688706,-3.416905,0.060641\H,0,5.002938,
3.413813,-0.052105\H,0,5.021195,-0.972384,0.012243\H,0,5.021179,0.9724
03,-0.012204\\Version=AM64L-G09RevA.02\State=2-A\HF=-1068.1828719\S2=0
.794516\S2-1=0.\S2A=0.750352\RMSD=4.825e-09\Dipole=1.0309951,-0.000031
3,0.0001527\Quadrupole=13.0417205,-1.0823839,-11.9593366,0.0001487,-0.
0006105,1.433405\PG=C01 [X(C21H13N2O2)]\\@

Table E–15. Output parameters for **3.5**, E_{anion}.

1\1\GINC-COMPUTE-0-16\SP\UB3LYP\6-311+G(d,p)\C23H13N2O2(1-)\BRYNND\10-
Sep-2010\0\\# ub3lyp/6-311+g(d,p)\\PyreneNN anion\\-1,1\N,0,1.307348,-
1.105762,-0.000527\C,0,2.139284,-0.000006,-0.000056\N,0,1.307359,1.105
747,0.000018\O,0,1.667737,-2.330666,-0.00103\O,0,1.667739,2.33066,0.00
0602\C,0,3.60267,-0.000009,0.000058\C,0,4.329817,-1.220511,0.003231\C,

0,4.329811,1.220498,-0.002931\C,0,5.728533,-1.209937,0.003442\H,0,3.79
6077,-2.159427,0.005401\C,0,5.728527,1.209933,-0.002723\H,0,3.796058,2
.159406,-0.005238\C,0,6.438961,0.,0.000469\H,0,6.263583,-2.155705,0.00
5975\H,0,6.263571,2.155705,-0.005033\H,0,7.525467,0.000003,0.000679\C,
0,-0.049611,0.689144,-0.000334\C,0,-1.24859,1.476619,0.000045\C,0,-0.0
49632,-0.689144,-0.0006\C,0,-2.47384,0.719461,0.000182\C,0,-1.282947,2
.886255,0.000119\C,0,-1.248621,-1.476619,-0.000607\C,0,-3.719948,1.428
306,0.000566\C,0,-2.473848,-0.719465,-0.000121\C,0,-2.514454,3.553425,
0.000464\H,0,-0.35155,3.436247,-0.000025\C,0,-3.717019,2.839393,0.0007
09\H,0,-2.531327,4.639442,0.00052\C,0,-2.514498,-3.553423,-0.000944\C,
0,-3.717044,-2.839381,-0.0004\C,0,-3.719957,-1.428287,0.000003\C,0,-1.
282969,-2.886245,-0.001069\H,0,-2.531341,-4.639438,-0.001295\H,0,-4.66
6311,-3.368626,-0.000286\H,0,-0.351589,-3.436261,-0.001479\H,0,-4.6662
79,3.368645,0.001009\C,0,-4.955042,-0.683215,0.000525\C,0,-4.955033,0.
683234,0.000789\H,0,-5.890213,-1.236866,0.0007\H,0,-5.890207,1.236879,
0.001174\\Version=AM64L-G09RevA.02\State=1-A\HF=-1144.5259116\S2=0.\S2
-1=0.\S2A=0.\RMSD=5.336e-09\Dipole=-1.6649297,-0.000028,0.0002147\Quad
rupole=-10.1779296,1.0916322,9.0862974,0.0000708,-0.0006472,-0.0193969
\PG=C01 [X(C23H13N2O2)]\\@

Table E–16. Output parameters for **3.5**, $E_{radical}$.

1\1\GINC-COMPUTE-0-14\SP\UB3LYP\6-311+G(d,p)\C23H13N2O2(2)\BRYNND\10-S
ep-2010\0\\# ub3lyp/6-311+g(d,p)\\PyreneNN radical\\0,2\N,0,1.307348,-
1.105762,-0.000527\C,0,2.139284,-0.000006,-0.000056\N,0,1.307359,1.105
747,0.000018\O,0,1.667737,-2.330666,-0.00103\O,0,1.667739,2.33066,0.00
0602\C,0,3.60267,-0.000009,0.000058\C,0,4.329817,-1.220511,0.003231\C,
0,4.329811,1.220498,-0.002931\C,0,5.728533,-1.209937,0.003442\H,0,3.79
6077,-2.159427,0.005401\C,0,5.728527,1.209933,-0.002723\H,0,3.796058,2
.159406,-0.005238\C,0,6.438961,0.,0.000469\H,0,6.263583,-2.155705,0.00
5975\H,0,6.263571,2.155705,-0.005033\H,0,7.525467,0.000003,0.000679\C,
0,-0.049611,0.689144,-0.000334\C,0,-1.24859,1.476619,0.000045\C,0,-0.0
49632,-0.689144,-0.0006\C,0,-2.47384,0.719461,0.000182\C,0,-1.282947,2
.886255,0.000119\C,0,-1.248621,-1.476619,-0.000607\C,0,-3.719948,1.428
306,0.000566\C,0,-2.473848,-0.719465,-0.000121\C,0,-2.514454,3.553425,
0.000464\H,0,-0.35155,3.436247,-0.000025\C,0,-3.717019,2.839393,0.0007
09\H,0,-2.531327,4.639442,0.00052\C,0,-2.514498,-3.553423,-0.000944\C,
0,-3.717044,-2.839381,-0.0004\C,0,-3.719957,-1.428287,0.000003\C,0,-1.
282969,-2.886245,-0.001069\H,0,-2.531341,-4.639438,-0.001295\H,0,-4.66
6311,-3.368626,-0.000286\H,0,-0.351589,-3.436261,-0.001479\H,0,-4.6662
79,3.368645,0.001009\C,0,-4.955042,-0.683215,0.000525\C,0,-4.955033,0.
683234,0.000789\H,0,-5.890213,-1.236866,0.0007\H,0,-5.890207,1.236879,
0.001174\\Version=AM64L-G09RevA.02\State=2-A\HF=-1144.4313128\S2=0.795
106\S2-1=0.\S2A=0.750363\RMSD=4.715e-09\Dipole=-1.0806566,-0.0000332,0
.0001341\Quadrupole=12.9025179,-0.1409421,-12.7615759,-0.0000858,-0.00
09627,-0.017\PG=C01 [X(C23H13N2O2)]\\@

Table E–17. Output parameters for **3.6**, E_{anion}.

1\1\GINC-COMPUTE-0-12\SP\UB3LYP\6-311+G(d,p)\C12H8N3O2(1-)\BRYNND\10-S
ep-2010\0\\# ub3lyp/6-311+g(d,p)\\4pyBNN anion\\-1,1\N,0,0.514317,1.12
0186,-0.000695\C,0,-0.304218,0.002735,-0.000205\N,0,0.526733,-1.11811,
0.000315\O,0,0.172446,2.351279,-0.001188\O,0,0.176856,-2.339506,0.0012
14\C,0,-1.765423,-0.001549,-0.000158\C,0,-2.49097,1.220462,0.001604\C,
0,-2.489098,-1.224383,-0.001669\C,0,-3.889332,1.20853,0.001769\H,0,-1.

955294,2.158789,0.002704\C,0,-3.887482,-1.214193,-0.001567\H,0,-1.9533
86,-2.162491,-0.002799\C,0,-4.597106,-0.003365,0.000155\H,0,-4.426319,
2.152983,0.003194\H,0,-4.423023,-2.159432,-0.002782\H,0,-5.683586,-0.0
04257,0.000272\C,0,1.886082,-0.687659,0.000209\C,0,1.864048,0.710736,-
0.000367\C,0,4.122674,-0.769959,0.000446\C,0,3.055196,1.429583,-0.0005
02\C,0,4.217703,0.639045,-0.000129\H,0,3.069178,2.513636,-0.000957\H,0
,5.198617,1.102468,-0.000267\H,0,5.026896,-1.373631,0.000705\N,0,2.961
816,-1.456669,0.000695\\Version=AM64L-G09RevA.02\State=1-A\HF=-776.946
7914\S2=0.\S2-1=0.\S2A=0.\RMSD=5.871e-09\Dipole=-0.4523069,0.7757901,-
0.0003817\Quadrupole=1.3089293,-9.0528501,7.7439208,5.0023078,-0.00299
25,0.0190791\PG=C01 [X(C12H8N3O2)]\\@

Table E–18. Output parameters for **3.6**, $E_{radical}$.

1\1\GINC-COMPUTE-0-12\SP\UB3LYP\6-311+G(d,p)\C12H8N3O2(2)\BRYNND\10-Se
p-2010\0\\# ub3lyp/6-311+g(d,p)\\4pyBNN radical\\0,2\N,0,0.514317,1.12
0186,-0.000695\C,0,-0.304218,0.002735,-0.000205\N,0,0.526733,-1.11811,
0.000315\O,0,0.172446,2.351279,-0.001188\O,0,0.176856,-2.339506,0.0012
14\C,0,-1.765423,-0.001549,-0.000158\C,0,-2.49097,1.220462,0.001604\C,
0,-2.489098,-1.224383,-0.001669\C,0,-3.889332,1.20853,0.001769\H,0,-1.
955294,2.158789,0.002704\C,0,-3.887482,-1.214193,-0.001567\H,0,-1.9533
86,-2.162491,-0.002799\C,0,-4.597106,-0.003365,0.000155\H,0,-4.426319,
2.152983,0.003194\H,0,-4.423023,-2.159432,-0.002782\H,0,-5.683586,-0.0
04257,0.000272\C,0,1.886082,-0.687659,0.000209\C,0,1.864048,0.710736,-
0.000367\C,0,4.122674,-0.769959,0.000446\C,0,3.055196,1.429583,-0.0005
02\C,0,4.217703,0.639045,-0.000129\H,0,3.069178,2.513636,-0.000957\H,0
,5.198617,1.102468,-0.000267\H,0,5.026896,-1.373631,0.000705\N,0,2.961
816,-1.456669,0.000695\\Version=AM64L-G09RevA.02\State=2-A\HF=-776.863
9364\S2=0.803889\S2-1=0.\S2A=0.750456\RMSD=2.270e-09\Dipole=0.5416074,
0.7777335,-0.0003426\Quadrupole=17.0511425,-10.7706682,-6.2804743,5.31
77824,-0.0030087,0.0153203\PG=C01 [X(C12H8N3O2)]\\@

Table E–19. Output parameters for **3.7**, E_{anion}.

1\1\GINC-COMPUTE-0-13\SP\UB3LYP\6-311+G(d,p)\C12H8N3O2(1-)\BRYNND\10-S
ep-2010\0\\# ub3lyp/6-311+g(d,p)\\5pyBNN anion\\-1,1\N,0,-0.512011,1.1
19363,0.000073\C,0,0.31347,0.001412,-0.000266\N,0,-0.514604,-1.113636,
-0.000236\O,0,-0.17177,2.349323,0.000203\O,0,-0.173947,-2.342142,-0.00
0537\C,0,1.774511,0.000664,-0.000294\C,0,2.498384,1.223116,-0.000591\C
,0,2.49786,-1.222162,0.000406\C,0,3.896816,1.211792,-0.000359\H,0,1.96
2609,2.161413,-0.000971\C,0,3.896144,-1.211438,0.000659\H,0,1.961707,-
2.160217,0.000694\C,0,4.604787,0.000067,0.000246\H,0,4.433581,2.156286
,-0.000666\H,0,4.432487,-2.156166,0.001161\H,0,5.691217,-0.000244,0.00
0517\C,0,-1.865144,-0.692776,0.000055\C,0,-1.862315,0.702567,0.000225\
C,0,-3.055516,1.416297,0.000267\C,0,-4.217274,0.619611,0.000131\H,0,-3
.087978,2.499161,0.000381\H,0,-5.193281,1.099309,0.000201\N,0,-4.23353
4,-0.730086,0.000086\C,0,-3.068159,-1.399418,-0.000105\H,0,-3.094942,-
2.484869,-0.000356\\Version=AM64L-G09RevA.02\State=1-A\HF=-776.9520663
\S2=0.\S2-1=0.\S2A=0.\RMSD=5.864e-09\Dipole=1.3476802,0.3244143,0.0002
067\Quadrupole=-8.774161,-2.0168108,10.7909718,-4.4049035,0.001406,-0.
0048748\PG=C01 [X(C12H8N3O2)]\\@

Table E–20. Output parameters for **3.7**, $E_{radical}$.

1\1\GINC-COMPUTE-0-12\SP\UB3LYP\6-311+G(d,p)\C12H8N3O2(2)\BRYNND\10-Se
p-2010\0\\# ub3lyp/6-311+g(d,p)\\5pyBNN radical\\0,2\N,0,-0.512011,1.1
19363,0.000073\C,0,0.31347,0.001412,-0.000266\N,0,-0.514604,-1.113636,
-0.000236\O,0,-0.17177,2.349323,0.000203\O,0,-0.173947,-2.342142,-0.00
0537\C,0,1.774511,0.000664,-0.000294\C,0,2.498384,1.223116,-0.000591\C
,0,2.49786,-1.222162,0.000406\C,0,3.896816,1.211792,-0.000359\H,0,1.96
2609,2.161413,-0.000971\C,0,3.896144,-1.211438,0.000659\H,0,1.961707,-
2.160217,0.000694\C,0,4.604787,0.000067,0.000246\H,0,4.433581,2.156286
,-0.000666\H,0,4.432487,-2.156166,0.001161\H,0,5.691217,-0.000244,0.00
0517\C,0,-1.865144,-0.692776,0.000055\C,0,-1.862315,0.702567,0.000225\
C,0,-3.055516,1.416297,0.000267\C,0,-4.217274,0.619611,0.000131\H,0,-3
.087978,2.499161,0.000381\H,0,-5.193281,1.099309,0.000201\N,0,-4.23353
4,-0.730086,0.000086\C,0,-3.068159,-1.399418,-0.000105\H,0,-3.094942,-
2.484869,-0.000356\\Version=AM64L-G09RevA.02\State=2-A\HF=-776.8629092
\S2=0.802865\S2-1=0.\S2A=0.750474\RMSD=7.530e-09\Dipole=0.3496769,0.42
34745,0.0001864\Quadrupole=6.7720075,-3.5797489,-3.1922587,-5.0880371,
0.0014691,-0.0037392\PG=C01 [X(C12H8N3O2)]\\@

Table E–21. Output parameters for **3.8**, E_{anion}.

1\1\GINC-COMPUTE-0-6\SP\UB3LYP\6-311+G(d,p)\C15H9N4O2(1-)\BRYNND\10-Se
p-2010\0\\# ub3lyp/6-311+g(d,p)\\QNN anion\\-1,1\N,0,-0.575604,1.12820
1,0.\C,0,-1.395696,-0.00008,0.\N,0,-0.575713,-1.128224,0.\O,0,-0.93352
2,2.349427,0.\O,0,-0.933511,-2.349442,-0.000001\C,0,-2.853729,-0.00000
3,0.\C,0,-3.579952,1.223609,-0.000001\C,0,-3.579996,-1.223597,0.000001
\C,0,-4.977441,1.211956,-0.000001\H,0,-3.044489,2.161591,-0.000002\C,0
,-4.977486,-1.21191,0.000001\H,0,-3.044575,-2.161605,0.000002\C,0,-5.6
85574,0.000035,0.\H,0,-5.514083,2.15641,-0.000002\H,0,-5.51416,-2.1563
47,0.000002\H,0,-6.772007,0.000052,0.\C,0,0.780047,-0.710096,0.\C,0,0.
780042,0.710103,0.\C,0,3.015611,0.725487,0.\C,0,3.015603,-0.725534,0.\
C,0,4.2577,1.418708,0.\C,0,5.448958,0.712367,0.\C,0,5.448988,-0.712347
,0.\C,0,4.25775,-1.418701,0.\H,0,4.232831,2.503918,0.\H,0,6.394531,1.2
46514,0.\H,0,6.394588,-1.24642,0.\H,0,4.232841,-2.503918,0.\N,0,1.8501
11,1.454831,0.\N,0,1.850041,-1.454816,0.\\Version=AM64L-G09RevA.02\Sta
te=1-A\HF=-946.6659655\S2=0.\S2-1=0.\S2A=0.\RMSD=7.052e-09\Dipole=0.45
94496,-0.000534,-0.0000005\Quadrupole=-1.1710274,-8.369198,9.5402254,0
.0002972,0.0000048,-0.0000086\PG=C01 [X(C15H9N4O2)]\\@

Table E–22. Output parameters for **3.8**, $E_{radical}$.

1\1\GINC-COMPUTE-0-7\SP\UB3LYP\6-311+G(d,p)\C15H9N4O2(2)\BRYNND\10-Sep
-2010\0\\# ub3lyp/6-311+g(d,p)\\QNN radical\\0,2\N,0,-0.575604,1.12820
1,0.\C,0,-1.395696,-0.00008,0.\N,0,-0.575713,-1.128224,0.\O,0,-0.93352
2,2.349427,0.\O,0,-0.933511,-2.349442,-0.000001\C,0,-2.853729,-0.00000
3,0.\C,0,-3.579952,1.223609,-0.000001\C,0,-3.579996,-1.223597,0.000001
\C,0,-4.977441,1.211956,-0.000001\H,0,-3.044489,2.161591,-0.000002\C,0
,-4.977486,-1.21191,0.000001\H,0,-3.044575,-2.161605,0.000002\C,0,-5.6
85574,0.000035,0.\H,0,-5.514083,2.15641,-0.000002\H,0,-5.51416,-2.1563
47,0.000002\H,0,-6.772007,0.000052,0.\C,0,0.780047,-0.710096,0.\C,0,0.
780042,0.710103,0.\C,0,3.015611,0.725487,0.\C,0,3.015603,-0.725534,0.\
C,0,4.2577,1.418708,0.\C,0,5.448958,0.712367,0.\C,0,5.448988,-0.712347
,0.\C,0,4.25775,-1.418701,0.\H,0,4.232831,2.503918,0.\H,0,6.394531,1.2
46514,0.\H,0,6.394588,-1.24642,0.\H,0,4.232841,-2.503918,0.\N,0,1.8501
11,1.454831,0.\N,0,1.850041,-1.454816,0.\\Version=AM64L-G09RevA.02\Sta

te=2-A\HF=-946.5790899\S2=0.811256\S2-1=0.\S2A=0.75061\RMSD=1.247e-09\
Dipole=0.5972331,0.0001036,-0.0000004\Quadrupole=23.3808168,-14.364069
6,-9.0167471,-0.0003392,0.0000036,-0.0000091\PG=C01 [X(C15H9N4O2)]\\@

Table E–23. Output parameters for **4.11a**; −180º dihedral angle.

N-N= 1.747253933543D+03 E-N=-9.835893603301D+03 KE= 1.958953933664D+03
1\1\GINC-COMPUTE-0-33\SP\UTD-B3LYP-FC\6-31G(d,p)\C17H11N2O2S1(2)\BRYNN
D\18-Apr-2010\0\\# td ub3lyp/6-31g(d,p) scrf=(solvent=thf,a0=5.29)\\bm
d139 in P2(1)/c -180 deg dihedral\\0,2\S,0,-4.319815,-1.574468,0.14733
3\N,0,1.567233,1.421309,-0.163202\O,0,2.213902,2.524024,-0.249115\N,0,
1.066727,-0.71592,-0.084724\O,0,1.151776,-1.989544,-0.026505\C,0,2.108
344,0.161042,-0.101558\C,0,0.162267,1.332104,-0.157321\C,0,-0.809643,2
.304164,-0.20649\H,0,-0.629567,3.201183,-0.222782\C,0,-2.114892,1.8634
92,-0.171787\H,0,-2.79894,2.472563,-0.182855\C,0,-2.458919,0.499242,-0
.087883\C,0,-1.450016,-0.467773,-0.063411\H,0,-1.624183,-1.384334,-0.0
52868\C,0,-0.154076,-0.012476,-0.102032\C,0,3.520193,-0.182092,-0.0096
13\C,0,4.404934,0.65457,0.662838\H,0,4.097509,1.380025,1.02359\C,0,5.7
29214,0.298063,0.780455\H,0,6.235677,0.822634,1.213468\C,0,6.195874,-0
.862003,0.221795\H,0,7.112295,-1.075459,0.32649\C,0,5.331072,-1.68987,
-0.461756\H,0,5.650231,-2.538934,-0.832302\C,0,4.000568,-1.365168,-0.5
71354\H,0,3.414802,-1.96204,-0.989275\C,0,-3.858012,0.079986,0.041991\
C,0,-4.991172,0.88793,0.046262\H,0,-4.932803,1.637687,-0.016325\C,0,-6
.174122,0.144735,0.131752\H,0,-7.055965,0.522284,0.140532\C,0,-5.96447
,-1.180524,0.192927\H,0,-6.578057,-1.890235,0.306544\\Version=AM64L-G0
9RevA.02\State=2-A\HF=-1312.0595638\S2=0.793294\S2-1=0.\S2A=0.750303\R
MSD=7.633e-09\PG=C01 [X(C17H11N2O2S1)]\\@

Table E–24. Output parameters for **4.11a**; −165º dihedral angle.

N-N= 1.747246082813D+03 E-N=-9.835863797900D+03 KE= 1.958948629278D+03
1\1\GINC-COMPUTE-0-4\SP\UTD-B3LYP-FC\6-31G(d,p)\C17H11N2O2S1(2)\BRYNND
\16-May-2010\0\\# td ub3lyp/6-31g(d,p) scrf=(solvent=thf,a0=5.40)\\bmd
139 in P2(1)/c -165 deg dihedral\\0,2\S,0,-4.308155,-1.534868,0.400112
\N,0,1.566279,1.42714,-0.108544\O,0,2.213206,2.532662,-0.137688\N,0,1.
065767,-0.711356,-0.135647\O,0,1.150742,-1.986312,-0.138147\C,0,2.1072
84,0.165328,-0.104351\C,0,0.16132,1.337856,-0.115057\C,0,-0.81049,2.31
1225,-0.12311\H,0,-0.630508,3.207979,-0.095281\C,0,-2.115826,1.869489,
-0.117133\H,0,-2.799925,2.478438,-0.102895\C,0,-2.460051,0.502808,-0.1
00804\C,0,-1.451107,-0.464339,-0.116964\H,0,-1.625144,-1.380337,-0.151
439\C,0,-0.15506,-0.007805,-0.126207\C,0,3.51865,-0.181925,-0.020842\C
,0,4.399327,0.621427,0.696091\H,0,4.089678,1.328749,1.089475\C,0,5.722
981,0.25959,0.804096\H,0,6.22683,0.762732,1.264707\C,0,6.193092,-0.872
352,0.19309\H,0,7.108938,-1.090654,0.292702\C,0,5.332416,-1.666388,-0.
534393\H,0,5.653881,-2.496706,-0.943425\C,0,4.002498,-1.336703,-0.6359
5\H,0,3.419275,-1.912783,-1.085416\C,0,-3.859783,0.0779,0.00072\C,0,-4
.999363,0.837609,-0.246357\H,0,-4.945329,1.561184,-0.453671\C,0,-6.176
027,0.092757,-0.106095\H,0,-7.060201,0.439008,-0.242527\C,0,-5.955722,
-1.187108,0.236571\H,0,-6.567745,-1.877215,0.442166\\Version=AM64L-G09
RevA.02\State=2-A\HF=-1312.0596966\S2=0.79332\S2-1=0.\S2A=0.750299\RMS
D=7.496e-09\PG=C01 [X(C17H11N2O2S1)]\\@

Table E–25. Output parameters for **4.11a**; −150º dihedral angle.

N-N= 1.746713107528D+03 E-N=-9.834245804524D+03 KE= 1.958939999946D+03
1\1\GINC-COMPUTE-0-17\SP\UTD-B3LYP-FC\6-31G(d,p)\C17H11N2O2S1(2)\BRYNN
D\18-Apr-2010\0\\# td ub3lyp/6-31g(d,p) scrf=(solvent=thf,a0=5.09)\\bm
d139 in P2(1)/c -150 deg dihedral\\0,2\S,0,-4.326555,-1.43557,0.649624
\N,0,1.56577,1.426516,-0.064912\O,0,2.211736,2.532828,-0.046369\N,0,1.
067592,-0.709612,-0.17976\O,0,1.15387,-1.983399,-0.232321\C,0,2.108018
,0.165953,-0.107573\C,0,0.160965,1.336466,-0.083254\C,0,-0.811767,2.30
8631,-0.058432\H,0,-0.632859,3.203715,0.006003\C,0,-2.116668,1.865988,
-0.077683\H,0,-2.801454,2.47336,-0.043343\C,0,-2.459598,0.499468,-0.11
7602\C,0,-1.449598,-0.465491,-0.166151\H,0,-1.622502,-1.379536,-0.2379
54\C,0,-0.153982,-0.00794,-0.149631\C,0,3.519221,-0.18324,-0.029572\C,
0,4.394863,0.591728,0.723843\H,0,4.082195,1.282648,1.143136\C,0,5.7182
26,0.226924,0.825224\H,0,6.218854,0.711792,1.308393\C,0,6.19306,-0.879
525,0.172591\H,0,7.108526,-1.100893,0.268871\C,0,5.337471,-1.644751,-0
.590878\H,0,5.662171,-2.457941,-1.030615\C,0,4.007839,-1.312334,-0.687
129\H,0,3.427846,-1.870586,-1.162523\C,0,-3.859471,0.069777,-0.041273\
C,0,-4.980611,0.732575,-0.531772\H,0,-4.915328,1.3984,-0.880878\C,0,-6
.158851,0.003703,-0.332994\H,0,-7.031364,0.291636,-0.608825\C,0,-5.957
549,-1.171042,0.286245\H,0,-6.578995,-1.818568,0.582226\\Version=AM64L
-G09RevA.02\State=2-A\HF=-1312.0594503\S2=0.793439\S2-1=0.\S2A=0.75029
1\RMSD=7.186e-09\PG=C01 [X(C17H11N2O2S1)]\\@

Table E–26. Output parameters for **4.11a**; −135º dihedral angle.

N-N= 1.745813265449D+03 E-N=-9.831526258195D+03 KE= 1.958934604049D+03
1\1\GINC-COMPUTE-0-27\SP\UTD-B3LYP-FC\6-31G(d,p)\C17H11N2O2S1(2)\BRYNN
D\18-Apr-2010\0\\# td ub3lyp/6-31g(d,p) scrf=(solvent=thf,a0=5.05)\\bm
d139 in P2(1)/c -135 deg dihedral\\0,2\S,0,-4.373754,-1.268913,0.88911
1\N,0,1.565477,1.420666,-0.043325\O,0,2.2091,2.527469,0.004424\N,0,1.0
72282,-0.713197,-0.210051\O,0,1.161429,-1.985282,-0.291253\C,0,2.1105,
0.162428,-0.111591\C,0,0.16099,1.328432,-0.072149\C,0,-0.813822,2.2979
51,-0.030904\H,0,-0.637098,3.191657,0.055086\C,0,-2.117694,1.853425,-0
.068114\H,0,-2.803891,2.458569,-0.02398\C,0,-2.457636,0.487539,-0.1413
75\C,0,-1.445429,-0.474162,-0.205952\H,0,-1.616068,-1.386644,-0.299706
\C,0,-0.150856,-0.014687,-0.171187\C,0,3.521912,-0.18582,-0.033146\C,0
,4.391495,0.573318,0.743059\H,0,4.07495,1.253863,1.176182\C,0,5.714961
,0.208763,0.843993\H,0,6.21173,0.683368,1.341134\C,0,6.195892,-0.88155
1,0.16905\H,0,7.111212,-1.103354,0.265724\C,0,5.346402,-1.63068,-0.616
862\H,0,5.675346,-2.432972,-1.073152\C,0,4.016702,-1.298634,-0.713447\
H,0,3.440671,-1.84693,-1.204972\C,0,-3.857073,0.053594,-0.083304\C,0,-
4.936089,0.563379,-0.799327\H,0,-4.844725,1.135302,-1.28308\C,0,-6.123
614,-0.129456,-0.537067\H,0,-6.971211,0.069006,-0.940129\C,0,-5.96972,
-1.130454,0.345161\H,0,-6.610917,-1.709344,0.728362\\Version=AM64L-G09
RevA.02\State=2-A\HF=-1312.0582147\S2=0.793629\S2-1=0.\S2A=0.750284\RM
SD=6.835e-09\PG=C01 [X(C17H11N2O2S1)]\\@

Table E–27. Output parameters for **4.11a**; −120º dihedral angle.

N-N= 1.744760542780D+03 E-N=-9.828349687662D+03 KE= 1.958933732316D+03
1\1\GINC-COMPUTE-0-35\SP\UTD-B3LYP-FC\6-31G(d,p)\C17H11N2O2S1(2)\BRYNN
D\18-Apr-2010\0\\# td ub3lyp/6-31g(d,p) scrf=(solvent=thf,a0=5.28)\\bm
d139 in P2(1)/c -120 deg dihedral\\0,2\S,0,-4.446428,-1.022958,1.10538
5\N,0,1.564962,1.411027,-0.057187\O,0,2.204634,2.520154,-0.01028\N,0,1

.079803,-0.725137,-0.217922\O,0,1.173626,-1.997243,-0.293317\C,0,2.114
529,0.154338,-0.117043\C,0,0.16098,1.314,-0.093825\C,0,-0.817254,2.280
432,-0.062299\H,0,-0.643991,3.17507,0.021007\C,0,-2.11941,1.83142,-0.1
05272\H,0,-2.807849,2.434453,-0.067659\C,0,-2.454404,0.464119,-0.17484
\C,0,-1.438665,-0.494468,-0.229512\H,0,-1.605736,-1.407892,-0.320469\C
,0,-0.145842,-0.030547,-0.189101\C,0,3.526601,-0.188884,-0.028915\C,0,
4.389115,0.576347,0.749192\H,0,4.067795,1.25762,1.177629\C,0,5.713165,
0.216619,0.859363\H,0,6.205446,0.694927,1.357419\C,0,6.201636,-0.87487
,0.191774\H,0,7.117102,-1.093223,0.29471\C,0,5.359238,-1.630066,-0.595
964\H,0,5.693495,-2.433138,-1.046988\C,0,4.029036,-1.302848,-0.701687\
H,0,3.457706,-1.855086,-1.194283\C,0,-3.852715,0.025762,-0.123137\C,0,
-4.868701,0.314556,-1.029346\H,0,-4.73822,0.749145,-1.632312\C,0,-6.07
2463,-0.318275,-0.69844\H,0,-6.883512,-0.247014,-1.205775\C,0,-5.99115
1,-1.062633,0.416605\H,0,-6.661005,-1.542062,0.879782\\Version=AM64L-G
09RevA.02\State=2-A\HF=-1312.0562094\S2=0.793845\S2-1=0.\S2A=0.750279\
RMSD=6.454e-09\PG=C01 [X(C17H11N2O2S1)]\\@

Table E–28. Output parameters for **4.11a**; −105º dihedral angle.

N-N= 1.743762104872D+03 E-N=-9.825337406432D+03 KE= 1.958936156501D+03
1\1\GINC-COMPUTE-0-2\SP\UTD-B3LYP-FC\6-31G(d,p)\C17H11N2O2S1(2)\BRYNND
\18-Apr-2010\0\\# td ub3lyp/6-31g(d,p) scrf=(solvent=thf,a0=5.28)\\bmd
139 in P2(1)/c -105 deg dihedral\\0,2\S,0,-4.539434,-0.69012,1.269063\
N,0,1.563735,1.396888,-0.116468\O,0,2.197698,2.510257,-0.10993\N,0,1.0
89924,-0.746394,-0.195603\O,0,1.190388,-2.019983,-0.220473\C,0,2.11977
3,0.141643,-0.124101\C,0,0.16046,1.29132,-0.156404\C,0,-0.82266,2.2532
3,-0.167852\H,0,-0.654233,3.151323,-0.118887\C,0,-2.122351,1.796225,-0
.199768\H,0,-2.813931,2.396742,-0.189382\C,0,-2.450256,0.425552,-0.217
257\C,0,-1.429549,-0.529236,-0.229053\H,0,-1.591652,-1.44637,-0.284894
\C,0,-0.139251,-0.057483,-0.20033\C,0,3.533027,-0.190628,-0.015375\C,0
,4.387653,0.608968,0.736436\H,0,4.060734,1.304888,1.136132\C,0,5.71285
2,0.260618,0.867389\H,0,6.200142,0.760626,1.348761\C,0,6.210195,-0.853
733,0.245699\H,0,7.126166,-1.063192,0.361789\C,0,5.375687,-1.643578,-0
.516028\H,0,5.71626,-2.462023,-0.933442\C,0,4.044472,-1.327569,-0.6412
9\H,0,3.478469,-1.901639,-1.114704\C,0,-3.846652,-0.01758,-0.155479\C,
0,-4.782926,-0.025292,-1.185128\H,0,-4.603011,0.22366,-1.874413\C,0,-6
.008602,-0.570356,-0.78558\H,0,-6.773892,-0.66786,-1.355748\C,0,-6.020
041,-0.965198,0.498155\H,0,-6.725396,-1.311316,1.023289\\Version=AM64L
-G09RevA.02\State=2-A\HF=-1312.0543191\S2=0.794016\S2-1=0.\S2A=0.75027
8\RMSD=6.091e-09\PG=C01 [X(C17H11N2O2S1)]\\@

Table E–29. Output parameters for **4.11a**; −90º dihedral angle.

N-N= 1.742975301043D+03 E-N=-9.822963242987D+03 KE= 1.958937813156D+03
1\1\GINC-COMPUTE-0-21\SP\UTD-B3LYP-FC\6-31G(d,p)\C17H11N2O2S1(2)\BRYNN
D\18-Apr-2010\0\\# td ub3lyp/6-31g(d,p) scrf=(solvent=thf,a0=5.08)\\bm
d139 in P2(1)/c -90 deg dihedral\\0,2\S,0,-4.646205,-0.296272,1.331703
\N,0,1.56144,1.375305,-0.209417\O,0,2.187983,2.490937,-0.275381\N,0,1.
102151,-0.771664,-0.146243\O,0,1.211146,-2.043334,-0.085276\C,0,2.1258
07,0.126225,-0.130901\C,0,0.159062,1.257656,-0.247048\C,0,-0.830356,2.
209854,-0.326406\H,0,-0.668075,3.110345,-0.337212\C,0,-2.126856,1.7428
16,-0.332102\H,0,-2.822434,2.337912,-0.364421\C,0,-2.445603,0.371834,-
0.258742\C,0,-1.418555,-0.574558,-0.202924\H,0,-1.574358,-1.494465,-0.
197679\C,0,-0.131532,-0.093084,-0.201436\C,0,3.540794,-0.188288,0.0047
7\C,0,4.387149,0.665777,0.70421\H,0,4.054062,1.38467,1.055186\C,0,5.71

4103,0.336108,0.86283\H,0,6.196179,0.870606,1.311265\C,0,6.221251,-0.8
13979,0.319021\H,0,7.138127,-1.008883,0.452077\C,0,5.394987,-1.658841,
-0.390896\H,0,5.742608,-2.501074,-0.751284\C,0,4.062209,-1.361099,-0.5
4169\H,0,3.501882,-1.969498,-0.977489\C,0,-3.839264,-0.075743,-0.17222
1\C,0,-4.684559,-0.432551,-1.218648\H,0,-4.448341,-0.403581,-1.934764\
C,0,-5.936165,-0.866804,-0.76707\H,0,-6.649567,-1.161047,-1.336936\C,0
,-6.054093,-0.844797,0.570695\H,0,-6.799249,-1.034105,1.120234\\Versio
n=AM64L-G09RevA.02\State=2-A\HF=-1312.0535188\S2=0.794085\S2-1=0.\S2A=
0.750277\RMSD=5.970e-09\PG=C01 [X(C17H11N2O2S1)]\\@

Table E–30. Output parameters for **4.11a**; −75º dihedral angle.

N-N= 1.742485934977D+03 E-N=-9.821483982117D+03 KE= 1.958936796289D+03
1\1\GINC-COMPUTE-0-32\SP\UTD-B3LYP-FC\6-31G(d,p)\C17H11N2O2S1(2)\BRYNN
D\18-Apr-2010\0\\# td ub3lyp/6-31g(d,p) scrf=(solvent=thf,a0=5.40)\\bm
d139 in P2(1)/c -75 deg dihedral\\0,2\S,0,-4.759237,0.08179,1.263367\N
,0,1.558001,1.34979,-0.294002\O,0,2.175755,2.463802,-0.431479\N,0,1.11
5706,-0.79219,-0.092234\O,0,1.234715,-2.056311,0.051202\C,0,2.132158,0
.113012,-0.13401\C,0,0.156667,1.218669,-0.325496\C,0,-0.840164,2.15572
5,-0.467551\H,0,-0.685036,3.054897,-0.536554\C,0,-2.132896,1.678884,-0
.444399\H,0,-2.833133,2.265016,-0.516024\C,0,-2.440845,0.313024,-0.282
636\C,0,-1.406393,-0.619462,-0.164405\H,0,-1.55488,-1.538317,-0.099685
\C,0,-0.123246,-0.128565,-0.192703\C,0,3.549378,-0.180646,0.02336\C,0,
4.387763,0.723758,0.666885\H,0,4.048392,1.461193,0.970125\C,0,5.717036
,0.415756,0.84804\H,0,6.194107,0.982069,1.261406\C,0,6.23421,-0.763055
,0.380534\H,0,7.152388,-0.941537,0.526977\C,0,5.41586,-1.658794,-0.274
021\H,0,5.770762,-2.519799,-0.578637\C,0,4.081004,-1.38219,-0.445302\H
,0,3.526252,-2.022057,-0.841354\C,0,-3.831041,-0.1392,-0.168831\C,0,-4
.580352,-0.831839,-1.115208\H,0,-4.284891,-1.015022,-1.78499\C,0,-5.86
0009,-1.15396,-0.64859\H,0,-6.518946,-1.635841,-1.152435\C,0,-6.090755
,-0.727038,0.603808\H,0,-6.877194,-0.766852,1.126319\\Version=AM64L-G0
9RevA.02\State=2-A\HF=-1312.0541939\S2=0.794026\S2-1=0.\S2A=0.750277\R
MSD=6.159e-09\PG=C01 [X(C17H11N2O2S1)]\\@

Table E–31. Output parameters for **4.11a**; −60º dihedral angle.

N-N= 1.742301228028D+03 E-N=-9.820924096462D+03 KE= 1.958934479294D+03
1\1\GINC-COMPUTE-0-29\SP\UTD-B3LYP-FC\6-31G(d,p)\C17H11N2O2S1(2)\BRYNN
D\18-Apr-2010\0\\# td ub3lyp/6-31g(d,p) scrf=(solvent=thf,a0=5.21)\\bm
d139 in P2(1)/c -60 deg dihedral\\0,2\S,0,-4.87066,0.375302,1.090089\N
,0,1.553686,1.33174,-0.334955\O,0,2.161934,2.445293,-0.512647\N,0,1.12
9568,-0.80537,-0.056926\O,0,1.259319,-2.062594,0.130937\C,0,2.13836,0.
106213,-0.132187\C,0,0.153461,1.187933,-0.359714\C,0,-0.851343,2.11105
4,-0.533332\H,0,-0.703825,3.008482,-0.634312\C,0,-2.140012,1.624591,-0
.491417\H,0,-2.845213,2.201977,-0.582682\C,0,-2.436329,0.262792,-0.281
008\C,0,-1.393972,-0.656291,-0.131418\H,0,-1.534689,-1.573486,-0.03403
1\C,0,-0.115011,-0.156044,-0.178957\C,0,3.558174,-0.169895,0.033364\C,
0,4.389727,0.763646,0.643267\H,0,4.044558,1.508495,0.920748\C,0,5.7217
44,0.473312,0.833227\H,0,6.194551,1.05784,1.225604\C,0,6.248207,-0.716
952,0.406924\H,0,7.168019,-0.882498,0.558224\C,0,5.436602,-1.642056,-0
.214339\H,0,5.798333,-2.510314,-0.488849\C,0,4.099277,-1.382799,-0.393
312\H,0,3.549427,-2.040865,-0.76567\C,0,-3.822557,-0.196674,-0.149225\
C,0,-4.477547,-1.155175,-0.916759\H,0,-4.124026,-1.504977,-1.484317\C,
0,-5.785411,-1.387196,-0.475539\H,0,-6.39109,-2.01674,-0.87189\C,0,-6.
127455,-0.63891,0.586102\H,0,-6.953778,-0.564209,1.038538\\Version=AM6

4L-G09RevA.02\State=2-A\HF=-1312.0559684\S2=0.793869\S2-1=0.\S2A=0.750
279\RMSD=6.517e-09\PG=C01 [X(C17H11N2O2S1)]\\@

Table E–32. Output parameters for **4.11a**; −45º dihedral angle.

N-N= 1.742352954645D+03 E-N=-9.821081767459D+03 KE= 1.958934994632D+03
1\1\GINC-COMPUTE-0-0\SP\UTD-B3LYP-FC\6-31G(d,p)\C17H11N2O2S1(2)\BRYNND
\18-Apr-2010\0\\# td ub3lyp/6-31g(d,p) scrf=(solvent=thf,a0=5.30)\\bmd
139 in P2(1)/c -45 deg dihedral\\0,2\S,0,-4.972827,0.57151,0.858134\N,
0,1.549072,1.326356,-0.329865\O,0,2.147994,2.44419,-0.512298\N,0,1.142
576,-0.813367,-0.045678\O,0,1.282776,-2.069149,0.144307\C,0,2.143992,0
.105813,-0.126841\C,0,0.149913,1.171694,-0.348784\C,0,-0.862669,2.0866
61,-0.520362\H,0,-0.722488,2.984984,-0.623807\C,0,-2.147366,1.590358,-
0.472329\H,0,-2.857361,2.162088,-0.562015\C,0,-2.432322,0.226764,-0.25
7893\C,0,-1.382314,-0.683928,-0.110499\H,0,-1.515556,-1.601971,-0.0106
33\C,0,-0.107454,-0.173927,-0.164147\C,0,3.566537,-0.158977,0.033672\C
,0,4.393248,0.78225,0.638321\H,0,4.043431,1.525002,0.915602\C,0,5.7282
07,0.50261,0.823619\H,0,6.198026,1.091603,1.212895\C,0,6.262167,-0.684
46,0.397735\H,0,7.18382,-0.84258,0.545742\C,0,5.455293,-1.617121,-0.21
837\H,0,5.822637,-2.483143,-0.492487\C,0,4.11531,-1.368573,-0.392596\H
,0,3.569098,-2.031655,-0.761394\C,0,-3.814429,-0.243106,-0.119664\C,0,
-4.383339,-1.386658,-0.672363\H,0,-3.976951,-1.850034,-1.107785\C,0,-5
.717678,-1.55714,-0.28572\H,0,-6.275031,-2.289042,-0.55765\C,0,-6.1617
96,-0.586203,0.52917\H,0,-7.023884,-0.436996,0.886424\\Version=AM64L-G
09RevA.02\State=2-A\HF=-1312.0579446\S2=0.793684\S2-1=0.\S2A=0.750285\
RMSD=7.091e-09\PG=C01 [X(C17H11N2O2S1)]\\@

Table E–33. Output parameters for **4.11a**; −30º dihedral angle.

N-N= 1.742512382293D+03 E-N=-9.821571088114D+03 KE= 1.958940398254D+03
1\1\GINC-COMPUTE-0-5\SP\UTD-B3LYP-FC\6-31G(d,p)\C17H11N2O2S1(2)\BRYNND
\18-Apr-2010\0\\# td ub3lyp/6-31g(d,p) scrf=(solvent=thf,a0=4.91)\\bmd
139 in P2(1)/c -30 deg dihedral\\0,2\S,0,-5.058862,0.686931,0.597844\N
,0,1.544917,1.330312,-0.29221\O,0,2.135695,2.455677,-0.453698\N,0,1.15
3576,-0.817675,-0.052599\O,0,1.3028,-2.076399,0.108916\C,0,2.148703,0.
109436,-0.119652\C,0,0.146661,1.167173,-0.30601\C,0,-0.872666,2.079198
,-0.451299\H,0,-0.738748,2.980449,-0.535848\C,0,-2.153913,1.57377,-0.4
06361\H,0,-2.868011,2.142784,-0.479154\C,0,-2.429004,0.204013,-0.22018
3\C,0,-1.372428,-0.702968,-0.099205\H,0,-1.499307,-1.623812,-0.018709\
C,0,-0.101138,-0.183786,-0.149396\C,0,3.573847,-0.14972,0.026354\C,0,4
.398405,0.783288,0.646482\H,0,4.045685,1.517537,0.942124\C,0,5.736213,
0.508183,0.817473\H,0,6.204754,1.091491,1.216722\C,0,6.27492,-0.665836
,0.362392\H,0,7.198446,-0.821275,0.501284\C,0,5.470073,-1.589904,-0.26
9121\H,0,5.84111,-2.447348,-0.564413\C,0,4.127505,-1.346157,-0.429695\
H,0,3.583164,-2.004471,-0.809633\C,0,-3.807261,-0.277588,-0.083898\C,0
,-4.304316,-1.536497,-0.407822\H,0,-3.853852,-2.068356,-0.697078\C,0,-
5.661706,-1.669549,-0.093487\H,0,-6.179047,-2.464783,-0.235713\C,0,-6.
191689,-0.560664,0.448268\H,0,-7.083048,-0.370138,0.697802\\Version=AM
64L-G09RevA.02\State=2-A\HF=-1312.0592393\S2=0.793537\S2-1=0.\S2A=0.75
0297\RMSD=7.557e-09\PG=C01 [X(C17H11N2O2S1)]\\@

Table E–34. Output parameters for **4.11a**; −15º dihedral angle.


```
N-N= 1.742622815394D+03 E-N=-9.821918905116D+03  KE= 1.958948639381D+03
 1\1\GINC-COMPUTE-0-18\SP\UTD-B3LYP-FC\6-31G(d,p)\C17H11N2O2S1(2)\BRYNN
 D\18-Apr-2010\0\\# td ub3lyp/6-31g(d,p) scrf=(solvent=thf,a0=5.30)\\bm
 d139 in P2(1)/c -15 deg dihedral\\0,2\S,0,-5.123117,0.738984,0.324347\
 N,0,1.541985,1.33819,-0.235896\O,0,2.126741,2.471231,-0.36168\N,0,1.16
 1568,-0.818706,-0.070076\O,0,1.317346,-2.081707,0.045258\C,0,2.152235,
 0.114654,-0.111687\C,0,0.144362,1.169387,-0.244706\C,0,-0.879901,2.081
 437,-0.349476\H,0,-0.750439,2.985721,-0.402841\C,0,-2.15862,1.568996,-
 0.312707\H,0,-2.875653,2.13704,-0.359629\C,0,-2.426479,0.192254,-0.173
 411\C,0,-1.365183,-0.713723,-0.093044\H,0,-1.487556,-1.63741,-0.044483
 \C,0,-0.09652,-0.187394,-0.134494\C,0,3.57956,-0.143159,0.013964\C,0,4
 .405054,0.77083,0.660604\H,0,4.051594,1.492485,0.984977\C,0,5.745311,0
 .495797,0.811328\H,0,6.21453,1.066593,1.227507\C,0,6.285342,-0.658826,
 0.310492\H,0,7.210578,-0.814981,0.43661\C,0,5.479431,-1.563386,-0.3473
 59\H,0,5.851727,-2.408086,-0.67592\C,0,4.134628,-1.320084,-0.488756\H,
 0,3.590079,-1.966864,-0.887728\C,0,-3.801585,-0.300067,-0.043756\C,0,-
 4.245944,-1.615875,-0.133412\H,0,-3.763131,-2.179521,-0.269996\C,0,-5.
 621554,-1.729793,0.098398\H,0,-6.109972,-2.555379,0.087233\C,0,-6.2154
 27,-0.552575,0.354284\H,0,-7.127689,-0.346767,0.490339\\Version=AM64L-
 G09RevA.02\State=2-A\HF=-1312.0597048\S2=0.793458\S2-1=0.\S2A=0.75031\
 RMSD=7.761e-09\PG=C01 [X(C17H11N2O2S1)]\\@
```


Table E–35. Output parameters for **4.11a**; 0º dihedral angle.


```
N-N= 1.742548766572D+03 E-N=-9.821704277984D+03  KE= 1.958952695418D+03
 1\1\GINC-COMPUTE-0-2\SP\UTD-B3LYP-FC\6-31G(d,p)\C17H11N2O2S1(2)\BRYNND
 \18-Apr-2010\0\\# td ub3lyp/6-31g(d,p) scrf=(solvent=thf,a0=5.36)\\bmd
 139 in P2(1)/c 0 deg dihedral\\0,2\S,0,-5.161993,0.737793,0.040274\N,0
 ,1.540867,1.346102,-0.170943\O,0,2.1224,2.484686,-0.254544\N,0,1.16588
 9,-0.816665,-0.091922\O,0,1.325,-2.083034,-0.030822\C,0,2.15444,0.1197
 9,-0.1034\C,0,0.143531,1.174747,-0.174273\C,0,-0.883294,2.088125,-0.23
 169\H,0,-0.755965,2.99413,-0.24841\C,0,-2.160694,1.571791,-0.204895\H,
 0,-2.879154,2.139724,-0.221633\C,0,-2.424779,0.18985,-0.120808\C,0,-1.
 361154,-0.71636,-0.087849\H,0,-1.481402,-1.641535,-0.076802\C,0,-0.093
 876,-0.185977,-0.118652\C,0,3.58331,-0.139909,-0.001415\C,0,4.412953,0
 .748107,0.675401\H,0,4.061129,1.454818,1.032775\C,0,5.755016,0.469965,
 0.802497\H,0,6.226941,1.023922,1.237925\C,0,6.292595,-0.661563,0.24907
 1\H,0,7.219217,-0.820814,0.360266\C,0,5.482415,-1.539646,-0.438727\H,0
 ,5.853261,-2.369079,-0.805592\C,0,4.135948,-1.293607,-0.557788\H,0,3.5
 88991,-1.924366,-0.978523\C,0,-3.797758,-0.310469,0.000492\C,0,-4.2117
 58,-1.630531,0.151771\H,0,-3.710191,-2.193933,0.17343\C,0,-5.59987,-1.
 739753,0.294011\H,0,-6.072239,-2.565663,0.416519\C,0,-6.23196,-0.55537
 7,0.252508\H,0,-7.155593,-0.356271,0.271141\\Version=AM64L-G09RevA.02\
 State=2-A\HF=-1312.0598395\S2=0.793425\S2-1=0.\S2A=0.750316\RMSD=7.946
 e-09\PG=C01 [X(C17H11N2O2S1)]\\@
```


Table E–36. Output parameters for **4.11a**; 15º dihedral angle.


```
N-N= 1.742244508545D+03 E-N=-9.820782093186D+03  KE= 1.958947725008D+03
 1\1\GINC-COMPUTE-0-35\SP\UTD-B3LYP-FC\6-31G(d,p)\C17H11N2O2S1(2)\BRYNN
 D\18-Apr-2010\0\\# td ub3lyp/6-31g(d,p) scrf=(solvent=thf,a0=5.15)\\bm
 d139 in P2(1)/c 15 deg dihedral\\0,2\S,0,-5.171588,0.68692,-0.236704\N
 ,0,1.541897,1.351796,-0.110088\O,0,2.123501,2.492527,-0.154942\N,0,1.1
```

66027,-0.812259,-0.111275\O,0,1.324735,-2.080107,-0.100614\C,0,2.15513
7,0.123545,-0.095595\C,0,0.14446,1.181256,-0.10726\C,0,-0.882158,2.096
582,-0.119949\H,0,-0.754304,3.002505,-0.10281\C,0,-2.159649,1.580109,-
0.101448\H,0,-2.877804,2.148551,-0.089658\C,0,-2.423996,0.196056,-0.06
8415\C,0,-1.360797,-0.711176,-0.080225\H,0,-1.481636,-1.636039,-0.1038
38\C,0,-0.093455,-0.180505,-0.102095\C,0,3.584681,-0.140473,-0.016791\
C,0,4.421132,0.72039,0.686221\H,0,4.073114,1.412902,1.073839\C,0,5.764
089,0.437007,0.790199\H,0,6.240382,0.973534,1.242375\C,0,6.295745,-0.6
72501,0.188569\H,0,7.223222,-0.836301,0.28505\C,0,5.478665,-1.523022,-
0.52521\H,0,5.845524,-2.337806,-0.927228\C,0,4.131353,-1.272028,-0.622
359\H,0,3.580107,-1.885836,-1.062135\C,0,-3.796188,-0.308028,0.046009\
C,0,-4.205306,-1.580788,0.432726\H,0,-3.700469,-2.113376,0.608651\C,0,
-5.598993,-1.698317,0.486016\H,0,-6.069857,-2.495046,0.738559\C,0,-6.2
39737,-0.565832,0.15295\H,0,-7.164116,-0.393575,0.058394\\Version=AM64
L-G09RevA.02\State=2-A\HF=-1312.0600307\S2=0.793425\S2-1=0.\S2A=0.7503
08\RMSD=7.809e-09\PG=C01 [X(C17H11N2O2S1)]\\@

Table E–37. Output parameters for **4.11a**; 30º dihedral angle.

N-N= 1.741773723409D+03 E-N=-9.819353811794D+03 KE= 1.958938979840D+03
1\1\GINC-COMPUTE-0-6\SP\UTD-B3LYP-FC\6-31G(d,p)\C17H11N2O2S1(2)\BRYNND
\18-Apr-2010\0\\# td ub3lyp/6-31g(d,p) scrf=(solvent=thf,a0=4.82)\\bmd
139 in P2(1)/c 30 deg dihedral\\0,2\S,0,-5.152469,0.583316,-0.504934\N
,0,1.544941,1.355465,-0.06265\O,0,2.129769,2.495299,-0.07991\N,0,1.162
178,-0.806553,-0.122502\O,0,1.316929,-2.074647,-0.149526\C,0,2.154364,
0.125505,-0.088682\C,0,0.147044,1.189022,-0.052497\C,0,-0.876721,2.107
349,-0.030008\H,0,-0.745837,3.012029,0.011939\C,0,-2.155645,1.594315,-
0.01514\H,0,-2.871855,2.164295,0.019192\C,0,-2.424108,0.210667,-0.0194
32\C,0,-1.363949,-0.698975,-0.066496\H,0,-1.487936,-1.622422,-0.115519
\C,0,-0.095157,-0.171623,-0.084237\C,0,3.583688,-0.144863,-0.02996\C,0
,4.428928,0.693041,0.690073\H,0,4.086485,1.375182,1.100382\C,0,5.77182
3,0.402849,0.774159\H,0,6.253717,0.924797,1.23733\C,0,6.294716,-0.6905
23,0.136393\H,0,7.222466,-0.859746,0.220038\C,0,5.468786,-1.517838,-0.
594276\H,0,5.829555,-2.321843,-1.022643\C,0,4.121491,-1.260203,-0.6724
26\H,0,3.564508,-1.859536,-1.12476\C,0,-3.796859,-0.292453,0.092499\C,
0,-4.225921,-1.463218,0.710608\H,0,-3.732909,-1.932711,1.036148\C,0,-5
.618247,-1.602473,0.678168\H,0,-6.101721,-2.338646,1.058393\C,0,-6.238
708,-0.584247,0.059903\H,0,-7.153551,-0.460038,-0.141895\\Version=AM64
L-G09RevA.02\State=2-A\HF=-1312.0597759\S2=0.793483\S2-1=0.\S2A=0.7502
94\RMSD=7.467e-09\PG=C01 [X(C17H11N2O2S1)]\\@

Table E–38. Output parameters for **4.11a**; 45º dihedral angle.

N-N= 1.741283310556D+03 E-N=-9.817871521419D+03 KE= 1.958932966374D+03
1\1\GINC-COMPUTE-0-6\SP\UTD-B3LYP-FC\6-31G(d,p)\C17H11N2O2S1(2)\BRYNND
\18-Apr-2010\0\\# td ub3lyp/6-31g(d,p) scrf=(solvent=thf,a0=5.12)\\bmd
139 in P2(1)/c 45 deg dihedral\\0,2\S,0,-5.10596,0.416393,-0.752725\N,
0,1.549555,1.35842,-0.041316\O,0,2.140332,2.49526,-0.052209\N,0,1.1547
84,-0.800882,-0.118698\O,0,1.302537,-2.069462,-0.158855\C,0,2.152172,0
.12556,-0.083538\C,0,0.150901,1.199276,-0.022229\C,0,-0.867736,2.12274
5,0.016622\H,0,-0.7317,3.026282,0.066124\C,0,-2.149242,1.616357,0.0362
58\H,0,-2.862113,2.189762,0.081352\C,0,-2.425134,0.23425,0.020922\C,0,
-1.370241,-0.680494,-0.042695\H,0,-1.499533,-1.602767,-0.0995\C,0,-0.0
98812,-0.159708,-0.064992\C,0,3.580426,-0.152901,-0.038115\C,0,4.43549
2,0.673661,0.683423\H,0,4.099779,1.353681,1.102716\C,0,5.777405,0.3755

94,0.754671\H,0,6.265531,0.890574,1.219114\C,0,6.289661,-0.71443,0.102
699\H,0,7.217089,-0.889337,0.177768\C,0,5.453881,-1.530405,-0.62952\H,
0,5.807132,-2.332207,-1.068158\C,0,4.107439,-1.264926,-0.695106\H,0,3.
543893,-1.856993,-1.148879\C,0,-3.799685,-0.262649,0.138411\C,0,-4.272
046,-1.267623,0.977308\H,0,-3.805113,-1.636182,1.441634\C,0,-5.656138,
-1.44484,0.868222\H,0,-6.165404,-2.083989,1.370622\C,0,-6.228845,-0.61
4046,-0.018228\H,0,-7.124518,-0.562772,-0.315261\\Version=AM64L-G09Rev
A.02\State=2-A\HF=-1312.0585408\S2=0.793621\S2-1=0.\S2A=0.750283\RMSD=
7.002e-09\PG=C01 [X(C17H11N2O2S1)]\\@

Table E–39. Output parameters for **4.11a**; 60º dihedral angle.

N-N= 1.740947229369D+03 E-N=-9.816858246849D+03 KE= 1.958932486613D+03
1\1\GINC-COMPUTE-0-35\SP\UTD-B3LYP-FC\6-31G(d,p)\C17H11N2O2S1(2)\BRYNN
D\18-Apr-2010\0\\# td ub3lyp/6-31g(d,p) scrf=(solvent=thf,a0=5.06)\\bm
d139 in P2(1)/c 60 deg dihedral\\0,2\S,0,-5.035093,0.171162,-0.957791\
N,0,1.555026,1.361644,-0.060032\O,0,2.153744,2.493788,-0.096479\N,0,1.
144592,-0.795874,-0.092834\O,0,1.283157,-2.066025,-0.108876\C,0,2.1486
77,0.123904,-0.081327\C,0,0.155412,1.212936,-0.030179\C,0,-0.856446,2.
144268,-0.003905\H,0,-0.713759,3.047603,0.027098\C,0,-2.141365,1.64756
2,0.032676\H,0,-2.849906,2.226836,0.070395\C,0,-2.42709,0.267433,0.045
994\C,0,-1.379055,-0.655921,-0.00541\H,0,-1.515172,-1.57818,-0.043385\
C,0,-0.104126,-0.144801,-0.04488\C,0,3.575162,-0.163844,-0.03825\C,0,4
.440073,0.67055,0.662231\H,0,4.111525,1.361046,1.069917\C,0,5.780226,0
.364324,0.731984\H,0,6.274572,0.884795,1.183549\C,0,6.281111,-0.741914
,0.098755\H,0,7.207688,-0.92196,0.172174\C,0,5.4355,-1.56607,-0.612719
\H,0,5.780617,-2.378828,-1.037449\C,0,4.090619,-1.292283,-0.676146\H,0
,3.520373,-1.889074,-1.115117\C,0,-3.804435,-0.217201,0.18073\C,0,-4.3
40449,-0.980105,1.213934\H,0,-3.912109,-1.202263,1.794133\C,0,-5.70988
1,-1.215706,1.046108\H,0,-6.256316,-1.714481,1.656763\C,0,-6.210581,-0
.660554,-0.069738\H,0,-7.078676,-0.712035,-0.439669\\Version=AM64L-G09
RevA.02\State=2-A\HF=-1312.0564853\S2=0.793807\S2-1=0.\S2A=0.750278\RM
SD=6.324e-09\PG=C01 [X(C17H11N2O2S1)]\\@

Table E–40. Output parameters for **4.11a**; 75º dihedral angle.

N-N= 1.740913872272D+03 E-N=-9.816760586421D+03 KE= 1.958935635348D+03
1\1\GINC-COMPUTE-0-2\SP\UTD-B3LYP-FC\6-31G(d,p)\C17H11N2O2S1(2)\BRYNND
\18-Apr-2010\0\\# td ub3lyp/6-31g(d,p) scrf=(solvent=thf,a0=5.25)\\bmd
139 in P2(1)/c 75 deg dihedral\\0,2\S,0,-4.944441,-0.156435,-1.081726\
N,0,1.560519,1.363229,-0.124537\O,0,2.168261,2.486949,-0.22172\N,0,1.1
32538,-0.789599,-0.043448\O,0,1.260769,-2.059954,0.006517\C,0,2.144064
,0.121214,-0.082753\C,0,0.159849,1.22783,-0.083138\C,0,-0.844352,2.167
575,-0.1028\H,0,-0.694262,3.070089,-0.119426\C,0,-2.133126,1.68407,-0.
036811\H,0,-2.836834,2.270346,-0.027477\C,0,-2.429967,0.308923,0.04937
7\C,0,-1.389606,-0.624467,0.043428\H,0,-1.5333,-1.546296,0.054063\C,0,
-0.110713,-0.126635,-0.02617\C,0,3.568303,-0.175646,-0.028593\C,0,4.44
2144,0.687031,0.624975\H,0,4.120482,1.400562,0.996921\C,0,5.779988,0.3
73826,0.706976\H,0,6.279952,0.913075,1.12938\C,0,6.269904,-0.768065,0.
131046\H,0,7.195221,-0.951666,0.211245\C,0,5.415411,-1.621252,-0.53408
5\H,0,5.752598,-2.4579,-0.91671\C,0,4.072597,-1.34007,-0.608061\H,0,3.
496157,-1.954249,-1.013694\C,0,-3.810757,-0.156639,0.213007\C,0,-4.426
46,-0.599355,1.379951\H,0,-4.046692,-0.628675,2.031393\C,0,-5.775634,-
0.915317,1.182688\H,0,-6.368069,-1.229712,1.868578\C,0,-6.184836,-0.72
6878,-0.082639\H,0,-7.018691,-0.910842,-0.487525\\Version=AM64L-G09Rev

A.02\State=2-A\HF=-1312.0545122\S2=0.79398\S2-1=0.\S2A=0.750276\RMSD=6
.093e-09\PG=C01 [X(C17H11N2O2S1)]\\@

Table E–41. Output parameters for **4.11a**; 90º dihedral angle.

N-N= 1.741272482472D+03 E-N=-9.817842337581D+03 KE= 1.958937890596D+03
1\1\GINC-COMPUTE-0-6\SP\UTD-B3LYP-FC\6-31G(d,p)\C17H11N2O2S1(2)\BRYNND
\18-Apr-2010\0\\# td ub3lyp/6-31g(d,p) scrf=(solvent=thf,a0=5.17)\\bmd
139 in P2(1)/c 90 deg dihedral\\0,2\S,0,-4.839881,-0.529463,-1.08656\N
,0,1.565246,1.360243,-0.213596\O,0,2.182161,2.469626,-0.38746\N,0,1.11
9629,-0.778372,0.014795\O,0,1.237442,-2.043324,0.151752\C,0,2.138587,0
.11926,-0.086651\C,0,0.163527,1.239515,-0.163294\C,0,-0.83293,2.183922
,-0.247532\H,0,-0.67544,3.08191,-0.325957\C,0,-2.125607,1.716685,-0.14
8813\H,0,-2.824474,2.307986,-0.179833\C,0,-2.4337,0.353167,0.03138\C,0
,-1.401041,-0.586952,0.089639\H,0,-1.552297,-1.504672,0.163413\C,0,-0.
118129,-0.105589,-0.013665\C,0,3.560359,-0.184882,-0.011982\C,0,4.4414
92,0.713357,0.581087\H,0,4.125836,1.453326,0.90318\C,0,5.776749,0.3955
26,0.684634\H,0,6.281277,0.958336,1.069179\C,0,6.257062,-0.787146,0.18
8436\H,0,7.180869,-0.972415,0.281218\C,0,5.39535,-1.67687,-0.416816\H,
0,5.725516,-2.540521,-0.74112\C,0,4.054864,-1.390395,-0.510163\H,0,3.4
73253,-2.026177,-0.872856\C,0,-3.818207,-0.08872,0.226263\C,0,-4.52427
4,-0.171307,1.422713\H,0,-4.199872,0.015787,2.077862\C,0,-5.848794,-0.
581343,1.231577\H,0,-6.492938,-0.68972,1.934144\C,0,-6.153042,-0.80789
2,-0.056878\H,0,-6.948179,-1.137963,-0.446621\\Version=AM64L-G09RevA.0
2\State=2-A\HF=-1312.0536333\S2=0.794074\S2-1=0.\S2A=0.750277\RMSD=6.3
31e-09\PG=C01 [X(C17H11N2O2S1)]\\@

Table E–42. Output parameters for **4.11a**; 105º dihedral angle.

N-N= 1.742017635685D+03 E-N=-9.820085311796D+03 KE= 1.958937044326D+03
1\1\GINC-COMPUTE-0-17\SP\UTD-B3LYP-FC\6-31G(d,p)\C17H11N2O2S1(2)\BRYNN
D\18-Apr-2010\0\\# td ub3lyp/6-31g(d,p) scrf=(solvent=thf,a0=5.24)\\bm
d139 in P2(1)/c 105 deg dihedral\\0,2\S,0,-4.73056,-0.87051,-0.98014\N
,0,1.568575,1.357133,-0.28383\O,0,2.193838,2.451467,-0.514094\N,0,1.10
7078,-0.763339,0.055336\O,0,1.215482,-2.020159,0.258789\C,0,2.13269,0.
1205,-0.090468\C,0,0.165916,1.24913,-0.230848\C,0,-0.82353,2.194838,-0
.367081\H,0,-0.659409,3.086334,-0.49212\C,0,-2.11975,1.742583,-0.24728
7\H,0,-2.814272,2.336369,-0.311082\C,0,-2.438042,0.392618,0.003425\C,0
,-1.412307,-0.550428,0.113582\H,0,-1.570326,-1.461917,0.235027\C,0,-0.
12574,-0.084239,-0.011558\C,0,3.552069,-0.189353,0.003697\C,0,4.438348
,0.732526,0.551062\H,0,4.127323,1.490598,0.833071\C,0,5.771053,0.41113
2,0.674563\H,0,6.278778,0.98977,1.030333\C,0,6.243923,-0.799325,0.2423
44\H,0,7.166167,-0.985999,0.347084\C,0,5.377152,-1.713478,-0.317586\H,
0,5.7018,-2.595277,-0.595274\C,0,4.03897,-1.422823,-0.429268\H,0,3.453
591,-2.072639,-0.759583\C,0,-3.826117,-0.028625,0.217685\C,0,-4.62523,
0.210453,1.331734\H,0,-4.35814,0.591798,1.925619\C,0,-5.92281,-0.28961
2,1.17287\H,0,-6.619794,-0.215611,1.827854\C,0,-6.117879,-0.891094,-0.
012109\H,0,-6.873162,-1.351106,-0.345314\\Version=AM64L-G09RevA.02\Sta
te=2-A\HF=-1312.0542542\S2=0.794046\S2-1=0.\S2A=0.750278\RMSD=6.193e-0
9\PG=C01 [X(C17H11N2O2S1)]\\@

Table E–43. Output parameters for **4.11a**; 120º dihedral angle.

N-N= 1.743114415481D+03 E-N=-9.823388903410D+03 KE= 1.958935255906D+03
1\1\GINC-COMPUTE-0-33\SP\UTD-B3LYP-FC\6-31G(d,p)\C17H11N2O2S1(2)\BRYNN
D\18-Apr-2010\0\\# td ub3lyp/6-31g(d,p) scrf=(solvent=thf,a0=5.01)\\bm
d139 in P2(1)/c 120 deg dihedral\\0,2\S,0,-4.619306,-1.148542,-0.80010
6\N,0,1.570387,1.361623,-0.314224\O,0,2.202947,2.447403,-0.564208\N,0,
1.095171,-0.748769,0.06634\O,0,1.195425,-2.001756,0.295938\C,0,2.12649
9,0.125999,-0.093207\C,0,0.166919,1.262775,-0.264953\C,0,-0.816441,2.2
1115,-0.424689\H,0,-0.646623,3.09894,-0.567262\C,0,-2.11575,1.768888,-
0.301124\H,0,-2.806538,2.365214,-0.37999\C,0,-2.442918,0.426193,-0.024
168\C,0,-1.423149,-0.520264,0.109596\H,0,-1.586967,-1.42815,0.249012\C
,0,-0.133389,-0.064124,-0.01964\C,0,3.543653,-0.189994,0.013263\C,0,4.
433033,0.737814,0.545369\H,0,4.125273,1.503279,0.810484\C,0,5.763327,0
.411381,0.681039\H,0,6.27295,0.994269,1.027023\C,0,6.230911,-0.810374,
0.275691\H,0,7.151616,-1.000147,0.388118\C,0,5.361135,-1.730826,-0.269
051\H,0,5.68178,-2.619979,-0.527256\C,0,4.025136,-1.434852,-0.3923\H,0
,3.437343,-2.087935,-0.711704\C,0,-3.834287,0.017398,0.192821\C,0,-4.7
26692,0.507464,1.141658\H,0,-4.517375,1.043029,1.630347\C,0,-5.995715,
-0.07184,1.027616\H,0,-6.745278,0.142426,1.586645\C,0,-6.080209,-0.972
38,0.034693\H,0,-6.795524,-1.535874,-0.218068\\Version=AM64L-G09RevA.0
2\State=2-A\HF=-1312.0560119\S2=0.793907\S2-1=0.\S2A=0.75028\RMSD=6.48
2e-09\PG=C01 [X(C17H11N2O2S1)]\\@

Table E–44. Output parameters for **4.11a**; 135º dihedral angle.

N-N= 1.744405352239D+03 E-N=-9.827281300309D+03 KE= 1.958936603205D+03
1\1\GINC-COMPUTE-0-16\SP\UTD-B3LYP-FC\6-31G(d,p)\C17H11N2O2S1(2)\BRYNN
D\18-Apr-2010\0\\# td ub3lyp/6-31g(d,p) scrf=(solvent=thf,a0=5.18)\\bm
d139 in P2(1)/c 135 deg dihedral\\0,2\S,0,-4.515921,-1.350275,-0.58392
7\N,0,1.570695,1.374883,-0.305765\O,0,2.209016,2.460614,-0.540875\N,0,
1.084807,-0.737448,0.049741\O,0,1.178697,-1.993226,0.266411\C,0,2.1205
49,0.134648,-0.095165\C,0,0.166595,1.281395,-0.264714\C,0,-0.812,2.235
535,-0.419294\H,0,-0.637782,3.124079,-0.551481\C,0,-2.113745,1.797423,
-0.307101\H,0,-2.801647,2.397447,-0.383096\C,0,-2.447882,0.453226,-0.0
46217\C,0,-1.432737,-0.49887,0.082599\H,0,-1.601021,-1.407501,0.211444
\C,0,-0.140454,-0.046782,-0.035164\C,0,3.535818,-0.188398,0.01514\C,0,
4.426277,0.729934,0.561683\H,0,4.120325,1.493802,0.833409\C,0,5.754496
,0.396499,0.700631\H,0,6.264738,0.973514,1.055433\C,0,6.219103,-0.8228
01,0.284608\H,0,7.138426,-1.01762,0.399688\C,0,5.348343,-1.733725,-0.2
74393\H,0,5.666633,-2.621402,-0.540469\C,0,4.01423,-1.430856,-0.401275
\H,0,3.425393,-2.078018,-0.730651\C,0,-3.842027,0.047968,0.159282\C,0,
-4.819779,0.708279,0.897412\H,0,-4.663603,1.351766,1.259343\C,0,-6.061
138,0.065085,0.831493\H,0,-6.858399,0.372302,1.267683\C,0,-6.04338,-1.
045666,0.076562\H,0,-6.722164,-1.682499,-0.0871\\Version=AM64L-G09RevA
.02\State=2-A\HF=-1312.0579476\S2=0.793707\S2-1=0.\S2A=0.750285\RMSD=6
.857e-09\PG=C01 [X(C17H11N2O2S1)]\\@

Table E–45. Output parameters for **4.11a**; 150º dihedral angle.

N-N= 1.745679619864D+03 E-N=-9.831130668797D+03 KE= 1.958942759103D+03
1\1\GINC-COMPUTE-0-34\SP\UTD-B3LYP-FC\6-31G(d,p)\C17H11N2O2S1(2)\BRYNN
D\18-Apr-2010\0\\# td ub3lyp/6-31g(d,p) scrf=(solvent=thf,a0=5.09)\\bm
d139 in P2(1)/c 150 deg dihedral\\0,2\S,0,-4.427607,-1.484162,-0.34924
4\N,0,1.569898,1.392429,-0.270571\O,0,2.2124,2.483354,-0.467081\N,0,1.

076429,-0.728867,0.014046\O,0,1.165776,-1.99123,0.190672\C,0,2.115275,
0.144505,-0.097006\C,0,0.165348,1.301644,-0.240265\C,0,-0.809834,2.263
034,-0.369409\H,0,-0.632523,3.154876,-0.471951\C,0,-2.113343,1.825226,
-0.278536\H,0,-2.799215,2.429331,-0.338944\C,0,-2.452497,0.474279,-0.0
62918\C,0,-1.440616,-0.484342,0.040742\H,0,-1.612028,-1.396169,0.13932
9\C,0,-0.146501,-0.032358,-0.0553\C,0,3.529044,-0.185932,0.010609\C,0,
4.418873,0.711805,0.591328\H,0,4.113437,1.467394,0.88583\C,0,5.745406,
0.37031,0.726759\H,0,6.255189,0.934157,1.102758\C,0,6.20909,-0.836277,
0.27424\H,0,7.127236,-1.037303,0.388035\C,0,5.339049,-1.726264,-0.3185
82\H,0,5.656463,-2.605814,-0.611357\C,0,4.006474,-1.41569,-0.442971\H,
0,3.417769,-2.050244,-0.796248\C,0,-3.848838,0.066566,0.121761\C,0,-4.
898205,0.829504,0.625345\H,0,-4.786869,1.541227,0.850103\C,0,-6.114807
,0.137686,0.608523\H,0,-6.951672,0.498708,0.907839\C,0,-6.010146,-1.10
7117,0.115047\H,0,-6.658417,-1.790989,0.043261\\Version=AM64L-G09RevA.
02\State=2-A\HF=-1312.0591576\S2=0.793506\S2-1=0.\S2A=0.750292\RMSD=7.
159e-09\PG=C01 [X(C17H11N2O2S1)]\\@

Table E–46. Output parameters for **4.11a**; 165º dihedral angle.

N-N= 1.746697754815D+03 E-N=-9.834211189243D+03 KE= 1.958950630032D+03
1\1\GINC-COMPUTE-0-21\SP\UTD-B3LYP-FC\6-31G(d,p)\C17H11N2O2S1(2)\BRYNN
D\18-Apr-2010\0\\# td ub3lyp/6-31g(d,p) scrf=(solvent=thf,a0=5.28)\\bm
d139 in P2(1)/c 165 deg dihedral\\0,2\S,0,-4.360629,-1.557652,-0.10389
4\N,0,1.568561,1.409129,-0.219975\O,0,2.213789,2.506607,-0.364076\N,0,
1.070335,-0.721879,-0.032917\O,0,1.156802,-1.991009,0.087803\C,0,2.111
09,0.153769,-0.099105\C,0,0.163728,1.319521,-0.201649\C,0,-0.809276,2.
287398,-0.293326\H,0,-0.630062,3.182613,-0.355039\C,0,-2.113929,1.8482
39,-0.229383\H,0,-2.79855,2.455623,-0.26668\C,0,-2.456308,0.48962,-0.0
7607\C,0,-1.446457,-0.47442,-0.009521\H,0,-1.619779,-1.389434,0.047385
\C,0,-0.151147,-0.020853,-0.078049\C,0,3.523731,-0.183585,0.001639\C,0
,4.411565,0.685854,0.62677\H,0,4.105576,1.428106,0.952914\C,0,5.736797
,0.336365,0.754318\H,0,6.245264,0.882023,1.157924\C,0,6.201264,-0.8496
73,0.251118\H,0,7.118448,-1.05716,0.361011\C,0,5.333298,-1.710865,-0.3
85648\H,0,5.651072,-2.577052,-0.715521\C,0,4.001916,-1.392748,-0.50357
6\H,0,3.414294,-2.009917,-0.888076\C,0,-3.854282,0.076509,0.082403\C,0
,-4.956661,0.886312,0.338963\H,0,-4.878719,1.63238,0.42123\C,0,-6.1532
79,0.161049,0.372372\H,0,-7.018986,0.544048,0.527715\C,0,-5.983116,-1.
153087,0.153059\H,0,-6.609102,-1.860754,0.17398\\Version=AM64L-G09RevA
.02\State=2-A\HF=-1312.0595154\S2=0.793359\S2-1=0.\S2A=0.7503\RMSD=7.4
83e-09\PG=C01 [X(C17H11N2O2S1)]\\@

Table E–47. Output parameters for **4.11a**; 180º dihedral angle.

N-N= 1.747253930527D+03 E-N=-9.835893592892D+03 KE= 1.958953933530D+03
1\1\GINC-COMPUTE-0-27\SP\UTD-B3LYP-FC\6-31G(d,p)\C17H11N2O2S1(2)\BRYNN
D\18-Apr-2010\0\\# td ub3lyp/6-31g(d,p) scrf=(solvent=thf,a0=5.25)\\bm
d139 in P2(1)/c 180 deg dihedral\\0,2\S,0,-4.319815,-1.574468,0.147333
\N,0,1.567234,1.421309,-0.163202\O,0,2.213902,2.524024,-0.249115\N,0,1
.066727,-0.71592,-0.084724\O,0,1.151776,-1.989544,-0.026505\C,0,2.1083
44,0.161042,-0.101558\C,0,0.162267,1.332104,-0.157321\C,0,-0.809643,2.
304164,-0.20649\H,0,-0.629567,3.201183,-0.222782\C,0,-2.114892,1.86349
2,-0.171787\H,0,-2.79894,2.472563,-0.182855\C,0,-2.458919,0.499242,-0.
087883\C,0,-1.450016,-0.467773,-0.063411\H,0,-1.624183,-1.384334,-0.05
2868\C,0,-0.154076,-0.012476,-0.102032\C,0,3.520193,-0.182092,-0.00961
3\C,0,4.404934,0.65457,0.662838\H,0,4.097509,1.380025,1.02359\C,0,5.72

9214,0.298063,0.780455\H,0,6.235677,0.822634,1.213468\C,0,6.195874,-0.
862003,0.221794\H,0,7.112295,-1.075459,0.32649\C,0,5.331072,-1.68987,-
0.461756\H,0,5.650231,-2.538934,-0.832302\C,0,4.000568,-1.365168,-0.57
1354\H,0,3.414802,-1.96204,-0.989275\C,0,-3.858012,0.079986,0.041991\C
,0,-4.991172,0.88793,0.046262\H,0,-4.932803,1.637687,-0.016325\C,0,-6.
174122,0.144735,0.131752\H,0,-7.055965,0.522284,0.140532\C,0,-5.96447,
-1.180524,0.192927\H,0,-6.578057,-1.890235,0.306544\\Version=AM64L-G09
RevA.02\State=2-A\HF=-1312.0595638\S2=0.793294\S2-1=0.\S2A=0.750303\RM
SD=7.633e-09\PG=C01 [X(C17H11N2O2S1)]\\@

Table E–48. Output parameters for **4.11a**; Onsager solvation, cyclohexane.

N-N= 1.741875852860D+03 E-N=-9.819503189043D+03 KE= 1.958930405568D+03
1\1\GINC-COMPUTE-0-26\SP\UTD-B3LYP-FC\6-31G(d,p)\C17H11N2O2S1(2)\BRYNN
D\20-May-2010\0\\# td ub3lyp/6-31g(d,p) scrf=(solvent=cyclohexane,a0=5
.25)\\bmd139 TDDFT cyclohexane\\0,2\S,0,9.1603,4.4877,0.7978\N,0,15.63
45,3.4905,2.4469\O,0,16.1333,2.3321,2.6724\N,0,15.3547,5.6655,2.3224\O
,0,15.555,6.9271,2.3538\C,0,16.2673,4.6975,2.613\C,0,14.311,3.7069,2.0
186\C,0,13.2965,2.8262,1.7235\H,0,13.3906,1.9164,1.7508\C,0,12.1045,3.
3841,1.3149\H,0,11.4037,2.8395,1.0884\C,0,11.913,4.7754,1.1958\C,0,12.
9546,5.6472,1.5254\H,0,12.8659,6.5758,1.5063\C,0,14.1354,5.0755,1.9342
\C,0,17.6619,4.913,2.971\C,0,18.6405,4.0139,2.56\H,0,18.4017,3.3271,2.
0886\C,0,19.961,4.2512,2.8676\H,0,20.5323,3.6921,2.5844\C,0,20.3248,5.
3521,3.5965\H,0,21.2431,5.4837,3.7856\C,0,19.361,6.2404,4.0237\H,0,19.
6178,7.049,4.5139\C,0,18.0396,6.0355,3.7081\H,0,17.4035,6.6741,3.9563\
C,0,10.6595,5.3225,0.6671\C,0,10.4796,6.5091,-0.0375\H,0,11.0631,6.964
1,-0.1857\C,0,9.1518,6.6925,-0.4404\H,0,8.8332,7.4454,-0.9423\C,0,8.33
98,5.6918,-0.0619\H,0,7.4046,5.5959,-0.1583\\Version=AM64L-G09RevA.02\
State=2-A\HF=-1312.0555218\S2=0.794939\S2-1=0.\S2A=0.750303\RMSD=3.838
e-09\PG=C01 [X(C17H11N2O2S1)]\\@

Table E–49. Output parameters for **4.11a;** Onsager solvation, carbon tetrachloride.

N-N= 1.741875881893D+03 E-N=-9.819521089427D+03 KE= 1.958931498934D+03
1\1\GINC-COMPUTE-0-3\SP\UTD-B3LYP-FC\6-31G(d,p)\C17H11N2O2S1(2)\BRYNND
\31-May-2010\0\\# td ub3lyp/6-31g(d,p) scrf=(solvent=ccl4,a0=5.25)\\bm
d139 TDDFT cyclohexane\\0,2\S,0,-5.158604,0.608893,-0.451944\N,0,1.544
181,1.354834,-0.070571\O,0,2.12812,2.495052,-0.092044\N,0,1.16326,-0.8
07745,-0.121209\O,0,1.319077,-2.075823,-0.14219\C,0,2.154637,0.125264,
-0.089969\C,0,0.146404,1.187303,-0.062013\C,0,-0.878137,2.104891,-0.04
5435\H,0,-0.748052,3.009859,-0.007392\C,0,-2.156671,1.590891,-0.03038\
H,0,-2.873396,2.160439,0.000147\C,0,-2.424012,0.20702,-0.028815\C,0,-1
.363043,-0.701966,-0.069946\H,0,-1.486204,-1.625727,-0.114966\C,0,-0.0
94649,-0.173669,-0.087956\C,0,3.584077,-0.143671,-0.027609\C,0,4.42742
6,0.698192,0.690017\H,0,4.083742,1.381918,1.096635\C,0,5.770411,0.4094
78,0.777686\H,0,6.251103,0.933923,1.239283\C,0,6.295259,-0.686365,0.14
5793\H,0,7.223003,-0.85445,0.231771\C,0,5.471229,-1.517672,-0.582485\H
,0,5.833367,-2.323328,-1.006574\C,0,4.123861,-1.261492,-0.664076\H,0,3
.568124,-1.863333,-1.11461\C,0,-3.796545,-0.2967,0.083098\C,0,-4.21962
8,-1.492825,0.655051\H,0,-3.723039,-1.977876,0.951002\C,0,-5.61279,-1.
626506,0.639411\H,0,-6.092612,-2.377636,0.994155\C,0,-6.239633,-0.5797
63,0.077804\H,0,-7.157207,-0.444002,-0.10307\\Version=AM64L-G09RevA.02
\State=2-A\HF=-1312.0559969\S2=0.794769\S2-1=0.\S2A=0.750302\RMSD=3.71
0e-09\PG=C01 [X(C17H11N2O2S1)]\\@

Table E–50. Output parameters for **4.11a**; Onsager solvation, 1,4-dioxane.

N-N= 1.741875852860D+03 E-N=-9.819519580171D+03 KE= 1.958931416613D+03
1\1\GINC-COMPUTE-0-19\SP\UTD-B3LYP-FC\6-31G(d,p)\C17H11N2O2S1(2)\BRYNN
D\03-Jun-2010\0\\# td ub3lyp/6-31g(d,p) scrf=(a0=5.25,solvent=1,4-diox
ane)\\bmd139 Onsager\\0,2\S,0,9.1603,4.4877,0.7978\N,0,15.6345,3.4905,
2.4469\O,0,16.1333,2.3321,2.6724\N,0,15.3547,5.6655,2.3224\O,0,15.555,
6.9271,2.3538\C,0,16.2673,4.6975,2.613\C,0,14.311,3.7069,2.0186\C,0,13
.2965,2.8262,1.7235\H,0,13.3906,1.9164,1.7508\C,0,12.1045,3.3841,1.314
9\H,0,11.4037,2.8395,1.0884\C,0,11.913,4.7754,1.1958\C,0,12.9546,5.647
2,1.5254\H,0,12.8659,6.5758,1.5063\C,0,14.1354,5.0755,1.9342\C,0,17.66
19,4.913,2.971\C,0,18.6405,4.0139,2.56\H,0,18.4017,3.3271,2.0886\C,0,1
9.961,4.2512,2.8676\H,0,20.5323,3.6921,2.5844\C,0,20.3248,5.3521,3.596
5\H,0,21.2431,5.4837,3.7856\C,0,19.361,6.2404,4.0237\H,0,19.6178,7.049
,4.5139\C,0,18.0396,6.0355,3.7081\H,0,17.4035,6.6741,3.9563\C,0,10.659
5,5.3225,0.6671\C,0,10.4796,6.5091,-0.0375\H,0,11.0631,6.9641,-0.1857\
C,0,9.1518,6.6925,-0.4404\H,0,8.8332,7.4454,-0.9423\C,0,8.3398,5.6918,
-0.0619\H,0,7.4046,5.5959,-0.1583\\Version=AM64L-G09RevA.02\State=2-A\
HF=-1312.0559573\S2=0.794783\S2-1=0.\S2A=0.750302\RMSD=3.720e-09\PG=C0
1 [X(C17H11N2O2S1)]\\@

Table E–51. Output parameters for **4.11a**; Onsager solvation, toluene.

N-N= 1.741875852860D+03 E-N=-9.819531824127D+03 KE= 1.958932179163D+03
1\1\GINC-COMPUTE-0-8\SP\UTD-B3LYP-FC\6-31G(d,p)\C17H11N2O2S1(2)\BRYNND
\11-Apr-2010\0\\# td ub3lyp/6-31g(d,p) scrf=(solvent=toluene,a0=5.25)\
\bmd139 TDDFT toluene\\0,2\S,0,9.1603,4.4877,0.7978\N,0,15.6345,3.4905
,2.4469\O,0,16.1333,2.3321,2.6724\N,0,15.3547,5.6655,2.3224\O,0,15.555
,6.9271,2.3538\C,0,16.2673,4.6975,2.613\C,0,14.311,3.7069,2.0186\C,0,1
3.2965,2.8262,1.7235\H,0,13.3906,1.9164,1.7508\C,0,12.1045,3.3841,1.31
49\H,0,11.4037,2.8395,1.0884\C,0,11.913,4.7754,1.1958\C,0,12.9546,5.64
72,1.5254\H,0,12.8659,6.5758,1.5063\C,0,14.1354,5.0755,1.9342\C,0,17.6
619,4.913,2.971\C,0,18.6405,4.0139,2.56\H,0,18.4017,3.3271,2.0886\C,0,
19.961,4.2512,2.8676\H,0,20.5323,3.6921,2.5844\C,0,20.3248,5.3521,3.59
65\H,0,21.2431,5.4837,3.7856\C,0,19.361,6.2404,4.0237\H,0,19.6178,7.04
9,4.5139\C,0,18.0396,6.0355,3.7081\H,0,17.4035,6.6741,3.9563\C,0,10.65
95,5.3225,0.6671\C,0,10.4796,6.5091,-0.0375\H,0,11.0631,6.9641,-0.1857
\C,0,9.1518,6.6925,-0.4404\H,0,8.8332,7.4454,-0.9423\C,0,8.3398,5.6918
,-0.0619\H,0,7.4046,5.5959,-0.1583\\Version=AM64L-G09RevA.02\State=2-A
\HF=-1312.0562838\S2=0.794667\S2-1=0.\S2A=0.750301\RMSD=9.918e-09\PG=C
01 [X(C17H11N2O2S1)]\\@

Table E–52. Output parameters for **4.11a**; Onsager solvation, diethyl ether.

N-N= 1.741875852860D+03 E-N=-9.819612548448D+03 KE= 1.958937326515D+03
1\1\GINC-COMPUTE-0-34\SP\UTD-B3LYP-FC\6-31G(d,p)\C17H11N2O2S1(2)\BRYNN
D\11-Apr-2010\0\\# td ub3lyp/6-31g(d,p) scrf=(solvent=diethylether,a0=
5.25)\\bmd139 TDDFT diethyl ether\\0,2\S,0,9.1603,4.4877,0.7978\N,0,15
.6345,3.4905,2.4469\O,0,16.1333,2.3321,2.6724\N,0,15.3547,5.6655,2.322
4\O,0,15.555,6.9271,2.3538\C,0,16.2673,4.6975,2.613\C,0,14.311,3.7069,
2.0186\C,0,13.2965,2.8262,1.7235\H,0,13.3906,1.9164,1.7508\C,0,12.1045
,3.3841,1.3149\H,0,11.4037,2.8395,1.0884\C,0,11.913,4.7754,1.1958\C,0,
12.9546,5.6472,1.5254\H,0,12.8659,6.5758,1.5063\C,0,14.1354,5.0755,1.9
342\C,0,17.6619,4.913,2.971\C,0,18.6405,4.0139,2.56\H,0,18.4017,3.3271
,2.0886\C,0,19.961,4.2512,2.8676\H,0,20.5323,3.6921,2.5844\C,0,20.3248

,5.3521,3.5965\H,0,21.2431,5.4837,3.7856\C,0,19.361,6.2404,4.0237\H,0,
19.6178,7.049,4.5139\C,0,18.0396,6.0355,3.7081\H,0,17.4035,6.6741,3.95
63\C,0,10.6595,5.3225,0.6671\C,0,10.4796,6.5091,-0.0375\H,0,11.0631,6.
9641,-0.1857\C,0,9.1518,6.6925,-0.4404\H,0,8.8332,7.4454,-0.9423\C,0,8
.3398,5.6918,-0.0619\H,0,7.4046,5.5959,-0.1583\\Version=AM64L-G09RevA.
02\State=2-A\HF=-1312.0584696\S2=0.793922\S2-1=0.\S2A=0.750299\RMSD=8.
445e-09\PG=C01 [X(C17H11N2O2S1)]\\@

Table E–53. Output parameters for **4.11a**; Onsager solvation, ethyl acetate.

N-N= 1.741875881893D+03 E-N=-9.819646738264D+03 KE= 1.958939565049D+03
1\1\GINC-COMPUTE-0-8\SP\UTD-B3LYP-FC\6-31G(d,p)\C17H11N2O2S1(2)\BRYNND
\01-Jun-2010\0\\# td ub3lyp/6-31g(d,p) scrf=(a0=5.25,solvent=ethyletha
noate)\\bmd139 TDDFT cyclohexane\\0,2\S,0,-5.158604,0.608893,-0.451944
\N,0,1.544181,1.354834,-0.070571\O,0,2.12812,2.495052,-0.092044\N,0,1.
16326,-0.807745,-0.121209\O,0,1.319077,-2.075823,-0.14219\C,0,2.154637
,0.125264,-0.089969\C,0,0.146404,1.187303,-0.062013\C,0,-0.878137,2.10
4891,-0.045435\H,0,-0.748052,3.009859,-0.007392\C,0,-2.156671,1.590891
,-0.03038\H,0,-2.873396,2.160439,0.000147\C,0,-2.424012,0.20702,-0.028
815\C,0,-1.363043,-0.701966,-0.069946\H,0,-1.486204,-1.625727,-0.11496
6\C,0,-0.094649,-0.173669,-0.087956\C,0,3.584077,-0.143671,-0.027609\C
,0,4.427426,0.698192,0.690017\H,0,4.083742,1.381918,1.096635\C,0,5.770
411,0.409478,0.777686\H,0,6.251103,0.933923,1.239283\C,0,6.295259,-0.6
86365,0.145793\H,0,7.223003,-0.85445,0.231771\C,0,5.471229,-1.517672,-
0.582485\H,0,5.833367,-2.323328,-1.006574\C,0,4.123861,-1.261492,-0.66
4076\H,0,3.568124,-1.863333,-1.11461\C,0,-3.796545,-0.2967,0.083098\C,
0,-4.219628,-1.492825,0.655051\H,0,-3.723039,-1.977876,0.951002\C,0,-5
.61279,-1.626506,0.639411\H,0,-6.092612,-2.377636,0.994155\C,0,-6.2396
33,-0.579763,0.077804\H,0,-7.157207,-0.444002,-0.10307\\Version=AM64L-
G09RevA.02\State=2-A\HF=-1312.0594154\S2=0.793615\S2-1=0.\S2A=0.750298
\RMSD=7.814e-09\PG=C01 [X(C17H11N2O2S1)]\\@

Table E–54. Output parameters for **4.11a**; Onsager solvation, tetrahydrofuran.

N-N= 1.741875852860D+03 E-N=-9.819663581274D+03 KE= 1.958940701117D+03
1\1\GINC-COMPUTE-0-12\SP\UTD-B3LYP-FC\6-31G(d,p)\C17H11N2O2S1(2)\BRYNN
D\20-May-2010\0\\# td ub3lyp/6-31g(d,p) scrf=(solvent=thf,a0=5.25)\\bm
d139 TDDFT cyclohexane\\0,2\S,0,9.1603,4.4877,0.7978\N,0,15.6345,3.490
5,2.4469\O,0,16.1333,2.3321,2.6724\N,0,15.3547,5.6655,2.3224\O,0,15.55
5,6.9271,2.3538\C,0,16.2673,4.6975,2.613\C,0,14.311,3.7069,2.0186\C,0,
13.2965,2.8262,1.7235\H,0,13.3906,1.9164,1.7508\C,0,12.1045,3.3841,1.3
149\H,0,11.4037,2.8395,1.0884\C,0,11.913,4.7754,1.1958\C,0,12.9546,5.6
472,1.5254\H,0,12.8659,6.5758,1.5063\C,0,14.1354,5.0755,1.9342\C,0,17.
6619,4.913,2.971\C,0,18.6405,4.0139,2.56\H,0,18.4017,3.3271,2.0886\C,0
,19.961,4.2512,2.8676\H,0,20.5323,3.6921,2.5844\C,0,20.3248,5.3521,3.5
965\H,0,21.2431,5.4837,3.7856\C,0,19.361,6.2404,4.0237\H,0,19.6178,7.0
49,4.5139\C,0,18.0396,6.0355,3.7081\H,0,17.4035,6.6741,3.9563\C,0,10.6
595,5.3225,0.6671\C,0,10.4796,6.5091,-0.0375\H,0,11.0631,6.9641,-0.185
7\C,0,9.1518,6.6925,-0.4404\H,0,8.8332,7.4454,-0.9423\C,0,8.3398,5.691
8,-0.0619\H,0,7.4046,5.5959,-0.1583\\Version=AM64L-G09RevA.02\State=2-
A\HF=-1312.0598879\S2=0.793465\S2-1=0.\S2A=0.750297\RMSD=7.492e-09\PG=
C01 [X(C17H11N2O2S1)]\\@

Table E–55. Output parameters for **4.11a**; Onsager solvation, methylene chloride.

N-N= 1.741875852860D+03 E-N=-9.819675810677D+03 KE= 1.958941524306D+03
1\1\GINC-COMPUTE-0-31\SP\UTD-B3LYP-FC\6-31G(d,p)\C17H11N2O2S1(2)\BRYNN
D\11-Apr-2010\0\\# td ub3lyp/6-31g(d,p) scrf=(solvent=dichloromethane,
a0=5.25)\\bmd139 TDDFT cyclohexane\\0,2\S,0,9.1603,4.4877,0.7978\N,0,1
5.6345,3.4905,2.4469\O,0,16.1333,2.3321,2.6724\N,0,15.3547,5.6655,2.32
24\O,0,15.555,6.9271,2.3538\C,0,16.2673,4.6975,2.613\C,0,14.311,3.7069
,2.0186\C,0,13.2965,2.8262,1.7235\H,0,13.3906,1.9164,1.7508\C,0,12.104
5,3.3841,1.3149\H,0,11.4037,2.8395,1.0884\C,0,11.913,4.7754,1.1958\C,0
,12.9546,5.6472,1.5254\H,0,12.8659,6.5758,1.5063\C,0,14.1354,5.0755,1.
9342\C,0,17.6619,4.913,2.971\C,0,18.6405,4.0139,2.56\H,0,18.4017,3.327
1,2.0886\C,0,19.961,4.2512,2.8676\H,0,20.5323,3.6921,2.5844\C,0,20.324
8,5.3521,3.5965\H,0,21.2431,5.4837,3.7856\C,0,19.361,6.2404,4.0237\H,0
,19.6178,7.049,4.5139\C,0,18.0396,6.0355,3.7081\H,0,17.4035,6.6741,3.9
563\C,0,10.6595,5.3225,0.6671\C,0,10.4796,6.5091,-0.0375\H,0,11.0631,6
.9641,-0.1857\C,0,9.1518,6.6925,-0.4404\H,0,8.8332,7.4454,-0.9423\C,0,
8.3398,5.6918,-0.0619\H,0,7.4046,5.5959,-0.1583\\Version=AM64L-G09RevA
.02\State=2-A\HF=-1312.0602331\S2=0.793357\S2-1=0.\S2A=0.750297\RMSD=7
.255e-09\PG=C01 [X(C17H11N2O2S1)]\\@

Table E–56. Output parameters for **4.11a**; Onsager solvation, acetone.

N-N= 1.741875852860D+03 E-N=-9.819711542818D+03 KE= 1.958943962863D+03
1\1\GINC-COMPUTE-0-26\SP\UTD-B3LYP-FC\6-31G(d,p)\C17H11N2O2S1(2)\BRYNN
D\20-May-2010\0\\# td ub3lyp/6-31g(d,p) scrf=(solvent=acetone,a0=5.25)
\\bmd139 TDDFT cyclohexane\\0,2\S,0,9.1603,4.4877,0.7978\N,0,15.6345,3
.4905,2.4469\O,0,16.1333,2.3321,2.6724\N,0,15.3547,5.6655,2.3224\O,0,1
5.555,6.9271,2.3538\C,0,16.2673,4.6975,2.613\C,0,14.311,3.7069,2.0186\
C,0,13.2965,2.8262,1.7235\H,0,13.3906,1.9164,1.7508\C,0,12.1045,3.3841
,1.3149\H,0,11.4037,2.8395,1.0884\C,0,11.913,4.7754,1.1958\C,0,12.9546
,5.6472,1.5254\H,0,12.8659,6.5758,1.5063\C,0,14.1354,5.0755,1.9342\C,0
,17.6619,4.913,2.971\C,0,18.6405,4.0139,2.56\H,0,18.4017,3.3271,2.0886
\C,0,19.961,4.2512,2.8676\H,0,20.5323,3.6921,2.5844\C,0,20.3248,5.3521
,3.5965\H,0,21.2431,5.4837,3.7856\C,0,19.361,6.2404,4.0237\H,0,19.6178
,7.049,4.5139\C,0,18.0396,6.0355,3.7081\H,0,17.4035,6.6741,3.9563\C,0,
10.6595,5.3225,0.6671\C,0,10.4796,6.5091,-0.0375\H,0,11.0631,6.9641,-0
.1857\C,0,9.1518,6.6925,-0.4404\H,0,8.8332,7.4454,-0.9423\C,0,8.3398,5
.6918,-0.0619\H,0,7.4046,5.5959,-0.1583\\Version=AM64L-G09RevA.02\Stat
e=2-A\HF=-1312.0612552\S2=0.793045\S2-1=0.\S2A=0.750296\RMSD=6.541e-09
\PG=C01 [X(C17H11N2O2S1)]\\@

Table E–57. Output parameters for **4.11a**; Onsager solvation, acetonitrile.

N-N= 1.741875852860D+03 E-N=-9.819723857774D+03 KE= 1.958944815120D+03
1\1\GINC-COMPUTE-0-26\SP\UTD-B3LYP-FC\6-31G(d,p)\C17H11N2O2S1(2)\BRYNN
D\20-May-2010\0\\# td ub3lyp/6-31g(d,p) scrf=(solvent=acetonitrile,a0=
5.25)\\bmd139 TDDFT cyclohexane\\0,2\S,0,9.1603,4.4877,0.7978\N,0,15.6
345,3.4905,2.4469\O,0,16.1333,2.3321,2.6724\N,0,15.3547,5.6655,2.3224\
O,0,15.555,6.9271,2.3538\C,0,16.2673,4.6975,2.613\C,0,14.311,3.7069,2.
0186\C,0,13.2965,2.8262,1.7235\H,0,13.3906,1.9164,1.7508\C,0,12.1045,3
.3841,1.3149\H,0,11.4037,2.8395,1.0884\C,0,11.913,4.7754,1.1958\C,0,12
.9546,5.6472,1.5254\H,0,12.8659,6.5758,1.5063\C,0,14.1354,5.0755,1.934
2\C,0,17.6619,4.913,2.971\C,0,18.6405,4.0139,2.56\H,0,18.4017,3.3271,2
.0886\C,0,19.961,4.2512,2.8676\H,0,20.5323,3.6921,2.5844\C,0,20.3248,5

.3521,3.5965\H,0,21.2431,5.4837,3.7856\C,0,19.361,6.2404,4.0237\H,0,19
.6178,7.049,4.5139\C,0,18.0396,6.0355,3.7081\H,0,17.4035,6.6741,3.9563
\C,0,10.6595,5.3225,0.6671\C,0,10.4796,6.5091,-0.0375\H,0,11.0631,6.96
41,-0.1857\C,0,9.1518,6.6925,-0.4404\H,0,8.8332,7.4454,-0.9423\C,0,8.3
398,5.6918,-0.0619\H,0,7.4046,5.5959,-0.1583\\Version=AM64L-G09RevA.02
\State=2-A\HF=-1312.0616127\S2=0.792938\S2-1=0.\S2A=0.750295\RMSD=6.28
9e-09\PG=C01 [X(C17H11N2O2S1)]\\@

Table E–58. Output parameters for **4.11a**; Onsager solvation, dimethyl sulfoxide.

N-N= 1.741875852860D+03 E-N=-9.819727870184D+03 KE= 1.958945094140D+03
1\1\GINC-COMPUTE-0-20\SP\UTD-B3LYP-FC\6-31G(d,p)\C17H11N2O2S1(2)\BRYNN
D\20-May-2010\0\\# td ub3lyp/6-31g(d,p) scrf=(solvent=dmso,a0=5.25)\\b
md139 TDDFT cyclohexane\\0,2\S,0,9.1603,4.4877,0.7978\N,0,15.6345,3.49
05,2.4469\O,0,16.1333,2.3321,2.6724\N,0,15.3547,5.6655,2.3224\O,0,15.5
55,6.9271,2.3538\C,0,16.2673,4.6975,2.613\C,0,14.311,3.7069,2.0186\C,0
,13.2965,2.8262,1.7235\H,0,13.3906,1.9164,1.7508\C,0,12.1045,3.3841,1.
3149\H,0,11.4037,2.8395,1.0884\C,0,11.913,4.7754,1.1958\C,0,12.9546,5.
6472,1.5254\H,0,12.8659,6.5758,1.5063\C,0,14.1354,5.0755,1.9342\C,0,17
.6619,4.913,2.971\C,0,18.6405,4.0139,2.56\H,0,18.4017,3.3271,2.0886\C,
0,19.961,4.2512,2.8676\H,0,20.5323,3.6921,2.5844\C,0,20.3248,5.3521,3.
5965\H,0,21.2431,5.4837,3.7856\C,0,19.361,6.2404,4.0237\H,0,19.6178,7.
049,4.5139\C,0,18.0396,6.0355,3.7081\H,0,17.4035,6.6741,3.9563\C,0,10.
6595,5.3225,0.6671\C,0,10.4796,6.5091,-0.0375\H,0,11.0631,6.9641,-0.18
57\C,0,9.1518,6.6925,-0.4404\H,0,8.8332,7.4454,-0.9423\C,0,8.3398,5.69
18,-0.0619\H,0,7.4046,5.5959,-0.1583\\Version=AM64L-G09RevA.02\State=2
-A\HF=-1312.0617298\S2=0.792903\S2-1=0.\S2A=0.750295\RMSD=6.207e-09\PG
=C01 [X(C17H11N2O2S1)]\\@

Table E–59. Output parameters for **4.11a**; CPCM solvation, cyclohexane.

N-N= 1.741875881893D+03 E-N=-9.819522742731D+03 KE= 1.958932286975D+03
1\1\GINC-COMPUTE-0-9\SP\UTD-B3LYP-FC\6-31G(d,p)\C17H11N2O2S1(2)\BRYNND
\01-Jun-2010\0\\# td ub3lyp/6-31g(d,p) scrf=(cpcm,solvent=cyclohexane)
\\bmd139 TDDFT CPCM model\\0,2\S,0,-5.158604,0.608893,-0.451944\N,0,1.
544181,1.354834,-0.070571\O,0,2.12812,2.495052,-0.092044\N,0,1.16326,-
0.807745,-0.121209\O,0,1.319077,-2.075823,-0.14219\C,0,2.154637,0.1252
64,-0.089969\C,0,0.146404,1.187303,-0.062013\C,0,-0.878137,2.104891,-0
.045435\H,0,-0.748052,3.009859,-0.007392\C,0,-2.156671,1.590891,-0.030
38\H,0,-2.873396,2.160439,0.000147\C,0,-2.424012,0.20702,-0.028815\C,0
,-1.363043,-0.701966,-0.069946\H,0,-1.486204,-1.625727,-0.114966\C,0,-
0.094649,-0.173669,-0.087956\C,0,3.584077,-0.143671,-0.027609\C,0,4.42
7426,0.698192,0.690017\H,0,4.083742,1.381918,1.096635\C,0,5.770411,0.4
09478,0.777686\H,0,6.251103,0.933923,1.239283\C,0,6.295259,-0.686365,0
.145793\H,0,7.223003,-0.85445,0.231771\C,0,5.471229,-1.517672,-0.58248
5\H,0,5.833367,-2.323328,-1.006574\C,0,4.123861,-1.261492,-0.664076\H,
0,3.568124,-1.863333,-1.11461\C,0,-3.796545,-0.2967,0.083098\C,0,-4.21
9628,-1.492825,0.655051\H,0,-3.723039,-1.977876,0.951002\C,0,-5.61279,
-1.626506,0.639411\H,0,-6.092612,-2.377636,0.994155\C,0,-6.239633,-0.5
79763,0.077804\H,0,-7.157207,-0.444002,-0.10307\\Version=AM64L-G09RevA
.02\State=2-A\HF=-1312.0565687\S2=0.794705\S2-1=0.\S2A=0.750301\RMSD=9
.624e-09\PG=C01 [X(C17H11N2O2S1)]\\@

Table E–60. Output parameters for **4.11a**; CPCM solvation, carbon tetrachloride.

N-N= 1.741875881893D+03 E-N=-9.819540909581D+03 KE= 1.958933427352D+03
1\1\GINC-COMPUTE-0-3\SP\UTD-B3LYP-FC\6-31G(d,p)\C17H11N2O2S1(2)\BRYNND
\01-Jun-2010\0\\# td ub3lyp/6-31g(d,p) scrf=(cpcm,solvent=ccl4)\\bmd13
9 TDDFT CPCM model\\0,2\S,0,-5.158604,0.608893,-0.451944\N,0,1.544181,
1.354834,-0.070571\O,0,2.12812,2.495052,-0.092044\N,0,1.16326,-0.80774
5,-0.121209\O,0,1.319077,-2.075823,-0.14219\C,0,2.154637,0.125264,-0.0
89969\C,0,0.146404,1.187303,-0.062013\C,0,-0.878137,2.104891,-0.045435
\H,0,-0.748052,3.009859,-0.007392\C,0,-2.156671,1.590891,-0.03038\H,0,
-2.873396,2.160439,0.000147\C,0,-2.424012,0.20702,-0.028815\C,0,-1.363
043,-0.701966,-0.069946\H,0,-1.486204,-1.625727,-0.114966\C,0,-0.09464
9,-0.173669,-0.087956\C,0,3.584077,-0.143671,-0.027609\C,0,4.427426,0.
698192,0.690017\H,0,4.083742,1.381918,1.096635\C,0,5.770411,0.409478,0
.777686\H,0,6.251103,0.933923,1.239283\C,0,6.295259,-0.686365,0.145793
\H,0,7.223003,-0.85445,0.231771\C,0,5.471229,-1.517672,-0.582485\H,0,5
.833367,-2.323328,-1.006574\C,0,4.123861,-1.261492,-0.664076\H,0,3.568
124,-1.863333,-1.11461\C,0,-3.796545,-0.2967,0.083098\C,0,-4.219628,-1
.492825,0.655051\H,0,-3.723039,-1.977876,0.951002\C,0,-5.61279,-1.6265
06,0.639411\H,0,-6.092612,-2.377636,0.994155\C,0,-6.239633,-0.579763,0
.077804\H,0,-7.157207,-0.444002,-0.10307\\Version=AM64L-G09RevA.02\Sta
te=2-A\HF=-1312.0570658\S2=0.794532\S2-1=0.\S2A=0.7503\RMSD=9.292e-09\
PG=C01 [X(C17H11N2O2S1)]\\@

Table E–61. Output parameters for **4.11a**; CPCM solvation, 1,4-dioxane.

N-N= 1.741875881893D+03 E-N=-9.819539474822D+03 KE= 1.958933337318D+03
1\1\GINC-COMPUTE-0-23\SP\UTD-B3LYP-FC\6-31G(d,p)\C17H11N2O2S1(2)\BRYNN
D\01-Jun-2010\0\\# td ub3lyp/6-31g(d,p) scrf=(cpcm,solvent=1,4-dioxane
)\\bmd139 TDDFT CPCM model\\0,2\S,0,-5.158604,0.608893,-0.451944\N,0,1
.544181,1.354834,-0.070571\O,0,2.12812,2.495052,-0.092044\N,0,1.16326,
-0.807745,-0.121209\O,0,1.319077,-2.075823,-0.14219\C,0,2.154637,0.125
264,-0.089969\C,0,0.146404,1.187303,-0.062013\C,0,-0.878137,2.104891,-
0.045435\H,0,-0.748052,3.009859,-0.007392\C,0,-2.156671,1.590891,-0.03
038\H,0,-2.873396,2.160439,0.000147\C,0,-2.424012,0.20702,-0.028815\C,
0,-1.363043,-0.701966,-0.069946\H,0,-1.486204,-1.625727,-0.114966\C,0,
-0.094649,-0.173669,-0.087956\C,0,3.584077,-0.143671,-0.027609\C,0,4.4
27426,0.698192,0.690017\H,0,4.083742,1.381918,1.096635\C,0,5.770411,0.
409478,0.777686\H,0,6.251103,0.933923,1.239283\C,0,6.295259,-0.686365,
0.145793\H,0,7.223003,-0.85445,0.231771\C,0,5.471229,-1.517672,-0.5824
85\H,0,5.833367,-2.323328,-1.006574\C,0,4.123861,-1.261492,-0.664076\H
,0,3.568124,-1.863333,-1.11461\C,0,-3.796545,-0.2967,0.083098\C,0,-4.2
19628,-1.492825,0.655051\H,0,-3.723039,-1.977876,0.951002\C,0,-5.61279
,-1.626506,0.639411\H,0,-6.092612,-2.377636,0.994155\C,0,-6.239633,-0.
579763,0.077804\H,0,-7.157207,-0.444002,-0.10307\\Version=AM64L-G09Rev
A.02\State=2-A\HF=-1312.0570268\S2=0.794546\S2-1=0.\S2A=0.7503\RMSD=9.
318e-09\PG=C01 [X(C17H11N2O2S1)]\\@

Table E–62. Output parameters for **4.11a**; CPCM solvation, toluene.

N-N= 1.741875881893D+03 E-N=-9.819551779411D+03 KE= 1.958934109331D+03
1\1\GINC-COMPUTE-0-31\SP\UTD-B3LYP-FC\6-31G(d,p)\C17H11N2O2S1(2)\BRYNN
D\01-Jun-2010\0\\# td ub3lyp/6-31g(d,p) scrf=(cpcm,solvent=toluene)\\b
md139 TDDFT CPCM model\\0,2\S,0,-5.158604,0.608893,-0.451944\N,0,1.544
181,1.354834,-0.070571\O,0,2.12812,2.495052,-0.092044\N,0,1.16326,-0.8

07745,-0.121209\O,0,1.319077,-2.075823,-0.14219\C,0,2.154637,0.125264,
-0.089969\C,0,0.146404,1.187303,-0.062013\C,0,-0.878137,2.104891,-0.04
5435\H,0,-0.748052,3.009859,-0.007392\C,0,-2.156671,1.590891,-0.03038\
H,0,-2.873396,2.160439,0.000147\C,0,-2.424012,0.20702,-0.028815\C,0,-1
.363043,-0.701966,-0.069946\H,0,-1.486204,-1.625727,-0.114966\C,0,-0.0
94649,-0.173669,-0.087956\C,0,3.584077,-0.143671,-0.027609\C,0,4.42742
6,0.698192,0.690017\H,0,4.083742,1.381918,1.096635\C,0,5.770411,0.4094
78,0.777686\H,0,6.251103,0.933923,1.239283\C,0,6.295259,-0.686365,0.14
5793\H,0,7.223003,-0.85445,0.231771\C,0,5.471229,-1.517672,-0.582485\H
,0,5.833367,-2.323328,-1.006574\C,0,4.123861,-1.261492,-0.664076\H,0,3
.568124,-1.863333,-1.11461\C,0,-3.796545,-0.2967,0.083098\C,0,-4.21962
8,-1.492825,0.655051\H,0,-3.723039,-1.977876,0.951002\C,0,-5.61279,-1.
626506,0.639411\H,0,-6.092612,-2.377636,0.994155\C,0,-6.239633,-0.5797
63,0.077804\H,0,-7.157207,-0.444002,-0.10307\\Version=AM64L-G09RevA.02
\State=2-A\HF=-1312.0573601\S2=0.794431\S2-1=0.\S2A=0.7503\RMSD=9.099e
-09\PG=C01 [X(C17H11N2O2S1)]\\@

Table E–63. Output parameters for **4.11a**; CPCM solvation, diethyl ether.

N-N= 1.741875881893D+03 E-N=-9.819629171538D+03 KE= 1.958938962842D+03
1\1\GINC-COMPUTE-0-15\SP\UTD-B3LYP-FC\6-31G(d,p)\C17H11N2O2S1(2)\BRYNN
D\01-Jun-2010\0\\# td ub3lyp/6-31g(d,p) scrf=(cpcm,solvent=diethylethe
r)\\bmd139 TDDFT CPCM model\\0,2\S,0,-5.158604,0.608893,-0.451944\N,0,
1.544181,1.354834,-0.070571\O,0,2.12812,2.495052,-0.092044\N,0,1.16326
,-0.807745,-0.121209\O,0,1.319077,-2.075823,-0.14219\C,0,2.154637,0.12
5264,-0.089969\C,0,0.146404,1.187303,-0.062013\C,0,-0.878137,2.104891,
-0.045435\H,0,-0.748052,3.009859,-0.007392\C,0,-2.156671,1.590891,-0.0
3038\H,0,-2.873396,2.160439,0.000147\C,0,-2.424012,0.20702,-0.028815\C
,0,-1.363043,-0.701966,-0.069946\H,0,-1.486204,-1.625727,-0.114966\C,0
,-0.094649,-0.173669,-0.087956\C,0,3.584077,-0.143671,-0.027609\C,0,4.
427426,0.698192,0.690017\H,0,4.083742,1.381918,1.096635\C,0,5.770411,0
.409478,0.777686\H,0,6.251103,0.933923,1.239283\C,0,6.295259,-0.686365
,0.145793\H,0,7.223003,-0.85445,0.231771\C,0,5.471229,-1.517672,-0.582
485\H,0,5.833367,-2.323328,-1.006574\C,0,4.123861,-1.261492,-0.664076\
H,0,3.568124,-1.863333,-1.11461\C,0,-3.796545,-0.2967,0.083098\C,0,-4.
219628,-1.492825,0.655051\H,0,-3.723039,-1.977876,0.951002\C,0,-5.6127
9,-1.626506,0.639411\H,0,-6.092612,-2.377636,0.994155\C,0,-6.239633,-0
.579763,0.077804\H,0,-7.157207,-0.444002,-0.10307\\Version=AM64L-G09Re
vA.02\State=2-A\HF=-1312.0593883\S2=0.79373\S2-1=0.\S2A=0.750298\RMSD=
7.788e-09\PG=C01 [X(C17H11N2O2S1)]\\@

Table E–64. Output parameters for **4.11a**; CPCM solvation, ethyl acetate.

N-N= 1.741875881893D+03 E-N=-9.819660096168D+03 KE= 1.958940904111D+03
1\1\GINC-COMPUTE-0-29\SP\UTD-B3LYP-FC\6-31G(d,p)\C17H11N2O2S1(2)\BRYNN
D\01-Jun-2010\0\\# td ub3lyp/6-31g(d,p) scrf=(cpcm,solvent=ethylethano
ate)\\bmd139 TDDFT cyclohexane\\0,2\S,0,-5.158604,0.608893,-0.451944\N
,0,1.544181,1.354834,-0.070571\O,0,2.12812,2.495052,-0.092044\N,0,1.16
326,-0.807745,-0.121209\O,0,1.319077,-2.075823,-0.14219\C,0,2.154637,0
.125264,-0.089969\C,0,0.146404,1.187303,-0.062013\C,0,-0.878137,2.1048
91,-0.045435\H,0,-0.748052,3.009859,-0.007392\C,0,-2.156671,1.590891,-
0.03038\H,0,-2.873396,2.160439,0.000147\C,0,-2.424012,0.20702,-0.02881
5\C,0,-1.363043,-0.701966,-0.069946\H,0,-1.486204,-1.625727,-0.114966\
C,0,-0.094649,-0.173669,-0.087956\C,0,3.584077,-0.143671,-0.027609\C,0
,4.427426,0.698192,0.690017\H,0,4.083742,1.381918,1.096635\C,0,5.77041

1,0.409478,0.777686\H,0,6.251103,0.933923,1.239283\C,0,6.295259,-0.686
365,0.145793\H,0,7.223003,-0.85445,0.231771\C,0,5.471229,-1.517672,-0.
582485\H,0,5.833367,-2.323328,-1.006574\C,0,4.123861,-1.261492,-0.6640
76\H,0,3.568124,-1.863333,-1.11461\C,0,-3.796545,-0.2967,0.083098\C,0,
-4.219628,-1.492825,0.655051\H,0,-3.723039,-1.977876,0.951002\C,0,-5.6
1279,-1.626506,0.639411\H,0,-6.092612,-2.377636,0.994155\C,0,-6.239633
,-0.579763,0.077804\H,0,-7.157207,-0.444002,-0.10307\\Version=AM64L-G0
9RevA.02\State=2-A\HF=-1312.060166\S2=0.793462\S2-1=0.\S2A=0.750297\RM
SD=7.272e-09\PG=C01 [X(C17H11N2O2S1)]\\@

Table E–65. Output parameters for **4.11a**; CPCM solvation, tetrahydrofuran.

N-N= 1.741875881893D+03 E-N=-9.819675102952D+03 KE= 1.958941847145D+03
1\1\GINC-COMPUTE-0-18\SP\UTD-B3LYP-FC\6-31G(d,p)\C17H11N2O2S1(2)\BRYNN
D\01-Jun-2010\0\\# td ub3lyp/6-31g(d,p) scrf=(cpcm,solvent=thf)\\bmd13
9 TDDFT CPCM model\\0,2\S,0,-5.158604,0.608893,-0.451944\N,0,1.544181,
1.354834,-0.070571\O,0,2.12812,2.495052,-0.092044\N,0,1.16326,-0.80774
5,-0.121209\O,0,1.319077,-2.075823,-0.14219\C,0,2.154637,0.125264,-0.0
89969\C,0,0.146404,1.187303,-0.062013\C,0,-0.878137,2.104891,-0.045435
\H,0,-0.748052,3.009859,-0.007392\C,0,-2.156671,1.590891,-0.03038\H,0,
-2.873396,2.160439,0.000147\C,0,-2.424012,0.20702,-0.028815\C,0,-1.363
043,-0.701966,-0.069946\H,0,-1.486204,-1.625727,-0.114966\C,0,-0.09464
9,-0.173669,-0.087956\C,0,3.584077,-0.143671,-0.027609\C,0,4.427426,0.
698192,0.690017\H,0,4.083742,1.381918,1.096635\C,0,5.770411,0.409478,0
.777686\H,0,6.251103,0.933923,1.239283\C,0,6.295259,-0.686365,0.145793
\H,0,7.223003,-0.85445,0.231771\C,0,5.471229,-1.517672,-0.582485\H,0,5
.833367,-2.323328,-1.006574\C,0,4.123861,-1.261492,-0.664076\H,0,3.568
124,-1.863333,-1.11461\C,0,-3.796545,-0.2967,0.083098\C,0,-4.219628,-1
.492825,0.655051\H,0,-3.723039,-1.977876,0.951002\C,0,-5.61279,-1.6265
06,0.639411\H,0,-6.092612,-2.377636,0.994155\C,0,-6.239633,-0.579763,0
.077804\H,0,-7.157207,-0.444002,-0.10307\\Version=AM64L-G09RevA.02\Sta
te=2-A\HF=-1312.0605368\S2=0.793335\S2-1=0.\S2A=0.750296\RMSD=7.022e-0
9\PG=C01 [X(C17H11N2O2S1)]\\@

Table E–66. Output parameters for **4.11a**; CPCM solvation, methylene chloride.

N-N= 1.741875881893D+03 E-N=-9.819685804532D+03 KE= 1.958942520147D+03
1\1\GINC-COMPUTE-0-17\SP\UTD-B3LYP-FC\6-31G(d,p)\C17H11N2O2S1(2)\BRYNN
D\01-Jun-2010\0\\# td ub3lyp/6-31g(d,p) scrf=(cpcm,solvent=dichloromet
hane)\\bmd139 TDDFT CPCM model\\0,2\S,0,-5.158604,0.608893,-0.451944\N
,0,1.544181,1.354834,-0.070571\O,0,2.12812,2.495052,-0.092044\N,0,1.16
326,-0.807745,-0.121209\O,0,1.319077,-2.075823,-0.14219\C,0,2.154637,0
.125264,-0.089969\C,0,0.146404,1.187303,-0.062013\C,0,-0.878137,2.1048
91,-0.045435\H,0,-0.748052,3.009859,-0.007392\C,0,-2.156671,1.590891,-
0.03038\H,0,-2.873396,2.160439,0.000147\C,0,-2.424012,0.20702,-0.02881
5\C,0,-1.363043,-0.701966,-0.069946\H,0,-1.486204,-1.625727,-0.114966\
C,0,-0.094649,-0.173669,-0.087956\C,0,3.584077,-0.143671,-0.027609\C,0
,4.427426,0.698192,0.690017\H,0,4.083742,1.381918,1.096635\C,0,5.77041
1,0.409478,0.777686\H,0,6.251103,0.933923,1.239283\C,0,6.295259,-0.686
365,0.145793\H,0,7.223003,-0.85445,0.231771\C,0,5.471229,-1.517672,-0.
582485\H,0,5.833367,-2.323328,-1.006574\C,0,4.123861,-1.261492,-0.6640
76\H,0,3.568124,-1.863333,-1.11461\C,0,-3.796545,-0.2967,0.083098\C,0,
-4.219628,-1.492825,0.655051\H,0,-3.723039,-1.977876,0.951002\C,0,-5.6
1279,-1.626506,0.639411\H,0,-6.092612,-2.377636,0.994155\C,0,-6.239633
,-0.579763,0.077804\H,0,-7.157207,-0.444002,-0.10307\\Version=AM64L-G0

9RevA.02\State=2-A\HF=-1312.0607986\S2=0.793244\S2-1=0.\S2A=0.750296\R
MSD=6.843e-09\PG=C01 [X(C17H11N2O2S1)]\\@

Table E–67. Output parameters for **4.11a**; CPCM solvation, acetone.

N-N= 1.741875881893D+03 E-N=-9.819716453840D+03 KE= 1.958944450464D+03
1\1\GINC-COMPUTE-0-31\SP\UTD-B3LYP-FC\6-31G(d,p)\C17H11N2O2S1(2)\BRYNN
D\01-Jun-2010\0\\# td ub3lyp/6-31g(d,p) scrf=(cpcm,solvent=acetone)\\b
md139 TDDFT CPCM model\\0,2\S,0,-5.158604,0.608893,-0.451944\N,0,1.544
181,1.354834,-0.070571\O,0,2.12812,2.495052,-0.092044\N,0,1.16326,-0.8
07745,-0.121209\O,0,1.319077,-2.075823,-0.14219\C,0,2.154637,0.125264,
-0.089969\C,0,0.146404,1.187303,-0.062013\C,0,-0.878137,2.104891,-0.04
5435\H,0,-0.748052,3.009859,-0.007392\C,0,-2.156671,1.590891,-0.03038\
H,0,-2.873396,2.160439,0.000147\C,0,-2.424012,0.20702,-0.028815\C,0,-1
.363043,-0.701966,-0.069946\H,0,-1.486204,-1.625727,-0.114966\C,0,-0.0
94649,-0.173669,-0.087956\C,0,3.584077,-0.143671,-0.027609\C,0,4.42742
6,0.698192,0.690017\H,0,4.083742,1.381918,1.096635\C,0,5.770411,0.4094
78,0.777686\H,0,6.251103,0.933923,1.239283\C,0,6.295259,-0.686365,0.14
5793\H,0,7.223003,-0.85445,0.231771\C,0,5.471229,-1.517672,-0.582485\H
,0,5.833367,-2.323328,-1.006574\C,0,4.123861,-1.261492,-0.664076\H,0,3
.568124,-1.863333,-1.11461\C,0,-3.796545,-0.2967,0.083098\C,0,-4.21962
8,-1.492825,0.655051\H,0,-3.723039,-1.977876,0.951002\C,0,-5.61279,-1.
626506,0.639411\H,0,-6.092612,-2.377636,0.994155\C,0,-6.239633,-0.5797
63,0.077804\H,0,-7.157207,-0.444002,-0.10307\\Version=AM64L-G09RevA.02
\State=2-A\HF=-1312.0615364\S2=0.79299\S2-1=0.\S2A=0.750295\RMSD=6.336
e-09\PG=C01 [X(C17H11N2O2S1)]\\@

Table E–68. Output parameters for **4.11a**; CPCM solvation, acetonitrile.

N-N= 1.741875881893D+03 E-N=-9.819726815566D+03 KE= 1.958945104162D+03
1\1\GINC-COMPUTE-0-12\SP\UTD-B3LYP-FC\6-31G(d,p)\C17H11N2O2S1(2)\BRYNN
D\01-Jun-2010\0\\# td ub3lyp/6-31g(d,p) scrf=(cpcm,solvent=acetonitril
e)\\bmd139 TDDFT CPCM model\\0,2\S,0,-5.158604,0.608893,-0.451944\N,0,
1.544181,1.354834,-0.070571\O,0,2.12812,2.495052,-0.092044\N,0,1.16326
,-0.807745,-0.121209\O,0,1.319077,-2.075823,-0.14219\C,0,2.154637,0.12
5264,-0.089969\C,0,0.146404,1.187303,-0.062013\C,0,-0.878137,2.104891,
-0.045435\H,0,-0.748052,3.009859,-0.007392\C,0,-2.156671,1.590891,-0.0
3038\H,0,-2.873396,2.160439,0.000147\C,0,-2.424012,0.20702,-0.028815\C
,0,-1.363043,-0.701966,-0.069946\H,0,-1.486204,-1.625727,-0.114966\C,0
,-0.094649,-0.173669,-0.087956\C,0,3.584077,-0.143671,-0.027609\C,0,4.
427426,0.698192,0.690017\H,0,4.083742,1.381918,1.096635\C,0,5.770411,0
.409478,0.777686\H,0,6.251103,0.933923,1.239283\C,0,6.295259,-0.686365
,0.145793\H,0,7.223003,-0.85445,0.231771\C,0,5.471229,-1.517672,-0.582
485\H,0,5.833367,-2.323328,-1.006574\C,0,4.123861,-1.261492,-0.664076\
H,0,3.568124,-1.863333,-1.11461\C,0,-3.796545,-0.2967,0.083098\C,0,-4.
219628,-1.492825,0.655051\H,0,-3.723039,-1.977876,0.951002\C,0,-5.6127
9,-1.626506,0.639411\H,0,-6.092612,-2.377636,0.994155\C,0,-6.239633,-0
.579763,0.077804\H,0,-7.157207,-0.444002,-0.10307\\Version=AM64L-G09Re
vA.02\State=2-A\HF=-1312.0617819\S2=0.792906\S2-1=0.\S2A=0.750295\RMSD
=6.167e-09\PG=C01 [X(C17H11N2O2S1)]\\@

Table E–69. Output parameters for **4.11a**; CPCM solvation, dimethyl sulfoxide.


```
N-N= 1.741875881893D+03 E-N=-9.819730170465D+03  KE= 1.958945315949D+03
 1\1\GINC-COMPUTE-0-24\SP\UTD-B3LYP-FC\6-31G(d,p)\C17H11N2O2S1(2)\BRYNN
 D\01-Jun-2010\0\\# td ub3lyp/6-31g(d,p) scrf=(cpcm,solvent=dmso)\\bmd1
 39 TDDFT CPCM model\\0,2\S,0,-5.158604,0.608893,-0.451944\N,0,1.544181
 ,1.354834,-0.070571\O,0,2.12812,2.495052,-0.092044\N,0,1.16326,-0.8077
 45,-0.121209\O,0,1.319077,-2.075823,-0.14219\C,0,2.154637,0.125264,-0.
 089969\C,0,0.146404,1.187303,-0.062013\C,0,-0.878137,2.104891,-0.04543
 5\H,0,-0.748052,3.009859,-0.007392\C,0,-2.156671,1.590891,-0.03038\H,0
 ,-2.873396,2.160439,0.000147\C,0,-2.424012,0.20702,-0.028815\C,0,-1.36
 3043,-0.701966,-0.069946\H,0,-1.486204,-1.625727,-0.114966\C,0,-0.0946
 49,-0.173669,-0.087956\C,0,3.584077,-0.143671,-0.027609\C,0,4.427426,0
 .698192,0.690017\H,0,4.083742,1.381918,1.096635\C,0,5.770411,0.409478,
 0.777686\H,0,6.251103,0.933923,1.239283\C,0,6.295259,-0.686365,0.14579
 3\H,0,7.223003,-0.85445,0.231771\C,0,5.471229,-1.517672,-0.582485\H,0,
 5.833367,-2.323328,-1.006574\C,0,4.123861,-1.261492,-0.664076\H,0,3.56
 8124,-1.863333,-1.11461\C,0,-3.796545,-0.2967,0.083098\C,0,-4.219628,-
 1.492825,0.655051\H,0,-3.723039,-1.977876,0.951002\C,0,-5.61279,-1.626
 506,0.639411\H,0,-6.092612,-2.377636,0.994155\C,0,-6.239633,-0.579763,
 0.077804\H,0,-7.157207,-0.444002,-0.10307\\Version=AM64L-G09RevA.02\St
 ate=2-A\HF=-1312.0618609\S2=0.792878\S2-1=0.\S2A=0.750295\RMSD=6.113e-
 09\PG=C01 [X(C17H11N2O2S1)]\\@
```


Table E–70. Output parameters for **4.11a**; SCI-PCM solvation, cyclohexane.


```
N-N= 1.741875881893D+03 E-N=-9.819522559036D+03  KE= 1.958937432461D+03
 1\1\GINC-COMPUTE-0-9\SP\UTD-B3LYP-FC\6-31G(d,p)\C17H11N2O2S1(2)\BRYNND
 \31-May-2010\0\\# td ub3lyp/6-31g(d,p) scrf=(scipcm,solvent=cyclohexan
 e)\\bmd139 TDDFT SCI PCM model\\0,2\S,0,-5.158604,0.608893,-0.451944\N
 ,0,1.544181,1.354834,-0.070571\O,0,2.12812,2.495052,-0.092044\N,0,1.16
 326,-0.807745,-0.121209\O,0,1.319077,-2.075823,-0.14219\C,0,2.154637,0
 .125264,-0.089969\C,0,0.146404,1.187303,-0.062013\C,0,-0.878137,2.1048
 91,-0.045435\H,0,-0.748052,3.009859,-0.007392\C,0,-2.156671,1.590891,-
 0.03038\H,0,-2.873396,2.160439,0.000147\C,0,-2.424012,0.20702,-0.02881
 5\C,0,-1.363043,-0.701966,-0.069946\H,0,-1.486204,-1.625727,-0.114966\
 C,0,-0.094649,-0.173669,-0.087956\C,0,3.584077,-0.143671,-0.027609\C,0
 ,4.427426,0.698192,0.690017\H,0,4.083742,1.381918,1.096635\C,0,5.77041
 1,0.409478,0.777686\H,0,6.251103,0.933923,1.239283\C,0,6.295259,-0.686
 365,0.145793\H,0,7.223003,-0.85445,0.231771\C,0,5.471229,-1.517672,-0.
 582485\H,0,5.833367,-2.323328,-1.006574\C,0,4.123861,-1.261492,-0.6640
 76\H,0,3.568124,-1.863333,-1.11461\C,0,-3.796545,-0.2967,0.083098\C,0,
 -4.219628,-1.492825,0.655051\H,0,-3.723039,-1.977876,0.951002\C,0,-5.6
 1279,-1.626506,0.639411\H,0,-6.092612,-2.377636,0.994155\C,0,-6.239633
 ,-0.579763,0.077804\H,0,-7.157207,-0.444002,-0.10307\\Version=AM64L-G0
 9RevA.02\State=2-A\HF=-1312.0553047\S2=0.794995\S2-1=0.\S2A=0.750303\R
 MSD=4.772e-09\PG=C01 [X(C17H11N2O2S1)]\\@
```


Table E–71. Output parameters for **4.11a**; SCI-PCM solvation, carbon tetrachloride.


```
N-N= 1.741875881893D+03 E-N=-9.819542887744D+03  KE= 1.958939410040D+03
 1\1\GINC-COMPUTE-0-3\SP\UTD-B3LYP-FC\6-31G(d,p)\C17H11N2O2S1(2)\BRYNND
 \31-May-2010\0\\# td ub3lyp/6-31g(d,p) scrf=(scipcm,solvent=ccl4)\\bmd
 139 TDDFT SCI PCM model\\0,2\S,0,-5.158604,0.608893,-0.451944\N,0,1.54
 4181,1.354834,-0.070571\O,0,2.12812,2.495052,-0.092044\N,0,1.16326,-0.
```

807745,-0.121209\O,0,1.319077,-2.075823,-0.14219\C,0,2.154637,0.125264
,-0.089969\C,0,0.146404,1.187303,-0.062013\C,0,-0.878137,2.104891,-0.0
45435\H,0,-0.748052,3.009859,-0.007392\C,0,-2.156671,1.590891,-0.03038
\H,0,-2.873396,2.160439,0.000147\C,0,-2.424012,0.20702,-0.028815\C,0,-
1.363043,-0.701966,-0.069946\H,0,-1.486204,-1.625727,-0.114966\C,0,-0.
094649,-0.173669,-0.087956\C,0,3.584077,-0.143671,-0.027609\C,0,4.4274
26,0.698192,0.690017\H,0,4.083742,1.381918,1.096635\C,0,5.770411,0.409
478,0.777686\H,0,6.251103,0.933923,1.239283\C,0,6.295259,-0.686365,0.1
45793\H,0,7.223003,-0.85445,0.231771\C,0,5.471229,-1.517672,-0.582485\
H,0,5.833367,-2.323328,-1.006574\C,0,4.123861,-1.261492,-0.664076\H,0,
3.568124,-1.863333,-1.11461\C,0,-3.796545,-0.2967,0.083098\C,0,-4.2196
28,-1.492825,0.655051\H,0,-3.723039,-1.977876,0.951002\C,0,-5.61279,-1
.626506,0.639411\H,0,-6.092612,-2.377636,0.994155\C,0,-6.239633,-0.579
763,0.077804\H,0,-7.157207,-0.444002,-0.10307\\Version=AM64L-G09RevA.0
2\State=2-A\HF=-1312.0557554\S2=0.794829\S2-1=0.\S2A=0.750302\RMSD=4.6
55e-09\PG=C01 [X(C17H11N2O2S1)]\\@

Table E–72. Output parameters for **4.11a**; SCI-PCM solvation, 1,4-dioxane.

N-N= 1.741875881893D+03 E-N=-9.819541265595D+03 KE= 1.958939251588D+03
1\1\GINC-COMPUTE-0-29\SP\UTD-B3LYP-FC\6-31G(d,p)\C17H11N2O2S1(2)\BRYNN
D\31-May-2010\0\\# td ub3lyp/6-31g(d,p) scrf=(scipcm,solvent=1,4-dioxa
ne)\\bmd139 TDDFT SCI PCM model\\0,2\S,0,-5.158604,0.608893,-0.451944\
N,0,1.544181,1.354834,-0.070571\O,0,2.12812,2.495052,-0.092044\N,0,1.1
6326,-0.807745,-0.121209\O,0,1.319077,-2.075823,-0.14219\C,0,2.154637,
0.125264,-0.089969\C,0,0.146404,1.187303,-0.062013\C,0,-0.878137,2.104
891,-0.045435\H,0,-0.748052,3.009859,-0.007392\C,0,-2.156671,1.590891,
-0.03038\H,0,-2.873396,2.160439,0.000147\C,0,-2.424012,0.20702,-0.0288
15\C,0,-1.363043,-0.701966,-0.069946\H,0,-1.486204,-1.625727,-0.114966
\C,0,-0.094649,-0.173669,-0.087956\C,0,3.584077,-0.143671,-0.027609\C,
0,4.427426,0.698192,0.690017\H,0,4.083742,1.381918,1.096635\C,0,5.7704
11,0.409478,0.777686\H,0,6.251103,0.933923,1.239283\C,0,6.295259,-0.68
6365,0.145793\H,0,7.223003,-0.85445,0.231771\C,0,5.471229,-1.517672,-0
.582485\H,0,5.833367,-2.323328,-1.006574\C,0,4.123861,-1.261492,-0.664
076\H,0,3.568124,-1.863333,-1.11461\C,0,-3.796545,-0.2967,0.083098\C,0
,-4.219628,-1.492825,0.655051\H,0,-3.723039,-1.977876,0.951002\C,0,-5.
61279,-1.626506,0.639411\H,0,-6.092612,-2.377636,0.994155\C,0,-6.23963
3,-0.579763,0.077804\H,0,-7.157207,-0.444002,-0.10307\\Version=AM64L-G
09RevA.02\State=2-A\HF=-1312.0557194\S2=0.794842\S2-1=0.\S2A=0.750302\
RMSD=4.647e-09\PG=C01 [X(C17H11N2O2S1)]\\@

Table E–73. Output parameters for **4.11a**; SCI-PCM solvation, toluene.

N-N= 1.741875881893D+03 E-N=-9.819555274010D+03 KE= 1.958940624404D+03
1\1\GINC-COMPUTE-0-18\SP\UTD-B3LYP-FC\6-31G(d,p)\C17H11N2O2S1(2)\BRYNN
D\31-May-2010\0\\# td ub3lyp/6-31g(d,p) scrf=(scipcm,solvent=toluene)\
\bmd139 TDDFT SCI PCM model\\0,2\S,0,-5.158604,0.608893,-0.451944\N,0,
1.544181,1.354834,-0.070571\O,0,2.12812,2.495052,-0.092044\N,0,1.16326
,-0.807745,-0.121209\O,0,1.319077,-2.075823,-0.14219\C,0,2.154637,0.12
5264,-0.089969\C,0,0.146404,1.187303,-0.062013\C,0,-0.878137,2.104891,
-0.045435\H,0,-0.748052,3.009859,-0.007392\C,0,-2.156671,1.590891,-0.0
3038\H,0,-2.873396,2.160439,0.000147\C,0,-2.424012,0.20702,-0.028815\C
,0,-1.363043,-0.701966,-0.069946\H,0,-1.486204,-1.625727,-0.114966\C,0
,-0.094649,-0.173669,-0.087956\C,0,3.584077,-0.143671,-0.027609\C,0,4.
427426,0.698192,0.690017\H,0,4.083742,1.381918,1.096635\C,0,5.770411,0

.409478,0.777686\H,0,6.251103,0.933923,1.239283\C,0,6.295259,-0.686365
,0.145793\H,0,7.223003,-0.85445,0.231771\C,0,5.471229,-1.517672,-0.582
485\H,0,5.833367,-2.323328,-1.006574\C,0,4.123861,-1.261492,-0.664076\
H,0,3.568124,-1.863333,-1.11461\C,0,-3.796545,-0.2967,0.083098\C,0,-4.
219628,-1.492825,0.655051\H,0,-3.723039,-1.977876,0.951002\C,0,-5.6127
9,-1.626506,0.639411\H,0,-6.092612,-2.377636,0.994155\C,0,-6.239633,-0
.579763,0.077804\H,0,-7.157207,-0.444002,-0.10307\\Version=AM64L-G09Re
vA.02\State=2-A\HF=-1312.0560307\S2=0.794728\S2-1=0.\S2A=0.750302\RMSD
=5.105e-09\PG=C01 [X(C17H11N2O2S1)]\\@

Table E–74. Output parameters for **4.11a**; SCI-PCM solvation, diethyl ether.

N-N= 1.741875881893D+03 E-N=-9.819648491978D+03 KE= 1.958949982249D+03
1\1\GINC-COMPUTE-0-15\SP\UTD-B3LYP-FC\6-31G(d,p)\C17H11N2O2S1(2)\BRYNN
D\31-May-2010\0\\# td ub3lyp/6-31g(d,p) scrf=(scipcm,solvent=diethylet
her)\\bmd139 TDDFT SCI PCM model\\0,2\S,0,-5.158604,0.608893,-0.451944
\N,0,1.544181,1.354834,-0.070571\O,0,2.12812,2.495052,-0.092044\N,0,1.
16326,-0.807745,-0.121209\O,0,1.319077,-2.075823,-0.14219\C,0,2.154637
,0.125264,-0.089969\C,0,0.146404,1.187303,-0.062013\C,0,-0.878137,2.10
4891,-0.045435\H,0,-0.748052,3.009859,-0.007392\C,0,-2.156671,1.590891
,-0.03038\H,0,-2.873396,2.160439,0.000147\C,0,-2.424012,0.20702,-0.028
815\C,0,-1.363043,-0.701966,-0.069946\H,0,-1.486204,-1.625727,-0.11496
6\C,0,-0.094649,-0.173669,-0.087956\C,0,3.584077,-0.143671,-0.027609\C
,0,4.427426,0.698192,0.690017\H,0,4.083742,1.381918,1.096635\C,0,5.770
411,0.409478,0.777686\H,0,6.251103,0.933923,1.239283\C,0,6.295259,-0.6
86365,0.145793\H,0,7.223003,-0.85445,0.231771\C,0,5.471229,-1.517672,-
0.582485\H,0,5.833367,-2.323328,-1.006574\C,0,4.123861,-1.261492,-0.66
4076\H,0,3.568124,-1.863333,-1.11461\C,0,-3.796545,-0.2967,0.083098\C,
0,-4.219628,-1.492825,0.655051\H,0,-3.723039,-1.977876,0.951002\C,0,-5
.61279,-1.626506,0.639411\H,0,-6.092612,-2.377636,0.994155\C,0,-6.2396
33,-0.579763,0.077804\H,0,-7.157207,-0.444002,-0.10307\\Version=AM64L-
G09RevA.02\State=2-A\HF=-1312.0581241\S2=0.793997\S2-1=0.\S2A=0.750299
\RMSD=8.719e-09\PG=C01 [X(C17H11N2O2S1)]\\@

Table E–75. Output parameters for **4.11a**; SCI-PCM solvation, ethyl acetate.

N-N= 1.741875881893D+03 E-N=-9.819688394297D+03 KE= 1.958954120047D+03
1\1\GINC-COMPUTE-0-0\SP\UTD-B3LYP-FC\6-31G(d,p)\C17H11N2O2S1(2)\BRYNND
\01-Jun-2010\0\\# td ub3lyp/6-31g(d,p) scrf=(scipcm,solvent=ethylethan
oate)\\bmd139 TDDFT SCI PCM model\\0,2\S,0,-5.158604,0.608893,-0.45194
4\N,0,1.544181,1.354834,-0.070571\O,0,2.12812,2.495052,-0.092044\N,0,1
.16326,-0.807745,-0.121209\O,0,1.319077,-2.075823,-0.14219\C,0,2.15463
7,0.125264,-0.089969\C,0,0.146404,1.187303,-0.062013\C,0,-0.878137,2.1
04891,-0.045435\H,0,-0.748052,3.009859,-0.007392\C,0,-2.156671,1.59089
1,-0.03038\H,0,-2.873396,2.160439,0.000147\C,0,-2.424012,0.20702,-0.02
8815\C,0,-1.363043,-0.701966,-0.069946\H,0,-1.486204,-1.625727,-0.1149
66\C,0,-0.094649,-0.173669,-0.087956\C,0,3.584077,-0.143671,-0.027609\
C,0,4.427426,0.698192,0.690017\H,0,4.083742,1.381918,1.096635\C,0,5.77
0411,0.409478,0.777686\H,0,6.251103,0.933923,1.239283\C,0,6.295259,-0.
686365,0.145793\H,0,7.223003,-0.85445,0.231771\C,0,5.471229,-1.517672,
-0.582485\H,0,5.833367,-2.323328,-1.006574\C,0,4.123861,-1.261492,-0.6
64076\H,0,3.568124,-1.863333,-1.11461\C,0,-3.796545,-0.2967,0.083098\C
,0,-4.219628,-1.492825,0.655051\H,0,-3.723039,-1.977876,0.951002\C,0,-
5.61279,-1.626506,0.639411\H,0,-6.092612,-2.377636,0.994155\C,0,-6.239
633,-0.579763,0.077804\H,0,-7.157207,-0.444002,-0.10307\\Version=AM64L

-G09RevA.02\State=2-A\HF=-1312.0590332\S2=0.793693\S2-1=0.\S2A=0.75029
8\RMSD=8.347e-09\PG=C01 [X(C17H11N2O2S1)]\\@

Table E–76. Output parameters for **4.11a**; SCI-PCM solvation, tetrahydrofuran.

N-N= 1.741875881893D+03 E-N=-9.819708331916D+03 KE= 1.958956218823D+03
1\1\GINC-COMPUTE-0-30\SP\UTD-B3LYP-FC\6-31G(d,p)\C17H11N2O2S1(2)\BRYNN
D\31-May-2010\0\\# td ub3lyp/6-31g(d,p) scrf=(scipcm,solvent=thf)\\bmd
139 TDDFT SCI PCM model\\0,2\S,0,-5.158604,0.608893,-0.451944\N,0,1.54
4181,1.354834,-0.070571\O,0,2.12812,2.495052,-0.092044\N,0,1.16326,-0.
807745,-0.121209\O,0,1.319077,-2.075823,-0.14219\C,0,2.154637,0.125264
,-0.089969\C,0,0.146404,1.187303,-0.062013\C,0,-0.878137,2.104891,-0.0
45435\H,0,-0.748052,3.009859,-0.007392\C,0,-2.156671,1.590891,-0.03038
\H,0,-2.873396,2.160439,0.000147\C,0,-2.424012,0.20702,-0.028815\C,0,-
1.363043,-0.701966,-0.069946\H,0,-1.486204,-1.625727,-0.114966\C,0,-0.
094649,-0.173669,-0.087956\C,0,3.584077,-0.143671,-0.027609\C,0,4.4274
26,0.698192,0.690017\H,0,4.083742,1.381918,1.096635\C,0,5.770411,0.409
478,0.777686\H,0,6.251103,0.933923,1.239283\C,0,6.295259,-0.686365,0.1
45793\H,0,7.223003,-0.85445,0.231771\C,0,5.471229,-1.517672,-0.582485\
H,0,5.833367,-2.323328,-1.006574\C,0,4.123861,-1.261492,-0.664076\H,0,
3.568124,-1.863333,-1.11461\C,0,-3.796545,-0.2967,0.083098\C,0,-4.2196
28,-1.492825,0.655051\H,0,-3.723039,-1.977876,0.951002\C,0,-5.61279,-1
.626506,0.639411\H,0,-6.092612,-2.377636,0.994155\C,0,-6.239633,-0.579
763,0.077804\H,0,-7.157207,-0.444002,-0.10307\\Version=AM64L-G09RevA.0
2\State=2-A\HF=-1312.0594912\S2=0.793544\S2-1=0.\S2A=0.750298\RMSD=7.9
57e-09\PG=C01 [X(C17H11N2O2S1)]\\@

Table E–77. Output parameters for **4.11a**; SCI-PCM solvation, methylene chloride.

N-N= 1.741875881893D+03 E-N=-9.819722795981D+03 KE= 1.958957756004D+03
1\1\GINC-COMPUTE-0-26\SP\UTD-B3LYP-FC\6-31G(d,p)\C17H11N2O2S1(2)\BRYNN
D\31-May-2010\0\\# td ub3lyp/6-31g(d,p) scrf=(scipcm,solvent=dichlorom
ethane)\\bmd139 TDDFT SCI PCM model\\0,2\S,0,-5.158604,0.608893,-0.451
944\N,0,1.544181,1.354834,-0.070571\O,0,2.12812,2.495052,-0.092044\N,0
,1.16326,-0.807745,-0.121209\O,0,1.319077,-2.075823,-0.14219\C,0,2.154
637,0.125264,-0.089969\C,0,0.146404,1.187303,-0.062013\C,0,-0.878137,2
.104891,-0.045435\H,0,-0.748052,3.009859,-0.007392\C,0,-2.156671,1.590
891,-0.03038\H,0,-2.873396,2.160439,0.000147\C,0,-2.424012,0.20702,-0.
028815\C,0,-1.363043,-0.701966,-0.069946\H,0,-1.486204,-1.625727,-0.11
4966\C,0,-0.094649,-0.173669,-0.087956\C,0,3.584077,-0.143671,-0.02760
9\C,0,4.427426,0.698192,0.690017\H,0,4.083742,1.381918,1.096635\C,0,5.
770411,0.409478,0.777686\H,0,6.251103,0.933923,1.239283\C,0,6.295259,-
0.686365,0.145793\H,0,7.223003,-0.85445,0.231771\C,0,5.471229,-1.51767
2,-0.582485\H,0,5.833367,-2.323328,-1.006574\C,0,4.123861,-1.261492,-0
.664076\H,0,3.568124,-1.863333,-1.11461\C,0,-3.796545,-0.2967,0.083098
\C,0,-4.219628,-1.492825,0.655051\H,0,-3.723039,-1.977876,0.951002\C,0
,-5.61279,-1.626506,0.639411\H,0,-6.092612,-2.377636,0.994155\C,0,-6.2
39633,-0.579763,0.077804\H,0,-7.157207,-0.444002,-0.10307\\Version=AM6
4L-G09RevA.02\State=2-A\HF=-1312.0598249\S2=0.793437\S2-1=0.\S2A=0.750
298\RMSD=7.826e-09\PG=C01 [X(C17H11N2O2S1)]\\@

Table E–78. Output parameters for **4.11a**; SCI-PCM solvation, acetone.

N-N= 1.741875881893D+03 E-N=-9.819765368696D+03 KE= 1.958962352815D+03
1\1\GINC-COMPUTE-0-28\SP\UTD-B3LYP-FC\6-31G(d,p)\C17H11N2O2S1(2)\BRYNN
D\31-May-2010\0\\# td ub3lyp/6-31g(d,p) scrf=(scipcm,solvent=acetone)\
\bmd139 TDDFT SCI PCM model\\0,2\S,0,-5.158604,0.608893,-0.451944\N,0,
1.544181,1.354834,-0.070571\O,0,2.12812,2.495052,-0.092044\N,0,1.16326
,-0.807745,-0.121209\O,0,1.319077,-2.075823,-0.14219\C,0,2.154637,0.12
5264,-0.089969\C,0,0.146404,1.187303,-0.062013\C,0,-0.878137,2.104891,
-0.045435\H,0,-0.748052,3.009859,-0.007392\C,0,-2.156671,1.590891,-0.0
3038\H,0,-2.873396,2.160439,0.000147\C,0,-2.424012,0.20702,-0.028815\C
,0,-1.363043,-0.701966,-0.069946\H,0,-1.486204,-1.625727,-0.114966\C,0
,-0.094649,-0.173669,-0.087956\C,0,3.584077,-0.143671,-0.027609\C,0,4.
427426,0.698192,0.690017\H,0,4.083742,1.381918,1.096635\C,0,5.770411,0
.409478,0.777686\H,0,6.251103,0.933923,1.239283\C,0,6.295259,-0.686365
,0.145793\H,0,7.223003,-0.85445,0.231771\C,0,5.471229,-1.517672,-0.582
485\H,0,5.833367,-2.323328,-1.006574\C,0,4.123861,-1.261492,-0.664076\
H,0,3.568124,-1.863333,-1.11461\C,0,-3.796545,-0.2967,0.083098\C,0,-4.
219628,-1.492825,0.655051\H,0,-3.723039,-1.977876,0.951002\C,0,-5.6127
9,-1.626506,0.639411\H,0,-6.092612,-2.377636,0.994155\C,0,-6.239633,-0
.579763,0.077804\H,0,-7.157207,-0.444002,-0.10307\\Version=AM64L-G09Re
vA.02\State=2-A\HF=-1312.0608159\S2=0.793126\S2-1=0.\S2A=0.750297\RMSD
=7.263e-09\PG=C01 [X(C17H11N2O2S1)]\\@

Table E–79. Output parameters for **4.11a**; SCI-PCM solvation, acetonitrile.

N-N= 1.741875881893D+03 E-N=-9.819780158870D+03 KE= 1.958963976985D+03
1\1\GINC-COMPUTE-0-23\SP\UTD-B3LYP-FC\6-31G(d,p)\C17H11N2O2S1(2)\BRYNN
D\31-May-2010\0\\# td ub3lyp/6-31g(d,p) scrf=(scipcm,solvent=acetonitr
ile)\\bmd139 TDDFT SCI PCM model\\0,2\S,0,-5.158604,0.608893,-0.451944
\N,0,1.544181,1.354834,-0.070571\O,0,2.12812,2.495052,-0.092044\N,0,1.
16326,-0.807745,-0.121209\O,0,1.319077,-2.075823,-0.14219\C,0,2.154637
,0.125264,-0.089969\C,0,0.146404,1.187303,-0.062013\C,0,-0.878137,2.10
4891,-0.045435\H,0,-0.748052,3.009859,-0.007392\C,0,-2.156671,1.590891
,-0.03038\H,0,-2.873396,2.160439,0.000147\C,0,-2.424012,0.20702,-0.028
815\C,0,-1.363043,-0.701966,-0.069946\H,0,-1.486204,-1.625727,-0.11496
6\C,0,-0.094649,-0.173669,-0.087956\C,0,3.584077,-0.143671,-0.027609\C
,0,4.427426,0.698192,0.690017\H,0,4.083742,1.381918,1.096635\C,0,5.770
411,0.409478,0.777686\H,0,6.251103,0.933923,1.239283\C,0,6.295259,-0.6
86365,0.145793\H,0,7.223003,-0.85445,0.231771\C,0,5.471229,-1.517672,-
0.582485\H,0,5.833367,-2.323328,-1.006574\C,0,4.123861,-1.261492,-0.66
4076\H,0,3.568124,-1.863333,-1.11461\C,0,-3.796545,-0.2967,0.083098\C,
0,-4.219628,-1.492825,0.655051\H,0,-3.723039,-1.977876,0.951002\C,0,-5
.61279,-1.626506,0.639411\H,0,-6.092612,-2.377636,0.994155\C,0,-6.2396
33,-0.579763,0.077804\H,0,-7.157207,-0.444002,-0.10307\\Version=AM64L-
G09RevA.02\State=2-A\HF=-1312.0611635\S2=0.793019\S2-1=0.\S2A=0.750296
\RMSD=7.254e-09\PG=C01 [X(C17H11N2O2S1)]\\@

Table E–80. Output parameters for **4.11a**; SCI-PCM solvation, dimethyl sulfoxide.

N-N= 1.741875881893D+03 E-N=-9.819784985268D+03 KE= 1.958964508543D+03
1\1\GINC-COMPUTE-0-17\SP\UTD-B3LYP-FC\6-31G(d,p)\C17H11N2O2S1(2)\BRYNN
D\31-May-2010\0\\# td ub3lyp/6-31g(d,p) scrf=(scipcm,solvent=dmso)\\bm
d139 TDDFT SCI PCM model\\0,2\S,0,-5.158604,0.608893,-0.451944\N,0,1.5
44181,1.354834,-0.070571\O,0,2.12812,2.495052,-0.092044\N,0,1.16326,-0

.807745,-0.121209\O,0,1.319077,-2.075823,-0.14219\C,0,2.154637,0.12526
4,-0.089969\C,0,0.146404,1.187303,-0.062013\C,0,-0.878137,2.104891,-0.
045435\H,0,-0.748052,3.009859,-0.007392\C,0,-2.156671,1.590891,-0.0303
8\H,0,-2.873396,2.160439,0.000147\C,0,-2.424012,0.20702,-0.028815\C,0,
-1.363043,-0.701966,-0.069946\H,0,-1.486204,-1.625727,-0.114966\C,0,-0
.094649,-0.173669,-0.087956\C,0,3.584077,-0.143671,-0.027609\C,0,4.427
426,0.698192,0.690017\H,0,4.083742,1.381918,1.096635\C,0,5.770411,0.40
9478,0.777686\H,0,6.251103,0.933923,1.239283\C,0,6.295259,-0.686365,0.
145793\H,0,7.223003,-0.85445,0.231771\C,0,5.471229,-1.517672,-0.582485
\H,0,5.833367,-2.323328,-1.006574\C,0,4.123861,-1.261492,-0.664076\H,0
,3.568124,-1.863333,-1.11461\C,0,-3.796545,-0.2967,0.083098\C,0,-4.219
628,-1.492825,0.655051\H,0,-3.723039,-1.977876,0.951002\C,0,-5.61279,-
1.626506,0.639411\H,0,-6.092612,-2.377636,0.994155\C,0,-6.239633,-0.57
9763,0.077804\H,0,-7.157207,-0.444002,-0.10307\\Version=AM64L-G09RevA.
02\State=2-A\HF=-1312.0612774\S2=0.792985\S2-1=0.\S2A=0.750296\RMSD=7.
773e-09\PG=C01 [X(C17H11N2O2S1)]\\@

Table E–81. Output parameters for **4.11a**; π dimer, singlet ground state.

1\1\GINC-COMPUTE-0-5\SP\UB3LYP\6-311+G(d,p)\C34H22N4O4S2\BRYNND\30-Aug
-2010\0\\# ub3lyp/6-311+g(d,p) guess=mix geom=connectivity\\bmd139 dim
er\\0,1\S,0,19.15,11.5622,2.7188\N,0,12.6758,10.5651,1.0697\O,0,12.177
,9.4067,0.844\N,0,12.9557,12.7402,1.1942\O,0,12.7553,14.0017,1.1626\C,
0,12.043,11.7721,0.9037\C,0,13.9993,10.7815,1.498\C,0,15.0138,9.9008,1
.7927\H,0,14.9199,8.9905,1.7653\C,0,16.2058,10.4587,2.2013\H,0,16.9071
,9.9144,2.4264\C,0,16.3974,11.85,2.3209\C,0,15.3558,12.7218,1.9911\H,0
,15.4443,13.6498,2.0115\C,0,14.1748,12.1501,1.5824\C,0,10.6484,11.9877
,0.5458\C,0,9.6699,11.0885,0.9565\H,0,9.9093,10.4012,1.4277\C,0,8.3494
,11.3258,0.6492\H,0,7.7784,10.7662,0.9354\C,0,7.9856,12.4268,-0.0802\H
,0,7.0679,12.5589,-0.2673\C,0,8.9492,13.3151,-0.5071\H,0,8.6923,14.123
8,-0.9987\C,0,10.2707,13.1102,-0.1913\H,0,10.9065,13.7489,-0.4431\C,0,
17.6508,12.3972,2.8491\C,0,17.8307,13.5838,3.5538\H,0,17.2477,14.0389,
3.6994\C,0,19.1585,13.7673,3.9568\H,0,19.4837,14.5172,4.459\C,0,19.970
5,12.7669,3.5784\H,0,20.903,12.6636,3.6783\S,0,19.1364,9.6617,6.2353\N
,0,12.6621,10.6588,4.5862\O,0,12.1633,11.8172,4.3605\N,0,12.942,8.4838
,4.7107\O,0,12.7416,7.2222,4.6791\C,0,12.0293,9.4519,4.4203\C,0,13.985
6,10.4425,5.0146\C,0,15.0001,11.3231,5.3092\H,0,14.9062,12.2335,5.2818
\C,0,16.1921,10.7652,5.7179\H,0,16.8934,11.3095,5.9429\C,0,16.3837,9.3
739,5.8374\C,0,15.3421,8.5022,5.5076\H,0,15.4306,7.5741,5.528\C,0,14.1
611,9.0738,5.099\C,0,10.6347,9.2362,4.0623\C,0,9.6562,10.1354,4.473\H,
0,9.8956,10.8228,4.9442\C,0,8.3357,9.8981,4.1657\H,0,7.7647,10.4577,4.
4519\C,0,7.9719,8.7972,3.4363\H,0,7.0542,8.665,3.2493\C,0,8.9356,7.908
9,3.0094\H,0,8.6786,7.1001,2.5178\C,0,10.2571,8.1138,3.3252\H,0,10.892
8,7.4751,3.0734\C,0,17.6371,8.8268,6.3656\C,0,17.817,7.6402,7.0703\H,0
,17.234,7.185,7.2159\C,0,19.1448,7.4567,7.4733\H,0,19.47,6.7068,7.9755
\C,0,19.9568,8.457,7.0949\H,0,20.8893,8.5603,7.1948\\Version=AM64L-G09
RevA.02\State=1-A\HF=-2624.621797\S2=1.084884\S2-1=0.\S2A=0.681602\RMS
D=2.643e-09\Dipole=1.4360929,-0.0260653,0.9887999\Quadrupole=26.024912
5,-15.4089507,-10.6159618,0.253944,10.4618504,-0.8920998\PG=C01 [X(C34
H22N4O4S2)]\\@

Table E–82. Output parameters for **4.11a**; π dimer, triplet ground state.

1\1\GINC-COMPUTE-0-20\SP\UB3LYP\6-311+G(d,p)\C34H22N4O4S2(3)\BRYNND\29
-Aug-2010\0\\# ub3lyp/6-311+g(d,p) geom=connectivity\\bmd139 dimer\\0,
3\S,0,19.15,11.5622,2.7188\N,0,12.6758,10.5651,1.0697\O,0,12.177,9.406
7,0.844\N,0,12.9557,12.7402,1.1942\O,0,12.7553,14.0017,1.1626\C,0,12.0
43,11.7721,0.9037\C,0,13.9993,10.7815,1.498\C,0,15.0138,9.9008,1.7927\
H,0,14.9199,8.9905,1.7653\C,0,16.2058,10.4587,2.2013\H,0,16.9071,9.914
4,2.4264\C,0,16.3974,11.85,2.3209\C,0,15.3558,12.7218,1.9911\H,0,15.44
43,13.6498,2.0115\C,0,14.1748,12.1501,1.5824\C,0,10.6484,11.9877,0.545
8\C,0,9.6699,11.0885,0.9565\H,0,9.9093,10.4012,1.4277\C,0,8.3494,11.32
58,0.6492\H,0,7.7784,10.7662,0.9354\C,0,7.9856,12.4268,-0.0802\H,0,7.0
679,12.5589,-0.2673\C,0,8.9492,13.3151,-0.5071\H,0,8.6923,14.1238,-0.9
987\C,0,10.2707,13.1102,-0.1913\H,0,10.9065,13.7489,-0.4431\C,0,17.650
8,12.3972,2.8491\C,0,17.8307,13.5838,3.5538\H,0,17.2477,14.0389,3.6994
\C,0,19.1585,13.7673,3.9568\H,0,19.4837,14.5172,4.459\C,0,19.9705,12.7
669,3.5784\H,0,20.903,12.6636,3.6783\S,0,19.1364,9.6617,6.2353\N,0,12.
6621,10.6588,4.5862\O,0,12.1633,11.8172,4.3605\N,0,12.942,8.4838,4.710
7\O,0,12.7416,7.2222,4.6791\C,0,12.0293,9.4519,4.4203\C,0,13.9856,10.4
425,5.0146\C,0,15.0001,11.3231,5.3092\H,0,14.9062,12.2335,5.2818\C,0,1
6.1921,10.7652,5.7179\H,0,16.8934,11.3095,5.9429\C,0,16.3837,9.3739,5.
8374\C,0,15.3421,8.5022,5.5076\H,0,15.4306,7.5741,5.528\C,0,14.1611,9.
0738,5.099\C,0,10.6347,9.2362,4.0623\C,0,9.6562,10.1354,4.473\H,0,9.89
56,10.8228,4.9442\C,0,8.3357,9.8981,4.1657\H,0,7.7647,10.4577,4.4519\C
,0,7.9719,8.7972,3.4363\H,0,7.0542,8.665,3.2493\C,0,8.9356,7.9089,3.00
94\H,0,8.6786,7.1001,2.5178\C,0,10.2571,8.1138,3.3252\H,0,10.8928,7.47
51,3.0734\C,0,17.6371,8.8268,6.3656\C,0,17.817,7.6402,7.0703\H,0,17.23
4,7.185,7.2159\C,0,19.1448,7.4567,7.4733\H,0,19.47,6.7068,7.9755\C,0,1
9.9568,8.457,7.0949\H,0,20.8893,8.5603,7.1948\\Version=AM64L-G09RevA.0
2\State=3-A\HF=-2624.6217761\S2=2.086055\S2-1=0.\S2A=2.003308\RMSD=3.8
38e-09\Dipole=1.4367108,-0.026744,0.9878972\Quadrupole=26.034263,-15.4
179205,-10.6163425,0.259826,10.4647306,-0.8899752\PG=C01 [X(C34H22N4O4
S2)]\\@

Table E–83. Output parameters for **4.11b**; π dimer, singlet ground state.

1\1\GINC-COMPUTE-0-33\SP\UB3LYP\6-311+G(d,p)\C30H18N4O4S4\BRYNND\29-Oc
t-2010\0\\# ub3lyp/6-311+g(d,p) guess=mix geom=connectivity\\pi-dimer
singlet\\0,1\C,0,-1.8024,14.7868,6.1673\C,0,-1.3649,14.4728,7.4762\C,0
,-2.8347,15.6883,5.919\H,0,-1.332,14.2958,5.3259\C,0,-1.9989,15.074,8.
5825\H,0,-3.1628,15.9213,4.9154\C,0,0.3808,12.7664,6.7161\H,0,-1.6929,
14.8788,9.6012\C,0,1.43,11.9657,7.2428\H,0,0.1238,12.7931,5.6658\C,0,1
.5919,12.1234,8.5904\O,0,-5.1112,17.7068,6.1506\H,0,2.0431,11.3065,6.6
427\H,0,2.3025,11.6451,9.2456\O,0,-3.7382,16.6648,10.4698\C,0,-6.9471,
18.6389,8.4111\C,0,-7.6981,19.5604,9.181\H,0,-7.2708,18.2044,7.4782\C,
0,-7.0504,19.9515,10.3206\H,0,-8.679,19.9163,8.8988\H,0,-7.3893,20.639
2,11.08\C,0,3.1494,14.7868,6.1673\C,0,2.1171,15.6883,5.919\H,0,3.6198,
14.2958,5.3259\C,0,4.6973,13.5357,7.6636\C,0,2.9529,15.074,8.5825\H,0,
1.7891,15.9213,4.9154\C,0,5.3327,12.7664,6.7161\S,0,5.4085,13.2558,9.2
415\H,0,3.2589,14.8788,9.6012\N,0,0.4628,17.1932,7.1351\C,0,6.3818,11.
9657,7.2428\H,0,5.0757,12.7931,5.6658\C,0,6.5438,12.1234,8.5904\N,0,1.
1124,16.7025,9.2035\O,0,-0.1593,17.7068,6.1506\H,0,6.9949,11.3065,6.64
27\H,0,7.2543,11.6451,9.2456\O,0,1.2137,16.6648,10.4698\S,0,-0.548,19.
2061,10.4914\C,0,-2.0985,19.9515,10.3206\H,0,-2.4374,20.6392,11.08\C,0
,1.5166,16.2635,7.0251\C,0,1.9248,15.9525,8.3177\C,0,0.2242,17.4517,8.
4645\C,0,-1.9952,18.6389,8.4111\H,0,-2.3189,18.2044,7.4782\C,0,-0.7702

,18.3356,8.9796\C,0,3.5869,14.4728,7.4762\C,0,-2.7462,19.5604,9.181\H,
0,-3.7272,19.9163,8.8988\S,0,0.4566,13.2558,9.2415\C,0,-0.2546,13.5357
,7.6636\C,0,-3.027,15.9525,8.3177\C,0,-3.4353,16.2635,7.0251\N,0,-4.48
9,17.1932,7.1351\N,0,-3.8395,16.7025,9.2035\C,0,-4.7276,17.4517,8.4645
\C,0,-5.7221,18.3356,8.9796\S,0,-5.4998,19.2061,10.4914\\Version=AM64L
-G09RevA.02\State=1-A\HF=-3266.8938947\S2=1.094084\S2-1=0.\S2A=0.77366
6\RMSD=6.367e-09\Dipole=1.2179816,-1.4000533,-0.8465792\Quadrupole=10.
7452493,0.6848205,-11.4300699,-23.7812685,-9.4683024,15.4466362\PG=C01
[X(C30H18N4O4S4)]\\@

Table E–84. Output parameters for **4.11b**; π dimer, triplet ground state.

1\1\GINC-COMPUTE-0-6\SP\UB3LYP\6-311+G(d,p)\C30H18N4O4S4(3)\BRYNND\29-
Oct-2010\0\\# ub3lyp/6-311+g(d,p) geom=connectivity\\pi-dimer triplet\
\0,3\C,0,0.120516,-2.761073,0.564625\C,0,-0.262368,-1.913833,-0.502523
\C,0,1.429924,-2.828012,1.034698\H,0,-0.625799,-3.396163,1.022868\C,0,
0.70986,-1.113182,-1.135791\H,0,1.713297,-3.479125,1.850114\C,0,-2.703
297,-2.674554,-0.516186\H,0,0.466165,-0.438895,-1.945383\C,0,-3.94459,
-2.358072,-1.131317\H,0,-2.589973,-3.451332,0.227901\C,0,-3.849635,-1.
31821,-2.012666\O,0,4.422051,-2.453963,1.501278\H,0,-4.870141,-2.87725
8,-0.920705\H,0,-4.623963,-0.871694,-2.616033\O,0,3.216201,0.306457,-2
.041657\C,0,6.722446,-1.243837,-0.108994\C,0,7.917536,-0.514946,-0.324
375\H,0,6.674297,-2.259758,0.25081\C,0,7.68998,0.753092,-0.784222\H,0,
8.904519,-0.917774,-0.145321\H,0,8.413234,1.515858,-1.028282\C,0,-4.12
1125,-0.536855,1.822265\C,0,-2.811717,-0.603794,2.292338\H,0,-4.86744,
-1.171945,2.280507\C,0,-5.9052,0.351106,0.329362\C,0,-3.531781,1.11103
6,0.121849\H,0,-2.52843,-1.254863,3.107779\C,0,-6.945024,-0.450291,0.7
41479\S,0,-6.474576,1.515959,-0.850828\H,0,-3.775476,1.785323,-0.68774
3\N,0,-0.498254,0.367776,1.86307\C,0,-8.186231,-0.133854,0.126323\H,0,
-6.831699,-1.227069,1.485566\C,0,-8.091362,0.906053,-0.755001\N,0,-1.0
64767,1.691274,0.169417\O,0,0.180324,-0.2297,2.758943\H,0,-9.111782,-0
.65304,0.336935\H,0,-8.865604,1.352524,-1.358393\O,0,-1.025526,2.53072
,-0.783992\S,0,1.76463,3.323485,0.287834\C,0,3.448253,2.977355,0.47344
3\H,0,4.171507,3.740121,0.229383\C,0,-1.88129,0.195711,1.652019\C,0,-2
.239432,1.021124,0.591552\C,0,-0.011604,1.278277,0.954656\C,0,2.480719
,0.980426,1.148671\H,0,2.432571,-0.035496,1.508475\C,0,1.343888,1.7101
66,0.847172\C,0,-4.504009,0.310385,0.755116\C,0,3.675809,1.709317,0.93
329\H,0,4.662878,1.306444,1.112319\S,0,-2.232849,-0.708304,-2.108493\C
,0,-1.663474,-1.873157,-0.928304\C,0,2.002209,-1.203094,-0.666087\C,0,
2.360437,-2.028552,0.394354\N,0,3.743387,-1.856442,0.60543\N,0,3.17695
9,-0.532989,-1.088248\C,0,4.230037,-0.945941,-0.302983\C,0,5.585615,-0
.514097,-0.410493\S,0,6.006271,1.099267,-0.969806\\Version=AM64L-G09Re
vA.02\State=3-A\HF=-3266.8940455\S2=2.099266\S2-1=0.\S2A=2.004462\RMSD
=5.183e-09\Dipole=-1.8628788,-0.8394636,0.1060818\Quadrupole=31.962891
1,-8.6300642,-23.3328268,13.341662,-3.0823819,-2.6604843\PG=C01 [X(C30
H18N4O4S4)]\\@

Table E–85. Output parameters for **4.11b**; O…C dimer, singlet ground state.

1\1\GINC-COMPUTE-0-13\SP\UB3LYP\6-311+G(d,p)\C30H18N4O4S4\BRYNND\28-Oc
t-2010\0\\# ub3lyp/6-311+g(d,p) guess=mix geom=connectivity\\O...C dim
er singlet\\0,1\C,0,3.4064,16.6438,-0.3279\C,0,3.8439,16.9578,0.9811\C
,0,2.3741,15.7423,-0.5761\H,0,3.8768,17.1348,-1.1692\C,0,4.9543,17.894
9,1.1685\C,0,3.2099,16.3566,2.0874\C,0,1.7736,15.1671,0.5299\H,0,2.046
1,15.5093,-1.5797\C,0,5.5897,18.6643,0.221\S,0,5.6655,18.1748,2.7464\C

,0,2.1818,15.4781,1.8225\H,0,3.5159,16.5518,3.1061\N,0,0.7198,14.2375,
0.64\C,0,6.6388,19.4649,0.7477\H,0,5.3327,18.6375,-0.8293\C,0,6.8008,1
9.3073,2.0953\C,0,0.4812,13.9789,1.9694\O,0,0.0977,13.7239,-0.3445\H,0
,7.2519,20.1241,0.1476\H,0,7.5113,19.7855,2.7505\C,0,-0.5132,13.095,2.
4844\C,0,-1.7382,12.7918,1.916\S,0,-0.291,12.2245,3.9962\C,0,-2.4892,1
1.8703,2.6859\H,0,-2.0619,13.2262,0.9831\C,0,-1.8415,11.4791,3.8254\H,
0,-3.4702,11.5143,2.4036\H,0,-2.1804,10.7915,4.5849\C,0,3.5869,14.4728
,7.4762\C,0,4.6973,13.5357,7.6636\C,0,2.9529,15.074,8.5825\C,0,1.5166,
16.2635,7.0251\C,0,5.3327,12.7664,6.7161\S,0,5.4085,13.2558,9.2415\C,0
,1.9248,15.9525,8.3177\H,0,3.2589,14.8788,9.6012\N,0,0.4628,17.1932,7.
1351\C,0,6.3818,11.9657,7.2428\H,0,5.0757,12.7931,5.6658\C,0,6.5438,12
.1234,8.5904\N,0,1.1124,16.7025,9.2035\C,0,0.2242,17.4517,8.4645\O,0,-
0.1593,17.7068,6.1506\H,0,6.9949,11.3065,6.6427\H,0,7.2543,11.6451,9.2
456\O,0,1.2137,16.6648,10.4698\C,0,-0.7702,18.3356,8.9796\C,0,-1.9952,
18.6389,8.4111\S,0,-0.548,19.2061,10.4914\C,0,-2.7462,19.5604,9.181\H,
0,-2.3189,18.2044,7.4782\C,0,-2.0985,19.9515,10.3206\H,0,-3.7272,19.91
63,8.8988\H,0,-2.4374,20.6392,11.08\H,0,1.7891,15.9213,4.9154\C,0,3.14
94,14.7868,6.1673\C,0,2.1171,15.6883,5.919\H,0,3.6198,14.2958,5.3259\O
,0,1.4707,14.7658,3.9746\N,0,1.3694,14.7281,2.7083\\Version=AM64L-G09R
evA.02\State=1-A\HF=-3266.8960011\S2=1.092619\S2-1=0.\S2A=0.735109\RMS
D=1.155e-09\Dipole=1.014126,-0.1377848,-2.0469192\Quadrupole=12.248407
1,-0.0105785,-12.2378286,5.4687743,-8.7734841,-9.3764882\PG=C01 [X(C30
H18N4O4S4)]\\@

Table E–86. Output parameters for **4.11b**; O…C dimer, triplet ground state.

1\1\GINC-COMPUTE-0-27\SP\UB3LYP\6-311+G(d,p)\C30H18N4O4S4(3)\BRYNND\28
-Oct-2010\0\\# ub3lyp/6-311+g(d,p) geom=connectivity\\O...C dimer trip
let\\0,3\C,0,3.4064,16.6438,-0.3279\C,0,3.8439,16.9578,0.9811\C,0,2.37
41,15.7423,-0.5761\H,0,3.8768,17.1348,-1.1692\C,0,4.9543,17.8949,1.168
5\C,0,3.2099,16.3566,2.0874\C,0,1.7736,15.1671,0.5299\H,0,2.0461,15.50
93,-1.5797\C,0,5.5897,18.6643,0.221\S,0,5.6655,18.1748,2.7464\C,0,2.18
18,15.4781,1.8225\H,0,3.5159,16.5518,3.1061\N,0,0.7198,14.2375,0.64\C,
0,6.6388,19.4649,0.7477\H,0,5.3327,18.6375,-0.8293\C,0,6.8008,19.3073,
2.0953\C,0,0.4812,13.9789,1.9694\O,0,0.0977,13.7239,-0.3445\H,0,7.2519
,20.1241,0.1476\H,0,7.5113,19.7855,2.7505\C,0,-0.5132,13.095,2.4844\C,
0,-1.7382,12.7918,1.916\S,0,-0.291,12.2245,3.9962\C,0,-2.4892,11.8703,
2.6859\H,0,-2.0619,13.2262,0.9831\C,0,-1.8415,11.4791,3.8254\H,0,-3.47
02,11.5143,2.4036\H,0,-2.1804,10.7915,4.5849\C,0,3.5869,14.4728,7.4762
\C,0,4.6973,13.5357,7.6636\C,0,2.9529,15.074,8.5825\C,0,1.5166,16.2635
,7.0251\C,0,5.3327,12.7664,6.7161\S,0,5.4085,13.2558,9.2415\C,0,1.9248
,15.9525,8.3177\H,0,3.2589,14.8788,9.6012\N,0,0.4628,17.1932,7.1351\C,
0,6.3818,11.9657,7.2428\H,0,5.0757,12.7931,5.6658\C,0,6.5438,12.1234,8
.5904\N,0,1.1124,16.7025,9.2035\C,0,0.2242,17.4517,8.4645\O,0,-0.1593,
17.7068,6.1506\H,0,6.9949,11.3065,6.6427\H,0,7.2543,11.6451,9.2456\O,0
,1.2137,16.6648,10.4698\C,0,-0.7702,18.3356,8.9796\C,0,-1.9952,18.6389
,8.4111\S,0,-0.548,19.2061,10.4914\C,0,-2.7462,19.5604,9.181\H,0,-2.31
89,18.2044,7.4782\C,0,-2.0985,19.9515,10.3206\H,0,-3.7272,19.9163,8.89
88\H,0,-2.4374,20.6392,11.08\H,0,1.7891,15.9213,4.9154\C,0,3.1494,14.7
868,6.1673\C,0,2.1171,15.6883,5.919\H,0,3.6198,14.2958,5.3259\O,0,1.47
07,14.7658,3.9746\N,0,1.3694,14.7281,2.7083\\Version=AM64L-G09RevA.02\
State=3-A\HF=-3266.8960249\S2=2.092614\S2-1=0.\S2A=2.003906\RMSD=4.097
e-09\Dipole=1.014287,-0.1373907,-2.046267\Quadrupole=12.2501428,-0.009
0126,-12.2411302,5.4659763,-8.7772008,-9.3774318\PG=C01 [X(C30H18N4O4S
4)]\\@

Table E–87. Output parameters for **4.11b**; Th…Th dimer, singlet ground state.

1\1\GINC-COMPUTE-0-28\SP\UB3LYP\6-311+G(d,p)\C30H18N4O4S4\BRYNND\28-Oc
t-2010\0\\# ub3lyp/6-311+g(d,p) guess=mix geom=connectivity\\Th-Th dim
er singlet\\0,1\C,0,3.1494,14.7868,6.1673\C,0,3.5869,14.4728,7.4762\C,
0,2.1171,15.6883,5.919\H,0,3.6198,14.2958,5.3259\C,0,4.6973,13.5357,7.
6636\C,0,2.9529,15.074,8.5825\C,0,1.5166,16.2635,7.0251\H,0,1.7891,15.
9213,4.9154\C,0,5.3327,12.7664,6.7161\S,0,5.4085,13.2558,9.2415\C,0,1.
9248,15.9525,8.3177\H,0,3.2589,14.8788,9.6012\N,0,0.4628,17.1932,7.135
1\H,0,5.0757,12.7931,5.6658\N,0,1.1124,16.7025,9.2035\C,0,0.2242,17.45
17,8.4645\O,0,-0.1593,17.7068,6.1506\O,0,1.2137,16.6648,10.4698\C,0,-0
.7702,18.3356,8.9796\C,0,-1.9952,18.6389,8.4111\S,0,-0.548,19.2061,10.
4914\C,0,-2.7462,19.5604,9.181\H,0,-2.3189,18.2044,7.4782\C,0,-2.0985,
19.9515,10.3206\H,0,-3.7272,19.9163,8.8988\H,0,-2.4374,20.6392,11.08\C
,0,1.0314,4.31,13.3181\C,0,0.5939,3.996,12.0092\C,0,2.0637,5.2114,13.5
664\H,0,0.561,3.8189,14.1595\C,0,-0.5164,3.0588,11.8218\C,0,1.2279,4.5
971,10.9029\C,0,2.6643,5.7867,12.4603\H,0,2.3918,5.4445,14.57\C,0,-1.1
518,2.2895,12.7693\S,0,-1.2276,2.7789,10.2439\C,0,2.256,5.4756,11.1678
\H,0,0.9219,4.4019,9.8842\N,0,3.718,6.7163,12.3503\C,0,-2.201,1.4888,1
2.2426\H,0,-0.8948,2.3162,13.8196\C,0,-2.3629,1.6465,10.895\N,0,3.0685
,6.2257,10.2819\C,0,3.9566,6.9749,11.0209\O,0,4.3402,7.2299,13.3348\H,
0,-2.8141,0.8296,12.8427\H,0,-3.0734,1.1682,10.2398\O,0,2.9672,6.1879,
9.0156\C,0,4.9511,7.8587,10.5058\C,0,6.1761,8.162,11.0743\S,0,4.7288,8
.7292,8.994\C,0,6.9271,9.0835,10.3044\H,0,6.4998,7.7276,12.0072\H,0,7.
908,9.4394,10.5866\C,0,6.2794,9.4747,9.1649\H,0,6.6183,10.1623,8.4054\
H,0,7.2543,11.6451,9.2456\C,0,6.3818,11.9657,7.2428\C,0,6.5438,12.1234
,8.5904\H,0,6.9949,11.3065,6.6427\\Version=AM64L-G09RevA.02\State=1-A\
HF=-3266.908208\S2=1.099527\S2-1=0.\S2A=0.788523\RMSD=4.560e-09\Dipole
=-0.1531255,-1.2634875,0.0139986\Quadrupole=8.0072741,0.4789519,-8.486
226,13.065321,-12.064546,-9.841441\PG=C01 [X(C30H18N4O4S4)]\\@

Table E–88. Output parameters for **4.11b**; Th…Th dimer, triplet ground state.

1\1\GINC-COMPUTE-0-1\SP\UB3LYP\6-311+G(d,p)\C30H18N4O4S4(3)\BRYNND\27-
Oct-2010\0\\# ub3lyp/6-311+g(d,p) geom=connectivity\\Th-Th dimer tripl
et\\0,3\C,0,3.1494,14.7868,6.1673\C,0,3.5869,14.4728,7.4762\C,0,2.1171
,15.6883,5.919\H,0,3.6198,14.2958,5.3259\C,0,4.6973,13.5357,7.6636\C,0
,2.9529,15.074,8.5825\C,0,1.5166,16.2635,7.0251\H,0,1.7891,15.9213,4.9
154\C,0,5.3327,12.7664,6.7161\S,0,5.4085,13.2558,9.2415\C,0,1.9248,15.
9525,8.3177\H,0,3.2589,14.8788,9.6012\N,0,0.4628,17.1932,7.1351\H,0,5.
0757,12.7931,5.6658\N,0,1.1124,16.7025,9.2035\C,0,0.2242,17.4517,8.464
5\O,0,-0.1593,17.7068,6.1506\O,0,1.2137,16.6648,10.4698\C,0,-0.7702,18
.3356,8.9796\C,0,-1.9952,18.6389,8.4111\S,0,-0.548,19.2061,10.4914\C,0
,-2.7462,19.5604,9.181\H,0,-2.3189,18.2044,7.4782\C,0,-2.0985,19.9515,
10.3206\H,0,-3.7272,19.9163,8.8988\H,0,-2.4374,20.6392,11.08\C,0,1.031
4,4.31,13.3181\C,0,0.5939,3.996,12.0092\C,0,2.0637,5.2114,13.5664\H,0,
0.561,3.8189,14.1595\C,0,-0.5164,3.0588,11.8218\C,0,1.2279,4.5971,10.9
029\C,0,2.6643,5.7867,12.4603\H,0,2.3918,5.4445,14.57\C,0,-1.1518,2.28
95,12.7693\S,0,-1.2276,2.7789,10.2439\C,0,2.256,5.4756,11.1678\H,0,0.9
219,4.4019,9.8842\N,0,3.718,6.7163,12.3503\C,0,-2.201,1.4888,12.2426\H
,0,-0.8948,2.3162,13.8196\C,0,-2.3629,1.6465,10.895\N,0,3.0685,6.2257,
10.2819\C,0,3.9566,6.9749,11.0209\O,0,4.3402,7.2299,13.3348\H,0,-2.814
1,0.8296,12.8427\H,0,-3.0734,1.1682,10.2398\O,0,2.9672,6.1879,9.0156\C
,0,4.9511,7.8587,10.5058\C,0,6.1761,8.162,11.0743\S,0,4.7288,8.7292,8.
994\C,0,6.9271,9.0835,10.3044\H,0,6.4998,7.7276,12.0072\H,0,7.908,9.43
94,10.5866\C,0,6.2794,9.4747,9.1649\H,0,6.6183,10.1623,8.4054\H,0,7.25

43,11.6451,9.2456\C,0,6.3818,11.9657,7.2428\C,0,6.5438,12.1234,8.5904\
H,0,6.9949,11.3065,6.6427\\Version=AM64L-G09RevA.02\State=3-A\HF=-3266
.9082132\S2=2.099717\S2-1=0.\S2A=2.004501\RMSD=4.105e-09\Dipole=-0.152
7367,-1.2644313,0.0142614\Quadrupole=8.0102659,0.4759514,-8.4862172,13
.0670954,-12.0651727,-9.8402561\PG=C01 [X(C30H18N4O4S4)]\\@

Table E–89. Output parameters for Table 5.1; R = benzene.

1\1\GINC-COMPUTE-0-27\SP\UTD-B3LYP-FC\6-311+G(d,p)\C13H9N2O2(2)\BRYNND
\05-Nov-2010\0\\# td ub3lyp/6-311+g(d,p) scrf=(cpcm,solvent=chloroform
) geom=connectivity\\PBNN TDDFT\\0,2\C,0,-0.000001,-4.218147,0.701492\
C,0,-0.000001,-4.218147,-0.701492\C,0,-0.000001,-3.027935,-1.433446\C,
0,-0.000001,-1.857762,-0.69385\C,0,-0.000001,-1.857762,0.69385\C,0,-0.
000001,-3.027935,1.433446\N,0,-0.000001,-0.505943,-1.107398\N,0,-0.000
001,-0.505943,1.107398\O,0,-0.000001,-0.162579,-2.333956\O,0,-0.000001
,-0.162579,2.333956\H,0,-0.000001,-5.163264,1.230484\H,0,-0.000001,-3.
012236,-2.514871\H,0,-0.000001,-3.012236,2.514871\H,0,-0.000001,-5.163
264,-1.230484\C,0,-0.000001,0.318959,0.\C,0,0.000001,2.499861,1.212505
\C,0,0.000002,3.890202,1.202749\C,0,0.000003,4.594789,0.\C,0,0.000002,
3.890202,-1.202749\C,0,0.000001,2.499861,-1.212505\C,0,0.000001,1.7754
06,0.\H,0,0.000001,1.969345,2.151041\H,0,0.000003,4.42424,2.146057\H,0
,0.000004,5.678738,0.\H,0,0.000003,4.42424,-2.146057\H,0,0.000001,1.96
9345,-2.151041\\Version=AM64L-G09RevA.02\State=2-A"\HF=-760.8368513\S2
=0.796723\S2-1=0.\S2A=0.750402\RMSD=4.509e-09\PG=CS [SG(C3H1),X(C10H8N
2O2)]\\@

Table E–90. Output parameters for Table 5.1; R = thiophene.

N-N= 1.140040958207D+03 E-N=-7.216122435343D+03 KE= 1.616003104580D+03
1\1\GINC-COMPUTE-0-26\SP\UTD-B3LYP-FC\6-311+G(d,p)\C11H7N2O2S1(2)\BRYN
ND\05-Nov-2010\0\\# td ub3lyp/6-311+g(d,p) scrf=(cpcm,solvent=chlorofo
rm) geom=connectivity\\ThBNN TDDFT\\0,2\C,0,-4.141796,-0.843233,0.0002
61\C,0,-4.231647,0.555293,0.000014\C,0,-3.089825,1.363271,-0.000301\C,
0,-1.874339,0.703407,-0.000436\C,0,-1.78529,-0.686715,-0.000187\C,0,-2
.905676,-1.497718,0.00021\N,0,-0.550108,1.204996,-0.000311\N,0,-0.4085
69,-1.008564,0.000074\O,0,-0.249872,2.442029,-0.000122\O,0,0.067309,-2
.190721,0.000473\H,0,-5.050388,-1.432673,0.000544\H,0,-3.145443,2.4435
07,-0.0005\H,0,-2.821821,-2.576134,0.000388\H,0,-5.208431,1.02315,0.00
0122\C,0,0.330008,0.147266,-0.000095\C,0,4.194434,-0.247696,-0.000304\
C,0,3.921566,1.094124,0.000328\C,0,2.532803,1.371584,0.000783\C,0,1.75
5052,0.225795,0.000467\H,0,5.158942,-0.733301,-0.000335\H,0,4.68596,1.
859428,0.000703\H,0,2.10329,2.361196,0.0012\S,0,2.763587,-1.215183,-0.
000483\\Version=AM64L-G09RevA.02\State=2-A\HF=-1081.604083\S2=0.799912
\S2-1=0.\S2A=0.750479\RMSD=3.178e-09\PG=C01 [X(C11H7N2O2S1)]\\@

Table E–91. Output parameters for Table 5.1; R = *p*-methoxybenzene.

N-N= 1.331137179979D+03 E-N=-7.041779578795D+03 KE= 1.306367218915D+03
1\1\GINC-COMPUTE-0-33\SP\UTD-B3LYP-FC\6-311+G(d,p)\C14H11N2O3(2)\BRYNN
D\07-Nov-2010\0\\# td ub3lyp/6-311+g(d,p) scrf=(cpcm,solvent=chlorofor
m) geom=connectivity\\pMeOPhBNN TDDFT\\0,2\C,0,-5.018719,0.548628,0.11
6944\C,0,-4.959882,-0.843571,-0.038876\C,0,-3.739113,-1.518489,-0.1346
18\C,0,-2.600953,-0.734594,-0.06666\C,0,-2.659372,0.646033,0.085597\C,
0,-3.859539,1.327647,0.182966\N,0,-1.231785,-1.084808,-0.132941\N,0,-1

.32474,1.114191,0.118022\O,0,-0.81868,-2.279819,-0.296453\O,0,-1.01320
7,2.340085,0.275889\H,0,-5.984831,1.033147,0.187783\H,0,-3.678502,-2.5
91819,-0.253961\H,0,-3.890002,2.402266,0.302174\H,0,-5.881488,-1.41060
9,-0.086088\C,0,-0.46227,0.050133,-0.018334\C,0,1.763771,-1.001332,0.3
21238\C,0,0.987242,0.113957,-0.036551\C,0,1.656461,1.298452,-0.415228\
C,0,3.037535,1.354082,-0.434651\C,0,3.80137,0.235587,-0.070371\C,0,3.1
53481,-0.944658,0.310233\H,0,1.279258,-1.923267,0.607171\H,0,3.548897,
2.262151,-0.730482\H,0,3.714705,-1.822819,0.59794\O,0,5.148444,0.39374
3,-0.11879\C,0,5.986774,-0.706444,0.24559\H,0,5.825834,-1.56061,-0.417
999\H,0,7.007623,-0.347194,0.134876\H,0,5.814795,-1.005294,1.283331\H,
0,1.086218,2.173709,-0.689165\\Version=AM64L-G09RevA.02\State=2-A\HF=-
875.3972189\S2=0.793132\S2-1=0.\S2A=0.750346\RMSD=3.164e-09\PG=C01 [X(
C14H11N2O3)]\\@

Table E–92. Output parameters for Table 5.1; R = 2-benzo[*b*]thiophene.

N-N= 1.538439462830D+03 E-N=-8.945146204104D+03 KE= 1.845478905393D+03
1\1\GINC-COMPUTE-0-6\SP\UTD-B3LYP-FC\6-311+G(d,p)\C15H9N2O2S1(2)\BRYNN
D\07-Nov-2010\0\\# td ub3lyp/6-311+g(d,p) scrf=(cpcm,solvent=chlorofor
m) geom=connectivity\\benzo2ThBNN TDDFT\\0,2\C,0,-5.269625,-0.617334,0
.000373\C,0,-5.259688,0.784687,0.000289\C,0,-4.063947,1.509315,0.00013
2\C,0,-2.898147,0.764375,0.00007\C,0,-2.908409,-0.628293,0.00015\C,0,-
4.083985,-1.357997,0.000303\N,0,-1.542396,1.17129,-0.000059\N,0,-1.558
802,-1.047899,0.000058\O,0,-1.157246,2.38424,-0.000155\O,0,-1.171962,-
2.260395,0.00015\H,0,-6.218103,-1.140142,0.000497\H,0,-4.042599,2.5907
18,0.000074\H,0,-4.077252,-2.439618,0.000369\H,0,-6.200843,1.320623,0.
000351\C,0,-0.739017,0.054778,-0.000118\C,0,4.033017,1.628185,-0.00011
3\C,0,2.90856,0.778368,-0.000267\C,0,3.106628,-0.623172,-0.00002\C,0,4
.389041,-1.180627,0.000377\C,0,5.479664,-0.321306,0.000517\C,0,5.3023,
1.075803,0.00027\H,0,3.896301,2.703712,-0.000275\H,0,4.531015,-2.25481
5,0.000496\H,0,6.482167,-0.733279,0.000779\H,0,6.171832,1.722734,0.000
38\C,0,0.689806,0.03576,-0.000311\C,0,1.523726,1.128222,-0.000554\S,0,
1.58677,-1.496882,-0.000536\H,0,1.151666,2.141103,-0.000637\\Version=A
M64L-G09RevA.02\State=2-A\HF=-1235.2883496\S2=0.802229\S2-1=0.\S2A=0.7
50521\RMSD=6.913e-09\PG=C01 [X(C15H9N2O2S1)]\\@

Table E–93. Output parameters for Table 5.1; R = 2,2′-bithiophene.

N-N= 1.764337204243D+03 E-N=-1.104280294007D+04 KE= 2.441960358259D+03
1\1\GINC-COMPUTE-0-34\SP\UTD-B3LYP-FC\6-311+G(d,p)\C15H9N2O2S2(2)\BRYN
ND\07-Nov-2010\0\\# td ub3lyp/6-311+g(d,p) scrf=(cpcm,solvent=chlorofo
rm) geom=connectivity\\BNN-bithiophene TDDFT\\0,2\C,0,-5.828417,-1.214
484,-0.000293\C,0,-6.076532,0.164614,-0.000254\C,0,-5.033481,1.097003,
-0.000174\C,0,-3.750954,0.579649,-0.000138\C,0,-3.50457,-0.791816,-0.0
00178\C,0,-4.525762,-1.724444,-0.000257\N,0,-2.492822,1.228562,-0.0000
55\N,0,-2.100642,-0.95549,-0.000124\O,0,-2.333758,2.491714,0.000006\O,
0,-1.492002,-2.075517,-0.000142\H,0,-6.664195,-1.903269,-0.000354\H,0,
-5.21116,2.16395,-0.000142\H,0,-4.320482,-2.786436,-0.000286\H,0,-7.10
0022,0.518836,-0.000284\C,0,-1.497058,0.277323,-0.000048\C,0,2.408904,
0.318174,0.00027\C,0,1.95699,1.624122,0.000277\C,0,0.554004,1.740668,0
.000133\C,0,-0.093932,0.515938,0.000032\H,0,2.618577,2.48042,0.00046\H
,0,0.019264,2.677635,0.00016\S,0,1.067331,-0.806824,0.000004\C,0,3.772
792,-0.164942,0.000417\C,0,4.232386,-1.464953,0.001677\S,0,5.128076,0.
952554,-0.001145\C,0,5.649621,-1.567504,0.001376\H,0,3.57477,-2.324718
,0.002843\C,0,6.270233,-0.349516,-0.000078\H,0,6.184643,-2.507759,0.00

2241\H,0,7.327075,-0.130404,-0.000589\\Version=AM64L-G09RevA.02\State=2-A\HF=-1633.4825844\S2=0.805508\S2-1=0.\S2A=0.750649\RMSD=8.745e-09\PG=C01 [X(C15H9N2O2S2)]\\@

Table E–94. Output parameters for Table 5.1; R = *N*-methylindole.

N-N= 1.565347248146D+03 E-N=-7.936874654335D+03 KE= 1.390428470967D+03
1\1\GINC-COMPUTE-0-21\SP\UTD-B3LYP-FC\6-311+G(d,p)\C16H12N3O2(2)\BRYNND\07-Nov-2010\0\\# td ub3lyp/6-311+g(d,p) scrf=(cpcm,solvent=chloroform) geom=connectivity\\NMeIndoleBNN TDDFT\\0,2\C,0,5.147905,0.369034,-0.254669\C,0,5.005919,-0.977881,0.103307\C,0,3.747226,-1.546548,0.329171\C,0,2.659973,-0.706068,0.176029\C,0,2.801049,0.632493,-0.177052\C,0,4.038008,1.20885,-0.401436\N,0,1.274596,-0.945178,0.341478\N,0,1.498998,1.180527,-0.236136\O,0,0.791076,-2.056672,0.736859\O,0,1.249695,2.399223,-0.526168\H,0,6.139574,0.771771,-0.420845\H,0,3.622914,-2.584078,0.608765\H,0,4.133163,2.251208,-0.674353\H,0,5.890075,-1.594429,0.209495\C,0,0.575366,0.20757,0.067474\C,0,-2.036615,-1.910878,-0.360936\C,0,-1.934901,-0.53887,-0.075099\C,0,-3.132286,0.216876,0.037271\C,0,-4.401093,-0.351561,-0.100956\C,0,-4.467939,-1.71185,-0.371015\C,0,-3.295743,-2.479145,-0.503613\H,0,-1.145934,-2.515973,-0.451505\H,0,-5.300219,0.2455,-0.007521\H,0,-5.435422,-2.187134,-0.484998\H,0,-3.378036,-3.538258,-0.720164\C,0,-1.435686,1.648775,0.296661\C,0,-0.844814,0.405148,0.106068\N,0,-2.791616,1.539802,0.2687\H,0,-0.959531,2.602362,0.446645\C,0,-3.735131,2.637035,0.426655\H,0,-3.179614,3.558394,0.591181\H,0,-4.346727,2.747828,-0.471616\H,0,-4.3877,2.458469,1.283928\\Version=AM64L-G09RevA.02\State=2-A\HF=-931.7666211\S2=0.791173\S2-1=0.\S2A=0.750318\RMSD=3.804e-09\PG=C01 [X(C16H12N3O2)]\\@

Table E–95. Output parameters for Table 5.1; R = *N*-ethylcarbazole.

N-N= 2.122329164949D+03 E-N=-1.027794110274D+04 KE= 1.678586497352D+03
1\1\GINC-COMPUTE-0-26\SP\UTD-B3LYP-FC\6-311+G(d,p)\C21H16N3O2(2)\BRYNND\07-Nov-2010\0\\# td ub3lyp/6-311+g(d,p) scrf=(cpcm,solvent=chloroform) geom=connectivity\\carbazoleBNN TDDFT\\0,2\C,0,-6.551227,-0.151728,0.331219\C,0,-6.345811,1.192315,-0.010309\C,0,-5.064771,1.698958,-0.250951\C,0,-4.020021,0.799776,-0.132198\C,0,-4.22392,-0.533695,0.203671\C,0,-5.484783,-1.049059,0.446086\N,0,-2.627026,0.972064,-0.308629\N,0,-2.950792,-1.149968,0.23673\O,0,-2.094059,2.079434,-0.64935\O,0,-2.771762,-2.374626,0.544172\H,0,-7.559423,-0.50466,0.510491\H,0,-4.891357,2.73348,-0.514843\H,0,-5.628387,-2.08862,0.708121\H,0,-7.198865,1.854973,-0.08985\C,0,-1.983388,-0.223238,-0.080956\C,0,-0.553214,-0.459274,-0.159838\C,0,-0.059316,-1.760614,-0.4367\C,0,0.352433,0.598329,0.034678\C,0,1.298755,-2.01982,-0.523274\H,0,-0.759363,-2.570838,-0.576221\C,0,1.718331,0.348996,-0.041181\H,0,-0.013144,1.594631,0.236684\C,0,2.191439,-0.960895,-0.325276\C,0,3.084254,2.541247,0.390926\C,0,2.890966,1.185094,0.111875\C,0,4.013814,0.34106,-0.087463\C,0,5.318972,0.833,-0.007112\C,0,5.484685,2.186998,0.272295\C,0,4.382546,3.035401,0.469827\H,0,2.235835,3.19886,0.544074\H,0,6.487761,2.592742,0.340125\H,0,4.548149,4.08422,0.686623\N,0,3.57166,-0.95095,-0.362323\C,0,4.42786,-2.115329,-0.572675\H,0,3.910823,-2.788756,-1.259226\H,0,5.327875,-1.7765,-1.089769\C,0,4.792777,-2.843911,0.723016\H,0,3.898641,-3.209797,1.232859\H,0,5.433119,-3.700952,0.498667\H,0,5.332242,-2.184325,1.406539\H,0,6.179369,0.191275,-0.15194\H,0,1.644099,-3.023894,-0.735319\\Version=AM64L-G09RevA.02\State=2-A\HF=-1124.7768988\S2=0.792281\S2-1=0.\S2A=0.750331\RMSD=9.933e-09\PG=C01 [X(C21H16N3O2)]\\@

Table E–96. Output parameters for Table 5.1; R = terthiophene.

N-N= 2.442607902947D+03 E-N=-1.503171871077D+04 KE= 3.267920182922D+03
1\1\GINC-COMPUTE-0-30\SP\UTD-B3LYP-FC\6-311+G(d,p)\C19H11N2O2S3(2)\BRY
NND\07-Nov-2010\0\\# td ub3lyp/6-311+g(d,p) scrf=(cpcm,solvent=chlorof
orm) geom=connectivity\\BNN-tert-thiophene TDDFT\\0,2\C,0,7.689495,-1.
262977,0.000106\C,0,7.952923,0.113264,0.000001\C,0,6.920333,1.057271,-
0.000067\C,0,5.632067,0.554343,-0.000025\C,0,5.37049,-0.814376,0.00007
9\C,0,6.381212,-1.758349,0.000147\N,0,4.381368,1.217261,-0.000073\N,0,
3.964974,-0.962518,0.000095\O,0,4.236328,2.482116,-0.000168\O,0,3.3438
03,-2.075599,0.000184\H,0,8.517529,-1.961052,0.000155\H,0,7.109952,2.1
22159,-0.000148\H,0,6.164069,-2.817988,0.000227\H,0,8.980312,0.456037,
-0.000027\C,0,3.374817,0.277081,0.000002\C,0,-0.530458,0.360149,0.0000
11\C,0,-0.063241,1.662416,-0.000115\C,0,1.339893,1.762889,-0.000128\C,
0,1.974921,0.530682,-0.000013\H,0,-0.71504,2.526183,-0.0002\H,0,1.8852
65,2.693717,-0.000221\S,0,0.799889,-0.780232,0.000127\C,0,-1.895479,-0
.105992,0.00005\C,0,-2.373548,-1.400081,0.000207\S,0,-3.23565,1.031018
,-0.000124\C,0,-3.783527,-1.488425,0.000238\H,0,-1.727839,-2.2687,0.00
0331\C,0,-4.419153,-0.264594,0.00009\H,0,-4.317143,-2.429869,0.0004\C,
0,-5.835826,0.027402,0.000082\C,0,-6.469423,1.251531,0.000621\S,0,-7.0
25114,-1.265962,-0.000693\C,0,-7.888074,1.158609,0.000425\H,0,-5.93501
3,2.192783,0.001173\C,0,-8.336359,-0.132209,-0.000246\H,0,-8.546885,2.
01676,0.000791\H,0,-9.353012,-0.494356,-0.000511\\Version=AM64L-G09Rev
A.02\State=2-A\HF=-2185.3611722\S2=0.80721\S2-1=0.\S2A=0.750721\RMSD=4
.499e-09\PG=C01 [X(C19H11N2O2S3)]\\@

Table E–97. Output parameters for Table 5.1; R = *p*-diaminophenylamine.

N-N= 2.576563711688D+03 E-N=-1.217479444880D+04 KE= 1.907996726761D+03
1\1\GINC-COMPUTE-0-27\SP\UTD-B3LYP-FC\6-311+G(d,p)\C25H18N3O2(2)\BRYNN
D\07-Nov-2010\0\\# td ub3lyp/6-311+g(d,p) scrf=(cpcm,solvent=chlorofor
m) geom=connectivity\\TriarylamineBNN TDDFT\\0,2\C,0,-7.391079,-0.4783
69,0.512244\C,0,-7.391032,0.478477,-0.512392\C,0,-6.199559,0.978486,-1
.047041\C,0,-5.029193,0.47543,-0.507111\C,0,-5.029239,-0.475424,0.5070
85\C,0,-6.199655,-0.978427,1.046956\N,0,-3.676229,0.754319,-0.811124\N
,0,-3.676302,-0.754365,0.811176\O,0,-3.315268,1.569138,-1.723027\O,0,-
3.315442,-1.569173,1.72313\H,0,-8.335855,-0.8397,0.899554\H,0,-6.18459
6,1.716965,-1.837205\H,0,-6.184765,-1.716904,1.837123\H,0,-8.335773,0.
83985,-0.89975\C,0,-2.857348,-0.000047,0.000037\C,0,-1.408394,-0.00004
8,0.000051\C,0,-0.679982,-1.095852,0.506989\C,0,-0.680018,1.095763,-0.
50692\C,0,0.704547,-1.094916,0.504464\H,0,-1.205506,-1.943794,0.920568
\C,0,0.70451,1.094866,-0.504419\H,0,-1.205576,1.943683,-0.920508\C,0,1
.428885,-0.000012,0.000023\H,0,1.233803,-1.949426,0.905967\H,0,1.23373
4,1.949386,-0.905944\N,0,2.834898,0.000002,0.000006\C,0,3.561097,1.217
525,0.164108\C,0,3.215742,2.119485,1.178675\C,0,4.637678,1.516469,-0.6
80107\C,0,3.928266,3.305586,1.334303\H,0,2.391117,1.888806,1.842404\C,
0,5.355944,2.697398,-0.508341\H,0,4.908995,0.822862,-1.466915\C,0,5.00
3291,3.600334,0.494963\H,0,3.649915,3.994347,2.124057\H,0,6.186647,2.9
16471,-1.169808\H,0,5.560254,4.521225,0.62243\C,0,3.56111,-1.217509,-0
.164113\C,0,3.215737,-2.119478,-1.178667\C,0,4.637717,-1.516439,0.6800
75\C,0,3.92827,-3.305571,-1.33431\H,0,2.39109,-1.888811,-1.842372\C,0,
5.355993,-2.697359,0.508293\H,0,4.909046,-0.822826,1.466874\C,0,5.0033
23,-3.600302,-0.494998\H,0,3.649906,-3.994339,-2.124052\H,0,6.186716,-
2.91642,1.169738\H,0,5.560293,-4.521188,-0.622477\\Version=AM64L-G09Re
vA.02\State=2-A\HF=-1278.4159886\S2=0.794393\S2-1=0.\S2A=0.750374\RMSD
=4.066e-09\PG=C01 [X(C25H18N3O2)]\\@

Table E–98. Output parameters for Table 5.1; R = *N*-tolylphenothiazine.

N-N= 3.064182052294D+03 E-N=-1.519024532220D+04 KE= 2.561424344733D+03
1\1\GINC-COMPUTE-0-2\SP\UTD-B3LYP-FC\6-311+G(d,p)\C26H18N3O2S1(2)\BRYN
ND\07-Nov-2010\0\\# td ub3lyp/6-311+g(d,p) scrf=(cpcm,solvent=chlorofo
rm) geom=connectivity\\phenothiazineBNN TDDFT\\0,2\C,0,7.606052,1.1311
63,-0.481154\C,0,7.714146,-0.086456,0.205542\C,0,6.583048,-0.810093,0.
595519\C,0,5.359527,-0.255339,0.264421\C,0,5.252196,0.952747,-0.414427
\C,0,6.361941,1.679455,-0.80797\N,0,4.042818,-0.710867,0.506792\N,0,3.
871732,1.210902,-0.582177\O,0,3.778962,-1.788138,1.135198\O,0,3.419734
,2.235813,-1.190673\H,0,8.507145,1.660437,-0.765766\H,0,6.651248,-1.75
064,1.125305\H,0,6.263301,2.617677,-1.337023\H,0,8.696878,-0.476835,0.
440004\C,0,3.140527,0.190568,-0.014261\C,0,1.695412,0.086163,0.025536\
C,0,0.875526,1.213778,-0.16079\C,0,1.064317,-1.151826,0.259325\C,0,-0.
506386,1.102791,-0.135448\H,0,1.320872,2.179911,-0.342596\C,0,-0.31775
3,-1.249165,0.315384\H,0,1.660868,-2.035307,0.43161\C,0,-1.143297,-0.1
28781,0.089373\H,0,-1.099777,1.992635,-0.288173\C,0,-3.204056,-3.88049
3,-0.441247\C,0,-2.579095,-2.697858,-0.049364\C,0,-3.198223,-1.452232,
-0.257557\C,0,-4.478644,-1.442911,-0.829188\C,0,-5.114832,-2.631269,-1
.183397\C,0,-4.479835,-3.856087,-1.001052\H,0,-2.693058,-4.823681,-0.2
84575\H,0,-4.98716,-0.503096,-0.99005\H,0,-6.109126,-2.588568,-1.61264
2\H,0,-4.965869,-4.781415,-1.285731\S,0,-1.036399,-2.793837,0.835177\C
,0,-3.332406,0.964031,0.180305\C,0,-3.612525,1.72152,-0.957663\C,0,-4.
375027,2.882389,-0.850695\C,0,-4.871512,3.31251,0.386033\C,0,-4.585129
,2.537424,1.515854\C,0,-3.823028,1.375086,1.41825\H,0,-3.236656,1.4028
86,-1.923315\H,0,-4.587665,3.461147,-1.743379\H,0,-4.963088,2.8439,2.4
85609\H,0,-3.607498,0.781568,2.299209\C,0,-5.66935,4.58818,0.501499\H,
0,-5.01286,5.437695,0.718678\H,0,-6.198203,4.812194,-0.427224\H,0,-6.4
02117,4.527556,1.309068\N,0,-2.545119,-0.244298,0.108954\\Version=AM64
L-G09RevA.02\State=2-A\HF=-1714.7513871\S2=0.795013\S2-1=0.\S2A=0.7503
86\RMSD=6.945e-09\PG=C01 [X(C26H18N3O2S1)]\\@

Table E–99. Output parameters for Table 5.1; R = tetrathiafulvalene.

N-N= 2.097458250395D+03 E-N=-1.461280986002D+04 KE= 3.519287992575D+03
1\1\GINC-COMPUTE-0-28\SP\UTD-B3LYP-FC\6-311+G(d,p)\C13H7N2O2S4(2)\BRYN
ND\07-Nov-2010\0\\# td ub3lyp/6-311+g(d,p) scrf=(cpcm,solvent=chlorofo
rm) geom=connectivity\\BNN TTF TDDFT\\0,2\C,0,6.077822,-1.424648,0.149
317\C,0,6.382532,-0.066779,0.32156\C,0,5.386003,0.913747,0.329486\C,0,
4.087652,0.466928,0.159001\C,0,3.785247,-0.882539,-0.011359\C,0,4.7619
45,-1.863184,-0.022543\N,0,2.866191,1.178969,0.115003\N,0,2.38372,-0.9
70195,-0.15694\O,0,2.765335,2.445757,0.235102\O,0,1.732375,-2.04568,-0
.347185\H,0,6.880396,-2.151755,0.149041\H,0,5.608045,1.964154,0.460463
\H,0,4.512705,-2.907155,-0.156759\H,0,7.415705,0.231139,0.45134\C,0,1.
83876,0.293454,-0.072448\C,0,-2.163332,0.367772,-0.220324\C,0,-0.04981
7,1.870299,-0.126343\C,0,0.444802,0.60963,-0.165406\H,0,0.570668,2.748
308,-0.029054\S,0,-0.749925,-0.710513,-0.387928\S,0,-1.765558,2.102104
,-0.283028\C,0,-3.420062,-0.095772,-0.062706\S,0,-3.813917,-1.834607,0
.014451\S,0,-4.847425,0.965126,0.086166\C,0,-5.489667,-1.585046,0.5041
5\C,0,-5.951342,-0.334146,0.536844\H,0,-6.070157,-2.46847,0.731358\H,0
,-6.96248,-0.050307,0.793881\\Version=AM64L-G09RevA.02\State=2-A\HF=-2
352.4319017\S2=0.803076\S2-1=0.\S2A=0.750597\RMSD=5.828e-09\PG=C01 [X(
C13H7N2O2S4)]\\@

Table E–100. Output parameters for **5.3e**; TDDFT on X-ray geometry.


```
N-N= 2.602518404755D+03 E-N=-1.225687036600D+04  KE= 1.914582966535D+03
 1\1\GINC-COMPUTE-0-1\SP\UTD-B3LYP-FC\6-311+G(d,p)\C25H18N3O2(2)\BRYNND
 \07-Nov-2010\0\\# td ub3lyp/6-311+g(d,p) scrf=(cpcm,solvent=chloroform
 ) geom=connectivity\\TDDFT on BNN-Ph3 Xray structure\\0,2\C,0,-2.83988
 2,0.040104,-0.072596\C,0,-5.014565,0.691887,0.047466\C,0,-6.193676,1.4
 05595,0.127563\H,0,-6.208637,2.35468,0.144021\C,0,-7.35888,0.646472,0.
 182761\H,0,-8.195797,1.091333,0.240382\C,0,-7.333788,-0.751107,0.15517
 \H,0,-8.152146,-1.230695,0.199606\C,0,-6.137296,-1.457392,0.063478\H,0
 ,-6.1116,-2.406277,0.036736\C,0,-4.991817,-0.690328,0.013358\C,0,1.416
 962,0.027358,-0.259145\C,0,0.739202,1.049119,0.41408\H,0,1.234356,1.74
 0152,0.838338\C,0,-0.645214,1.065318,0.469025\H,0,-1.090963,1.769539,0
 .925513\C,0,-1.393288,0.050378,-0.143535\C,0,-0.714559,-0.972084,-0.82
 3653\H,0,-1.207158,-1.664181,-1.248175\C,0,0.663975,-0.977643,-0.88009
 2\H,0,1.109921,-1.674299,-1.347122\C,0,3.568844,1.194688,-0.116252\C,0
 ,3.440928,2.245702,-1.019446\H,0,2.886053,2.150007,-1.784387\C,0,4.125
 432,3.43451,-0.801686\H,0,4.021907,4.160697,-1.405898\C,0,4.961297,3.5
 60151,0.298448\H,0,5.424588,4.375742,0.452279\C,0,5.120152,2.498497,1.
 170894\H,0,5.712508,2.578173,1.909358\C,0,4.418821,1.31682,0.973248\H,
 0,4.520469,0.594693,1.582522\C,0,3.515572,-1.240158,-0.137788\C,0,4.67
 9491,-1.490889,-0.866007\H,0,4.975029,-0.869842,-1.520406\C,0,5.403632
 ,-2.651985,-0.630666\H,0,6.206026,-2.811602,-1.113387\C,0,4.966849,-3.
 583224,0.304569\H,0,5.464966,-4.376288,0.461235\C,0,3.797565,-3.340982
 ,1.004901\H,0,3.486267,-3.981187,1.635006\C,0,3.073694,-2.174006,0.797
 846\H,0,2.279444,-2.012704,1.293355\N,0,-3.670622,1.127774,0.003985\N,
 0,-3.63653,-1.076043,-0.052899\N,0,2.822393,-0.007975,-0.332508\O,0,-3
 .322006,2.361681,0.037639\O,0,-3.250321,-2.296061,-0.070222\\Version=A
 M64L-G09RevA.02\State=2-A\HF=-1278.1458561\S2=0.791508\S2-1=0.\S2A=0.7
 50325\RMSD=5.559e-09\PG=C01 [X(C25H18N3O2)]\\@
```


Table E–101. Output parameters for **5.3e**; D–A dimer, singlet.


```
1\1\GINC-COMPUTE-0-12\SP\UB3LYP\6-311+G(d,p)\C50H36N6O4\BRYNND\08-Nov-
 2010\0\\# ub3lyp/6-311+g(d,p) guess=mix geom=connectivity\\singlet\\0,
 1\C,0,7.1267,13.1192,6.8639\H,0,6.289,13.3141,7.2657\C,0,7.6978,13.949
 6,5.904\H,0,7.2343,14.7354,5.6408\C,0,8.9333,13.6615,5.3165\H,0,9.2847
 ,14.2528,4.662\C,0,9.6616,12.5282,5.6685\H,0,10.5048,12.3287,5.2799\C,
 0,9.0802,11.7141,6.6184\C,0,8.9447,6.4419,10.3395\C,0,7.6886,6.9216,9.
 9539\H,0,6.9075,6.4358,10.1924\C,0,7.5701,8.0965,9.229\H,0,6.7093,8.41
 2,8.9795\C,0,8.7109,8.823,8.8607\C,0,9.9711,8.3455,9.2516\H,0,10.7533,
 8.8288,9.0141\C,0,10.0806,7.1784,9.9793\H,0,10.94,6.8691,10.2401\C,0,7
 .9767,4.7486,11.8259\C,0,7.4882,5.4855,12.9007\H,0,7.9106,6.2987,13.15
 04\C,0,6.383,5.0307,13.6083\H,0,6.0351,5.5437,14.3286\C,0,5.7881,3.825
 8,13.2629\H,0,5.0273,3.5173,13.742\C,0,6.3023,3.0742,12.2218\H,0,5.908
 9,2.2376,12.0034\C,0,7.3907,3.5357,11.4939\H,0,7.7326,3.0228,10.7708\C
 ,0,10.1108,4.3182,10.7342\C,0,10.7474,3.5975,11.7458\H,0,10.5379,3.767
 7,12.656\C,0,11.6883,2.631,11.4168\H,0,12.1062,2.1279,12.1056\C,0,12.0
 249,2.3915,10.0894\H,0,12.6698,1.7303,9.8694\C,0,11.4091,3.1281,9.092\
 H,0,11.646,2.9789,8.1835\C,0,10.4492,4.0824,9.4028\H,0,10.0242,4.573,8
 .7092\N,0,7.5707,10.9392,8.0923\N,0,9.5251,10.4958,7.173\N,0,9.0899,5.
 2534,11.0801\O,0,6.4963,10.8687,8.7892\C,0,9.4407,3.6718,-0.1585\C,0,8
 .6913,1.7167,-1.0443\C,0,7.963,0.5916,-1.3757\H,0,7.1252,0.3967,-0.973
 9\C,0,8.534,-0.2388,-2.3356\H,0,8.0705,-1.0247,-2.5988\C,0,9.7695,0.04
 93,-2.9231\H,0,10.1209,-0.542,-3.5776\C,0,10.4979,1.1826,-2.5711\H,0,1
 1.3411,1.382,-2.9597\C,0,9.9164,1.9967,-1.6212\C,0,9.7809,7.2689,2.099
```

9\C,0,8.5248,6.7892,1.7143\H,0,7.7438,7.2749,1.9528\C,0,8.4063,5.6143,
0.9894\H,0,7.5455,5.2987,0.7399\C,0,9.5471,4.8878,0.6211\C,0,10.8073,5
.3653,1.012\H,0,11.5895,4.8819,0.7745\C,0,10.9168,6.5323,1.7397\H,0,11
.7762,6.8417,2.0006\C,0,8.8129,8.9622,3.5864\C,0,8.3244,8.2253,4.6611\
H,0,8.7468,7.412,4.9108\C,0,7.2192,8.6801,5.3687\H,0,6.8713,8.167,6.08
9\C,0,6.6243,9.8849,5.0233\H,0,5.8635,10.1935,5.5024\C,0,7.1385,10.636
5,3.9822\H,0,6.7451,11.4732,3.7638\C,0,8.227,10.175,3.2543\H,0,8.5688,
10.688,2.5312\C,0,10.947,9.3925,2.4946\C,0,11.5836,10.1132,3.5063\C,0,
12.5246,11.0797,3.1772\H,0,12.9424,11.5828,3.866\C,0,12.8611,11.3192,1
.8498\H,0,13.506,11.9805,1.6298\C,0,12.2453,10.5827,0.8525\H,0,12.4822
,10.7319,-0.056\C,0,11.2854,9.6283,1.1633\H,0,10.8604,9.1378,0.4697\N,
0,8.4069,2.7716,-0.1473\N,0,10.3614,3.215,-1.0665\N,0,9.9261,8.4573,2.
8405\O,0,7.3325,2.8421,0.5496\O,0,11.4571,3.7846,-1.4025\H,0,11.3742,9
.943,4.4164\C,0,8.6045,10.0389,8.081\C,0,7.855,11.9941,7.1953\O,0,10.6
208,9.9261,6.837\\Version=AM64L-G09RevA.02\State=1-A\HF=-2556.2682611\
S2=1.088157\S2-1=0.\S2A=0.699034\RMSD=1.149e-09\Dipole=-0.0937512,-0.0
756002,0.0245314\Quadrupole=-20.5596328,23.4513911,-2.8917583,-0.01176
91,1.6292779,-1.3408082\PG=C01 [X(C50H36N6O4)]\\@

Table E–102. Output parameters for **5.3e**; D–A dimer, triplet.

1\1\GINC-COMPUTE-0-13\SP\UB3LYP\6-311+G(d,p)\C50H36N6O4(3)\BRYNND\07-N
ov-2010\0\\# ub3lyp/6-311+g(d,p) geom=connectivity\\triplet\\0,3\C,0,7
.1267,13.1192,6.8639\H,0,6.289,13.3141,7.2657\C,0,7.6978,13.9496,5.904
\H,0,7.2343,14.7354,5.6408\C,0,8.9333,13.6615,5.3165\H,0,9.2847,14.252
8,4.662\C,0,9.6616,12.5282,5.6685\H,0,10.5048,12.3287,5.2799\C,0,9.080
2,11.7141,6.6184\C,0,8.9447,6.4419,10.3395\C,0,7.6886,6.9216,9.9539\H,
0,6.9075,6.4358,10.1924\C,0,7.5701,8.0965,9.229\H,0,6.7093,8.412,8.979
5\C,0,8.7109,8.823,8.8607\C,0,9.9711,8.3455,9.2516\H,0,10.7533,8.8288,
9.0141\C,0,10.0806,7.1784,9.9793\H,0,10.94,6.8691,10.2401\C,0,7.9767,4
.7486,11.8259\C,0,7.4882,5.4855,12.9007\H,0,7.9106,6.2987,13.1504\C,0,
6.383,5.0307,13.6083\H,0,6.0351,5.5437,14.3286\C,0,5.7881,3.8258,13.26
29\H,0,5.0273,3.5173,13.742\C,0,6.3023,3.0742,12.2218\H,0,5.9089,2.237
6,12.0034\C,0,7.3907,3.5357,11.4939\H,0,7.7326,3.0228,10.7708\C,0,10.1
108,4.3182,10.7342\C,0,10.7474,3.5975,11.7458\H,0,10.5379,3.7677,12.65
6\C,0,11.6883,2.631,11.4168\H,0,12.1062,2.1279,12.1056\C,0,12.0249,2.3
915,10.0894\H,0,12.6698,1.7303,9.8694\C,0,11.4091,3.1281,9.092\H,0,11.
646,2.9789,8.1835\C,0,10.4492,4.0824,9.4028\H,0,10.0242,4.573,8.7092\N
,0,7.5707,10.9392,8.0923\N,0,9.5251,10.4958,7.173\N,0,9.0899,5.2534,11
.0801\O,0,6.4963,10.8687,8.7892\C,0,9.4407,3.6718,-0.1585\C,0,8.6913,1
.7167,-1.0443\C,0,7.963,0.5916,-1.3757\H,0,7.1252,0.3967,-0.9739\C,0,8
.534,-0.2388,-2.3356\H,0,8.0705,-1.0247,-2.5988\C,0,9.7695,0.0493,-2.9
231\H,0,10.1209,-0.542,-3.5776\C,0,10.4979,1.1826,-2.5711\H,0,11.3411,
1.382,-2.9597\C,0,9.9164,1.9967,-1.6212\C,0,9.7809,7.2689,2.0999\C,0,8
.5248,6.7892,1.7143\H,0,7.7438,7.2749,1.9528\C,0,8.4063,5.6143,0.9894\
H,0,7.5455,5.2987,0.7399\C,0,9.5471,4.8878,0.6211\C,0,10.8073,5.3653,1
.012\H,0,11.5895,4.8819,0.7745\C,0,10.9168,6.5323,1.7397\H,0,11.7762,6
.8417,2.0006\C,0,8.8129,8.9622,3.5864\C,0,8.3244,8.2253,4.6611\H,0,8.7
468,7.412,4.9108\C,0,7.2192,8.6801,5.3687\H,0,6.8713,8.167,6.089\C,0,6
.6243,9.8849,5.0233\H,0,5.8635,10.1935,5.5024\C,0,7.1385,10.6365,3.982
2\H,0,6.7451,11.4732,3.7638\C,0,8.227,10.175,3.2543\H,0,8.5688,10.688,
2.5312\C,0,10.947,9.3925,2.4946\C,0,11.5836,10.1132,3.5063\C,0,12.5246
,11.0797,3.1772\H,0,12.9424,11.5828,3.866\C,0,12.8611,11.3192,1.8498\H
,0,13.506,11.9805,1.6298\C,0,12.2453,10.5827,0.8525\H,0,12.4822,10.731
9,-0.056\C,0,11.2854,9.6283,1.1633\H,0,10.8604,9.1378,0.4697\N,0,8.406
9,2.7716,-0.1473\N,0,10.3614,3.215,-1.0665\N,0,9.9261,8.4573,2.8405\O,

0,7.3325,2.8421,0.5496\O,0,11.4571,3.7846,-1.4025\H,0,11.3742,9.943,4.
4164\C,0,8.6045,10.0389,8.081\C,0,7.855,11.9941,7.1953\O,0,10.6208,9.9
261,6.837\\Version=AM64L-G09RevA.02\State=3-A\HF=-2556.2682616\S2=2.08
8167\S2-1=0.\S2A=2.003469\RMSD=4.029e-09\Dipole=-0.0937291,-0.0757175,
0.0243944\Quadrupole=-20.559778,23.4508263,-2.8910483,-0.0116067,1.629
1302,-1.3403749\PG=C01 [X(C50H36N6O4)]\\@